PROCEEDINGS OF THE INTERNATIONAL CONFERENCE
ON HYDRO-TECHNICAL ENGINEERING
FOR PORT AND HARBOR CONSTRUCTION

HYDRO-PORT'94

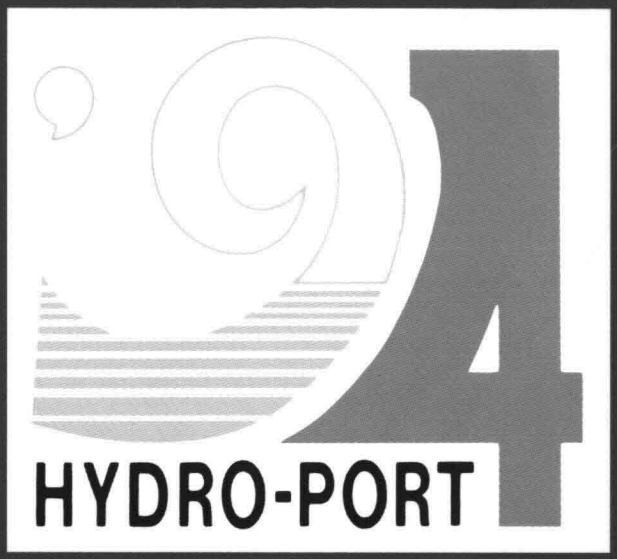

Edited by
Port and Harbour Research Institute
Ministry of Transport

(VOLUME 2)

OCTOBER 19-21, 1994
YOKOSUKA, JAPAN

HYDRO-PORT'94

PROCEEDINGS OF THE INTERNATIONAL CONFERENCE

ON HYDRO-TECHNICAL ENGINEERING

FOR PORT AND HARBOR CONSTRUCTION

Sponsored by

Port and Harbour Research Institute, Ministry of Transport

Coastal Development Institute of Technology

under the auspices of

The Japan Society of Civil Engineers

Yokosuka City

(VOLUME 2)

OCTOBER 19-21,1994
YOKOSUKA,JAPAN

Complete set of two volumes ISBN 4-900302-04-X

Edited by Port and Harbour Research Institute, Ministry of Transport
Published by Coastal Development Institute of Technology

CONTENTS

PREFACE i
MEMBERS OF COMMITTEES iii
CONFERENCE TIMETABLE v

KEYNOTE LECTURE

A Plea for Engineering-minded Research Efforts in Harbor and Coastal Engineering
Professor Yoshimi Goda, Yokohama National University, Japan 1

SPECIAL LECTURES

Management of Coastal Waters in Western Australia:The Use of Integrated Models
Dr. Desmond A.Lord, Director of D.A.Lord and Associates, Australia 23

Engineering Devices for a Smooth Port Operation with Focus on Developing Countries
Professor Isao Irie, Kyushu University, Japan 43

Theme 1. ACQUISITION AND ANALYSIS OF WAVE INFORMATION FOR STRUCTURAL DESIGN

Introduction of Japanese NOWPHAS System and its Recent Topics (Nationwide Ocean Wave information network for Ports and HArbourS)
T.Nagai, K.Sugahara, N.Hashimoto, T.Asai, S.Higashiyama and K.Toda, Japan 67

Wave Monitoring System of the Korea Maritime and Port Administration
K.S.Park, D.Y.Lee, C.S.Kim, S.W.Kang, K.S.Bahk, K.C.Jeon, S.I.Kim, J.S.Shim and B.C.Oh, Korea 83

Cooperation on the Improvement of the Wave Measurement and Analysis Technology between PHRI and KORDI
D.Y.Lee [1], *K.S.Bahk* [1], *K.S.Park* [1], *B.C.Oh* [1], *K.D.Seo* [1], *T.Nagai* [2], *N.Hashimoto* [2], *T.Asai* [2] *and T.Horie* [2]; [1] *Korea,* [2] *Japan* 93

Reliability of Wave Forecasting by Autoregressive Model Represented in Wave Energy
H.Ohashi, S.Akamura, M.Suzuki and H.Inada, Japan 107

On the Extreme Wave Height Analysis
H.F.Burcharth and Z.Liu, Denmark 123

Evaluation of Directional Wave Measurements – a Comparative Field Exercise
A.van Tonder and J.Davies, South Africa 143

Measured Transformation of Deep Water Wave Spectra Across a Shallow Coral Reef Flat
D.D.McGehee, U.S.A. 165

Applicability of Surface Displacement Recovery Methods from Pressure Gauge for Irregular Waves
J.G.Kwon and Y.M.Yang, Korea 175

A Classification of the Explored Techniques for Detecting Offshore Waves
S.Nakamura, Japan 187

Investigation of the Harbour Tranquillity Based on Wave Group Characteristics
T.Nagai, N.Hashimoto, T.Asai, I.Tobiki, K.Ito, T.Toue, A.Kobayashi and T.Shibata, Japan 203

A Wave Forecasting Model by Multiple Regression with Coastal Wave Observation Data
N.Sato, T.Aono and C.Goto, Japan 217

On the Development of a Global Ocean Wave Model JWA3G
Y.Suzuki, I.Isozaki and T.Tanahashi, Japan 227

Theme 2. WAVE TRANSFORMATION ANALYSIS FOR PORT CONSTRUCTION

Field Application of Angular Spectrum Model to Directional Wave Transformation
K.D.Suh, B.C.Oh and J.S.Shim, Korea 239

Time Domain Simulation of Directional Wave Propagation into Harbours
O.G.Nwogu and E.P.D.Mansard, Canada 253

The Development and Application of a Computational Model of Directional Wave Transformation in Harbours
N.P.Tozer and J.V.Smallman, U.K. 267

Applicability of Multi-directional Wave Experiment for Port Design
Y.Suzuki, T.Hiraishi, T.Takayama and N.Ikeda, Japan 281

Field Applicability of Wave Models to Estimating the Wave Fields Outside and Inside a Harbor
T.Shimizu, A.Ukai, Y.Kubo and M.Shimada, Japan 303

Development and Application of a Numerical Model for Wave Diffraction through Breakwater Gaps
D.Anand and V.Sundar, India 317

Penetration of Long Waves into a Lagoon Harbour and Resulting Ship Motions
V.Barthel, E.P.D.Mansard and D.D.MacDonald, Canada 333

Wave Height Distribution around a Vertical Circular Cylinder in Multi-Directional Random Seas
T.Ikeya, K.Iwase and J.Minami, Japan 353

Field Observation on Wave Dissipation and Reflection by an Artificial Reef with Varying Crown Width
S.Ohnaka and T.Yoshizawa, Japan 365

Characteristics of Wave Deformation on the Reef
Y.Okuyama, K.Adachi, S.Miyazaki and M.Teruya, Japan 377

Slope Effect on Wave Overtopping Rate of Block Armored Seawall
T.Sekimoto, H.Kunisu and T.Yamazaki, Japan 393

Study of Wave Overtopping on a Breakwater of Marina
T.Kono, Z.Amin and H.Tsuda, Japan 405

Random Model and Simulation for Nonlinear Interaction of Irregular Waves and Vertical Wall
H.Guangwen and F.Weibing, China 423

Estimation of Wharf Operation Efficiency of All-Weather Berth Based on Ship Motions
S.Ueda, S.Shiraishi, T.Kawahara, T.Akahoshi and S.Sugiura, Japan 443

Theme 3. DESIGN WAVE FORCES ON COMPOSITE BREAKWATERS

Caisson Breakwaters: Integrated Design and Wave Load Specifications
H.Oumeraci, A.Kortenhaus and P.Klammer, Germany 453

Experimental Study and Theoretical Comparison of Irregular Wave Pressures on Deepwater Composite Breakwaters
H.S.Hou, Y.D.Chiou and C.H.Chien, Chinese Taipei 473

A Proposal of Impulsive Pressure Coefficient for the Design of Composite Breakwaters
S.Takahashi, K.Tanimoto and K.Shimosako, Japan 489

A Comparative Study on Wave Forces and Overtopping of Caisson Breakwaters
J.Juhl, Denmark 505

Design of Harbour Entrances: Breakwater Design and Vessel Safety
M.W.McBride, J.V.Smallman and N.W.H.Allsop, U.K. 525

A New Type of Breakwater with a Step-Shaped Slit Wall
R.Fujiwara, T.Yoshida, K.Kurata, S.Kakuno and K.Oda, Japan 543

Hydraulic Experiments for Basic Design of Offshore Breakwater for Protecting Artificial Island
D.S.Lee, W.S.Park, K.D.Suh and Y.M.Oh, Korea 563

New Types of Breakwater Two Projects in MONACO
R.Bouchet, P.Cellario and J.L.Isnard, Monaco 581

Field Demonstration Test on a Semi-Circular Breakwater
H.Sasajima, T.Koizuka, H.Sasayama, Y.Niidome and T.Fujimoto, Japan 593

Design of Coastal Structures – an overview –
K.W.Pilarczyk, Netherlands 617

Hydraulic Model Test on Stability of a Low Crest Breakwater with Tetrapod Armour Layer
A.B.Widagdo, Sudarpo and D.C.Istiyanto, Indonesia 641

Berm Breakwaters in Iceland, Practical Experiences
S.Sigurdarson and G.Viggosson, Iceland 651

Hydraulic Characteristics of Breakwaters with Rear Parapets
H.Funakoshi, N.Simizu, S.Tsuda, K.Sano and T.Yoshida, Japan 673

Field Sliding Test of Double Cylinder Caisson Breakwater
R.Ojima, T.Owaki, N.Yamagata and Y.Komoto, Japan 691

Development of Wave-Dissipating Block-Embedded Double-Box Caisson for Breakwaters
A.Mutoh, H.Fujisaki, H.Geshi and S.Mori, Japan 707

Study of Deep Water Breakwater Design Factors
H.S.Hou, C.C.Chen and T.M.Hu, Chinese Taipei 721

Hydraulic Characteristics of a Sloping Top Caisson – Wave forces acting on the sloping top caisson –
S.Takahashi, T.Hosoyamada and S.Yamamoto, Japan 733

Wave Pressure on a Perforated Wall Caisson
S.Takahashi and K.Shimosako, Japan 747

Experimental Studies on Tsunami Flow and Armor Block Stability for the Design of a Tsunami Protection Breakwater in Kamaishi Bay
S.Hitachi, M.Kawada and H.Tsuruya, Japan 765

Theme 4. HARBOR WATER QUALITY AND SEAWATER QUALITY IMPROVEMENT

Characteristics of Wind Induced Upwelling in Tokyo Bay based on Analysis of NOAA-AVHRR data
S.Ueno, K.Nadaoka, H.Ohtani and H.Katsui, Japan 785

3-Dimensional Modelling of Heated Water Discharges into Coastal Waters of Yellow Sea
S.W.Kang and T.S.Jung, Korea 805

Development of Water–Intake Works with Submerged Mound (WWSM)
A.Nakayama, M.Yamamoto, J.Yamamoto and A.Moriguchi, Japan 823

Water Quality in Penang Harbor
P.M.Sivalingam and S.V.Charles, Malaysia 843

Environmental Monitoring of the Lagunar Complex of the South Region of the Santa Catarina State
D.Accetta, W.S.S.Dias, B.M.Vargas and J.A.dos.Santos, Brazil 871

Channel Experiments on Coastal Water Purification by Stone Bed with Biofilm
Y.Hosokawa, T.Ootsuki and C.Niwa, Japan 885

Sand Covering for Improving Quality of Bottom Sediments in Japanese Harbors
S.Inoue, T.Horie, K.Murakami, Y.Hosokawa, S.Sato and Y.Sega, Japan 907

Water Exchange Mechanisms in Enclosed Coastal Seas influenced by Marine Structure
K.Murakami, K.Shimizu and K.Yamada, Japan 921

Development of model by soil diffusion within Dam
M.S.Shin, J.N.Lee and S.K.Hong, Korea 941

A Physical–Biological Simulation on a Nutrient Absorption Process by Seaweed in the Bay
K.Furukawa and Y.Hosokawa, Japan 953

Red Water in Nippon–maru Memorial Park and Countermeasures against it
E.Yauchi, K.Yokobori, I.Iida and T.Uesugi, Japan 967

A Study of Sandy Beach Surf Zone as Nursery Grounds for Marine Organisms
M.Gomyoh, Y.Suda, M.Nakagawa, T.Otsuki, J.Higano, K.Adachi and K.Kimoto, Japan 977

Theme 5. BEACH STABILIZATION IN THE VICINITY OF A HARBOR

Change of the Ag.Nikolaos Beach in the Vicinity of a New Harbor for Small Crafts
C.I.Moutzouris, Greece 987

Protection against Shore Erosion and Channel Shoaling at Port Madero, MEXICO
J.M.Montoya R. [1], *J.R.Vera.S.* [1] *and S.Sato* [2]; [1] *Mexico,* [2] Japan 999

Control of Littoral Drift in Caldera Port, Costa Rica
J.G.Rodoriguez P. [1] *and K.Katoh* [2]; [1] *Costa Rica,* [2] *Japan* 1019

Physical Impact of Bilbao Harbour New Breakwater on Adjacent Beaches
J.P.Sierra, J.A.Jiménez, A.Sánchez-Arcilla, J.M.Picó, A.Viñuales and E.J.Villanueva, Spain 1041

Littoral Drift in Fishing Ports and Approach Channels: Problems and Countermeasures
M.Fukuya, N.Takaki, K.Ota, S.Harikai and M.Ikeda, Japan 1059

Stabilization of Beach in Integrated Shore Protection System
K.Katoh, S.Yanagishima, S.Nakamura and M.Fukuta, Japan 1077

Scour around the Head of a Vertical-Wall Breakwater
T.Gökçe, B.M.Sumer and J.Fredsøe, Denmark 1097

Stability of Beaches Protected with Detached Breakwaters
Y.Kuriyama, K.Katoh and Y.Ozaki, Japan 1117

Gros Beach Nourishment(San Sebastian, SPAIN)
J.M.M.Villaverde, Spain 1131

Development and Application of a Numerical Model for Shoreline Simulation
K.Janardanan and V.Sundar, India 1141

Drifting Characteristics of Littoral Sand Around Submerged Breakwater (Field Survey on Niigata West Coast)
H.Funakoshi, T.Shiozawa, A.Tadokoro and S.Tsuda, Japan 1157

Investigation of Current and Particle Velocity near the Surf Zone
C.-K.Chang and F.-T.Chang, Chinese Taipei 1179

Two Dimensional Change of Swash Slope
S.Kubota, Y.Hida and M.Takezawa, Japan 1193

Theme 6. COUNTERMEASURES AGAINST SHOALING DUE TO SILTATION AND SEDIMENTATION IN THE HARBOR AND WATERWAY

Criteria and Methods to Determine Navigable Depth in Hyperconcentrated Sediment Layers
W.R.Parker and P.M.Hooper, U.K. 1211

Field Surveys on Siltation–Prevention Effects in Waterway and Anchorage by Submerged Walls
T.Kihara, H.Sasajima, K.Yoshinaga, T.Koizuka, H.Sasayama, H.Yoshinaga and T.Fujimoto, Japan 1225

Case Study on Channel Improvement in the Mouth of the Yongjiang River
J.Jiang, China 1243

Field Survey on Estuarine Mud Transport Process around Navigation Channel, Banjarmasin, Indonesia
H.Tsuruya, K.Murakami, K.Nagai and I.Irie, Japan 1253

Modelling Cohesive Sediment Transport in Tidal Waters
K.P.P.Pathirana, C.S.Yu and J.Berlamont, Belgium 1271

Viscous Damping of Irregular Waves Propagating over Mud Seabeds
Z.Zhao and H.Li, China 1291

AUTHOR INDEX 1301

Theme 4

HARBOR WATER QUALITY AND SEAWATER QUALITY IMPROVEMENT

HYDRO-PORT'94
International Conference on Hydro-Technical
Engineering for Port and Harbor Construction
October 19 - 21, 1994, Yokosuka, Japan

Characteristics of Wind Induced Upwelling in Tokyo Bay based on Analysis of NOAA-AVHRR data

Seizo Ueno [1]
Kazuo Nadaoka [2]
Hideo Ohtani [1]
Hidehiro Katsui [1]

[1] Technology Research Center, Taisei corporation
344-1, Nasemachi, Totsukaku, Yokohama, 245
[2] Department of Civil Engineering, Tokyo Institute of Technology
2-12-1, Ohokayama, Meguroku, Tokyo, 152

ABSTRACT

Spatial patterns of the upwelling in Tokyo bay induced by the wind forces were investigated using infrared images taken by the advanced very high resolution radiometer (AVHRR) on the NOAA satellite platforms. The generation-propagation processes of the upwelling were also examined through the satellite data analysis and numerical experiments. The processes of the upwelling strongly depend on the wind conditions, and consist of two stages as follows: 1) during the northern wind blowing, the upwelling is generated at the region stretched along the east coast from the northern head of the bay to southern bay mouth. This generation process can be explained as a part of the vertical circulation system induced by wind forces and this was basically suggested by Ohtubo and Muraoka (1988). 2) after the northern wind stops blowing, the upwelling region propagates anticlockwise along the coast, and is localized in the northern head of the bay. This propagation process is in agreement with that of the internal Kelvin wave which was previously suggested by Unoki (1990) and Matsuyama et al. (1990).

Key Words: Internal Kelvin Wave, Satellite Infrared Image, Sea Surface Temperature, Aoshio, Little dissolved oxygen water

1. INTRODUCTION

Although the coastal upwelling in the open ocean, for example, off Peru and off California, is recognized as an important physical factor in coastal environment, the roles of the upwelling in bays on the water quality changes have not yet well understood because its intermittent occurrence makes observations difficult. In the sea areas enclosed by land, such as bays, the upwelling is easily generated by the wind forces with very short response time, and brings the water mass near

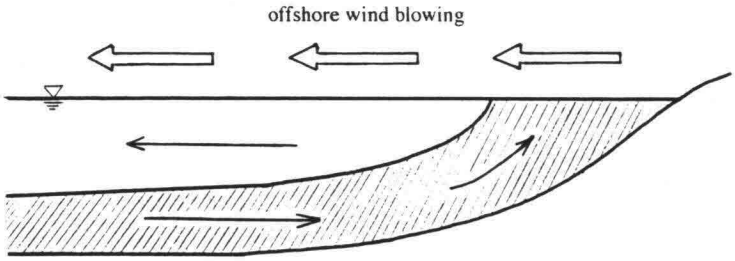

(a) upwelling generated by the offshore wind blowing

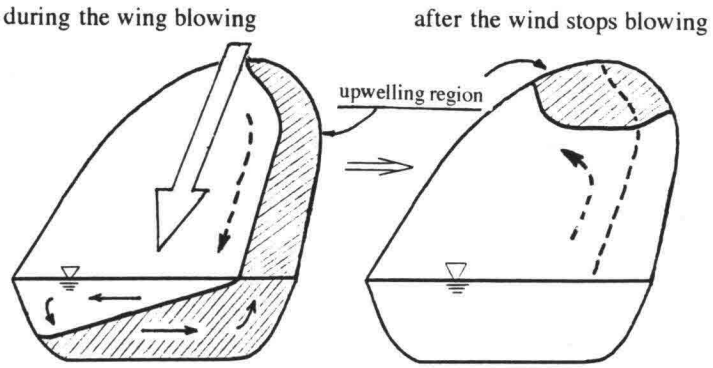

(b) upwelling associated with the internal Kelvin wave

Figure 1 Two mechanisms of the upwelling in Tokyo bay: (a) upwelling generated as a part of the vertical circulation induced by the offshore wind blowing (Ohtubo and Muraoka, 1988), (b) upwelling associated with the internal Kelvin wave which is generated as the interface setup during the wind blowing and propagates anticlockwise along the coast after the wind stops blowing (Unoki,1990; Matsuyama et al.,1990).

the sea bottom to the sea surface which contains the rich nutrient and the little dissolved oxygen in the eutophicated bays. Therefore, it is suggested that the upwelling in bays causes the rapid change of the water qualities in the coastal area.

As one of the water quality problems in Japan which are directly influenced by the upwelling, the phenomenon called 'Aoshio' gives us a good example. Aoshio is the phenomenon which upwells the little dissolved oxygen water near the sea bottom to the coastal region. In the case of Tokyo bay, Aoshio occurs mainly at the end of summer and its occurrence periods tend to correspond with those of the northern wind blowing. During the Aoshio occurrence, shellfish and fish inhabiting the coastal region often suffer sever damage because they are exposed to the almost no oxygen water brought by Aoshio. The detail of Aoshio is mentioned in section 2.

The mechanisms of the upwelling causing Aoshio have been investigated by many researchers in Japan under the simple condition of the two layered sea area because Tokyo bay is strongly stratified in summer as described in section 2. Those mechanisms can be classified into the following two types according the wind force conditions inducing the upwelling. Ohtubo and

Muraoka(1988) considered the condition of the steady offshore wind blowing, and showed that the upwelling is generated at the upwind side of the bay as a part of the vertical circulation system driven by the offshore wind blowing (Figure 1(a)). On the other hand, the mechanism proposed by Unoki(1990) and Matsuyama et al.(1990) includes the unsteady characteristics of the wind forces, and consists of two stages related with the wind conditions (Figure 1(b)). The first stage proceeds during the wind blowing, in which the upwelling is generated at the upwind side of the bay and extended along the left-hand coast to the direction of the wind blowing. This upwelling pattern can be explained by the former mechanism by Ohtubo and Muraoka(1988) if the effects of the Coriolis force are introduced into their mechanism. After the wind stops blowing the second stage starts, in which the upwelling region generated during the wind blowing propagates along the coast in the anticlockwise direction. This propagation pattern of the upwelling region can be interpreted as the oscillation of the density interface affected by the Coriolis forces, what is called, the internal Kelvin wave. The internal Kelvin wave rotates anticlockwise in the northern hemisphere about the amphidromic center with amplitudes increasing from zero at the center to a maximum at the boundary of the bay. Consequently, the upwelling generated at the large amplitude region propagates in the same way.

It should be noted that there is the apparent difference in the upwelling patterns led by these two mechanisms, i.e., regarding the upward direction in Figure 1(b) as the north, while the former mechanism suggests that the upwelling region is stretched southward along the east coast as the northern wind blows, the latter suggests that the upwelling region propagates northward after the wind stops blowing.

Giving a focus on this difference in the upwelling patterns, Ueno et al. (1992) investigated the relationship between the upwelling regions and the wind conditions in Tokyo bay using the satellite infrared images, and showed that some upwelling patterns are in agreement with the later mechanism proposed by Unoki(1990) and Matsuyama et al.(1990). In the present study, a large number of infrared images taken by the advanced very high resolution radiometer (AVHRR) on the satellite platforms of NOAA were collected and further investigation to Ueno et al.(1992) was made to show the general characteristics of the wind-induced upwelling in Tokyo bay. A brief background of Tokyo bay and Aoshio is presented in section 2. Descriptions of the satellite infrared data and data processing are given in section 3. In section 4 the upwelling patterns obtained from the infrared images are shown and related to the wind conditions. In section 5 the processes of the generation and the propagation of the upwelling are examined by the numerical experiments. The general characteristics of the upwelling in Tokyo bay are also discussed in section 5. Finally, the conclusions of this study are summarized in section 6.

2. BACKGROUND of TOKYO BAY and AOSHIO

Tokyo bay is the sea area almost enclosed by two peninsulas. It is approximately 50km long and 30km wide and is connected with the Pacific Ocean through the bay mouth of 7km wide at the south side of the bay(Figure 2). The depth increases from about 10m at the northern head of the bay up to about 70m at the southern bay mouth and the average depth is 17m. The feature of quasi-enclosed topography of Tokyo bay keeps the weak water exchange between the bay and the ocean. The land area faced on Tokyo bay has been so fully industrialized and heavily populated that a large amount of industrial waste water and urban sewage has been flowing into Tokyo bay. As a result of the weak water exchange and the high loading, the processes of the eutrophication

in the bay have proceeded causing many problems in the water environment, for instances, the occurrence of the red tides, the generation of the little dissolved oxygen water and so on.

Seasonal changes of the vertical profiles for the density and the dissolved oxygen concentration at the center of Tokyo bay reported by Unoki(1985) are shown in Figure 3. During summer, the strong stratification is generated due to the high solar radiation and the high precipitation. The the dissolved oxygen concentration near the sea bottom decreases as the stratification becomes strong because the strong stratification restricts the vertical flux of the dissolved oxygen; besides, the dissolved oxygen is consumed at the high rate under the eutrophication condition. Thus, the stratification as well as the weak water exchange is considered as an important physical factor which influences the processes of the water quality change in Tokyo bay.

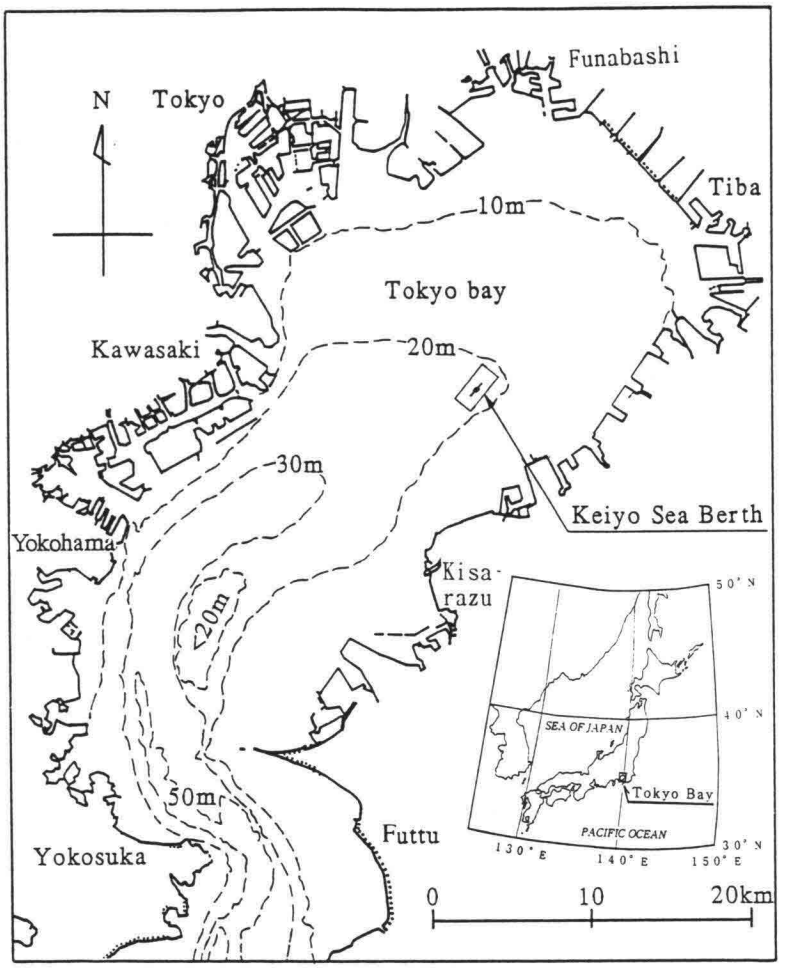

Figure 2 Topography and location map of Tokyo bay.

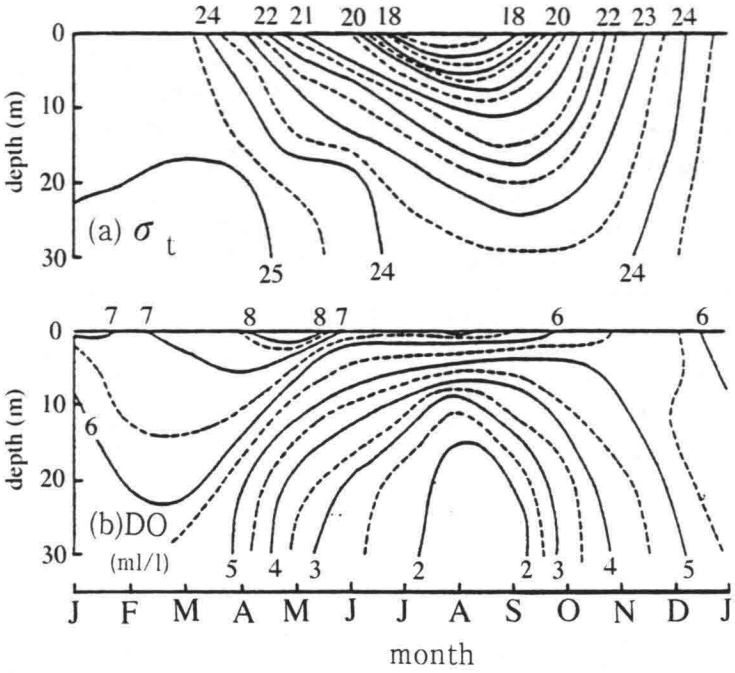

Figure 3 Seasonal changes of the vertical profiles of (a) the density, σt and (b) the dissolved oxygen concentration, DO observed at the center of Tokyo bay (Unoki, 1985).

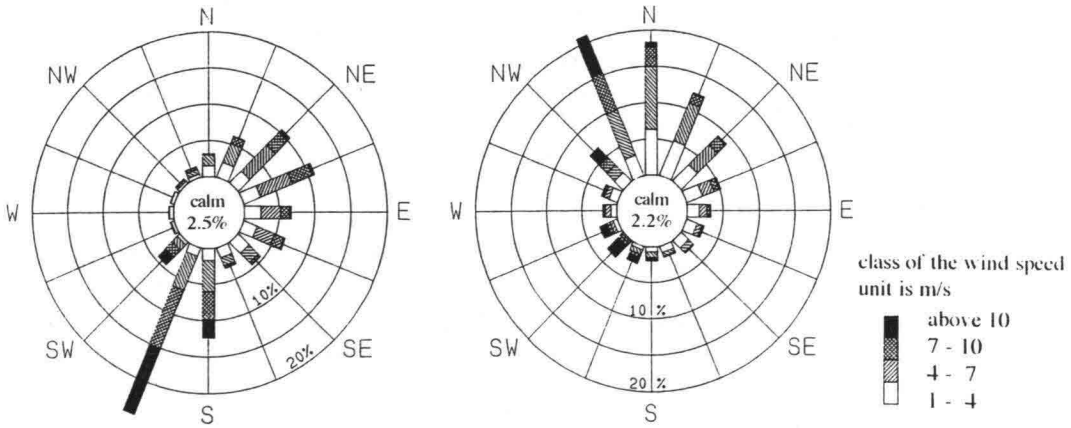

(a) summer (b) winter

Figure 4 Wind roses measured for 6 years at the Keiyo Sea Berth near the center of Tokyo bay for (a) summer form June to August and (b) winter from December to February.

Wind roses at the center of Tokyo bay during summer and winter are represented in Figure 4. During winter, the northern winds become dominant and act as the main driving force to keep the anticlockwise residual current in the bay. During summer, although the dominant wind direction can be estimated as the south, its dominant tendency is weaker than that in winter. Therefore, the stable residual current system can be hardly observed in summer. The unsteady currents which quickly respond to the change of the wind forces with a response time of less than one day, have been observed in stead (Morikawa and Murakami,1986; Odamaki et al.,1990; Ueno et al.,1993). Thus, for the study of the upwelling as well as the residual currents, the unsteady characteristics of the wind forces must be considered.

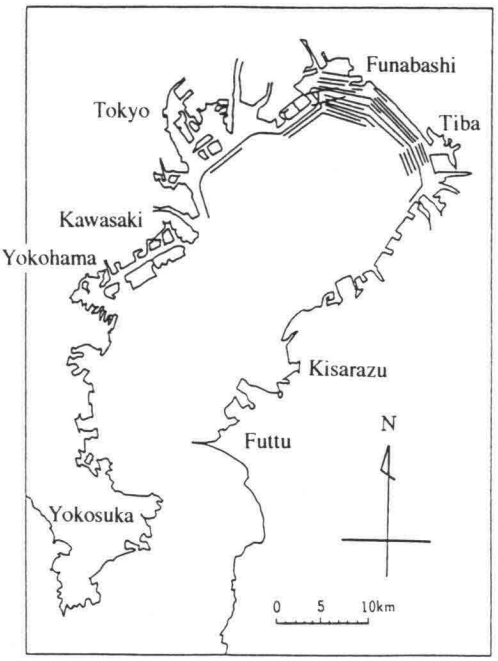

Figure 5 Regions where the occurrences of Aoshio have been reported (Kataoka et. al., 1988). Note that Aoshio has been sometimes observed off Kisarazu.

Aoshio is a symbolic example of the processes of the water quality change strongly depending on the upwelling. The meaning of 'Aoshio' can be translated to English as ' blue tides ' because the sea water color changes to milky-blue due to the colloidal sulfur particles which are produced by chemical reaction from the dissolved sulfide brought by Aoshio. Aoshio occurs from June to October, especially, at the end of summer of almost every year. Main regions where the occurrence of Aoshio has been reported are shown in Figure 5 (Kataoka et al.,1988). Aoshio occurs mainly at the northern head of the bay off Funabashi. It should be added that Aoshio has been sometimes observed at the east side of the bay off Kisarazu, in spite of no description in Figure 5. Since Aoshio is often observed when the northern wind blows, it is roughly explained that the cause of Aoshio is the upwelling induced by the northern wind. This explanation can be supported by either of the two mechanisms described in section 1, because the upwelling periods led by those two mechanisms are relatively close to those of the northern wind blowing. However, the detail of the mechanism has not yet well examined. Many inhabitants near the coast, such as shellfish, crabs and flounders, suffer severe damage under little oxygen condition caused by Aoshio, at the worst, almost none of them survives.

3. SATELLITE INFRARED DATA and WIND DATA

Since satellite infrared imagery has proven to be a useful tool in the study of the coastal upwelling (for example, Kelly, 1985), the same technique used in the coastal upwelling analysis was applied to detect the upwelling in Tokyo bay, i.e., the regions where the sea surface temperatures (SSTs) are locally lower than the global SST over the bay are regarded as the upwelling regions.

To select the infrared images suitable for the upwelling analysis, we, first, searched all images of quick-look type from 1984 till 1992 which have been stored at Touhoku university, and selected the images which are relatively cloud-free and of which the passing time is close to the period of the northern wind blowing. The selected images were processed at the Japan Weather Association, and checked again the inadequate cloud masking over the bay. Finally, a total of 19 images were used in the analysis (Table 1). It might be considered that the selection rate, 19 images out of the 9 years of images, is too small. This is due to the weather condition that Tokyo bay is subjected to the cloud masking in the periods of the northern wind blowing.

The SSTs were estimated using the Multi-Channel Sea Surface Temperature (MCSST) algorithms (McClain,1985; Japan Weather Association,1992) for the AVHRR data of NOAA 7, 9, 11 and 12 and the conventional black radiation theory for NOAA 10. Some SSTs images, however, showed rather large temperature biases of about 2℃ probably due to the effects of aerosols and fogs. Therefore, the qualitative patterns of the upwelling are mainly discussed in this study, since the quantitative analysis using absolute SSTs is not acceptable in some images affected by large temperature biases.

Table 1 List of satellite infrared images used in the upwelling analysis

Year	Date	Time	Satellite No.	Wind condition	Upwelling pattern	Remark
1984	21 Sept.	20:48	7	during NE	No	*
1986	9 June	14:36	9	during SW	No	Figure 8
	12 June	14:03	9	after NE	LN	Figure 8
	30 July	19:44	9	during SW	No	a little cloudy
	4 Aug.	20:28	9	during N	SE	
	5 Aug.	20:17	9	during N	SE	
	25 Aug.	14:15	9	after N	LN	Figure 11
1987	14 Sept.	13:56	9	after N	LN	a little cloudy
	20 Sept.	20:21	9	during N	No	*
1988	31 July	13:03	10	after N	LN	
1989	6 Aug.	13:34	10	after N	LN	
	25 Sept.	13:17	10	after N	No	*
	4 Oct.	13:16	10	during N	No	*
1990	2 Aug.	13:04	11	during S	No	Figure 9
	7 Aug.	2:27	11	after N	LN	Figure 9
	7 Aug.	13:51	11	after N	LN	Figure 9
	15 Aug.	14:04	11	during SW	No	Figure 6
1991	15 Aug.	20:16	11	during N	SE	Figure 7
	25 Aug.	20:01	11	during N	SE	

Year, Date and Time, satellite passing time in standard time of Japan; Satellite No., NOAA satellite platform number; Wind condition, for examples, during N:during the north wind blowing, after N: after the north wind stops blowing; Upwelling pattern, No:No upwelling in the bay, SE:upwelling generated mainly at region Stretched the along the East coast, LN:upwelling generated mainly at the region Localized in the Northern head of the bay, see section 4.1 in the text; Remark, reference of figure and additional condition, *:the estimated upwelling pattern is not reliable because the passing time is too late for period of stratification that the upwelling may not be detected by the SSTs pattern.

The wind data were measured at the Keiyo Sea Berth near the center of the bay (Figure 2) and the wind velocities and directions averaged over one hour were used. The records of the Aoshio occurrence off Funabashi observed by the Funabashi fishermem's cooperative were also used.

4. UPWELLING PATTERNS RELATED TO WIND CONDITIONS

4.1 Classification of Upwelling Patterns

The upwelling patterns estimated from the SSTs images are listed in Table 1. The upwelling patterns are strongly related on the wind conditions and classified into the following three types: 1) no upwelling during the southern wind blowing (marked by No in Table 1), 2) upwellings generated at the region stretched along the ease coast the from the northern head of the bay to the southern bay mouth during the northern wind blowing (SE), and 3) upwellings generated at the relatively local region in the north part of the bay after the northern wind stops blowing (LN).

In the following sections, typical examples of these three types of the upwelling are represented with the SSTs images and the wind conditions. The direction and the speed of the propagation of the LN type of the upwelling are also examined. In addition, An example in which the reflection rate of the visible rays band, albedo, increased after the Aoshio occurrence is reported.

4.2 No Upwelling during the Southern Wind Blowing

Time series of the wind velocity vectors from 9 through 18 August 1990 and the SSTs spatial pattern on 15 August 1990 are represented in Figure 6. The SSTs pattern was taken when the stable and almost steady southwestern wind blew. The SSTs pattern shows that SSTs continuously increase with distance from the southern bay mouth and highest SST occurs at the northern head of the bay. This is the typical SSTs pattern in summer which has been observed in field surveys. In this case, it can be considered that no upwelling is generated because no local region showing lower SSTs exists in the bay.

4.3 Upwelling during the Northern Wind Blowing

Wind data from 10 through 19 August 1991 and the SSTs pattern on 15 are shown in Figure 7. The SSTs pattern was taken during the stable northeastern wind blowing. The SSTs pattern shows that particularly low SSTs region is stretched along the east coast from the northern head to the southern bay mouth. Off the north coast, the low SSTs region tends to be deformed along the north coast. These shows that during the northern wind blowing the large scale upwelling is generated along the north and east coasts. This upwelling pattern is similar to that formed by the vertical circulation induced by the wind force as has been described in section 1 (Figure 1).

4.4 Upwellings after the Northern Wind Stops Blowing

The wind velocities from 4 through 15 June 1986 and the SSTs patterns on 9 and 12 are shown in Figure 8. The strong northern wind blew from 4 through 7 and Aoshio occurred off Funabashi from 5 to 7. The wind direction changed to the southwest from 8 and the SSTs pattern was taken on 9. Then, the wind direction changed again and the northeast wind blew till morning of 12. After then, when the wind became weak the other SSTs pattern was taken.

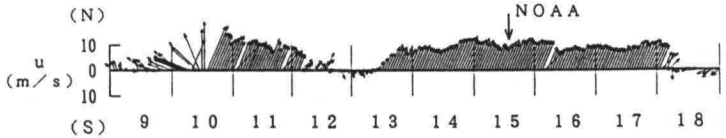

(a) Time series of the wind velocity vectors

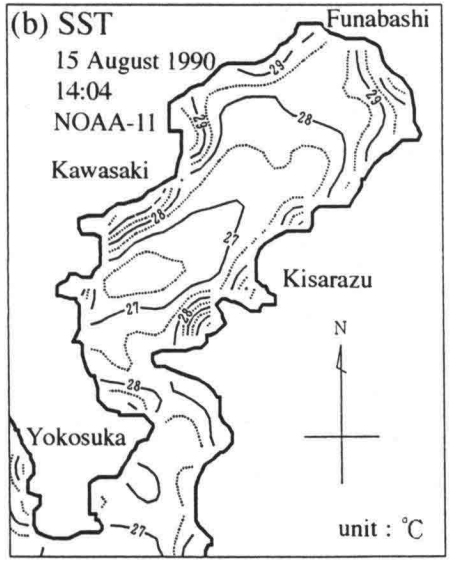

Figure 6 (a) Time series of the wind velocities from 9 through 18 August 1990 and (b) SST's pattern on 15 August 1990 during the southwestern wind blowing. No upwelling was generated.

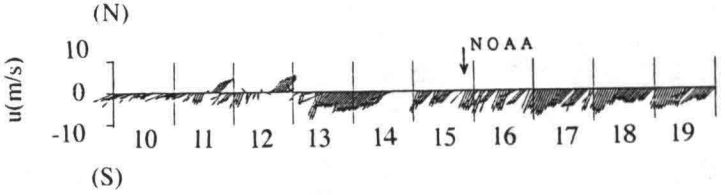

(a) Time series of the wind velocity vectors

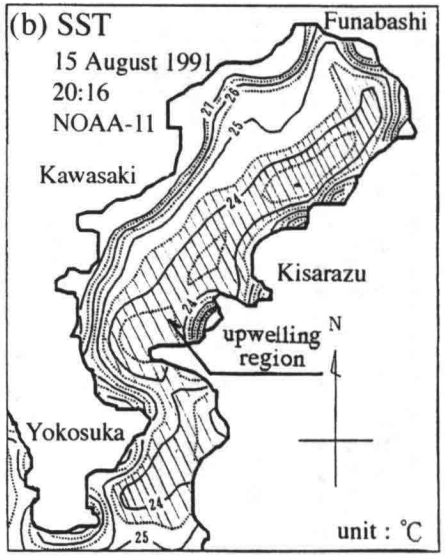

Figure 7 (a) Time series of the wind velocities from 10 through 19 August 1991 and (b) SST's pattern on 15 August 1991 during the northeastern wind blowing. The upwelling region is stretched along the north and the east coasts of the bay.

As compared between these two SSTs pattern, the drastic change of the SSTs pattern within three days can be found. The SSTs pattern on 9 is the typical one in summer in which SSTs are low at the bay mouth and high at the northern head, as shown in Figure 6(b) which is taken also during the southern wind blowing. On the other hand, the SSTs pattern on 12 is completely different from that on 9, that is, the relatively low SSTs region appeared in the north part of the bay and stayed along the east and north coasts. This region is rather localized in the northern head of the bay as compared with that of Figure 7 which was taken during the northern wind blowing. In the period from 9 to 12, there were no significant meteorological events, such as the heavy rainfalls and the floodwater discharge from rivers, but 2 days of the northern wind blowing.

The other example of the upwelling after the northern wind stops blowing is shown in Figure 9. The weak southwestern wind blew from afternoon of 1 through 2 August 1990 and the SSTs pattern was taken on 2. Then, the strong northern wind began to blow and from afternoon of 5 the wind became much weaker. The two SSTs patterns were taken on 7 during the period when

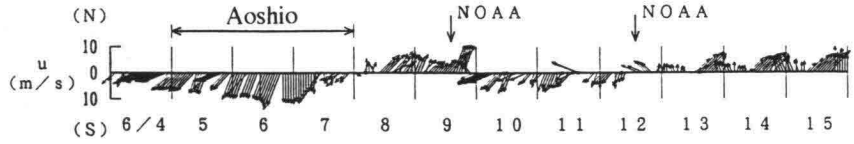

(a) Time series of the wind velocity vectors

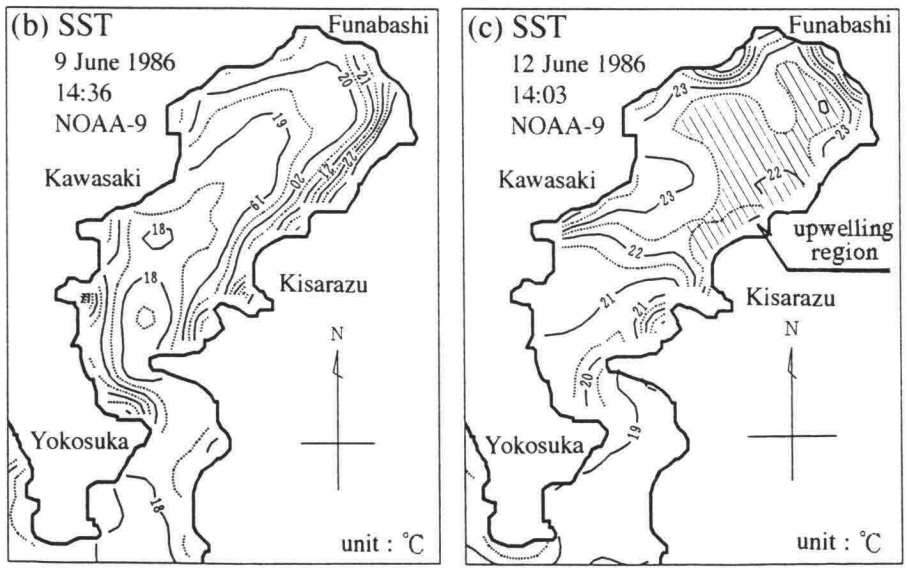

Figure 8 (a) Time series of the wind velocities from 4 through 15 June 1986, SST's patterns (b) on 9 June 1986 during the southwestern wind blowing, and (c) on 12 June 1986 after the northeastern wind stopped blowing. The upwelling region is relatively localized in the north part of the bay.

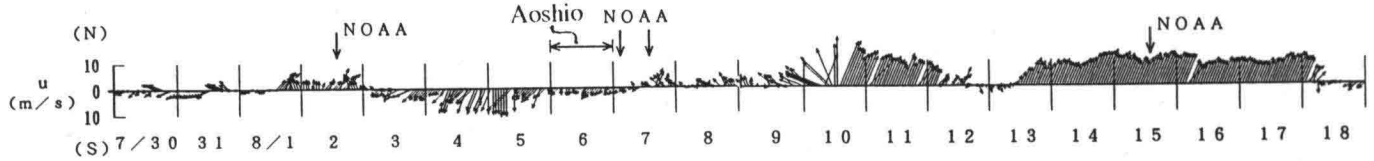

(a) Time series of the wind velocity vectors

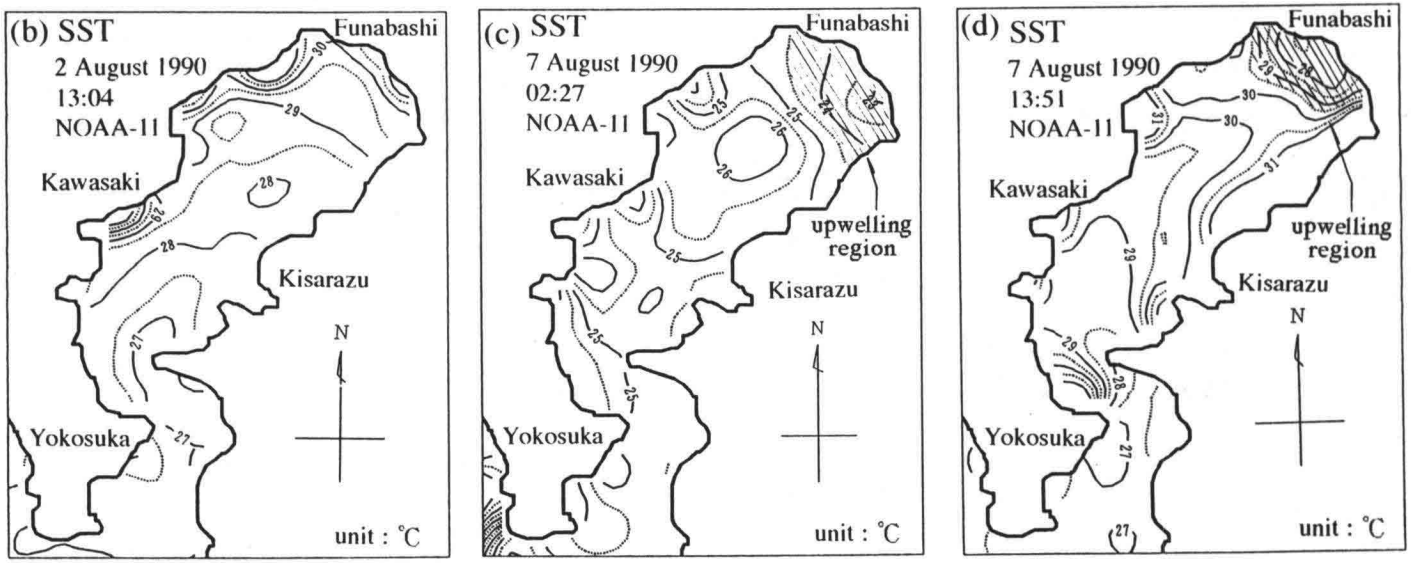

Figure 9 (a) Time series of the wind velocities from 30 July through 18 August 1990, SST's patterns (b) on 2 August 1990 during the southwestern wind blowing, (c) at 2:27, and (d) at 13:51 on 7 August 1990 after the northern wind stopped blowing. The upwelling region is localized in the northern head of the bay. Note that the upwelling region moves anticlockwise along the coast.

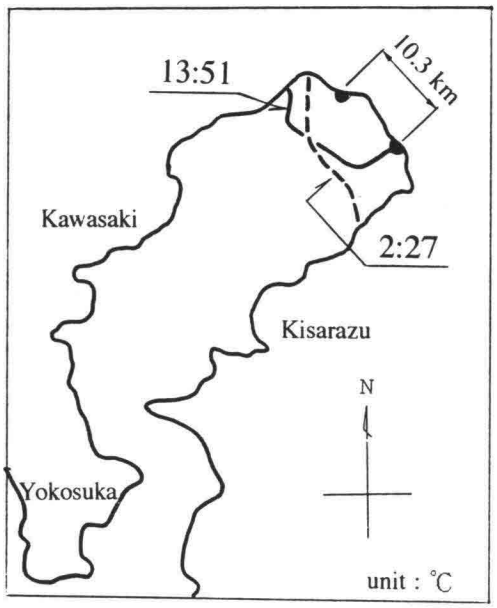

Figure 10 The movement of the upwelling region traced from two SST's patterns at 2:27 and at 13:51 on 7 August 1990 after the northern wind stopped blowing. The movement speed is estimated as approximately 25cm/s which is close to the phase velocity of the internal Kelvin wave.

the northern wind blowing was getting stopped. Aoshio was observed off Funabashi on 6 just before these two SSTs patterns were taken. From 8 the southern wind began to blow and became stronger. The SSTs pattern on 15 has been already shown in Figure 6(b).

While the SSTs pattern on 2 is the typical one during the southern wind blowing, as well as Figure 6(b) and 8(b), the two SSTs patterns on 7 show quite different patterns in which the low SSTs region is localized in the northern head of the bay. This dramatic change in SSTs pattern was achieved within 5 days without any significant rainfalls and floods except about 4 days of the northern wind blowing.

As the common feature of the upwelling pattern after the northern wind stops blowing obtained from Figure 8 and 9, it can be pointed out that the upwelling region is localized in the north part of the bay, at least, in the sense of comparison with that observed during the northern wind blowing (Figure 7(b)). This upwelling pattern corresponds to that associated the internal Kelvin wave as has been described in section 1 (Figure 1(b)) and will be examined in section 5.1.

4.5 Direction and Speed of Upwelling Propagation

Comparing between the upwelling regions in Figure 9(c) and (d), it is apparent that this upwelling region moves northward. To estimate the direction and the speed of the upwelling movement, the regions and the center points of the upwellings are traced in figure 10. Here, the center points are determined to refer to the lowest SST point inside the upwelling region. The direction of the

upwelling movement is anticlockwise, and agrees with that of the propagation of the internal Kelvin wave as described in section 1. The distance between the upwelling centers is about 10.3km resulting in that the movement speed is approximately 25cm/s. This speed is very close to the phase velocity of the internal Kelvin wave, as well as the propagation speed of the density interface setup in Tokyo bay which was calculated by Matsuyama et al.(1990). Thus, from a viewpoint of the upwelling propagation, it is emphasized that the upwelling observed on 7 August 1990 is in agreement with that associated with the internal Kelvin wave.

4.6 High Albedo Pattern after Aoshio

The albedo is estimated using the data of AVHRR channel 1 whose sensitive frequencies belong to the visible rays band (Japan Weather Association,1992). The value of albedo is often reported to show good correlation with the turbidity of the water.

As an example of the high albedo pattern observed after the Aoshio occurrence, SSTs and albedo patterns on 25 August 1986 are shown in Figure 11. Before 25, the northern wind blew from 22 till morning of 24 and Aoshio occurred off Funabashi from 23 till 24. The patterns show the high albedo at the northern head of of the bay as well as the upwelling at the almost same region.

Onizuka et al.(1987) reported that the occurrences of the red tides in which the water color changes due to the increase of plankton, are sometimes observed after Aoshio. Referring to this report, there is some possibility that the high albedo pattern observed here may be due to the red tides. It is suggested that the upwelling may become important for not only physical processes but also biological processes such as the growth of plankton.

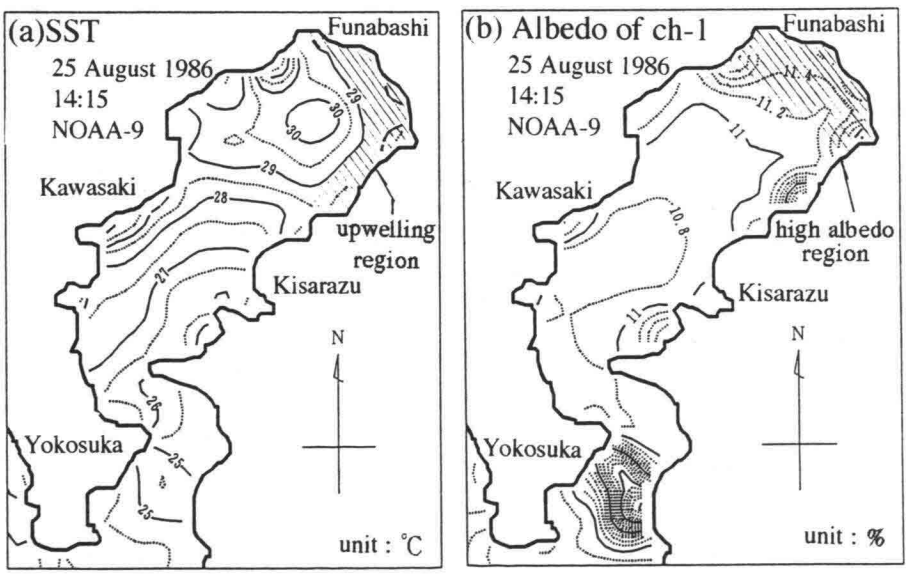

Figure 11 (a) SST's patterns and (b) Albedo pattern estimated by using AVHRR ch 1 on 25 August 1986 after the occurrence of Aoshio off Fnabashi. Note the high albedo pattern at the northern head of the bay.

5. UPWELLING PROCESSES

5.1 Numerical Experiments for the Upwelling Processes

The processes of the generation and the propagation of the upwelling and their mechanisms are investigated through the numerical experiments by Matsuyama et al.(1990) and Ueno et al.(1992).

First, to examine the generation process of the upwelling, the numerical experiment for the upwelling in the rectangular basin which is 45km long, 20km wide and 20m deep was implemented using the two levels model (Ueno et al.,1992). The attention was paid on the transient process of the upwelling after the wind begins to blow. The north wind of 5m/s was acted under no stratified condition. The level model used here is the conventional type with constant horizontal and vertical eddy viscosities. The details are referred to Shibayama(1992).

The results calculated at 1 and 3 hours after the wind begins to blow are shown in Figure 12. It was confirmed that the steady state was achieved in the results after 3 hours. The results after 1 hour show that the directions of the horizontal velocities are relatively parallel to the wind direction resulting in that the upwelling is generated along the north side of the basin. On the other hand, in the results after 3 hours, the upwelling region extends from the north side to east side of the basin because the velocity directions are inclined by the effects of the coriolis force. The upwelling velocities after 3 hours become larger that those after 1 hour. The developing pattern of the upwelling regions is shown in Figure 13. The upwelling regions are defined to the regions where vertical velocities exceed 10^{-3}cm/s. The upwelling region is localized in the north side of the basin until 1.7 hours, and then, stretched along the east side. Finally, at 2.8 hours later, the upwelling region is fully developed along the north and the east sides of the basin. This final region is quite similar to that observed in Tokyo bay during the northern wind blowing (Figure 7).

Matsuyama et al.(1990) calculated the upwelling patterns in Tokyo bay the using the two layers model, and showed that the propagation patterns of the density interface setup corresponds with those of the internal Kelvin wave. To show the propagation process of the upwelling region after the wind stops blowing, one of their results is quoted in Figure 14. The lines in Figure 14 show the upwelling region and numerals on lines is elapsed time after the wind begins to blow. The northeastern wind was generated for 24 hours and then stopped. The upwelling region at 24 hour extends along the north and the east coasts of the bay, which is the almost same pattern calculated by two level model (Figure 13, 2.8h) and observed in Tokyo bay (Figure 7). After the wind stops blowing, the upwelling region propagates anticlockwise along the coast. Some of the upwelling patterns in Figure 14 are quite similar to those in Figure 8(c), Figure 9(c)(d), and Figure 11(b) which were taken after the northern wind stopped blowing.

The main mechanisms in the processes of the upwelling can be explained as follows: In the generation process during the northern wind blowing, the upwelling is generated as a part of the vertical circulation system induced by the wind forces. The upwelling region are influenced by the effects of the coriolis force, i.e., as the effects of the coriolis force become significant, the upwelling region is stretched southward along the east coast. In the propagation process after the northern wind stops blowing, the interface setup propagates anticlockwise along the coast in the same way of the internal Kelvin wave. Consequently, the upwelling associated with the internal Kelvin wave also propagates anticlockwise (Matsuyama et al.,1990).

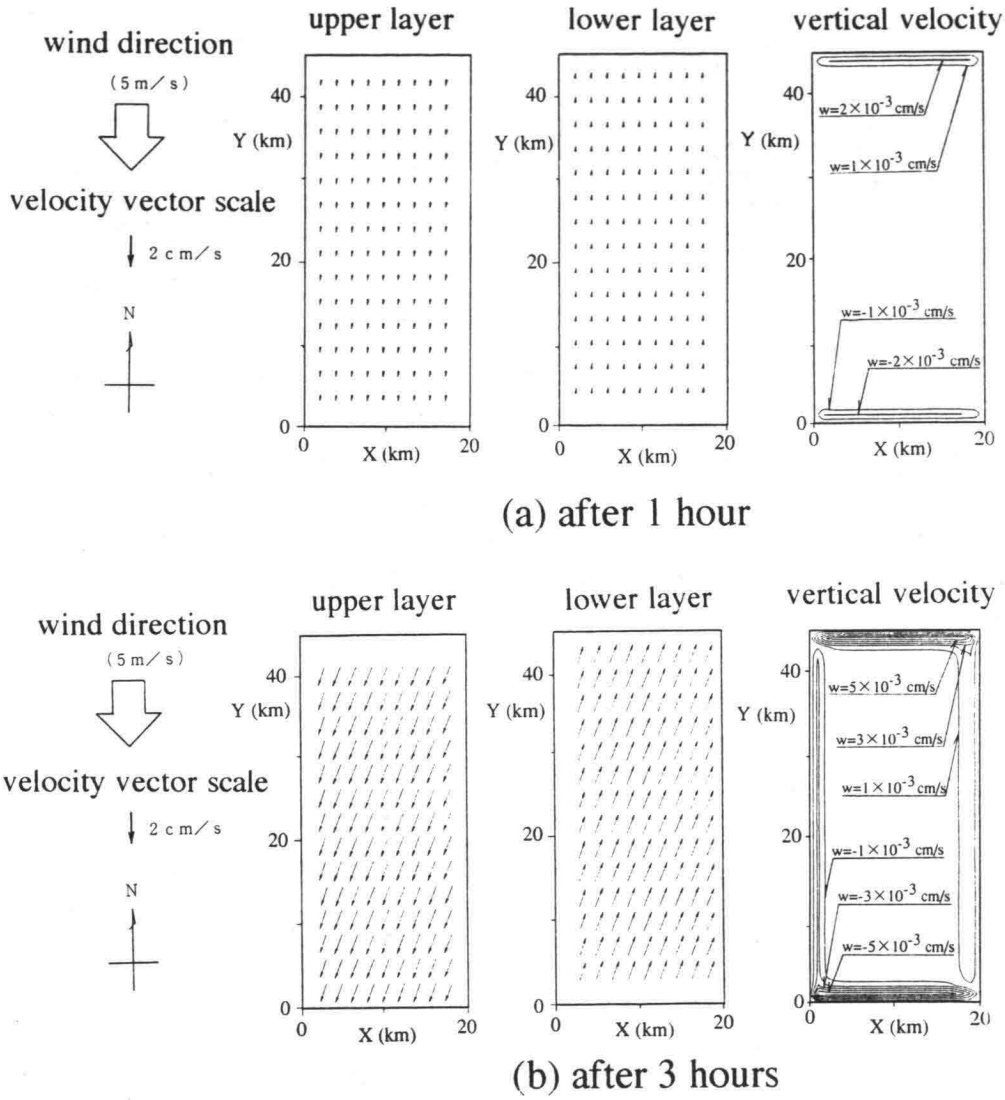

Figure 12 Spatial patterns of horizontal velocities at the upper and lower layer and vertical velocities through the interface calculated by the two levels model at (a) 1 hour and (b) 3 hours after the northern wind stops blowing.

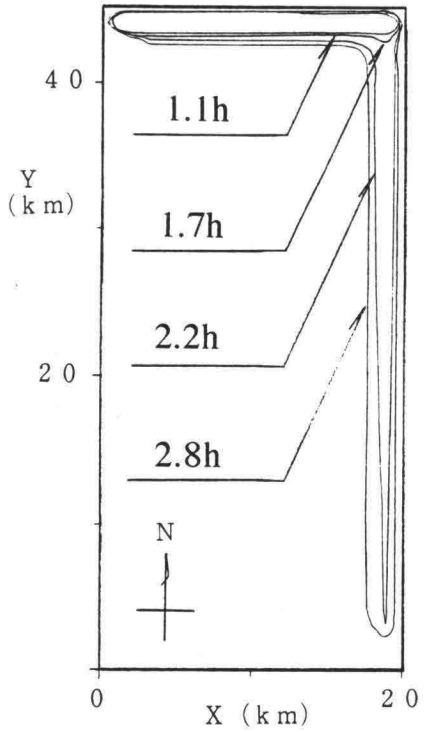

Figure 13 Developing process of the upwelling regions after the northern wind begins to blow obtained through the numerical experiments using the two levels model.

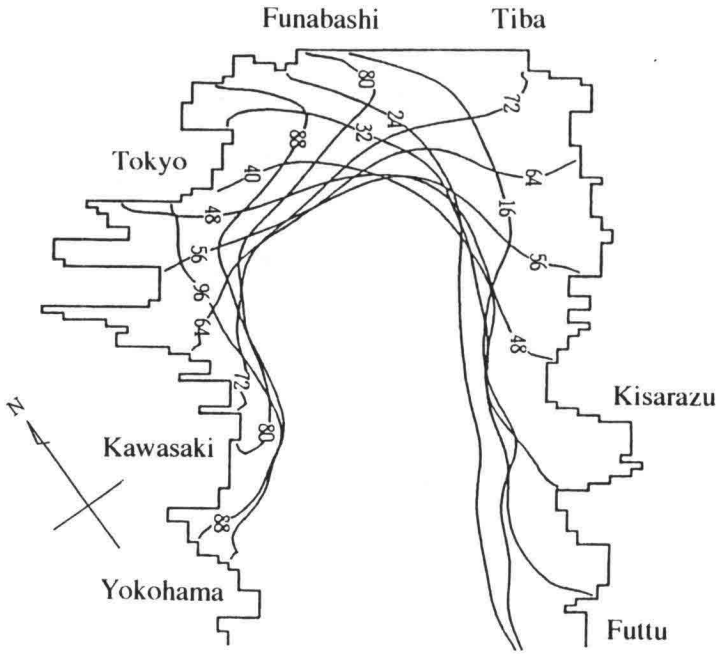

Figure 14 Propagation process of the upwelling regions after the northern wind stops blowing obtained through the numerical experiments by the two layers model (Matsuyama et al.,1990). The lines show the regions where the level of the interface rises to 75cm and the numerals on the line are the elapsed time after the northeastern wind begins to blow. The wind is generated for 24 hours.

5.2 General Characteristics of Upwelling in Tokyo Bay

Using results obtained from the proceeding sections, the general characteristics of the upwelling in Tokyo bay is attempted to be schematized in Figure 15. The several days of the northern wind blowing are assumed here.

Each stage in the upwelling processes is explained in the following:

(a) At the beginning of the wind blowing, the weak upwelling is locally generated along the northern coast of the bay.
(b) As the wind blows, the upwelling region is stretched along the east coast. At the steady state, the strong upwelling is generated at the large region extending along the north and the east coasts.
(c) After the wind stops blowing, the upwelling region propagates anticlockwise along the east coast.
(d) As time passes after the wind stops blowing, the upwelling region propagates further and is localized in the north head of the bay.
(e) As the upwelling propagates, upwelling region will become unclear due to the mixing and the energy loss.

The stages from (a) to (b) are generated as a part of the vertical circulation system induced by wind forces under the effects of the coriolis forces. This mechanism was based on that previously suggested by Ohtubo and Muraoka(1988). The stage of (a) is estimated from the result through the numerical experiments (Figure 12(a)), the stage of (b) is depends on the results from the satellite data analysis as well as the numerical experiments (Figure 7 and 13). The stages from (c) to (d) follow the propagation pattern of the internal Kelvin wave as suggested by Unoki (1990) and Matsuyama et al. (1990). The examples of the stage of (c) are shown in Figure 8, 11 and 14, and the stage of (d) in Figure 9 and 14. The stage of (e) is based on results from neither the satellite data analysis nor the numerical experiments. However, since the bottom friction and the mixing at the interface dissipate the energy of the internal wave and make the interface unclear, the internal wave can no longer exist at last. In order to investigate the fate of the internal Kelvin wave, it is necessary to study the quantitative characteristics of the upwelling as well as the energy dissipation and the mixing processes of the internal Kelvin wave.

The other conditions which were not considered in the present study but will be of importance to the upwelling processes, are briefly described below.

Only two types of wind conditions, during the wind blowing and after the wind stops blowing, were considered in this study. However, in order to generate the internal Kelvin wave, to stop the wind blowing is not always necessary. Correctly speaking, the changes of the wind forces acted on the sea surface, for examples, the wind speed change and the wind direction change, are needed to generate the internal oscillations. When wind conditions, such as speed and direction, change periodically and the period is close to that of the internal seiches, the resonant oscillations will be developed resulting in the strong upwelling. Since the period of the internal standing wave in Tokyo bay is estimated as 1 to 3 days, which is relatively close to the time scale of the change of the wind conditions, the possibility of the resonant internal oscillations can not be ignored.

Topography conditions of the bay will be also important to the propagation patterns of the internal Kelvin wave. In Tokyo bay, water depths at the north part are shallower than those at the south

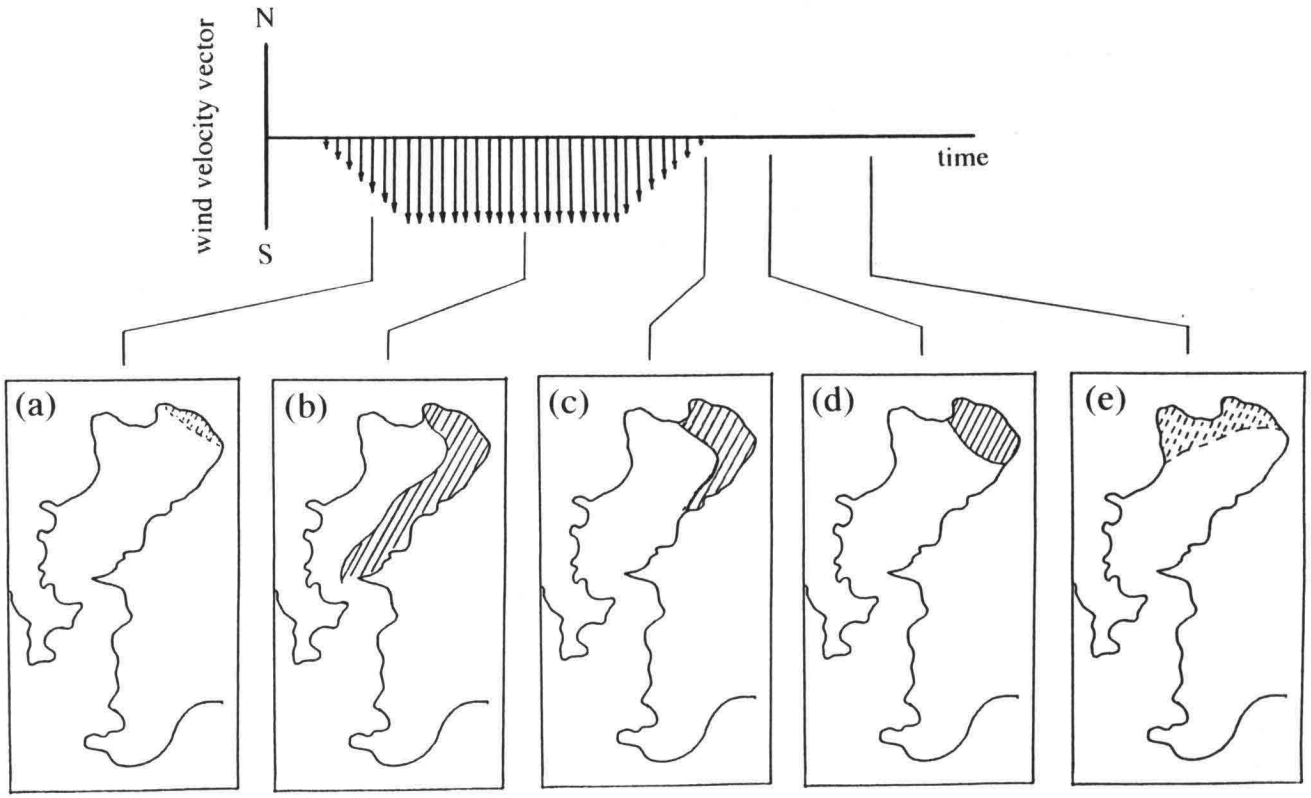

Figure 15 Schematic example for the general characteristics of the upwelling in Tokyo bay. The explanations for each stages from (a) to (e) are referred to section 5.2 in the text.

part. Thus, when the internal Kelvin wave propagates from the south part into the north part, the shoaling, the increasing and the steepening of the wave height, occurs. Besides, under critical conditions, the internal Kelvin wave may break. Since the shoaling and the breaking will make the mixing stronger, the upwelling characteristics included these phenomena should be examined.

6. CONCLUSIONS

The spatial patterns of the upwelling induced by the wind forces in Tokyo bay were investigated using the satellite infrared images taken by the NOAA AVHRR. The processes of the upwelling generation and propagation were also examined through the satellite data analysis and the numerical experiments.

The upwelling patterns obtained from the satellite infrared images are classified into the three types according the wind conditions, i.e.,

1) No upwelling generated during the southern wind blowing.
2) Upwellings generated at the region stretched along the east coast from the northern head of the bay to the southern bay mouth during the northern wind blowing.
3) Upwellings generated at the relatively local region in the northern head of the bay after the northern wind stops blowing.

The processes of the upwelling consist of two parts driven by the different two mechanisms, i.e.,

1) The first process proceeds during the northern wind blowing. At the beginning of the wind blowing the weak upwelling is generated along the north coast of the bay, then, the upwelling region is stretched along the east coast, and finally, the strong upwelling is generated at the region extending along the north and the east coasts. This generation process of the upwelling is explained as a part of the vertical circulation system induced by wind forces. The basic mechanism in this process was suggested by Ohtubo and Muraoka (1988).
2) The second process is generated after the northern wind stops blowing. The density interface setup along the north and the east coasts which has been completed during the northern wind blowing, propagates anticlockwise along the coast. The propagation pattern of the interface setup follows that of the internal Kelvin wave. As the result, the upwelling associated with the internal Kelvin wave also propagates anticlockwise along the coast. This mechanism was previously suggested by Unoki (1990) and Matsuyama et al. (1990).

ACKNOWLEDGEMENTS

The authors would like to acknowledge the assistance of Japan Weather Association for satellite data processing. We especially with to thank Associate Professor S. Saitoh of Hokkaido university for comments on satellite data analysis. The cooperation of Professor M. Sawamoto of Tohoku university enabled us to select the useful satellite data and is gratefully acknowledged. The wind data was made available through Keiyo Sea Berth Co. and the record of Aoshio was provided by Funabashi fishermem's cooperative. We are grateful for their cooperation. Out thanks go also to Professor T . Shibayama of Yokohama National university for offering the level model. The stimulating discussions and comments provided by Professor G.S. Stelling and Dr. R. Uittenbogaard of Delft Hydraulics are appreciated.

REFERENCES

Ueno, S., K. Nadaoka, A. Ishimura and H. Katsui (1992): Analysis of wind induced upwelling in Tokyo Bay using NOAA-AVHRR, Proc. of Coastal Eng., JSCE, Vol.39, pp256-260 (in Japanese).

Ueno, S., K. Nadaoka, H. Katsui and H. Ohtani (1993): On the rapid change in the density, currents and water qualities profiles, and high-frequency internal waves observed in Tokyo bay during stratification season, Proc. of Coastal Eng., JSCE, Vol.40, pp.246-250 (in Japanese).

Unoki, S. (1985) : Tokyo bay, 2.Physics, Coastal Oceanography of Japan, Tokai publishing company, pp.344-361 (in Japanese).

Unoki, S. (1990) : Upwelling and Aoshio in Tokyo bay, Proc. of the Autumn Conference of Japan Oceanography Association, pp.156-157 (in Japanese).

Kataoka, S. A. Komatsu and Y. Fuse (1988): Aoshio in Tokyo bay, Reclamation and Dredging, No. 143, pp.12-19 (in Japanese).

Kelly, K. A.(1985): The influence of winds and topography on the sea surface temperature patterns over the northern California slope, J. Geophys. Res., 90, pp.11783-11798.

Matsuyama, M., M. Touma and A. Ohwaki (1990): Numerical experiments of upwelling in Tokyo Bay, Bulletin on Coastal Oceanography, Vol.28, pp.63-74(in Japanese).

McClain, E. P. (1985): Comparative performance of AVHRR-based multichannel sea surface temperature, J. Geophys. Res., 90, pp.11587-11601.

Morikawa, M. and K. Murakami (1986): Fluctuation characteristics of long-period current in Tokyo bay - investigation by field observation data in the bay -, Tech. Note of Port and Harbour Res. Inst., No. 550, pp.3-50 (in Japanese).

Sibayama, T. and P. K. Leung (1992): Multi-level model for hydrodynamic circulation and dispersion process in bays, Coastal Engineering in Japan, Vol. 35, No. 1, pp.49-66.

Odaomaki, M., H. Sato and N. Shimohira (1990): Investigation and estimation methods for currents and transports induced by winds in the semi-enclosed sea areas (Currents in Tokyo bay in summer), Proc. of the Autumn Conference of Japan Oceanography Association, pp.154-155 (in Japanese).

Ohtubo, K. and H. Muraoka (1988) : A discussion on physical mechanism of the generation of Aoshio, Proc. of 22nd Annual Conference of Water Quality and Pollution Association in Japan、pp.193-194 (in Japanese).

Onizuka, M., T. Samukawa, K. Ohta and K. Nagaoka (1987): Discussions on sea conditions related to Aoshio on August 1985, Pollution, Vol.23、No.2、pp.1-21(in Japanese).

JAPAN WEATHER ASSOCIATION (1992): The Handbook for using NOAA satellite data, Ver. 1.1 (in Japanese).

HYDRO-PORT'94
International Conference on Hydro-Technical
Engineering for Port and Harbor Construction
October 19 - 21, 1994, Yokosuka, Japan

3-Dimensional Modelling of Heated Water Discharges into Coastal Waters of Yellow Sea

See Whan Kang
Tae Sung Jung

Korea Ocean Research and Development Institute
Ansan P.O.Box 29, Seoul 425-600

ABSTRACT

A three-dimensional numerical model for thermal plume with computational efficiency has been developed to simulate the coastal currents, the thermal jets from outfall, and the excess temperature fields in the shallow coastal waters. The model adopts computational meshes with horizontally variable and vertically stretched grid system. Because of large water-level changes, the model takes into account of tidal flats along the coastline. The computed currents and thermal plume patterns changing in time and space were compared with the observed field data including the Landsat images.

Key Words : 3-Dimensional Model, Thermal Plume, Mode-Splitting

1. INTRODUCTION

Most of nuclear and fossil power plants in Korea are located on the coast area and their heated water from the generation units discharges into the coastal waters. Recently, many power plants have been constructed, and the use of the sea water as cooling water has increased rapidly. The heated waters from the power plant have caused many environmental problems due to the increase of the surrounding water temperatures in the coastal waters. Therefore, it is very important to predict the behaviour of thermal plume and assess its environmental impacts in the coastal waters.

As a part of environmental impact assessment, a thermal plume study was conducted for a nuclear power plant sited at Yeong-Kwang on the west coast of Korea. The power plant of two generation units has been in operation since 1987, discharging the cooling waters of 115 m^3/sec directly into the coastal surface water. The excess water temperature of ΔT = 8-9℃ is discharged from once-through system. Because of strong tidal currents in the order of 1m/sec parrallel to the coastal line, the heated water masses discharged from the power plant are mostly transported along the coast.

In order to understand the transport phenomena of thermal plume at Yeong-Kwang coast, we carried out field survey including tides, currents, and vertical profilings of water temperature on the seasonal basis in 1991-1992. The analyzed data from Landsat

images was also used to verify the dispersed patterns of thermal plume which are changed due to tidal actions.

In this study, a three-dimensional numerical model has been established to simulate the tidal currents and the excess temperature fields due to thermal jets and tidal actions. The computed currents and excess temperature fields were compared with the field surveyed data and the Landsat images.

2. FIELD MEASUREMENTS

In order to obtain the thermal plume data, extensive field survey including tides, currents, and vertical profilings of water temperatures at 30 different locations (Figure 1) was conducted on the seasonal basis in 1991-1992. The remote sensing images observed by Landsat were also analyzed to obtain the dispersed patterns of thermal plume. Figure 1 shows the depth profiles and the location map of field measurements. The vertical profiling of water temperatures were performed at more than 30 points twice per every three month interval. The survey area covers 16Km radius distance from the outfall of the nuclear power plant.

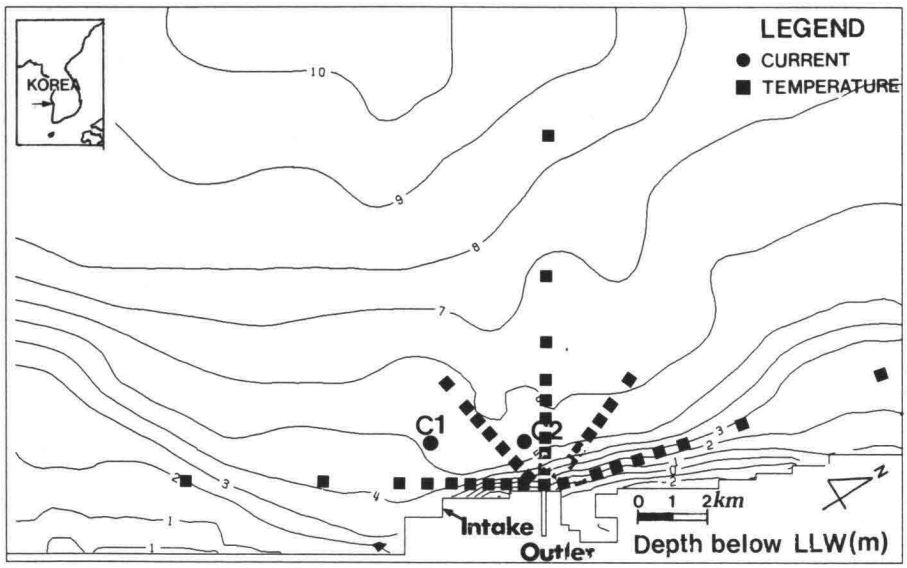

Figure 1 Location map of thermal plume study at Yeong-Kwang coast of Korea

Two current meters, the Aanderaa RCM-4's, were deployed at about 3 meter above the sea bottom at the stations C1 and C2 to measure the currents, water temperature and salinity. Tides were measured for one month at 5 stations situated at the open boundaries of numerical model, by mooring the pressure-type gauge's. Sampling intervals for tides and currents were fixed at 10 minutes. The mean tidal range in the study area is approximately 540cm during spring tide and 220cm during Neap tide. Semi-diurnal tides are dominant and tidal flats are wide along the coast.

3. NUMERICAL MODEL

A 3-dimensional model were developed for this study. The model (Jung, 1993) uses fully nonlinear, time-dependent, three-dimensional, σ-tranformed equations of motion and equation of heat transport. The governing equations together with their boundary

conditions are transformed by non-dimensional variables and solved by a finite difference method. An implicit numerical scheme in the vertical direction and a mode-splitting technique in time have been adopted for computaional efficiency. Surface elevation was calculated by an elliptic-type finite difference equation and the variable rectangular grid system was employed for differencing in the horizontal directions. To resolve tidal flats, a treatment technique for moving boundaries were employed.

(1) Governing equations

Two simplifing approximation are used for Reynolds averaged eqautions of motion and equation of heat : first, it is assumed that the weight of the fluid identically balances the pressure (hydrostatic assumption), and second, density differences are neglected unless the differences are multiplied by gravity (Boussinesq approximation). Consider a system of orthogonal Cartesian coordinate with x increasing northward, y increasing eastward, and z increasing vertically downward. The surface located at $z=-\eta(x, y, t)$ and the bottom is at $z=h(x, y)$.

The continuity equation is

$$\frac{\partial u}{\partial x}+\frac{\partial v}{\partial y}+\frac{\partial w}{\partial z}=0 \tag{1}$$

where (u, v, w) are velocity components in the (x, y, z) directions.
The Reynolds averaged momentum eqations are

$$\frac{\partial u}{\partial t}+\frac{\partial (u^2)}{\partial x}+\frac{\partial (uv)}{\partial y}+\frac{\partial (uw)}{\partial z}+fv=-\frac{1}{\rho_0}\frac{\partial p}{\partial x}+\frac{\partial}{\partial x}(A_H\frac{\partial u}{\partial x})$$
$$+\frac{\partial}{\partial y}(A_H\frac{\partial u}{\partial y})+\frac{\partial}{\partial z}(A_V\frac{\partial u}{\partial z}) \tag{2}$$

$$\frac{\partial v}{\partial t}+\frac{\partial (uv)}{\partial x}+\frac{\partial (v^2)}{\partial y}+\frac{\partial (vw)}{\partial z}-fu=-\frac{1}{\rho_0}\frac{\partial p}{\partial y}+\frac{\partial}{\partial x}(A_H\frac{\partial v}{\partial x})$$
$$+\frac{\partial}{\partial y}(A_H\frac{\partial v}{\partial y})+\frac{\partial}{\partial z}(A_V\frac{\partial v}{\partial z}) \tag{3}$$

$$\frac{\partial p}{\partial z}=\rho g \tag{4}$$

where f is the Coriolis parameter, ρ_0 is the refence density, p is the water pressure, A_H is the horizontal momentum exchange coefficient, A_V is the vertical momentum exchange coefficient, g is the gravitatioal acceleration, and ρ is the in situ density.

The advection-diffusion equation for water temperature T is

$$\frac{\partial T}{\partial t}+\frac{\partial (uT)}{\partial x}+\frac{\partial (vT)}{\partial y}+\frac{\partial (wT)}{\partial z}=\frac{\partial}{\partial x}(B_H\frac{\partial T}{\partial x})$$
$$+\frac{\partial}{\partial y}(B_H\frac{\partial T}{\partial y})+\frac{\partial}{\partial z}(B_V\frac{\partial T}{\partial z}) \tag{5}$$

where B_H is the horizontal exchange coefficient of temperature, and B_V is the vertical exchange coefficient of temperature.
The density of sea water ρ is computed by an equation of state of the form (Eckart,

1958)

$$\rho = (5890+38T-0.375T^2+3S)/[(1779.5+11.25T-0.0745T^2) +(3.8+0.01T)S+0.698(5890+38T-0.375T^2+3S)] \quad (6)$$

where S is the salinity. In this study, the salinity is specified as the seasonal mean value (constant) based on field survey.
The governing equations (1), (2)-(4), and (5) are transformed by nondimensional variables on σ-coordinate (Figure, 2; Freeman et al., 1972) (all asterisks will be dropped for notation convenience).

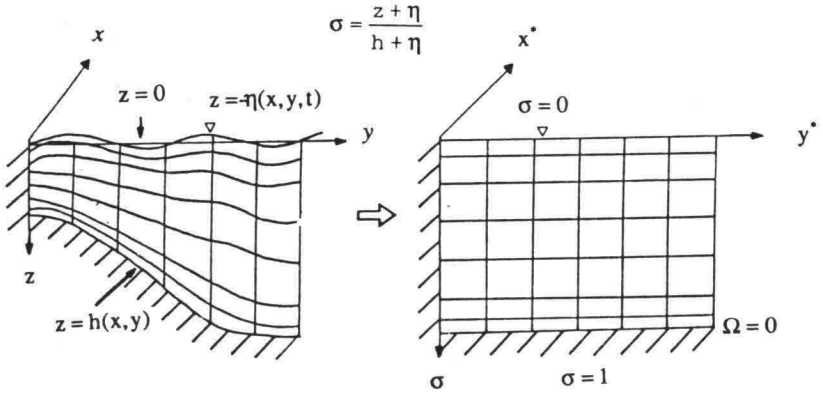

Figure 2 Nomalization of z-coordinate

$$\frac{1}{H}\frac{\partial \eta}{\partial t}+\frac{K}{H}\left(\frac{\partial (Hu)}{\partial x}+\frac{\partial (Hv)}{\partial y}\right)+K\frac{\partial \Omega}{\partial \sigma}=0 \quad (7)$$

$$\frac{1}{H}\frac{\partial (Hu)}{\partial t}+R_e\left(\frac{1}{H}\frac{\partial (Huu)}{\partial x}+\frac{1}{H}\frac{\partial (Huv)}{\partial y}+\frac{\partial (\Omega u)}{\partial \sigma}\right)+R_0 v = -\frac{\partial p_a}{\partial x}-\frac{\partial \eta}{\partial x}-\frac{R_e}{F_r^2}\left[\frac{\partial}{\partial x}\left(H\int_0^\sigma \rho d\sigma\right)-\sigma\frac{\partial H}{\partial x}\rho\right] +\frac{1}{H}\frac{\partial}{\partial x}\left(H\frac{\partial u}{\partial x}\right)+\frac{1}{H}\frac{\partial}{\partial y}\left(H\frac{\partial u}{\partial y}\right)+\left(\frac{b_0}{h_0}\right)^2\frac{1}{H^2}\frac{\partial}{\partial \sigma}\left(\gamma\frac{\partial u}{\partial \sigma}\right) \quad (8)$$

$$\frac{1}{H}\frac{\partial (Hv)}{\partial t}+R_e\left(\frac{1}{H}\frac{\partial (Huv)}{\partial x}+\frac{1}{H}\frac{\partial (Hvv)}{\partial y}+\frac{\partial (\Omega v)}{\partial \sigma}\right)-R_0 u = -\frac{\partial p_a}{\partial y}-\frac{\partial \eta}{\partial y}-\frac{R_e}{F_r^2}\left[\frac{\partial}{\partial y}\left(H\int_0^\sigma \rho d\sigma\right)-\sigma\frac{\partial H}{\partial y}\rho\right] +\frac{1}{H}\frac{\partial}{\partial x}\left(H\frac{\partial v}{\partial x}\right)+\frac{1}{H}\frac{\partial}{\partial y}\left(H\frac{\partial v}{\partial y}\right)+\left(\frac{b_0}{h_0}\right)^2\frac{1}{H^2}\frac{\partial}{\partial \sigma}\left(\gamma\frac{\partial v}{\partial \sigma}\right) \quad (9)$$

$$P_r\left[\frac{1}{H}\frac{\partial (HT)}{\partial t}+R_e\left(\frac{1}{H}\frac{\partial (HuT)}{\partial x}+\frac{1}{H}\frac{\partial (HvT)}{\partial y}+\frac{\partial (\Omega T)}{\partial \sigma}\right)\right]= \frac{1}{H}\frac{\partial}{\partial x}\left(H\frac{\partial T}{\partial x}\right)+\frac{1}{H}\frac{\partial}{\partial y}\left(H\frac{\partial T}{\partial y}\right)+\left(\frac{b_0}{h_0}\right)^2\frac{1}{H^2}\frac{\partial}{\partial \sigma}\left(\beta\frac{\partial T}{\partial \sigma}\right) \quad (10)$$

where b_0 is the reference distance, h_0 is the reference depth, u_0 is the reference velocity, velocity components (u^*, v^*, Ω^*) are $(u, v, \Omega b_0)/u_0$, time t^* is t/t_0, distances (x^*, y^*, Ω^*) are $(x, y, \sigma b_0)/b_0$, reference time t_0 is b_0^2/A_H, water depth H^* is H/h_0, reference Reynolds number R_e is $u_0 b_0/A_H$, R_0 is fb_0/A_H, F_r^2 is u_0^2/gh_0, F_r is the reference Froude number, γ is A_V/A_H, β is B_V/B_H, surface elevation η^* is $\eta/(A_H u_0/gb_0)$, K is $gb_0^2 h_0/(A_H^2)$, Prandtl number P_r is A_H/B_H, vertical velocity Ω is $d\sigma/dt$, σ is $(\eta+z)/H$, total depth $H(x, y, t)$ is $h+\eta$, and $h(x, y)$ is the mean water depth.

Rearranging of (8) and (9) with neglected atmospheric pressure gives

$$\frac{1}{H}\frac{\partial (Hu)}{\partial t}+R_0 v-\left(\frac{b_0}{h_0}\right)^2\frac{1}{H^2}\frac{\partial}{\partial \sigma}\left(\gamma\frac{\partial u}{\partial \sigma}\right)=c(u,v,\Omega)-\frac{\partial \eta}{\partial x} \tag{11}$$

$$\frac{1}{H}\frac{\partial (Hv)}{\partial t}-R_0 u-\left(\frac{b_0}{h_0}\right)^2\frac{1}{H^2}\frac{\partial}{\partial \sigma}\left(\gamma\frac{\partial v}{\partial \sigma}\right)=d(u,v,\Omega)-\frac{\partial \eta}{\partial y} \tag{12}$$

where $c(u,v,\Omega)$ = rest of terms in x-momentum equation, and $d(u,v,\Omega)$ = rest of terms in y-momentum equation.

By integrating (7) from $\sigma=\sigma$ to $\sigma=1$(sea bottom) and rearranging, the vertical component Ω_σ of velocity is obtained as

$$\Omega_\sigma=\frac{(\sigma-1)}{H}\int_0^1 ADV d\sigma+\frac{1}{H}\int_\sigma^1 ADV d\sigma \tag{13}$$

where $ADV=\frac{\partial (Hu)}{\partial x}+\frac{\partial (Hv)}{\partial y}$.

(2) Boundary conditions

The boundary conditions at the free surface $z=-\eta(x, y)$ are

$$\gamma\left(\frac{\partial u}{\partial \sigma}, \frac{\partial v}{\partial \sigma}\right)=\gamma_1 H(\tau_x^*, \tau_y^*) \tag{14}$$

$$\beta\frac{\partial T}{\partial \sigma}=\frac{K_T h_0}{\rho_0 C_p B_H}H(T-T_e) \tag{15}$$

where (τ_x^*, τ_y^*) are the nondimensionalized surface wind stresses, (τ_x^*, τ_y^*) = $(\tau_x, \tau_y)/\tau_0$, $\tau_0=(\rho_0 u_0 A_H)/h_0$, τ_x and τ_y are the surface wind stress in the x and y direction respectively, γ_1 is the non-dimensionalized vertical momentum exchange coefficient at water surface, K_T is the surface haet transfer coefficient, T_e is the equlibrium water temperature, and C_p is the specific heat of water at constant pressure.

The boundary conditions at the sea bottom and the side wall are

$$u=v=\Omega=0 \tag{16}$$

$$\frac{\partial T}{\partial \sigma}=0 \tag{17}$$

Surface elevations are specified at the open boundaries and Neumann condition is used for determining u, v, and T at the open boundaries. At the outlet of heated waters, the velocity and water temperatute were specified.

(3) Finite difference formulation

A numerical algorithm, based on SMAC(simplified marker and cell method, Amsden and Harlow, 1970) with mode-splitting technique(Paul and Lick, 1985), was used for computational efficiency. The surface elevation was solved by an elliptic-type finite diference equation to avoid time-step restriction by CFL (Courant-Levy-Fredrich) condition that time step must be less than the ratio of horizontal grid size to long wave propagation speed ($\sqrt{gH}$). The relative positions of the variables on the staggered "B" grid are shown in Figure 3. The equations of motion, (11) and (12) are differnced as follows.

$$\frac{H^{n+1}}{H^n}u_i^{n+1}-u_i^n+\Delta t\frac{H^{n+1}}{H^n}[\theta_1 H_c R_0 v_i^{n+1}-(\frac{b_0}{h_0})^2\frac{\theta_2}{(\Delta\sigma)^2}H_v[\gamma_{i+1/2}^{n+1}(u_{i+1}^{n+1}-u_i^{n+1})$$

$$-\gamma_{i-1/2}^{n+1}(u_i^{n+1}-u_{i-1}^{n+1})]]=\Delta t[c_i^n-\theta_3\frac{\partial\eta^{n+1}}{\partial x}-(1-\theta_3)\frac{\partial\eta^n}{\partial x}+(\frac{b_0}{h_0})^2\frac{1-\theta_2}{(H^n)^2}$$

$$[\gamma_{i+1/2}^n(u_{i+1}^n-u_i^n)-\gamma_{i-1/2}^n(u_i^n-u_{i-1}^n)]-R_0(1-\theta_1)v_i^n] \tag{18}$$

$$\frac{H^{n+1}}{H^n}v_i^{n+1}-v_i^n-\Delta t\frac{H^{n+1}}{H^n}[\theta_1 H_c R_0 u_i^{n+1}+(\frac{b_0}{h_0})^2\frac{\theta_2}{(\Delta\sigma)^2}H_v[\gamma_{i+1/2}^{n+1}(v_{i+1}^{n+1}-v_i^{n+1})$$

$$-\gamma_{i-1/2}^{n+1}(v_i^{n+1}-v_{i-1}^{n+1})]]=\Delta t[c_i^n-\theta_3\frac{\partial\eta^{n+1}}{\partial y}-(1-\theta_3)\frac{\partial\eta^n}{\partial y}+(\frac{b_0}{h_0})^2\frac{1-\theta_2}{(H^n)^2}$$

$$[\gamma_{i+1/2}^n(v_{i+1}^n-v_i^n)-\gamma_{i-1/2}^n(v_i^n-v_{i-1}^n)]+R_0(1-\theta_1)u_i^n] \tag{19}$$

where i is the vertical node number that is 1 at the water surface and L+1 at the sea bottom, n is the present time step, $n+1$ is the furture time step, (θ_1, θ_2, θ_3) are the weightinf factors each for Coriolis terms, vertical momentum exchange terms, and water surface gradients; 0 means explicit, 1(used in this study) means fully implicit, 0.5 means Crank-Nicolson type, $H_c=H^n/H^{n+1}$, and $H_v=H^n/(H^{n+1})^3$.

Equations (18) and (19) exist at all horizontal grid points. c_i^n and d_i^n are diffrenced by centered space method at time level n.

Equations (18) and (19) can be rewritten in vector form as

$$A\vec{u}+\theta_1 H_c R_0\vec{v}=\vec{G}+\vec{U}-\theta_3\frac{\partial\eta^{n+1}}{\partial x}\vec{I} \tag{20}$$

$$A\vec{v}-\theta_1 H_c R_0\vec{u}=\vec{F}+\vec{V}-\theta_3\frac{\partial\eta^{n+1}}{\partial y}\vec{I} \tag{21}$$

where $A=\begin{bmatrix}\alpha_1 & -\beta_1 & & & \\ -\xi_2 & \alpha_2 & -\beta_2 & & \\ & & & -\xi_{L-1} & \alpha_{L-1} & -\beta_{L-1} \\ & & & & -\xi_L & \alpha_L\end{bmatrix}$, $\vec{u}=\frac{H^{n+1}}{H^n}\begin{pmatrix}u_1^{n+1}\\ u_2^{n+1}\\ \cdot\\ \cdot\\ u_L^{n+1}\end{pmatrix}$, $\vec{v}=\frac{H^{n+1}}{H^n}\begin{pmatrix}v_1^{n+1}\\ v_2^{n+1}\\ \cdot\\ \cdot\\ v_L^{n+1}\end{pmatrix}$, $\vec{G}=\begin{pmatrix}G_1^n+c_1^n\\ G_2^n+c_2^n\\ \cdot\\ \cdot\\ G_L^n+c_L^n\end{pmatrix}$,

$$\vec{F}=\begin{pmatrix} F_1^n+d_1^n \\ F_2^n+d_2^n \\ . \\ . \\ F_L^n+d_L^n \end{pmatrix},\quad \vec{U}=\frac{1}{\Delta t}\begin{pmatrix} u_1^n \\ u_2^n \\ . \\ . \\ u_L^n \end{pmatrix},\quad \vec{V}=\frac{1}{\Delta t}\begin{pmatrix} v_1^n \\ v_2^n \\ . \\ . \\ v_L^n \end{pmatrix},\quad I=\begin{pmatrix} 1 \\ 1 \\ . \\ . \\ 1 \end{pmatrix},$$

α_i, β_i, ξ_i = coefficients dependent on differencing, Δt = time step,

$$G_1^n=-(1-\theta_3)\frac{\partial \eta^n}{\partial x}-R_0(1-\theta_1)v_1^n+\left(\frac{b_0}{h_0}\right)^2\frac{1}{(H^n)^2}\frac{2}{\Delta\sigma}[-\gamma_1(\theta_2\tau_x^{n+1}H^n+(1-\theta_2)\tau_x^nH^n)+(1-\theta_2)\gamma_{3/2}^n\frac{u_2^n-u_1^n}{\Delta\sigma}],$$

$$G_i^n=-(1-\theta_3)\frac{\partial \eta^n}{\partial x}-R_0(1-\theta_1)v_i^n+\left(\frac{b_0}{h_0}\right)^2\frac{1}{(H^n)^2}\frac{(1-\theta_2)}{(\Delta\sigma)^2}[\gamma_{i+1/2}^n(u_{i+1}^n-u_i^n)-\gamma_{i-1/2}^n(u_i^n-u_{i-1}^n)] \text{ for } 2\le i\le L,$$

$$F_1^n=-(1-\theta_3)\frac{\partial \eta^n}{\partial y}+R_0(1-\theta_1)u_1^n+\left(\frac{b_0}{h_0}\right)^2\frac{1}{(H^n)^2}\frac{2}{\Delta\sigma}[-\gamma_1(\theta_2\tau_y^{n+1}H^n-(1-\theta_2)\tau_y^nH^n)+(1-\theta_2)\gamma_{3/2}^n\frac{v_2^n-v_1^n}{\Delta\sigma}],$$

$$F_i^n=-(1-\theta_3)\frac{\partial \eta^n}{\partial y}+R_0(1-\theta_1)u_i^n+\left(\frac{b_0}{h_0}\right)^2\frac{1}{(H^n)^2}\frac{(1-\theta_2)}{(\Delta\sigma)^2}[\gamma_{i+1/2}^n(v_{i+1}^n,-\gamma_{i-1/2}^n(v_i^n-v_{i-1}^n)] \text{ for } 2\le i\le L,$$

$\Delta\sigma$ = the vertical grid size.

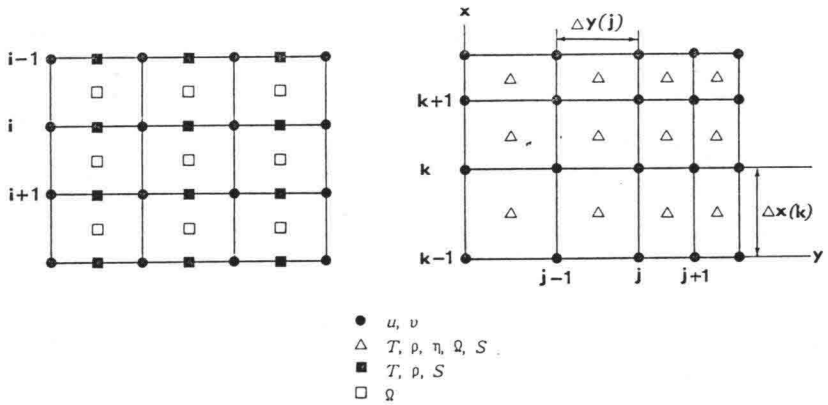

Figure 3 Computational mesh

Now, write equations (20) and (21) as

$$B\vec{\Gamma}=\vec{\Gamma}_1-\vec{\Gamma}_2 \tag{22}$$

where $B=\begin{bmatrix} A & \theta_1 H_c R_0 \vec{I} \\ -\theta_1 H_c R_0 \vec{I} & A \end{bmatrix}$, $\vec{\Gamma}=\begin{pmatrix} \vec{u} \\ \vec{v} \end{pmatrix}$, $\vec{\Gamma}_1=\begin{pmatrix} \vec{G}+\vec{U} \\ \vec{F}+\vec{V} \end{pmatrix}$, $\vec{\Gamma}_2=\begin{pmatrix} \theta_3\frac{\partial \eta^{n+1}}{\partial x}\vec{I} \\ \theta_3\frac{\partial \eta^{n+1}}{\partial y}\vec{I} \end{pmatrix}$.

Write

$$\vec{\Gamma}=\vec{\Gamma}^*+\vec{\Gamma}^o \tag{23}$$

such that

$$B\vec{\Gamma}^*=\vec{\Gamma}_1 \tag{24}$$

$$B\vec{\Gamma}^o=\vec{\Gamma}_2. \tag{25}$$

This splitting is valid since we are working with a liniear equation in $\vec{\Gamma}$. Equation (24) is a tridiagonal matrix and solved by Thomas algorithm.
Formally, the solutions to (25) are

$$\vec{P}=Q\vec{L} \tag{26}$$

where $\vec{P}=\begin{pmatrix}\vec{u^o}\\ \vec{v^o}\end{pmatrix}$, $Q=\begin{bmatrix}\theta_1\Delta t H_c R_0\theta_3\dfrac{\partial\eta^{n+1}}{\partial y} & -\theta_3\dfrac{\partial\eta^{n+1}}{\partial x}\\ -\theta_1\Delta t H_c R_0\theta_3\dfrac{\partial\eta^{n+1}}{\partial x} & -\theta_3\dfrac{\partial\eta^{n+1}}{\partial y}\end{bmatrix}$, $\vec{L}=\begin{pmatrix}\vec{\lambda^A}\\ \vec{\lambda^B}\end{pmatrix}$,

$R\vec{\lambda^A}=\dfrac{1}{\Delta t}\vec{I}$, $R\vec{\lambda^B}=A\vec{I}$, $R=(\theta_1 H_c R_0)^2 I+AA$, I is the a matrix with unity on the diagonal.
Now, integrate the equations (20) and (21) over the vertical coordinate, i.e., sum them up vertically using the following summation scheme:

$$\sum_{i=1}^{L}\Psi_i X_i \tag{27}$$

where X_i is the appropriate equation and $\Psi_i=\begin{pmatrix}\Delta\dfrac{\sigma}{2} & ,i=1\\ \Delta\sigma & ,2\le i\le L\end{pmatrix}$.

The result is

$$\frac{1}{\Delta t}\sum_i\Psi_i(un_i^{n+1}-u_i^n)+\theta_2\phi un_L^{n+1}+\theta_1 H_c R_0\sum_i\Psi_i vn_i^{n+1}=-\chi\theta_3\frac{\partial\eta^{n+1}}{\partial x}+\sum_i\Psi_i G_i^n \tag{28}$$

$$\frac{1}{\Delta t}\sum_i\Psi_i(vn_i^{n+1}-v_i^n)+\theta_2\phi vn_L^{n+1}-\theta_1 H_c R_0\sum_i\Psi_i un_i^{n+1}=-\chi\theta_3\frac{\partial\eta^{n+1}}{\partial y}+\sum_i\Psi_i F_i^n \tag{29}$$

where $\chi=\sum_i\Psi_i=\dfrac{L-1/2}{L}=(L-\dfrac{1}{2})\Delta\sigma$, $\phi=(\dfrac{b_0}{h_0})^2\dfrac{H_v}{\Delta\sigma}\gamma_{L+1/2}^{n+1}$, un_i^{n+1} is $\dfrac{H^{n+1}}{H^n}u_i^{n+1}$, and vn_i^{n+1} is $\dfrac{H^{n+1}}{H^n}v_i^{n+1}$.

Next, take the numerical divergence of these two equations, first multiplying the equations by the total depth. This is equivalent to

$$\frac{1}{\Delta x(k+1)}[HA_{j+1,k+1}+HA_{j,k+1}-HA_{j+1,k}-HA_{j,k}]$$
$$+\frac{1}{\Delta y(j+1)}[HB_{j+1,k+1}+HB_{j+1,k}-HB_{j,k+1}-HB_{j,k}] \tag{30}$$

where $HA=H^n\times(28)$, $HB=H^n\times(29)$.
Diffrencing the vertically summed continuity equation by Leap-frog method gives

$$H^n\Omega^n_{1,j+1/2,k+1/2}=\frac{(\eta^{n+1}-\eta^{n-1})_{j+1/2,k+1/2}}{2K\Delta t}$$

$$+\sum_i \Psi_i \frac{(Hu)^n_{i,j+1,k+1}+(Hu)^n_{i,jk+1}-(Hu)^n_{i,j+1,k}-(Hu)^n_{i,jk}}{2\Delta x(k+1)}$$

$$+\sum_i \Psi_i \frac{(Hv)^n_{i,j+1,k+1}+(Hv)^n_{i,j+1,k}-(Hv)^n_{i,jk+1}-(Hv)^n_{i,jk}}{2\Delta y(j+1)} \tag{31}$$

where $\Delta x(k+1)$ is the grid size between node k and node $k+1$ and $\Delta y(j+1)$ is the grid size between node j and node $j+1$. In the case of using depth-averaged equation, the first term $H^n\Omega_{1,j+1/2,k+1/2}$ is neglected.
Using (31) in (30), get

$$\theta_2\tau^{n+1}_{Bx}+\theta_2\tau^{n+1}_{By}+\theta_1 H_c R_0 v^{n+1}_x-\theta_1 H_c R_0 u^{n+1}_y=-\chi\theta_3\nabla^2\eta^{n+1}+\overline{G}+\overline{F}-\frac{\eta^{n+1}-\eta^{n-1}}{K\Delta t^2} \tag{32}$$

where $\tau^{n+1}_{Bx}=\dfrac{[(H^n\phi un^{n+1}_L)_{j+1,k+1}+(H^n\phi un^{n+1}_L)_{jk+1}-(H^n\phi un^{n+1}_L)_{j+1,k}-(H^n\phi un^{n+1}_L)_{jk}]}{\Delta x(k+1)}$,

$$\tau^{n+1}_{By}=\frac{[(H^n\phi vn^{n+1}_L)_{j+1,k+1}+(H^n\phi vn^{n+1}_L)_{j+1,k}-(H^n\phi vn^{n+1}_L)_{jk+1}-(H^n\phi vn^{n+1}_L)_{jk}]}{\Delta y(j+1)},$$

$$v^{n+1}_x=\frac{\sum_i \Psi_i[(H^n vn^{n+1}_i)_{j+1,k+1}+(H^n vn^{n+1}_i)_{jk+1}-(H^n vn^{n+1}_i)_{j+1,k}-(H^n vn^{n+1}_i)_{jk}]}{\Delta x(k+1)},$$

$$u^{n+1}_y=\frac{\sum_i \Psi_i[H^n un^{n+1}_i)_{j+1,k+1}+(H^n un^{n+1}_i)_{j+1,k}-(H^n un^{n+1}_i)_{jk+1}-(H^n un^{n+1}_i)_{jk}]}{\Delta y(j+1)},$$

$$\nabla^2\eta^{n+1}=\frac{(H^n\frac{\partial\eta^{n+1}}{\partial x})_{j+1,k+1}+(H^n\frac{\partial\eta^{n+1}}{\partial x})_{jk+1}-(H^n\frac{\partial\eta^{n+1}}{\partial x})_{j+1,k}-(H^n\frac{\partial\eta^{n+1}}{\partial x})_{jk}}{\Delta x(k+1)}$$

$$+\frac{[H^n\frac{\partial\eta^{n+1}}{\partial y})_{j+1,k+1}+(H^n\frac{\partial\eta^{n+1}}{\partial y})_{j+1,k}-(H^n\frac{\partial\eta^{n+1}}{\partial y})_{jk+1}-(H^n\frac{\partial\eta^{n+1}}{\partial y})_{jk}]}{\Delta y(j+1)},$$

$$\overline{G}=\frac{1}{\Delta x(k+1)}\sum_i \Psi_i[(HG)^n_{i,j+1,k+1}+(HG)^n_{i,jk+1}-(HG)^n_{i,j+1,k}-(HG)^n_{i,jk}],$$

$$\overline{F}=\frac{1}{\Delta y(j+1)}\sum_i \Psi_i[(HF)^n_{i,j+1,k+1}+(HF)^n_{i,j+1,k}-(HF)^n_{i,jk+1}-(HF)^n_{i,jk}].$$

The corresponding equation in terms of $\overrightarrow{u^*}$ and $\overrightarrow{v^*}$ is

$$-\frac{2}{\Delta t}H^n\Omega^*_{1,j+1/2,k+1/2}{}^n+\theta_2\tau^*_{Bx}+\theta_2\tau^*_{By}+\theta_1 H_c R_0 v^*_x-\theta_1 H_c R_0 u^*_y=\overline{G}+\overline{F} \tag{33}$$

Subtracting (33) from (32) and using (23) and (26), get

$$-\frac{2}{\Delta t}(H^n\Omega^*_{1,j+1/2,k+1/2}{}^n+\frac{\eta^{n+1}-\eta^{n-1}}{2K\Delta t})=[\frac{\chi+\varepsilon}{\Delta x(k+1)}+\frac{\delta}{\Delta y(j+1)}]\theta_3(H^n\frac{\partial\eta}{\partial x})^{n+1}_{j+1,k+1}$$

$$+[\frac{\chi+\varepsilon}{\Delta x(k+1)}-\frac{\delta}{\Delta y(j+1)}]\theta_3(H^n\frac{\partial\eta}{\partial x})^{n+1}_{jk+1}-[\frac{\chi+\varepsilon}{\Delta x(k+1)}-\frac{\delta}{\Delta y(j+1)}]\theta_3(H^n\frac{\partial\eta}{\partial x})^{n+1}_{j+1,k}$$

$$-[\frac{\chi+\varepsilon}{\Delta x(k+1)}+\frac{\delta}{\Delta y(j+1)}]\theta_3(H^n\frac{\partial\eta}{\partial x})^{n+1}_{j,k}+[\frac{\chi+\varepsilon}{\Delta y(j+1)}-\frac{\delta}{\Delta x(k+1)}]\theta_3(H^n\frac{\partial\eta}{\partial y})^{n+1}_{j+1,k+1}$$

$$+[\frac{\chi+\varepsilon}{\Delta y(j+1)}+\frac{\delta}{\Delta x(k+1)}]\theta_3(H^n\frac{\partial\eta}{\partial y})^{n+1}_{j+1,k}-[\frac{\chi+\varepsilon}{\Delta y(j+1)}-\frac{\delta}{\Delta x(k+1)}]\theta_3(H^n\frac{\partial\eta}{\partial y})^{n+1}_{j,k+1}$$

$$-[\frac{\chi+\varepsilon}{\Delta y(j+1)}-\frac{\delta}{\Delta x(k+1)}]\theta_3(H^n\frac{\partial\eta}{\partial y})^{n+1}_{j,k} \tag{34}$$

where $\varepsilon_{j,k}=-\theta_2\phi\lambda^B_{L,j,k}-\Delta t(\theta_1 H_c R_0)^2\sum_i\Psi_i\lambda^A_{i,j,k}$, $\delta_{j,k}=-\Delta t\theta_1 H_c R_0\theta_2\phi\lambda^A_{L,j,k}+\theta_1 H_c R_0\sum_i\Psi_i\lambda^B_{i,j,k}$.

The diffrence forms for the water surface gradient terms are

$$\frac{\partial\eta}{\partial x})_{j,k}=\frac{\eta_{j+1/2,k+1/2}+\eta_{j-1/2,k+1/2}-\eta_{j+1/2,k-1/2}+\eta_{j-1/2,k-1/2}}{\Delta x(k+1)+\Delta x(k)} \tag{35}$$

$$\frac{\partial\eta}{\partial y})_{j,k}=\frac{\eta_{j+1/2,k+1/2}+\eta_{j+1/2,k-1/2}-\eta_{j-1/2,k+1/2}+\eta_{j-1/2,k-1/2}}{\Delta y(j+1)+\Delta y(j)} \tag{36}$$

Equation (34) was solved by Point-SOR(successive over-relaxation) method. Equation (34) is only for the interior grid points, away from all boundaries. Near a boundary, a similar equation is derived; however, instead of using the summed horizontal momemtum equations at the boundary points, the appropriate boundary condition is used.

For the transport equation of temperture, the similar method with (18) was used for differencing and the resulting tridiagonal matrix was solved by Thomas algorithm.

4) Stability Constraints

The differece method for advective terms and horizontal diffusion terms limits the time step of circulation model. By neglecting vertical advection term, get the stability criteria as

$$\frac{[R_e(u_0+v_0)]^2\Delta t}{4}\leq 1,\ \frac{\Delta t}{\Delta x^2}\leq\frac{1}{4} \tag{37}$$

For the stability criteria of transport model of temperature, we can get by mutiplying Pr to the left hane side for the second constraint of (37).

4. APPLICATION TO YEONG-KWANG SITE

The grid system for numerical computation were shown in Figure 4. The horizontal grid size varies from 60m near the outlet to 1000m at off-shore boundary. There are 34×41 rectangular meshes. The water column was divided into 5 layers equally ($\Delta\sigma$= 0.2) to resolve the vertical variations of currents and temperature. The water depth (Figure 1) at every grid point was read from the hydrographic chart of this area. The numerical time step for computation was determined as 20sec.

The initial condition was $\eta=u=v=\Omega=0$ and the precomputation for η, u, v, Ω during 3 tidal cycles was performed before computing water temperature fields. The circulation and water temperatures were computed for more than 10 tidal cycles to reach quasi-steady state. The boundary conditions at the open boundaries were specified with the tidal heights combined with 5 major consitituents (M_2, S_2, K_1, O_1, N_2) analyzed from the tidal measurements. The outlet conditions were specified with the designed discharge (2units×57.5 m^3/sec) and the excess temperature (8.2℃). A value of 30 Watt/m^2/℃ was chosen as the heat exchange coefficient.

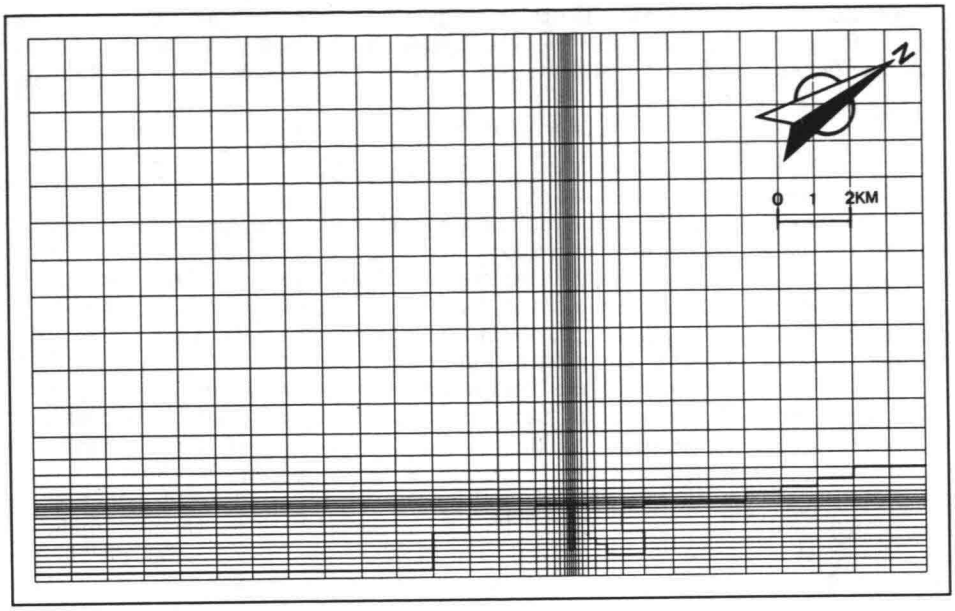

Figure 4 Numerical grid system of 3-D model

The vertical exchange coefficients, A_V and B_V (Officer, 1976) are determined as

$$A_V = A_{V0} f(R_i) \tag{38}$$

$$B_V = B_{V0} g(R_i) \tag{39}$$

where A_{V0} is the vertical exchange coefficient of momentum under neutral state, B_{V0} is the vertical exchange coefficient of water temperature under neutral state, and $f(R_i)$ and $g(R_i)$ are the stability fuctions respectively. Comparative evaluations for 5 stability fuctions shown in Table 1 were conducted by Jung (1993).

Table 1 Examples of stability function

Researcher	$f(R_i)$	$g(R_i)$
Munk and Anderson (1948)	$(1+10R_i)^{-0.5}$	$(1+3.33R_i)^{-1.5}$
Mamayev (1958)*	$e^{-0.4R_i}$	$e^{-0.8R_i}$
Delft Hydraulic Lab. (1974)*	$e^{-1.5R_i}$	$e^{-3.0R_i}$
Officer (1976)	$(1+R_i)^{-1}$	$(1+R_i)^{-2}$
Vreugdenhil*	$(1+30R_i)^{-1}$	$1.17(1+6.53R_i)^{-1.5}$

* referenced from Leendertse and Liu (1975)

A three-dimensional model was applied to the heated water discharges into the stagnant water with the same conditions with hydraulic experiments of Pande and Rajaratnam (1977). The calculated velocity decay and temperature decay along surface center-line were compared with the hydraulic experimental data set. The numerical simulation results were not affected by the form of stability function but the exchnge

coefficients under neutral state. In this study the stability function of Munk and Anderson (1948) were adopted for the application to YeongKwang area. The vertical exchange coefficients under neutral state are computed by Bowden et al. (1959) as

$$A_{V0} = B_{V0} = 0.0025HU[4(1-\sigma)\sigma] \tag{40}$$

where U is the depth averaged velocity.

To check the performance of the circulation model, the computed tidal currents at 5 layers were compared with the observations at St. C1 and St. C2 as shown in Figure 5.The velocity magnitude and the general trends of variations are in good agreements with the observations. Figure 6 shows the distribution of computed tidal currents during spring tide. In Figure 6, symbol * means the dried area of tidal flats. The tidal flats were treated appropriately by the model. The basic concept for the treatment of tidal flats is to consider as a land in the calculations when the water depth is less than 10cm. The flood and ebb currents far from the outlet flow parallel to the coastline.

Figure 7 shows the comparison of the spatial distribution of the excessive water temperature with the field observations during a neap tide in the February of 1992. General patterns of the thermal plume and excessive temperature distribution are in good agreement with the observations. To check the simulation results qualitively, a Landsat image (Figure 8) was analyzed. Figure 9 shows the spatial distributons of surface water temperature in spring tide for the present case of 2 units operation. The isolines of the heated water temperature are moved toward the northern coast during flood tide, while they are turned toward the southern coast during ebb tide. Figure 8 is a Landsat image at low water in spring tide, and the pattern of thermal plume is in a good agreement compared with the compued results of Figure 9(a). In this area the additional two units are under the construction. The change of excess temperature distrbution by additional 2 units (totally 4 units) operation was predicted as shown in Figure 10.

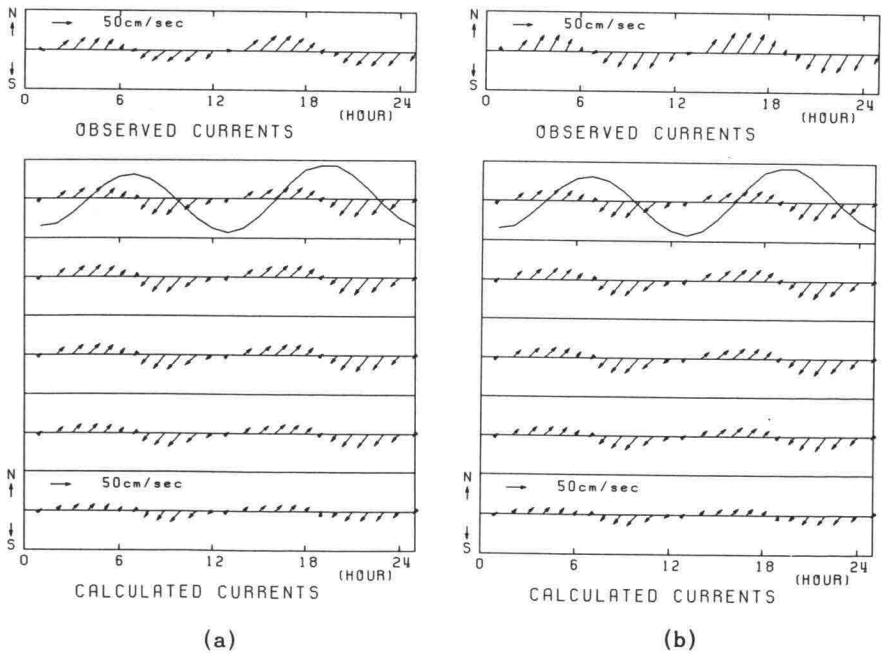

Figure 5 Comparison of tidal currents at C1(a) and C2(b) stations

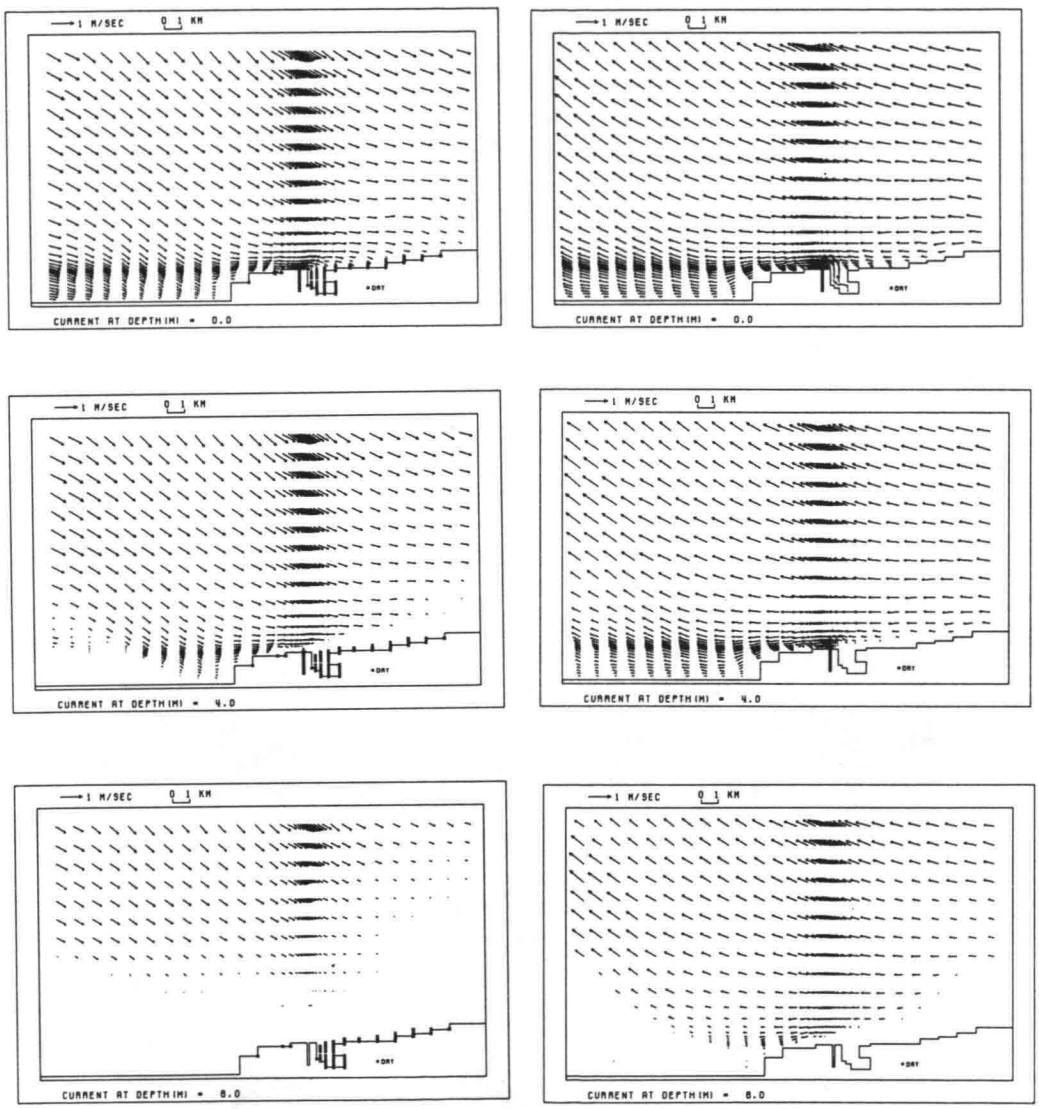

(a) (b)

Figure 6 Computed currents at 3-layers during the flood(a) and ebb(b) cycles in Spring Tide

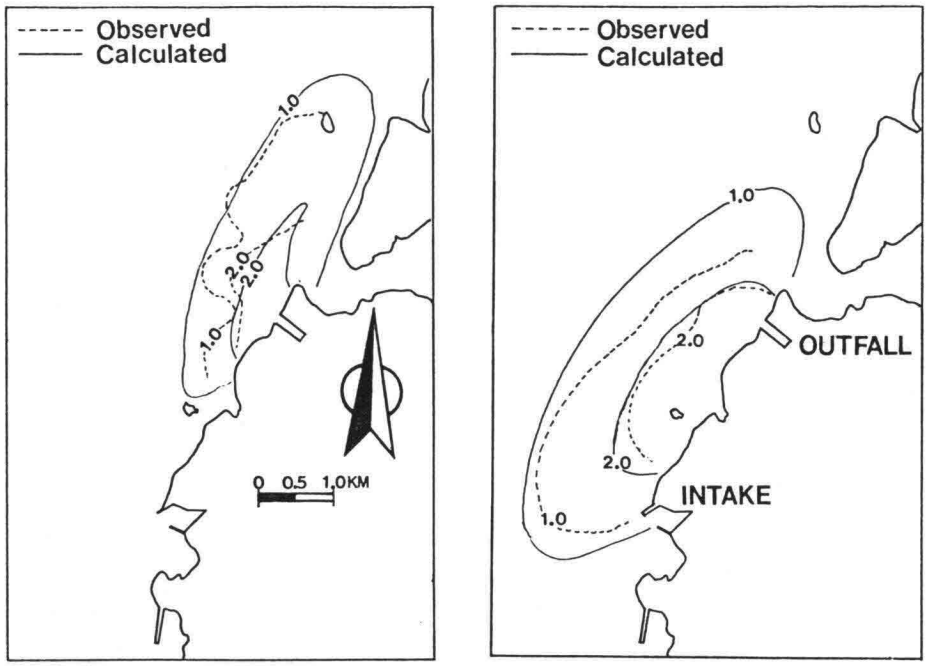

Figure 7 Comparison of the excessive temperature field during the flood(a) and ebb(b) cycles in Neap Tide

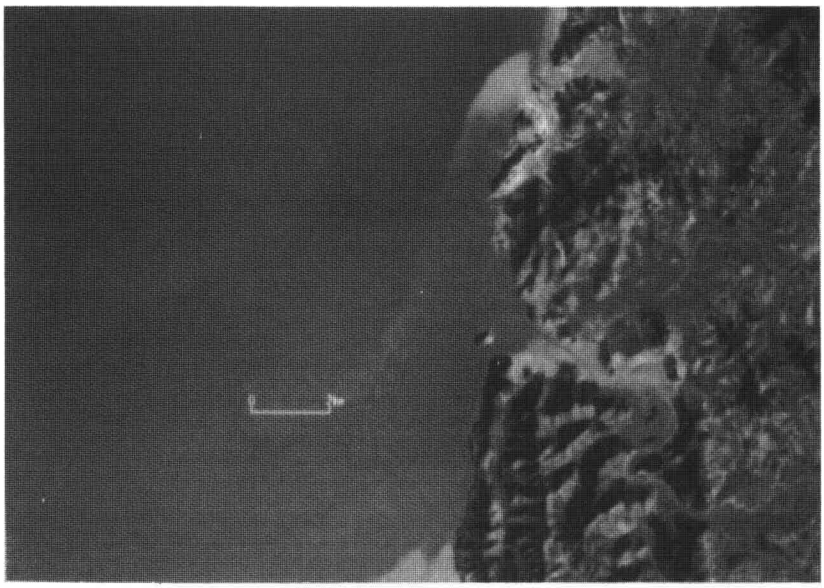

Figure 8 LANDSAT TM image of the Yeong-Kwang coast on October 27, 1987

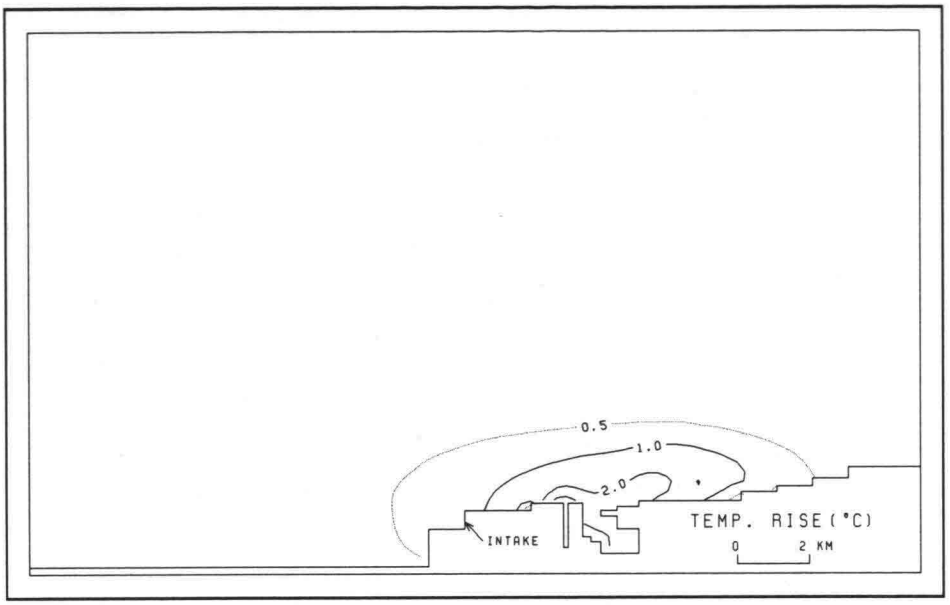

(a)

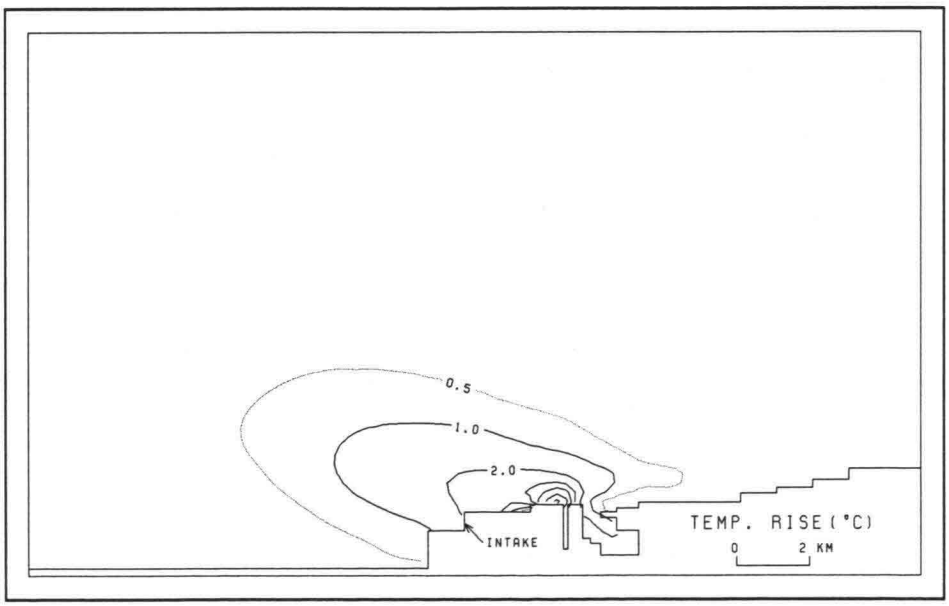

(b)

Figure 9 Computed excessive temperature fields during the flood(a) and ebb(b) cycles in Spring Tide

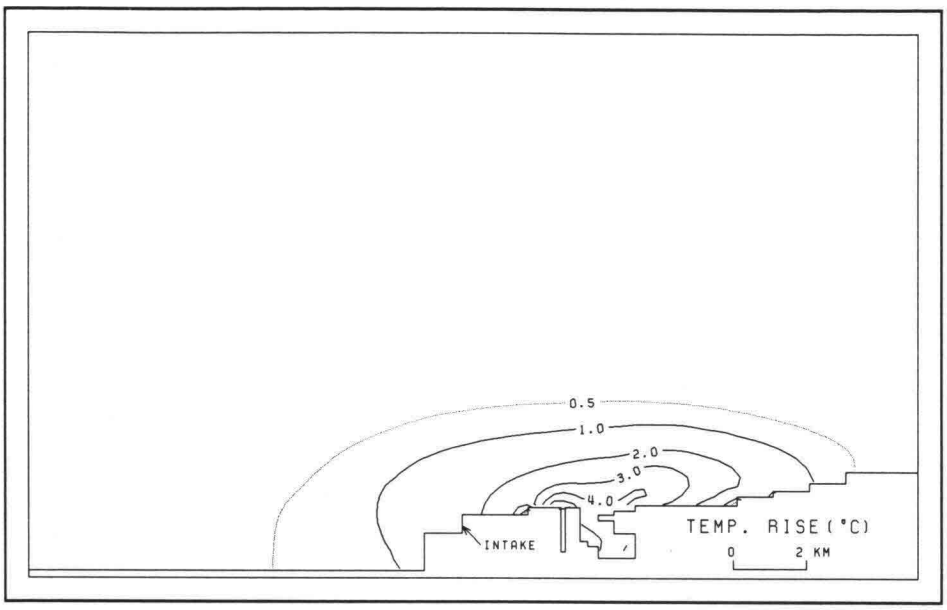

(a)

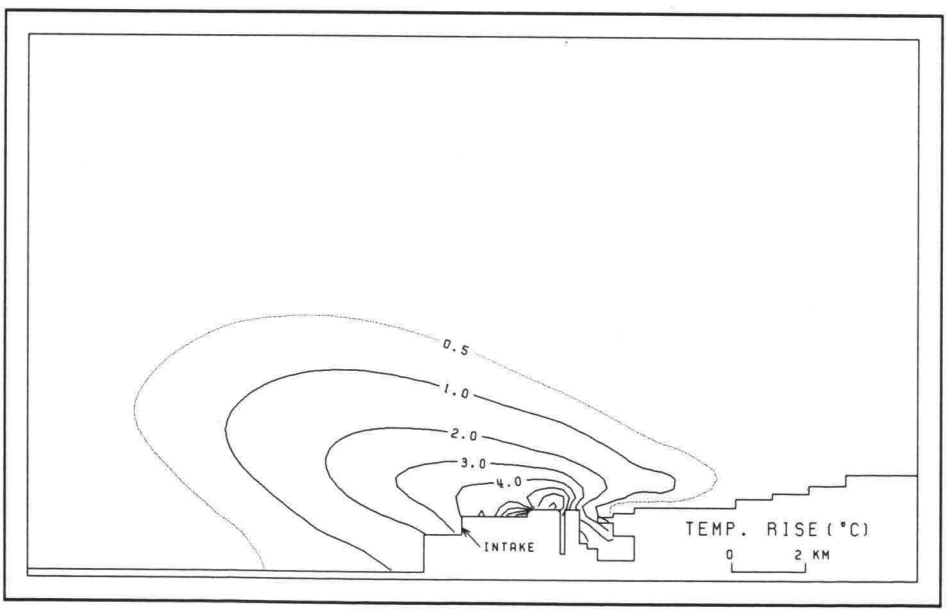

(b)

Figure 10 Computed excessive temperature fields during the flood(a) and ebb(b) cycles in Spring Tide for the case of 4-units operation (under construction)

5. CONCLUSIONS

In this study, a three-dimensional numerical model with computational efficiency was developed and applied to simulate the circulation and transport of heated water dicharged from the Yeong-Kwang nuclear power plant of Korea. The model results are in a good agreement comparing with the field obsevations. The tidal currents are the major forcing factors to transport the thermal plume along the Yeong-Kwang coast of the Yellow Sea.

ACKNOWLEDGEMENTS

This study was conducted as a part of the environmental assessment funded by the Korea Power Engineering Company. The authors wish to thank the members of Korea Ocean Research and Development Institute who participated in field survey and data analysis.

REFERENCES

Amsden, A. A. and F. H. Harlow (1970): The SMAC method: A numerical technique for calculating incompressible fluid flows, LA-4370, Los Alamos Scientific Lab., Los Alamos, N. M., 84p..

Bowen, K. F., L. A. Fairbairn and P. Hughes (1959): The prediction of shearing stresses in tidal current, Geophys. J. R. Astro. Soc., Vol. 2, pp. 288-305.

Delft Hydraulics Laboratory (1974): Momentum and mass tranfer in stratified flow, Report R880, Delft Hydraulics Lab.

Freeman, N. G., A. M. Hale and M. B. (1972): A modified sigma equations' approach to the numerical modelling of Great Lake hydrodynamics, J. of Geophys. Res., Vol. 77, No. 6, pp. 1050-1060.

Jung, T. S. (1993): Numerical analysis of surface buoyant jets by a 3-dimensional numerical model on σ-coordinate, Korea Ocean Research & Development Institue Report BSPE 00334-541-2, 73p. (in Korean).

Leendertse, J. J. and S-K. Liu (1975): A three-dimensional model for estuaries and coastal seas, Vol. II: Aspects of computation, R-1764-OWRT, Rand Corp., Santa Monica, 1975, 123p..

Mamayev, O. I. (1958): The influence of stratification on vertical turbulent mixing in the sea, Izv. Geophys. Ser., pp. 870-875.

Munk, W. H. and E. R. Anderson (1948): Notes on the theory of the thermocline, J. of Mar. Res., Vol. 1, pp. 276-295.

Officer, C. B. (1976): Physical oceanography of estuaries and associated coastal waters, Wiley-Interscience, New York, ...

Pande, B. B. L. and N. Rajaratnam (1977): An experimental study of bluff buoyant turbulent surface jets, J. Hyd. Res., Vol. 15, pp. 261-272.

Paul, J. F. and W. Lick (1985): Numerical model for three-dimensional, variable-density, rigid-lid hydrodynamic flow, Grant No. 803704, Env. Res. Lab., Office of Res. and Dev., U. S. Environmental Protection Agency, Duluth, Minesota, 1985.

HYDRO-PORT'94
International Conference on Hydro-Technical
Engineering for Port and Harbor Construction
October 19 - 21, 1994, Yokosuka, Japan

Development of Water-Intake Works with Submerged Mound (WWSM)

Akiyoshi Nakayama [1]
Masaaki Yamamoto [1]
Jun Yamamoto [1]
Akihiko Moriguchi [2]

[1] National Research Institute of Fisheries Engineering
Ebidai, Hasaki-machi, Kashima-gun, Ibaraki
[2] Hokkaido Development Agency
Kasumigaseki 3-1-1, Chiyoda-ku, Tokyo

ABSTRACT

WWSM is a system for bringing seawater into a basin by using wave power. It was reported from field survey that WWSM was able to exchange sufficient amount of seawater and it was useful for purifying the basin water. In this report, the authors proposed a method to plan WWSM regarding applicability, required quantity of seawater inflow, layout of the submerged mound and training channels. Moreover,a calculation method of deciding its structure and scale in order to get enough amount of seawater inflow, was proposed.

Key Words: Water-intake works,Water Purifying

1.INTRODUCTION

In Japan, most of calm basins in fishing ports are used for live fish stock which supply fresh and valuable fish to japanese people. Moreover these basins are requested to be used for nursery culture before seed liberation. So improvement and conservation of seawater quality in basins is increasing its importance.

In order to improve and conserve seawater quality in basins, it is necessary to construct wastewater treatment works and training facilities which bring clean seawater to basins. Training facilities are not always necessary at every fishing port. But at the fishing port of which scale is small or medium and seawater exchange efficiency is not so high, WWSM is effective. For bringing clean seawater to a basin, it is economical to utilize natural powersuch as tide, wind waves, internal waves. Some methods have been studied up to now, but almost studies are about utilizing tidal power.

Authors have been studying WWSM which is effective to exchange seawater by utilizing wind waves even if wave height is relatively small[1]. WWSM is composed of a breakwater with training channels, a seawater pool, and a remote submerged mound(Fig.1). Wind waves breaking at the remote submerged mound cause wave-set up at the seawater pool between the breakwater and the submerged mound. So mean seawater level at the seawater pool is higher than the one at the basin behind the breakwater. And seawater flow from the seawater pool to the basin through the training channels.

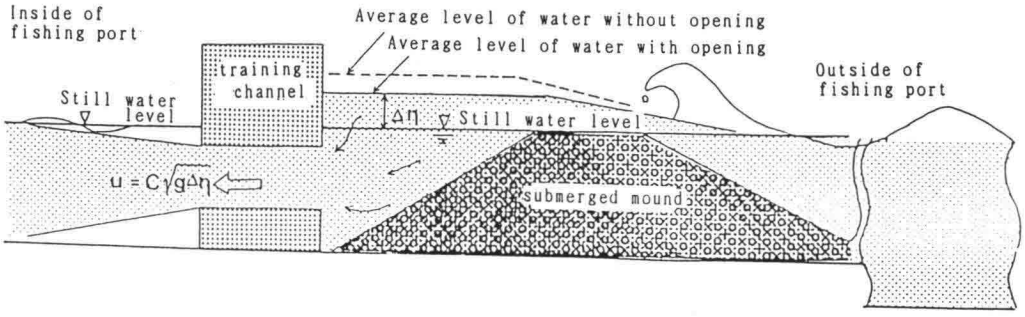

Fig.1 Schematic drawing of WWSM

Layout and scale of the submerged mound, wave force acting on the breakwater, and flow pattern in the basin have been investigated experimentally. Conclusions of these studies are as follows.

(1)Quantity of seawater inflow canbe estimated by wave height.

(2)The impermeable submerged mound is more effective than the permeable one. Its crown height should be nearly equal to mean seawater level. And its slope should be 1/1-1/3.

(3)The training channels should be under seawater level not to increase transmitted wave height.

(4)Plural channels increase mixing seawater in the basin

By designing WWSM to satisfy these conclusions, improving seawater quality in the basin becomes possible even if wave height is small.

Recently WWSM's are constructed or under construction at several fishing ports in Japan, for example, Yokata fishing port (Toyama pref.), Oshima fishing port, Sikanoshima fishing port (both Fukuoka pref.),and so on.
Field surveys were carried out at above three fishing ports. The outline of field survey on Yokata fishing port is described later.

In this report, on the basis of these experimental studies and field surveys, planning and design of WWSM are investigated for the purpose of improving seawater quality in fishing ports and breeding fishes in a closed sea area.

Fig.2 shows the process of planning and designing WWSM.

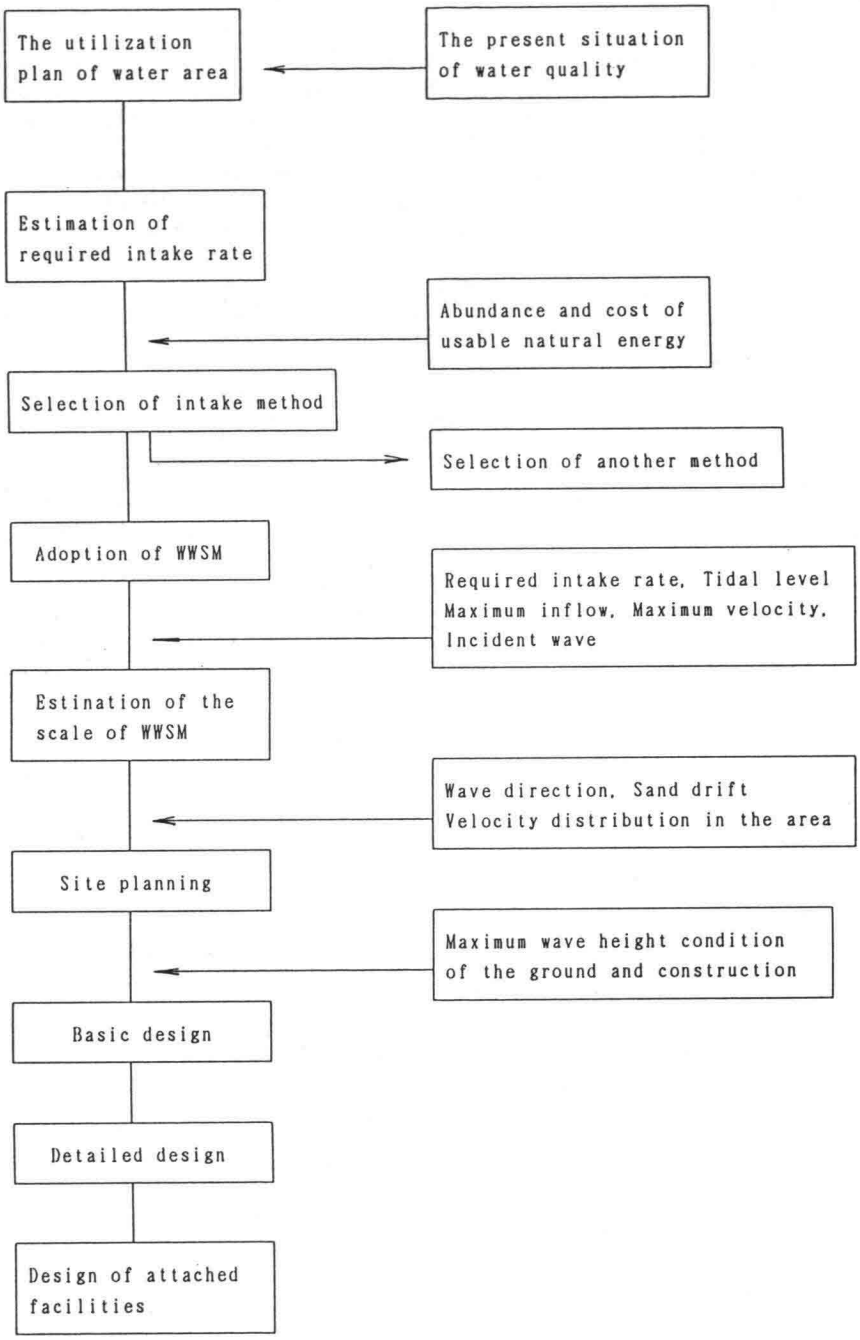

Fig.2 Flow chart of planning and designing WWSM

2. ESTIMATION OF PLAN SCALE AND ENVIRONMENTAL CONDITIONS

2.1 PLAN TARGETS

Planning targets for improving seawater quality are depend on how to use the supposed area. For example, one is improving seawater quality and sediments for fishing port environment, the other is improving or keeping seawater quality to breed fishes and stock live fishes. The former is enough to consider mean (long time scale) seawater quality. But the latter needs to consider more severe conditions not to be below the survival limit in a short time. In case of the closed nursery culture ground with embankments, scale and type of facilities for improving seawater quality should be selected on the basis of not also construction cost but also management cost.
Generally the planning condition is most severe environmental condition during breeding fishes. Phenomena which may have possibility of improving sea water quality by exchange seawater are as follows.

(1) Lack of dissolved oxygen (DO) for fishes

Lack of dissolved oxygen occurs from late spring to early summer when weather is mild and aquatic organism become active, or from late summer to autumn when dissolved oxygen decrease gradually. These Phenomena are related to biological consumption and generation of oxygen, oxygen supply by seawater circulation and oxygen supply from the surface which depend on wind speed.

Generally at a closed shallow sea , DO reaches saturation during day-time by photosynthesis of phytoplankton. But DO is decreasing during night and reaches minimum value at dawn. So severe status occurs at dawn on the next day when it is rainy or cloudy and calm.

On the other hand, in a deep bay, seawater becomes stratified from spring to summer because of decrease in salinity and water temperature rise at the upper layer. So oxygen supply from the upper layer to the bottom layer is cut off, and DO at the bottom layer reaches minimum value in early autumn.

Salinity of the seawater brought by WWSM may be high. And DO is also high be cause wave breaking at the submerged mound will cause aeration. Possibility of improving seawater quality by utilizing these characteristics should be investigated.

(2)High seawater temperature ,or low seawater temperature

In a shallow sea, seawater is also easy to be heated and cooled. So troubles on breeding fishes may occur because of severe seawater temperature changes. Seawater is mainly heated by radiant energy from the sun -short wave radiation-, and is cooled by radiant energy from the seawater surface to the atmosphere -long wave radiation- and water evaporation energy which is in proportion to wind speed.

Short wave radiation depends on permeability of the sunlight which is changed by the amount of clouds and humidity, and an angle of the sun. In case of high seawater temperature, possibility of cooling seawater by bringing outside seawater should be investigated. In case of low seawater temperature, we should investigate possibility of heating seawater by bringing outside seawater.

(3)rapid salinity reduction due to rainfall

Direct rainfall to the sea area, inflow from rivers and underground water decrease seawater salinity. Seawater brought by external force, such as tide, supply salinity to this area. Especially in the of rivers discharging this area, salinity reduction is remarkable. In such cases, it is necessary to improve efficiency of exchanging seawater.

2.2 METHODS TO EXCHANGE SEAWATER

According to the Design manual of Facilities for Improving Coastal Fishing Ground[9], "As natural forces, we can utilize tide, current, wind waves,internal wave, wind, long-period wave, water oscillation in bay and so on. And We must investigate these forces quantitatively." Wind waves are generally most powerful of these forces, and tide is the next. But there are few methods to utilize wind wave for exchanging seawater. Because wind waves are too irregular to utilize their force easily (shown table 1).

Table.1 Wave power and tidal power

	Tide	Wave
Wave height	～0.4m in the Japan Sea 0.5～3m in the Pacific Ocean	0～10m, violent, variation
Prediction	Regular variation with a period of half month	Not predictable because of irregularity
Displacement of a water particle	Long in shallow region	Short, less than 10m

Moreover, excursion length of water particle is calculated by eq.(1) which is derived under long wave condition. As an order of calculated value is only 1 meter, the effective region by only training channels is very narrow in comparison with a fishing port or a nursery culture ground.

$$l=H.T.(g/d)^{1/2}/(2.\pi) \qquad \text{----------(1)}$$

H ; Wave height T ; wave period
g ; gravity acceleration d ; water depth

But in the case of the bay of which shape is similar to a suck, displacement of a water particle is calculated by eq.(2)

$$l=H.T.(g/d)^{1/2}/(2.\pi)\sin(2.\pi.x/L) \qquad \text{----------(2)}$$

x ; distance from reflection phase
L ; wave length

According to eq.(2) excursion length of water particle will become short if

longitudinal length of the bay is short. In such a case, it is possible to increase exchanging seawater by constructing jetties and water-routes.

On the other hand, if we can change even small waves to flow, excursion length of water particle will become long. So in a narrow sea area, wind wave will be come effective force for exchanging seawater.

2.3 MAXIMUM SEAWATER INFLOW

Seawater inflow -Qin- by WWSM is depend upon wave height, tidal level, cross section area of training channels and so on. According to authors' experiments (fig.3), maximum seawater inflow by WWSM is about $1/5.(g.H^3)^{1/2}$. "$(g.H^3)^{1/2}$" is an index of overtopping rate. Qin can be calculated by eq.(3).

$$Qin=Cin.(g.H^3)^{1/2} \qquad \text{----------(3)}$$

$$Cin=0.2.\tanh(4.0.A/BH)$$

A; Cross section area of a training channel
B; length of a submerged mound
H; Incident wave height

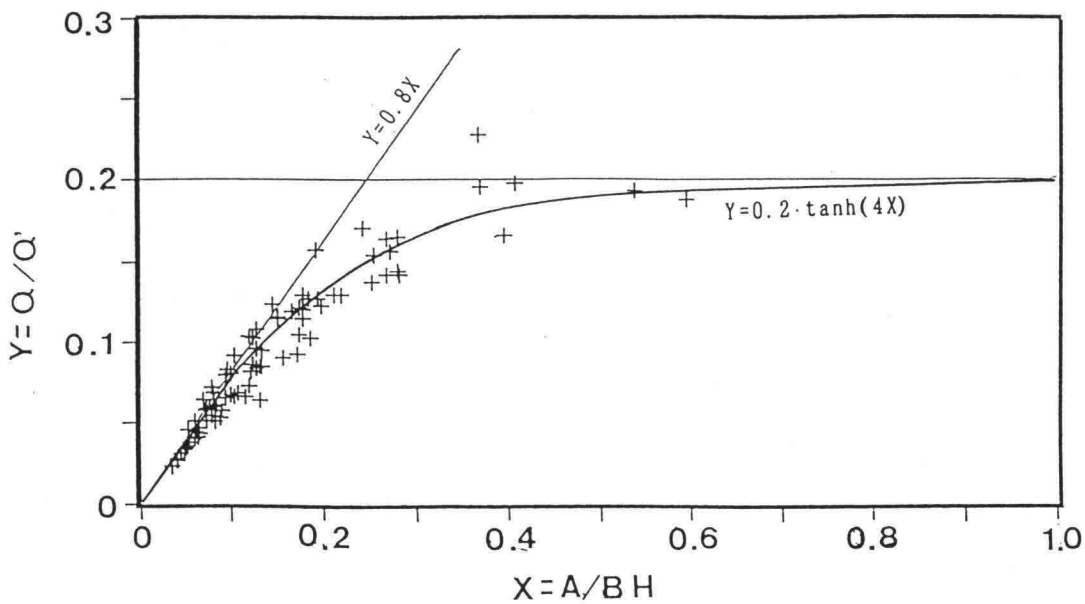

Fig.3 Efficiency of seawater inflow

If the submerged mound works effectively, seawater inflow will be $200m^3$/hour every 1 meter of the submerged mound ,when incident wave height is 0.2 meter. In such a case, Oxgen supplied by seawater inflow will be about 40 kg/hour. In another words, seawater inflow by 1 meter submerged mound is equal to the quantity of exchanging seawater in $2400m^2$ sea area by tidal wave of which amplitude is 1 meter. If incident wave height is 1 meter, seawater inflow is

eleven times as much as the above case. At a nursery culture ground or an aquaculture pond, assuming that difference between DO inflow and discharge is 2.0ml/l and fishes can use 0.5ml/l in 2.0ml/l DO, seawater inflow by WWSM will be good enough to breed 200-500 kg fishes,when wave height is 0.2m. But the capacity should be actually estimated at about 100-250kg fish.

2.4 DESIGN WAVE HEIGHT

In a bay or a fishing port, sludge and sediments at the sea bottom have a great influence on seawater quality. And wave energy change seasonally. So the monthly mean wave should be adopted as the design wave for improving seawater quality and sediments.

In a narrow sea area, seawater quality such as DO change every day. In case of breeding fishes, it is important to investigate the hourly variation of seawater quality. In general, DO is mainly consumed in the night and DO reaches minimum at dawn. According to this phenomenon, the minimum wave in the night should be adopted as the design wave. But the Japan Sea often continues to be calm for a few days from spring to summer. Only seawater inflow by WWSM may not be able to recover the lack of DO under such a calm condition. And minimum of useful wave height to WWSM is about 20cm. If wave height continues to be less than 20cm for a long time, countermeasures should be taken to recover the lack of DO. Some countermeasures are as follows.

(1)While seawater inflow is zero, nursery culture grounds or aquaculture ponds have enough room for DO consumption in order to keep minimum DO for fishes. In another words, culture density need to be less than the standard.

(2)Aeration equipments or feeding pumps need to be prepared for DO supply to nursery grounds or ponds.

(3)In order to restrain biological DO consumption, the amount of feed need to be reduced.

3. REQUIRED SEAWATER INFLOW AND PLAN OF WWSM

3.1 REQUIRED SEAWATER INFLOW

Required seawater inflow, for keeping seawater quality good ,is calculated by balance equation on DO[3]. From this equation, the equation on required seawater inflow is as follows.

$$V\cdot dC/dt-Q\cdot(C0-C)+K1\cdot R\cdot V-K2\cdot(Cs-C)\cdot A+K'1\cdot C\cdot A+(\alpha 0-\alpha 1)\cdot V+k\cdot Wb\cdot N=0 \qquad (4)$$

V,A ; Volume and area of the supposed sea area
C,C0,Cs ; DO inside and outside of the supposed sea area, saturated DO
K1,K2,K'1; Coefficient of DO consumption, DO supply, and DO consumption at the sea bottom
R ; Biological oxygen demand
Q ; Seawater inflow
$\alpha 0, \alpha 1$; DO consumption and DO production per unit volume in the sea
k ; DO consumption rate by fishes per unit weight
Wb,N ; Weight of fish, number of fish
t ; Time

Every term shows DO variation rate, DO supply from outside by seawater inflow Q, DO consumption and supply underwater, DO consumption at the sea bottom, DO consumption by plankton and DO production by phytoplankton, and DO consumption by fishes.

Planning conditions at a narrow sea are as follows.

(1) wind speed is equal to zero.
(2) DO variation is independent of time

And C is replaced with C* that is required DO in eq.(4). So eq.(4) is simplified as follows.

$$Q=K1.R.V+K1.C.A+\alpha 0.V+k.Wb.N/(C0-C^*) \qquad \text{----------(5)}$$

This equation is based on the assumption that DO is homogeneous , and this phenomenone is stationary. In order to know DO distribution , numerical simulation, such as box model and finite difference equation, need to be used.

In order to decide required seawater inflow on the basis of required DO, DO consumption rate must be observed in the field. But in case of closing sea area, giving baits to fishes or exchanging seawater, the environment of the sea area change rapidly. For this reason, it becomes hard to estimate DO consumption rate. For examples, floating seaweed with seawater inflow was brought to the nursery pond ,in which flounder juveniles wrere stocked, and the seaweed sunk in that pond. Under such condition, DO consumption rapidly increased. On the other hand, seawater inflow by WWSM might purify sediments in Sikanoshima fishing port (Fukuoka pref.), and the severe DO reduction in the night have never occurred since WWSM was completed.

Assuming that DO consumption and supply is equilibrium, oxygen required to decompose organic matters brought into the sea area, is supposed to be multi plier of useful DO=(DO in seawater inflow)-(necessary DO for the sea area) and seawater inflow.

Proteinic matter such as plankton is decomposed to carbonic acid gas and nitric acid by oxygen. In this process, oxygen need 1.24 times as much as protein. So feed for fishes need the same amount of oxygen supply. For example, assuming that weight of feed in a day is equal to 5% of fish weight and useful DO is 5mg/l, required seawater inflow in a day is calculated as follows.

$$1{,}000{,}000g \times 0.05(g/day)/5(g/m^3)=10{,}000(m^3/day)$$

Pollution sources are feed, filthy water, organic matters in sediments and so on.

3.2 SEAWATER INFLOW

Seawater inflow can be calculated by eq.(3) ,if the submerged mound is im permeable and its crown height is equal to mean seawater level. In this sec tion, authors proposed a method of calculating seawater inflow in case of tide level changing and the permeable submerged mound.

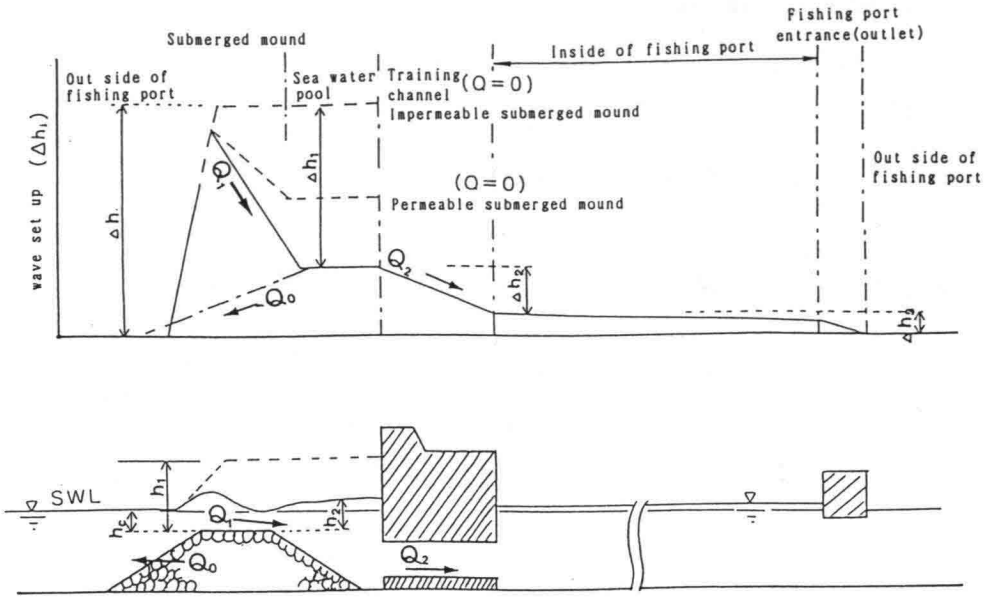

Fig.4 Explanation on method to calculate quantity of seawater inflow

WWSM is hydraulically composed of three parts which is the submerged mound, the inlet and the outlet (show fig.4). Wave-setup Δh generated by wave breaking at the submerged mound is divided to three above part $\Delta h1, \Delta h2, \Delta h3$.

$$\Delta h=\Delta h1+\Delta h2+\Delta h3 \qquad \text{----------(6)}$$

Applying the formula on the submerged sluice gate[6] to relationship between inflow Q and $\Delta h1$, the equation is as follows.

$$Q=(C1.h1.B).(2.g.\Delta h1)^{1/2} \qquad \text{----------(7)}$$

h1,h2; sea level at front edge and end edge of the submerged mound
C1 ; Coefficient of inflow rate
B ; length of the submerged mound

From the results of experiments on impermeable submerged mound, Coefficient of inflow rate is calculated by eq.(8).

$$h2/h1<0.71 \quad C1=0.32$$
$$h2/h1>0.71 \quad c1=0.45.h2/h1 \qquad \text{----------(8)}$$

Relationship between $\Delta h1$ and flow rate Q1 is calculated by eq.(9).

$$\Delta h1=1/\{2.g(C1.h1.B)^2\}.Q1^2=R1.Q1^2 \qquad \text{----------(9)}$$

R1 ; resistance Coefficient

In case of the permeable submerged mound, return flow in the submerged mound

exist. It is calculated by eq.(10)

$$Q0=(C0.hd.B).(2.g.\Delta ho)^{1/2} \qquad \text{----------(10)}$$

$$C0=(2.\beta lm)^{-1/2} \qquad \text{----------(11)}$$

β ; $\beta 0(1-\lambda)/(\lambda^3.d)$
$\beta 0$; 2.2
lm; width of the permeable submerged mound
λ ; void ratio(=0.4)
d; diameter of stone

So relationship between head loss $\Delta h0$ and resistance in the permeable mound is as follows.

$$\Delta h0=1/\{2.g.(C0.hd.B)^2\}.Q0^2=R0.Q0^2 \qquad \text{----------(12)}$$

Head loss $\Delta h2$, $\Delta h3$ at the inlet and the outlet are calculated by eq.(13),(14).

$$\Delta h2=1/\{2.g.(C2.A)^2\}.Q2^2=R2.Q2^2 \qquad \text{----------(13)}$$

$$\Delta h3=R3.Q2^2 \qquad \text{----------(14)}$$

The relation ship between $\Delta h1$, $\Delta h2$, $\Delta h3$ is shown schematically fig.3. So in flow Q1 above the submerged mound is divided into effective inflow Q1 and return flow Q0.

$$Q1=Q2+Q0 \qquad \text{----------(15)}$$

$$\Delta h2+\Delta h3=(R2+R3).Q2^2=R0.Q0^2=R_{2+3,0}.Q1^2 \qquad \text{----------(16)}$$

Substituting eq.(16) for eq.(15), coupled resistance Coefficient R is derived as follows.

$$1/R_{2+3,0}^{1/2}=1/(R2+R3)^{1/2}+1/R0^{1/2} \qquad \text{----------(17)}$$

$$R_{2+3,0}^{1/2}=(R2+R3)^{1/2}.R0^{1/2}/\{(R2+R3)^{1/2}+R0^{1/2}\} \qquad \text{----------(18)}$$

So total resistant Coefficient R is expressed eq.(19)

$$R=R1+R_{2+3,0} \qquad \text{----------(19)}$$

$$Q1^2=\Delta h1/R \qquad \text{----------(20)}$$

Substituting eq.(19) for eq.(9), eq.(20) is derived.

$$\Delta h1=R1.Q1^2=(R1/R)\Delta h \qquad \text{----------(21)}$$

From eq.(6), eq.(22) is derived.

$$\Delta h2+\Delta h3=(R_{2+3,0}/R).\Delta h \qquad \text{----------(22)}$$

So seawater inflow can be calculated by eq.(23).

$$Q2=\{(R_{2+3,0}/R).\Delta h/(R2+R3)\}^{1/2} \qquad \text{----------(23)}$$

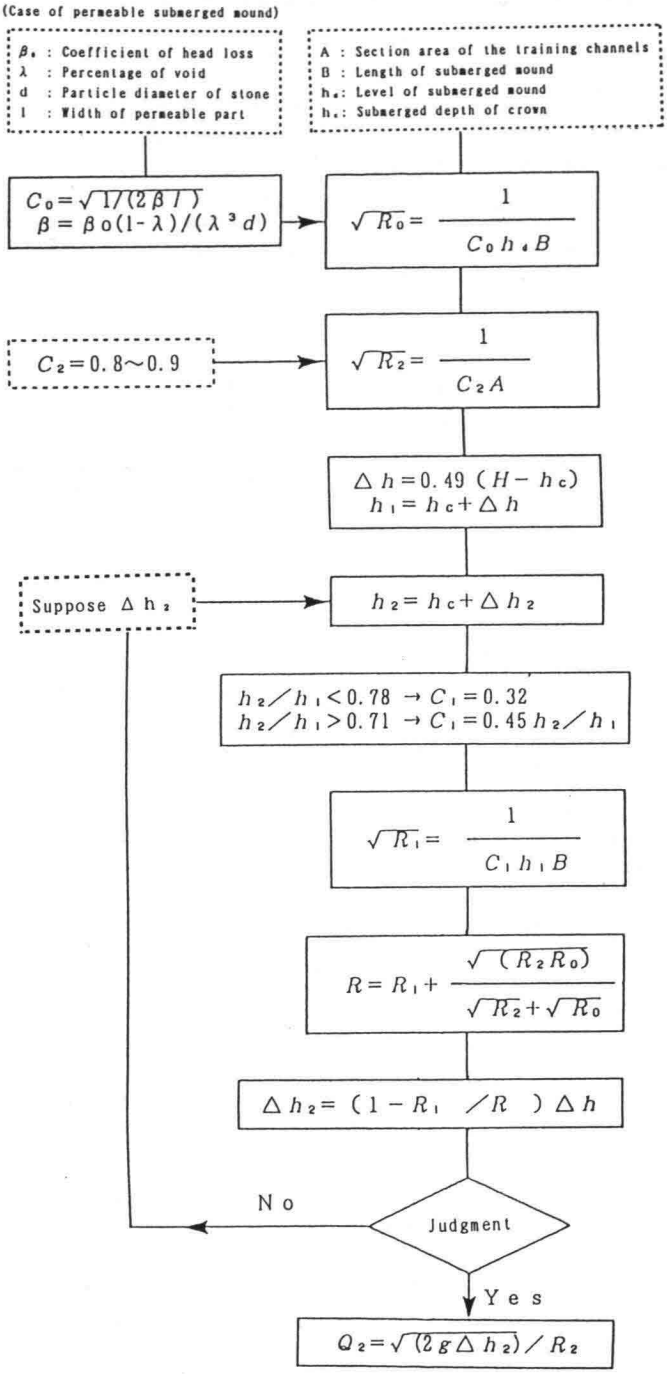

Fig.5 Flow-chart to calculate seawater inflow

Wave-setup at the seawater pool can be calculated by eq.(24).

$$\Delta h = 0.49.(H0' - hc)$$

$$\Delta h = 0 \quad H0' < 0.78.h \text{ or } hc < -H0' \qquad \text{----------(24)}$$

H0; equivalent deepwater wave height

Using these equations, seawater inflow can be calculated (shown fig.5). Fig.6 shows the comparison of calculated inflow and experimental one. From this figure, this method is sufficiently applicable.

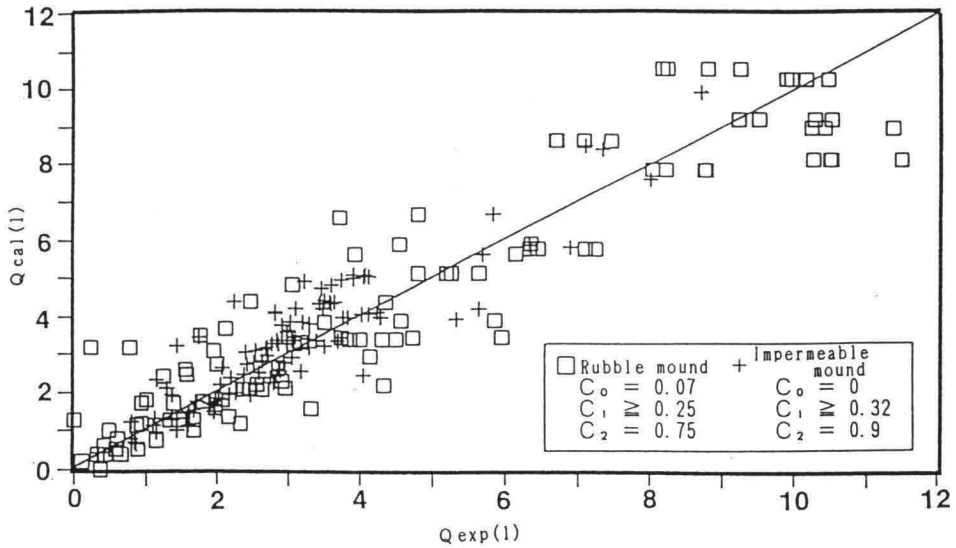

Fig.6 Comparison of inflow between in calculation and in experiment

In authors' experiments, regular waves are used as external forces. So it is necessary to convert irregular wave height to regular wave one. Relationship between regular wave and irregular one is as follows.

$$H0' = 0.66Hs \qquad \text{----------(25)}$$

Hs ; significant wave height

In case of wave not acting normal to WWSM, length of the submerged mound should be corrected to its length normal to wave direction.

3.4 TRANSMISSION COEFFICIENT

For ensuring seawater inflow at a wave height, there is some choices in designing the submerged mound and the training channel. For instance, one is

to design a short submerged mound and a large training channel, and the another is to design a long submerged mound and a small training channel. For designing WWSM, it is important to estimate transmitted waves. From authors' experiments, transmission Coefficient is about 0.15-0.3 (shown fig.7). Trans mission Coefficient is depend upon cross section of the inlet and depth of the inlet, height of the submerged mound, incident wave period and height. Trans mission Coefficient is calculated by eq.(26), (27). Eq.(27) is for WWSM having plural training channels.

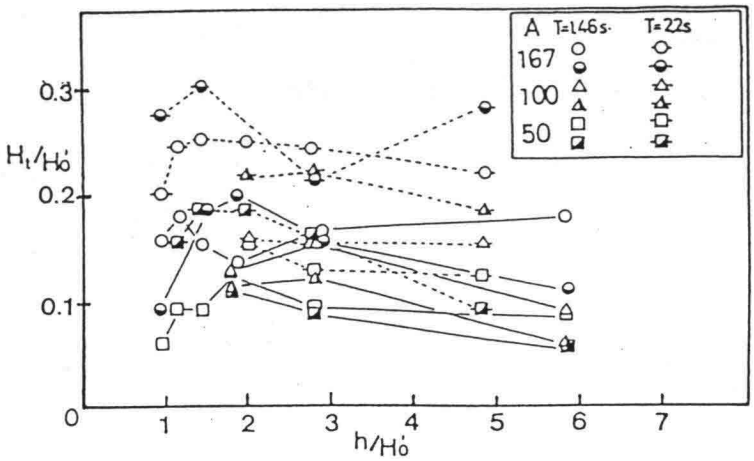

Fig.7 Wave transmission coefficient in WWSM

$$Ht=Kt.(b0/\pi r)^{1/2}.H \qquad \text{----------(26)}$$

$$Ht=Kt.(\Sigma b0/l)^{1/2}.H \qquad \text{----------(27)}$$

b0 ; Width of a training channels
l ; Length of a submerged mound
r ; Distance from the end of training channel
Kt ; Transmission Coefficient at the end of training channel(shown fig.7)

In case that the ratio of b0 and l is 0.1, averaged transmission Coefficient is less than 0.1. For fishing port, small transmitted waves is better. But transmitted waves are sometime useful to removed sediments such as sludge, silt and baits sunk.

4. LAYOUT PLANNING

4.1 POSITION OF THE SUBMERGED MOUND

Position of the submerged mound should be decided from the following points.

(1)Incident wave height is big enough to get required seawater inflow by the submerged mound when seawater quality becomes worst in the fishing port or the nursery culture ground.

(2)The submerged mound is normal to incident wave direction.

(3)Sediment transport is a little at the submerged mound.

(4)Depth at the submerged mound is larger than double the design wave height which is not for its stability but for its function.

(5)The sea bottom is stable.

4.2 SUPPLEMENTAL FACILITIES TO THE SUBMERGED MOUND

If incident waves is too big, velocity of seawater inflow will be too large, and transmitted wave will be too big. So countermeasures to control inflow and transmitted wave are necessary. One of them is a remote submerged mound in front of the main submerged mound for reducing only big waves.

If incident wave height is not enough big, it is necessary to plan following supplemental facilities in order to strengthen the function of the submerged mound.

(1)Jetties

Two jetties are in front of the submerged mound for concentrating incident waves. Their angle to wave direction is about 25 degree. But they are unsuitable in case that wave direction often changes. The amplification ratio by them can be calculated by eq.(28).

$$H/H'=(B'/B)^{1/2} \qquad \text{----------(28)}$$

H ; Wave height in front of the submerged mound
H'; Wave height in front of jetties
B'; Distance between front edges of jetties
B ; length of the submerged mound

(2) Submerged mound in shape of lens

This is in front of the main submerged mound for concentrating incident waves by using wave refraction. To amplify wave height to double, its length needs at least four times as long as the main submerged mound length.

4.3 INLETS

Outflow from the inlet diffuse at an angle α ($\tan\alpha=1/4$) to flow axis[10]. In the case of one inlet, velocity reduction along flow axis is not so large, and outflow reaches relatively in the distance. But circulation flow and dead water region is generated.

On the other hand, in the case of plural inlets, flow diffusion is large, and velocity reduction along flow axis is relatively large. From authors'experiments, scale of flow diffusion by two inlets ,of which distance is 10 times as long as the inlet width, is double the one by only one inlet.

So in case of planning plural inlets, it is necessary to estimate the extent of flow diffusion comparing with scale of the supposed sea area.

When stormy weather, nets of cages in the sea area are fluttered by strong current. This phenominone is inconvenient to cultured fishes in cages. In a fishing port, current speed at the quay wall, which is against the inlets, should be less than 1.0m/sec for fishing boat moored at this quay wall. Velocity of jet is calculated by eq.(29).[11]

$$Um/U0=2.5(X/b0)^{1/2} \qquad \text{----------(29)}$$

Um ; velocity at the supposed point
U0 ; velocity at an inlet
b0 ; width of an inlet
X ; distance from an inlet to the supposed point

If inflow velocity, or transmitted wave height exceed the limit value or a large amount of sand with inflow is brought through this facility, it is necessary to take countermeasures such as a gate.

4.4 OUTLETS

For a fishing port, an outlet of WWSM is just equal to fishing port entrance. But for a nursery culture ground or an aquaculture ground, layout of an outlet is very important to get enough seawater inflow effectively. Layout of an out let should be decided from considering the followings.

An outlet should not be against wave direction. If outflow velocity against wave direction is large, wave height will become large because of the interaction between outflow and wave, and wave breaking may cause wave-setup at the outlet. So sea level difference between the inlet and the outlet will be reduced and inflow from the inlet may be almost zero.

5. THE OUTLINE OF THE FIELD SURVEY AT YOKATA FISHING PORT

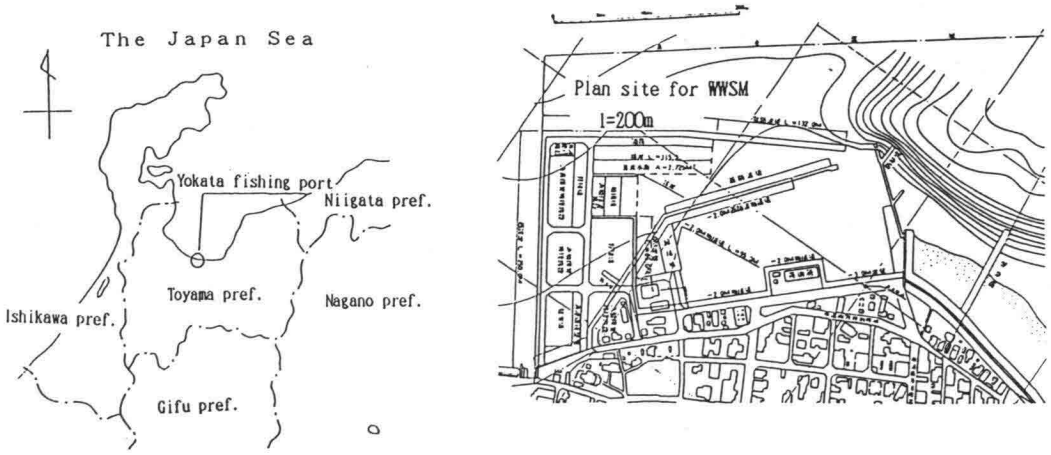

Fig.8 Position and plan of Yokata fishing port

Authors carried out the field survey on WWSM constructed in Yokata fishing port cooperating with the Toyama city office in 1991. Yokata fishing port is located in Toyama prefecture as shown fig.8. This fishing port is up to now under construction for its enlargement, and live fish stock in its new basin is planned. For this reason, WWSM was constructed with the main breakwater in 1990 (shown fig.9,10). Incident waves, sea level variations at the sea water pool, velocity in the training channel were measured from Dec. 4th to Dec. 22th in 1991.

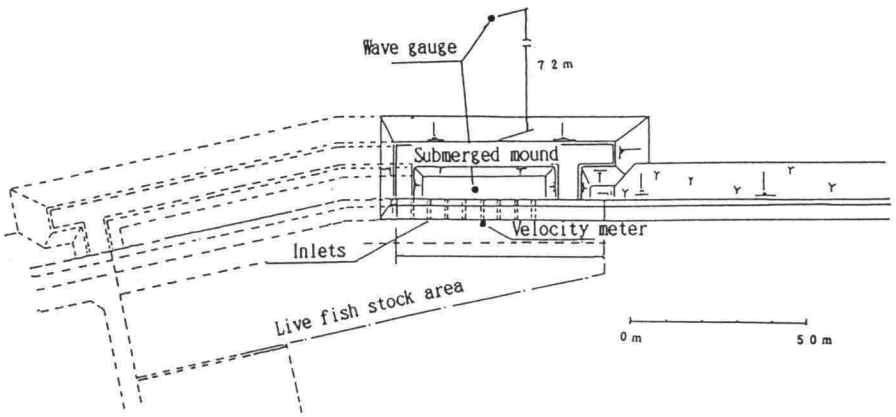

Fig.9 Plan of WWSM

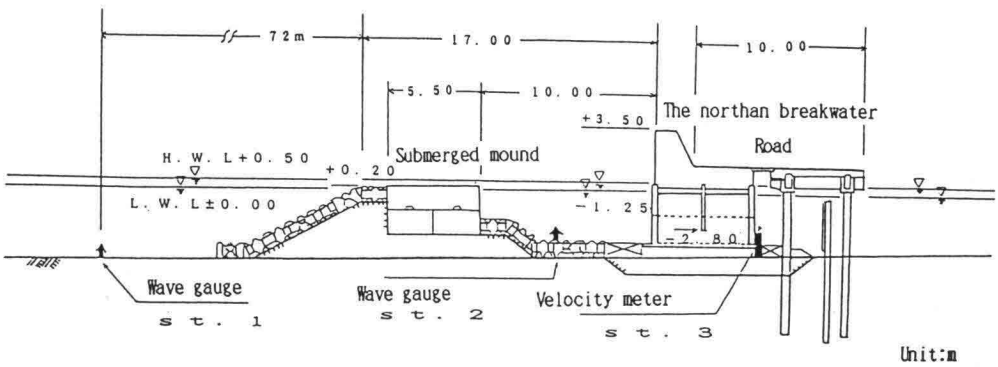

Fig.10 Cross section of WWSM

Fig.11 shows variations of the tide level, incident wave height (significant wave height) and mean inflow velocity. In this figure, the dashed line is the level of the submerged mound crown. Maximum incident wave height was 1.5m at 1:00 Dec. 19th and maximum velocity was 1.2m/sec at the same time.

From this figure, it is found that inflow velocity is closely related to incident wave height. But, although incident wave height was nearly constant 0.6m from 18:00 Dec. 19th to 13:00 Dec. 20th, inflow velocity changed 0-0.6m/sec. Comparing the tide level with the level of the submerged mound crown in this period, it is clear that inflow velocity became large at the time when the tide level was nearly equal to the level of the submerged mound crown. On the other hand, inflow velocity reduction was great when the tide level was below the submerged mound crown. So inflow velocity is also depend upon the tide level and the level of the submerged mound crown.

Fig.12 shows the comparison between measured velocity and calculated one by using the above mentioned method. Measured velocity almost agree with calcu lated one. So authors' method is enough applicable to prototype.

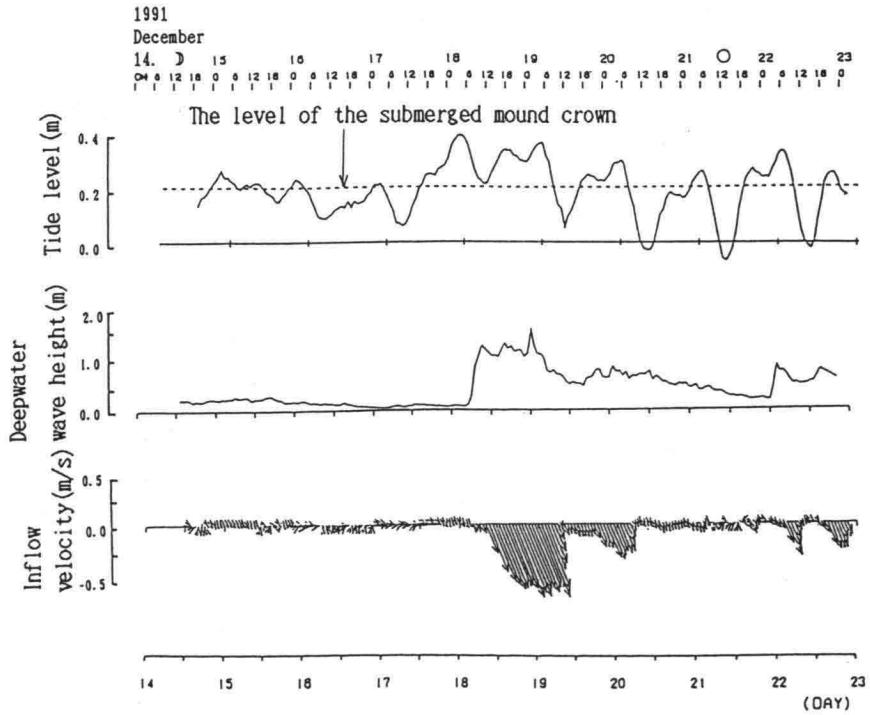

Fig.11 Variations of tide level, wave height and inflow velocity

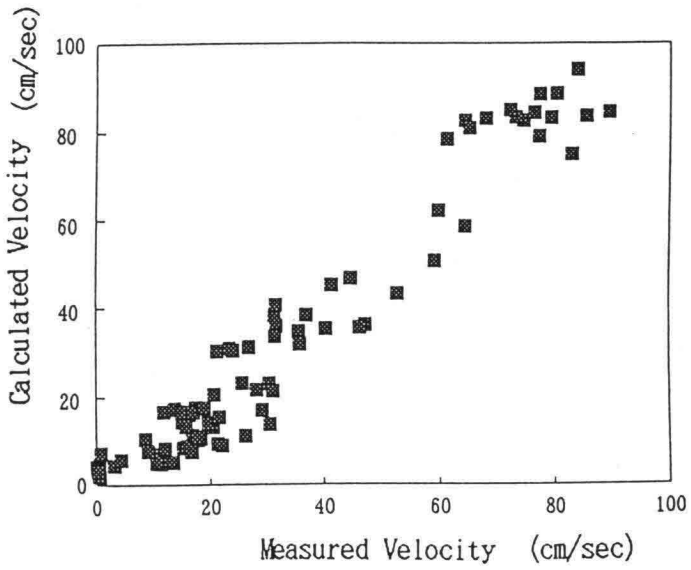

Fig.12 Comparison between measured velocity and calculated one

6.SUMMARY

Authors proposed the method of planning and designing WWSM, such as its scale for requested seawater inflow, layout of submerged mound, training channel and outlet,and applicability to purifying seawater in a fishing port. Moreover WWSM may have applicability to improving seawater quality in the bay which is much larger than a fishing port.

Hereafter, authors will investigate countermeasures in case that tide amplitude is large, because the performance of WWSM is sensitive to the tide level.

REFERENCES

1) Yamamoto,M., Nakaizumi,M. and Moriguchi,A.: Development of the breakwater with submerged mound for sea water interchange, Bulletin of national research institute of fisheries engineering, No.13, March 1992.
2) Proceedings of the 1992 conference for promoting fisheries engineering re search, pp.11-17, 1992.
3) National coastal fishery development association: Design manual of facilities for improving coastal fishing ground, pp.248-252, 1993.
4) National coastal fishery development association: Design manual of facilities for improving coastal fishing ground, pp.253-255, 1993.
5) Fujiwara,M., Kubo,S. and Takeuchi,T.: Development of numerical model for prediction of water quality in a nursery aqua culture pond constructed at sandy coast,Fisheries engineering Vol.27 No.1,March. 1991
6) Japan society of civil engineers: Manual of hydraulic formulae,1985.
7) Kondo,Y. and Takeda,H.: Wave absorbing structures, Morikita-shuppan,Tokyo,1983

8) Yamamoto,M., Manabe,M. and Nakaizumi,M.: Development of the break water with remote submerged rubble mound for the purpose of interchanging sea water (1)-Investigation on its function and the form of the submerged rubble mound-, Technical report of national research institute of fisheries engineering, aqua culture and fishing port engineering, No.10, March 1988.
9) Same as 8)
10) Same as 1)
11) Manabe,M., Nakaizumi,M. and Yamamoto,M.: Development of the break water with remote submerged rubble mound for the purpose of interchanging sea water(2), Proceedings of coastal engineering, Vol.35, pp.632-636, 1988.
12) Yamamoto,M.: Experimental study on wave and water level on a reef, Techni cal report of national research institute of fisheries engineering, aqua cul ture and fishing port engineering, No.8, March 1987.
13) Nakayama,A. and Yamamoto,M.: Wave deformation behind submerged -Influence for fairway-, Proceedings of 29th conference of research for construction of fishing port, pp.1-17, 1984
14) Same as 8)
15) Editorial committee of reference manual for construction of coastal protection works: Reference manual for construction of coastal protection works and its explanation, National coastal association, (Tokyo), pp.59, 1987.
16) Nakaizumi,M., Yamamoto,M. and Manabe,M: An experimental study on wave force against break water with remote submerged mound, Proceedings of coastal engineering, Vol.35, pp.632-636, 1988.
17) Yamamoto,M.: Deformation of wave around a reef joined to slope and induced phenomenon, Technical report of national research institute of fisheries en gineering, aqua culture and fishing port engineering, No.12, March 1990.
18) Same as 8)
19) National coastal fishery development association: Design manual of facilities for improving coastal fishing ground, pp.156, 1993.

HYDRO-PORT'94
International Conference on Hydro-Technical
Engineering for Port and Harbor Construction
October 19 - 21, 1994, Yokosuka, Japan

Water Quality in Penang Harbor

P.M. Sivalingam
S.V. Charles

School of Biological Sciences
The University of Sciences Malaysia
Minden, 11800 Penang

ABSTRACT

Penang Harbor, located at the northern most enterance point of the Malacca Straits is historically one of the oldest and largest port in Western Peninsular Malaysia. The paper will discuss to what extent the port is polluted due to its activities hand-in-hand with other impacts and inputs, arising as a consequence of human activities in the vicinity, in conjunction with its hydrography. Heavy metals, PCBs, pesticides as well as hydrocarbon contamination will also be considered in related areas. Microbial contamination in oysters, the green-lipped mussel, etc., in relation to age dependence will also be pondered.

Words: Water Quality, Penang Harbor, Biological Impact, Pollution.

1. INTRODUCTION

Penang harbor, situated within the Northern and Southern Channels accommodates the pressure of been the second most busiest international waterways in the world - the Malacca Straits. The Straits of ca. 1,000. Km in length is plyed by ca. 3,000 vessels daily out of which a majority of them call in Penang Harbor. The Penang Harbor, is so contained whereby it is engulfed by the Swettenham Pier, Butterworth's Container Wharf, Prai Industrial Estate, Prai Electric Plant, The Penang Free Trade Zone, etc., inclusive of vast inputs from municiple solid and liquid discharges together with river inflows from the Sungai Pinang, Sungai Prai, Sungai Juru and Sungai Jelawi.

As a forerunner, the volume of vessels arriving at the Penang Harbour in 1992 were as follows: container carriers; 715 (GRT - 4,537,902) lash; 6 (GRT - 115,691), roro; 77 (GRT - 265,433), naval vessels; 90 (GRT - 379,190), passenger vessels; 81 (GRT - 456,825) oil tankers; 585 (GRT-2,329,391), other tankers; 268 (GRT-1,515,791), dry bulk carriers; 333 (GRT-3,070,476), others; 2,442 (GRT-5,240,662) and emergency vessels (=75 GRT); 1,669 (GRT-227,299). Hence, the total tonnage handled by the port in 1992 amounted to 18,138,660 GRT. In conjunction with this, the Penang Ferry System carried 7,412,917 passengers, 185,974 bycycles, 2,597,107 motorcycles, 983,470 motorcars, 186,057 lorries, 154 goods items etc., and issuance of tickets amounting to 19,670 for the same year using 6 new and 2 old ferries. The ferry systems by itself had an income of ca. RM 12,434,903/- in 1992. Based on the above, it is evident that the port is heavily taxed with traffic.

2. HYDROGRAPHY OF PENANG HARBOR

The port of Penang between the Ferry Terminal and the island is ca. 1.7 nautical miles. The depth of the port varies from 6 meters to 28 meters. The Northern Channel is located between longitude 100^{0} 21'E, latitude 5^{0} 25.2 'N. In this connection, the Southern Channel is between longitude 100^{0} 20'E, latitude 5^{0} 5.5'N and longitude 100^{0} 11'E latitude 5^{0} 5.5'N and longitude 100^{0} 11'E latitude 5^{0} 16'N. This topographical layout is as indicated in Figure 1.

The diurnal tidal and seasonal salinity variations in the straits of Penang are as indicated in Figures 2 and 3.

Since large amounts of sediments are brought into the Straits by the Kuala Muda in the tune of 500 tons/yr, 50% incident light is absorbed in the first meter resulting in very little penetration at 9 meters depth (Figure 4).

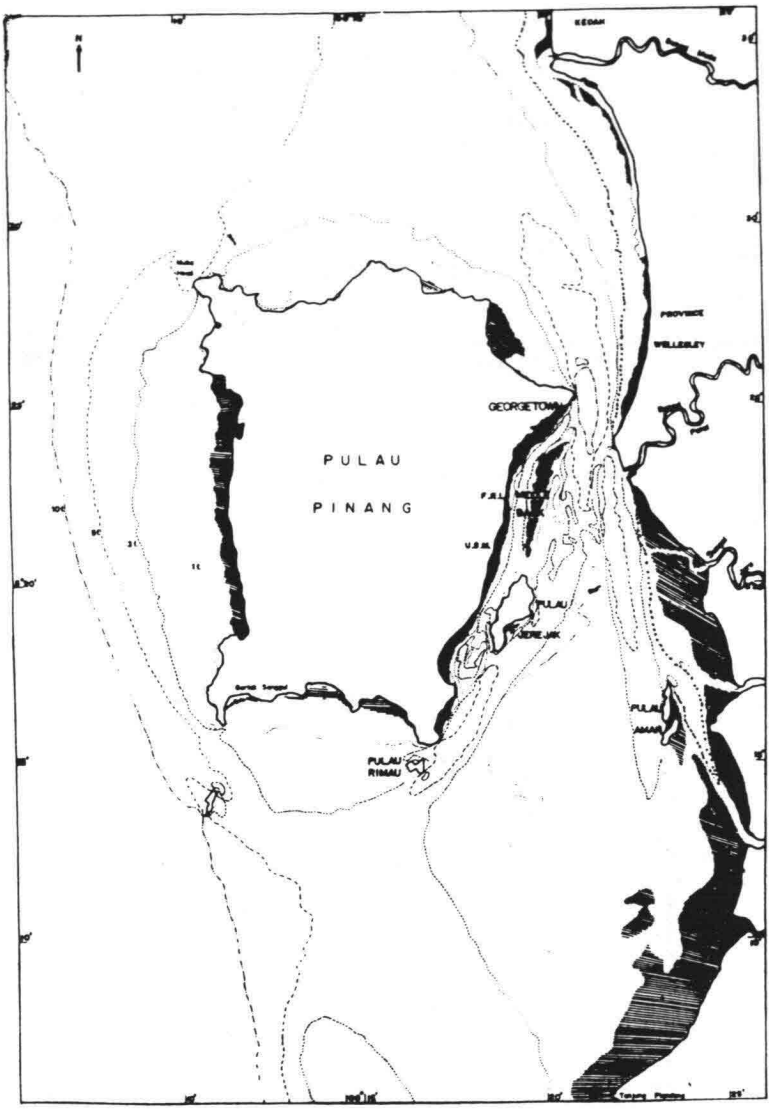

Figure 1. Physical features of the Penang Harbor between the Northern and Southern Channels

The Straits of Penang harbour are relatively shallow covered extensively with mudflats stretching North to South. The Great Kra Flat in the Southern Straits is formed by silt deposition contributed by the Krian, Muda and Tengah rivers of the mainland. Most parts of the Straits are shallow under 3 fathoms (6 m) at Spring low tide. The North and South Channels are between 4 - 5 fathoms (8 - 10 m) whilst near the deepest part of the Straits near the Ferry Terminal 11 - 14 fathoms (22 - 28 m).

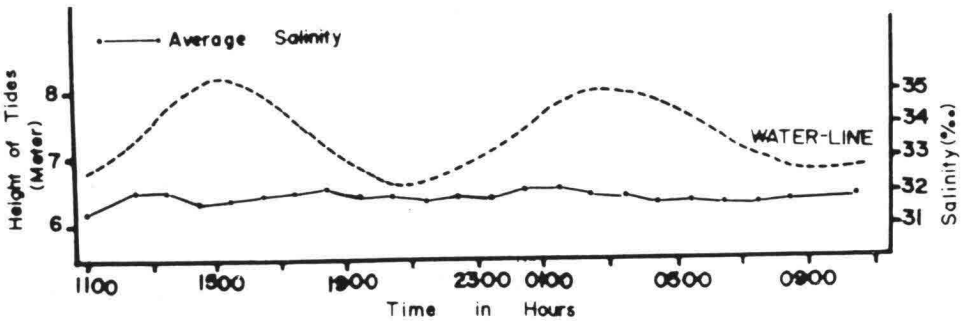

Figure 2. Diurnal tidal variation of salinity in Penang Harbor

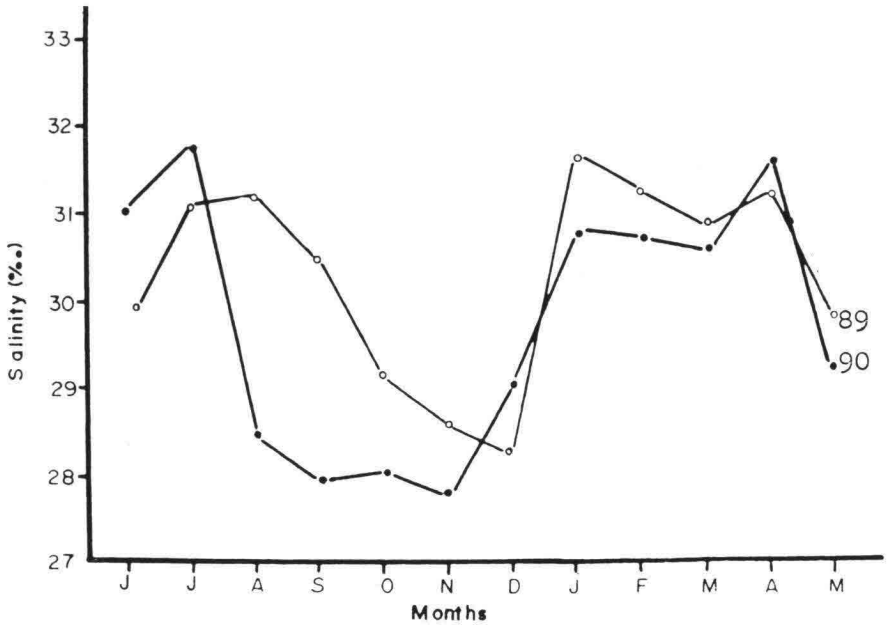

Figure 3. Seasonal variations in salinity in the Straits of Penang

Based on figures 2 & 3, it is obvious that the harbour experiences a daily diurnal tidal system which is normal to this region and is not one of any pecularity. In addition, the salinities are lowest between the months of April to December probably due to the fact in large inputs of fresh water from adjacent rivers as a consequence of the rainy seasons prevailing at this time of the year.

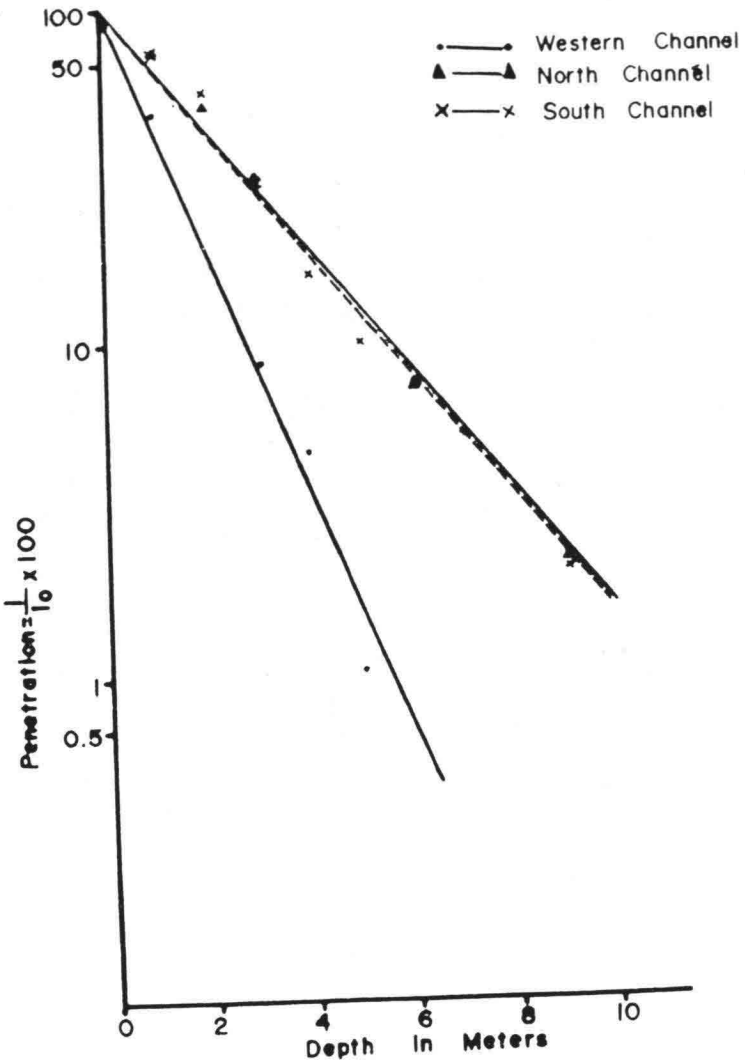

Figure 4. Actinic light penetration in the Straits of Penang.

Figure 4 illustrates that at least 50% of the incident light is absorbed in the first 1 meter, while in the Western Channel > 90% at a depth of 3 meters. In comparison, this is ca. 80% in the Southern Channel. Take note, too, that at 9 meters depth relatively little light is detected. Hence, the waters in the Western Channel are much turbid than that of both the North and South Channels.

On a similar basis the tidal current characteristics at the Western Channel of the Straits over a complete tidal cycle are as illustrated below.

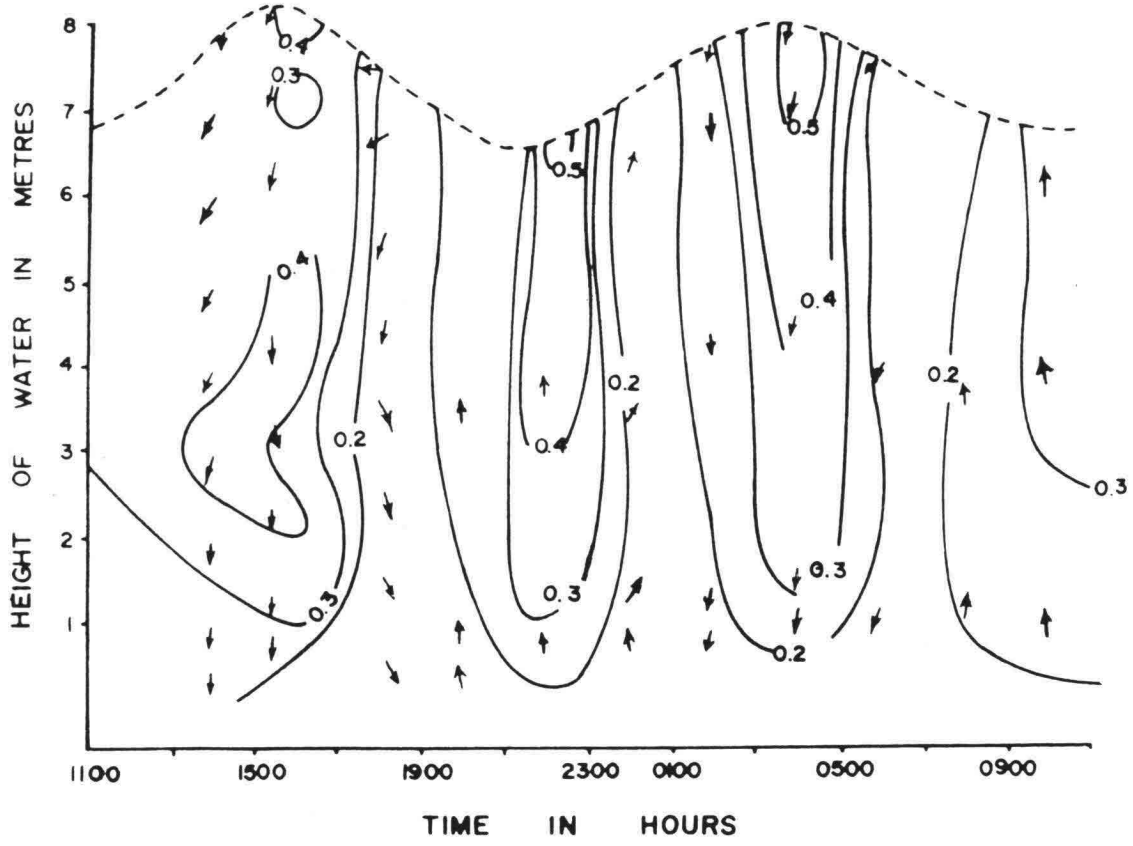

Figure 5. Tidal characteristics of the Western Channel

It is apparent that the Straits of Penang experiences a semi-diurnal tidal pattern with a Mean High Water Spring (MHWS) at 2.5 m, Mean High Water Neap (MHWN) at 1.8 m, Mean Low Water Spring (MLWS) at 0.6 m and Mean Low Water Neap (MLWN) at 2.3 m. Water flows into the Straits from the North at rising tide and recedes in the opposite direction. In the Western channel, where it is rather shallow at the centre, i.e. 6 - 10 m, there is no counter current. The water mass moves in one direction generated by tidal current and changes direction twice a day in a tidal cycle.

The isothermal distribution in the Straits of Penang are as indicated below, while the Port area is between 30 - 31.5^{o}C.

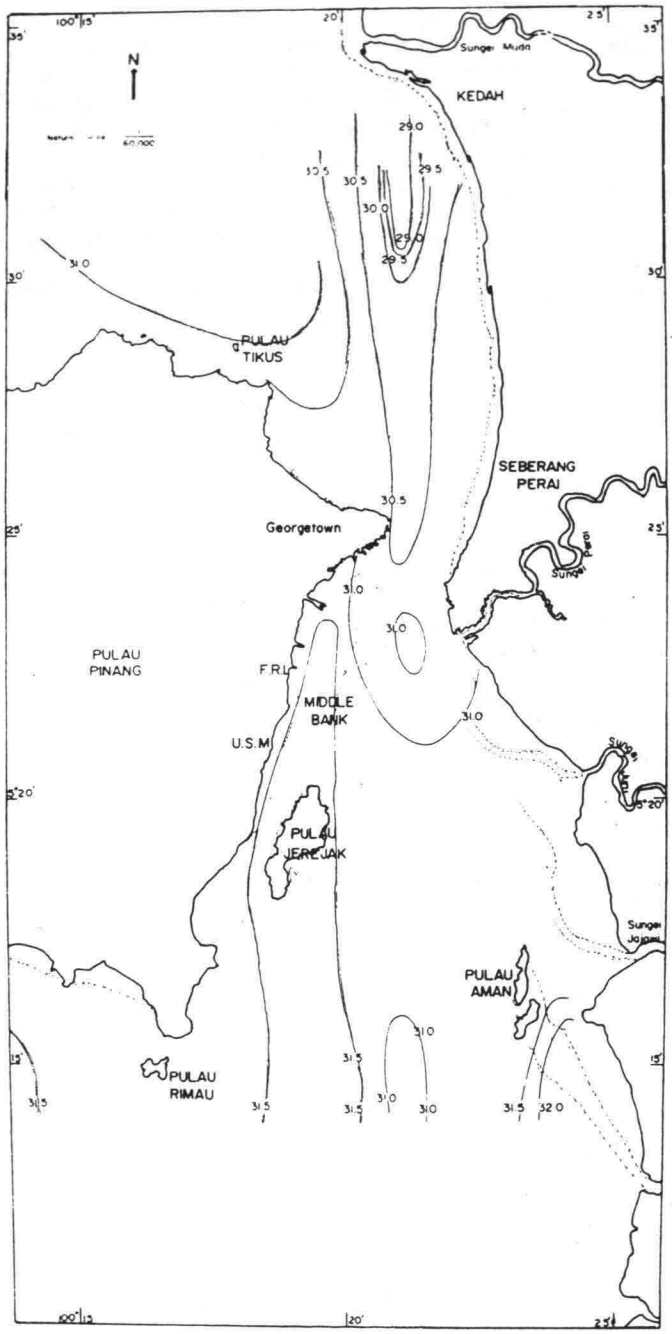

Figure 6. Isothermal distribution in the Straits of Penang.

No distinct diurnal variation in water temperature of the Penang Channels was observed though a slight drop of 0.5^{o}C to 1.0^{o}C was detected for surface waters during the night and early morning hours. The observable maximum range of water temperature within a day is 1.4^{o}C at the surface while below 1^{o}C at bottom waters. Nevertheless, throughout the whole year the maximum and minimum water temperatures recorded in the Straits of Penang was 32.1^{o}C and 27^{o}C, respectively, deriving an annual range of 5.1^{o}C. The annual mean water temperature is 29.5^{o}C. There is evidently a significant seasonal variation in water temperature in the Straits of Penang demonstrating two periods of high temperatures in the months of June and January /February. On the contrary, a slight drop of mean temperature is recorded during April and a dramatic decline noticed at the end of the year, i.e. November/December months when the temperature drops to below 28^{o}C. This seasonal trend is rather consistent.

The vertical stratification of temperature of the water mass in the harbour is not detected. The fluctuation in water temperature between the surface and bottom is within the region of 1.1^{o}C.

On the whole, the distribution variations of isotherms of surface waters at the Straits of Penang overall is small though interestingly a slight lower temperature is recorded at the North Channel, i.e. 29^{o}C - 30.5^{o}C, while a slightly higher temperature in the vicinity of Penang Harbour and the South Channel, i.e. 30.5^{o}C - 31.5^{o}C.

On a similar basis Figure 7 illustrates the DO (cc/l) distribution in the Straits of Penang.

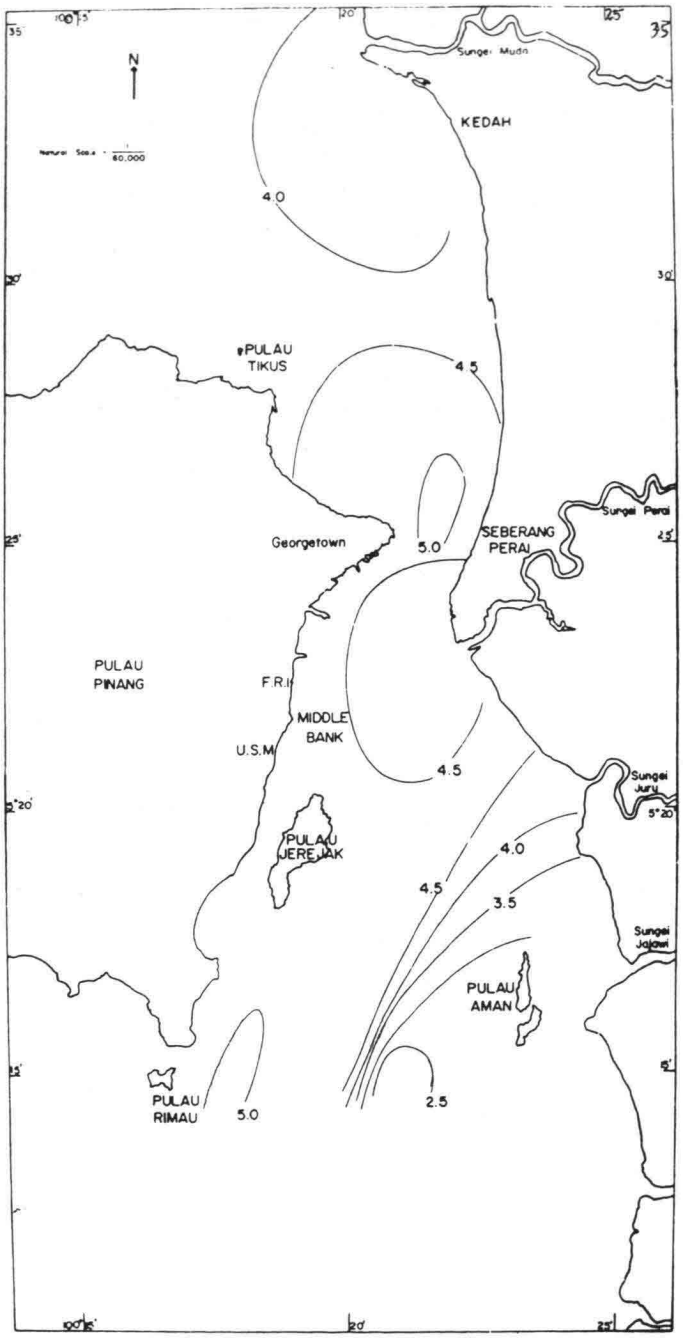

Figure 7. DO distribution in the Straits of Penang.

The dissolved oxygen content in the Straits of Penang is usually well above 3 cc/L, which is about 58% its saturation. In most cases, the dissolved oxygen content fluctuates within the region of 3 cc/L and 5cc/L, i.e. ranging from 58% to 100% saturation.

Regarding surface dissolved oxygen content in the Western Channel, it fluctuates in the region of 20% between the highest and lowest values. The oxygen content is higher during daylight as compared to darkness as a consequence of photosynthetic processes.

The mean monthly surface dissolved oxygen content in the Straits is well above 58% saturation while in the Western Channel it varies from 3,87cc/L to 5.84 cc/L. Further, it demonstrates a seasonal trend, being high in the months of May/June and hence decreasing slightly to 3.5 - 4.0 cc/L in the months of July/August. The dissolved oxygen content increases again after September and reaches peak values of 5 - 6 cc/L in November/December while dropping again to 3.8 - 4.0 cc/L in March/April.

In general, the horizontal distribution of surface dissolved oxygen content in the Straits of Penang, especially in the North Channel and the harbour limits are fairly uniform, i.e. in the region of 4 - 4.5 cc/L. It is interesting to note here that the dissolved oxygen content in the Great Kra Mudflat is slightly lower ranging between 2.5 cc/L to 3.5 cc/L. However, in the South Channel proper near Pulau Rimau, the dissolved oxygen content is much higher, i.e. 5 cc/L.

Maximum B.O.D. value in the Straits of Penang is 4.36 $cc O_2/L$, near the Ocean Sewage Outfall, while the lowest is 0.18 $cc O_2/L$ at the North Channel. The average B.O.D. value being 1.84 cc O_2/L. It is noted that the B.O.D. value is rather high in the Penang Harbour between latitudes 5^0 20′ and 5^0 25′, along the eastern end of the Great Kra Mudflat and river mouths. This is relatively lower in both the North and South Channels proper.

Taking into consideration of the large phosphate (PO4; 2.37 mg-at-P/L) and possibly high NO_3 (12.39 ppm) input from the sewage outfall at Jelutong, Figures 8 & 9 demonstrate the phytopigment (highest; 25-50 mg/m^3) and zooplankton (0.28 - 1.2 g/m^3) distribution patterns in the Straits of Penang, respectively.

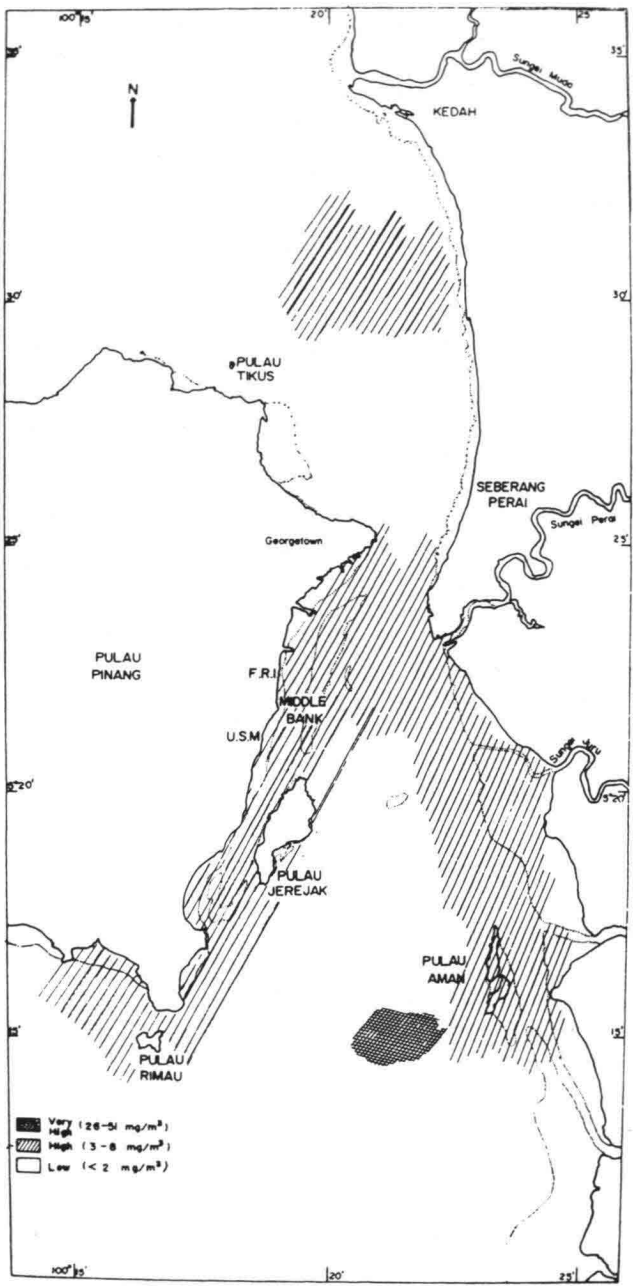

Figure 8: Distribution patterns of Chlorophyll -a in the Straits of Penang.

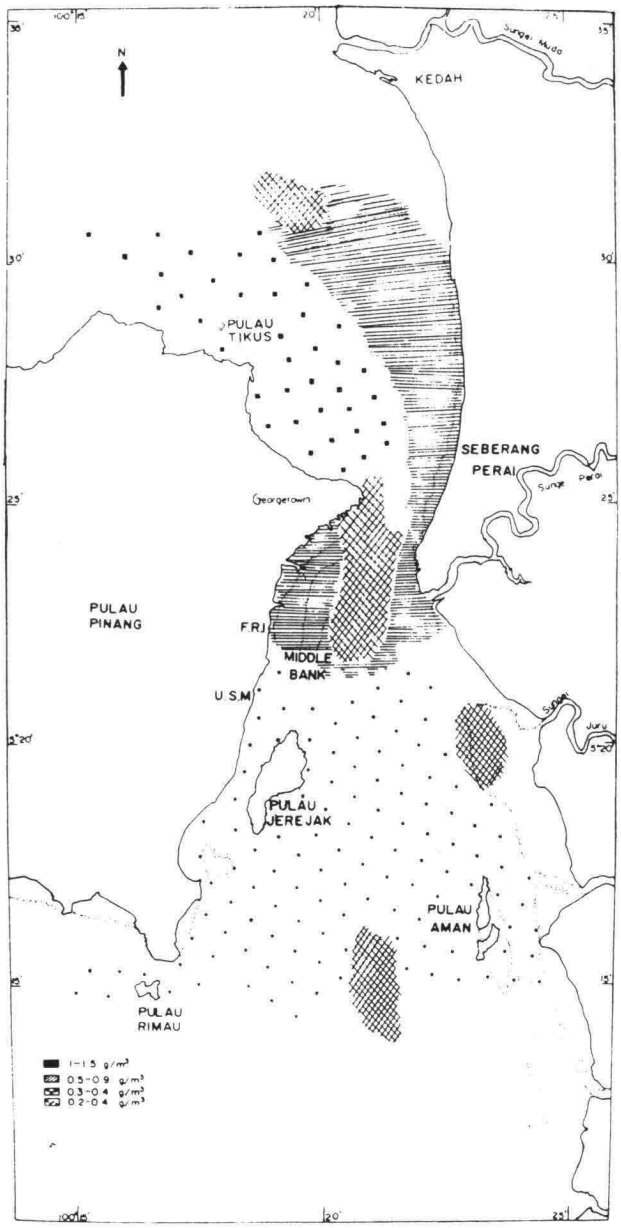

Figure 9: Distribution patterns of zooplankton biomass in the Straits of Penang

High concentrations of Chlorophyll-a has beeen recorded along the Straits coastline, with a value usually above 2 mg/m^3. The water columns between the Ferry Terminals, Middle Bank and the Prai River mouth are high in Chlorophyll-a content in the region of 3.85 - 7.82 mg/m^3. This enriched phytoplankton characteristic extends further along the coast of Province Wellesley spreading over the adjacent mudflats where the highest concentrations range between 25 - 50 mg/m^3. In the North Channel the average is lower than that of the South Channel. However, lower concentrations are recorded for deeper parts of the Straits. Disregarding nanoplankton, the bulk of the phytoplankton from the Straits of Penang consist of diatoms, dinoflagellates and blue-green algae. Diatoms are by far the largest group, consisting of 49 spesies belonging to 24 genera. Additionally, 7 genera and 15 species of dinoflagellates and 2 genera of blue-green algae are detectable in the straits.

The average standing crop of zooplankton in the Straits is in the region of 0.64 g/m^3. Its biomass varies from 0.28 g/m^3 - 1.20 g/m^3 by net weight and 0.31 ml/m^3 - 4.59 ml/m^3 by volume. High standing crop is recorded between Penang Harbour and the Middle Bank, Juru River mouth, Great Kra Mudflat southwest of Pulau Awam and along the Northern beaches of Province Wellesley. A high standing crop is also recognizable south of the Muda River mouth. On the whole, the zooplankton standing crop is higher in the North Channel as compared to the South Channel. Over 80% of the zooplankton population belongs to the order of Crustacea, which constitutes the most important group of planktonic forms in the Straits environment.

3. HYDROCARBON CONTAMINATION IN THE STRAITS OF PENANG

Hydrocarbon content in the harbor (= Glugor Naval Base) ranges between 30 - 50 ug/l as compared to that in Teluk Bahang; 10-80 ug/l and Teluk Kumbar; 70 - 120 ug/l. These values in comparison to the East Coast are fairly low:- Bachok; 90 ug/l, Dungun; 70-80 ug/l, Kota Baru; 110 ug/l, Kuala Besut; 40 - 80 ug/l, Kuala Trengganu; 50-70 ug/l, Marang; 70-130 ug/l, Rantau Abang; 30-50 ug/l and Tumpat; 50-70 ug/l.

4. MICROBIAL CONTAMINATION IN THE STRAITS OF PENANG

While most adjoining rivers of the Straits of Penang funnel lots of microbial flora into it besides other sources, there is still prevalent of one culprit, which is the 40 year old Jelutong Ocean Outfall-constructed during the colonial days - flowing into the Western Channel bringing into the waters of the harbour ca. 60% of Georgetowns untreated raw sewage. The biochemical characteristics of this sewer is as indicated in Table 1.

Table 1: Biochemical characteristics of raw sewage discharged at the Jelutong Ocean Outfall.

Parameters	Values
Moisture Content	99.95%
Org. Matter	0.04%
Inorg. Matter	0.01%
pH	7.05
Daily Disch. Vol.	16.75×10^6 Gal.
BOD / Day	6.3×10^9 ppm.
COD / Day	1.1×10^2 ppm.
Nitrate	12.39 ppm.
NH_3- N	8.01 ppm.
Total - P	2.32 ppm.

The coliform, *E. coli*, total aerobic and total spore formers counts (/100ml) of the dischare are, 4.9×10^7, 1.6×10^7, 1.3×10^8 and 2.3×10^3, respectively. Further, it harboured in 250 ml ca. 2,375 eggs of *Ascarus lumbricoides*, 308 eggs of *Trichurus trichura*, 108 eggs of hookworms and 50 eggs of *Toxocora canis*. The precise bacterial composition of the discharge (log MPN/100 ml) itself is: -*E. coli*; 10.1 $\pm$ 0.8, *Klebsiella* sp.; 8.6 $\pm$ 0.4, *Shigella dysentriae*; 6.5 $\pm$ 0.8, *Salmonella paratyphii* A; 7.3 $\pm$ 0.7, *Vibrio parahaemolyticus*; 8.1 $\pm$ 0.2, *Vibrio alginolyticus*; 8.5 $\pm$ 0.4, *Vibrio vulnificus*; 6.2 $\pm$ 0.9, *Vibrio cholerae*; 5.2 $\pm$ 0.3 and *Flavobacterium* sp.; 7.8 $\pm$ 0.2. As an input of this microbial flora the composition of them in adjacent waters as compared to a clean area is indicated in Figure 10.

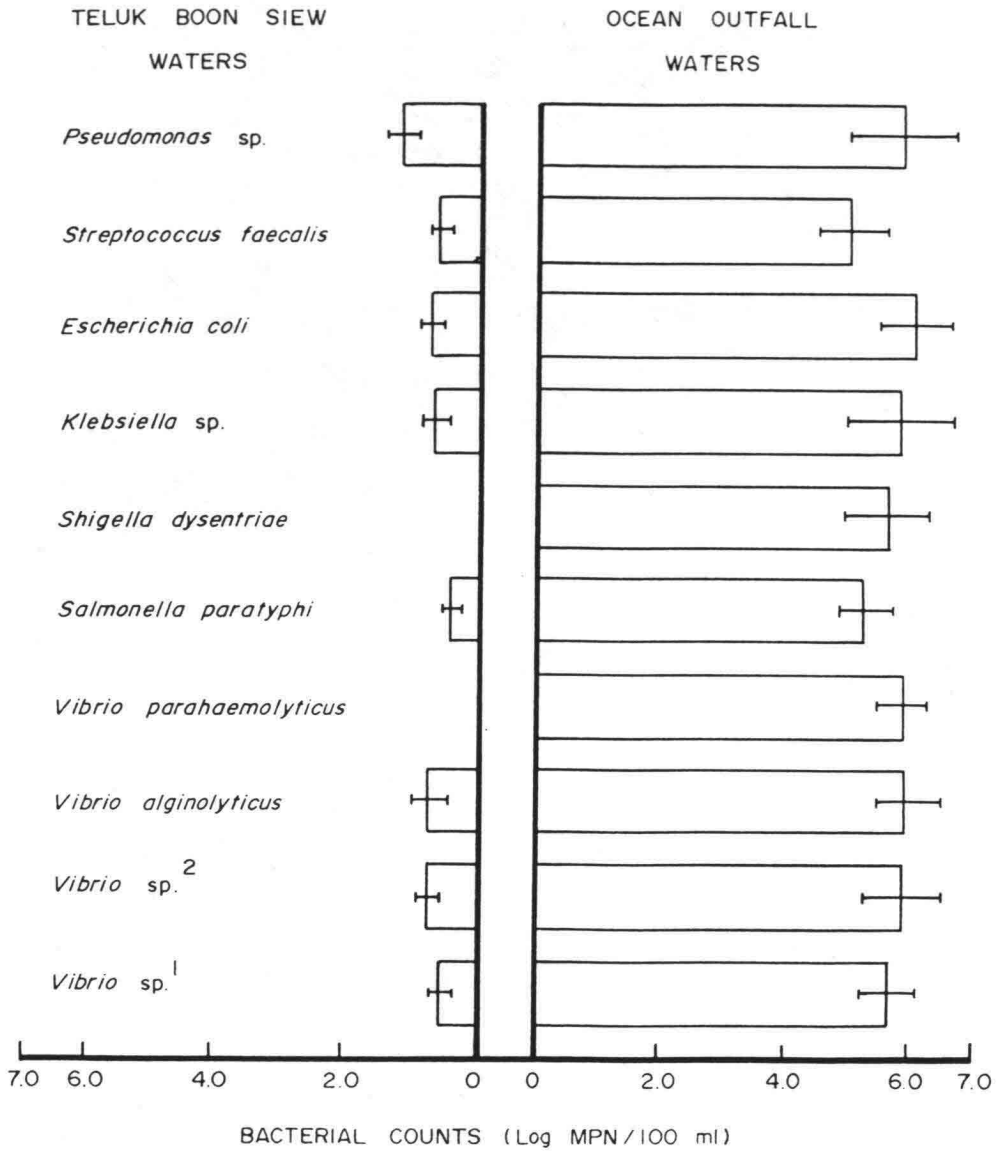

Figure 10: Microbial composition of coastal waters adjacent to the Ocean Outfall

As a consequence of this it has also been noted that the *E. coli* counts in the port ranged between 4.1×10^4 - 2.3×10^5 counts /100 ml while coliforms 1.5×10^5 - 7.1×10^5 (Figure 11).

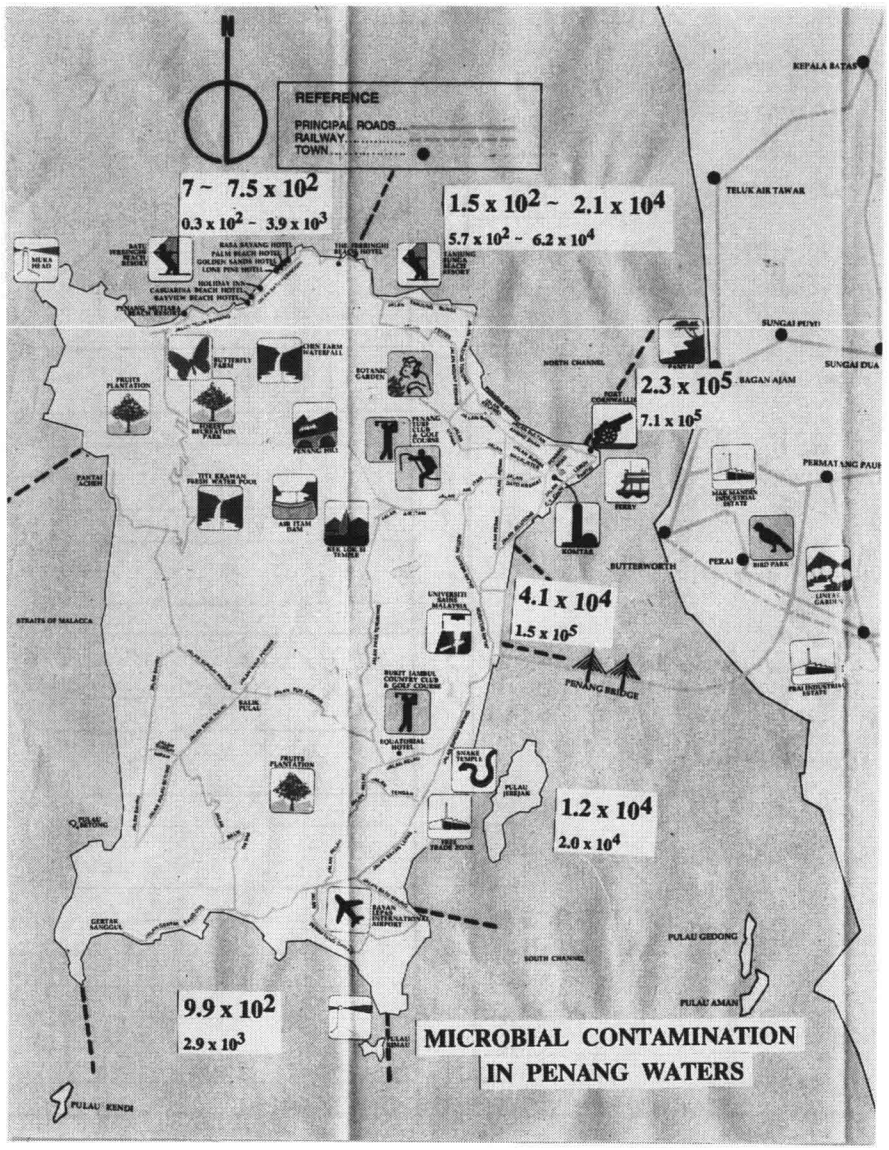

Figure 11. Comparative microbial contamination of waters in the Port to those around the island.

The impact of these microbial contaminants on oyster spat settlement are illustrated in Figure 12. Here it is noticeable that the oyster spat settlement at the Port is only 900 as compared to that in the clean shores of Muka Head where the number is 3,300.

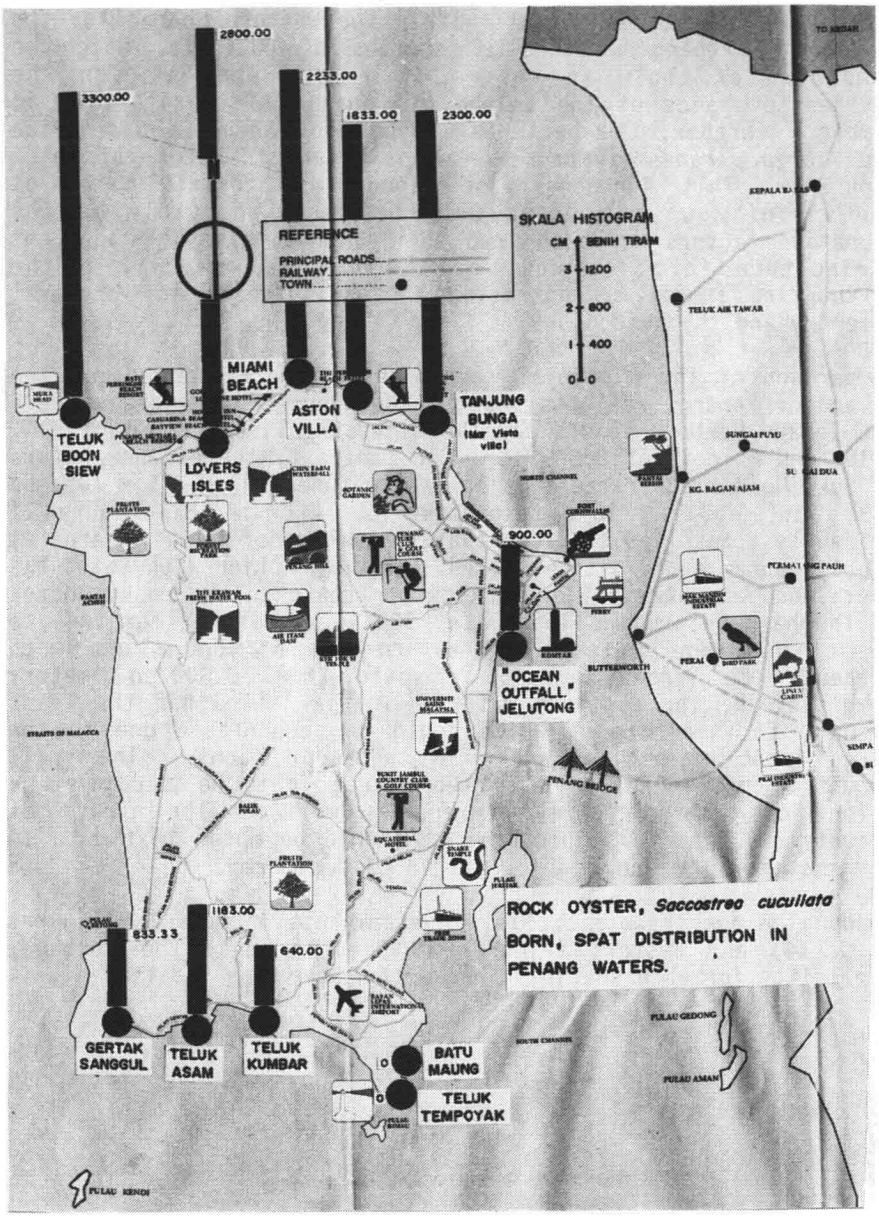

Figure 12: Oyster spat settlement in relation to microbial contamination.

As illustrated in Figure 10 it is obvious that the waters in the vicinity of the Ocean Outfall within the Western Channel of the Straits of Penang harbours 10 species of bacteria, which on comparion of those in waters of Teluk Boon Siew on the northeastern side of the Island of Penang is several folds in number. Further, the bacterial species of *Shigella dysentriae* and *Vibrio parahaemolyticus* are not existent in waters of Teluk Boon Siew. This high density of pathogenic bacteria in waters of the vicinity of the Ocean Outfall could posssibly be the causative factors for both "red boil" fish-disease in adjacent mariculture farms as well as the human community in the surrounding shores demonstrating a high intensity of cholera, dysentry and thyphoid cases.

Comparison of the microbial contamination in waters around the Island of Penang, reflects that the Northern Channel areas where the Penang Harbour exists has the highest coliform count of 7.1. x 10^5 and *E. coli* of 2.3 x 10^5. In contrast, the cleaner waters of Muka Head illustrated figures in the tune of 7 - 7.5 x 10^2 and 0.3 x 10^2 - 3.9 x 10^3, respectively. All in all, Figure 11 evidently transpires the fact that the waters of the Port area is highly contaminated with microbes. In conjunction with this, the prevalence and survival of rock oyster spats in the rocky shores of the harbour are the least i.e. 900/sq. meter, as compared to the clean waters in the northeastern side of the island which harbours the largest amount of spats, i.e. 3,300/sq. meter. Nevertheless, the southern waters of the Island had the least amount of oyster spats, which could be accountable due to the large input of piggery muck from adjacent farms. The small amount of oyster spats in the Port area could be a cumulative effect of both microbial numbers as well as the impact of tributyltin. At this juncture, it should be noted that data on the content of tributyltin is yet to be decifered.

Pending on age these microbial contaminants in mussels (Figures 13 & 14) and oysters (Figures 15 & 16) convey the message, explicitly for each species along with harvesting locality.

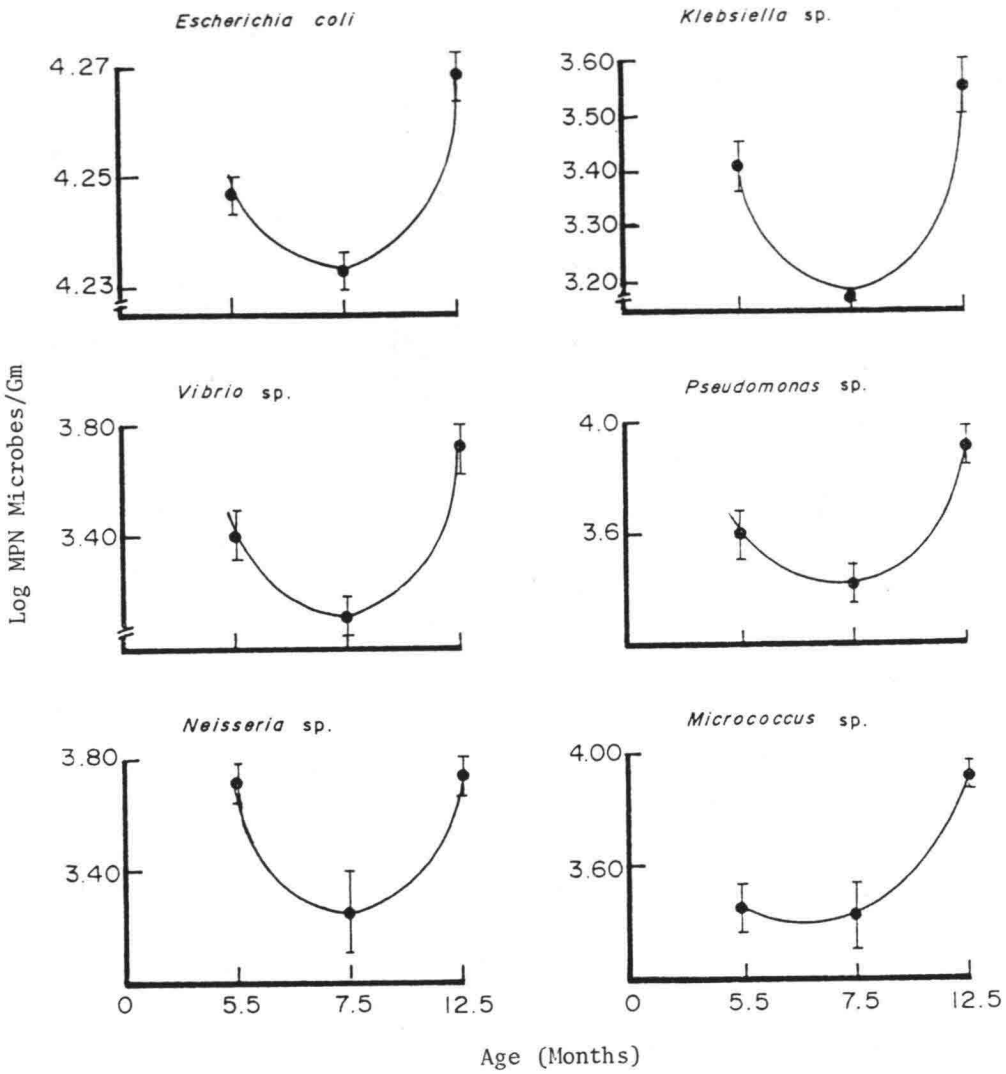

Figure 13: Variation in microbial flora in the green-lipped mussel, *Perna viridis* Linnaeus, from the Port area.

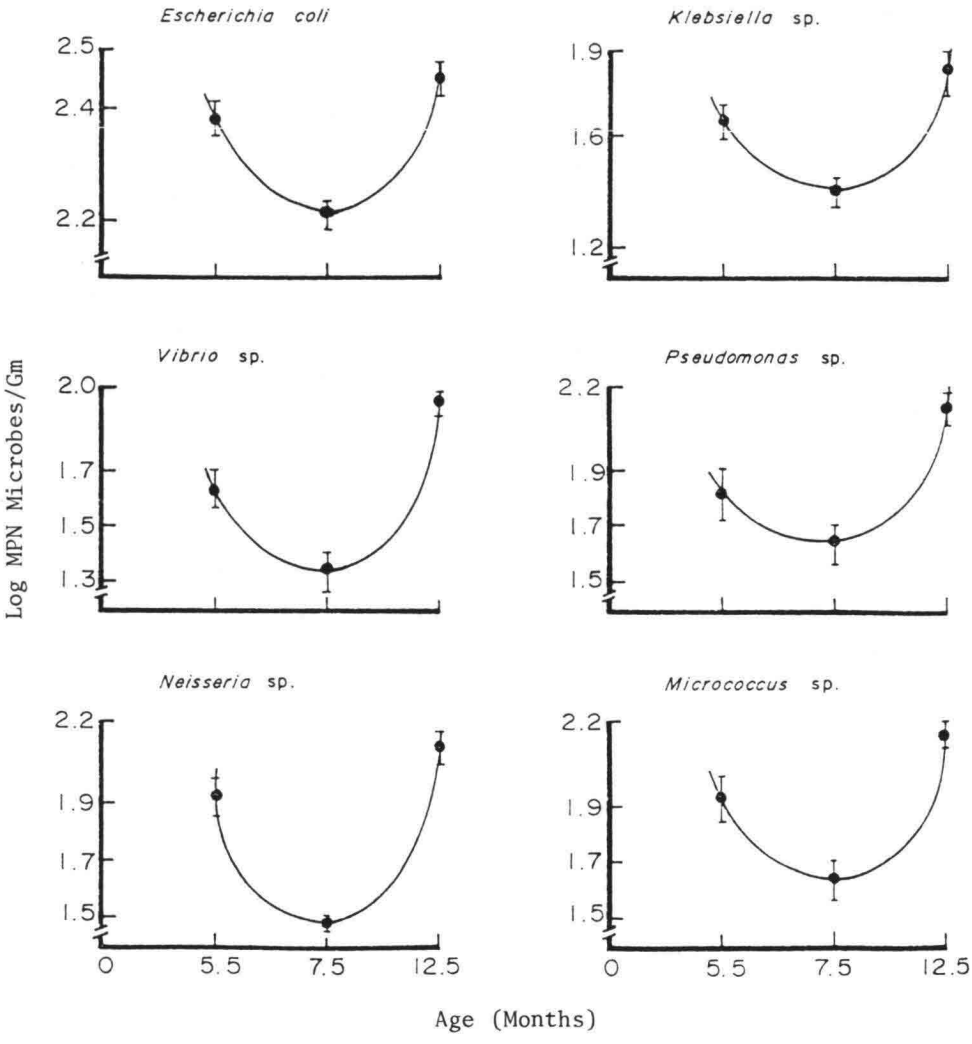

Figure 14: Variation in microbial flora in the green - lipped mussel, *Perna viridis* Linnaeus, from Teluk Aling, a clean area.

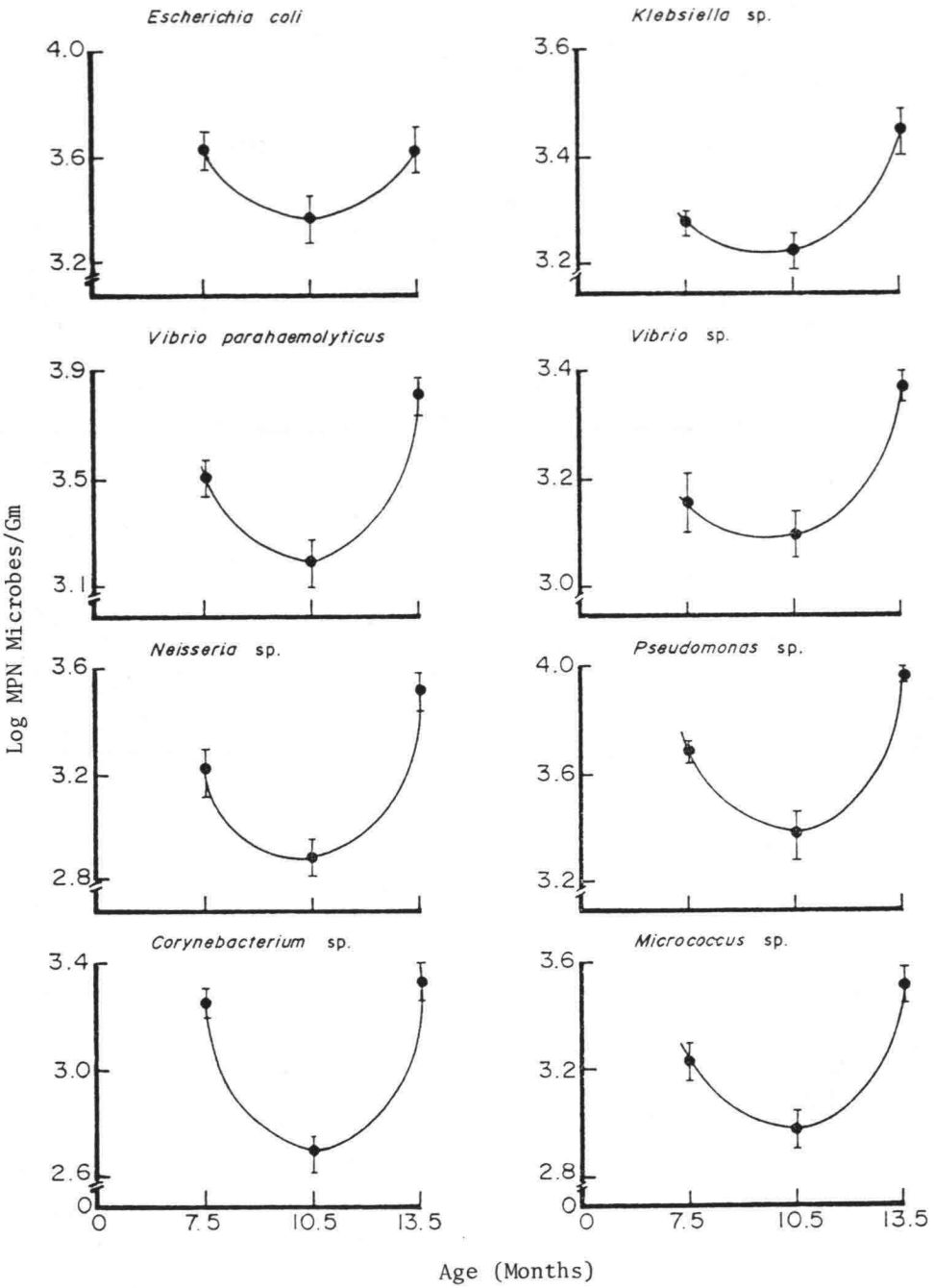

Figure 15: Variation in microbial flora in the rock-oyster, *Saccostrea cucullata* **BORN**, from the Port area.

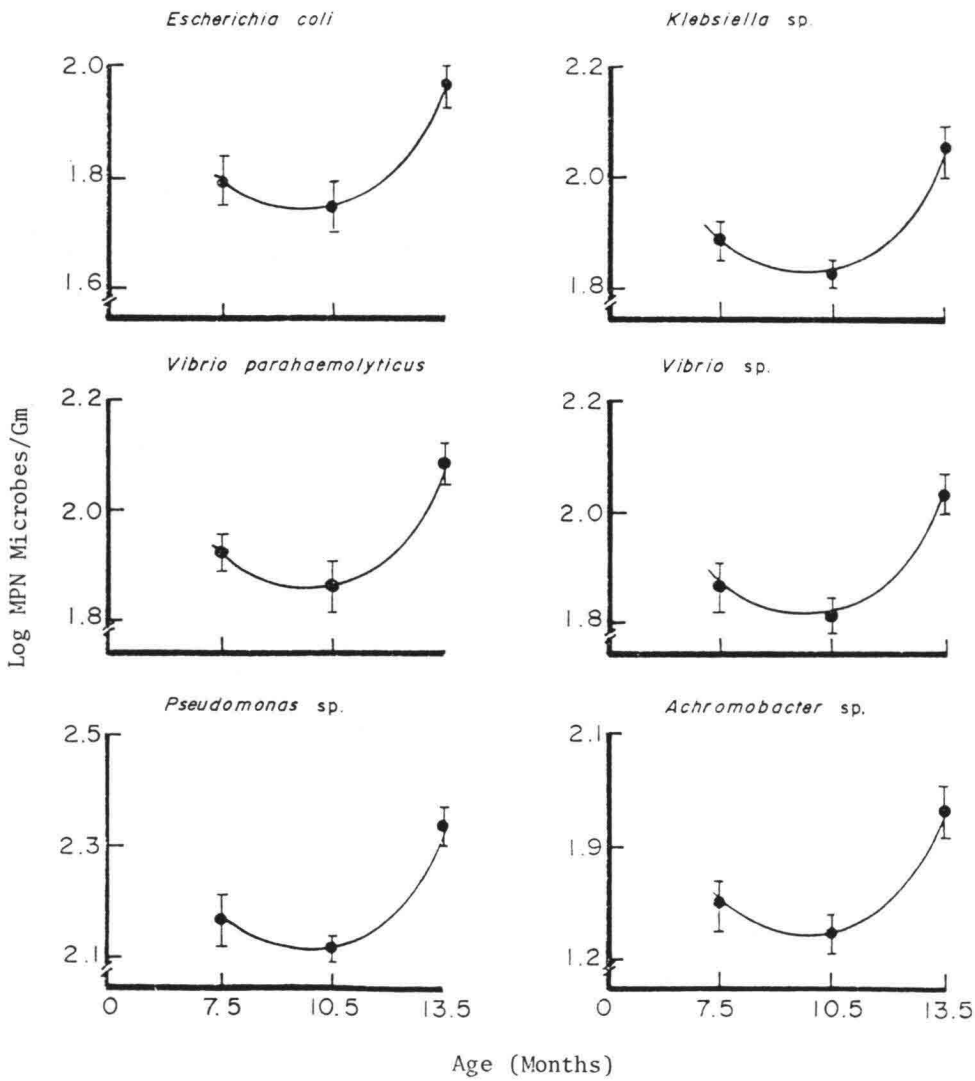

Figure 16: Variation in microbial flora in the rock oyster, *Saccostrea cucullata* BORN, from Teluk Aling, a clean area.

Under these considerations Figure 17 demonstrates the microbial flora distribution in parrot-fish, *Liza dussumieri*, from the Port area.

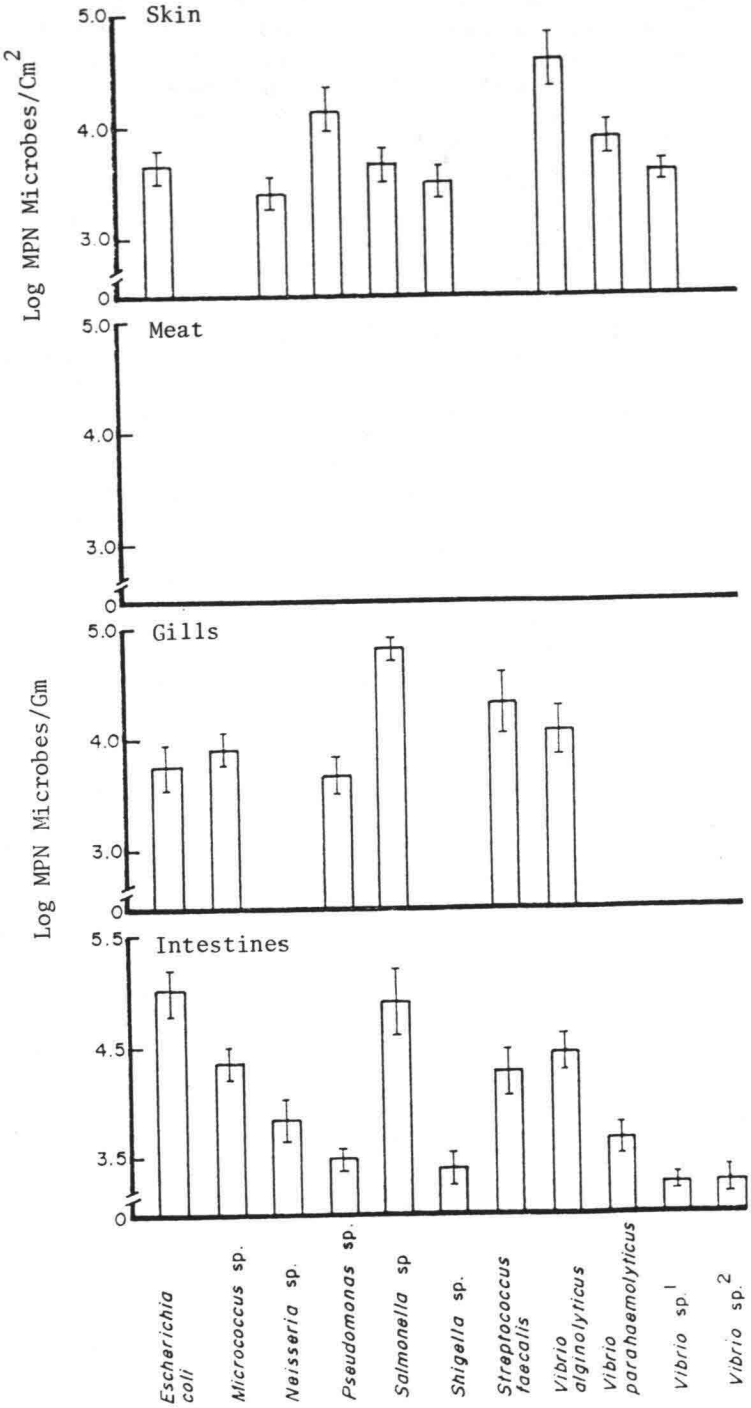

Figure 17: Microbial flora distribution in parrot-fish, *Liza dussumieri*.

It is noticeable in both Figures 13 & 14 that the microbial flora of *E. coli*, *Klebsiella* sp., *Vibrio* sp., *Pseudomonas* sp., *Neisselia* sp. and *Micrococcus* sp. exist commonly in the green-lipped mussel, *Perna viridis* L., harvested from both localities of the Port area as well as Teluk Aling. However, the ratio in distribution of MPN/gm is ca. 2 folds in samples from the Port area. With age, too, it is explicitly noticeable that these microbial flora are least in number in the age groups of 7.5 months, indirectly transpiring the fact that in general the harvesting months of these organisms should fall at this age when it is least contaminated.

With regard to the rock-oyster species, *Saccostrea cucullata* BORN, the samples from the Port area harboured 9 species of bacteria, viz. *E. coli*, *Klebsiella* sp., *V. parahaemolyticus*, *Vibrio* sp., *Neisseria* sp., *Pseudomonas* sp., *Corynebacterium* sp. and *Micrococcus* sp., while those from Teluk Aling only *E. coli*, *Klebsiella* sp. *V. parahaemolyticus*, *Vibrio* sp., *Pseudomonas* sp. and *Achromobacter* sp. (Figures 15 & 16). It should be noted that samples from the Port area harboured no *Achromobacter* sp. Almost identical to mussels, the intensity of bacteria in samples from the Port area are 2 fold, while the least bacterial counts at both sites prevailed at the age groups of 10.5 months.

In Figure 17, the distributional patterns of microbial flora in parrot - fish, *Liza dussumieri*, from waters of the Harbour indicate the non-existence of them in finfish meat, while in the skin; *E. coli*, *Neisseria* sp., *Pseudomonas* sp., *Salmonella* sp., *Shigella* sp., *Vibrio alginolyticus*, *V. parahaemolyticus* and *Vibrio* sp[1]., in the gills; all the above excepting *Neisseria* sp., *Shigella* sp., *V. parahaemolyticus* and *Vibrio* sp.[1] and harbouring additionally *Streptococcus faecalis* and *Micrococcus* sp., and in the intestines; all the above mentioned species inclusive of additionally *Vibrio* sp.[2]. This reflects the high intensity of contamination by bacterial species in finfish from the Harbour area.

5. PCBs AND PERSISTENT PESTICIDAL CONTAMINATION

Although the levels of PCBs and persistent pesticidal residues were not detectable in water samples the levels of PCBs (KC - 400) in *Anadara granosa* ranged between 174.45 - 335.31 ppbs, *Barbatia bicolorata*; 472.25 ppb, *Atrina* vexillum; 519.79 ppb, *Pinctada vulgaris*; 467.25 ppb, *Saccostrea cucullata*; 461.57 ppb and mussels; 99.9 - 599.9 ppbs. In the green-lipped mussel, *Perna viridis* L., p, p' - DDE ranged between 3.69 - 17.38 ppbs while no p, p'DDD was detected. In other shellfish species, mentioned previously, these contaminants were absent excepting cockle samples from Batu Maung with a p,p'DDE content of 9.24 ppb.

Table 2: PCBs and persistent peoticides in the green-lipped mussel.

Locality	Date	Species	*pp'*-DDE[a]	*pp'*-DDD[a]	ΣDDT[a]	PCBs[a] (KC–400)[b]	Source
Malaysia (present study)							
Weld Quay (old pier)		*Perna viridis*	12·46	ND	12·46	400·9	This study
Marine Depot		*Perna viridis*	17·38	ND	17·38	442·3	This study
Permatang Damar Laut		*Perna viridis*	3·69	ND	3·69	99·9	This study
Batu Maung		*Perna viridis*	17·15	ND	17·15	480·7	This study
Gertak Sanggul		*Perna viridis*	16·17	ND	16·17	495·9	This study
Pulau Jerejak		*Perna viridis*	10·12	ND	10·12	599·9	This study
Singapore (present study)							
Ponggol area		*Perna viridis*	7·11	ND	7·11	170·4	This study
Selatar area		*Perna viridis*	8·12	ND	8·12	256·9	This study
Serangoon area		*Perna viridis*	7·82	ND	7·82	139·8	This study
USA (west coast)	1976						
Bogeda Head		*Mytilus californianus*	17–34·6	7–23	NG	10–50	Goldberg *et al.* (1978)
Tillamook Bay		*M. edulis*	<3–17	<2–44	NG	9–25	Goldberg *et al.* (1978)
San Pedro harbour		*M. edulis*	330–17 000	150–<1200	NG	440–8700	Goldberg *et al.* (1978)
Puget Sound		*M. edulis*	<2	<2	<4	41	Goldberg *et al.* (1978)
San Diego harbour		*M. edulis*	29–57	NG	NG	360–1400	Goldberg *et al.* (1978)
USA (east coast)	1976						
Narragabsett, Rhode Island		mussel	25·6–37·2	NG	NG	281–626	Goldberg *et al.* (1978)
Portland		mussel	<7·88	NG	NG	94·6	Goldberg *et al.* (1978)
Boston		mussel	<44·4	NG	NG	635	Goldberg *et al.* (1978)
New Haven		mussel	<7·43	NG	NG	129	Goldberg *et al.* (1978)
Herod Point		mussel	17·6	NG	NG	316	Goldberg *et al.* (1978)
Northwestern Mediterranean	1973–1974	*M. galloprovincialis*	NG	NG	88	268	Marchand *et al.* (1976)
Baltic Sea	1966–1968	*M. edulis*	NG	NG	30	30	Jensen *et al.* (1969)
Archipelago of Stockholm	1966–1967	*M. edulis*	NG	NG	40	37	Jensen *et al.* (1969)
Holland Coast (Rhine)	1965–1968	*M. edulis*	NG	NG	100–250	600–1100	Koeman and Van Genderen (1972)
Sweden	1972	*M. edulis*	NG	NG	95	13	ICES (1974)
Germany	1972	*M. edulis*	NG	NG	25	90	ICES (1974)
Holland	1972	*M. edulis*	NG	NG	9	237	Ten Berge and Hillebrand (1974)
Canadian Atlantic Coast	1970	*M. edulis*	NG	NG	20	140	Zitko (1971)
Norway	1972	*M. edulis*	NG	NG	25	30	ICES (1974)

[a] Concentration in ppb on dry weight basis [b] Kanechlor 400 *Note.* ND = not detected; NG = not given

6. HEAVY METALS CONTAMINATION IN PENANG PORT WATERS.

The heavy metal input into the Straits of Penang by the Ocean Outfall is indicated in Table 3. The large input of the various heavy metals is noticeable.

Table 3: Heavy metals input by Jelutong's Ocean Outfall.

Metal sp.	Kg / Day
Cd	14.32
Co	3.4×10^2
Cr	2.01×10^2
Cu	3.44×10^2
Fe	3.41×10^4
Mn	7.45×10^2
Ni	6.01×10^2
Pb	1.29×10^4
Zn	2.46×10^3

Comparison of the levels of these metals as compared to Boon Siew Bay, a clean area, is reflected in Table 4.

Table 4: Heavy metals content in Port waters as compared to Boon Siew Bay.

Metal sp.	Outfall	Boon Siew Bay
Cd	0.163± 0.005	0.192± 0.002
Co	0.95 ± 0.06	0.27 ± 0.03
Cr	BDL	BDL
Cu	0.342± 0.022	0.342 ± 0.22
Fe	1.74 ± 0.043	0.877 ± 0.021
Mn	1.161± 0.004	0.098 ± 0.008
Ni	0.70 ± 0.050	0.362 ± 0.040
Pb	0.141± 0.001	0.073 ± 0.006
Zn	0.44 ± 0.001	0.22 ± 0.002

The biodeposited heavy metals in *Perna viridis* L. from the Port area as compared to other areas is indicated in Table 5, while for finfish in Table 6.

Table 5: Heavy metals in *Perna viridis* L. from the Port area as compared to those from other areas.

STATION	Metal concentration ($\mu g\ g^{-1}$)								
	Cd	Co	Cr	Cu	Fe	Mn	Ni	Pb	Zn
Ocean outfall at Penang	3.23	25.98	11.91	12.38	2166.33	75.15	81.21	21.04	162.36
Telok Aling	5.27	17.69	BDL*	BDL	271.05	12.05	22.39	9.40	144.54
Batu Ferringhi	5.26	17.65	BDL	BDL	458.61	24.04	27.98	9.38	216.35
Port Weld	4.85	10.83	BDL	BDL	365.28	27.67	10.31	8.65	133.02
Marine Depot	3.97	8.85	BDL	BDL	314.35	22.62	16.85	7.07	126.87
Permatang Damar Laut	5.31	11.86	BDL	BDL	653.10	36.35	28.28	9.48	145.77
Gertak Sanggul	5.60	11.48	6.52	BDL	489.11	23.50	21.85	18.34	117.51
Telok Asam	8.36	18.66	BDL	BDL	563.08	38.22	17.76	14.91	152.78

Table 6: Heavy metals in *Liza subviridis* L. as compared to other species.

Fish	Metal concentration ($\mu g\ g^{-1}$)								
	Cd	Co	Cr	Cu	Fe	Mn	Ni	Pb	Zn
Liza subviridis L.	2.6	56.0	18.9	34.4	2713.9	38.8	118.5	106.3	269.2
Stromateus cinereus (Black pomfret)	ND*	ND	ND	0.7	10.8	ND	ND	1.4	12.0
Stromateus cinereus (White pomfret)	ND	ND	ND	0.4	10.3	ND	ND	1.1	6.7
Stolephorus commersonii	ND	ND	ND	0.6	11.8	ND	ND	2.5	28.0
Megalaspis cordyla	ND	ND	ND	2.3	34.4	ND	ND	1.0	22.0
Rastrelliger kanagurta	ND	ND	ND	1.4	17.9	ND	ND	1.2	19.3
Polynemus spp.	ND	ND	ND	0.7	5.4	ND	ND	1.2	4.1
Dasyatidae spp.	ND	ND	ND	0.3	3.9	ND	ND	0.5	7.5
Soleidae spp. (sole)	ND	ND	ND	1.2	40.3	ND	ND	0.6	8.0
Selaroides leptolepis	ND	ND	ND	1.3	13.7	ND	ND	1.3	19.5
Polynemus tetradactylus	ND	ND	ND	0.9	10.5	ND	ND	4.0	15.4
Soleidae spp. (flatfish)	ND	ND	ND	0.4	6.5	ND	ND	0.8	7.6
Scomberomorus spp.	ND	ND	ND	0.0	2.2	ND	ND	0.7	7.3
Chirocentrus dorab	ND	ND	ND	0.3	24.1	ND	ND	0.1	8.1
Osphromenus trichopterus	ND	ND	ND	0.3	5.6	ND	ND	0.9	14.9

Regarding PCBs, as shown in Table 2, the levels found in mussels from the harbour area are high (KC - 400) along with pp'DDE as compared to those found worldwide. Table 3 illustrates the very high input daily of most heavy metals via the Jelutong Ocean Outfall and this is visualized as high concentrations of Co, Fe, Mn, Ni, Pb and Zn in adjacent waters as compared to Boon Siew Bay (Table 4). Based on this input the bioaccumulated levels of heavy metals in the green-lipped mussel (Table 5) and finfish of *Liza subviridis* L. in harbour waters are also high as compared to other species around the Island of Penang/marketed ones (Table 6).

7. CONCLUSIONS

Thusfar, we have noticed that *in lieu* of contaminants originating from overtaxing effects of Port usage, the waters of the Straits of Penang is immensely influenced by river input and wantom sewage discharge. It is apparent at this juncture to note that in order to maintain water quality there is an urgent need to have proper wastewater treatment plants in conjunction with well oriented civic minded educational aspects objectively to revive the contaminated and dead rivers. Environmental laws should also be much more stringently promulgated hand-in-hand with acidness in its implementation so as to maintain the healthiness of them. If contrary, the tourist industry would be greatly effected besides the health of the future and present generation. Obviously, this will boomerang also on the fisheries landings in the long run.

The levels of PCBs, DDTs and oil contamination also appear to be high in harbour waters and this necessitates indepth extensive studies. Further, the practicing of mariculture of both finfish and shellfish in harbour waters should also be not encouraged. Since the harbour experiences heavy usage by commercial vessels, studies should also be extended to evaluate the levels of tributyltin and its biological effects on spats/fingerlings of marine organisms. Appropriate measures should also be taken so as to prevent heavy siltation within the harbour to maintain safety depthness of its waters concomitantly protecting valuable breeding grounds therein.

PMS/khaa
fn:water2.qly
08041994

HYDRO-PORT'94
International Conference on Hydro-Technical
Engineering for Port and Harbor Construction
October 19 - 21, 1994, Yokosuka, Japan

Environmental Monitoring of the Lagunar Complex of the South Region of the Santa Catarina State

Dominico Accetta
Wagner S. Scisinio Dias
Berenice Mota Vargas
José Antonio dos Santos

Waterways Research Institute - INPH
Companhia Docas do Rio de Janeiro
Rua General Gurjão 166, Caju
Cep: 20.931- 040- Rio de Janeiro

ABSTRACT

Besides the prosperity resulting from the exploration of coal, the south region of the Santa Catarina state has serious problems concerning its environment. With about 220 km square, the lagunar complex situated in that region receives contributions from the hydrical net formed by the hydrographic basin that integrate the catarinense coal basin. This paper presents some important results obtained in two years of environmental monitoring of the lagunar complex.

Key Words: Hydrographic Survey, Hydrodynamic Survey, Biologic Measurements.

1. INTRODUCTION

1.1 Presentation of the Problem

Santa Catarina State, in Brazil, has achieved great prosperity due to the coal mining activity, but nowadays the catarinense natural resources are suffering from serious environmental problems, which affect the life of the major part of the population.

The lagunar system of the region has a surface area of approximately 220 km^2 and it gets all the river discharges from the so-called "catarinense coal hydrographic basins". The daily rate of acid effluents discharged in these basins approximately 300.000 m^3.

The acid effluents carried by the Tubarão river and by the Lavrador of Capivari have accelerated the environmental degradation process within the lagoons of Santo Antonio, Imaruí and Mirim, causing serious social and economical problems for the region.

In order to have an idea of the problem, in the last decade there was an 80% reduction in the production of shrimps. Consequently, 20.000 fishermen families had there annual income diminished.

The environmental impact caused by the coal mining activity has been affecting all the south region lagoons and particularity the lagoons of Santo Antonio, Imaruí and Mirim, where the pollution reached high levels, causing damage to the aquatic life, to the fishery and to the touristic activities.

1.2 Aim of the Study

The aim of the short-time studies (1991-1993) proposed by INPH for the environmental survey of the lagunar system was to find out the present situation of the lagoons of Mirim, Imaruí, Santo Antonio, Ribeirão Grande, Santa Marta, Camacho, Garopaba do Sul e Manteiga (Figure 1), concerning to its environment.

The studies comprises the determination of the hydraulic and sedimentologic behaviour of the lagoons, the determination of the degree of chemical pollution, as well as the determination of the present situation of the biological resources.

The field survey will make it possible for the Government of Santa Catarina to contract the medium-time studies (1993 to 1995) - flow motion, pollution dispersion and salt intrusion simulations - that will help in the decision about what to do in order to improve the environmental conditions of the lagunar system, according to the PROVIDA - SC Program.

In summary, it were performed the following activities:

- Hydrographic survey of the lagunar system, which comprises a surface area of 220 km^2.

- Hydrodynamic survey of the lagoons, chemical measurements, to check for the presence of heavy metal and other substances.

- Biologic measurements, regarding the existing aquatic fauna the flora.

2. STUDIES AND FIELD MEASUREMENTS PERFORMED

2.1 - Hydrographic Survey

The hydrographic survey was based upon the IBGE Datum and it was referred to the Horizontal Datum of Córrego Alegre.

Based upon this hydrographic survey it were drawn 18 bottom contour maps, 17 of them in the scale of 1:10000 and the remaining one (Ribeirão Grande lagoon) in the scale of 1:5000.

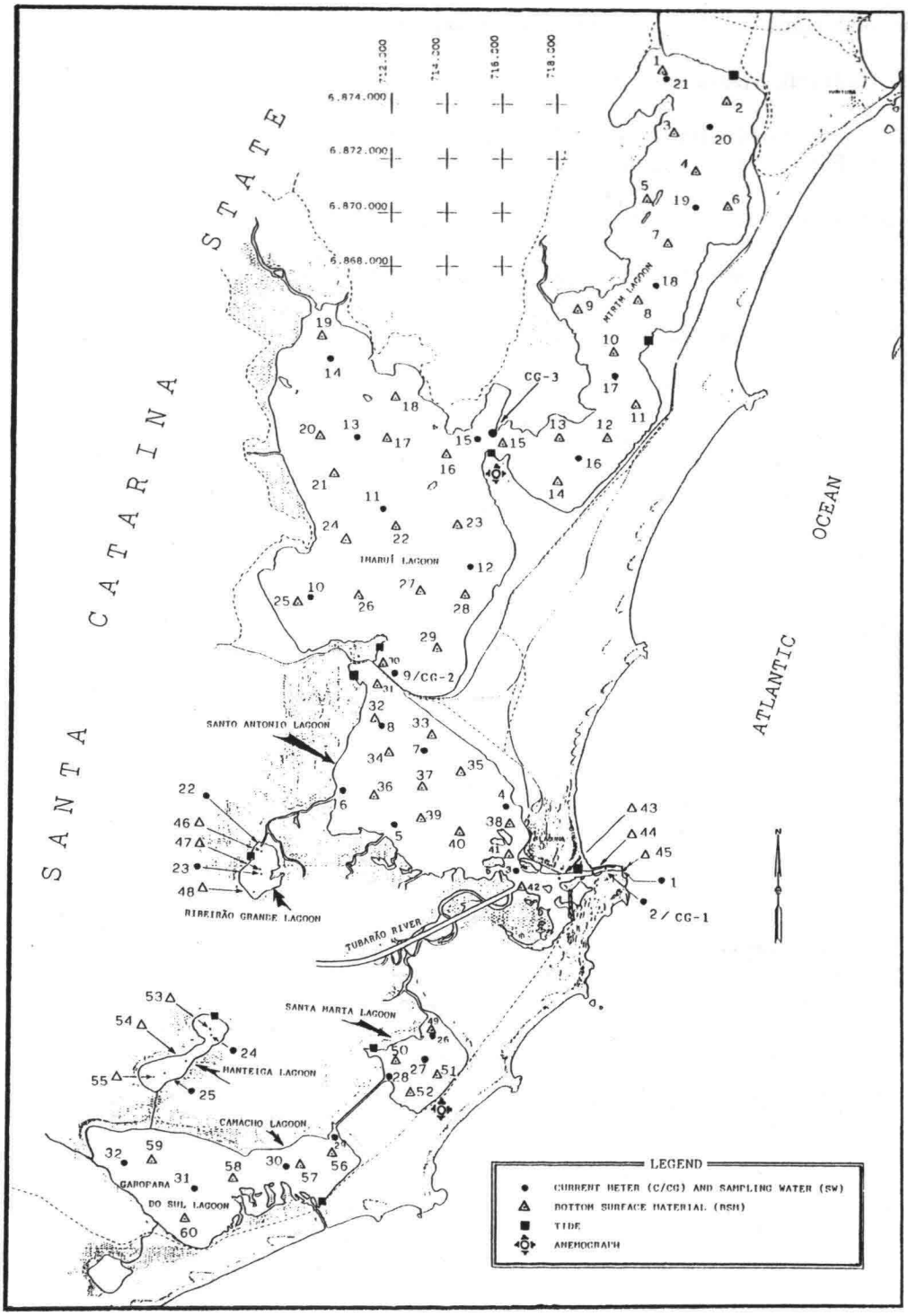

FIGURE 1: MEASUREMENT STATIONS LOCALIZATION

The south-catarinense lagunar system is shown in Figure 1.

2.2 - Hydraulic Measurements

For the perfect understanding of the dynamics of the flow motion in the lagunar system, it were performed the following studies:

- Currents measurements

- Salinity, water temperature and suspended matter concentrations measurements

- Meteorological measurements

- Tide and water level measurements

2.3 - Meteorological, Tide and Water Level Measurements

The local wind climate in the regions was established by using the data measured by the 2 meteorological stations shown in Figure 1. To analyze the water level variation in the lagoons, 4 tide gages and 6 tide staffs were installed at the points marked on Figure 1.

For the duration of the field measurements, i.e. 01/03/92 to 30/11/92, it was possible to verify that the lagoons located to the south, present a still water level smaller (± 15 to 20 cm) than the others, because there is no significant tide penetration in these lagoons. The tide amplitude in the lagoons is comparatively smaller than the one measured at the Port of Laguna, due to the tide damping at the entrance chance).

As an example, Figure 2 shows the water level and the wind variations measured at several stations. Starting on 15/06/92, it is possible to verify that the Northeast wind causes the still water level to drop down.

2.4 - Hydraulic-Sedimentologic Measurements

In general the velocities of the currents in the lagunar system are very small, getting to almost zero as far as the measured point is from the entrance channel.

Although we have detected tidal influences in the lagunar system, they have a significant value only in that places located in the vicinity of the entrance channel, i.e., the Santo Antonio lagoon, which has shown the biggest flow motion of all the lagunar system. The major physical parameter enveloped in the problem is the meteorological one, caused by the wind climate and by the atmospheric pressure of south region of the country, which is directly related to the atmospheric changes in the Antarctic Continent.

When a cold front is moving to, or when it reaches the south region, the most frequent winds become those coming from SSE to WSW. These winds push the sea towards the coast, causing the still water level to raise and, as a consequence, more sea water enters the lagoons. On the other hand, when there is no cold fronts in the region, or when there is a hot front, the most frequent wind directions become those from NNE to ENE, which cause the flow to move towards the sea (Figure 2).

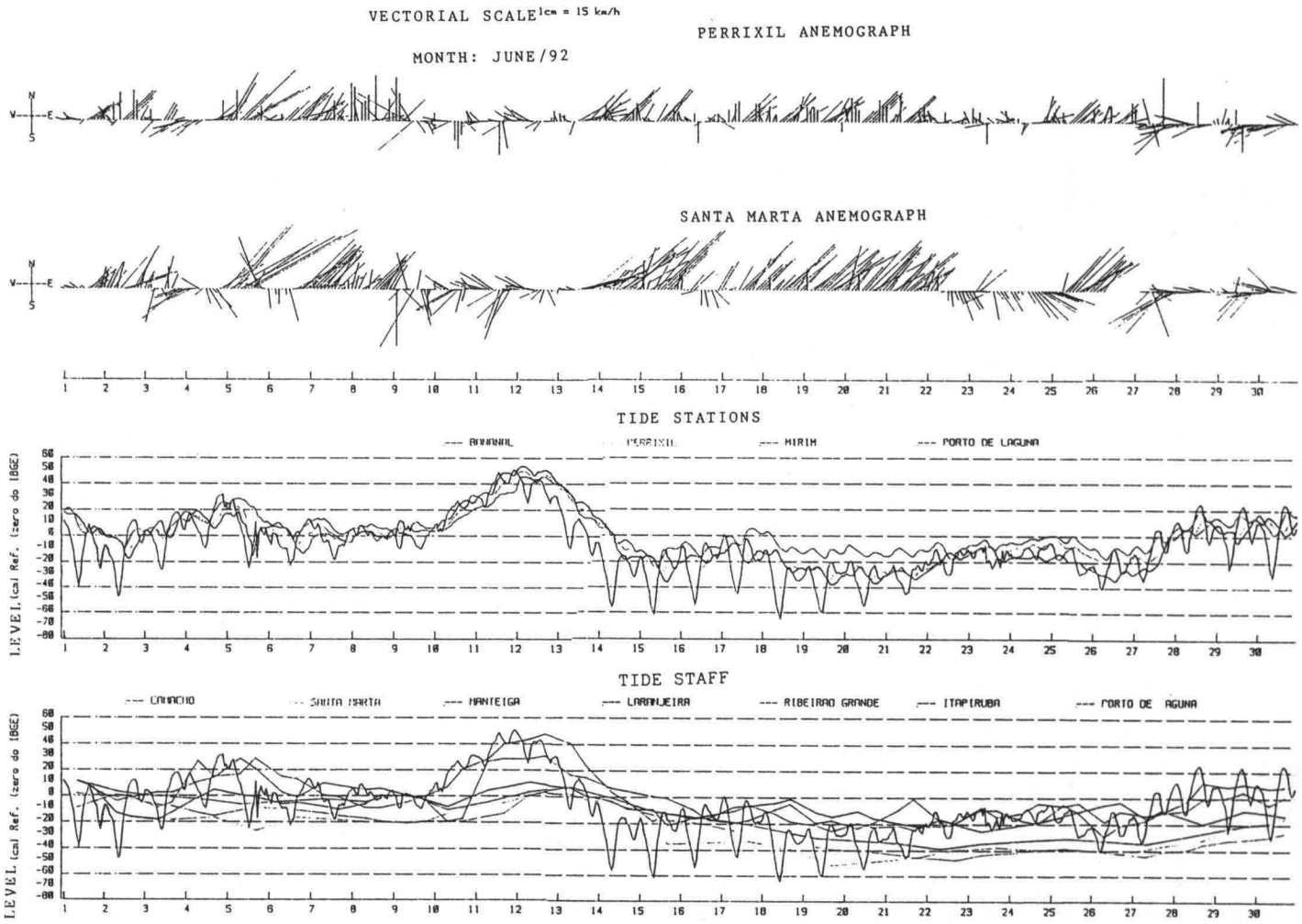

FIGURE 2 - WATER LEVEL AND WIND MEASUREMENTS

This behaviour of the lagunar system is shown by the correlation between the winds and currents directions at the boundaries of the system: Barra, Ponte de Cabeçudas e Perrexil. At these places, due to its morphological situation, one can observe an intense flow interchange with the sea, as well as at the boundary between Santo Antonio and Imaruí lagoons, and at the boundary between Imaruí and the Mirim lagoon (Figure 4).

Another indication of this behaviour is given by the salinity, temperature and suspended matter concentrations measured along the longitudinal path of the lagunar system (Figure 3).

When the south wind is blowing, it was observed an increasing of the salinity and a decreasing of the temperature, as well as of the suspended matter concentrations, in the main flow motion regions, indicating salt water penetration in the lagoons.

On the other hand, when the NE wind is blowing it becomes clear the dropping down of the salinity and the increasing of the two other parameters, indicating a flow motion toward the sea.

3. PHYSICAL-CHEMICAL MEASUREMENTS

From the results obtained, we can notice, based on the parameter oil/grease, the strong antropic action that there is at the regions located near the urban centers; however, the COD - chemical oxygen demand - parameter is relatively high at the C6, C7, C26 point, where there is also potassium concentration (Figure 5).

It seems that there are two situations: the values measured at C6 and C7 probably are due to the currents, which carry organic matter to this areas, as well as to the influence of Cabeçudas and Laguna cities; the values measured at C26 seems to be much more related to the presence of organic material. The bottom material collected at MF 36 point confirms that this is a dead zone.

The points C15 and C21 are located at the two boundaries of the Mirim Lagoon, and they are those where were measured the highest amounts of coliforms.

The fact that point C21 has higher concentration of coliforms than point C15, located near the city of Imaruí, does not invalidate the antropic influence. This is a lagoon, that has no significant current velocities, is less marshed, and has its margins occupied by houses and gas stations.

Concerning to the bottom material, we can verify that the Imaruí and Mirim lagoons present a high correlation between the iron and manganese concentrations; the same happens with the lagoons of Santa Marta and Ribeirão Grande. This phenomenon happens less frequently at the lagoons of Santo Antonio, and it almost doesn't happen at the lagoons of Manteiga, Camacho and Garopaba do Sul (Figure 5), showing that these are places where fine material sedimentation occur, while the Santo Antonio lagoon is a place where occurs the deposition of the largest grains material.

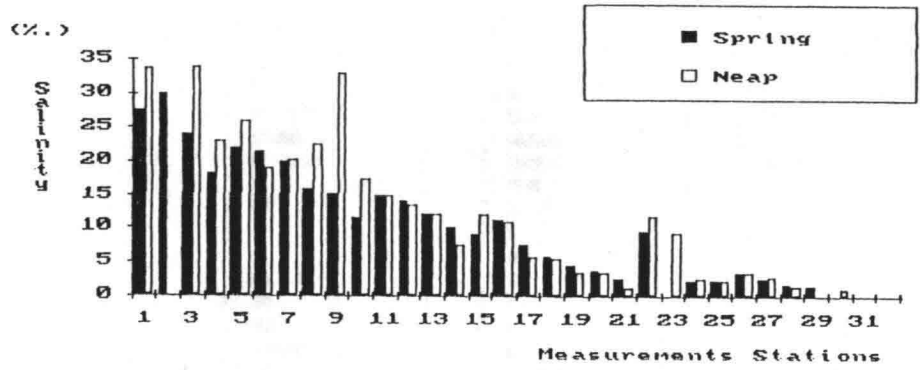

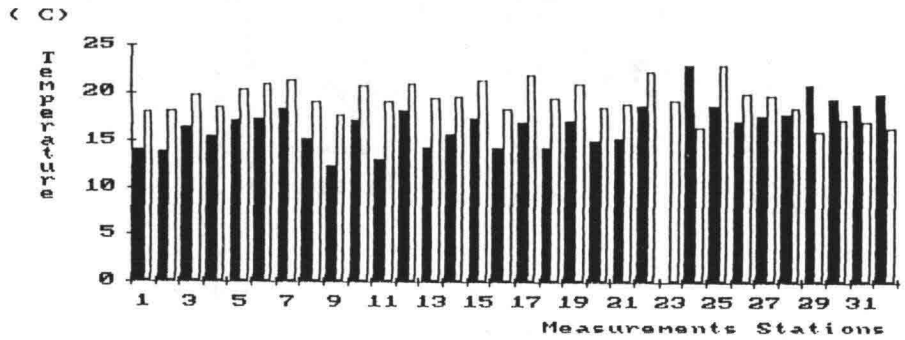

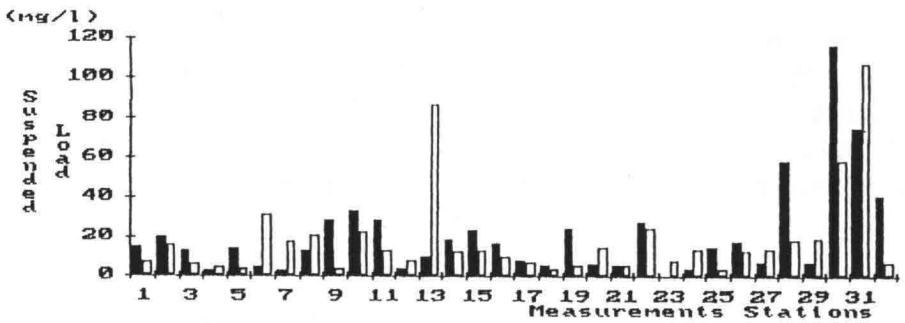

Stations	Lagoon
1 to 8	Santo Antonio
9 to 15	Imarui
16 to 21	Mirim
22 to 23	Ribeirao Grande
24 to 25	Manteiga
26 to 28	Santa Marta
29 to 32	Camacho / Garopaba do Sul

Figure 3: Salinity, Temperature and Suspended Load on 1/2 Depth

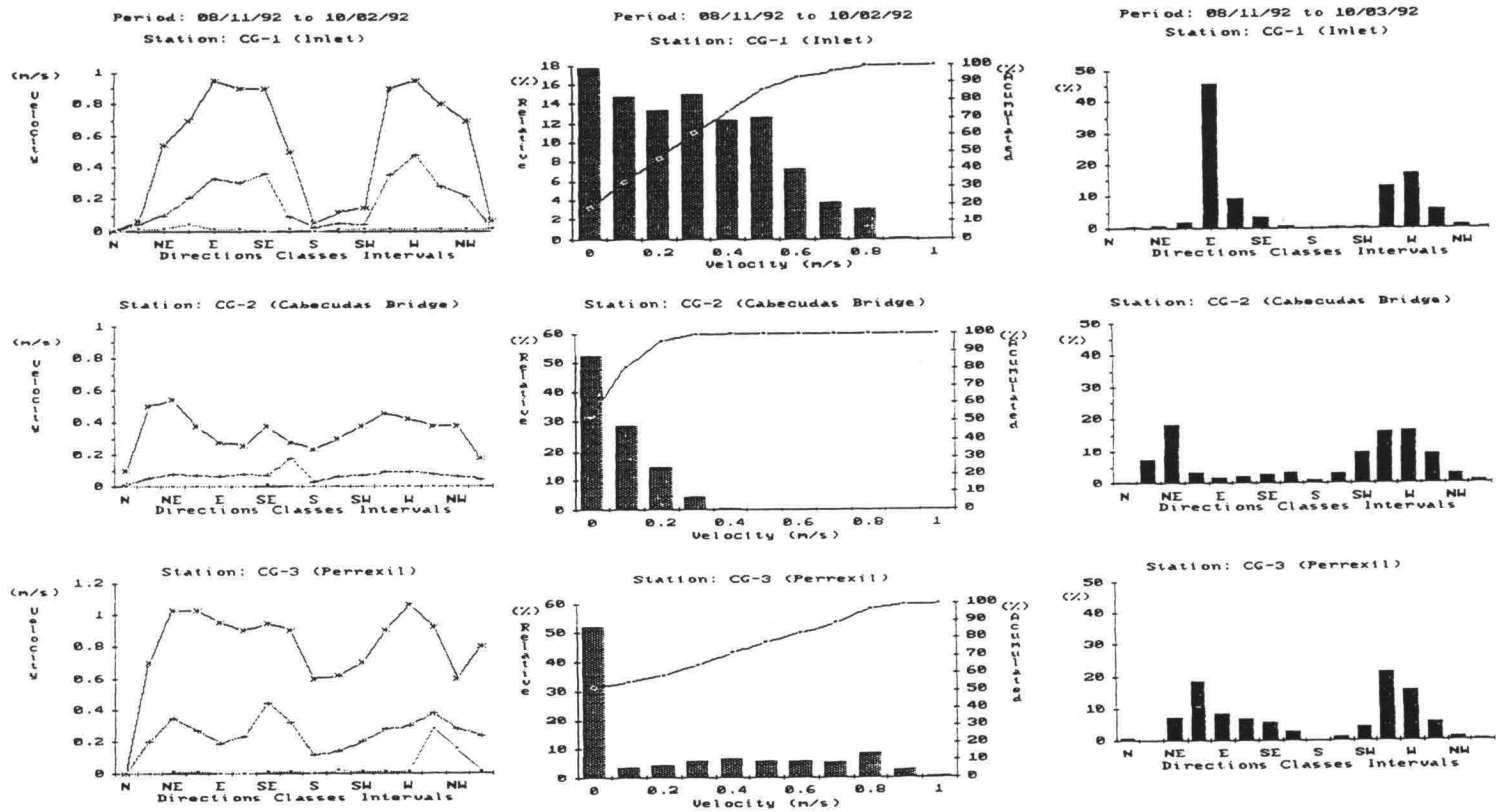

FIGURE 4: MAIN CHARACTERISTICS OF CURRENT MEASUREMENTS

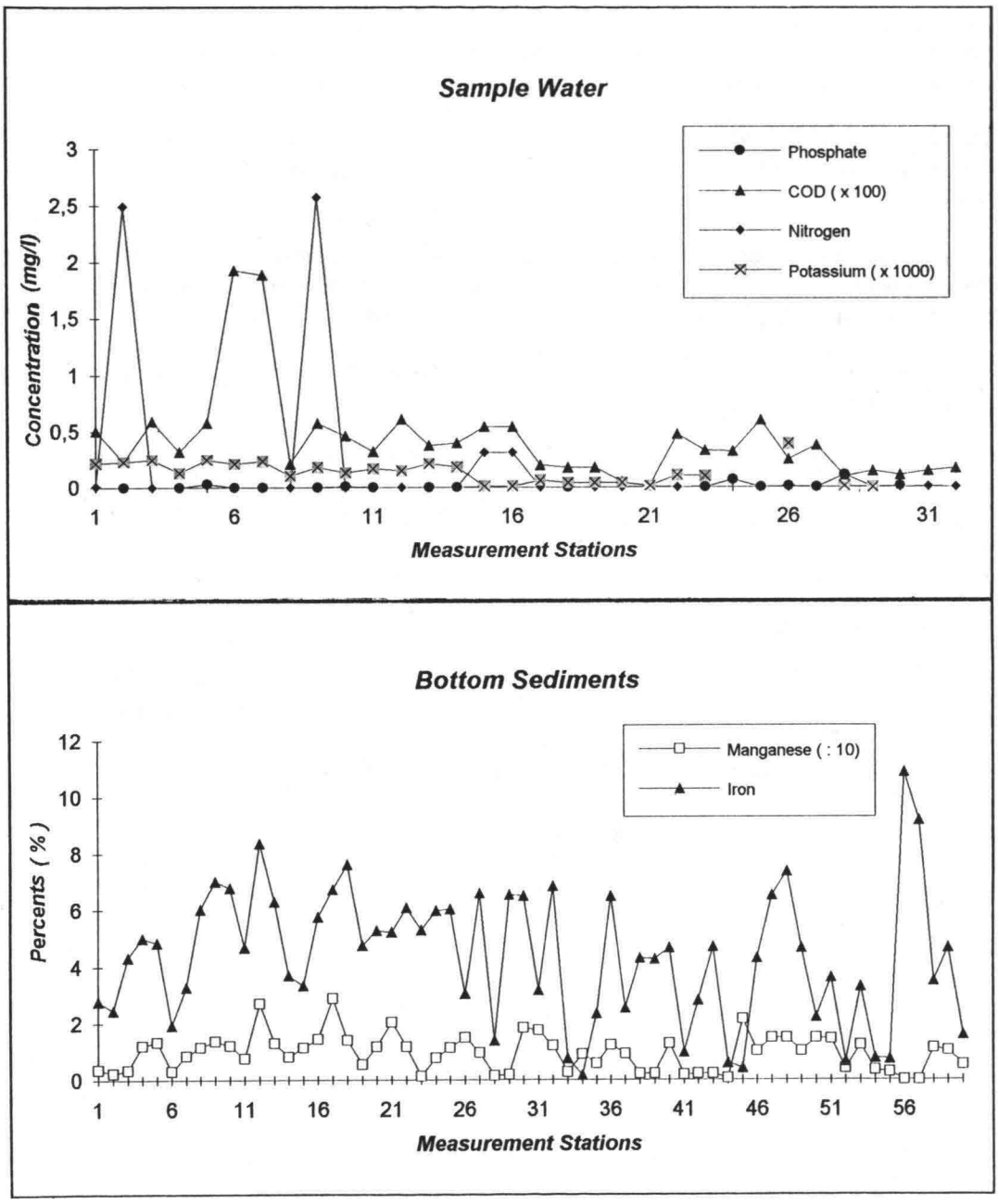

FIGURE 5 - PHYSICAL-CHEMICAL MEASUREMENTS

4. BIOLOGICAL MEASUREMENTS

Those measures have by objective diagnostic ate of the present situation of the aquatic habitat that occur on the lagoon complex from the south of the state of Santa Catarina contributing with subsidy to obtain a global vision of the ecosystem from the region.

This lagoon system as others geographical regions, develop a function of critical biotic for the survival of juvenile form of migrant species which are live resources of economics interest.

Between them the complex Mirim - Imaruí - Santo Antonio is the most important system for the state with a natural production of shrimp and crabs that achieve of 500 kg/year, which means a participation of until 30 % of all the non industrialized.

The location of the stations and zones of biological sampling as coincident with the punctual stations showed on the Figure 1.

On this campaign could be verified inside the benthonic community, that the space distribution of the crustaceans on the lakes show the same concentrations on Imaruí, where was collected 34,5 % of all the samples on the lagoon Mirim of 12,8 % and Santo Antonio of 12,6 %.

5. NUMERIC MODELS

INPH pretends, with the data gathered and analyzed from the lagunar system during the summer and winter campaigns (presented on this paper), to encourage the Santa Catarina State Government on conducting a program on the improvement of water quality at the lagunar ecosystem in the south region of the State of Santa Catarina.

As an example, we will focus on the studies related to the opening and fixation of the Camacho bar, situated on the south side of the lagunar system where the Camacho and Garopaba do Sul lagoons, with an area of approximately 24,52 km^2 and depth around 1,5 meters (IBGE) may be considered as a fresh body due to the results of the measurements conducted by INPH.

The study, therefore, to determine the salt concentrations in the lagoon, close to the Congonhas river, after the opening and fixation of the bar channel. The channel that links the lagoon with the open sea will be 1 km long by 40 meters wide, and about 2 meters in depth.

Studies were conducted for conditions of wind absence and wind blowing from a given direction. With no wind the circulation occurs with greater intensity at the Camacho lagoon and in its inside (Garopaba do Sul lagoon) with low circulation.

With the presence of wind, the circulation was significant on both lagoons and presenting the vortex phenomena. Regarding the salt concentrations, the mathematical model indicated that the salt wedge will penetrate up the inner most part of the Garopaba do Sul lagoon, and the water will be marsh waters.

Figures 6 and 7 shows the current circulation pattern and salinity concentrations in the case wind action coming from NE and S directions, respectively.

6. CONCLUSIONS

Based upon the winter's field survey data (1st campaign) we can come up to the following conclusions:

Hydraulic Parameters

- The meteorological conditions play an important role upon the water flow motion within the lagunar system, because there are strict interactions between the winds and the water levels within the lagunar system . In opposition to the climatic actions, the morphological configuration of the system, characterized by small depths, and the presence of some narrow transversal flow sections, is responsible for the difficulty the waters find to flow within the lagunar system (almost all the current velocities measured were equal or less than 0.15 m/s).

- When the NE wind is blowing the data showed a decreasing in the lagoon's still water level, even though with a time lag for the inner places. For the SW wind the phenomenon happens on the other way around.

- As far as the measurement point was from the mouth of the system, smaller was the degree of salinity measured. This is an indication of the salt wedge difficulty to reach these places, taking into account not only the astronomic tide wave but also the meteorological one, which most of the time is the main force acting on the water flow motion within the lagunar system. In the occasions when it were possible to measure both the water salinity and temperature, and also the suspended matter concentrations under NE and SW wind conditions, it was observed that:

  . The salinity always reached higher values when the SW wind was blowing;

  . Except for the Sta. Marta lagoon, the water temperature was always smaller when the SW wind was blowing;

  . the suspended matter concentration was smaller when the SW wind was blowing.

Physical - Chemical Parameters

- There are important evidences of antropic contributions (via organic matter and coliforms);

- The Tubarão river must have an influence on the industrial antropic contributions (coal, oil and grease);

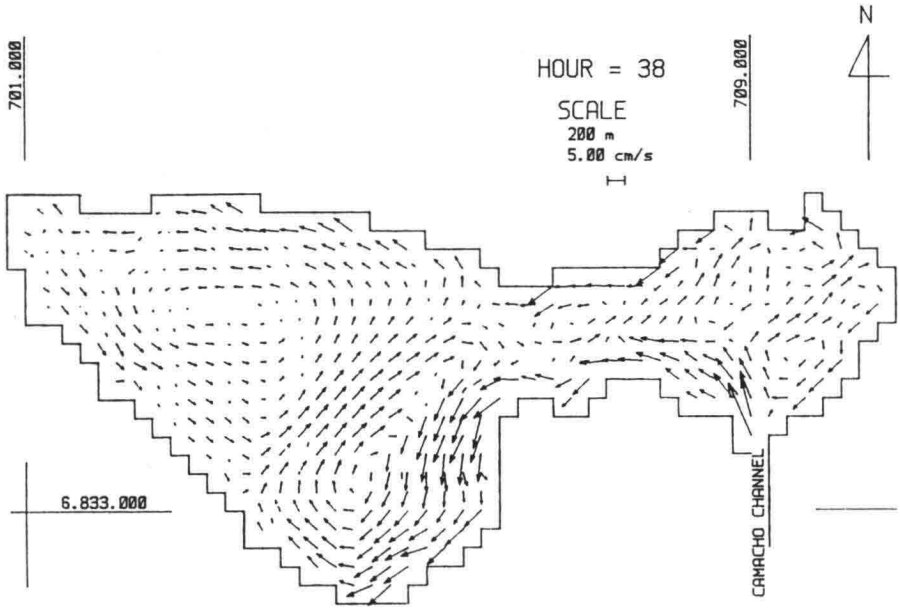

CURRENTS GENERATED BY TIDE AND A NE WIND

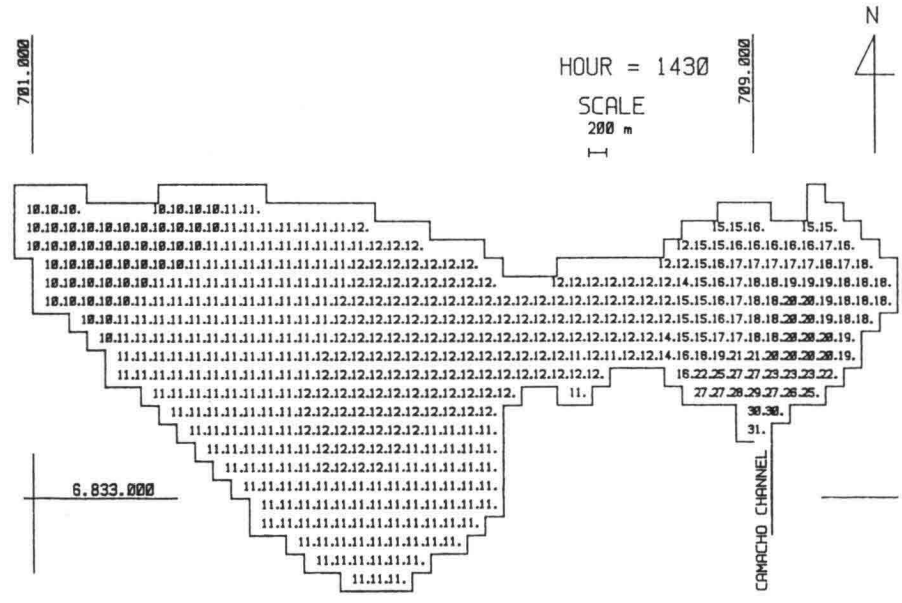

SALINITY CONCENTRATIONS FOR A NE WIND

FIGURE 6 - CAMACHO LAGOON NUMERIC SIMULATION

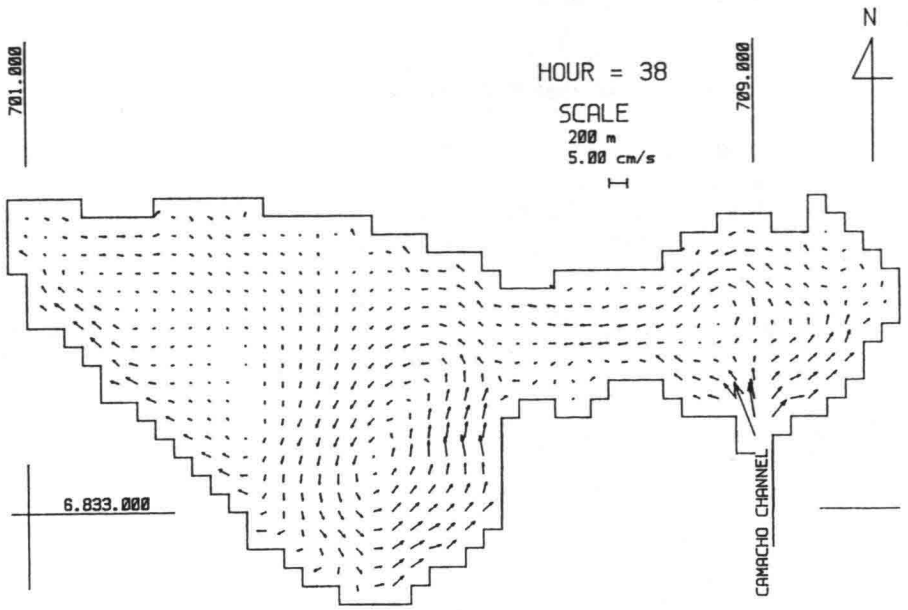

CURRENTS GENERATED BY TIDE AND A S WIND

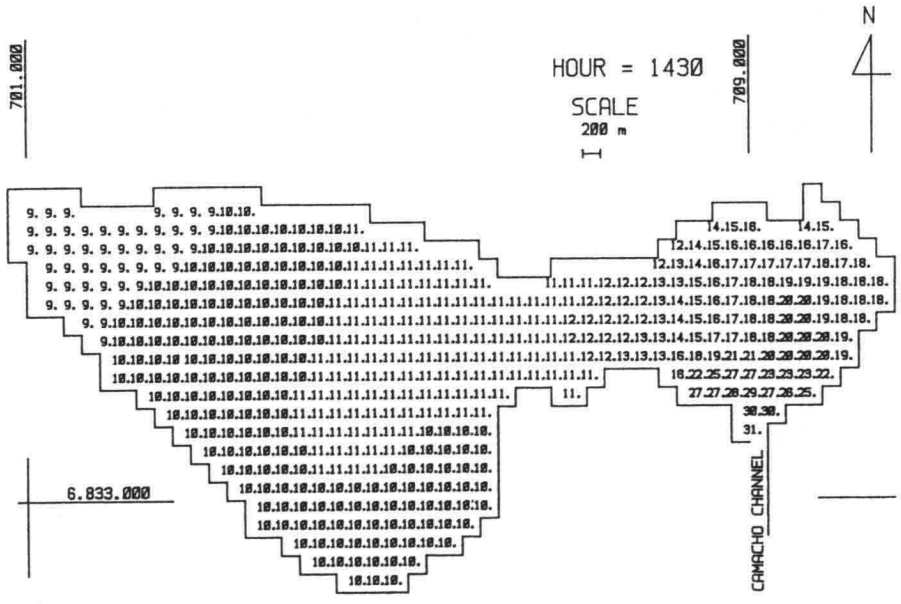

SALINITY CONCENTRATIONS FOR A S WIND

FIGURE 7 - CAMACHO LAGOON NUMERIC SIMULATION

- There is a accumulation of heavy metals (iron and manganese) in the lagoons of Imaruí and Ribeirão Grande, via deposition of gel and other metals adsorbed.

Biological Parameters

In general the results of the field survey allow us to corroborate the biological importance of the south-catarinense lagunar system, in particular concerning to the behaviour of the lagoons of Imaruí, Mirim and Santo Antonio as habitat for migratory estuarine specimens like the shrimps and the mullet fish, which region's fishery activity. The maximum size not only of the migratory specimens, but also of the already settled aquatic populations, shows the presence of young specimens, confirming the natural raising up behaviour of the ecosystem, and, consequently, its importance for the maintenance of profitable levels for the fishery activity in the region.

Finally, by using these data, as well as the data collected during the summer's field survey, INPH will be able to calibrate mathematical models and to perform simulations which will indicate us what to do in order to get lower pollution levels in the south-catarinense lagunar system, as well as what type of civil engineering works will give the best results for improving the water quality of the lagunar ecosystem.

ACKNOWLEDGMENTS

Authors would like to thank the State of Santa Catarina Government, specially Deputy - Governor Antonio Carlos Konder Reis, for his effort on the development of the studies related to the PROVIDA-SC Project, and also a special thanks to Eng° Antonio Paulo dos S. Pinto and João Luiz P. Lemos for the support given, and to Mrs. Marlene R. Peres for the administrative arrangements.

REFERENCES

Accetta, D. (1988). Araruama Lagoon; Measurements Hydraulic-sedimentologycal - Second Survey. Rio de Janeiro, INPH-69/88. (In Portuguese).

Ledo, Blanca Sienna (1993). Biological Study to Lagunar Complex of South Catarinense Region. First Biological Survey: (In Portuguese).

Masson, T.A, A, Martins L.A.B. (1987) - Araruama Lagoon: Measurements of Hydraulic-sedimentologycal - First Survey. Rio de Janeiro. INPH-113/87. (In Portuguese).

Pucci, L. C, Casaroli, L. F. R. (1993): Provida-SC Plan; Measurements of Water Level and wind in Lagunar Complex of South of Santa Catarina State. Rio de Janeiro. INPH-29/93. (In Portuguese).

University of South of Santa Catarina. Chymical Survey in Lagunar Complex of South of Santa Catarina State. (In Portuguese).

Vargas, B. M. (1993). Simulations of Unsteady Flow by Tide and Salt Concentration in Camacho and Garopaba do Sul lagoons. Rio de Janeiro. INPH-21/93. (In Portuguese).

HYDRO-PORT'94
International Conference on Hydro-Technical
Engineering for Port and Harbor Construction
October 19 - 21, 1994, Yokosuka, Japan

Channel Experiments on Coastal Water Purification by Stone Bed with Biofilm

Yasushi Hosokawa [1]
Tadashi Ootsuki [2]
Chiaki Niwa [3]

[1] Port and Harbour Research Institute, Ministry of Transport
1-1, 3chome, Nagase, Yokosuka, 239
[2] Ex- Toa Construction Co.,Ltd.
5 Yonban-cho, Chiyoda-ku, Tokyo, 102
[3] Institute of Technology, Shimizu Construction Co.,Ltd.
4-17, 3chome, Etchujima, Kohtou-ku, Tokyo, 135

ABSTRACT

Large scale model channels (30m long, 1m wide and 1.3m deep, 6 parallel channels) were constructed for contact-purification experiments at the inner coast of Tokyo Bay. Each channel was filled with crushed stones which were expected to be coated with natural biofilm. Coastal saline water was pumped up to pass through the interstitial space in each channel. Different sets of hydraulic retention time(HRT) of the flow (HRT: 1-5 hours) and stone size(d_{50}: 2-11cm) were applied for each channel. After one year's monitoring, removal rate and removal mass of Suspended Solids(SS) and Chemical Oxygen Demand(COD) were analyzed. Supplemental experiments were also conducted for hydraulic characteristics and particles settling.
Even for saline coastal water with lower organic concentration than that in waste water or effluent from waste water treatment plants, biofilm was developed on the surface of stones. Organic particles were effectively removed by settling and biological uptake. SS was removed well by 60-90% after the film development, though the removal rate for COD was 15-30%. Effluent from channels became clearer with longer HRT and smaller stone size, while the maximum removal mass was obtained for the highest hydraulic loading ($15m^3/h$). The inclination of water surface was a good index for the detection of clogging which were developed among stones by the accumulation of resuspended film sludge. Maximum limits of the appropriate surface loading is estimated for SS and COD removal. Preferable values of such basic design parameters as HRT and stone size are proposed for the channel-type purification facility.

Key Words: biofilm, contact purification channel, coastal water, SS removal, COD removal, hydraulic loading, surface loading, clogging, stone size

1. INTRODUCTION

Most of the large cities are located at the inner bottom end of enclosed bays in Japan. Waterfront areas of these cities are expected to provide amenity space for citizens. People wish to enjoy the open space with wide scenery, fresh wind and good water quality. On the other hand, inner water surface of an enclosed bay is often stagnant and more vulnerable to the contamination. Technological developments are required for water quality improvement of this area.

Comparing to waste water, we can find following characteristics of coastal water that influence treatment technologies;
a). containing salinity: Salinity gives the coagulation effect for particles and the buffer effect to pH change.
b). tidal and wave movement of water: Target water is moving around and total volume of water to be treated becomes enormous.
c).low level of contaminant concentration: Present and required concentration of the coastal water is 1-2 order lower in organic matter and nutrients than that of waste water influent. It is not economical to apply conventional waste water treatment technology directly to the coastal water.
d). rich in biological activity and biodiversity: When certain environment is given, suitable species easily grow there as the sea water contains various species of microbe. If the area has gradient and diversity in environment, different species can live along the gradient. The set of various species with different trophic level will give the ecological stability against the environmental fluctuation.

Accordingly, one of the practical options for water quality improvement at coast will be the utilization and enhancement of biological purification activities. Biofilm technology was originally developed from the analogy of the microbial purification activity on the surface of river bed materials. This method requires very little electricity and reagent.

2. BIOFILM TREATMENT METHOD

2.1 Principle of Biofilm Treatment Method

Microbial treatment is a process that microbes utilize organic particles as a food source, get energy from them, and assimilate them into their microbe body. Biofilm treatment method is a kind of microbial treatment and utilizes attached biofilm on the surface of bed materials. Two types of bed materials are common for waste water treatment, those are; 1) crushed stones are used in the trickling filtration, and 2) flat disks are applied for the rotating disk method. Contact between biofilm and water is made by either the movement of bed in stagnant water or by the water flow running among the interstitial space of fixed bed materials.

Biofilm consists of various microorganisms such as bacteria, germs, plankton, and microanimals (Protozoa and Metazoa). As they are attaching on the bed surface, species of slower reproduction rate can also survive in the biofilm without flushing out by water flow. These species sometimes includes large sessile animals. Attached biofilm becomes thick, as it grows. Thick biofilm consists of two layers; aerobic layer near the film surface and anaerobic

layer inside the film near the bed. The aerobic layer consumes oxygen for the degradation of taken organic mater. Thick film can easily peel off and be resuspended from the bed by the friction stress of contact flow. If resuspended materials are accumulated at a certain open space, then the space becomes narrower and difficult for water passing. Biofilm system is said to have less production rate of the excess sludge than suspended activated-sludge system. It is because uptaken organic matters are utilized and degraded more easily owing to the complex foodchain network including the co-existing large animals in biofilm system. Sludges from the biofilm system are also said to settle faster than those from suspended system.

Different from the above-mentioned biological degradation activity, settling and sedimentation is another function for the removal of suspended particles. Particles in inflow water settle down on to the biofilm during passing through the interstitial space, and are caught by the film. Resuspension of individual particles from the bed surface is very small due to the adhesive biofilm, while scraching-off of the film materials may occur with high friction stress on the bed surface.

2.2 Channel Type Contact Method

Various types of design are possible for biofilm treatment methods. Trickling filter and rotating disk contactor are the most typical for waste water treatment. Here, we chose a channel-type contact method with crushed stones inside. Water comes into one end of the channel and flows down among the stones along the channel to the other end. Biofilm is expected to develop naturally on the wet surface of the stones inside the channel. This method has an advantage of low cost for construction and maintenance because of its simplicity. Expecting saline ecosystem inside, simple design with environmental gradient is preferable and flexible for the fluctuation of the natural environmental conditions. As water treatment facilities for saline waste with low organic concentration like sea water, we have not enough experiences nor design criteria for any types of biofilm reactors yet. Applicability and efficiency of SS and organic removal of the channel type facility were unknown for coastal water. As it is difficult to scale up from a small size model to a prototype facility for the biological processes, large scale channels with natural sea water are preferable for designing research.

3. EXPERIMENT FACILITIES

3.1 Experiment Channels

Experimental yard and channels were located beside a small waterway of inner bottom end of Tokyo Bay as shown in Fig.-1. Six channels with 30m long x 1m wide x 1.3m high were constructed in parallel. Crushed stones were filled up to 1.2m high in each channel. Coastal water was taken from the waterway by a submerged pump and introduced to the entrance pit of each channel through a flow regulator. Water flowed down inside the stone layer. Water surface of the flow was beneath the top of the stone layer. Shading sheets covered the channels to prevent stones from being exposed to the sunlight. Effluent from each channel was returned back to the waterway again.
At every entrance pit, aeration was made by an air compressor to improve DO concentration. Water in only the channel #6 received aeration during flowing down.

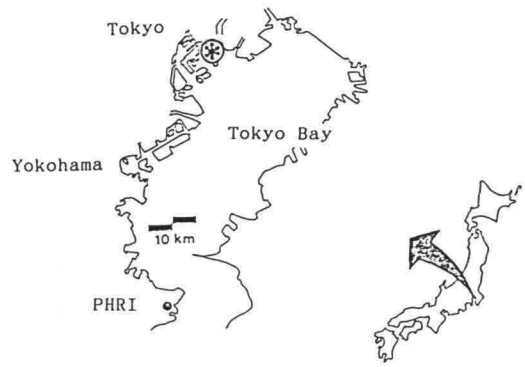

Fig.-1 Location of experiment channels

3.2 Experiment Cases and Seasons

Different set of stone size and flow velocity was applied to each channel. Mean diameter of filled stones, porosity, water discharge and hydraulic retention time(HRT) were listed in Table-1. Difference of the conditions between channels #1 and #6 was aeration during the flow. Hydraulic retention time of one hour for 30m long is equivalent to the current of 0.8 cm/s (= 3000cm/3600s). Taking the stone diameter as representative length, Reynolds' number of the interstitial flow is in the order of 10^2 to 10^3.

Table-1 Experiment cases

channel	1	2	3	4	5	6
stone media						
diameter(mm)	100-150	100-150	100-150	40-80	20-30	100-150
d50 (mm)	113.0	113.0	113.0	42.2	24.6	113.0
relative surface(m^2/m^3)	31.7	31.7	31.7	53.8	216.	31.7
porosity of clean bed(-)	.487	.487	.487	.466	.459	.487
flow rate(m^3/hr)						
Oct'90-Feb'91	3.0	6.1	11.0	5.6	5.8	3.0
Feb'91-Oct'91	3.8	7.6	15.5	7.0	6.9	3.8
hydraulic retention time(hr)						
Oct'90-Feb'91	5.0	2.5	1.4	2.6	2.4	5.0
Feb'91-Oct'91	4.0	2.0	1.0	2.0	2.0	4.0
line aeration	none	none	none	none	none	done
washing stones	none	Apr.'91	Apr.'91	Apr.'91	Apr.'91	none

Channel experiments were started from September 3, 1990. For the first one month, hydraulic characteristics was checked. During this month, water was supplied only when the experiments were conducted. From October 1 on, treatment experiment was conducted with continuous flow for thirteen months until October 18, 1991. On April 16 and 17, 1991, in the middle of the continuous flowing, stones in the channels #2,3,4 and 5 were washed by sea water and attached excess solids were removed for the recovery of easier water flow.

More over, on June 27,1991, stones at the entrance two meters (0-2m) in channels #4 and 5 only were replaced to new stones with equivalent diameter due to heavy clogging by attached bivalves.

3.3 Observation

Fig.-2 shows the conceptual arrangement of sampling pits for water and stones. Water quality such as Suspended Solids(SS), Total Organic Carbon(TOC), Chemical Oxygen Demand(COD), Dissolved Oxygen(DO), Transparency, Water Temperature and Salinity were monitored as well as Water Discharge(Q). Water samples were taken at sampling pits including influent head-pit and effluent end-pit. Observations were made 1-3 days a week from October 1990 to October 1991. Samples were taken from two channels per every observation day. So, three observation days were necessary for sampling from all six channels. Inflow water was taken at ten o'clock in the morning. After that, water was sampled at each sampling pit at the moment equivalent to the traveling time from 10:00.

Biological monitoring was made almost once every two months. Attached microalgae, microanimals and sessile as well as biofilm were observed on stone samples. Numbers of species and individuals were counted.

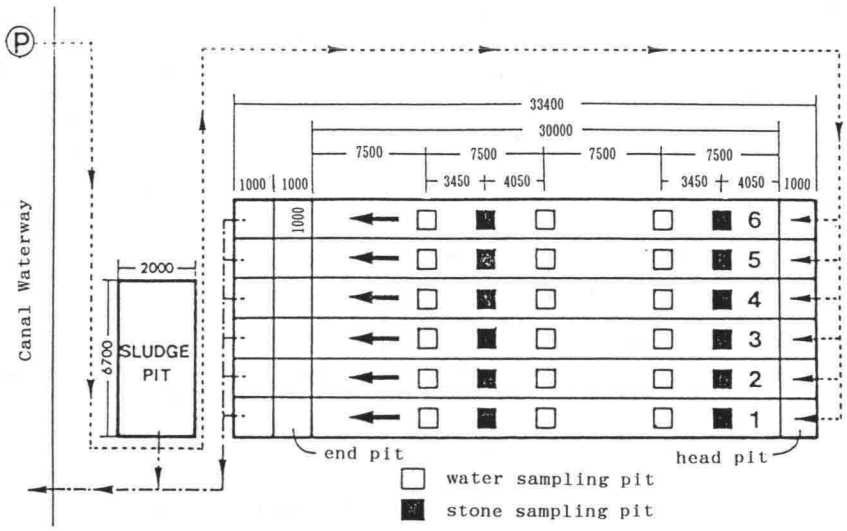

Fig.-2 Conceptual diagram of six channels and sampling pits arrangement (unit:mm)

3.4 Associated Experiments and Supplemental Observation

Hydraulic measurements for the initial condition were conducted prior to the full-year continuous monitoring. Porosity, water surface gradient along the channel, mass transport velocity and horizontal diffusibility by the tracer experiment were measured. Besides the regular monitoring for water quality, biofilm condition and flow resistance were measured when necessary. When clogging was evident in spring, supplemental observation was made for the flow resistance and attached bivalves. After the regular monitoring was over in

October 1991, a settling experiment was made using Kaolin particles as tracers.

4. OBSERVATION RESULTS

4.1 Hydraulic Characteristics

Porosity in the layer of media stones was estimated by counting the volume of filled water inside each channel. Results are already shown in Table-1. Hydraulic gradient and permeability (transmission coefficient) were observed for media stones of each size for flow ranging from such relatively slow as applied to the channel experiment up to fast flow within the water surface inside the stone layer. Obtained permeability ranged 5-20 cm/s for bare stones without biofilm. Even for the shortest HRT case of channel #3, water surface gradient was observed as less than 0.001 (several centimeters for 30m of the channel length).

Using the porosity, we can guess the flow velocity inside the stone layer. This velocity could be compared with mass transport velocity by the result of a tracer experiment. Mass transport velocity was observed using sodium chloride (NaCl) as a tracer. Electric conductivity was monitored at two layers in each sampling pit for two times longer period than HRT from the injection. Though there happened some troubles like density stratification of initial flow after the instantaneous dumping of tracer, mass transport velocity was very close to the calculated hydraulic velocity. Horizontal diffusibility was also estimated by the first-order moment method to the monitoring data and estimated as the order of 10^1 cm^2/s.

4.2 Water Quality of Inflow Water

Water quality of original inflow ranged 10-25 $\%_0$ for salinity, 1-15 mg/l for SS and 3-7 mg/l for COD. The relatively low salinity suggests that this waterway receives fresh water discharge from the land area. High SS concentration was sometimes observed after a strong storm. COD changed as high as 6-7mg/l in summer (June - August) and low in late autumn. This fluctuation along with high concentration of nutrients (annual mean: T-N 6mg/l, T-P 0.4mg/l) indicates that the waterway is eutrophic. Chlorophyll-a reached as high as 7-34 mg/m^3 in spring and summer.

4.3 Biofilm Development and Attached Fauna and Flora

a)Biofilm development
Biofilm attached within a month and developed for a few months (Hosokawa et al., 1992). The color of the biofilm indicated the degree of assimilation activity.

Observed color was usually light brownish, which showed a rather small load of organics. Temporal change of collected dry mass (SS) on the unit surface is shown in Fig.-3 for channels #1,3 and 6(Mouri et al., 1993). Stones in the 4m-pit near the entrance were always covered with larger mass than that in the 19m-pit behind. In channel #1, attached mass became larger up to $75g/m^2$ until June, 1991. Then, the dry mass were suddenly dropped down in the next three months. Contrary to this channel, channel #3 with short HRT and high inflow lord reached the maximum dry weight of over $150g/m^2$ within four

months of operation and dropped down to the stable mass of around 50g/m^2. It means that earlier and larger development was observed for the higher inflow load condition. Between the dry mass in channels #1 and 6, observed mass was relatively smaller in channel #6. Attached dry mass fluctuated within the range of 10-50g/m^2 for channel #6 and 10-75g/m^2 for channel #1. Aeration effect to the biofilm growth was not significant for this experiment condition.

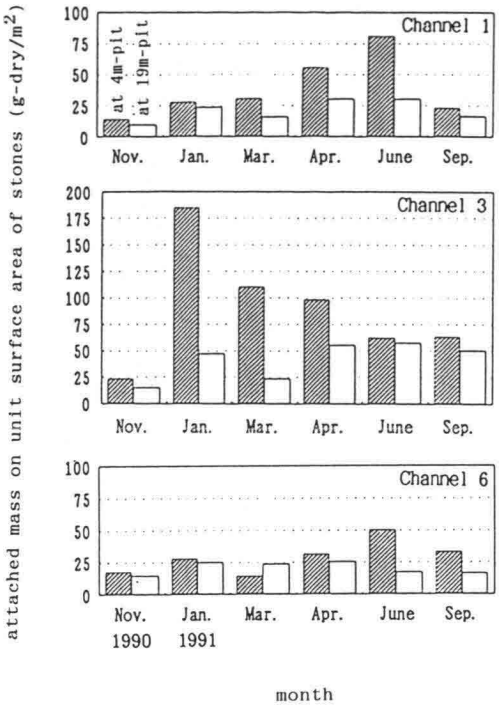

Fig.-3 Temporal changes of attached dry mass on unit surface of stone media

b)Biofilm components
Collected biofilm was examined for 1).VSS per unit volume of stone media, 2).organic component ratio in unit dry weight (VSS/SS), and 3).DO uptake rate (r_r). Results are summarized on Table-2. At the initial stage of November,1990, though VSS/SS ratio was low due to the low organic load at the initial stage, r_r per unit VSS weight was estimated as high as that of facilities for waste treatment. At this stage, biofilm was developed with high activity among large amount of inorganic particles settled. After a half year elapsed, in March, VSS/SS ratio grew up to 30-40%, and 30-60% in September. This ratio is close to that observed on the bottom bed or flat plates in eutrophic rivers(Nakamura et al.,1990).

c)Attached fauna and flora
For attached microalgae, diatoms such as Aphanotheca sp. and Skeletonema sp. were dominant species. All dominant species are marine inhabiting. Density was not large due to the light shadowing.

Table-2 Attached biomass and DO consumption rate at 20 ^{o}C

channel	sampling pit(m) /days	VSS in unit volume (kg/m^3) 31	184	337	VSS/SS ratio 31	184	337	oxygen uptake rate r_r(mg/l/hr/g) 31	184	337
#1	4	.11	1.44	1.51	.13	.40	.50	65.1	19.0	8.5
	19	-	.80	1.80	-	.43	.58	-	9.5	3.1
#2	4	-	1.76	2.67	-	.31	.45	-	13.0	4.4
	19	-	1.09	3.01	-	.34	.27	-	8.1	.9
#3	3	.17	1.94	2.09	.17	.35	.61	53.7	15.1	13.9
	18	-	1.32	2.57	-	.35	.36	-	39.3	9.6
#4	4	.40	2.13	4.00	.11	.30	.58	14.3	15.5	2.7
	19	-	1.33	1.67	-	.19	.32	-	7.9	7.8
#5	4	.24	4.63	NA	.10	.34	NA	32.3	6.8	NA
	19	-	3.27	NA	-	.08	NA	-	7.5	NA
#6	4	.07	.81	1.02	.22	.37	.98	73.4	8.4	4.0
	19	-	.54	.70	-	.41	.73	-	8.2	4.3

A total of 36 species of microanimals in Protozoa and Metazoa were observed in the attached biofilm during the experimental thirteen months(Suda et al., 1994). In November, Carchesium sp. was dominant among 1771 N/cm^2, and then Vorticella sp. took after the dominant specie for the total number of individuals 5115 N/cm^2 in January. These two species are well known as dominant species in biofilm facilities for fresh water. In March, among the similar number density (4929 N/cm^2) as that in January, Zoothamnium sp. became dominant. In June, total individual number decreased rapidly to 1479 N/cm^2 and the dominant specie was Peritrichida sp. Rapid succession was observed in the channels for one year. As for the spatial distribution in one channel, microanimals were always larger in number in the head part (at 4-m pit) than that in the lower part (at 19-m pit). Among the channels #1,2 and 3, highest number was observed at the maximum discharged channel #3. Not so significant difference was seen among the channels with different stone sizes nor between the channels with and without aeration.

Large size sessile and benthic animals of marine species were found in the biofilm and spaces among stones. Those were Neanthes japonica, Serpulidae sp., Ficopomatus enigmaticus, Mytilus edulis and others. These animals are expected to consume organic particles or biofilm materials and to reduce the total volume of the accumulated sludge.

In the flowing water, one marine diatom named Skeletonema costatum was dominant as the concentration order of 10^3 cells/ml whole through one year.

4.4 Water Quality Improvement

Fig.s-4 and -5 are plotted from the data obtained after the first 31 days' operation. SS concentration and turbidity decreased along the channel flow as seen in Fig.-4. In this figure, SS and turbidity is expressed as relative turbidity based on the inflow concentration (C_0). Transparency was also improved along the flow. Removal of turbid particles is clear. An example is shown in Fig.-5 for the change of the diameter distribution of suspended solids along the flow. We can see that larger particles were removed fast and mean diameter shifted to the smaller size as water traveled along the channel.

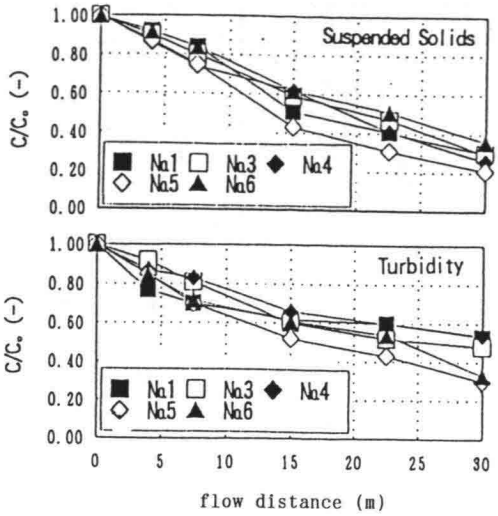

Fig.-4 Change of relative SS and turbidity along the channel

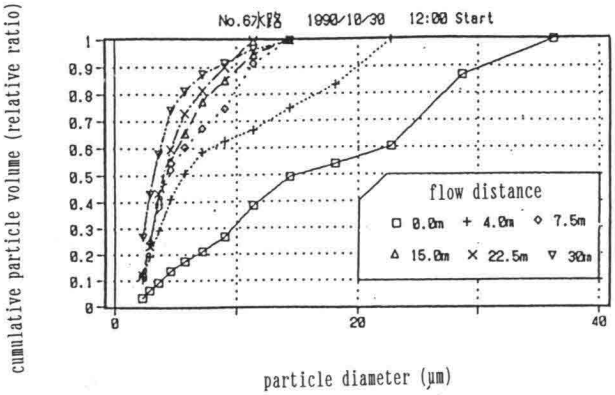

Fig.-5 An example of change of diameter distribution of suspended solids along the channel flow (channel #6)

Monthly change of SS concentration is shown in Fig.-6 for each channel. Channel #5 stopped receiving water after August 20,1991 due to heavy clogging. Though the inflow concentration fluctuate widely, effluent was clean to maintain almost below 2mg/l of SS. High transparency was obtained.

4.5 Oxygen Uptake and DO Deficit

A typical DO profile in the channel is shown in Fig.-7 after one month's operation. Sudden drop of DO at the first 5m occurred due to active DO uptake by attached fresh biofilm. Contribution of inflow water itself to DO uptake was very small. Channel #5 with the smallest stones showed the fastest decrease of DO concentration among the channels #2,4 and 5 of the similar HRT. Effluent from each channel, except channel #6, always showed low DO.

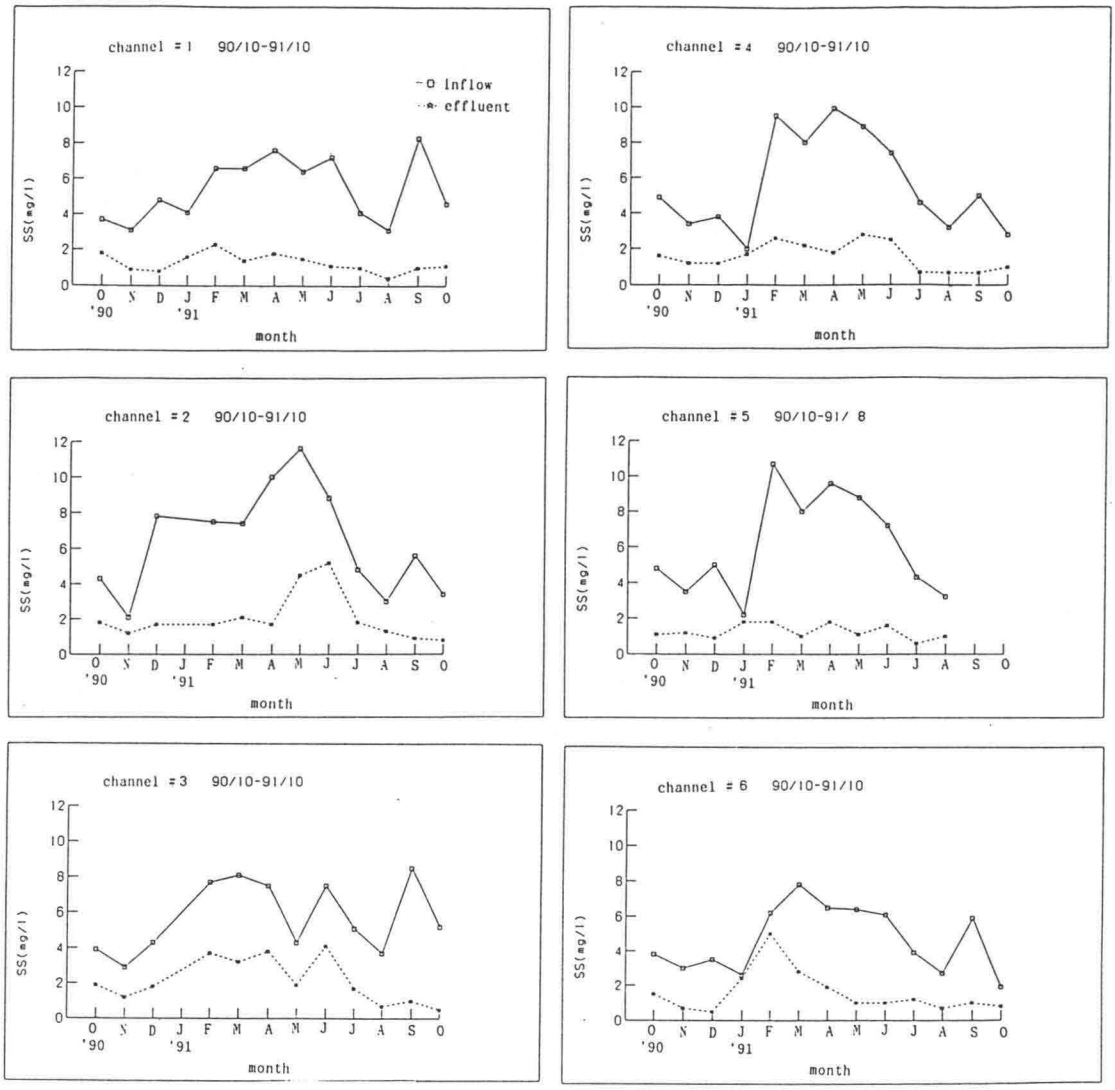

Fig.-6 Monthly fluctuation of SS concentration in inflow and effluent water (SS at head & end pits is averaged for each month. As observation dates were different, mean inflow concentration is slightly different among channels.)

Using detailed DO profile in Fig.-7 and oxygen uptake rate(r_r) in Table-2, VSS in unit volume of each channel can be estimated. Calculated results are presented in Fig.-8 (Hosokawa et al.,1992). Applying observation data of VSS/SS ratio, stocked volume of total solid (VSS+SS) can also be evaluated assuming relative weight of VSS as 1.1 and SS as 2.1. The lower part in Fig.-8 expresses longitudinal distribution along each channel. Biofilm (VSS) started developing from the entrance section within the first one month. Solids (VSS+SS) were also accumulated from the entrance section for all channels except channel #6. In channel #6, solids were held evenly in all sections along the flow due probably to the internal mixture by aeration.

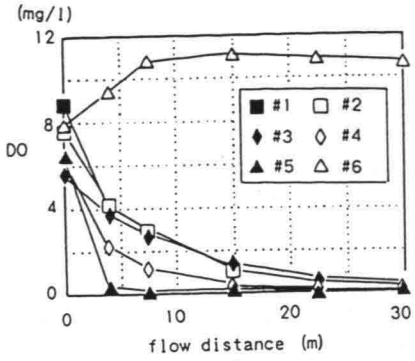

Fig.-7 DO profile along channel in November after one month's operation

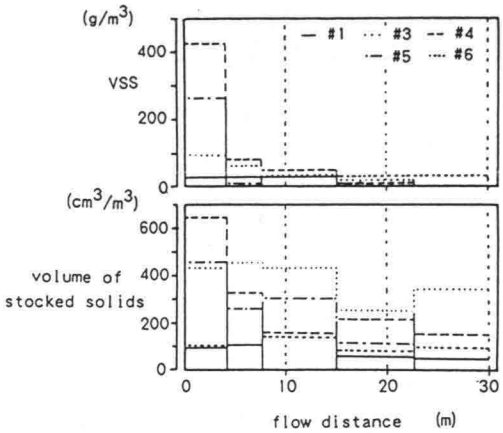

Fig.-8 Developed biofilm(VSS) in unit volume of each channel (unit:g/m^3) and longitudinal distribution of stocked solids (unit:cm^3/m^3) after one month

4.6 SS and Organic Removal Rate and Mass Flux

Product of 'flow discharge rate' and 'inflow concentration' gives an inflow loading rate at the influent pit of each channel. Integration of this loading rate for a certain observation time period gives total loading weight of a contaminant. If we apply the effluent concentration in stead of the inflow concentration, then we can get total effluent weight which expresses the mass weight of a contaminant flowing out from the channel effluent pit. Ratio 'total effluent weight' over 'total loading weight' for a certain duration is defined here as passing rate. Unity (1) minus passing rate gives removal rate. This removal rate indicates overall efficiency of water quality improvement for the large scale experiment with some fluctuation of both flow rate and initial concentration.

For the appropriate temporal integration, total observation duration can be divided into three stages, those are, the first 'developing stage' from Oct. to Jan., the next 'cool season' from Feb. to May, and the final 'warm season' from Jun. to Oct. Calculation results for SS and COD are plotted separately.

Removal rate of SS for each channel is shown in Fig.-9. It became larger up to 60-90% after 50-70% of the initial development stage. On the other hand, removal rate of COD can be seen in Fig.-10 as 5-10% at the initial period and 15-30% after the biofilm development. Particle components were removed effectively.

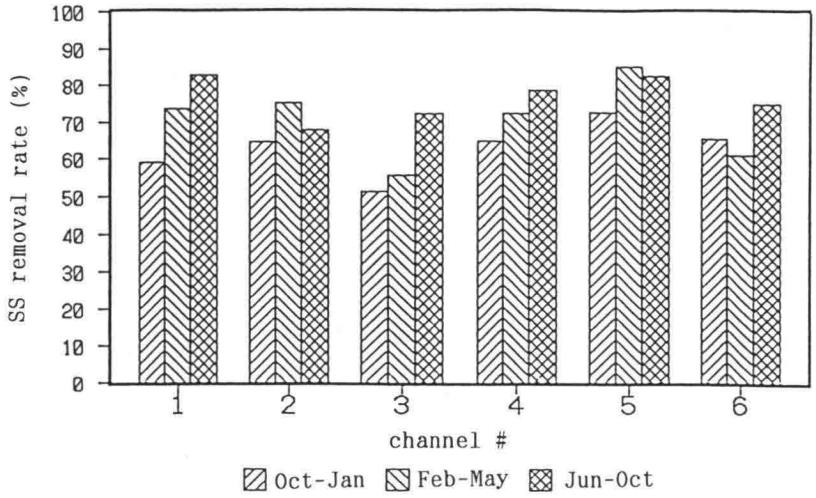

Fig.-9 Removal rate of SS at each channel

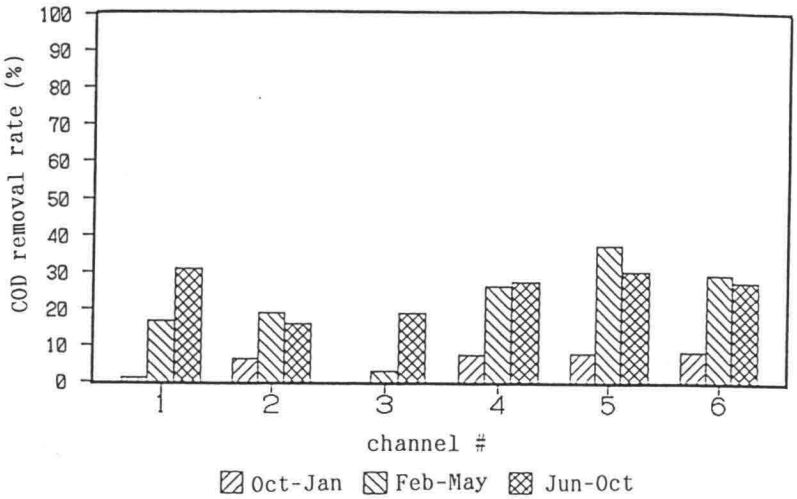

Fig.-10 Removal rate of COD at each channel

Fig.-9 also suggests that removal rate is altered by media size and HRT. For the same size of contact stones in the channels #1,2 and 3, removal rate of channel #1 was higher and stable. Hydraulic retention time of channel #1 was set as around 4 hours, the longest among the three. Similar tendency can be seen for COD removal in Fig.-10. Among the channels #2,4 and 5 for the same HRT of 2 hours, channel #5 always removed SS and COD most effectively. Channel #5 held the smallest stones inside. Removal rates decrease as the increase of the stone size. Aeration effect was not significant between channels #1 and 6 for SS and COD removal. Within the assigned experimental conditions, we can

guess that a channel with slower flow among narrower space gives higher removal rate of particles and organics.

For the water quality improvement of natural water surface, channel contactors are expected to remove larger amount of mass weight of pollutants efficiently from the water area for a certain time period. Removed mass is another important index for the facility evaluation. Difference between 'total loading weight' and 'total effluent weight' was calculated as 'total removed mass weight' for each channel. Fig.-11 shows total inflow mass and removed mass of SS. Mass weight of inflow was almost proportional to the water discharge rate, though the daily fluctuation of inflow SS concentration was large. Among the channels, channel #3 received largest mass weight of SS (700kg in 13 months) and removed largest mass(400kg for 13 months). Removal rate of this channel was lowest among the six channels but maintained 50-70% still, as seen in Fig.-9. In spite of receiving four times (x4) larger flow rate than the smallest one of the channel #1, channel #3 kept high removal rate, much higher than one quarter (1/4) of that of channel #1 (60-85%). Almost 30-40kg of SS were removed every month by channel #3, while 10kg/month by channel #1. In the first half year until spring, channel #5 with smallest media stones also showed high removal mass flux of 20kg/month. But this channel started clogging in late spring to decrease removal efficiency and increase flow resistance. Within the range of the experimental conditions, the channel of the shortest HRT with large stones maintained highest mass weight of SS removal.

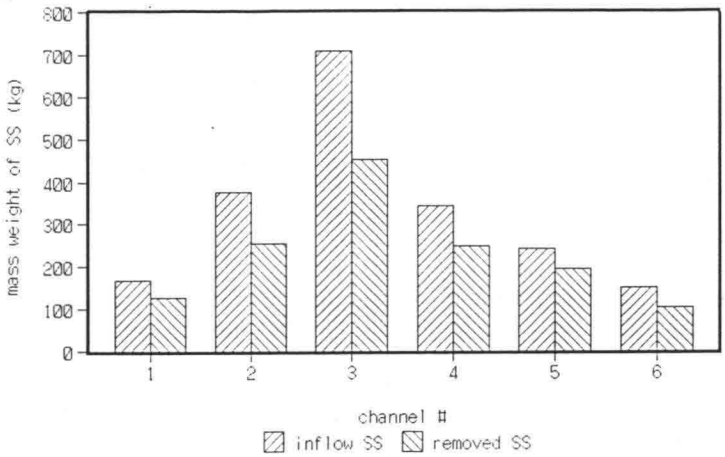

Fig.-11 Mass weight of inflow and removal of SS
(Weight for channel #5 is the integration result for 8.5 months until June.)

4.7 Flow Resistance and Clogging

Clogging can be detected by the change of hydraulic gradient. Two types of clogging were observed during the experiment. One was the clogging by separated biofilm from stone surface, and the other by the dense attach and growth of bivalves in spring and early summer.

a)Clogging by separated film
As the particles removed from flowing water and accumulated on the surface of stones, films became thick and easy to be separated by the stress of water

flow. After 60-80 days of operation, higher SS concentration was sometimes observed at latter pit than SS at the entrance. SS profile of averaged concentration over five months from Dec. 1990 to Apr. 1991 is shown in Fig.-12 for channels #1,#2,#3 and #6 with the largest size of media stones. Considering the SS removal along the flow as seen in Fig.-4 and the longitudinal distribution of captured solid mass shown in Fig.-8, we can guess that film develops its thickness from the front part of channel and that thick film at the front part is easy to peel off from stones into the flow. This high SS concentration at 7.5m pit in channel #3 can be considered as 'self-turbidity' due to the separation and resuspension of film sludge from the stone surface.

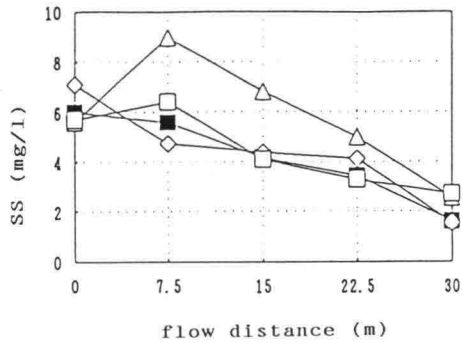

Fig.-12 SS profile of averaged concentration for five months (December, 1990 - April, 1991)

Accumulated solid mass of removed SS for 192 days (from Oct.'90 to Apr. '91) is shown in Fig.-13 for channels #1,#2,#3 and #6 of the same stone size. Among them, channel #3 removed and captured over 180kg of solids and is expected to receive the separation effect heavily inside the channel due to the fastest current. Hydraulic gradient profiles on the 192nd day (Apr. 1991) can be seen in Fig.-14 for the same four channels. Maximum gradient is found downward as removed mass in the channel becomes larger(channel #1 < #2 < #3). That is, clogging was significant at the latter part in channel #3 with highest inflow load, while max. gradient at the entrance part in channel #1. Flow resistance can be converted into the occupied volume of the clogging solids under the assumption of the relation of Fair-Hatch equation between hydraulic gradient and apparent diameter. Maximum gradient value in each channel on the figure is estimated as -50% occupation of the open space among the stones. Removed solid mass in channels #1 and #6 is similar as shown in Fig.-14, but hydraulic gradient in channel #1 was higher at every part than that in channel #6. All these results suggest that:

1). separation of film will easily occur as it becomes thicker after the accumulation of solids on the stone surface,

2). after separation, solid film body will be resuspended and transported by the flow towards the downward, but as film body is larger and bulky than the inflow SS, it is easily caught inside the stone layer again,

3). recaptured film body will interfere the flow and clog the open space among stones, and

4). this separation and recapture cycle will bring the clogging point downward along the flow.

Aeration in the channel along the flow contributes to the resuspension and dispersion of film and to less clogging. After one year operation on 344th

day, hydraulic gradient values at some points decreased than those on 192nd day. In channel #1, all the hydraulic gradient on Sep. 1991 (after 344 days of operation) became lower than the data on Apr. 1991. Local mass of the clogging solids, and so is the local hydraulic gradient, is thought to be influenced by the combination of following processes;
1). accumulation of settling solids from inflow water onto the surface film,
2).separation of film solids, and
3).re-accumulation and re-separation of the separated materials, as well as
4).biological digestion and utilization of the accumulated organics.

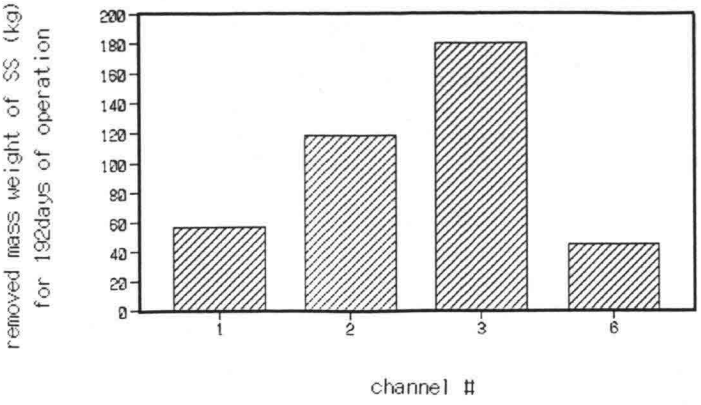

Fig.-13 Total accumulated mass of removed solids in channels #1,2,3 and 6 after 192 days operation (unit:kg)

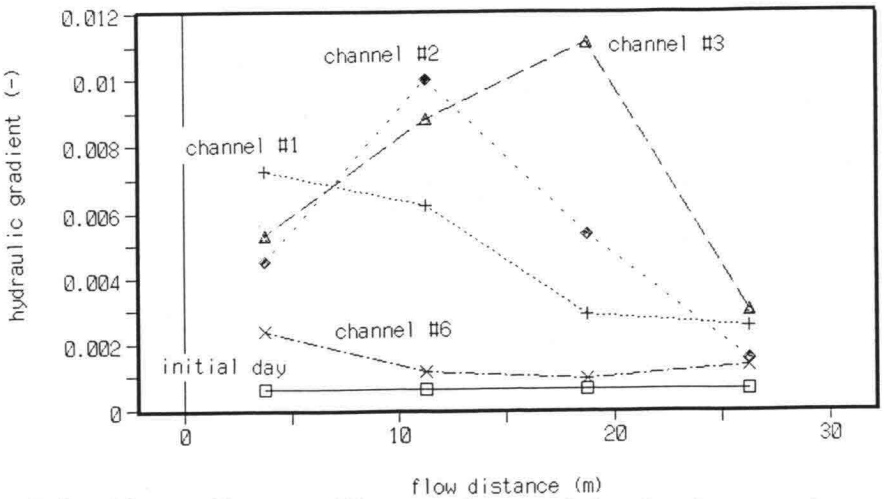

Fig.-14 Hydraulic gradient profiles on the 192nd day in channels #1,2,3 and 6

b)Clogging by bivalves
In June 1991, water surface in channel #4 and #5 was found to rise extremely over the top of the stone layer near the entrance. On the surface of stones near the head pit and on the flow-regulation wall of the head pit, dense mussels (Mytilus edulis), rock barnacles and worms were observed. Shell

length of Mytilus was 4-22mm. Mussels attached to stones or other shells firmly by their strong threads with sludges. We could not remove them by normal washing by aeration nor water flushing. So, media stones of these two channels were replaced by new ones for 0-2m section on June 27, 1991. After this replacement, mussels started attaching again on the new stones at the entrance section. Hydraulic gradient after 42 days from the replacement is presented in Fig.-15 for the heading 0-12m of the two channels. In this figure, hydraulic gradient on the restarting day of operation (Jun. 28, '91) is plotted together. Gradient is calculated by the difference of water surface elevation between neighboring two pits. Gradient data are plotted against the center of the observed two pits in the figure. We can easily understand that clogging by attached mussels for 42 days in this season gave far more impact to the transmissibility of water flow than those by the separated biofilm for a half year's operation as shown in Fig.-14. Clogging by mussels was significant for the entrance area within 0-3m. Flow was interfered more severely in the channel #5 with smallest stones. If a channel facility of this type is planned to operate for years for eutrophic coastal water, size of media stones should not be smaller than that for channel #1.

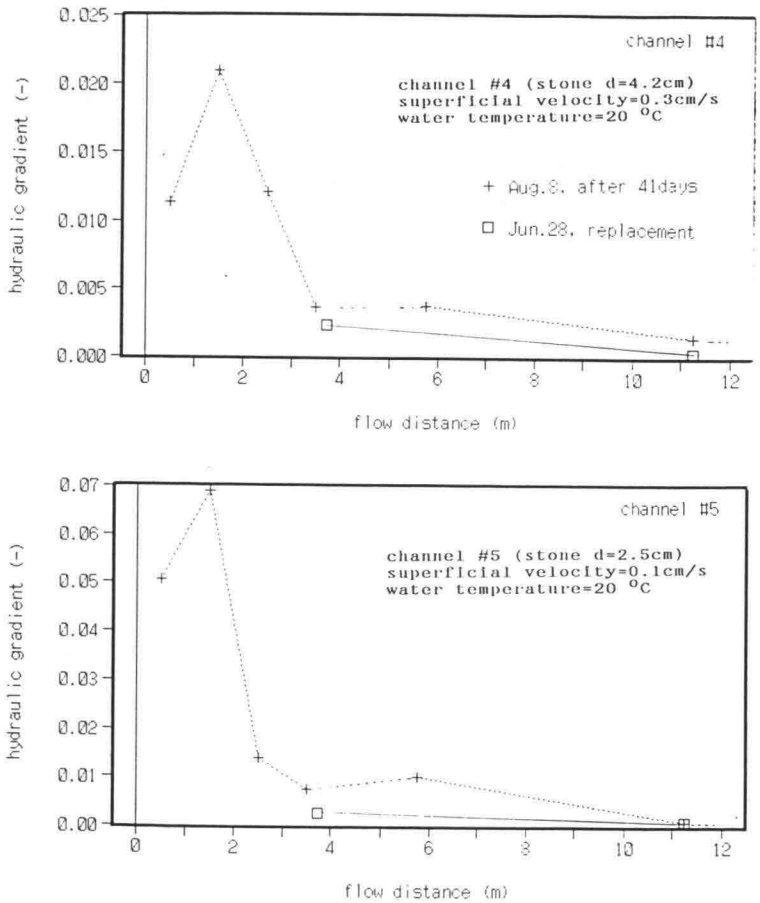

Fig.-15 Distribution of hydraulic gradient at the entrance section (clogging effect by attached bivalves)

4.8 Other Indices

Removal of the bacteria was observed significantly high (around 90%). E.Coliform and chlorophyll were also removed effectively. Though particulate phosphorous was removed with SS, nitrification and denitrification were not significant without aeration for these HRT conditions.

4.9 Apparatus Settling Depth

Solid removal in the stone layer was dominantly driven by settling and filtration as well as biological effects. For the settling tank analysis, tracer experiment is often applied with particles of known settling velocity as tracers. Here, we conducted a removal experiment with Kaolin as a tracer in Sep. 1991. The same flow rate of $13m^3/m$ was selected for every channel as the experiment condition. Channel #5 could not be used due to heavy clogging. Assigning the settling velocity distribution of Kaolin particles, apparatus settling depth among media stones was estimated by the data of travel time and removed rate at observation points (head pit, pits at 4m,7.5m, 15m and 22.5m). This analysis is based on the assumption of the ideal settling tank model. A typical example of temporal change of tracer concentration at each observation pit is shown in Fig.-16. Calculated results for apparatus settling depth are tabulated in Table-3. The apparatus settling depth obtained is ranging between similar to the diameter of media stones and one-quarter(1/4) of it. These results of settling depth is thought to be the reasonable order of magnitude but a little smaller than the actual physical opening. Filtration and biological uptake may contribute to the removal of Kaolin tracers other than settling mechanism.

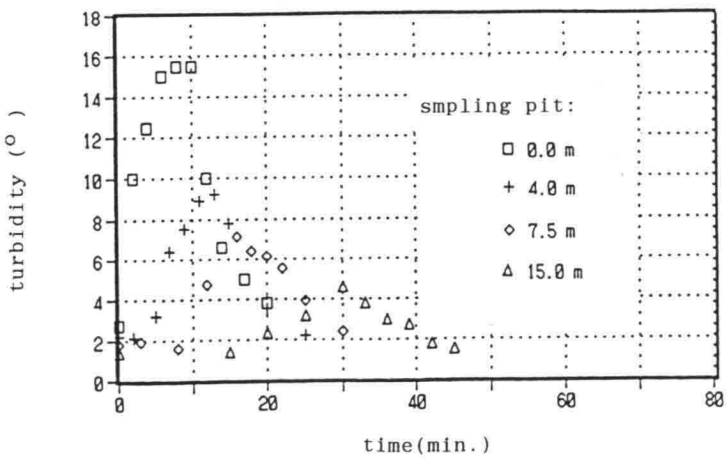

Fig.-16 A typical example of temporal change of Kaolin concentration at each observation pit (case for channel #1)

Table-3 Apparatus settling depth caluculated from Kaolin experiments

channel	d50 (cm)	SS passing weight (g) head-pit	4m-pit	7.5m-pit	overflow rate(mm/s) 0-4m	0-7.5m	settling depth(cm) 0-4m	0-7.5m
#1	11.3	72.9	38.2	33.1	.079	.054	10	12
#2	11.3	73.8	27.0	17.1	.034	.016	4	4
#3	11.3	37.6	10.2	7.1	.02	.013	3	3
#4	4.2	63.1	18.7	13.0	.023	.014	3	3
#6	11.3	72.9	40.2	34.0	.092	.058	12	13

Experiments were made at the constant flow rate of 13.2m^3/hr for all channels.

5.DESIGNING PROCEDURES

5.1 Surface Loading

As seen in the previous section, removal of suspended solids is effectively conducted in the stone layer of the channels. Surface load is defined as the inflow load per unit surface area of the stones per a day. This index expresses the strength of load on the unit film area. Biofilm is said to regulate its own biomass by depending on its food source. Biofilm develops its biomass by rapid uptake of organics, if organic load to the unit film increases. This smooth response makes it possible to maintain high removal rate against load fluctuation. But, overall removal rate will decrease when biofilm receives excess load over its adaptability. Relationships between surface load vs removal rate are presented in Fig.-17 for SS and Fig.-18 for COD. For SS, surface load over 1g/m^2/d makes the removal rate decrease. Surface load exceeding 0.5g/m^2/d for COD makes the removal rate down. These numbers may be one of the critical values for designing sound biofilm development though our experimental conditions were limited.

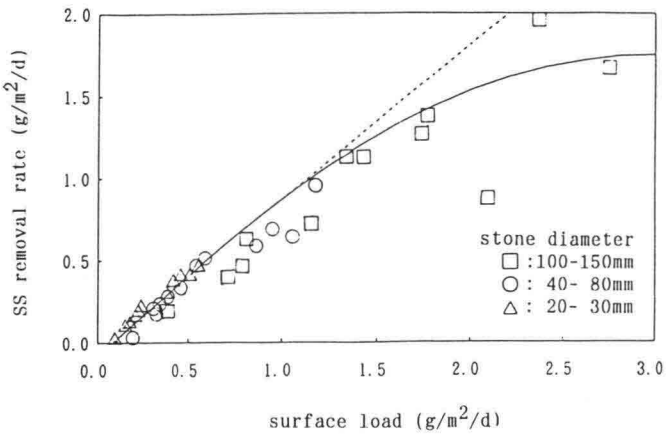

Fig.-17 Relation between surface load and removal rate for SS

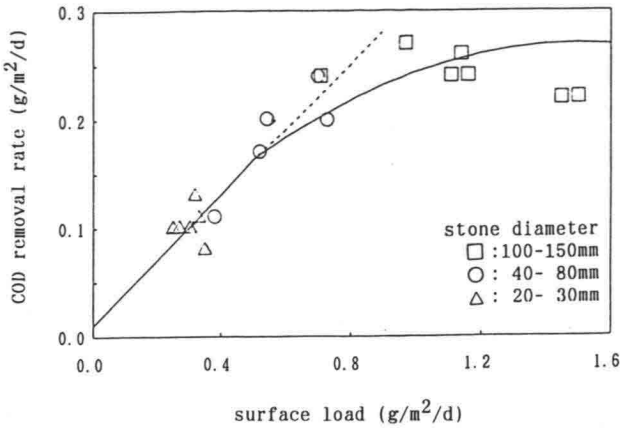

Fig.-18 Relation between surface load and removal rate for COD

5.2 Retention Time Requirement

Shorter hydraulic retention time with high flow rate decreases the removal rate of SS and organics. But, so long as this decrease is not so large comparing to the increase of flow rate, removed mass per unit time increases. At the extreme condition of zero hours for retention time, removed mass is expected to be none. Removal rate vs retention time is plotted on Fig.-19 for spring data (Feb. 1991 to May 1991) and on Fig.-20 for summer data (Jun. 1991 to Oct. 1991). Plotted data are for channels with largest stones. High removal rate even for short HRT can be recognized in Fig.-20, which might be partially due to the fluctuation of both solids size (settling velocity) and concentration of inflow SS by a summer storm. Within the range of 1 to 5 hours HRT in both figures, we cannot find a critical value below which removal rate and removal mass are both dropped. Within this range, shortest retention time is preferable so long as no interferences occur for the treatment and the management. More than one hour might be preferable for HRT.

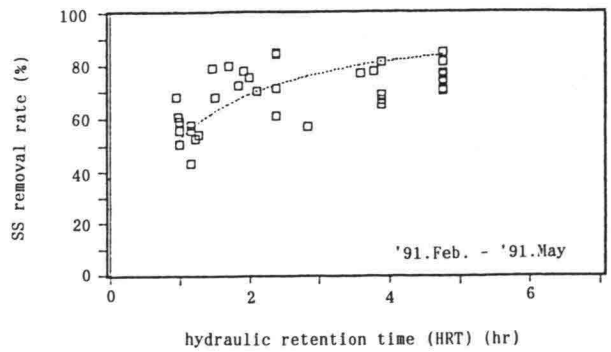

Fig.-19 Relation between removal rate vs retention time for spring data (Feb. 1991 to May 1991)

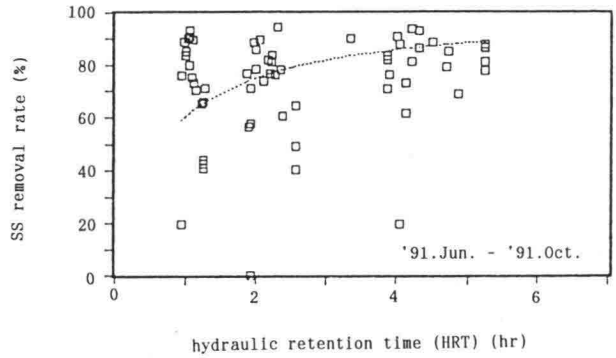

Fig.-20 Relation between removal rate vs retention time for summer data (Jun. 1991 to Oct. 1991)

5.3 Necessary Considerations

For the prevention of clogging by attached bivalves, larger media like rocks might be effective for the first few meters from the entrance head pit. If clogging by resuspension solids is expected, longer length is necessary to compensate self turbidity by the detachment and to maintain the required removal rate. Operation experience of channel #1 for larger stones suggests that moderate flow rate with lower organic load gives long life of its removal ability without clogging nor washing. We could not yet analyze the critical friction stress which makes surface film peel off, nor size distribution of resuspended film. Effluent from the channel facility requires the recovery of dissolved oxygen concentration. End pits gave some contribution to the hydraulic aeration for the effluent. Necessary capacity of aeration for DO recovery is not evaluated yet. Problems of offensive odor did not occur during the channel experiment for one year.

5.4 Design Procedure

Recommended design procedure is proposed as follows:
First, assign inflow concentration and required removal mass of pollutants. Then, flow discharge rate and removal rate are decided. Necessary retention time is estimated from the removal rate.
Select media materials of proper diameter.
Then, necessary volume of the stone layer can be calculated by the required surface load.
Assuming a set of dimension (length x width x depth) of the stone layer and the channel, we can evaluate cross-sectional velocity of flow. Applying this velocity, we can check retention time and head loss. Necessary initial water head is compared with the dimension assumed.
Details for the entrance and end of the channel is designed.

6.CONCLUSIONS

Large scale channels were used for the experiment on coastal water purification. After one year's operation, followings are understood:
a). Even for saline coastal water with lower organic concentration than that

in waste water or effluent from waste water treatment plants, biofilm was developed on the surface of stones.
b). Organic particles were effectively removed by settling and biological uptake. SS was removed well by 60-90% after the film development, though the removal rate for COD was 15-30%.
c). Effluent became clearer with longer HRT and smaller stone size, while the maximum removal mass was obtained for the highest hydraulic loading ($12m^3/h$).
d). Permeability ranged between 5-20 cm/s for initial bare stones. The inclination of water surface was a good index for the detection of clogging which were developed among stones by the accumulation of resuspended film sludge. For small stone media below 10cm diameter, acute clogging by attaching bivalves in spring and summer gave fatal effect for water flow.
e). Maximum limits of the appropriate surface loading was estimated for SS and COD removal. Preferable values of such basic design parameters as HRT and stone size are proposed for the channel-type purification facility.

This channel experiment was conducted as a cooperative study between Port and Harbour Research Institute and Sea-Blue Technology Research association. The association consisted of the following 17 private companies; Daito Kogyo Co. Ltd., Fudogikenn Co., Ltd., Fujita Corporation, Honma Corporation, Kumagai Gumi Co., Ltd., Kurita Water Industries Ltd., Mitsui Harbour and Urban Construction Co., Ltd., Obayashi Corporation, Penta Ocean Construction Co. Ltd., Rinkai Construction Co. Ltd., Saeki Kensetsu Kogyo Co. Ltd., Shimizu Construction, Taiyo Kogyo Corporation, Takenaka Civil Eng. & Construction Co. Ltd., Toa Corporation, Toyo Construction Co. Ltd., and Wakachiku Construction Co. Ltd. The authors express their sincere appreciation for kind arrangements of PHRI and for the enthusiastic participation of the member companies. The authors also appreciate Dr. Horie , Director of Marine Hydraulic Division, PHRI for his advises. Some parts of the research results have already presented to academic journals. The authors appreciate IAWQ and Pergamon Press for the reprint permission of two figures from Water Science and Technology, and Japan Society on Water Environment for the reprint approval from its Journal.

REFERENCES

Harris,V.A.(1990):Sessile Animals of the Sea Shore, Chapman and Hall,vii+379p.

Hashimoto, K. and Y.Teranishi (1988): Water purification by attached film in channels, Jour. Japan Sewage Works Assoc., 25(285), 41-52. (in Japanese)

Hosokawa,Y., T.Ootsuki and C.Niwa(1992): Channel experiments on coastal water purification by porous bed using crushed stones, Wat. Sci. Tech.,26(9-11), 2007-2010.

Inamori,Y., N.Hayashi, and R.Sudo(1990): Direct purification of polluted river water by channel type facility, Water & Waste Water, 32(8), 32-37. (in Japanese)

Mouri,M., Y.Suda, I.Uehara, N.Kadokura, Y.Tanaka and Y.Hosokawa(1993): Deposit ratio distribution and clogging in rock bed contact-purification channel, Jour. Japan Society on Water Environment,16(7), 516-525. (in Japanese)

Nakamura,E. and K.Sakai(1987): Water purification by rock-bed contact filtration, Civil Engineering, 29(10), 534-539. (in Japanese)

Suda Y., H.Hamabata and Y.Hosokawa (1994): The sea blue plan experiment of sea water purification by porous bed contact purification method, Proc. 15th US/Japan Experts Meeting on Management of Bottom Sediments Containing Toxic Substances, US Army Corps of Engineers, WES, Vicksburg. (in Press)

HYDRO-PORT'94
International Conference on Hydro-Technical
Engineering for Port and Harbor Construction
October 19 – 21, 1994, Yokosuka, Japan

Sand Covering for Improving Quality of Bottom Sediments in Japanese Harbors

Satoshi Inoue [1]
Takeshi Horie [2]
Kazuo Murakami [2]
Yasushi Hosokawa [2]
Seiji Sato [1]
Yasuhiro Sega [1]

[1] Ports and Harbours Bureau, Ministry of Transport
2-1-3, Kasumigaseki, Chiyoda-ku, Tokyo, 100
[2] Port and Harbour Research Institute, Ministry of Transport
3 Chome 1-1, Nagase, Yokosuka, Kanagawa, 239

ABSTRACT

This paper describes field measurement results of sand covering work to purify sea bottom sediments in Mikawa Bay, Japan. A great amount of nutrients are released from polluted sea bottom sediments. The nutrients cause eutrophication in enclosed coastal seas. In order to reduce the release rate of nutrient salts from the sediments, sand covering, that is the covering work over the organic bottom sediments with non-polluted sea sand, was conducted. The sand covering area was 150m in length, 100m in width and 0.5m in thickness. The sand covering showed favorable effects on improving sediment quality and recovering ecological condition for benthos.

Key Words: sand covering, polluted sediment, nutrient salt, benthos, water quality

1. INTRODUCTION

Water quality in enclosed seas is contaminated due to various causes such as oil spills, floating garbage, sewage discharge, etc. Great efforts have been paid on such measures as the advancement of sewage treatment systems and total pollution load regulation policy in major enclosed bays in Japan. Table 1 shows the outline of ports and marine environment improvement works administrated by the Ministry of Transport. Among them, main works are described briefly as follows:

- Waste Oil Disposal Work : The work constructs a facility for waste oil disposal. Since the establishment of this work in 1967, 81 port management bodies in Japan constructed the facilities by the work.
- Port Pollution Prevention Work : This work began at 1972 in Minamata Bay, where contaminated sediments with organic mercury were removed by dredging and reclaimed. At present, contaminated sediments in 52 ports have been dredged by the work.
- Marine Clean-Up Work : This work began at 1974. Several ships were constructed to collect floating garbage and spilling oils in coastal seas.
- Wide Area Reclamation Site Construction Work : A remarkable concentration of population and industry in coastal region causes several difficult problems. Among them, the most serious problem is the treatment of waste disposal produced from urban and industrial areas. In order to dispose these wastes, it is necessary to construct new reclamation lands with a area of 3120 hectares with a capacity of 410 million cubic meters.

Above mentioned works have been carried out by the Ministry of Transport to prevent water pollution and to conserve marine environment in Japan, whereas Marine Environmental Creating Work is recently introduced as the work to improve water quality. The Ministry of Transport carried out the pilot work of the sand covering in Mikawa Bay, and investigated the effect of the sand covering on bottom sediments quality, ecological conditions of benthos, etc.

2. WATER QUALITY IN MIKAWA BAY

Many works to conserve marine environment were carried out by several organizations. In spite of these efforts, however, the compliance ratio of the water quality standard in terms of COD (Chemical Oxygen Demand) is still low as shown in Figure 1. Several causes of sea water contamination are considered as follows:

- A large amount of sewage is discharged into these coastal seas from rivers, factories, farms, houses, etc.,
- Nutrient salts are released from contaminated bottom sediments, and
- internal production of phyto-plankton by photosynthesis.

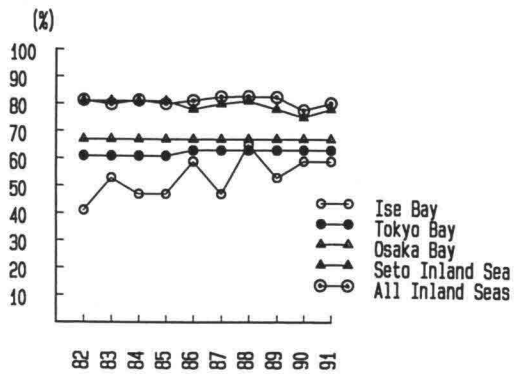

Fig.1 Compliance ratio of water quality standard in enclosed coastal seas in Japan.

Table 1 Outline of ports and marine environment improvement works administrated by the Ministry of Transport.

Classification	Item	Beginning	Outline of the Work
1. Prevent Pollution in the Port	Port Pollution Prevention Work	1972	1) Dredging work or water conveying work to be carried out based on a pollution control program or by the order of the Home Affairs Minister and the sand covering stipulated by other cabinet order. 2) Work to construct or improve the port pollution prevention facility.
	Marine Clean-Up Work	1974	Work to recover floating refuse and oil in the inner sea and inner bay (excluding ports and fishing ports areas, etc.).
	Construction of Cleaning Ships	1974	Work to construct cleaning ships needed to perform clean the water in the port.
	Waste Oil Disposal Work	1967	Work to construct or improve waste oil disposing facilities (by port authorities and private companies, etc.).
	Marine Waste Disposal Facility Construction Work	1973	Work to construct or improve the acceptance facility, incineration and crushing facilities for waste which from ships and ocean facilities and waste produced during the work by the port authority.
	Disposal of Sunken Ships	1974	Work to dispose of unidentified sunken ships in the port.
	Stockpiling of Materials to Remove Port Contamination	1975	Work to stockpile the oil fences required to remove the oil contamination in the port.
	Designing and Research for Sediment Purification	1979	Designing and research necessary to implement sediment purification (by dredging or covering) at in the area where sea-bed contamination is pronounced.
2. Maintenance of Waste Reclamation Site	Waste Reclamation Revetment Construction Work	1973	Work to construct or improve the revetment for reclaiming the waste to be disposed of.
	Wide Area Recramation Site Construction Work	1982	Work to construct or improve the waste reclamation site for wide area waste (generated in coastal areas and broader areas inland) disposal.
3. Environmental Improvement of the Port	Green Zone Facilities Construction Work	1973	Work to construct or improve port environment improvement facilities such as the park or green zone.
	Marine Environment Creating Work	1988	Work such as the sand covering or improvement of the beach in order to create refreshing space for public access to the sea by improving the water bed quality.

Table 2 Fctors of water contamination of five representative enclosed coastal seas in Japan.

No	Name of Sea		Tokyo Bay	Mikawa Bay	Osaka Bay	Hiroshima	Suo-Nada
1	Area(km^2)		1000	510	1400	1000	3000
2	Volume($10^9 m^3$)		18	4.6	38	25	72
3	Mean Depth(m)		18	9.2	27	25	24
4	River Discahrge ($10^6 m^3$/day)		26	12	60	11	16
5	Discharged Load (ton/day)	COD	285	50	285	70	50
		TP	22	4	30	3	1.1
6	Released Load (ton/day)	COD	96	43	131	42	477
		PO_4P	6.3	3.3	13.7	13	9.7
7	Volume/Discharge (No.2/No.4)		692(day)	383	633	2270	4500
8	COD : Ratio of No.6/No.5		0.34	0.86	0.46	0.60	9.5
9	PO_4P : Ratio of No.6/No.5		0.29	0.83	0.46	4.3	8.8

Fig.2 Locations of enclosed coastal seas in Table 2.

Table 2 shows the characteristic indices of water contamination of five representative enclosed seas in Japan. The locations of these seas are shown in Figure 2. In the table, the values of row 8 show the ratio of the amount of COD discharged from surrounding rivers to the one released from bottom sediments. These values range between 0.34 to 0.86 except the case of the Sea of Suo-Nada. This means that the amount of COD load released from sediments is about a half of the one discharged from surrounding rivers. In case of inorganic phosphorus(PO_4-P), the ratios are almost the same as of COD. It is said that the nutrient

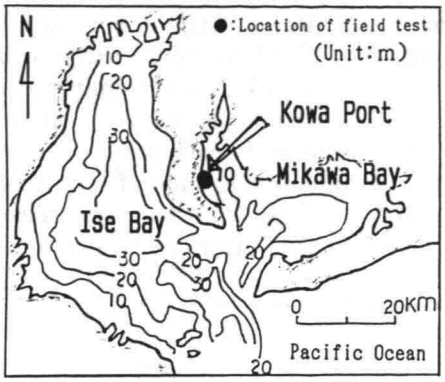

Fig.3 Location of Kowa Port in Mikawa Bay.

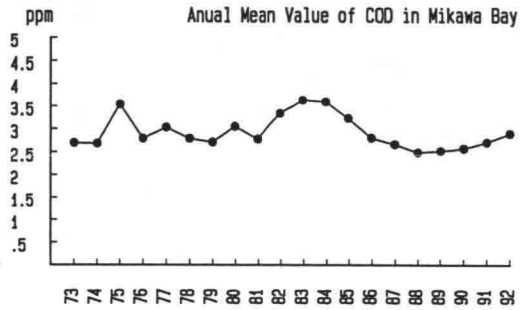

Fig.4 Time series of anual mean concentrations of COD of water in Mikawa Bay.

released from polluted bottom sediments is one of the main causes of sea water contamination.

In the paper, we describe the results of field measurements concerned with the effect of sand covering on improvements of water quality and marine environmental conditions in Mikawa Bay. Mikawa Bay, with a surface area of 510 km^2, is located at the central part of Japan, and is connected to Ise Bay as shown in Figure 3. With an average depth of 9.2 meter, the bay is characterized as shallow and semi-enclosed coastal sea.

Figure 4 shows the yearly trend of annual mean concentrations of COD of Mikawa Bay. The total load of COD is decreasing because of total pollution load regulation policy, but the concentration of COD still remains at contaminated level. The reason why the water quality in Mikawa Bay is still contaminated is considered that the large amount of nutrient salts are released from contaminated sea bottom sediments.

Figure 5 shows the horizontal distributions of COD of bottom surface sediments in the bay. From the figure, almost all values of COD exceed 20 mg/g in dry weight, so the bottom sediments in Mikawa Bay are considered as very contaminated situation. We carried out laboratory tests in order to know nutrient release rates from contaminated bottom sediments. The nutrient release rate from bottom sediments is the function of the concentration of nutrient of bottom sediments and the concentration of DO (Dissolved Oxygen) of bottom water as shown in Figures 6 and 7. In Figure 6, black circles show the release rate of PO_4-P from the sediments 50 to 80 cm below the bottom surface, and white circles show the one of

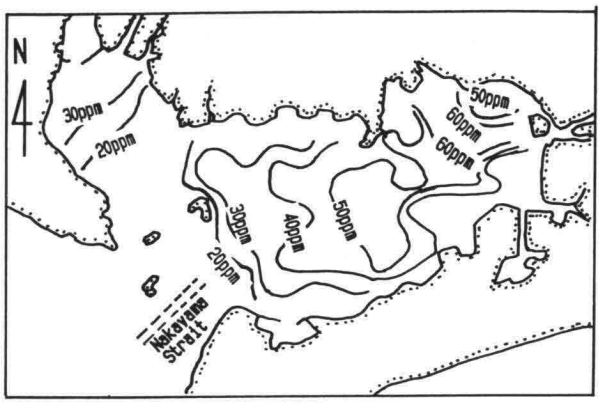

Fig.5 Contour lines map of COD of bottom sediment.
(unit : mg/g in dry weight)

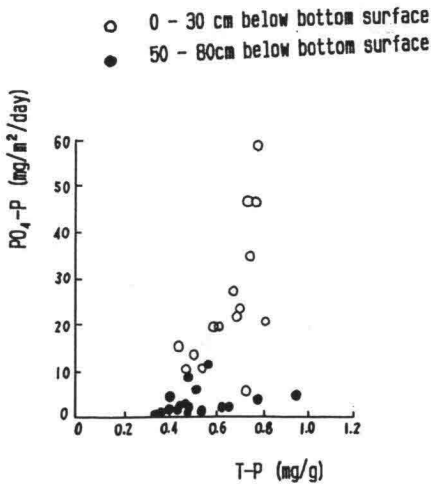

Fig.6 Relationship between the release rate of phosphorus and concentration of T-P of bottom sediment.

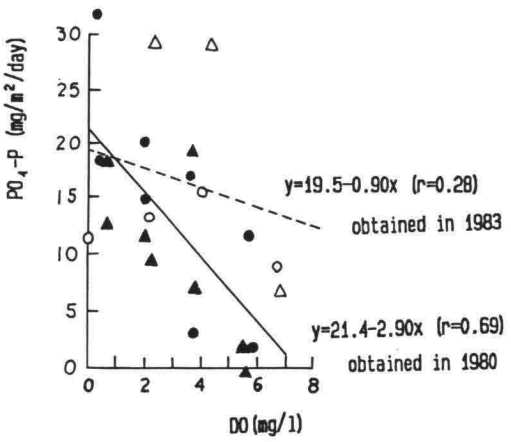

Fig.7 Relationship between the release rate of phosphorus and concentration of DO of bottom water.

the sediments from the bottom surface. Figure 6 shows that the release rates of phosphorus from the bottom surface sediments are much larger than the one from the sediments 50 to 80 cm below the bottom surface. Figure 7 shows the release rates decrease as the concentrations of DO in bottom water increase. For non-polluted sand, which is used as the sand covering material, the concentration of T-P of the sand is very small, and the sand does not consume oxygen in bottom water. Therefore, it is considered that the release rate of phosphorus is almost zero from the sediments covered with non-polluted sand. These laboratory test results say that sand covering or dredging works have large effect on reduce the nutrient release rate from the polluted bottom sediments.

3. SAND COVERING WORK AT OFF-KOWA PORT IN MIKAWA BAY

Since 1979, the Ministry of Transport has been studied polluted bottom sediment purification techniques. The study was carried out in five enclosed coastal seas in Japan as shown in Figure 2. Among them, we describe the field investigation results in Mikawa Bay as an example. Sand covering work to cover the polluted sediments with non-polluted sea sand was conducted at off-Kowa Port in Mikawa Bay. The area of test works of sand covering is located in Western part of Mikawa Bay. The outlines of the test field are shown in Table 3 and Figure 8. Contaminated sediments were covered with non-polluted sea sand with 0.5 meter in thickness in the area of 150 meter long and 100 meter wide. In order to avoid the

Table 3 Outline of test field.

Name of Sea	Mikawa Bay
Location of test field	Kowa Port (Fig. 8)
Water Depth	5m below datum line
Date of sand covering work	June, 1987
Sand covering area	1.5 ha (100m x 150m)
Thickness of sand covering	50 cm
Sand covering technique	Unloader barge

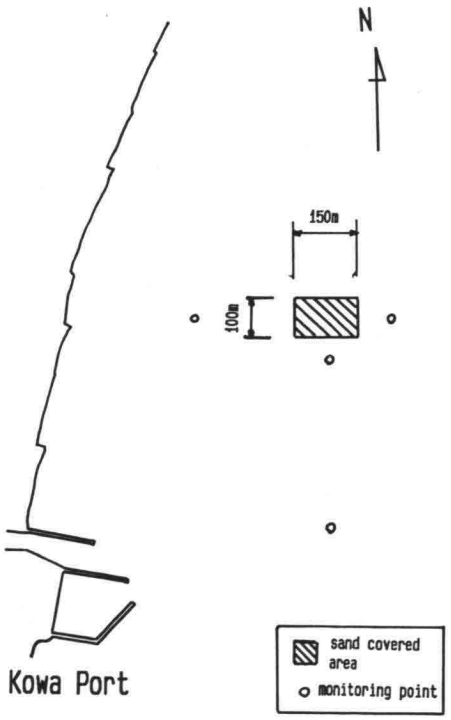

Fig.8 Location of sand covering test field.

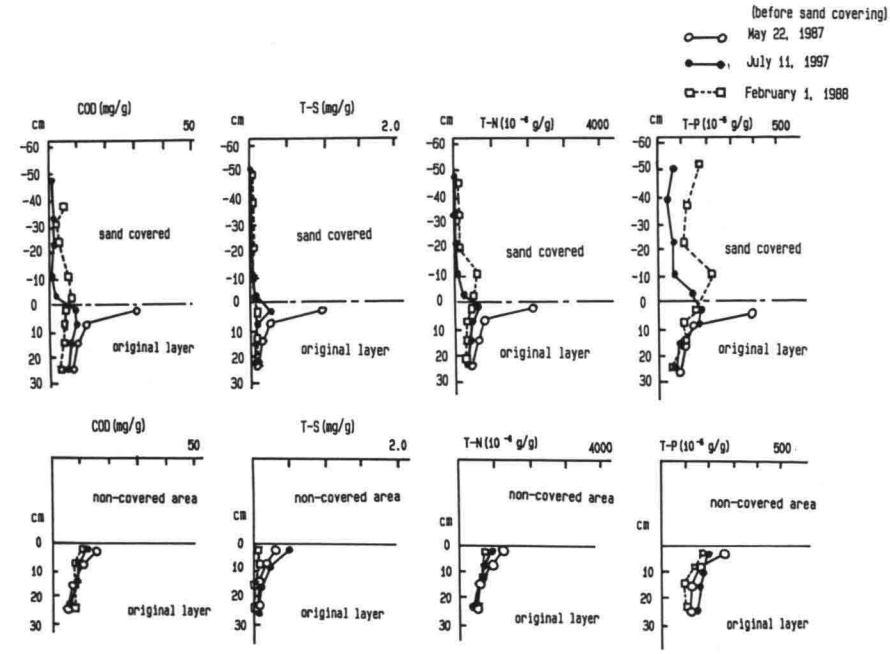

Fig.9 Temporal change of vertical distributions of COD, T-S, T-N and T-P of bottom sediment(upper:sand covered area, lower:non-covered area).

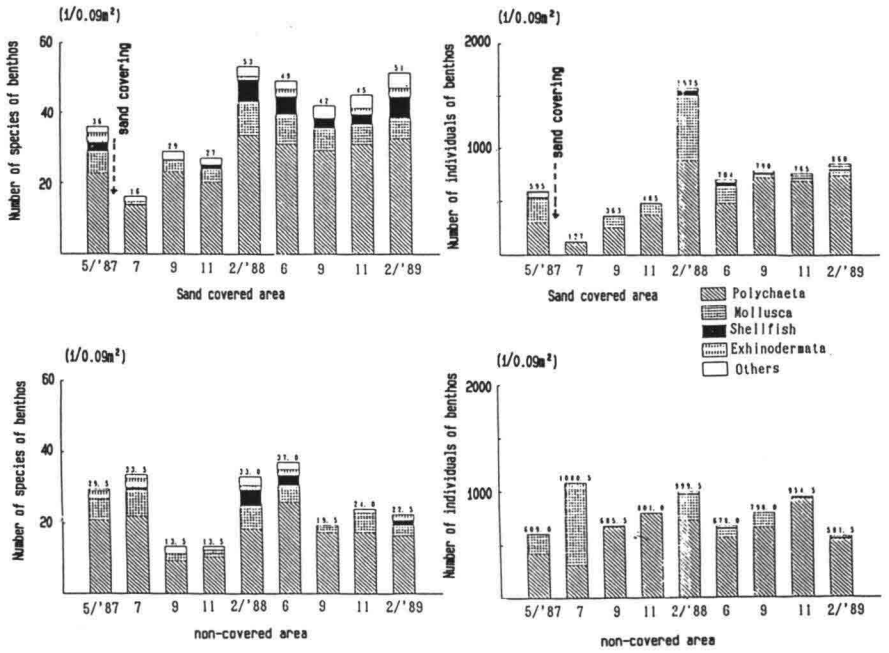

Fig.10 Comparisons of individual number and species number of benthos in bottom sediments between with sand covering and without one. (upper:sand covered area, lower:non-covered area).

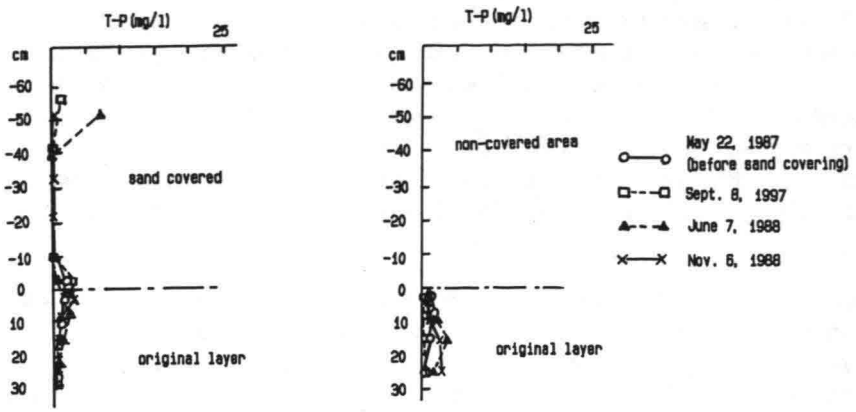

Fig.11 Temporal change of vertical distributions of T-P of interstitial water in bottom sediment(left:sand covered area, right:non-covered area).

extreme disturbance of the contaminated sediments during sand covering works, improved unloader barge was employed for the construction.

The sand covering was carried out in June 1987. After the covering, the follow up measurements were carried out to know the effect of sand covering on environmental improvements for water quality, sediment quality, benthos, etc. Figure 9 shows the temporal change of vertical distributions of COD concentrations , total sulphate(T-S), total nitrogen(T-N), and total phosphorus(T-P) of the bottom sediments. In the figure, white circles show the data before the sand covering, white triangles show the one after one month, and white squares show the one after 20 months from the construction. From the figure, it is shown that the COD of the surface sediment is greatly reduced at the covered area compared to that at the non-covered area immediately after the site work.

Due to the sedimentation, gradual increase of sediment COD is obtained at the surface of sand covering area, but the values show that the quality of the sediment is still improved condition. The improvement of sediment quality changes the ecological conditions of benthos in the sea bottom sediments of the sand covering area. Figure 10 shows the comparisons of individual number and species number of benthos in the sea bottom sediments between with sand covering and without one. After the sand covering construction, number of species of benthos in the sand covered area is larger than the one in the non-covered area. Generally, the species number of benthos is small in the contaminated sediments compared to non-contaminated sediment(Odum,1971). Therefore, it can be concluded that the sand covering improves the ecological conditions for benthos.

The most important effect of sand covering with non-polluted sand on water quality is to reduce the release rate of nutrient salts from contaminated bottom sediments. Figure 11 shows the comparison between the concentration of total phosphate(T-P) of interstitial water in the bottom sediment with sand covered area and the one without sand covered area.

From the figure, it is shown that the concentrations of T-P of interstitial water in sand covered layer are almost zero except bottom surface layer. This fact says that the release rate of nutrient salts from the sediment with sand covered area is smaller than the one without sand covered area. As described before in Figures 6 and 7, release rate of nutrient salts is the function of sediment quality and DO concentration, and small release rate from bottom sediment covered with non-polluted sand is obtained by laboratory test. These facts imply that environmental conditions for benthos life are improved by the sand covering work.

Unfortunately, the sand covering area is very small compared to the area of Mikawa Bay, so it is very difficult to show the fact of water quality improvement due to the sand covering with non-polluted sand. In order to estimate the effect of sand covering work on improvement of water quality, following numerical simulations are carried out by using nutrient cycle mathematical model. In the model, we treat only phosphorus cycle, because the phosphorus is a limiting factor to the nutrient cycle in eutrophic bays. The model consists of mass conservation equations of organic phosphorus, inorganic phosphorus, COD, and DO. Flow field is divided into three layers in vertical. Detailed description of the model is written in the Horie's paper(1987). The reader who wants to know the model in detail had better read his paper.

By using the model, we carried out two cases of numerical simulation of water quality in Mikawa Bay. These are present condition case and sand covering condition case. In case of present condition, the release rates of phosphorus and COD from bottom sediments are adopted as shown in Figure 12, which are based upon laboratory tests. While in case of sand covering condition, we assume that the release rates are zero from the sediments for whole area of the bay.

Computational results of the simulation are shown in Figures 13 and 14. Figure 13 shows the contour lines of computed COD concentration in case of present condition, and Figure 14 shows the same one in case of sand covering condition. These figures show that the concentration of COD in case of sand covering condition is less than half of the one in case of present condition. This result indicates that the sand covering for whole area of the bay has large effect on water quality improvement.

Marine environmental improvement work has been systematically pursued since 1988 based upon the results of the study of bottom sediment purification. The work aims at improving water quality and recovering marine environment through sand covering with non-polluted sand. From the viewpoint of economical aspects, it is desirable to use high quality sand which is produced by dredging works in waterways or anchorages. In case of Mikawa Bay, non-polluted sand for covering was transported from the entrance of the bay, where dredging work was carried out to construct the waterway of Nakayama Strait. At present, 3 projects for coastal seas and 7 projects for harbors of Marine Environment Improvement work have been developing by the Ministry of Transport and some local governments. The concept of the marine environmental improvement work by sand covering is shown in Figures 15 and 16. Figure 15 shows the environmental image of coastal seas on condition of contaminated bottom sediments, and Figure 16 shows the environmental image of coastal seas after the

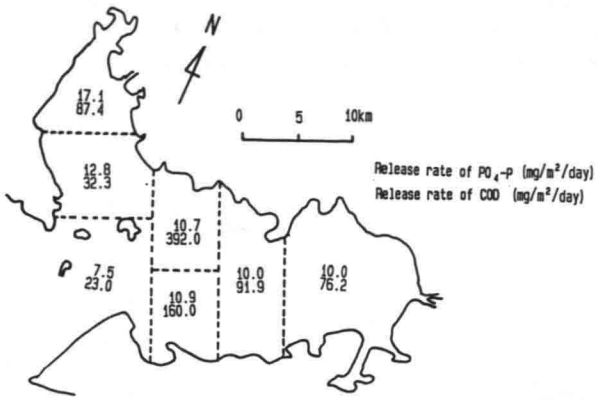

Fig.12 Release rate values of PO_4-P and COD from bottom sediments, which are based upon laboratory tests.

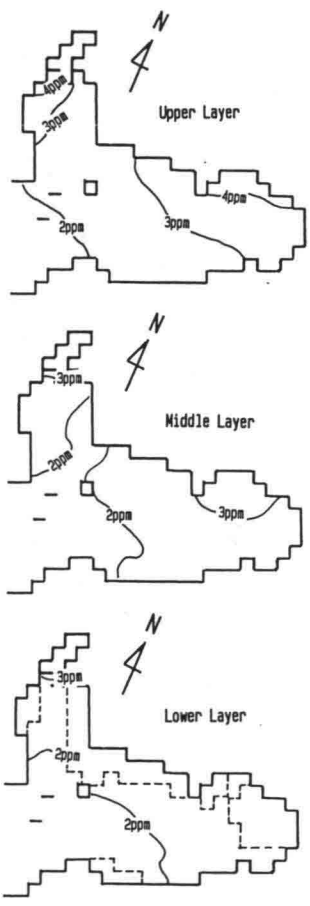

Fig.13 Contour lines of computed COD concentration in case of present condition. (release rates are shown in Fig.12)

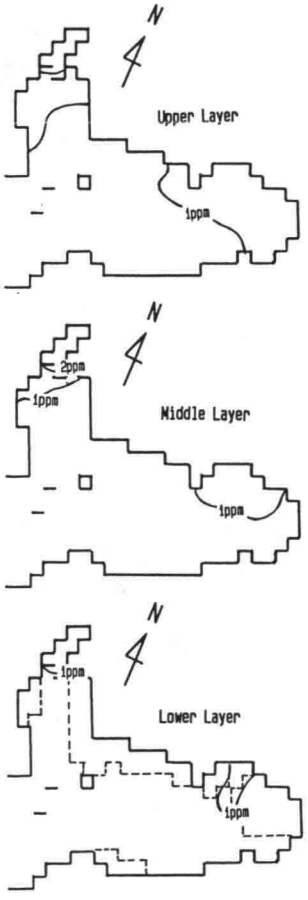

Fig.14 Contour lines of computed COD concentration in case of sand covering condition. (release rates are zero for whole area)

improvement of sediment quality by sand covering with non-polluted sand. A favorable marine environmental conditions, which are improved sediment quality and increased DO concentration at the sea bottom, is obtained for fish and benthos by sand covering work.

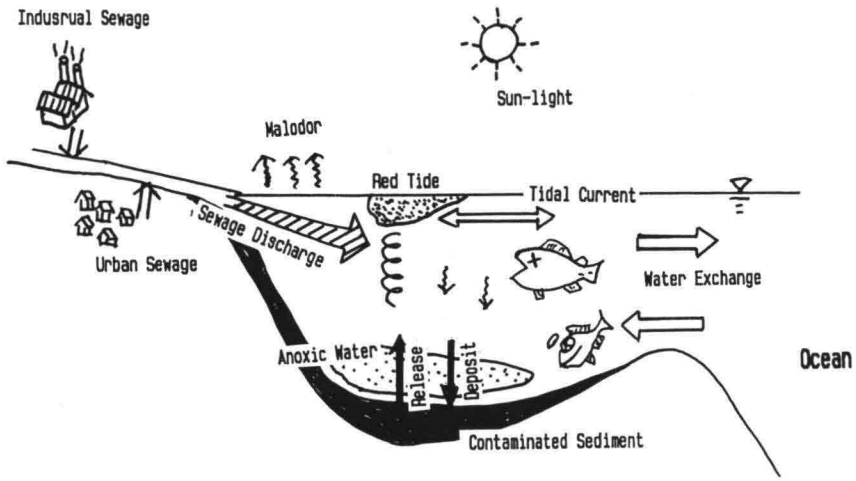

Fig.15 Environmental image of coastal seas on condition of contaminated bottom sediment.

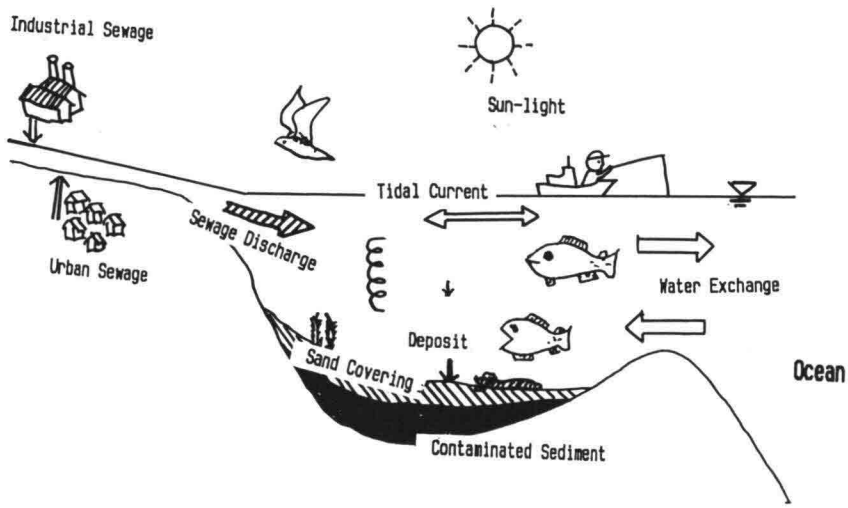

Fig.16 Environmental image of coastal seas on condition of after improvement of sediment quality by sand covering.

4. CONCLUDING REMARKS

Field measurement studies were carried out in order to know the effect of sand covering work over polluted sediments with non-polluted sea sand on water quality, sediment quality, and ecological conditions for benthos at off-Kowa Port in Mikawa Bay. Several results are obtained as follows:

(1) By the sand covering works, the COD concentration of surface sediment was greatly reduced at the covered area compared to at the non-covered area.

(2) The number of species of benthos in the sand covering area is larger than the one in the non-covered area. This means that the sand covering improves the ecological conditions for benthos.

(3) The interstitial total phosphate of the bottom sediment in sand covering area is smaller than the one in the non-covered area. This means that the nutrient release rate from bottom sediments is effectively reduced by the sand covering work.

ACKNOWLEDGEMENT

This observational study was carried out by the Fifth District Port Construction Bureau, Ministry of Transport. The authors express their greatest thanks to the persons in charge of field measurements.

REFERENCES

Horie, T.(1987): Modeling for the prediction of the effects of sea bed sediment treatment on the improvements of ecological conditions and seawater quality, Report of the Port and Harbour Research Institute, Vol. 26, No.5, pp.175-214.

Odum, E.P.(1971): Fundamentals of ecology, Third Edition, Saunders, pp.148-154.

HYDRO-PORT'94
International Conference on Hydro-Technical
Engineering for Port and Harbor Construction
October 19 - 21, 1994, Yokosuka, Japan

Water Exchange Mechanisms in Enclosed Coastal Seas influenced by Marine Structure

Kazuo Murakami
Katsuyoshi Shimizu
Kuniaki Yamada

Port and Harbour Research Institute, Ministry of Transport
3 Chome 1-1, Nagase, Yokosuka, Kanagawa, 239

ABSTRACT

Breakwaters located at the bay entrance have a role to protect the area from natural disasters such as tsunami waves or typhoon storm surges. However, water quality deterioration is feared due to the reduction of the cross sectional area of the entrance by the breakwaters. In this paper, the authors investigate the effect of horizontal circulation and vertical circulation flows on water exchange, and the influence of the breakwaters on water exchange by using hydraulic and mathematical model experiments. Experimental results show following conclusions: The existence of the breakwaters promotes water exchange because a horizontal circulation flow is generated behind the breakwaters, but reduces the exchange because the vertical circulation flow is suppressed by the breakwaters. One-way flow generated by the layout of breakwaters or by gate operation in a channel has a large effect on water exchange.

Keywords: Water exchange, Hydraulic model experiment, Horizontal circulation, Vertical circulation, Enclosed coastal seas

1. INTRODUCTION

Enclosed coastal seas are utilized for many purposes such as port, fishery, marine leisure, etc., because the region is tranquil. Many large cities in Japan are located in the hinterland of enclosed seas. Thus a great amount of sewage from the urban and industrial areas is discharged into the region. Water exchange between contaminated bay water and clean ocean water plays a great role in determining the water quality of the region. The enclosed coastal sea, however, has a low water exchange ratio because the cross sectional area of the entrance is small. Due to the large amount of sewage discharge and the small water exchange property, the water quality in enclosed coastal seas is generally contaminated.

Japanese coastal areas were often damaged by tsunami waves and typhoon storm surges. In order to protect the coastal areas from these kinds of natural disasters, breakwaters were

constructed at the entrance of the region. By the construction of the breakwaters, the cross sectional area of the entrance decreases. This means that the region protected by the breakwaters becomes an enclosed coastal sea. Since the area of the entrance section is reduced by the breakwaters, many persons fear the degradation of the water quality in the region. Prior to the construction of the breakwaters, we must investigate the influence of the breakwaters on water exchange as well as on tsunami wave height.

Water exchange is caused by several mechanisms such as turbulent mixing, horizontal circulation flow, and vertical circulation flow. Effect of these mechanisms on water exchange is dependent upon the flow field of the area concerned and configuration of the entrance. In this paper, the authors describe the water exchange mechanisms in enclosed coastal seas and comments on how to consider the influence of marine structures on water exchange between enclosed region and ocean water bodies. The authors investigate water exchange enhancement techniques by generating a one-way flow and the horizontal circulation flow.

2. WATER QUALITY IN ENCLOSED COASTAL SEAS

The grade of enclosed property of coastal seas is defined simply by the following expression.

$$E.I. = \frac{\sqrt{S_a}}{D_{p1}} \cdot \frac{W}{D_{p2}} \tag{1}$$

in which, $E.I.$ is the enclosed index, S_a the area of coastal sea, W the width of the entrance, D_{p1} the mean depth of the coastal sea, and D_{p2} the mean depth at the entrance cross section. Table 1 shows the $E.I.$ values of the representative Japanese inland seas as shown in Fig. 1.

Table 1 Enclosed Index(E.I.) values of the representative Japanese inland seas.

Type	Current	Name of Bay	S_a(km^2)	D_{p1}(m)	W(km)	D_{p2}(m)	E.I.
Enclosed Sea E.I.>2	Tidal Current	Kinkowan Bay	250	136	2.1	33	31.0
		Ohmura Bay	320	14.8	0.33	32.2	25.3
		Ofunato Bay	7.9	14.9	0.2	16	13.1
		Ariake Bay	1700	20	4.4	50	3.7
		Kagoshima Bay	1130	100	10	70	4.8
		Kamaishi Bay	7.9	30	0.5	13.5	12.5
		Suzaki Bay	3.3	10	0.3	15	3.8
		Mutsu Bay	1720	32.6	10.5	62.7	2.1
		Tokyo Bay	1160	15.8	7.3	32.6	2.3
		Osaka Bay	1400	30	8.8	58	2.2
		Mikawa Bay	500	6.8	13.3	8.2	1.3
Semi-Enclosed Sea 2>E.I.>1	Tidal -Ocean Current	Ise Bay	1600	18.7	11.4	41	1.6
		(Ofunato Bay)	7.9	14.9	0.8	40	1.4
		Hakata Bay	125	12	5.4	15	1.7
		Beppu Bay	430	35.8	27	46.2	0.6
		Funka Bay	2270	59	29.7	63.1	1.5
		(Kamaishi Bay)	7.9	30	2.3	42	0.9
		(Suzaki Bay)	3.3	10	1.6	15	0.8
Open Sea E.I.<1	Ocean Current	Shibushi Bay	400	35	20	70	0.5
		Suruga Bay	2300	880	56	1000	0.7
		Akita Bay	800	30	50	50	0.3

( ) Before the construction of the breakwaters.

In general, the water quality in enclosed coastal seas is contaminated due to small water exchange. Figures 2(a) and 2(b) show the time series of the annual mean concentration of COD(Chemical Oxygen Demand) of Tokyo Bay from 1974 to 1988 and the total load of COD discharged into the bay. The total load of COD is slightly decreasing owing to several water quality controls. However, the concentration of COD still remains at the contaminated level.

Japanese coastal areas were damaged by tsunami waves and typhoon storm surges. Table 2 shows the representative tsunami waves and typhoon storm surges, and the damages suffered from these disasters. Ofunato Bay is located at the Pacific Ocean side of the Northern part of Japan. The bay has been seriously damaged by tsunami disasters several times. Especially, the bay was damaged by Chilean Tsunami in 1964. After the serious disaster, Ministry of Transport constructed the tsunami breakwaters at the bay entrance in order to reduce the tsunami wave height. By the construction of the break waters, the enclosed index of the bay increased from 1.4 to 13.1. Figure 3 shows the time series of the depth of transparency in Ofunato Bay. From the figure, it is considered that the water quality became considerably poorer after the construction. The contamination is seemed to be caused by several factors such as over feeding of fishery farming, small water exchange due to the breakwaters, etc.

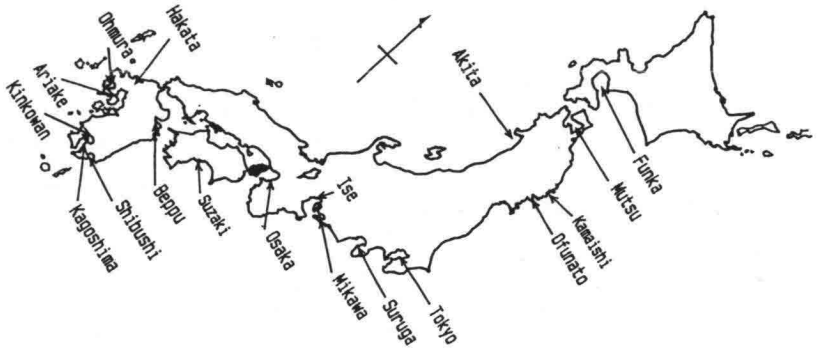

Fig.1 Representative enclosed seas in Japan.

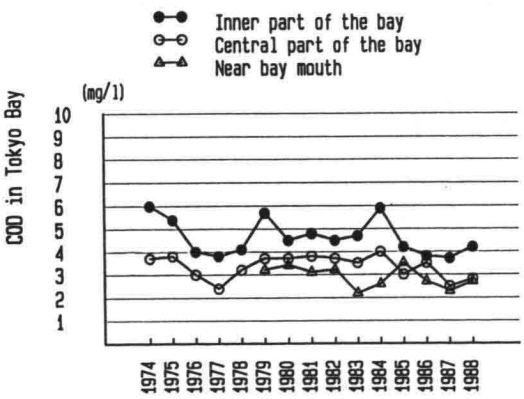

Fig.2(a) Annual mean concentration of COD in Tokyo Bay from 1974 to 1988.

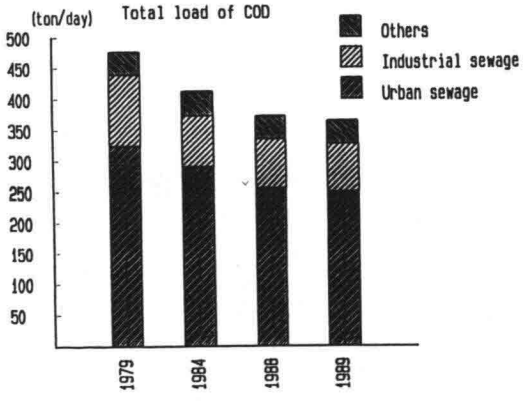

Fig.2(b) Total load of COD in Tokyo Bay.

Table 2 Disasters by tsunamis and typhoons of Japan.

	Name of Disaster	Year	No. of killed
Tsunami	Nankai	1946	1330 (102)
	Chilean	1960	119 (20)
	Nihonkai Chubu	1983	100
	Hokkaido Nanseiok	1993	201 (29)
Typhoon	Muroto	1934	2866 (200)
	Isewan	1956	4759 (282)
	Second Muroto	1961	194 (8)

( ) unknown

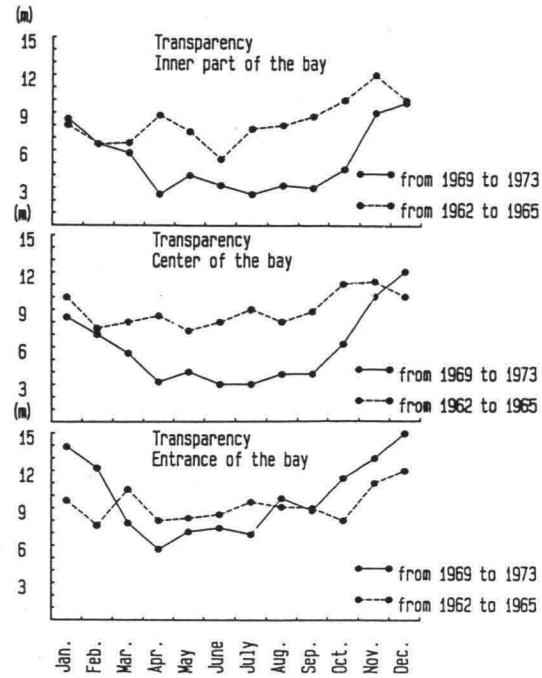

Fig.3 Transparency in Ofunato Bay before(dotted) and after(real) the breakwater construction.

3. WATER EXCHANGE MECHANISM

3.1 Mechanism

The tidal cycle average of mass transport along the axis of an estuary or a bay is expressed by

$$\dot{M} = \frac{1}{T}\int_0^T \int_A uC \; dA \; dt \tag{2}$$

in which, velocity u and concentration C profiles are decomposed by Fischer(1972) as follows:

$$u = u_0 + u_1 + u_{st} + u_{sv} + u'_t + u'_v \tag{3}$$

$$C = C_0 + C_1 + C_{st} + C_{sv} + C'_t + C'_v \tag{4}$$

Then the mass transport $\dot{M}$ is expressed by the following expression.

$$\dot{M} = A_0 u_0 C_0 + C_0\langle A_1 u_1\rangle + A_0(\langle\overline{u_{st}C_{st}}\rangle + \langle\overline{u_{sv}C_{sv}}\rangle + \langle\overline{u'_t C'_t}\rangle + \langle\overline{u'_v C'_v}\rangle) \tag{5}$$

in which, u , C : instantaneous velocity and concentration profiles, u_o, C_o : average velocity and concentration over cross sectional and a tidal cycle, u_1, C_1 : cross sectional averages at any time during the tidal cycle, minus the tidal cycle averages, u_{st}, C_{st} : the horizontal variation of the vertical mean, u_{sv}, C_{sv} : the vertical variation of the vertical mean, u'_t, C'_t : the horizontal deviation from the vertical mean, u'_v, C'_v : the vertical deviation from the vertical mean.

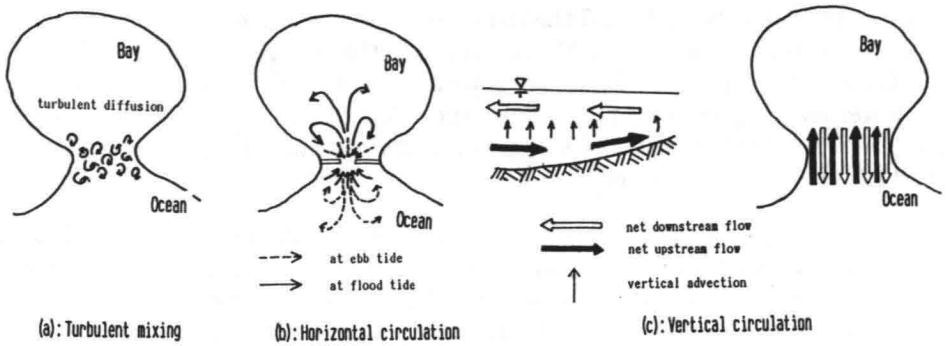

Fig.4 Water exchange mechanism[(a):turbulent diffusion, (b):horizontal circulation, (c):vertical circulation]

The first two terms in Eq. (5) may be combined to give $C_o Q_f$, when Q_f is the discharge of one-way flow of the cross section. $A_o\langle\overline{u_{st}C_{st}}\rangle$, $A_o\langle\overline{u_{sv}C_{sv}}\rangle$, $A_o\langle\overline{u_t'C_t'}\rangle$, $A_o\langle\overline{u_v'C_v'}\rangle$ represent respectively mass transport by the horizontal circulation flow, the vertical circulation flow, the horizontal oscillatory shear and the vertical oscillatory shear. The last two terms are considered as the turbulent diffusion transport. According to above consideration of mass transport decomposition, the net mass transport components that pass through the bay entrance are composed of the one-way flow term and the other water exchange terms such as the horizontal circulation flow, the vertical circulation flow and the turbulent diffusion.

Water exchange is a very important phenomenon which dilutes the contaminated bay water with clean ocean water. Water exchange mechanisms are schematically explained as shown in Fig.4(Murakami,1992). In the figure, the mechanism (a) is caused by turbulent mixing, (b) is caused by horizontal circulation flow, and (c) is caused by vertical circulation flow. Turbulent mixing is caused by turbulent flow. This is the fundamental mechanism of water exchange caused by oscillatory tidal current. Horizontal circulation flow is caused by tidal residual flow, which is generated by the non-linearity property of tidal current. When breakwaters are constructed at the entrance of a bay, tidal velocity is increased because of the reduction of the cross sectional area. Therefore, horizontal circulation flow is generated behind the breakwater by relatively strong tidal velocity. The horizontal circulation flow has an effect on water exchange between two water bodies. The water exchange mechanism caused by horizontal circulation flow is explained as tidal pumping by Fischer et al.(1979).

Vertical circulation flow also has an effect on water exchange between two water bodies. The vertical circulation flow is generated by density current or wind driven current. In a small bay, abrupt rising of water temperature occurs frequently due to strong tidal current(so called Kyucho). It is thought that the phenomenon of the Kyucho is caused by vertical circulation flow induced by density current. The abrupt water temperature rising implies that the water exchange occurs abruptly.

3.2 Water Exchange Ratio and Averaged Residence Time

The water exchange phenomenon is explained in two ways. One is the water exchange ratio (tidal exchange ratio) investigated by Parker et al.(1972). And the other is the averaged residence time investigated by Bolin et al.(1973). The former considers the mixing process of

materials at the bay entrance. And the latter considers the amount of the remnant materials in the enclosed region. Parker et al. investigated the concept of water exchange ratio at Golden Gate in San-Francisco Bay. They defined the water exchange ratio as the fraction of new water entering the bay on the flood tide. The water which passes through the bay entrance on a flood tide consists of water which has been in the bay before (old water) and water which has not (new water).

Bolin et al. investigated the concept of residence time in natural reservoirs. The residence time means the duration which a particle spends the region before removal to adjacent region. The short residence time is the same meaning of large water exchange ratio. The averaged residence time is expressed by the following equation (Takeoka,1984).

$$\tau_r = \int_0^\infty \frac{R(t)}{R_0} dx = \int_0^\infty r(t) dt \tag{6}$$

in which , τ_r : average residence time, $R(t)$: the amount of material which still remains in the region at a time t, R_o : the amount of material at t=0, $r(t)$: remnant function $(= R(t)/R_o)$.

This concept is suitable for water exchange studies by using physical model experiments and numerical simulations. In this paper, the author utilizes the concept of the remnant function of the average dye concentration of enclosed region and the average residence time.

4. HYDRAULIC AND MATHEMATICAL MODEL EXPERIMENTS ON WATER EXCHANGE

4.1 Hydraulic Model Experiment Procedure

In order to predict the influence of reclamation lands or breakwaters on tidal current and substance dispersion, hydraulic model experiments are generally utilized. Water exchange is also investigated by hydraulic model experiment. Hydraulic model experiment of water exchange is carried out by the following procedure as shown in Fig.5

At the first stage, water is filled in the model basin up to the mean water level. Then the water is divided into inner bay water and outer ocean water by the barrier board installed at the cross section of the bay entrance. Fluorescein sodium dye is used as the tracer of contaminated substance. The dye is put into the inner bay water, and mixed up sufficiently

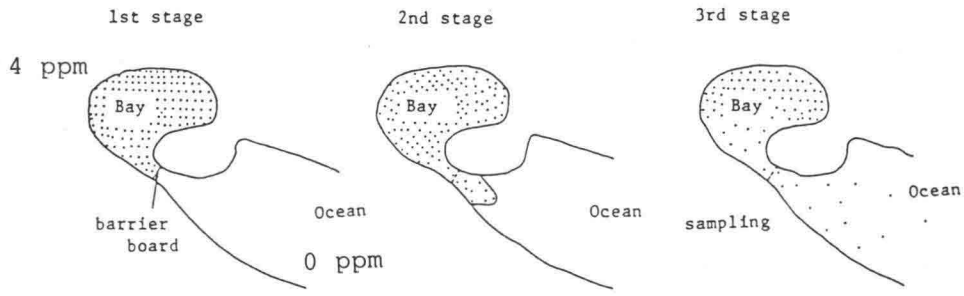

Fig.5 Experimental procedure of water exchange by physical model.

Table 3 Experimental cases and maximum current vellocity at the entrance.
(Suzaki Bay model)

Exp.	Exp. Condition		Flood Tide	Ebb Tide	Compu.
Cases	Breakwater	Density	(cm/s)	(cm/s)	Cases
Run-A	without	without	1.6	0.8	Case-03
Run-B	with	without	10.5	8.9	Case-04
Run-C	without	with	2.9	2.3	Case-01
Run-D	with	with	6.0	13.8	Case-02

until the water becomes a homogeneous dye concentration. At the second stage, the barrier board is removed from the cross section which divides into two regions. At the same time, the operation of tide generator starts. Then the mixing between two water bodies begins due to tidal current and turbulent diffusion. At the third stage of the experiment, a small volume of water is picked up from each gathering station distributed in the model basin in order to measure the dye concentration distribution every several tidal cycles. Eighty pieces of water gathering equipment can collect water samples from each station simultaneously.

4.2 Horizontal Circulation Flow

As described before, horizontal circulation flow has a large effect on water exchange between two water bodies. Figures 6(a) and 6(b) show the float trajectories for two tidal cycles in case of "with" and "without" breakwaters at bay entrance, which are experimental results of the Suzaki Bay model basin (Murakami,1988). From the figures, it is shown that the horizontal circulation flow is generated behind the breakwaters. Tidal amplitudes in inner region for both cases show almost the same values. This result means that the net volume of water entering into enclosed region from the outside during flood tide is almost the same under the experimental condition of with and with out breakwaters.

Table 3 shows the maximum current velocities measured by ultra-sonic current meter installed at the center between two breakwaters. The maximum velocity in case of with breakwaters is much higher than the velocity in case of without breakwater. This high velocity current generates the horizontal circulation flow behind breakwater, which is the tidal residual flow caused by non-linearity of tidal current.

Fig.6(a) Float trajectories for 2 tidal cycles. (with breakwater without density current)

Fig.6(b) Float trajectories for 2 tidal cycles. (without breakwater without density current)

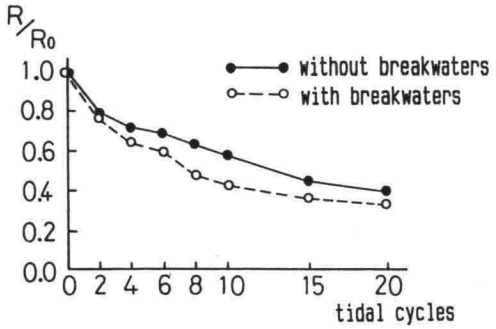

Fig.7 Decay curves of remnant function of average dye concentration. (without density current : Suzaki Bay Mmodel)

Figure 7 shows the decay curves of the remnant function of the averaged dye concentration whole over the enclosed region in case of with breakwaters plotted by white circles and without breakwaters plotted by black circles. According to the figure, water exchange is promoted by existence of the breakwaters at the bay entrance. This depends upon the horizontal circulation flow generated by tidal residual flow. This experimental result shows that the horizontal circulation flow has an effect on water exchange promotion.

The concept of water exchange is applied to other coastal seas. Kagoshima Bay is an extremely enclosed region as shown in Fig.8. The effect of the new channel excavation, as shown in the enlarged part of the figure, on water exchange is studied by hydraulic model experiment. Water exchange experiments are carried out by using the Kagoshima Bay model basin (Murakami et al.,1986). Experimental cases are shown in Table 4. In order to generate horizontal circulation flow in enclosed region, a gate which is installed in the new channel of the model is repeatedly operated in the following way. The gate is opened while the tide is flood (or ebb), and closed while the tide is ebb (or flood). Enforced unidirectional flow is thus generated in the new channel. As a result, enforced circulation flow is generated in the area of inner bay. Figures 9(a) and 9(b) show the pattern of the average tidal velocity obtained by float movements for two tidal cycles of Flood-Only and Ebb & Flood cases. It is clearly shown that counter clockwise horizontal circulation flow is generated by the operation of the

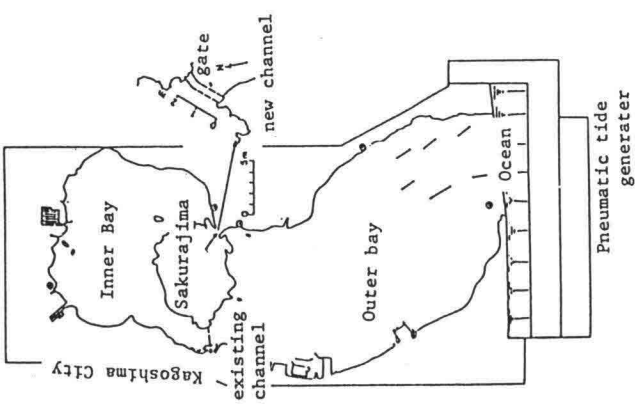

Fig.8 Hydraulic model basin of Kagoshima Bay

Table 4 Experimental cases of Kagoshima Bay model.

Case No.	Name	Experimental Conditions
Case I	Present	No new channel
Case II	Ebb & Flood	With new channel, but no gate operation
Case III	Flood-Only	Gate is opende during flood tide
Case IV	Ebb-Only	Gate is opened during ebb tide

Fig.9(a) Average flow pattern(Ebb & Flood)

Fig.9(b) Average flow pattern(Flood-Only)

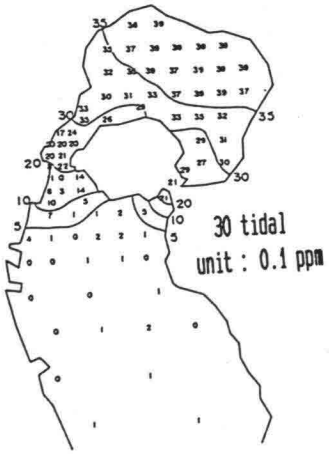

Fig.10(a) Horizontal distribution of dye tracer concentration(Ebb & Flood)

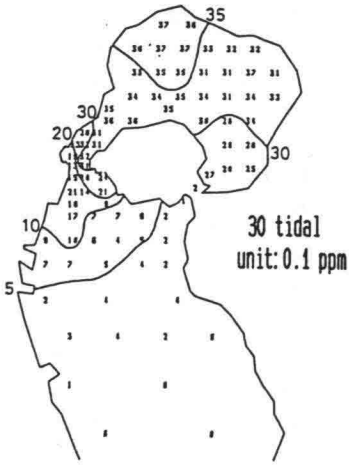

Fig.10(b) Horizontal distribution of dye tracer concentration(Flood-Only)

gate which is opened while the tide is flood. Figures 10(a) and 10(b) show the horizontal distributions of dye tracer concentration after the 30 tidal cycles from the initial condition, which is set up 4 ppm in the dye concentration for the inner bay water and 0 ppm for the outer ocean water. In case of Ebb & Flood, the most inner part of water is diluted due to the excavation of the new channel, but the inner bay water does not diffuse to outer bay region through the existing channel very much. On the other hand in case of Flood-Only, the inner

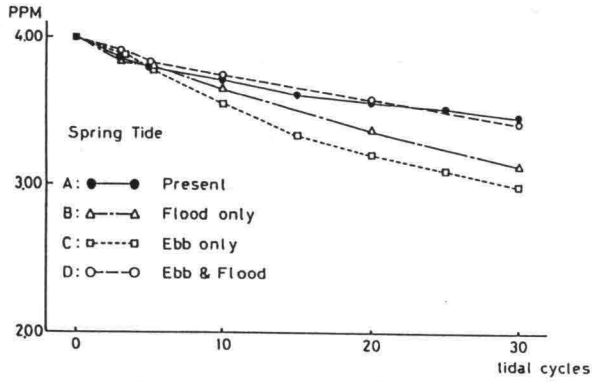

Fig.11 Decay curves of remnant function of average dye concentration. (Kagoshima Bay model)

bay water is transported to the outer bay region passing through the existing channel.

The decay curves of the remnant function in cases of Flood-Only and Ebb & Flood are shown in Fig. 11. From the figure, it is found that the average concentration in case of Flood-Only decreases more quickly than the concentration of Ebb & Flood case. This result implies that the enforced horizontal circulation flow generated by the gate operation has a large effect on water exchange between two water bodies.

The reason why the new channel excavation does not have an effect on water exchange in case of the Kagoshima Bay model experiment is thought as follows: Tidal amplitude measured by wave gauge does not change whether the new channel is excavated or not. These results mean that the net volume entering into inner region during flood tide does not change whether the new channel exists or not. Therefore, the total volume that passes through the existing channel decreases due to the new channel excavation, and the new channel does not generate horizontal circulation flow in inner bay region.

As described before, the horizontal circulation flow generated by the gate operation or by tidal residual current behind the breakwaters has an effect on water exchange between contaminated inner bay water and clean ocean water. Several ideas proposed by some researchers to promote water exchange are based upon the effect of horizontal circulation flow on water exchange. In this section, the authors only considered horizontal circulation flow because the hydraulic model experiments are generally carried out by homogeneous water condition. The method does not consider the vertical circulation flow induced by density current or wind driven current.

4.3 Vertical Circulation Flow

So far, the authors have not mentioned vertical circulation flow. In an enclosed region, vertical circulation flow is generated by density current or wind driven current. For hydraulic model experiments, the density current and wind driven current are usually ignored, because it is very difficult to control both currents precisely in the model basin.

When we consider well mixed conditions for enclosed region, the narrow entrance causes the high speed current velocity which generates the horizontal circulation flow in the region. As described before, the horizontal circulation flow has an effect on water exchange. Therefore,

the narrow entrance does not contribute to water contamination in enclosed region if the flow is in a well mixed condition. However, the water in enclosed coastal seas is generally contaminated. Several reasons are considered for the water contamination of enclosed regions. Among them, small water exchange ratio is one of the most important reasons. Therefore, the vertical circulation flow should be considered as well as the horizontal circulation flow when we consider the water exchange problems in enclosed coastal seas.

Considering above mentioned viewpoints, the author carried out hydraulic model experiments of water exchange on the condition of the flow field with and without density current by using the Suzaki Bay model basin (Murakami & Shirai,1990). For without density current, the experimental results are already described in Figs. 6 and 7. The consideration of density current in the hydraulic model basin is carried out in the following way. At the first stage, seawater in the basin is divided into inner bay water and outer ocean water by the barrier board. Then the inner bay water is mixed well with freshwater up to homogeneous salinity, which is 0.05% less than the salinity of ocean water. The other procedure is the same as the experiment without density current.

By the density difference between inner bay water and outer ocean water, density current is induced in the model basin. The water in upper layer flows from the bay to the ocean, while the water in lower layer flows from the ocean to the bay. Table 3 shows the maximum velocities at the bay entrance measured by current meter. According to these results, the maximum velocity with breakwaters is much higher than the velocity in case of without breakwaters, and the horizontal circulation is generated behind the breakwaters. These flow patterns are considerably similar to that of without density current.

Figure 12 shows the decay curves of the remnant function in case of with breakwater plotted by white circles and without breakwaters plotted by black circles. As compared with Fig. 7, it is evident that the water exchange with density current is much larger than that of without density current. As to with density current, water exchange is decreased due to the existence of the breakwaters at the bay entrance. This is mainly due to the reduction of cross sectional area of the bay entrance. This implies that the influence of the breakwaters on water exchange is negative whether the density current exists or not.

Thus, the existence of the breakwaters at the bay entrance enhances the water exchange by horizontal circulation flow, but decreased the exchange owing to the suppressed vertical

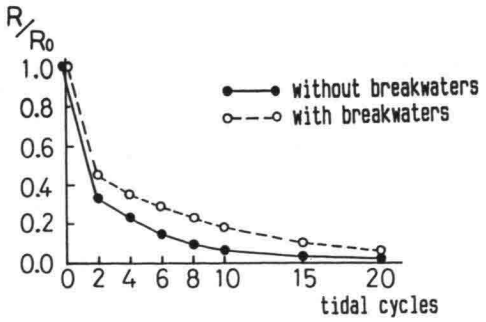

Fig.12 Decay curves of remnant function of average dye concentration.
(with density current : Suzaki Bay Mmodel)

circulation flow.

4.4 Mathematical Model Experiments on Water Exchange

Water exchange experiment by hydraulic model technique with density current has a problem, which is the unrealistic still water and homogeneous high density distribution in the enclosed region at the initial stage of the experiment. Therefore, a very strong vertical circulation is generated just after the removal of the barrier board which divides lighter inner bay water and heavier ocean water.

In order to avoid this unrealistic conditions, we carried out mathematical model experiments on water exchange by using a simple rectangular bay with constant depth. Experimental conditions are the same as in Table 3, that is, Case-01 for without breakwater and with density current, Case-02 for with breakwater and with density current, Case-03 for without breakwater and without density current, and Case-04 for with breakwater and without density current.

Three-dimensional mathematical model is employed in order to consider the vertical circulation flow induced by density current and the horizontal circulation flow generated by tidal residual current. The computational condition is shown in Table 5. In this computation, water depth is divided to 5 layers by sigma stretching coordinate technique. The mode splitting technique is employed, so time step for external mode is 30 seconds, and for internal mode is 300 seconds. Salinity conditions at initial stage and along the open boundary are fixed as 32.0 ppt, and fresh water is discharged into the inner part of the enclosed region.

The density difference between freshwater and saltwater induces the density current. According to computational results, vertical circulation flow is generated in case of with density different, and horizontal circulation flow is generated in case of with breakwaters.

Figures 13(a) to 13(d) show the horizontal distributions of the contents of inner bay water after 30 tidal cycles computation from the initial condition. And Figure 14 shows the decay curves of the remnant function of the inner bay water contents calculated by mathematical model. From these figures, it is shown that the horizontal circulation induced by breakwaters has an effect on water exchange, and the vertical circulation induced by density current has an also effect on water exchange by the mathematical model experiment, too. And, the density current is decreased by the existence of the breakwaters.

Table 5 Computational conditions of mathematical model experiments.

Variables	Computational conditions
Time interval	external:30s, internal 300s
Initial condition	u=v=0.0, salinity=3.20%
Boundary condition	salinity=3.20%, amplitude=1.2m
Number of layers	5 layers
Fresh discharge	10 m3/s for each colume
Bottom friction	γ_b^2 = 0.0043
Viscosity coefficients	horizontal:5000cm2/s,vertical:8cm2/s
Diffusion coefficients	horizontal:5000cm2/s,vertical:1cm2/s
Exchange tracer	Inner bay c=0.0, Outer bay c=1.0

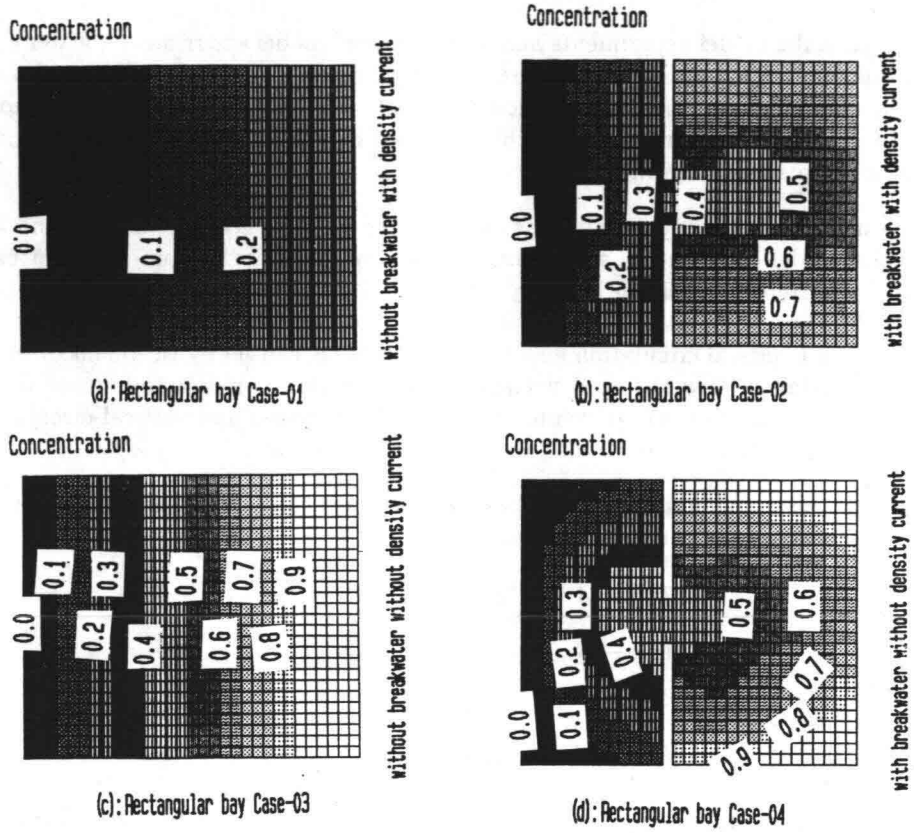

Fig.13 Horizontal distributions of the content of inner bay water
(after 30 tidal cycles from the initial condition)

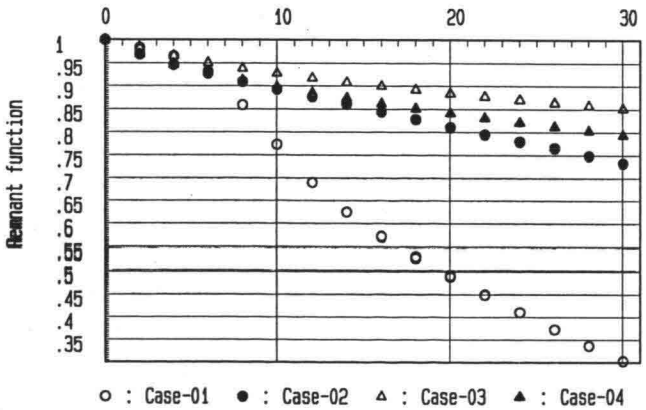

Fig.14 Decay curves of remnant function of average inner bay water content.

4.5 Discussion

By using hydraulic model experiments and mathematical model experiments, water exchange mechanisms in enclosed coastal seas were investigated. The influence of breakwaters on water exchange has two aspects in relation to density current condition. The authors tried to explain this contradictory result of the influence of breakwaters on water exchange by using the concepts as shown in Fig. 4.

Hydraulic model experimental conditions are shown in Table 3. Water exchange mechanisms in hydraulic model experiments are assumed as follows. In case of Run-A, water exchange is caused by turbulent diffusion (a) only. In case of Run-B, water exchange is caused by turbulent diffusion (a) and horizontal circulation flow (b), Run-C is caused by turbulent diffusion (a) and vertical circulation flow (c), and Run-D is caused by turbulent diffusion (a), horizontal circulation flow (b), and vertical circulation flow (c). Furthermore, the author assumes that the water exchange volume by turbulent diffusion and vertical circulation flow are proportional to the cross sectional area of the bay entrance.

According to these assumptions, the volume of water exchange of each experimental run is expressed respectively in the following equations.

$$Run-A \quad : \quad q_1 = \alpha \cdot Q \tag{7}$$

$$Run-B \quad : \quad q_2 = (\alpha \frac{s'}{S}) \cdot Q \tag{8}$$

$$Run-C \quad : \quad q_3 = (\alpha + \beta) \cdot Q \tag{9}$$

$$Run-D \quad : \quad q_4 = (\alpha \frac{s'}{S} + \beta + \gamma \frac{s'}{S}) \cdot Q \tag{10}$$

where, α is the water exchange ratio by turbulent diffusion, β is the ratio by horizontal circulation flow, γ is the ratio by vertical circulation flow, Q is the volume of water entering into a bay during flood tide or ebb tide, s' is the cross sectional area of bay entrance with breakwaters, and S is the area of bay entrance without breakwaters

$$r(t) = \exp\left\{-A_d \cdot t_d^{B_d}\right\} \tag{11}$$

where, $r(t)$ is the remnant function, t_d is the number of tidal cycles, A_d, B_d are empirical constants. Average residence time is defined by Eq.(6), and empirical constants A_d and B_d are obtained in Table 6 of each experimental run. From the table, water exchange ratios for one tidal cycle of each run can be estimated. By substituting these exchange ratios into Eqs.(7) to (10), water exchange ratios of each mechanism are obtained as α =0.199 from Run-A, β=0.198 from Run-B, and γ=0.433 from Run-C. These values are substituted into Eq.(10), and the water exchange ratio in case of Run-D is estimated as 39.1%.

Table 6 Average residence time and the value of empirical constants.

Case	A_d	B_d	τ_d (days)
Run-A	0.143	0.63	15.3
Run-B	0.201	0.57	13.2
Run-C	0.688	0.58	1.3
Run-D	0.358	0.68	2.7

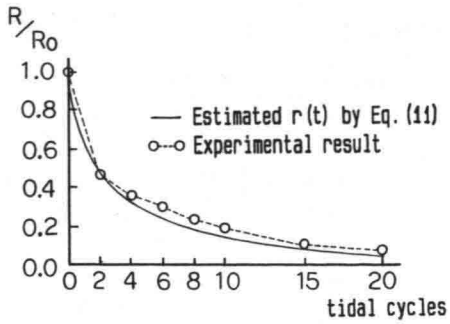

Fig.15 Comparison between experimental results and estimated results of remnant function in case of Run-D

This value is relatively close to the value of 43.6% obtained by the result of Run-D. By substituting the water exchange ratio and average empirical constant B_d into Eq.(11), the remnant function for Run-D is estimated. Figure 15 shows the comparison between the experimental result and the estimated result of the remnant function for Run-D. The estimated remnant function agrees with the experimental result.

From these considerations and very rough assumptions, different water exchange behaviors between with density current and without one can be explained successfully. Especially the contradictory effect of the influence of the breakwaters located at a bay entrance on water exchange is explained successfully.

5. PROMOTION OF WATER EXCHANGE BY CONFIGURATION OF THE ENTRANCE

In this chapter, the authors consider the water exchange mechanism induced by horizontal circulation flow only. As described before, the water exchange induced by vertical circulation flow is also very important. However the reduction of cross sectional area at bay entrance by breakwaters is absolutely necessary in order to protect the sheltered region from natural disasters such as tsunami waves or typhoon storm surges. Based upon these situations, the author investigated the water exchange promotion techniques by using hydraulic model experiments under the condition of a well mixed flow field.

The hydraulic model experiments of water exchange are carried out for several experimental conditions as shown in Table 7. The hydraulic model basin used here is a rectangular shape of 5.4m in length, 5.4m in width and 0.15m in depth. In the table, width (W) and length (L) of the entrance, number of entrances, and the layout of the breakwaters are alternated in order to investigate the effect on water exchange. The tidal amplitude of each experimental case is 0.5cm, 1.0cm, and 3.0cm, respectively.

Figure 16 shows the velocity vectors of the tidal residual flows, which are the average values of tidal velocities for one tidal cycle, and the decay curves of the remnant function of the averaged dye concentration in enclosed region in case of Run-10, and Fig.17 shows the same graphs in case of Run-30. At first, the comparison for entrance width W is carried out. Tidal amplitudes at inner region for both cases show almost the same values in spite of the different entrance width. Tidal residual flow in case of Run-10 is much larger than the flow

Table 7 Experimental cases of the rectangular model basin.

No.	Entrance	Width	Length
Run-10	1: center	90 cm	0 cm
Run-11	1: center	90 cm	180 cm
Run-20	1: center	180 cm	0 cm
Run-30	1: center	270 cm	0 cm
Run-40	1: right end	90 cm	0 cm
Run-50	2:both sides	45x2cm	0 cm
Run-60	2:both sides	45x2cm	jetties

of Run-30. The remnant function of the averaged dye concentration in inner region in case of Run-10 decreases more quickly than that of Run-30. This is the same effect of the horizontal circulation flow on water exchange as described in Section 4.2.

Next consideration is the effect of the entrance length L. Figure 18 shows the same graphs in case of Run-11. At the entrance, the cross sectional average current velocities in cases of Run-11 and Run-10 are almost the same values for both ebb and flood tides, because the volume of water entering from outside during flood tide and the entrance width are almost the same for both experimental conditions. In spite of same current velocity at the entrance, the tidal residual flow in case of Run-11 is much smaller than the flow of Run-10, and the dye concentration reduction curve in case of Run-11 decays slowly compared to Run-10.

The above difference is seemed to be caused by the following reason. In case of Run-10, there is no channel with length L=0cm, so the cross sectional area changes rapidly from outside to inside. For this entrance condition, the large vorticity is generated by the tidal current at the entrance. In case of Run-11 with the channel length L=180cm, the velocity profile of flood flow is refined due to the friction of the training walls, so the relatively weak vorticity is generated by the tidal current at the entrance. By above mentioned reasons, the relatively weak tidal residual flow is generated in case of Run-11, and the average dye concentration decay curve decreases more slowly compared to the decay curve of Run-10.

Next the authors consider the location of the entrance. Figure 19 shows the velocity vectors of tidal residual flow and the averaged dye concentration decay curve in case of Run-40 whose entrance is located at the right end with W=90cm width and L=0cm length. The average dye concentration decay curve in case of Run-40 decreases slightly slower than the decay curve of Run-10. The reason for this is considered to be that the tidal residual flow in case of Run-40 is slightly weaker than the flow of Run-10 because the distance of the left-hand part of the inner region in case of Run-40 is much far from the entrance compared to the distance of Run-10. But the difference of the average residence time between Run-10 and Run-40 is very small.

Next consideration is the number of entrances. Figure 20 shows the results of Run-50. In case of Run-50, there are two entrances with 45cm width and 0cm length. The average dye concentration decay curve in case of Run-50 decreases slightly slower than that of Run-10. In case of Run-50, both entrances generate horizontal circulation flows in opposite directions. Therefore, the energy of the horizontal circulation flow generated by one entrance is dissipated by the opposite direction of the horizontal circulation flow generated by the other entrance.

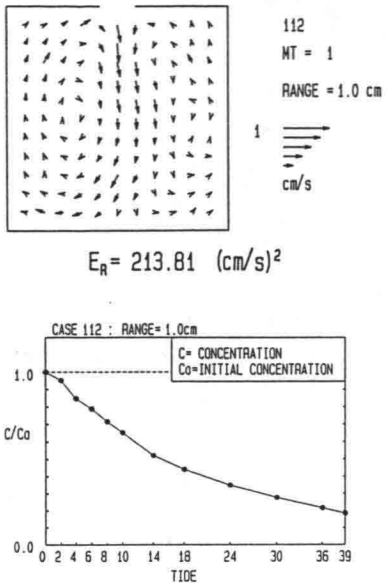

Fig.16 Tidal residual flow and decay curve of remnant function (Run-10).

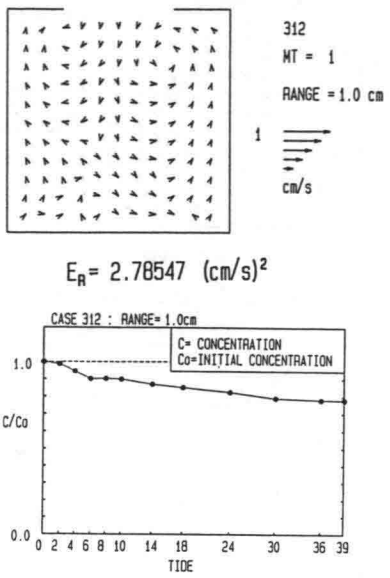

Fig.17 Tidal residual flow and decay curve of remnant function (Run-30).

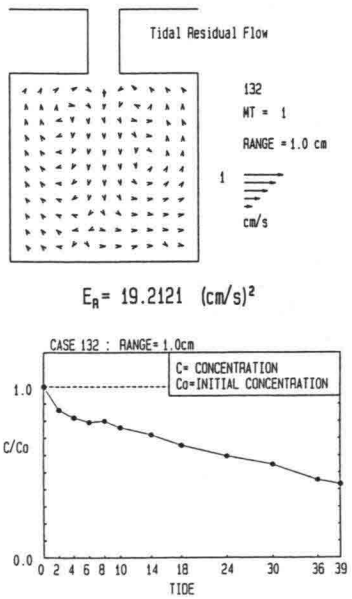

Fig.18 Tidal residual flow and decay curve of remnant function (Run-11).

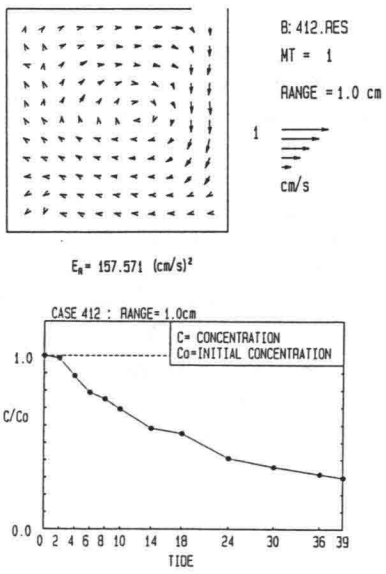

Fig.19 Tidal residual flow and decay curve of remnant function (Run-40).

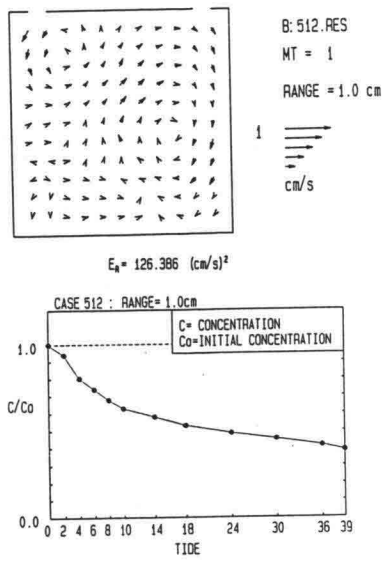

Fig.20 Tidal residual flow and decay curve of remnant function (Run-50).

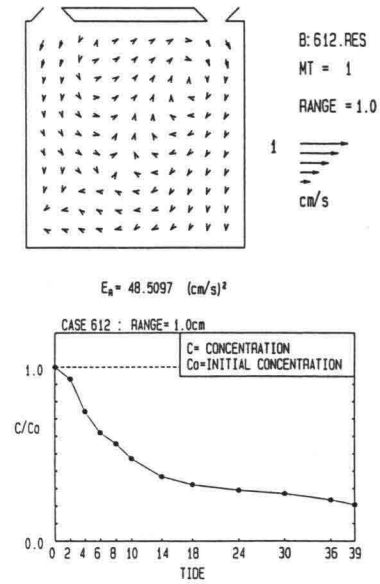

Fig.21 Tidal residual flow and decay curve of remnant function (Run-60).

This is why the water exchange in case of Run-50 is slightly smaller than the case of Run-10.

Until now from Run-10 to Run-50, the experimental conditions has been one entrance or two entrances symmetrically. By these conditions, the horizontal tidal residual flow is generated by the vorticity at the entrance, but the one-way flow at the entrance is not generated. Cross sectional average flood flow velocity is almost the same as the ebb flow velocity, so there is no significant net volume of water passing through the entrance. In order to promote water exchange, one-way flow is generated by the layout of the breakwaters as shown in Fig. 21. The right hand side of the entrance shape has the property of which the water is easy to enter from the outside, and the left hand side one has the opposite property. Therefore, weak clock-wise horizontal circulation flow is generated in the whole region. Figure 21 shows the velocity vectors of the tidal residual flow and the average dye concentration decay curve in case of Run-60. In case of Run-60, the tidal current is refined by the training jetties. Therefore a weak vorticity is generated around these entrances, and one-way flow from right-hand side entrance to left-hand side entrance is generated by the existence of the training jetties. In this way, a relatively weak tidal residual flow and one-way flow are generated as shown in Fig.21. The average dye concentration decay curve decreases relatively faster than the decay curve of other cases even if the tidal residual flow is weak. This result implies that the one-way flow generated by the training jetties has a large effect on water exchange between inner and outer water bodies. According to these experimental results, the average residence time (Eq.6), the total energy of tidal residual flow (Eq.12), and the total value of the circulation (Eq.13) in enclosed region are estimated.

$$E_R = \frac{1}{2}\Sigma\left(u_R^2 + v_R^2\right) \tag{12}$$

$$L_R = \Sigma\left(\left|\frac{\partial v_R}{\partial x} - \frac{\partial u_R}{\partial y}\right|\right) \tag{13}$$

where, E_R : the total energy of the tidal residual flow in enclosed region, L_R : the total value of the circulation in enclosed region, u_R : the velocity of the tidal residual flow in x-direction, v_R : the velocity of the tidal residual flow in y-direcrion.

Figure 22 shows the relationship between the total energy of the tidal residual flow (E_R) and the total value of the circulation (L_R). A good relationship between these values is obtained for every experimental case. This means that the tidal residual flow in the enclosed region is generated by the convection of vorticity which is released at the entrance of the region. In cases of Run-11 and Run-60, the total energy of the tidal residual flow is smaller than other cases because the shape of the entrance for both cases has training jetties or training channel, which generates relatively weak vorticity at the entrance.

Figure 23 shows the relationship between the average residence time and the total value of the circulation for each experimental case. From the figure, the following characteristics of the average residence time are obtained. The average residence time decreases as the total value of the circulation increases. In case of the same amplitude experimental conditions, the average residence time becomes small as the width of the entrance decreases and the length of the entrance channel decreases. One-way flow in case of Run-60 has a large effect on water exchange even if the total value of the circulation is not large.

6. CONCLUDING REMARKS

In this paper, the author investigated the water exchange mechanisms in enclosed coastal seas by using hydraulic model experiments. Especially, the influence of the breakwaters located at the bay entrance on water exchange is examined. Conclusions obtained from these experiments are summarized as follows:
(1) The tidal residual flow is generated by the vorticity which is formed at the entrance of the region. (2) Water exchange is promoted by the total value of the circulation. The

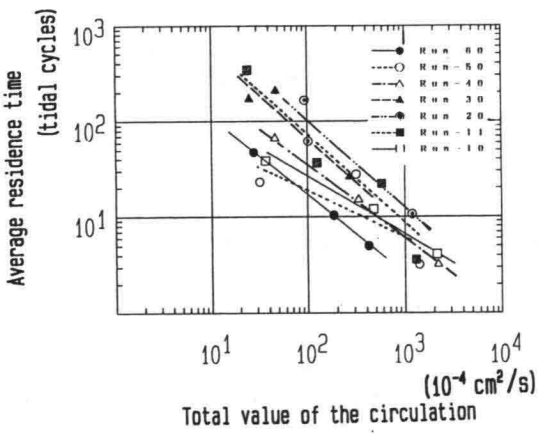

Fig.22 Relationship between the total energy of the tidal residual flow and the total value of circulation.

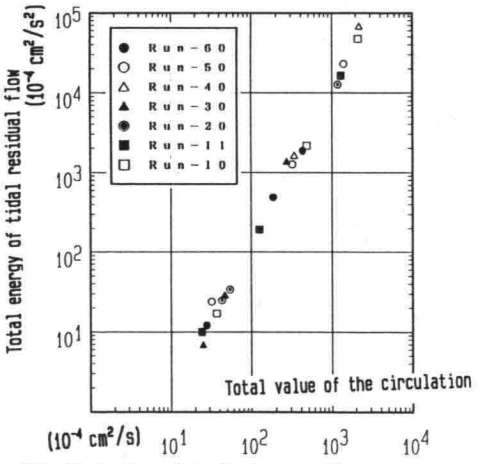

Fig.23 Relationship between the average residence time and the total value of circulation.

total value of the circulation increases as the width of the entrance decreases and the length of the entrance channel decreases. (3) To excavate the new channel without gate operation affects water dilution only near the channel, but does not have effect on water exchange for whole over the enclosed region. (4) One-way flow generated by the training jetties or the gate operation in the new channel has large effect on water exchange. The generation of enforced horizontal circulation flow induced by the gate operation has a large effect on water exchange promotion between contaminated inner bay and clean ocean water bodies. (5) Influence of the breakwaters located at the bay entrance on water exchange has two aspects. As to the case without density current, the existence of the breakwaters promotes the water exchange because the horizontal circulation flow is generated behind the breakwaters. On the other hand in case of with density current, water exchange decreases due to the existence of the breakwaters because the vertical circulation flow is suppressed by the breakwaters. (6) Based on some very rough assumptions, this contradictory result of influence of breakwaters on water exchange is explained successfully. (7) When we predict the influence of marine structures on water exchange, we must consider both configuration conditions and detailed flow field conditions of concerned area.

These considerations are carried out by using hydraulic model experiments. Water exchange experiment by this model has a fundamental problem, which is the unrealistic still water in the enclosed region at the initial stage of the experiment. The author would like to continue the investigation by using mathematical model experiments for stratified flow condition.

REFERENCES

Bolin, B. and H. Rohde (1973): A note on the concepts of age distribution and transit time in natural reserviors, Tellus, Vol.25, No.1, pp.58-62.

Fischer H. B. (1972): Mass transport mechanismsin stratified estuaries, Journal of Fluid Mechanics, Vol.53, pp.671-687.

Fischer H. B., et al.(1979): Mixing in inland and coastal waters, Academic Press, 483 p.

Murakami, K., M. Moriawa, M. Shirai and E. Sato (1986): Physical model experiments on the increase tidal exchange by an enforced tidal circulation - Investigation using Kagoshima Bay model -, Tech. Note of Port & Horbour Research Institute, No.544, 31 p.(in Japanese)

Murakami, K.: Hydraulic model experiments on water exchange for enclosed inner bay, International Symposium on Scale Modeling, Tokyo, Japan, pp.301-307

Murakami, K. and M. Shirai (1990): Investigations on water exchange with density current by hydraulic model experiments, Tech. Note of Port & Harbour Research Institute, No.625, 29 p.(in Japanes)

Murakami, K.(1992): Tidal exchange mechanism in enclosed regions, 2nd Int'l Conf. on Hydraulic and Environmental Modelling of Coastal, Estuarine and River Waters, Univ. of Bradford, Vol.1, pp.111-120.

Parker, D. S., D. P. Norris and A. W. Nelson (1972): Tidal exchange in at Golden Gate, Proc. of ASCE, Vol.98, SA2, pp.305-323.

Takeoka, H.(1984): Fundamental concepts of exchange and transport time scales in a coastal sea, Continental Shelf Research, Vol.3, No.3, pp.311-326.

HYDRO-PORT'94
International Conference on Hydro-Technical
Engineering for Port and Harbor Construction
October 19 - 21, 1994, Yokosuka, Japan

Development of Model by Soil Diffusion within Dam

Moon Seup Shin [1]
Jong Nam Lee [2]
Sung Kun Hong [3]

[1] Dept. of Ocean Civil Engineering, Kunsan National University
1044-2 So Ryung Dong Kusan Chon Buk
[2] Dept. of Civil Engineering, Kyunghee University
1 Hoe Gi Dong Seoul
[3] Dept. of Fisheries, Kunsan National University
1044-2 So Ryung Dong Kusan Chon Buk

ABSTRACT

Field survey and monte carlo method finite difference method was conducted to estimate the soil diffusion for point of dredging work and outlet of muddy water in the Euam Dam in Kang Won-Do, Korea. As a result of comparing the values of on-the-spot survey and the two theoretical method, the following conculusions can be obtained. 1) We see the possibility of modelling about the diffusion of moving flow by Monte Carlo method which pursuits the volume of flow, time, and the number of particles using the sampling of random number not solving the Fick's diffusion equations. 2) In the Lagrangian approach by Monte Carlo method which focus on the movement of particles, the density and the range of diffusion of sediment using the regular random number are almost same as in case of using the uniform random number. 3) We see the high stability of calcualtion, the non-accumulation of error, the high precision by increasing the number of random sampling, and the simple application even in complex boundary conditions, if we use the Monte Carlo method in the

prediction of the diffusion of turbid water due to desilting and reclamation according to the developement of Boongeuh island within Yeuam lake.4) As a results of estimation of the sediment density and the diffusion range of the drained sediment at the desilting spot and at the drainage of desilting sediment, the obtain ed three sediment densities which are one by on-the-spot survey, by the Monte Carlo method and by the difference method for the solution of diffussion equation almost same within the range 10-20 % error.

1. INTRODUCTION

The purpose of this papaer is the development of the prediction model of the density and the diffusion range of floating dust which occurs around the cutter and the turbid water which discharges from drain tile and spillway due to desilting and reclamation within lake.

The numerical prediction and on-the-spot survey are carried out about the density of turbid water due to the developement of Boongeuh island within Yeuam-Dam lake. On -the-spot survey is conducted at the desilting spot and at the outlet of turbid water. The numerical prediction methods are the difference method which is one of the deterministic method transforms the basic equationas to the dispersion value, and the Monte Carlo Method which is one of the probability method pursuit s the volume of flow, time, and the number of particles using the randomness not solving the differential equations.

2. FIELD SURVEY

2.1 Outline of survey

On the purpose of the developement of Boongeuh island within the Yeuam-Dam lake, Choonchon City, Kangwon Province, the desilting work is to perform from August 1991 to December 1992. The area of developement is 96,000 pyung. The pump desilting ship is used. The average working time of desilting is 17 hours per day. The maximum amount of desilting is about 3,000 m^3 per day. The physical properties of desilting ship are as follows; Length: 22 m, Width: 7 m, Diameter of drain pipe: 350 mm.

Four spots are selected to investigate the distribution of bottom material.

2.2 Method of survey

In order to investigate the distribution of bottom material within Yeuam lake, the sampling is performed using the sampler at four spots which indicated on figure 2-1.

In order to investiagte the distribution of turbid water due to desilting, the turbidity measurement is conducted in the topstratum and the meddle-stratum at the desilting spots, and at outlet of turbid water as shown figure 2-1.

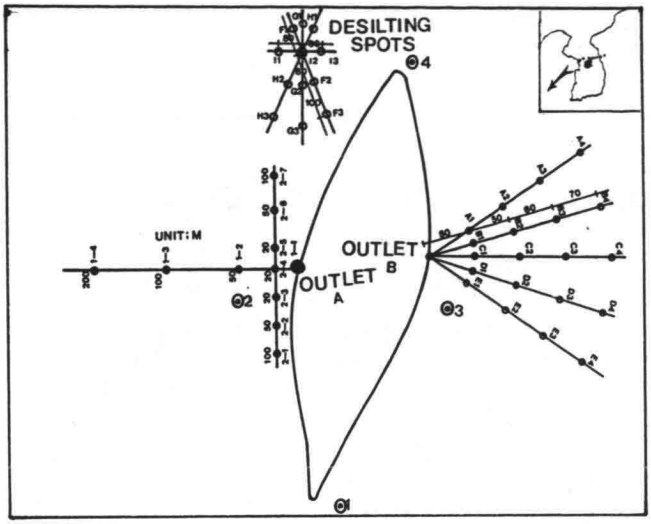

Fig. 2-1 Point of turbidity

2.3 Analysis of results

The results of grain size analysis of bottom material at four spots within Yeuam lake as follows: the bottom materials of Yeuam lake are sand and gravel, the distribution percentage of silt is less than 4%. At No. 4 spot the size of sampled gravel is 30mm-70mm.

The results of analysis of turbid water collected at desilting spots as follows: the density of turbid water collected at desilting spots is 40-250 mg/l, the one of the outlet at spot 'A' is 3-912 mg/l, and the one of the outlet at spot 'B' is 2-60 mg/l.

3. DIFFUSION OF TURBID WATER DUE TO PUMP DESILTING

3.1 Diffusion of turbid water by Monte Carlo Method

The methods of numerical analysis of diffusion model are the Eulerian method(deterministic method) represented by finite difference method and the Lagrangian method(probability method) represented by Monte Carlo method that we focus on the movement of particle. The prediction method of the diffusion of turbid

water due to desilting and reclamation according to the developement of Boongeuh island within Yeuam lake is the Monte Carlo method which contains the conservation of mass, the high stability of calcualtion, the non-accumulation of error, the high precision by increasing the number of random sampling, and the simple application even in complex boudary conditions. The dispersion of movement is appeared as figure 3-1.

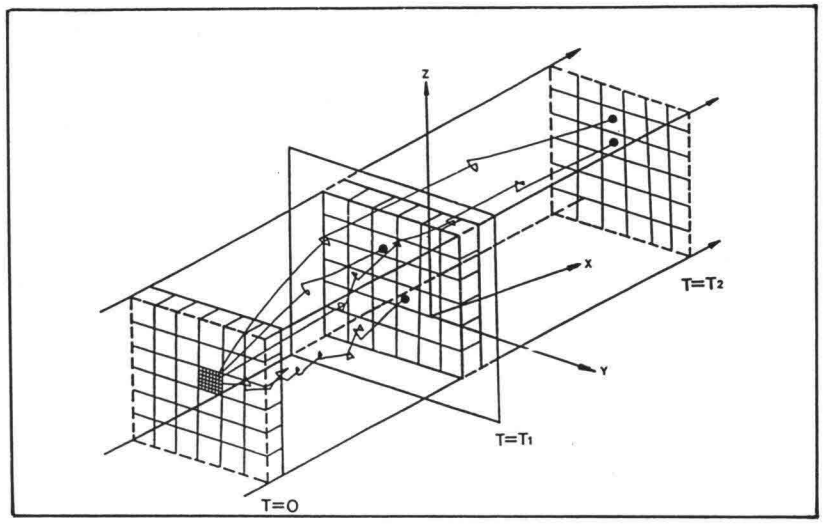

Fig. 3-1 variance of particles

3.2 Diffusion model by sampling of random number

The one dimensional flow describes as:

$$u = U + \beta y + \gamma z$$

where U is the average velocity in x direction

β, γ are the linear distribution functions in the directions y and x respectively

At time $t=n\triangle t$, the particle moves from $(x^{(n)}, y^{(n)}, z^{(n)})$ to $(x^{(n+1)}, y^{(n+1)}, z^{(n+1)})$ after time $\triangle t$. The distances of movement in directions x, y, z which correspond to vortex diffusion term due to sampling of random number are l_x, l_y, l_z respectively. Then:

$$\begin{aligned} x^{(n+1)} &= x^{(n)} + l_x + (U + \beta y^{(n+(1/2))} + \gamma z^{(n+(1/2))})\triangle t \\ y^{(n+1)} &= y^{(n)} + l_y \\ z^{(n+1)} &= z^{(n)} + l_z \end{aligned} \qquad (3\text{-}1)$$

where

$$\begin{aligned} y^{(n+1/2)} &= (y^{(n+1)} + y^{(n)})/2 \\ z^{(n+1/2)} &= (z^{(n+1)} + z^{(n)})/2 \end{aligned} \qquad (3\text{-}2)$$

l_x, l_y, l_z : Each has different value for each time step. In order to determine the distances of movement l_x, l_y, l_z, the uniform random number used. The sampling range

of random numbers a, b, c is -0.5 - 0.5. The random numbers a, b, c are different each other. Then A, B, C are expressed as:

$$A = \frac{a}{(a^2 + b^2 + c^{2)}}$$

$$B = \frac{b}{(a^2 + b^2 + c^{2)}} \qquad (3\text{-}3)$$

$$C = \frac{c}{(a^2 + b^2 + c^{2)}}$$

In equ.(3-3), the average value of A, B, C is zero. Because the dispersion is ⅓ distribution, the relation of the dispersion of distance of movement σ^2 and the coefficient of diffusion is expressed as:

$$K = \sigma^2/2\triangle t \qquad (3\text{-}4)$$

and using the equation (3-4), the distances of movement are discribed as:

$$\begin{aligned} l_x &= A\times(3\times2\times\triangle t\times k_x)^{1/2} \\ l_y &= B\times(3\times2\times\triangle t\times k_y)^{1/2} \\ l_z &= C\times(3\times2\times\triangle t\times k_z)^{1/2} \end{aligned} \qquad (3\text{-}5)$$

In case of normal random numbers A, B, C, the average is 0 and the disprsion is 1.0. Then the distances of movement of particle can be written:

$$\begin{aligned} l_x &= A\times(2\times\triangle t\times k_x)^{1/2} \\ l_y &= B\times(2\times\triangle t\times k_y)^{1/2} \\ l_z &= C\times(2\times\triangle t\times k_z)^{1/2} \end{aligned} \qquad (3\text{-}6)$$

The calculation of density is carried out by considering the number of particles which get in the grid at time (t) = t, assumed that N particles started from time t=0, x=0, y=o.

In the process of calculation of density, it makes the dispersion small as average because the dispersion of particles is great in case of small number of particles. The dispersion of turbidity can be considered about only two procedures of moving

flows and diffusion in those four procedures of moving flow, plunging, diffusion, and refloatation. The number of sampling in random numbers A, B, C is 20,400 respectively. The table 1 shows the conditions used in the estimation of the diffusion of turbid water at the outlet of drainage and the spot of desilting.

Table 1 condition of calculation

mean velocity	4cm/sec
diffusion coefficient(kx)	4,300 cm2/sec
diffusion coefficient(ky)	4,300 cm2/sec
diffusion coefficient(kz)	500 cm2/sec
mesh size(△x)	50 m
mesh size(△y)	50 m
mesh size(△z)	1 m
sampling volume of turbid water at the desilting spot	7,111 mg/sec
point of sampling	x=11, y=11, z=1
sampling volume of turbid water at outlet(A)	912 mg/sec
sampling volume of turbid water at outlet(B)	362 mg/sec
point of sampling	x=1, y=11, z=1
time interval(△t)	60 sec
working time	1920 sec

3.3 Numerical analysis by Monte carlo Method

The figures 3.3.1-2 show the horizontal distributions of the density calculated using the uniform random number and the normal random number after the working time 1920 seconds at the outlet of turbid water (A),(B), and the figure 3.3.3 shows it at the spot of desilting.

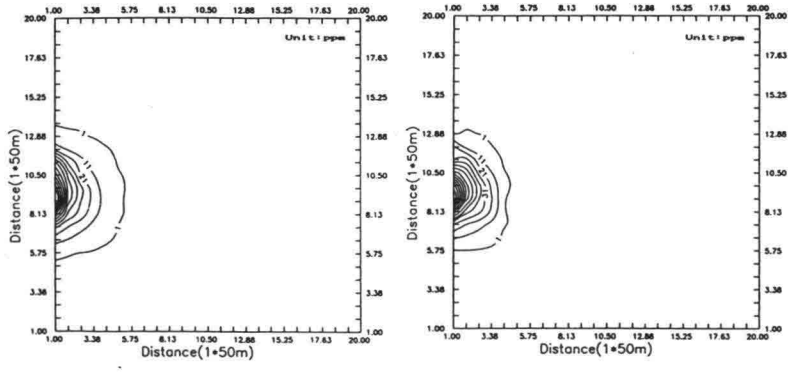

uniform random number normal random number

Fig.3.3.1 distribution of concentration for turbid water at outlet(A)

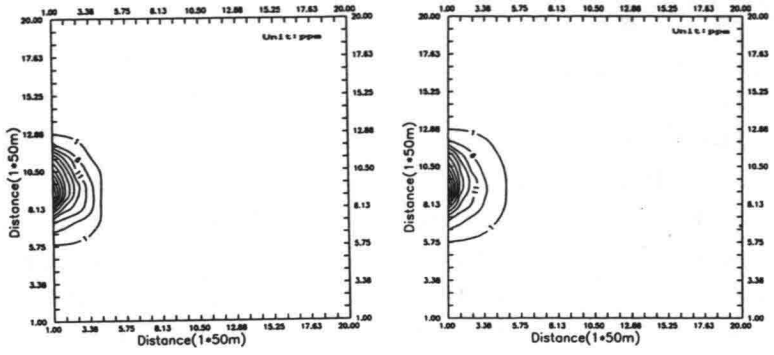

uniform random number normal random number

Fig. 3. 3. 2 distribution of concentration for turbid water at outlet(B)

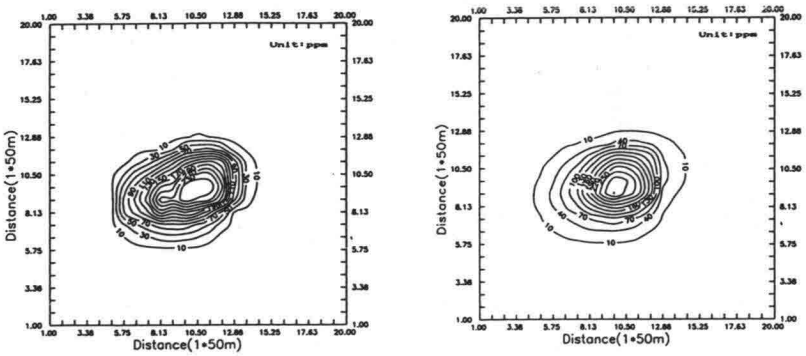

uniform random number normal random number

Fig. 3. 3. 3 distribution of concentration for turbid water at the desilting spot

3.4 Equation of diffusion

The diffusions of suspension material, warm-water drainage, salinity at lake, river, sea area mainly due to the moving flow by the movement of diffusion, dispersion and average flow. There are two diffusions, namely, the particle diffusion due to the difference of density and the turbulence diffusion due to the turbulence of flow.

The classic theory of diffusion is established by Fick. The diffusion equation about the sediment due to the desilting in Yeuam-Dam lake can be expressed by the Fick type equation about the two dimensional flow.

$$\frac{\partial c}{\partial t} + u\frac{\partial c}{\partial x} + v\frac{\partial c}{\partial y} = k_x\frac{\partial^2 c}{\partial x^2} + k_y\frac{\partial^2 c}{\partial y^2} \qquad (3\text{-}7)$$

Considering the plunging of sediment, the above equation could be

$$\frac{\partial c}{\partial t} + u\frac{\partial c}{\partial x} + v\frac{\partial c}{\partial y} = k_x\frac{\partial^2 c}{\partial x^2} + k_y\frac{\partial^2 c}{\partial y^2} - W_0 C \qquad (3\text{-}8)$$

where W_0 : the velocity of plunging

3.4.1 Difference equation

In the soluton process of diffusion equation, the foreward difference method used in the difference of time term, which obtain the unknown variable at time $t=(n+1)\triangle t$ from known variable at time $t=n\triangle t$ and leap-frog method used in the difference of moving flow term. The figure 3.4.1 shows the results of calculation of the density distribution of turbid water after working time 1920 seconds at the desilting spot and the outlet of drainage (A),(B).

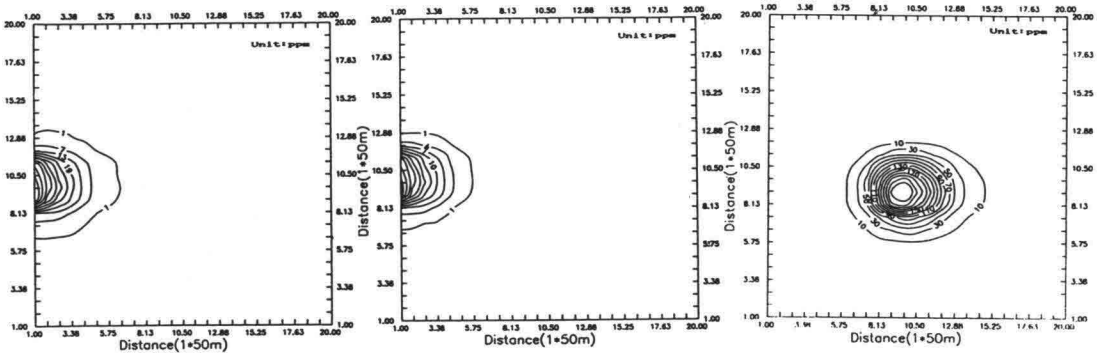

point of outlet(A) point of outlet(B) desilting spot

Fig.3.4.1 distribution of concentration for turbid water by difference method

4. RESULTS AND DISCUSSION

4.1 Discussion of the application of model

In order to investiage the application of prediction model for the sediment density and the range of diffusion about the drained sediment at the desilting spot and the outlet of drainage, the three sediment densities which obtained by on-the-spot survey, by the two Monte Carlo method(uniform random number, regular random number) and by the difference method for the solution of diffussion equation compared as shown in figures 4.1-2. In the figure, (○:uniform random number), (●:regular random number), (X:difference method), (□:on-the-spot survey) indicate the densities after working time 1920 seconds.

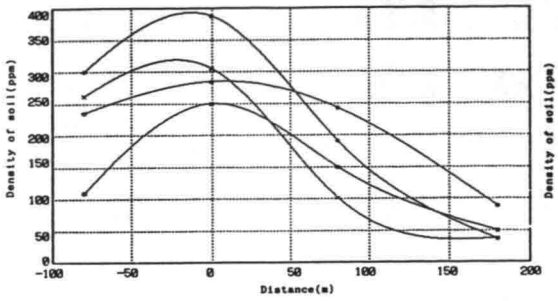

desilting spot(G-3)

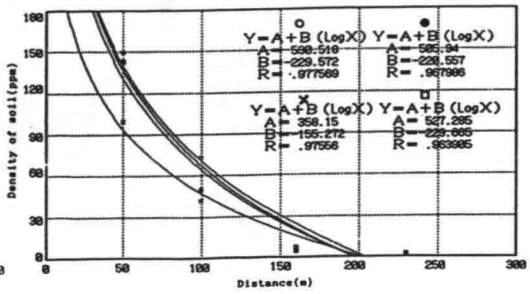

point(2.5-7) of outlet(A)

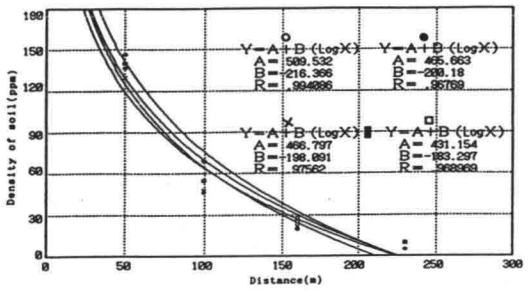

point(2.1-3) of outlet(A)

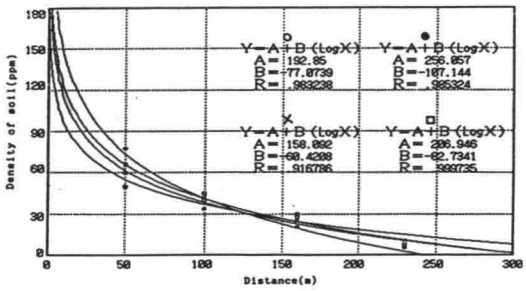

point(1.2-4) of outlet(A)

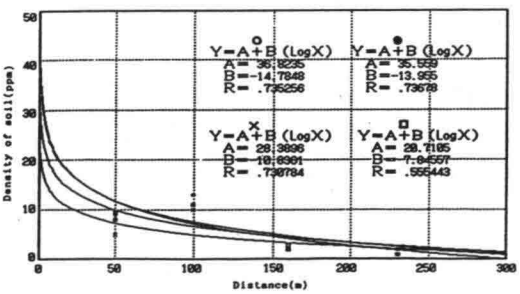

point(A1-4) of outlet(B)

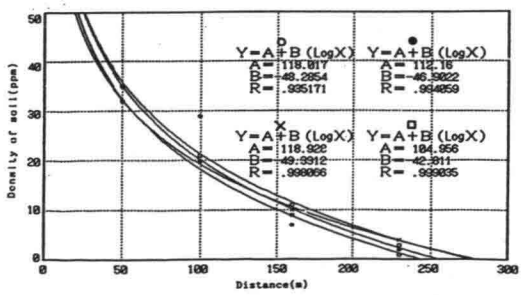

point(B1-4) of outlet(B)

Fig.4.1 distribution of concentration for turbid water at each point

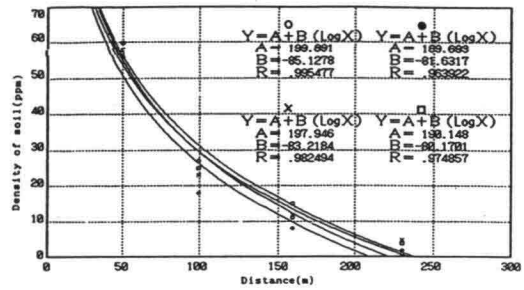

point(C1-4) of outlet(B)

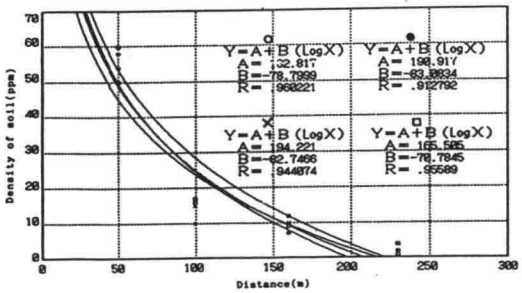

point(D1-4) of outlet(B)

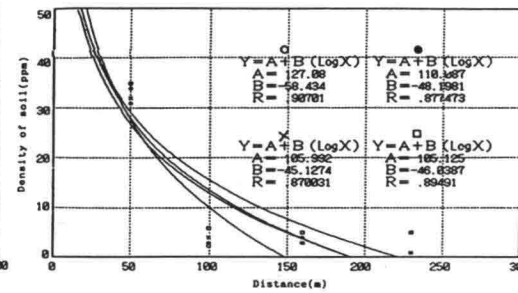

point(E1-4) of outlet(B)

Fig.4.2 distribution of concentration for turbid water at each point

5. CONCLUSIONS

In order to estimate the densities and the range of diffusion of floating material due to desilting and plunging, on-the-spot survey carried out at the desilting spot and the outflow area of turbid water, and the numerical prediction was conducted by the difference method that the basic equation which is one of the deterministic method transforms as the dispersion value and the Monte Carlo Method which is one of the probability method such that it pursuits the volume of flow, time, and number of particles using the randomness not solving the differential equations.

As a result of comparing the values of on-the-spot survey and the two theoretical method, the following conculusions can be obtained.

1. We see the possibility of modelling about the diffusion of moving flow by Monte Carlo method which pursuits the volume of flow, time, and the number of particles

using the sampling of random number not solving the Fick's diffusion equations.

2. In the Lagrangian approach by Monte Carlo method which focus on the movement of particles, the density and the range of diffusion of sediment using the regular random number are almost same as in case of using the uniform random number.

3. We see the high stability of calcualtion, the non-accumulation of error, the high precision by increasing the number of random sampling, and the simple application even in complex boundary conditions, if we use the Monte Carlo method in the prediction of the diffusion of turbid water due to desilting and reclamation according to the developement of Boongeuh island within Yeuam lake.

4. As a results of estimation of the sediment density and the diffusion range of the drained sediment at the desilting spot and at the drainage of desilting sediment, the obtained three sediment densities which are one by on-the-spot survey, by the Monte Carlo method and by the difference method for the solution of diffussion equation almost same within the range 10-20 % error.

REFERANCES

1. Im, Yeong Chun. Shin, Dong Su. Shin, Moon Seup. (1988). Reclmation Engineering. Keyng moon sa.
2. Lee, Jong Nam & Shin Moon Seup. (1987), Fisheries civil engineering, Keyng moon sa.
3. Shin, Moon Seup(1990), A study on the behavior of muddy waer lumps caused by dropping soil in coastal areas, Thsis of Ph. D, Kyung hee university.
4. Lee, Jong Nam & Shin Moon Seup. (1990). An Experimental Study on the Behavior of Muddy Water Lumps caused by Dropping Soil in Coastal Areas, Journal of Korean Society of Coastal and Ocean Engineers, Vol. 2, No. 4.
5. Shin Moon Seup, Ko Byung Wook. (1990). A Study on a analysis of unsteady flow, Repts. of Kunsan National Fisheries Junior College, Vol. 24. pp. 9-15.
6. Shin Moon Seup. (1990). A Study on the Behavior of Brine Lumps caused by Dropping Brine in Coastal Areas, Bulletin of Fisheries Science Institute Vol. 6.
7. Lee, Jong Nam., K. Nakatsuji & Shin Moon Seup. (1991). A Study on the Behavior of Brine Lumps caused by Dropping Brine in Coastal Areas, Journal of Korean Society of Coastal and Ocean Engineers, Vol. 3.
8. Shin Moon Seup, Lee Jong Nam. (1991). An Analysis of Diffusion by probability Method, Journal of Korean Society of Coastal and Ocean Engineers, 8.
9. Shin Moon Seup, Lee Jong Nan, Ko Byeng Uk, Park Sang Bai. (1992). Diffusion pre-estimate of soil by Punp Dredging Work, 34 Korean Society of Hydrology.
10. Shin Moon Seup, Lee Jong Nan, Ko Byeng Uk, Park Sang Bai, Jang In Kyu. (1992). Diffusion pre-estimate of soil caused by a tidal embankment

construction, 34 Korean Society of Hydrology.

11. Takeshi Horie. (1987). Mathematical modeling on the fate of suspended particles caused by marine works and application of the models to environmental monitoring, Report of the port and harbour research institute vol. 26.
12. Hino, M. (1965). Digital computer simulation of turbulent diffusion. Proc. 11th Congress of the , Vol. 2, pp. 1-11.
13. Hino, M. (1965). Digital computer simulation of random phenomena , Trans of JSCE, No. 123, Nov. 1965, pp. 33-43.
14. J. A. Fleck, J. D. Cummings. (1971). An Implicit Monte Carlo Scheme for Calculating Time and Frequency Dependent Nonlinear Radiation Transport, Jour. of Computational Physics 8, pp. 313-342.
15. J. E. Cermak. (1962). Lagrangian similarity hypothesis applied to diffuion in turbulent shear flow, Fluid of Mech. 15, pp. 49-64.
16. J. W. Elder. (1958). The dispersion of marked fluid in turbulent shear flow. Fluid of Mech. 5, pp. 544-560.
17. K. W. Bedford, O. W. Charles, M. Libicki, R. V. Evra. (1987). Sediment entrainment and deposition measurements in long island sound, J. of Hydraulic Engineering, 113 , No. 10, ASCE. pp. 1325-1342.
18. R. V. Ahilan, F. A. Sleath. (1987). Sediment transport in oscillatory flow over flat beds. J. of Hydraulic Engineering, 113, No. 3, ASCE. pp. 308-322.
19. J. Akiyama, H. Stefan. (1985). Turbidty current with erosion and deposition. J. of Hydraulic Engineering, 111, No. 12, ASCE. pp. 1473-1496.

HYDRO-PORT'94
International Conference on Hydro-Technical
Engineering for Port and Harbor Construction
October 19 - 21, 1994, Yokosuka, Japan

A Physical-Biological Simulation on a Nutrient Absorption Process by Seaweed in the Bay

Keita Furukawa
Yasushi Hosokawa

Port and Harbour Research Institute, Ministry of Transport
1-1, Nagase 3-chome, Yokosuka, Kanagawa, 239

ABSTRACT

A physical-biological model for Tokyo Bay was employed to calculate an effect of a nutrient absorption process by seaweed in a shallow water region. The numerical model is effective for the estimation of water quality distribution controlled interactively by biologic and hydraulic processes. The biological model contained 8 biological compartments. The physical model predicted 3D flow in the bay. It had 1 km mesh resolution in the horizontal plain and 3 levels' layers in the vertical axis. We carried out simulations for 3 different boundary conditions. Those were 1) a present condition, 2) a past condition, and 3) a tentative condition. In the past condition, a tidal exchange rate was assigned bigger than that in the present condition. The standing mass of nitrogen in the bay was decreased by this effect. In the tentative condition: the seaweed vegetated more than that in the present condition, and absorption rate of nitrogen was bigger than that in the present condition. The standing mass of nitrogen in the bay was also decreased. By using analysis, we could estimate the spatial effect of the nutrient absorption by seaweed was compared with the spatial distribution of residence time.

Key Words: Numerical Simulation, Sensitivity Analysis, Residence Time, Tokyo Bay, Nutrient Capacity in the Bay

1. INTRODUCTION

In 1936, the water surface of Tokyo Bay was about 1140 km^2 inside the boundary line connecting Futsu and Yokosuka. The area of shallow water region (less than 10 m depth) was about 450 km^2. After many reclamation projects were completed, those areas were decreased to about 900 km^2 and 180 km^2 in 1984.

Tokyo Bay's ecosystem is dominated by phosphorus as introduced by Sasaki(1991). Sasaki(1991) also pointed out the absorption process in the shallow water region plays an important role for nutrient circulation. The shallow water region is potential habitat of seaweed. Seaweed can absorb nutrients. The local reduction of the shallow water region will decrease the nutri-

ent assimilation capacity in the bay. A physical-biological model was employed for making a trial calculation to estimate this effect.

In the section 2., the physical-biological modeling is introduced. The model can be written as two parts. One is a part of biological reaction process. The other is a part of physical (hydraulic) process. A residence time analysis method is also described in this section for the estimation of the nutrient circulation in the bay.

In the section 3., some results obtained through the model calculations are described. 1) We applied sensitivity analysis of the biological model, 2) Comparisons among the results under the different conditions with 3D model and 3) results of remnant time analysis.

2. A PHYSICAL-BIOLOGICAL MODEL AND RESIDENCE TIME ANALYSIS

2.1 Biological Model

(1) Outline of the Model

The biological model was constructed for the simulation of the nutrient circulation as Hosokawa *et al.*(1993). The model contains eight compartments as: Phytoplankton (PHY), Zooplankton (ZOO), Dissolved Organic Carbon (DOC) for detritus, Particulate Organic Carbon (POC), Dissolved Inorganic Phosphorus (DIP), Dissolved Inorganic Nitrogen (DIP), Dissolved Oxygen (DO) and Chemical Oxygen Demand (COD). Kremer *et al.*(1987) showed a masterpiece of biological modeling for Narragansett Bay. Nakata(1993) improved the Narragansett Bay model and introduced new model parameters. Our model stands on these valuable works, but it is simplified. A schematic view of the model is shown in Fig. 1.

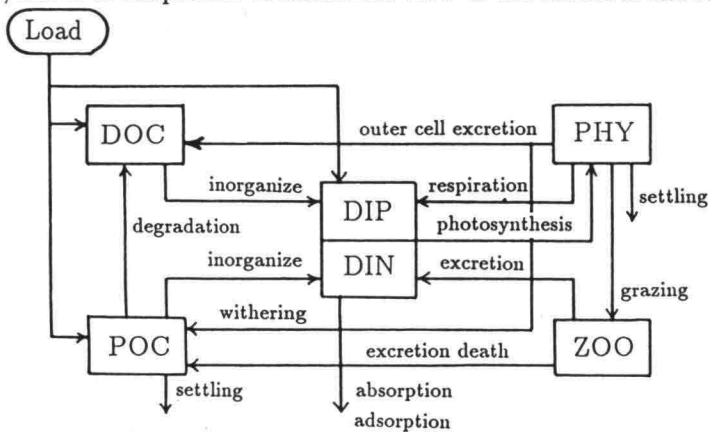

Figure 1: Schematic View of Biological Model

Loads come from rivers and bottom sediment in the form of DOC, POC, DIP and DIN. Nutrients circulate in the system through PHY and ZOO compartments. DO and temperature (T) restrict the each reaction rate in this system. In this model, temperature is assumed as a function of the depth of the each layer.

(2) DIN Absorption Processes
In the shallow water region, DIN is absorbed by seaweed and adsorbed by bed materials. The adsorption rate from overlaying sea water to the bottom sediment (v_b)[mg atm /(m^2 · day)] is written as,

$$v_b = 0.021 \cdot NO_3^{1.13}. \quad (1)$$

NO_3 value is assumed as NO_3 = DIN / 2. The Eq.(1) was based on the observation data obtained in the deep water region. So, we used three times bigger adsorption rate for the shallow water less than 10 m depth.

The absorption rate from sea water to seaweed was assumed as a function of the depth. In the region that 0-5 m depth, the absorption rate is $v_{s5} = 20.7$[mg atm /(m^2 · day)]. In the region that 5-10 m depth, the absorption rate is $v_{s10} = 29.2$[mg atm /(m^2 · day)].

2.2 Physical Model

(1) Outline of the Model
The physical model was constructed for the prediction of the 3D flow in the bay. It is required that the model can treat:

- density stratified flow,
- enough spatial resolution to describe the geographical boundary condition, and
- tidal current is controlled by water elevation at the open boundary at bay mouth.

For the first request, we employed the level-model for the treatment of density stratified flow with some simplification.

For the second request, the model has 1 km mesh resolution in the horizontal plain and 3 leveled layers in the vertical axis.

For the last matter, the simple open boundary condition is set at the bay mouth. We assign:

- water elevation is fluctuated as a sinusoidal curve, and
- velocity vector does not change when across the open boundary.

(2) Governing Equations
Figure 2 shows coordinate system for governing equations. Governing equations are based on Navier-Stokes Equation and a mass conservation equation. Simplification was made assuming:

- fluid is not compressible,
- horizontal velocity speed exceeds vertical one,
- spatial density variation is small,
- pressure is described by hydrostatic pressure, and
- buoyant effect can be treated by Boussinesq's approximation.

The continuity equation described as:

$$\frac{\partial u}{\partial x} + \frac{\partial v}{\partial y} + \frac{\partial w}{\partial z} = 0. \quad (2)$$

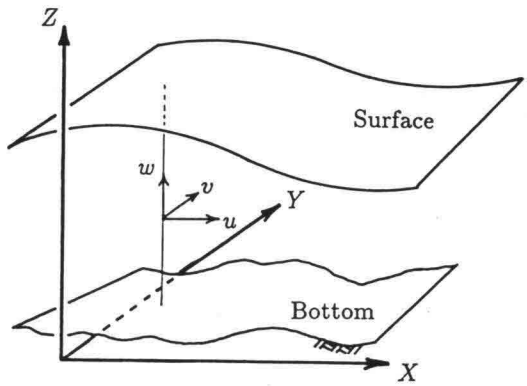

Figure 2: Coordinate System

The momentum mass transport equation described as:

$$\begin{aligned}
\frac{\partial u}{\partial t} &+ u\frac{\partial u}{\partial x} + v\frac{\partial u}{\partial y} + w\frac{\partial u}{\partial z} \\
&= vF - \frac{1}{\rho_0}\frac{\partial P}{\partial x} + \nu_h\left(\frac{\partial^2 u}{\partial x^2} + \frac{\partial^2 u}{\partial y^2}\right) + \nu_z\left(\frac{\partial^2 u}{\partial z^2}\right), \qquad (3) \\
\frac{\partial v}{\partial t} &+ u\frac{\partial v}{\partial x} + v\frac{\partial v}{\partial y} + w\frac{\partial v}{\partial z} \\
&= -uF - \frac{1}{\rho_0}\frac{\partial P}{\partial y} + \nu_h\left(\frac{\partial^2 v}{\partial x^2} + \frac{\partial^2 v}{\partial y^2}\right) + \nu_z\left(\frac{\partial^2 v}{\partial z^2}\right), \qquad (4) \\
\text{and} \quad 0 &= -g\frac{\rho_0 - \rho}{\rho_0} - \frac{1}{\rho}\frac{\partial P}{\partial z}. \qquad (5)
\end{aligned}$$

Where u, v and w are velocity components parallel to x, y and z axis. ρ is density of the fluid that is determined by density diffusion equation and ρ_0 is the fixed reference value of density. ν_h and ν_v are kinetic viscosity for the horizontal direction and the vertical direction. F is Coriolis force.

Governing equations (Eq.(2)$\sim$(5)) were integrated for each vertical layer. For solving these equations by the ADI method as Kaneko(1975), each equation was differentiated using a staggered mesh system.

2.3 Residence Time Analysis

Residence time (τ_r) is a life time indicator for an entrained object in a designated region as described by Takeoka(1984). It was defined as:

$$\tau_r = \int_0^\infty r(t)\mathrm{d}t. \qquad (6)$$

Where, $r(t)$ is a remnant function of the object normalized by initial concentration r_0.

If we assume a simple first order reaction process for $r(t)$, $r(t)$ is written as

$$\frac{dr}{dt} = -\alpha \cdot r \tag{7}$$

$$\text{and} \quad r(t) = \exp(-\alpha t). \tag{8}$$

In this case, Eq.(6) can be easily integrated as $\tau_r = 1/\alpha$.

3. RESULTS AND DISCUSSIONS

3.1 Sensitivity Analysis of Biological Model

A sensitivity analysis for the biological process was conducted by using one box model. A basic case was selected as to express Tokyo Bay's configuration as shown in Table 1.

Table 1: Model Parameter for One Box Model

Parameter	Value
Total Volume of Water Mass	13.8 km^3
Mean Depth	13.8 m
Shallow Water Region	
0~5 m depth	90 km^2
5~10 m depth	91 km^2
Tidal Exchange Ratio	0.4 % / day
Load from River	
POC	81.6 t-C / day
DOC	101.9 t-C / day
DIP	0.17 t-atm / day
DIN	14.3 t-atm / day

(1) Tidal Exchange Rate
Figure 3 shows the result of sensitivity analysis for the tidal exchange rate. The horizontal axis denotes relative input value of tidal exchange rate based on the tidal exchange rate at the basic case. The vertical axis denotes the relative values of iterated output for the standing mass of PHY, ZOO, DIP and DIN based on the output at the basic case.

The most sensitive output is DIN. The standing mass of DIN has nearly linear relationship with the tidal exchange rate. Contrary, the standing mass of PHY is least changeable by the tidal exchange rate. Nevertheless, an approaching speed to the steady value is more fast when the tidal exchange rate is assigned larger value.

The standing mass of ZOO is responding as non-linear relationship with the tidal exchange rate. It seems to be caused by the interaction with PHY, ZOO and DIP as follows. ZOO is dominated by PHY not only its standing mass but also its decaying speed. When the DIP is enough to feed PHY, PHY is decayed slowly. It causes that ZOO can graze PHY and can

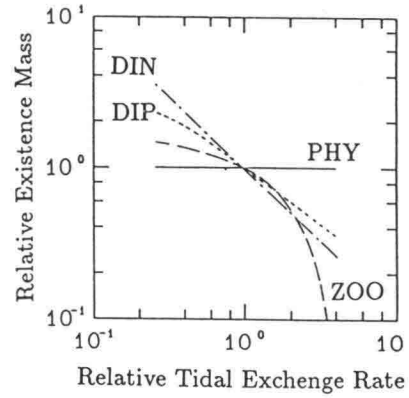

Figure 3: Sensitivity Analysis for Tidal Exchange Rate

support DIP. Once DIP is not enough to feed PHY owing to the rapid tidal exchange, PHY decays very rapidly. Then, ZOO is decays more rapidly and DIP is partially supported by the death of ZOO and decays more slowly.

(2) Dominant Parameter of DIN

Fig.4 shows the sensitivity analysis result of the standing mass of DIN for various conditional variables. The variables are tidal exchange rate, temperature of sea water, absorption rate of seaweed and adsorption rate of bottom sediment. The horizontal axis denotes input of variables compare to the basic case's value. The vertical axis denotes iterated output values for DIN based on the basic case's one.

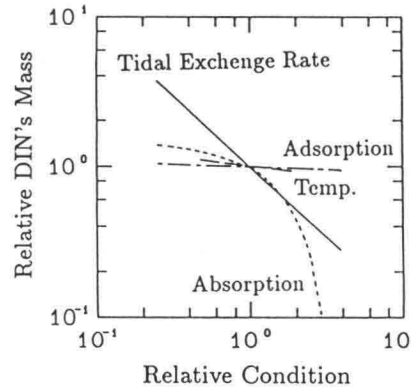

Figure 4: Sensitivity Analysis of DIN's Existence Rate for Various Incidents

The tidal exchange rate influences the standing mass of DIN most dominantly within the whole region in these cases. The absorption rate of seaweed becomes a more influential parameter for DIN when it has big value.

From this figure, increase of the capacity of DIN in the bay will be achieved by increase of the tidal exchange rate. Furthermore, vegetated area of seaweed in the bay will be expected also an important factor to increase the capacity of DIN.

3.2 Comparisons of DIN by 3D Model

We carried out numerical simulation to three different boundary conditions. Those were 1) the present condition, 2) the past condition, and 3) a tentative condition. In a tentative condition, we increased a shallow water area (seaweed vegetated area) without the modification of the present shoreline's location. By the comparison with 1) and 2), the nutrient capacity in the past condition can be estimated. By the comparison with 1) and 3), the ability of recovering the nutrient capacity by seaweed vegetation can be estimated.

The model had 1 km mesh resolution in the horizontal plain and 3 leveled layers in the vertical axis (0-5 m, 5-10 m and over 10 m depth). By the hydraulic model, we obtained velocity distribution vectors data for one tide cycle. By the biological model, we obtained spatial distribution of the standing mass of each compartment after 60 tides' computation.

(1) Flow Field
Boundary conditions of three types of Tokyo Bay are shown in Fig.5 for the configuration and summarized in Table 2.

Table 2: Summary of Boundary Conditions for Hydraulic Model

Case #	Total Vol. (km^3)	Mean Depth (m)	Shallow Water Area* (km^2)
1	13.6	15.2	181
2	14.6	12.8	447
3	12.1	13.5	341

$*$: The depth is $0 \sim 10$ m

Examples of obtained surface velocity fields are shown in Fig.6. These figures show the surface flow field in the ebb tide, the flood tide, and the residual flow of the case 1. In the ebb tide, the flow is more rapid than the flow in the flood tide. A strong residual circulation near the Cape Huttsu can be seen in the figure.

Figure 7 shows a comparison for the scalar values of surface velocity vectors at ebb tide to the flow in the case 1. In the case 2, the flow is accelerated almost all region in the bay. The accelerated ratio is about +0.5 in the center of the bay up to +5.0 near the coast. In the case 3, the flow is accelerated along the west coast and the top of the bay. The accelerated ratio is almost +0.2 in the center of the bay up to +0.8 in the top of the bay. It is hard to draw the conclusion directly from these figures, because the configuration of the bay is different among 3 cases. Nevertheless, we can guess that the tidal exchange rate increase in the case 2 and 3 relative to the case 1.

(2) Distribution of DIN
According to the sensitivity analysis for the simplified one-box model, DIN is one of the most sensitive parameters. So, we compared distribution of DIN for the each case.

Figure 8 shows the distribution of DIN for the case 1. The unit is μg-atm/l.

Figures 9 and 10 shows the distribution of increase of DIN in the Cases 2 and 3. Those values are obtained by the subtraction of Case 1 from that for each case.

Table 3 shows a comparison of the total amount of the standing mass of DIN in the bay. The standing mass of DIN is reduced by almost 30 % due to the change of geographical configuration of the bay.

In the Cases 2 and 3, the reduction is clear along the west coast. In the Case 2, the reduction is significant in the whole layers. This means that the change of tidal exchange system is affecting DIN distribution in the Case 2. In the Case 3, the reduction is significant only in the bottom layer. This shows that DIN distribution in the Case 3 is mainly controlled by the absorption process of seaweed. To clarify this argument, we conducted the residence time analysis in the next subsection.

3.3 Comparison of Residence Time

For the estimation of the effect of the configuration change, the residence time was calculated for sea water and DIN in the bay. The sequence for the residence time analysis in this paper is:

1. obtain the spatial distribution at steady state for each compartment,
2. mark up existence water and DIN in the bay by the tracer,
3. cut the load from the land off,
4. reset a time counter as t=0,

Figure 5: Boundary Conditions of Tokyo Bay : Depth (m)
(left: Case 1 center: Case 2 right: Case 3)

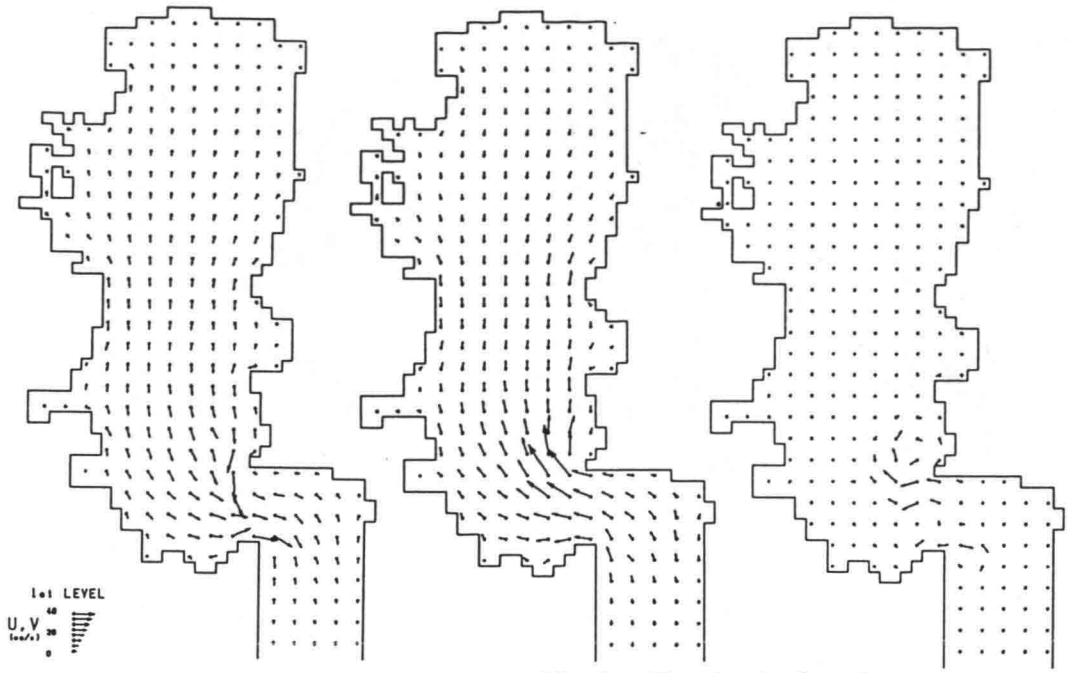

Figure 6: Velocity Vector of Surface Flow in the Case 1

(left: flow in the ebb tide center: flow in the flood tide right: tidal residual flow)

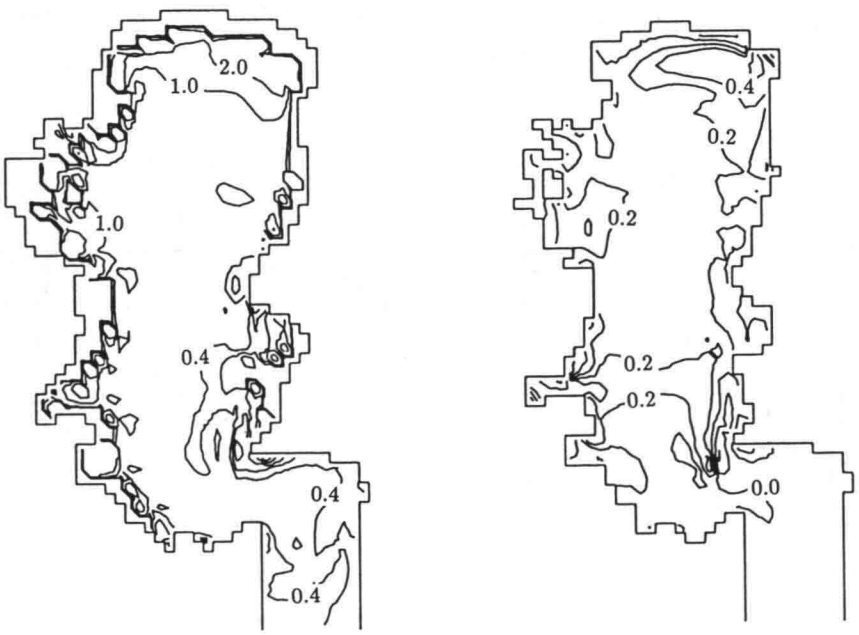

Figure 7: Comparisons for Intensity of Velocity Vector to the Case 1

(left: case 2 - case 1 right: case 3 - case 1)

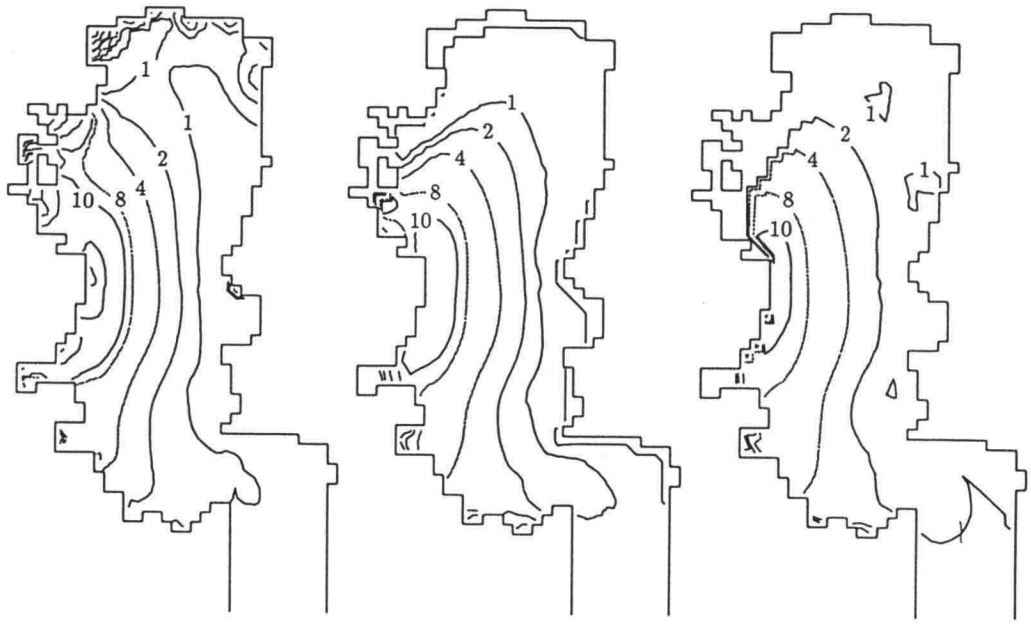

Figure 8: DIN's Distribution in the Case 1 (unit:[μg-atm/l])
(left: surface level center: middle level right: bottom level)

Figure 9: Relative DIN's Distribution in the Case 2 (unit:[μg-atm/l])
(left: surface level center: middle level right: bottom level)

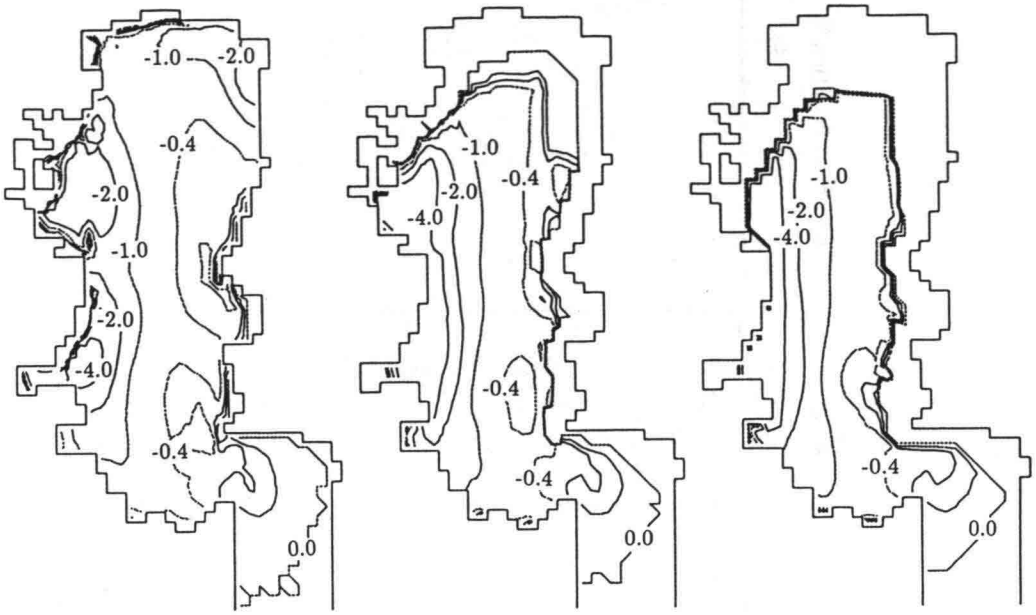

Figure 10: Relative DIN's Distribution in the Case 3 (unit:[μg-atm/l])
(left: surface level center: middle level right: bottom level)

Table 3: Total Amount of DIN's Mass in the Bay

Case #	Mass (t-atm)	Rate
1	66.2	1.0
2	48.0	0.73
3	42.0	0.63

5. continue the physical-biological model calculation,
6. obtain the remnant function $r(t)$ for the water and DIN, and
7. calculate the residence time τ_r by Eq.(6).

(1) Residence Time of the Sea Water
Fig.11 shows the remnant function of the water in the whole bay for each case.

Residence times of the sea water are estimated as 250 days for the Case 1, 142 days for the Case 2 and 200 days for the Case 3. By the comparison with the Case 1, change of the residence time is more significant for Case 2 than Case 3. The tidal exchange is more promoting in Case 2.

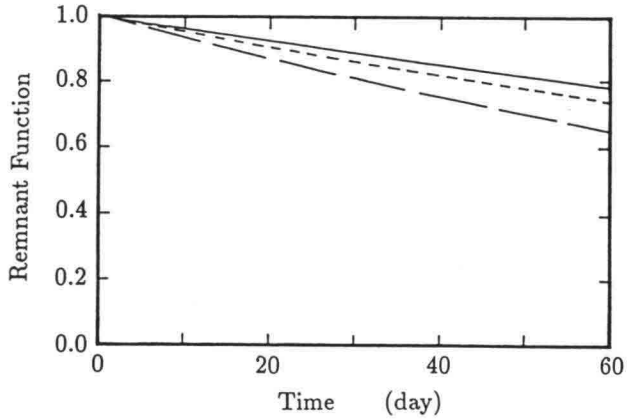

Figure 11: Remnant Function for the Water in the Bay
(solid line: Case 1 dashed line: Case 2 doted line: Case 3)

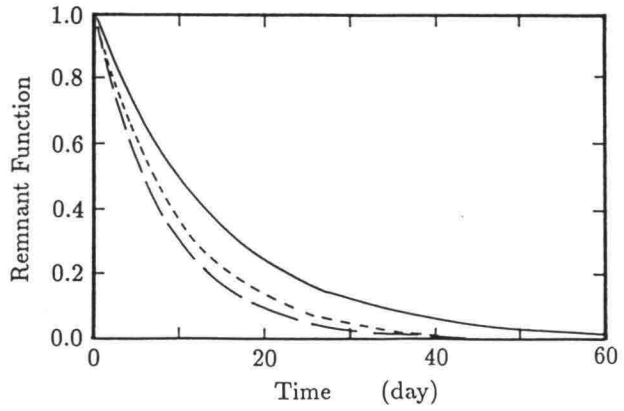

Figure 12: Remnant Function for the DIN's mass in the Bay
(solid line: Case 1 dashed line: Case 2 doted line: Case 3)

(2) Residence Time of DIN
Fig.12 shows the remnant function of the standing mass of DIN in the whole bay for each case.

Residence times of DIN are 14 days for the Case 1, 8 days for the Case 2 and 10 days for the Case 3. By the comparison with the Case 1, change is also more significant for Case 2 than Case 3. But, the residence time in Case 3 is close to that of Case 2. It can be said that other factors except the tidal exchange rate are affecting in Case 3.

In Case 3, the shallow water region is expanded as Table 2. It rose larger absorption rate along the coastal line by seaweed. That may be a dominant factor in the Case 3.

According to the Table 3, the highest capacity for DIN is obtained for Case 3. It is caused by the process of absorption for seaweed. This result shows a possibility to use a seaweed absorption process instead of a tidal exchange process to improve the capacity of DIN in the bay.

(3) Spatial Residence Time of DIN

We conduced a spatial residence time analysis to estimate which region's absorption process is more significant. The bay is divided into 7 regions as shown in Fig.13. The sequence of the analysis is the same with the residence time analysis but marks up the tracer for each region.

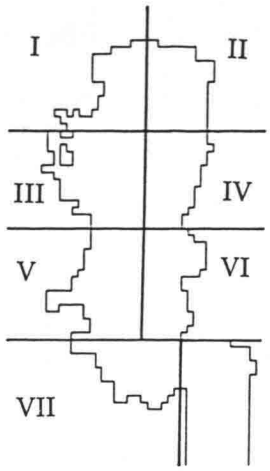

Figure 13: Regions Used in Spatial Residence Time Analysis

Table 4: Configurations and Results for Spatial Residence Time Analysis

region #	loads from river	residence time for water mass (day)	residence time for DIN (day)
I	high	333	2
II	low	333	25
III	high	333	5
IV	low	250	17
V	high	143	10
VI	low	100	17
VII	low	500	17

Results are tabulated in Table 4. From these results, regions that a) high loads comes from river, and b) long residence time for the water mass cause short residence time for DIN (regions I and III). These conditions should be considered when we would utilize seaweed to absorb DIN and improve DIN concentration more efficiently in the bay.

4. CONCLUSIONS

We coded the simplified physical-biological model for the calculation on nutrient circulation in the bay. In conclusion, we obtained the understanding of its basic system responses and

the experience of its application to Tokyo Bay as follows:

- The most sensitive output variable in this model was DIN.
- DIN was controlled mainly by tidal exchange rate.
- If the standing mass of DIN exceeded certain value, it was also controlled by an absorption process of seaweed.
- In the past Tokyo Bay's condition, water exchange rate is almost 1.8 times bigger than that in the present Tokyo Bay's condition.
- DIN's capacity is controlled dominantly by tidal exchange rate in the past Tokyo Bay's condition.
- If we make shallow water region and vegetate seaweed in the present Tokyo Bay's condition, DIN's capacity is controlled by absorption rate of seaweed.
- The absorption process in the high loaded and stagnated area is effective to improve the DIN's capacity in the bay.

The physical-biological model that we employed here is required to improve for application to get quantitative information. The more field data correction will be essential to improve the accuracy of biological parameters.

ACKNOWLEDGMENTS

We would like to thank Dr. M. Kishi of Tokyo Univ. for helpful information on the ecological modeling. We would like to thank Mr. K. Murakami of P.H.R.I. for helpful discussions and comments on the hydraulic modeling. We also would like to thank Dr. T. Horie of P.H.R.I. and Prof. T. Sugimoto of Tokyo Univ. for their supporting to this research.

REFERENCES

Kermer, J.N. and S.W.Nixon (1987): A Coastal Marine Ecosystem, Ecological Studies, Vol.24, Springer-Verlag Press, 227p.

Hosokawa, Y., K. Furukawa and M. Kishi (1993): A Physical-Biological model calculation in Tokyo Bay, Proc. of Coastal Engineering, Vol.40, pp.1101-1105, (in Japanese).

Sasaki, K (1991): Nitrogen and Phosphorus Circulation related with the Plankton Communities in Tokyo Bay, Bulletin on Coastal Oceanography, Vol.28, No.2, pp.129-139, (in Japanese).

Murakami, K (1990): Calculations of Vertical Circulation in Stratified Waters by Two-Level and Two-Layer Models, Tech. Note of P.H.R.I., No.665, pp.1-33, (in Japanese).

Kaneko, Y., T. Horie and K. Murakami (1975): Numerical Simulation on Tidal Currents and Pollutant Dispersion due to Alternating Direction Implicit Method, Rept. of P.H.R.I., Vol.14, No.1, pp.3-61, (in Japanese).

Takeoka, H. (1984): Fundamental Concepts of Exchange and Transport Time Scales in a Coastal Sea, Continental Shelf Research, Vol.3, pp.311-326.

Nakata, K. (1993): The Scale of Physical Processes and the Estimation of Material Flux between Coastal Region and Open Ocean, Bulletin on Coastal Oceanography, Vol.30, No.2, pp.139-152, (in Japanese).

HYDRO-PORT'94
International Conference on Hydro-Technical
Engineering for Port and Harbor Construction
October 19 - 21, 1994, Yokosuka, Japan

Red Water in Nippon-maru Memorial Park and Countermeasures against it

Eiji Yauchi [1]
Koichi Yokobori [2]
Isao Iida [2]
Tadao Uesugi [3]

[1] TOA CORPORATION, Design Department
5, Yonbancho, Chiyoda-ku, Tokyo, 102
[2] ditto. Yokohama Branch
18, Nihon-Odori, Naka-ku, Yokohama, Kanagawa, 231
[3] Yokohama City Office
3, Nishikicho, Naka-ku, Yokohama, Kanagawa, 231

Abstract

Intermittent aeration devices were installed at a pavilion in Nippon- Maru Memorial Park as a remedial measure against the red water phenomenon at Yokohama Port in Japan. Field observations show that intermittent aeration devices have prevented the appearance of red water and, also, improved the transparency of the water at the park.

Key Words: Red Water, Red Tide, Aeration, Transparency

1. INTRODUCTION

In 1989, an international exposition was held in Yokohama City. A sailboat pavilion was constructed at the Nippon-Maru Memorial Park using seawater of Yokohama Port. During the exposition, plans were made to control the predictable occurrences of red water.

This paper presents the results of a two-year investigation of the occurrences of red water. It, also, investigates the efficacy of countermeasures designed to prevent these occurrences.

2. FACILITIES OF THE PAVILION

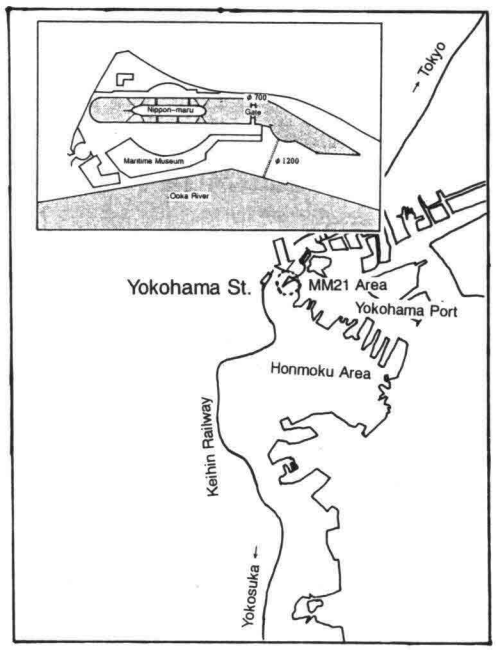

Figure 1: Location of Nippon-maru Memorial Park

Figure 1 shows the exposition site at Yokohama Port. The Nippon-Maru Memorial Park pavilion was used to exhibit classic sailboats in a 200 m long, 25 m wide, and 10 m deep dock. Two 1200 mm diameter pipes were used to pump water in and out from the dock from and into Yokohama Port. Pollution at the dock was kept low by draining the waste water generated at Nippon-Maru into the public sewer system.

In the past, red water used to appear when there was continuous insolation in the months June to September. A pump with discharge rate of 0.25 m^3/s was installed in 1986 and the seawater from the innermost part of the dock was drained. However, the pump was unable to control the appearance of red water in the dock.

3. EXPERIMENTAL METHOD AND COUNTERMEASURES FOR THE RED WATER

3.1 EXPERIMENTAL METHOD

Field observations were conducted to investigate the mechanism of the red water phenomenon and estimate the efficacy of countermeasures against it. Fifteen thermometers were used to measure vertical profiles of water temperature at four different points as shown in Figure 2.

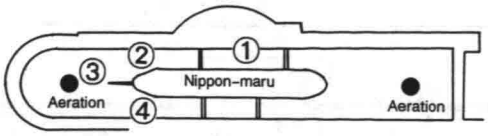

Figure 2: Locations of measuring points

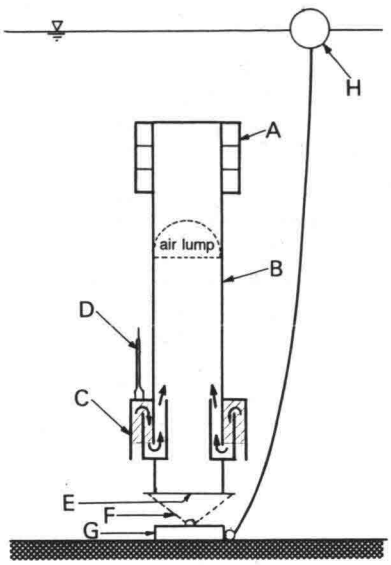

Figure 3: Intermittent aeration device

In addition, at the times of occurrence of red water and its clearing away, water quality at three depths, surface, middle and bottom layers, was examined and the number of plankton measured. Daily measurements were made of the transparency of the water which serves as an index of red water.

3.2 COUNTERMEASURES FOR THE RED WATER

An intermittent aeration device was used as a countermeasure against the red water because of the limited size of the facility at the park, and the main cause of red water was believed to be a thermocline. The components of the intermittent aeration device installed at the park are shown in Figure 3, namely, a buoy for maintaining upright position, a pipe for lift, an air room, an air tube, an absorption mouse, mooring chains, a sinker, and a marker buoy.

The mechanism of aeration can be outlined as follows:

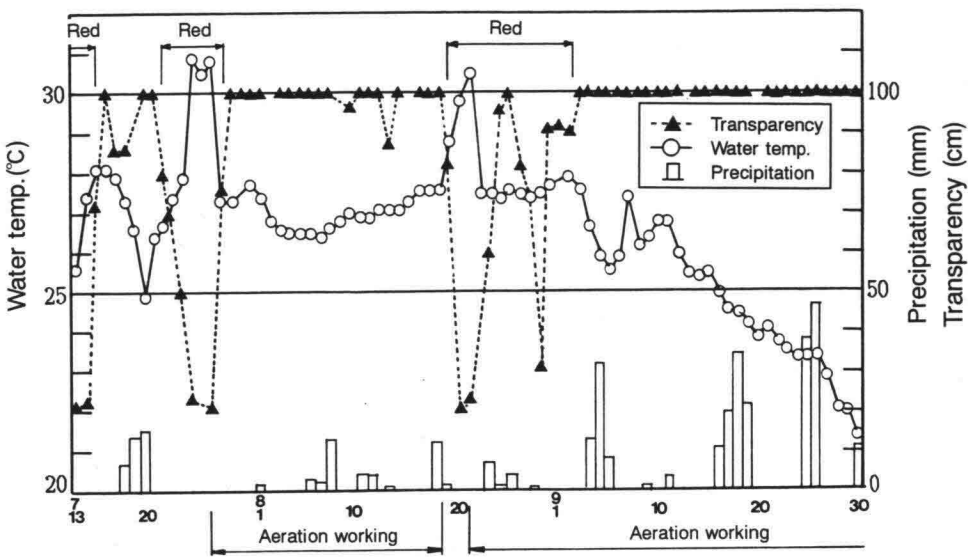

Figure 4: Change of transparency and water temprature

(1) air is transmitted to an air box and the box is filled with air as shown by an oblique line in Figure 3, and

(2) air lump gushes out from an upper outlet.

Two aeration devices were placed at the stem and stern of Nippon-Maru as shown in Figure 2.

4. RESULTS

4.1 CHANGE OF WATER TEMPERATURE

Figures 4 shows the temperature and transparency of the surface water. In Figure 4, the transparency shows a decrease with increase in water temperature because of the clear weather from July 22 onwards. The transparency decreased to a low of 22 cm on July 25.

On this worst transparency day, the intermittent aeration device was activated, after which transparency increased to 1 m, water temperature decreased to 27 °C, and red water disappeared in two days time. Transparency was maintained in the range 90 cm to 1 m while the intermittent aeration devices were working and the red water was controlled.

Figure 5 shows the vertical distribution of water temperature. When the red water appeared, a thermocline was observed at a depth of 1.4 m and its thermal difference was 3 °C, as shown in Figure 5(a). Figure 5 (b) shows the thermal distribution on the worst transparency day. On this day an even stronger thermocline with a temperature difference exceeding 30 °C existed above the 1.4 m deep thermocline.

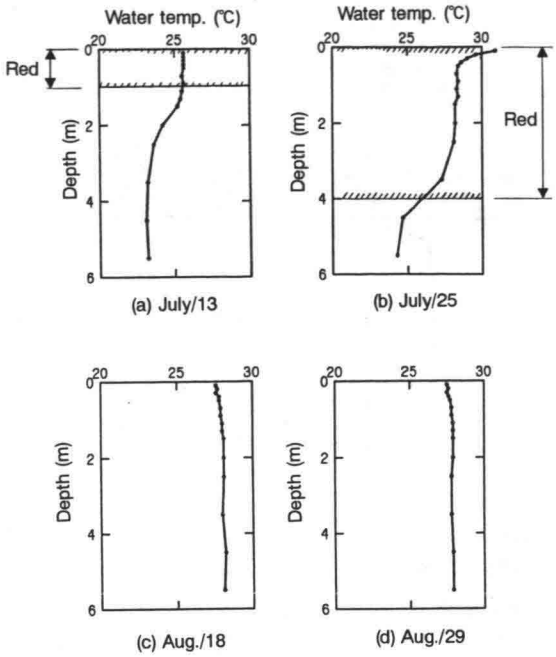

Figure 5: Vertical distribution of water temperature and red water height

Figure 5 (c) shows the thermal distribution when the aeration devices were working. On this day, the transparency was 1 m and red water did not appear. In addition, there were no thermoclines as the seawater in the dock was mixed by the action of the intermittent aeration devices.

Figure 6 shows the vertical distribution of water temperature when the surface temperature was maximum at the four measuring points. At the side of Nippon-Maru (no. 1), a 40 cm deep thermocline occurred and another 70 cm deep thermocline occurred at the near stem of the right hand side of Nippon-Maru. Therefore, it appears that the seawater of the dock was not mixed vertically at these two points.

At point no. 3, at a distance of 10 m from the closer intermittent aeration device, a complete vertical mixing of the seawater was achieved though the temperature at its bottom was the highest among the four instrumented points.

4.2 CHANGE OF WATER AND SEDIMENT QUALITY

The results of the analyses of water and bottom sediments in the dock are listed in Table 1. All water quality data satisfied the existing environmental quality standards. In all cases the dissolved oxygen (DO) was remarkably high because of the photosynthesis of plant plankton which was, also, the cause of red water.

On bottom sediments, total nitrogen (TN) exceeded 2 mg/g which was considered the result of an eutrophic state which has a bearing on the appearance and disappearance of red

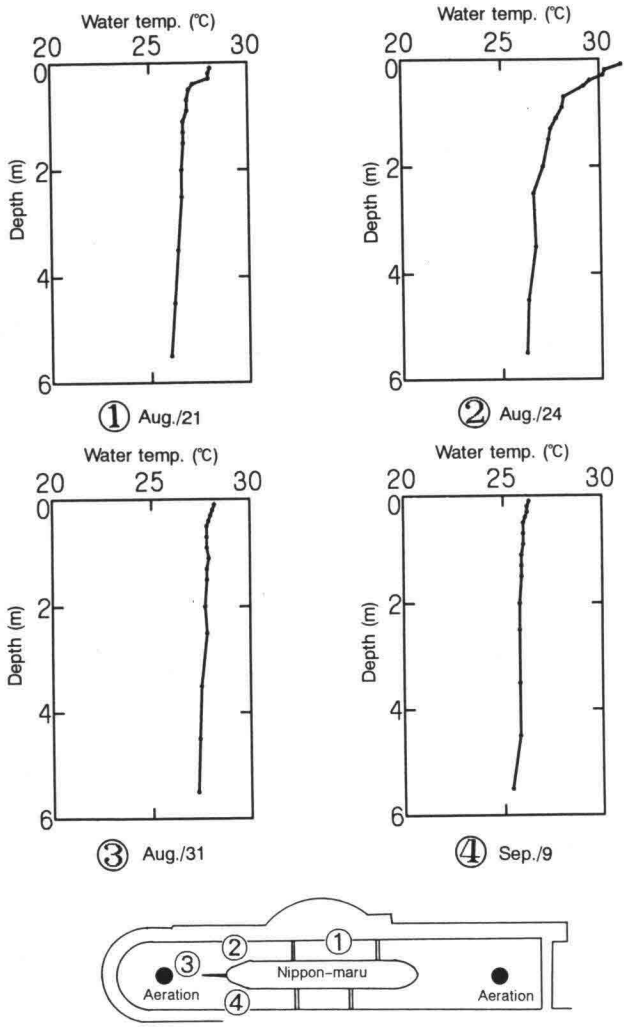

Figure 6: Vertical distribution of maximum water temperature

Table 1: Analyses of water and bottom sediments

Items	Measuring Point / Date	1987 July/13 ③	1987 July/13 ①	1987 Augst/18 ③	1987 Augst/18 ①	1988 June/27 ③	1988 June/27 ①
Water Quality	COD (mg/l)	1.4	1.8	1.2	1.0	2.8	2.8
	T-N (mg/l)	1.09	3.98	0.84	0.73	1.27	0.98
	T-P (mg/l)	0.08	0.10	0.12	0.11	0.12	0.12
	Salinity Content (%)	2.87	2.79	2.87	2.92	2.56	–
	pH	7.8	7.8	7.8	7.9	7.4	–
	DO (mg/l)	16.3	15.9	7.7	6.5	8.0	–
Bottom Mud	Ignition loss (%)	14.0	15.7	14.7	12.0	4.8	–
	COD (mg/g)	45.2	46.8	51.7	45.5	44.5	–
	T-N (mg/g)	4.27	3.74	3.55	3.01	4.41	–
	T-P (mg/g)	1.17	0.88	1.04	0.70	1.58	–
	pH	7.6	7.6	7.8	7.7	7.5	–
Transparency (cm)		21.5		100.0		100.0	
Water Temp. (upper) (℃)		25.8		27.6		22.8	

water. These measurements indicate that the water quality did not change by the action of the intermittent aeration devices.

4.3 CHANGE OF PLANKTON NUMBER

Table 2 shows the results of the analyses of planktons in the dock. Plankton is the cause of red water and it was found to belong to the prorocentrum species. A number of plant planktons, both diatoms and dinophyta were seen at all times, and some zoo planktons which fed on plant planktons were, also, observed. However, at the time of red water 95 % of plant plankton was of the Dinophyta type, and zoo plankton decreased by one fifth when red water cleared away.

Figure 7 shows the ratio of plant and zoo planktons at the surface layer. The ratio was less than 10^5 when the water was clear but it increased by about 10^6 when red water appeared. These results indicate a drastic imbalance in the number of plant and zoo planktons.

5. CONCLUSIONS

A countermeasure against the phenomenon of red water at Yokohama Port in Japan was studied. A pavilion housing a dock in Nippon-Maru Memorial Park with water pumped from Yokohama port was used as a test site. Intermittent aeration devices were used at the dock to test its efficacy in preventing the appearance of red water. Field observations confirmed that the installed equipment was able to prevent the appearance of red water and, in addition, improved the transparency of the water at the park.

Table 2: Analyses of planktons

Items		Measuring Date and Point	1987 ③			1988 ① : 6/27			② : 8/22			③ : 9/5			④ : 9/12		
			8/18	9/2	10/27	Upp.	Mid.	Low.	Upp.	Mid.	Low.	Upp.	Mid.	Low.	Upp.	Mid.	Low.
Plant Plankton	Diatoms	Bacillariophyceae	555	20	215	319	372	134		48	11	3	3	1	54	79	330
	Lafid	Heterosigma sp.				4	6										
	Dinophyta	Gonyaulax triacantha					1	3									
		Prorocentrum sp.							2,661	1,491	804	605	815	246	46	9	7
		Dinoflagellates	1,926	6,353		30	2		55	33		7	1		3	6	7
	Euglenophyta	Englenophyceae	77		2	95	5		4	7							
	Others	Micro-flagellates	9		426	1,590	533	206	256	141	122	35	68	46	256	485	300
	Number of cells	(cells/ml)	2,567	6,373	643	2,039	921	340	2,976	1,720	944	643	887	293	359	579	644
	Number of kinds		7	4	16	7	7	3	5	6	6	3	6	5	9	6	6
Zoo Plankton	Ciliates	Mesodinium rubrum				19.0	34.0	34.0									
		Tintinnopsis radix				0.2											
		Tintinnopsis sp.				2.4	9.2	8.8							0.4	0.4	
		Ciliata				2.4	4.8	4.4									
	Polychaetes	Polychaeta larva				0.2	0.4	0.8	0.4	0.8	1.0	4.2	2.8	2.8	0.8	1.6	16.0
	Nematades	Nematoda						0.4							128.0	0.4	0.4
	Crustaceans	Copepodite of Oithona						1.2	0.4	0.4	0.2	0.4			0.4		1.2
		Nauplius of Copepoda				0.4				0.2	2.0	3.6	2.0	49.6	1.2	2.4	
		Nauplius of Balanomorpha				0.6		0.4	1.6	2.0	0.6	5.2	5.6	3.2	23.2	33.6	2.8
	Urochorda	Appendicularia larva						0.4									
	Others		30.1	6.0	7.0				1.2			1.6	1.2	1.2	19.8	2.0	13.6
	Number of individual (indi./l)		30.1	6.0	7.0	25.2	48.4	50.4	3.6	3.2	2.0	13.4	13.2	9.2	173.0	39.2	36.4
	Number of kinds		4	3	2	7	4	9	4	3	4	6	5	5	12	7	8
Transparency (cm)			100	80	100	100			67			100			100		

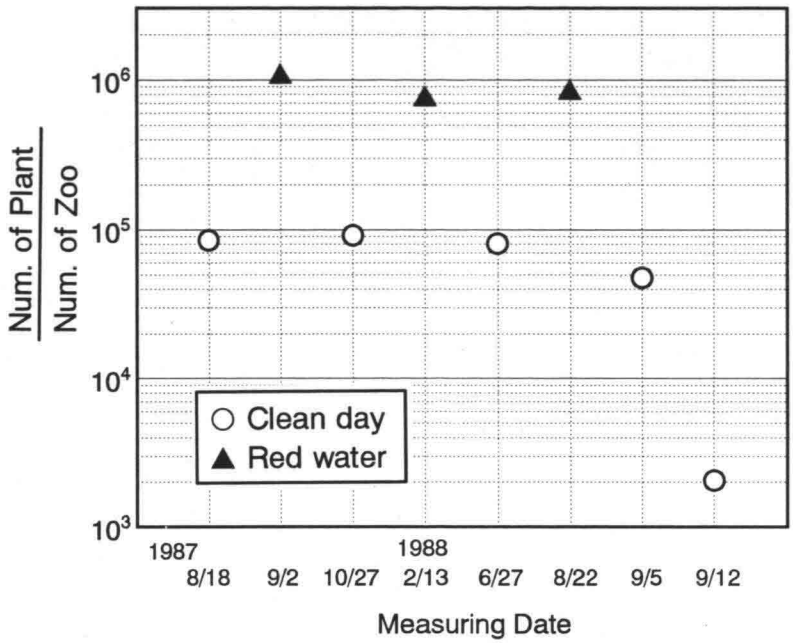

Figure 7: Ratio of plant and zoo planktons

These results indicate that in small enclosed bodies of water such as reported in this study, intermittent aeration devices are effective in preventing red water because these devices lead to a thorough vertical mixing of the water.

References

[1] Yauchi,E., Koichi Yokobori, Isao Iida, and Tadao Uesugi : Red Water in Yokohama-Port and Countermeasures against it, Proc. of Coastal Engineering, JSCE, vol.37, pp.813-817, 1990.(in Japanese)

HYDRO-PORT'94
International Conference on Hydro-Technical
Engineering for Port and Harbor Construction
October 19 - 21, 1994, Yokosuka, Japan

A Study of Sandy Beach Surf Zone as Nursery Grounds for Marine Organisms

Michio Gomyoh [1]
Yusuke Suda [2]
Masayuki Nakagawa [1]
Tadashi Otsuki [1]
Junya Higano [3]
Kumiko Adachi [3]
Katsunori Kimoto [3]

[1] Toa Corporation, 5, Yonbancho, Chiyodaku, Tokyo
[2] Shimonoseki University of Fisheries
7-1, Nagatahonmachi 2-chome, Shimonoseki, Yamaguchi
[3] National Research Institute of Fisheries Engineering
Ebidai, Hasakimachi, Kashimagun, Ibaraki

ABSTRACT

In order to understand the mechanism of the sandy beach surf zone as a nursery ground, a series of investigations for distribution of fish larvae and juveniles has been carried out as well as natural conditions at Hasaki Beach, a typical exposed sandy beach. It was found that there are many fish larvae and juveniles in the surf zone of exposed sandy beach, and that the distribution of several dominant fish larvae and juveniles is dependent on the tide level and diurnal time. In particular, ayu sweetfish *Plecoglossus altivelis* and mullet *Mugil cephalus* are pointed out as residents or seasonal migrants in common with a sheltered beach. The role of surf zone as a shelter from predators is discussed for a nursery grounds for fish larvae and juveniles.

Key Words: Sampling, Fish Larvae and Juveniles, Exposed Sandy Beach, Hasaki Beach

1. INTRODUCTION

Sandy beach surf zone has not been interested in as a nursery ground for marine organisms in contrast with tranquil environments such as tidal flat, seagrass bed and estuary because of strong wave action, wave driven current and heavy sand transport as well as difficulty of in-situ investigation and observation.

As reported by Higano (1990), however, the benthic community with diversity was observed in the exposed sandy beach. Lasiak (1986), and Brown and McLachlan (1990) also suggested that the surf zone of the sheltered sandy beach is an nursery ground for fish larvae and juveniles. The same indication was also reported for this area in Japan (Senta & Kinoshita, 1985).

However, there are little information or studies on the distribution of fish larvae and juveniles in the surf zone of the exposed sandy beach. In order to study this subject, Suda et al.

(1992a,b) began to investigate about the distribution of marine organisms in the surf zone of the exposed sandy beach located at Hasaki, the central part of Honshu Island in Japan, from October 1991. They firstly investigated the relationship between the distribution of organisms and the sea bottom topography. They found that density and diversity of the phytoplankton in the offshore direction increase at the breaking point. They also found that lots of fish larvae and juveniles like mullet *Mugil cephalus* and ayu sweetfish *Plecoglossus altivelis* inhabit in the swash zone which is located at the most onshore-ward within the surf zone.

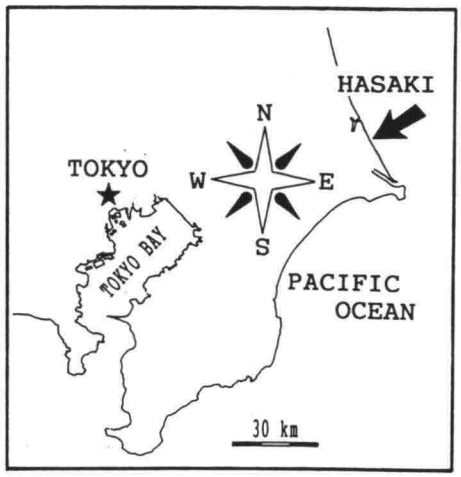

Figure 1 Proposed site for investigation

On the other hand, many tidal flats and seagrass beds being important places as the nursery grounds have been reclaimed and disappeared at the estuarine coast of Japan. Coastal development will be gradually extended to the open sea coast. It is an important subject to understand appropriately the function of the surf zone as a nursery ground in order to provide a valuable information for coastal management and conservation.

From these points of view, the authors have been carrying out a series of investigation at Hasaki Beach, typical surf zone at the exposed sandy beach, up to the present time in order to evaluate the relationship between the distribution of fish larvae and juveniles and natural conditions. In this paper, natural conditions of the sampling site are firstly described, and then the distribution of fish larvae and juveniles is presented and discussed in relation to wave condition, current, beach topography, time and tide levels.

2. INVESTIGATION METHODS

The proposed site for this investigation is located on the central part of Hasaki Beach, Ibaraki prefecture as shown in Figure 1. Various investigations were carried out in the surf zone near the Hasaki Oceanographical Research Facility (HORF) of Port and Harbor Research Institute, of which site is presented in Figure 2.

Figure 2 Site view of the HORF

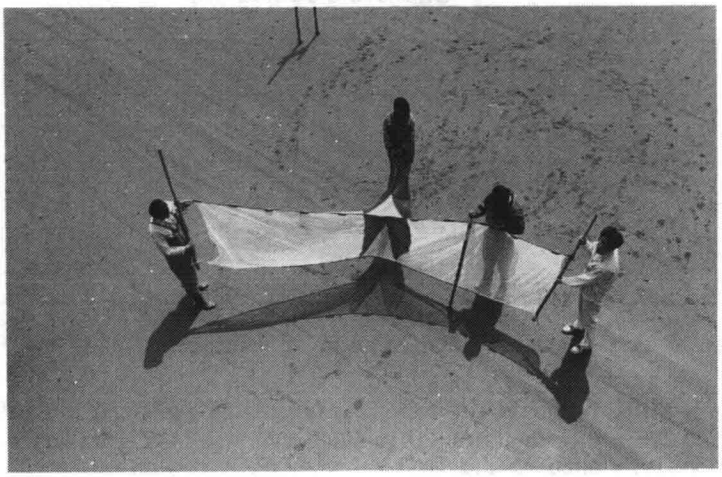

Figure 3 Photograph of net sampler

Figure 4 Photograph of sampling with net sampler

The net sampler with 1m in height and 5m in width equipped with the central cod end (mesh size 1mm) was used for sampling fish larvae and juveniles as indicated in Figure 3, and the net operation in the sampling is as also shown in Figure 4.

The sampling was carried out to investigate the distribution patterns of fish larvae and juveniles due to 1) diurnal and tidal changes in the surf zone and 2) difference between the cusp horn and bay under the beach cusp condition. The investigations for the former were done 7 times, April 21, May 22, June 3, August 24 to 26, October 12 to 13, December 7 to 8 in 1992 and January 12 to 14, 1993. The net was towed for 50m parallel to the shore line in the surf zone where the water depth was ranging from 0.5 to 1m. The investigation for the latter was done at the beach cusp located at 250m north of the HORF at both low and high tide on July 14–15, 1992.

In addition, net sampling was also conducted at several places in order to investigate the fish larvae and juveniles fauna in the proposed site.

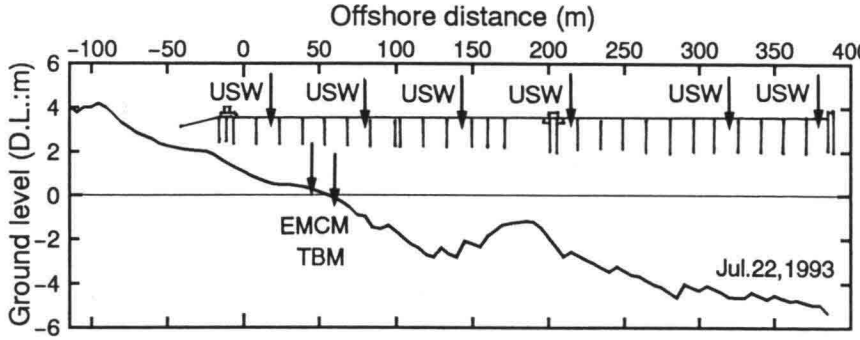

Figure 5 Bed topography and location of instruments along the HORF

Natural conditions at the proposed site were investigated as explained in the following. Wave height and period were measured for 20 minutes every 1 hour intervals with 6 ultrasonic wave gages (USW) installed at the pier deck of the HORF as shown in Figure 5. The beach profile along the pier was surveyed once a day with a lead from the pier deck and a surveyor's staff and level. Current field and turbidity in the surf zone where sampling was done were investigated with the two pairs of electromagnetic current meter (EMCM) and turbidity meter (TBM) installed at 47m and 63m away from the base of the pier as indicated in Figure 5.

The topography of the beach cusp was directly surveyed by rod leveling during the low tide. Furthermore, a simple measurement of current was carried out with floats and a tethered float during the low and high tides.

3. RESULTS OBTAINED FROM INVESTIGATION

3.1 Natural Conditions

The offshore and the nearshore significant wave heights, H_0 and $H_{1/3}$ on the sampling days are presented in Figure 6. The values of H_0 are ranged from 0.6 to 2.3m. The sampling sites are located in the surf zone within the area from 0m to 90m from the base of the pier. The significant wave heights in the sampling site are estimated to be less than 50cm.

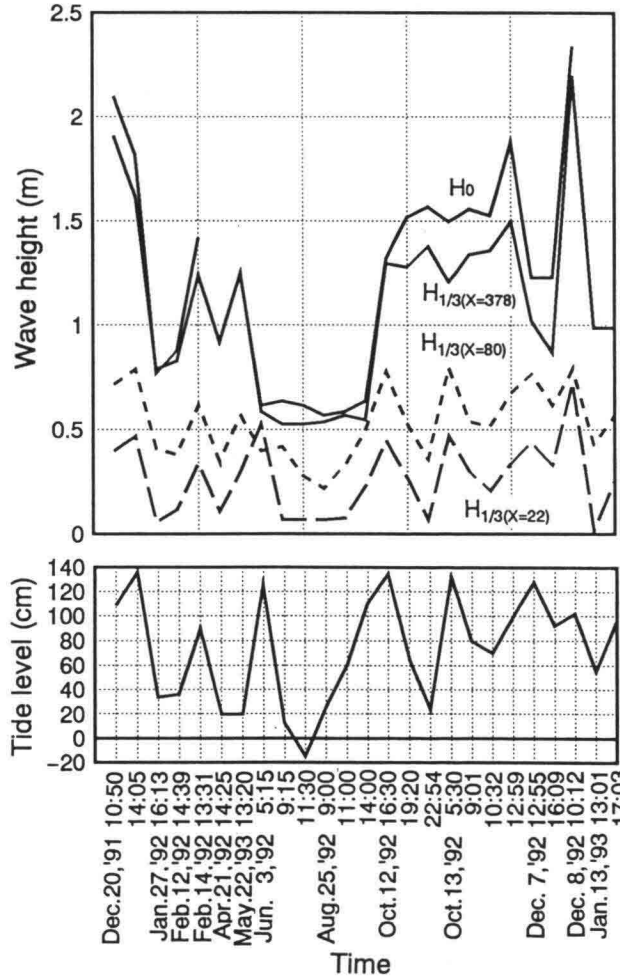

Figure 6 Wave characteristics and tide level on the sampling days

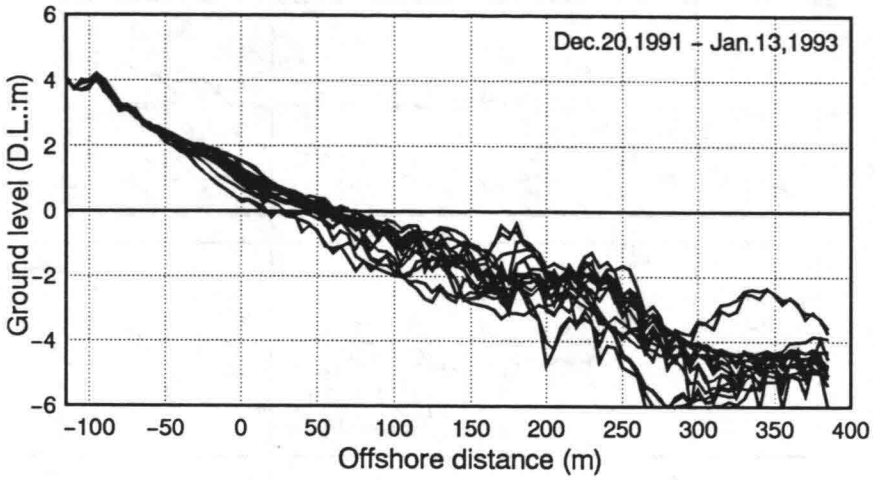

Figure 7 Overlapping of bed profiles on the sampling days

In Figure 7 are shown the bed profiles on the sampling days. The ground elevation at the sampling site varies by 0.8 to 1.5m through 1 year. It can be seen that the location of the D.L.±0m moves about 70m for this time.

The offshore and the nearshore significant wave heights and wave periods, the averaged velocity, the on-offshore and longshore current velocities, averaged current direction and tide level measured during January 18 to 22 in 1993 are summarized in Figure 8. It is found that the wave height in the surf zone is affected by the tide level consequently being dependent on the water depth and that the average current direction is parallel to the shoreline. It can also be said that a longshore current with a velocity of 40 to 80 cm/sec is generated at the investigation time. These phenomena are closely related to incident wave conditions and beach topography, and indicated different behaviors at each sampling date in Figure 6.

The turbidity measured at the same location for current velocity indicated an average value of about 100ppm with 2300ppm in maximum, and significantly differed from that in the trough, 50 to 60 ppm measured by using thrown-type turbidity meter.

Beach cusps are formed seasonally on Hasaki Beach, and there is a trend for generating local longshore current and rip current. In Figure 9 are shown the topography and the current field at high and low tides at the investigation time. The wavelength of the cusp was about 100m and the water depth in the bay is deeper than in the horn. It was also found that the shore shows a straight line without a clear rip current in high tide, while both clear current toward the bay and rip current are observed in low tide.

3.2 Fish Larvae and Juveniles

48 species and 1158 individuals of fish larvae and juveniles were totally collected as summarized in Table 1. The dominant species were *M. cephalus* (n=410), *P. altivelis* (259), *Engraulis japonicus* (126), *Terapon jarbua* (80) and *Salangichthys ishikawae* (68). The growth stages of the samples were postlarva and juvenile except for *S. ishikawae*, *Eleutherochir mirabilis* and *Paraplagusia japonica* in the adult stage.

The minimum and maximum body length specified by the total length were 4.3mm for *Nibea mitsukurii* and 207mm for *P. japonica*, respectively.

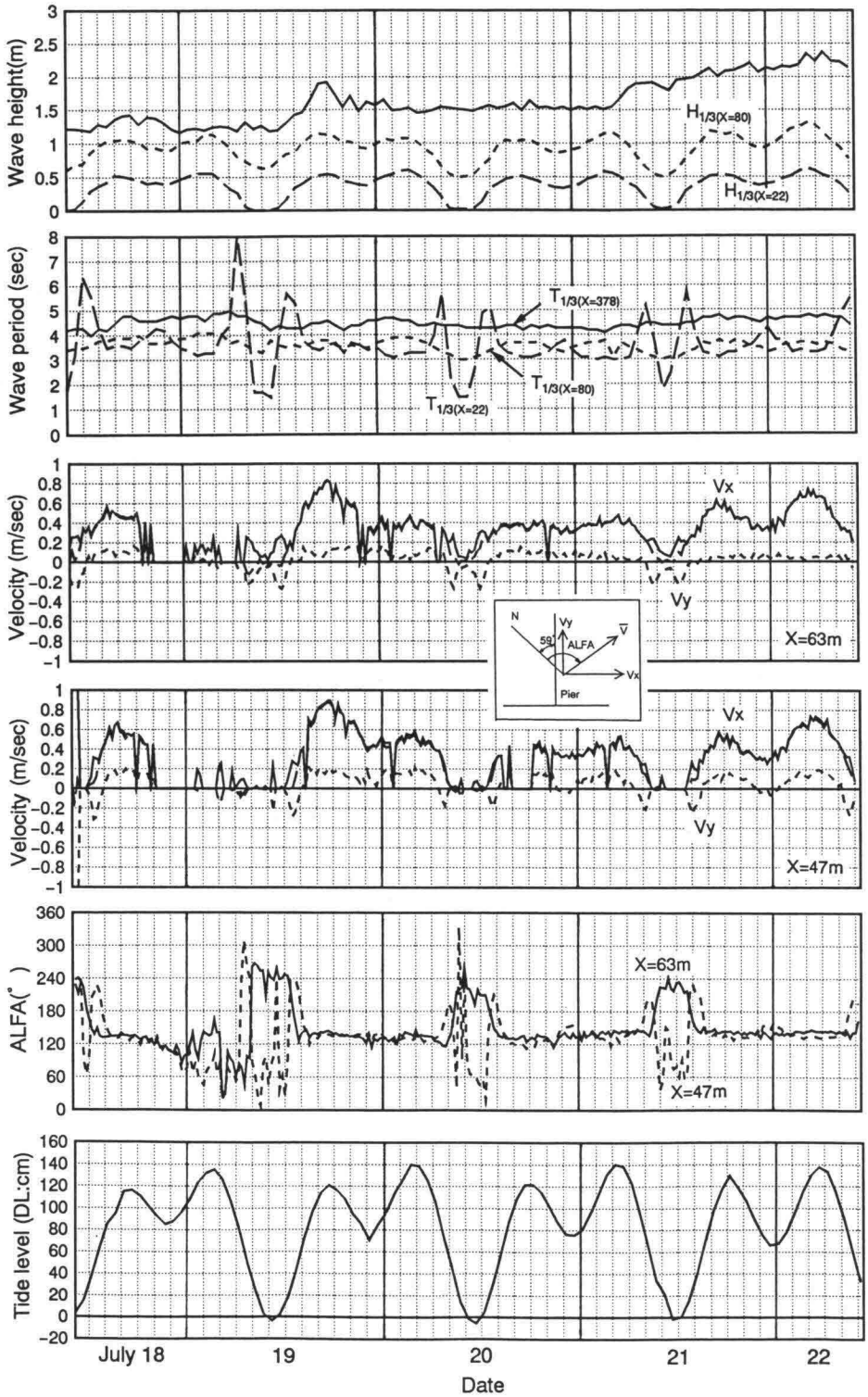

Figure 8 Wave, current and tide level measured during July 18–22, 1993

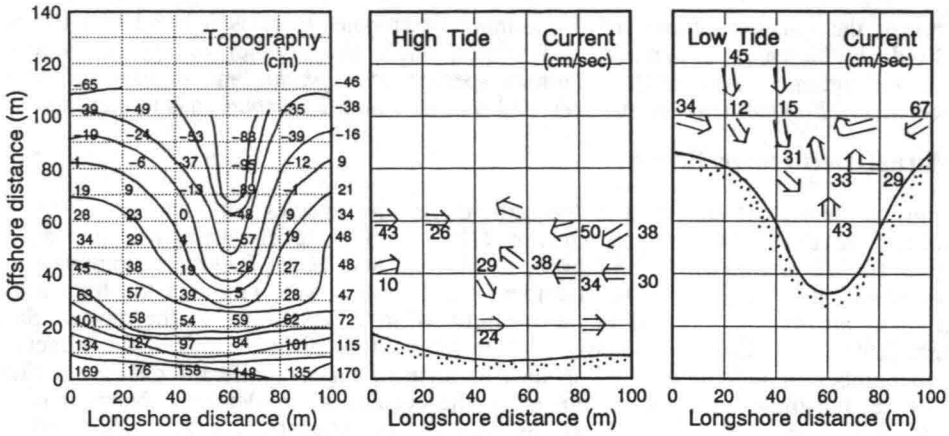

Figure 9 Topography and current distribution in the cusp

Table 1 Numbers of fish larvae and juveniles from the surf zone of Hasaki Beach (SL:standard length, TL:total length)

Scientific name	Total	'91 Oct	Nov	Dec	'92 Jan	Feb	Mar	Apr	May	June	July	Aug	Oct	Dec	'93 Jan	Body length range (mm)
Sardinella zunasi	1												1			SL29.2
Konosirus punctatus	1												1			SL23.5
Engraulis japonicus	126								10	6	15	28	56	11		TL5.5-SL39.4
Anguilla japonica	1														1	TL62.4
Salangichthys ishikawae	68							2	8		2	2	51		3	SL10.5-63.0
Plecoglossus altivelis	259			15										225	19	SL16.2-41.0
Cololabis saira	1										1					SL12.5
Hyporhamphus intermedius	9												9			SL101.3-130.4
Halicampus grayi	1													1		SL23.3
Syngnathus schlegeli	1													1		SL77.7
Syngnathidae sp.	1										1					TL46.9, SL45.0
Valamugil seheli	4											2	2			SL11.9-22.9
Mugil cephalus	410			336	5	18		1		2				46	2	SL13.7-99.4
Liza haematocheila	9								1	6	2					SL7.9-22.3
Lateolabrax japonicus	4			1	1	1				1						TL9.6-SL41.0
Sillago japonica	2											2				SL9.0, 11.5
Trachinotus baillonii	1											1				SL14.6
Caranx lugubris	1											1				SL63.5
Coryphaena hippurus	1												1			SL19.2
Gerres oyena	12											10	2			SL7.5-10.6
Rhyncopelatus oxyrhynchus	19											19				SL8.1-9.6
Terapon jarbua	80										1	72	7			SL10.0-13.4
Acanthopagrus latus	1												1			SL9.2
Acanthopagrus schlegeli	3										1	2				SL8.1-17.0
Evynnis japonica	1												1			SL17.0
Nibea mitsukurii	22											22				TL4.3-6.3
Girella punctata	4										4					SL15.1-16.4
Mugiloididae sp.	7				1						2		4			SL7.5-11.0
Pseudolabras japonicus	1			1												SL13.0
Scomber japonicus	2									1		1				SL13.2, 22.9
Tetragonurus cuvieri	1											1				TL6.2
Tridentiger trigonocephalus	7											7				SL10.8-14.5
Acanthogobius flavimanus	2							1	1							SL12.9, 14.4
Sagamia geneionema	1							1								SL15.0
Luciogobius guttatus	3								1			2				SL10.6-13.4
Gobiidae sp.	13												13			SL7.2-20.4
Pictyblennius yatabei	6										1	4	1			SL11.3-14.6
Scartella cristata	1									1						SL15.2
Blenniidae sp.	1											1				SL13.7
Blenniidae sp.	1												1			SL12.2
Sebastes thompsoni	2										2					SL30.6, 38.8
Hexagrammos otakii	1				1											TL13.6
Platycephalus indicus	43											6	37			SL7.1-10.4
Eleutherochir mirabilis	12					1		4	5			1	1			SL6.3-52.2
Pseudorhombus sp.	1											1				TL9.4
Paraplagusia japonica	8					1		2	1		2	1	1			TL14.3-207.0
Rudarius ercodes	1												1			SL8.8
Canthigaster rivulata	1									1						SL10.2-20.6
Total	1158	0	0	353	8	21	0	11	27	18	34	186	191	284	25	

In terms of the seasonal change of the number of sample, there is a trend that the number of individuals increases in autumn and winter, while the number of species increases in summer and autumn. Among the dominant species, *M. cephalus* and *P. altivelis* are largest in December, *E. japonicus* in summer and autumn, and *T. jarbua* in summer alone.

3.3 Diurnal Occurrence Change

The diurnal change of the number of individuals and species on October 12 to 13 and December 7 to 8 in 1992 are presented in Table 2. Tide level during the time are shown in Figure 10. *E. japonicus*, *S. ishikawae*, *P. altivelis* and *M. cephalus* are dominant in these two investigations. In October, the number of individuals were larger at the high tide level. *E. japonicus* are mostly sampled in the evening, while *S. ishikawae* in the dawn. Sampling numbers in the day time was scare. In December, it is difficult to say the effect of tide level on number of individuals and species because of the insignificant change in tide level from 7 to 8, but these numbers are largest in the evening as in October. Number of species was few in any time. The preliminary investigation on August 25 in 1992 indicated that the number of individuals increased with rising tide with the number of 66, 92 and 225 at low, middle, and high tide times, respectively.

Table 2 Diurnal change of the number of individuals of dominant species

Dominant species	Oct.12,1992			Oct.13				Dec.7,1992		Dec.8
	16:30-16:56 #1	19:20-19:42 #2	22:36-23:17 #3	05:13-5:47 #4	08:33-9:03 #5	10:32-10:45 #6	12:59-13:01 #7	12:45-13:05 #8	15:58-16:23 #9	10:12-10:42 #10
Engraulis japonicus	54	0	0	0	2	0	0	0	5	0
Salangichthys ishikawae	1	0	1	49	1	0	0	0	0	0
Plecoglossus altivelis	0	0	0	0	0	0	0	0	221	0
Mugil cephalus	0	0	0	0	0	0	0	11	4	30

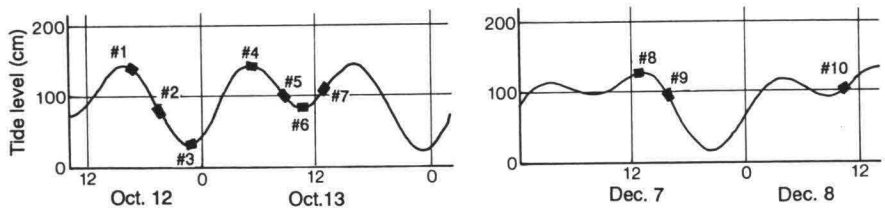

Figure 10 Change of tide level during Oct.12–13, Dec.7–8, 1992

3.4 Difference of the Occurrence within the Cusp

Because only a few fish were collected at the cusp, the number of the mysid shrimps are discussed here. In Table 3 are shown the number of individuals in the towing area of N/100m^2 . There is no clear difference between the horn and the bay at low tide times where the cusp is clearly formed and there is a trend that the number of individuals at high tide, where the cusp is unclear, are greater in the bay part than in the horn part.

Table 3 Difference of the number of mysid shrimp between cusp horn and bay

	Horn		Bay	
	#1	#2	#1	#2
July 14, 1992 11:25-11:39	12	7	5	
July 14, 1992 14:20-15:00	15	4	957	187
July 14, 1992 18:00-18:27	8	4	192	475
July 15, 1992 04:59-05:41	704	81	1569	958
July 15, 1992 09:58-10:36	11	3	8	10

4.DISCUSSION

4.1 Comparison with the Fish Species in the Sheltered Beach

Kinoshita (1984) reported 86 species of fish larvae and juveniles from the surf zone of a sheltered sandy beach located at the Tosa Bay, Shikoku Island. Although about half species of the present study are also collected in Tosa Bay, the dominant species were different in these two sites. The dominant species were *Konosirus punctatus, P. altivelis, Crenimugil crenilabis, Takifugu niphobles* and *Gerres oyena* in Tosa Bay among which only *P. altivelis* was dominant in Hasaki Beach.

4.2 Resident, Seasonal Migrant or Stray ?

In order to understanding the function of the surf zone as an important nursery ground for marine organisms, it is necessary to classify the fish larvae and juveniles found at this zone into the residents, seasonal migrants or strays as proposed by Brown and McLachlan (1990). The residents and seasonal migrants require the surf zone environment at least in a part of their life history, whereas the strays are those accidentally coming into the surf zone by wave action or current.

When the species obviously classified to the strays according to the atlas edited by Okiyama(1988), the surf zone residents or seasonal migrants at Hasaki Beach will be *Sardinella zunasi, K. punctatus, S. ishikawae, P. altivelis*, mullet *M. cephalus, Lateolabrax japonicus, G. oyena, Rhyncopelatus oxyrhynchus, T. jarbua, Acanthopagrus latus, Acanthopagrus schlegeli, N. mitsukurii*, gobii and *Platycephalus indicus*. Kinoshita (1984) pointed out that *K. punctatus, S. zunasi, P. altivelis, Chanos chanos*, silver sides, mullets (*M. cephalus, M. affinis, C. crenilabis*), *Lateolabrax latus, N. mitsukurii, G. oyena, Sparus sarba, A. schlegeli, A. latus, Cottus kazika, P. indicus* and *T. niphobles* are the resident species in the surf zone in Tosa Bay. Thus, *P. altivelis* and *M. cephalus* are common residents or seasonal migrants in both sites.

4.3 Function of Sandy Beach of Sandy Beach Surf Zone as Nursery Ground

Brown and McLachlan (1990) pointed out that plenty of feed and a role of shelter from the predators would be important factors for the sandy beach surf zone as a nursery ground. Among them, a brief discussion on the sheltering mechanism is given based on the facts obtained from this study. First point is that the decrease of the transparency of sea water induced by suspended sediment at the breaking point is suggested to work as a barrier against predators. Furthermore, floating seagrasses, macrophytes and gabages are supposed to play an important role as a shelter for the fish larvae and juveniles in the surf zone.
Second point is that the larger fish (predators) would be hard to control their action in the surf zone with shallow water depth and strong water turbulence, which could result in difficulty in catching feed. Although the strong wave in the surf zone may be disadvantage to small juveniles because of injury by turbulence (Lasiak, 1986), it is suggested that the condition acts as one of the protection factors from predators.

In this study, we didn't discuss the feed supply for the juveniles fishes. In the future, further studies about the distribution of microorganisms such as phyto– and zoo–plankton and gut contents of the fish juveniles are desirable.

5.CONCLUSIONS

The following conclusions can be made from the present study.

1) The sampling at the proposed site clearly indicated that there are many fish larvae and juveniles in the surf zone of the exposed sandy beach.

2) The distribution of several dominant fish larvae and juveniles suggested to be dependent on the tide level and diurnal time.

3) The residents or seasonal migrants at the proposed surf zone are presented, and *P. altivelis* and *M. cephalus* are common one both in the proposed and Tosa Bay sites.

4) The surf zone could play an important role as the shelters against the predators.

ACKNOWLEDGEMENT

The cooperation by the Littoral Drift Laboratory, Port Harbor Research Institute, Ministry of Transport, Japan is greatly acknowledged in carrying out the site investigation and providing the data of physical environment presented in this paper.

REFERENCES

Brown, A. C. and A. McLachlan (1990): Ecology of sandy shores, Elsevier, 328 p.

Higano, J. (1990): Ecosystem of Nearshore Coast, Fisheries Engineering, Vol.26, No.1,pp.37–44., (in Japanese).

Kinoshita, I. (1984): Occurrence of larval and juvenile fishes in the surf zones facing Tosa Bay, Kaiyo to Seibutsu, Vol. 6, No. 6, pp. 409–415., (in Japanese).

Lasiak, T. (1986): Juveniles, food and the surf zone habitat: Implications for teleost nursery areas, South African Journal of Zoology, Vol. 21, pp. 51– 56.

Okiyama, M.(Ed.) (1988): An atlas of the early stage fishes in Japan, Tokai University Press, 1154p.

Senta, T. and I. Kinoshita (1985): Larval and juvenile fishes occurring in surf zones of western Japan, Transactions of the American Fisheries Society, Vol. 114, pp. 609–618.

Suda, Y., J. Higano, K. Adachi and K. Kimoto (1992a): Occurrence of marine organisms in the surf zone of Kashima–nada, Japan, Proceedings of the Japanese Society of Fisheries Engineering, 1992, pp. 59–60.,(in Japanese).

Suda, Y., J. Higano, K. Adachi and T. Otsuki (1992b): Occurrence of marine organisms in the surf zone of the exposed sandy beach, Proceedings of the Japanese Association for Coastal Zone Studies, 1992, pp. 46–47. (in Japanese).

Theme 5

BEACH STABILIZATION IN THE VICINITY OF A HARBOR

HYDRO-PORT'94
International Conference on Hydro-Technical
Engineering for Port and Harbor Construction
October 19 - 21, 1994, Yokosuka, Japan

Change of the Ag.Nikolaos Beach in the Vicinity of a New Harbor for Small Crafts

C.I. Moutzouris

National Technical University of Athens, Civil Engineering Department
5, Iroon Polytechniou, 15773 Athens

ABSTRACT

A new harbor for small crafts was recently built on the sea front of Aghios Nikolaos, a popular touristical center of the island of Crete, Greece. The two moles of the harbor modified the nearshore processes and caused extensive erosion to the beach adjacent to the town. In 1992 a study was commissioned by the relevent public authority aiming at restoring the urgently needed municipal beach.

A pattern of nearshore mechanisms was established after evaluation of results from direct measurements and computations . A system of two detached breakwaters was designed to provide protection to the beach. The location and orientation of the structures were also dictated by the entrance to the harbor. The coastal protection and restoration scheme was completed by a beach replenishment programme. The granulometry of the replenishing sediment was prescribed following the sediment investigation mentioned above.

Key words:

1. INTRODUCTION

Ag.Nikolaos is a popular tourist town on the northeastern coast of the island of Crete, Greece. Among the main attractions of the area is the coastline, combined with a mild climate.

In 1991-92, the National Tourist Organisation of Greece (NTOG) built a new marina on the southern coast of the town, aimed at providing facilities for local and visiting yachts. Two moles protect the marina basin from waves approaching from the NE to S sector. The new marina is less than 200 metres from the town's traditional sandy beach, which in the past was used mainly by the local inhabitants.

The construction of the new marina modified the nearshore physical processes and caused rapid destructive modification of the beach. In less than a year, a major part of the beach was damaged and nearby properties were threatened. More than 150m of the beach vanished completely.

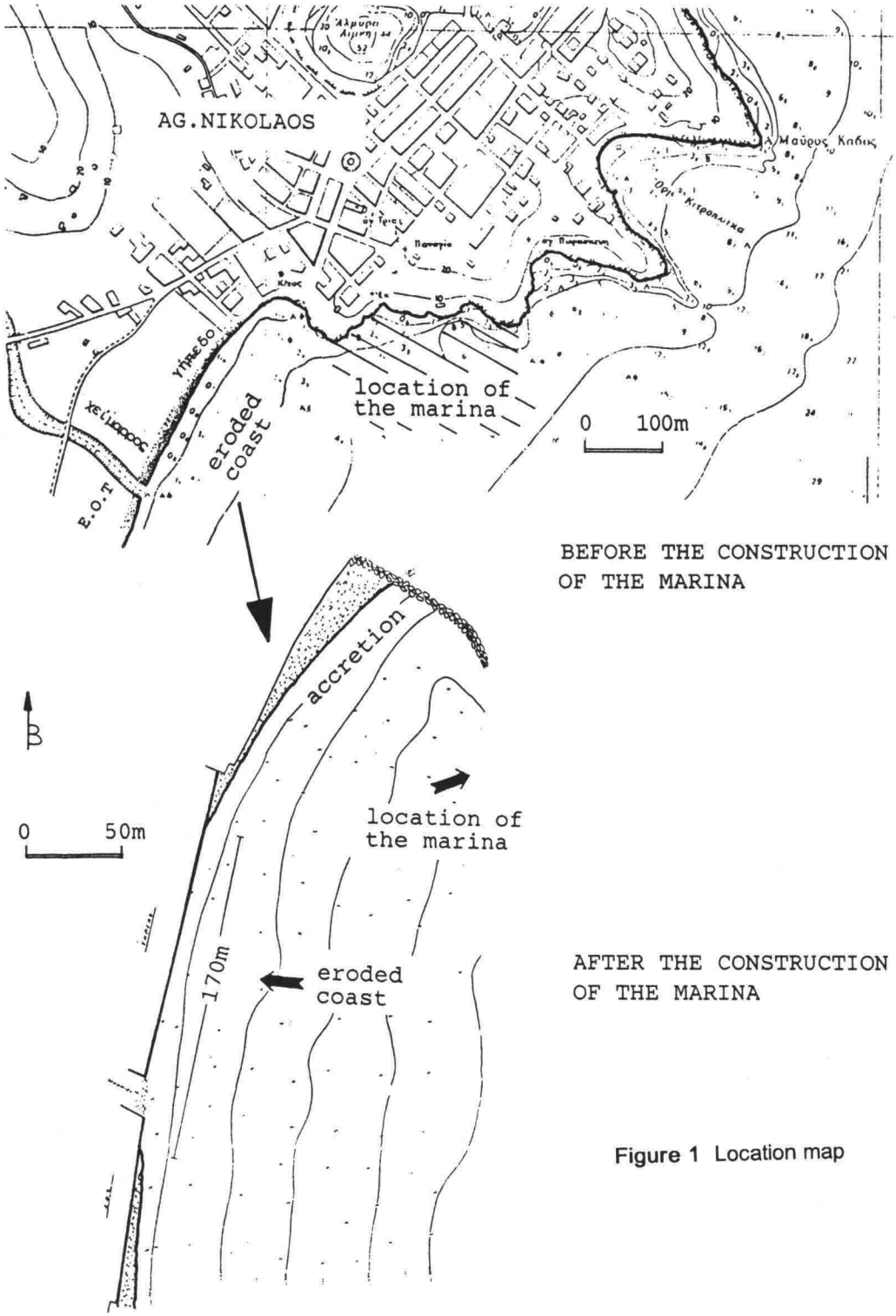

Figure 1 Location map

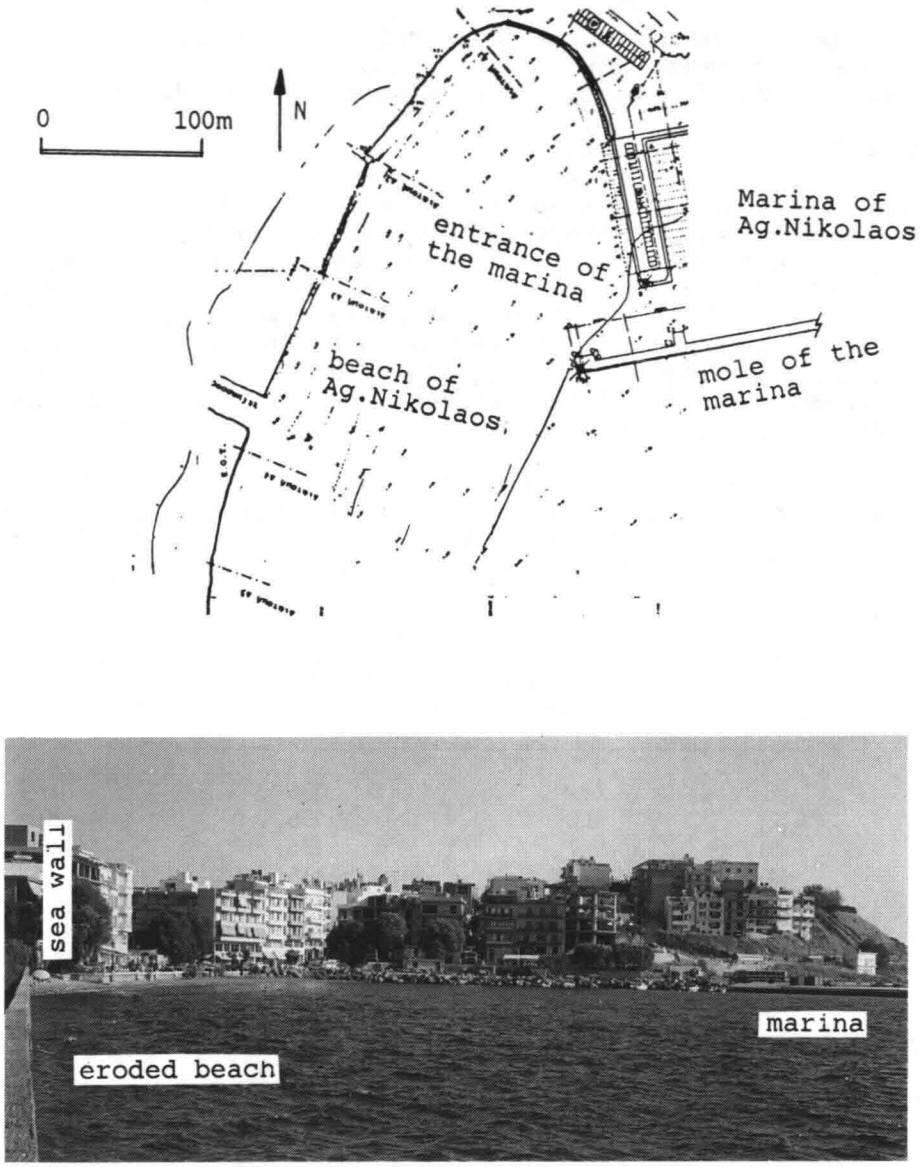

Figure 2 The eroded beach of Ag.Nikolaos

A sea wall was urgently built to provide "protection" to a neighboring soccer field but created considerable problems at the entrance of the marina, due to wave energy reflected on the wall. Figures 1 and 2 show the location of the marina and the eroded beach.

In 1992 NTOG commissioned a study, aimed at restoring the much needed (and remembered) municipal beach. The study included various field measurements and mathematical modeling, in order to obtain a sound insight to the physical mechanisms causing the coastal instability. As a result of this study a program of coastal works were proposed.

This paper presents the methodology of the study, and a description of the structures recommended. As these structures are currently under construction, it is expected that the results and observations from their performance will be discussed when this paper is presented.

2. DESCRIPTION OF THE STUDIES

A programme of sediment sampling from the sea bed of the eroding zone and the adjacent coast was executed. Sediment samples were collected from characteristic locations (1,2,3 and 4) along various transverse sections. Statistical parameters such as the mean diameter Mz, the standard deviation σ, skewness S and kurtosis K of the grain populations were computed and compared (see Fig.3). As expected, the coarsest grain population was found along the eroded zone. The finest grains accumulated in the zone of accretion and gave the coastline the typical shape of an accretion line. Examination of grain-size distributions, prior to their erosion, showed that sediment could easily be transported by the waves, and in some cases, by the currents in the area.

Sea currents induced by mechanisms other than waves were measured along the study area. Current-meters were deployed and collected data for periods of 20 days. Figure 4 shows typical histograms of current speeds and directions.The study determined that dominant current-induced flow is in the longshore direction to the right of the coast (southwards). Maximum observed current speeds are as follows:

	Current speed (cm/sec)	Direction (azimuth) (o)
(1)	24,4	135
(2)	19,6	165
(3)	18,7	135
(4)	18,3	135
(5)	17,8	195
(6)	17,4	300
(7)	17,2	195
(8)	16,9	135
(9)	16,7	195
(10)	16,5	240

Statistical analysis of existing wind data showed that dominant winds in the study area are as follows:

Wind direction	Annual frequency percentage	Maximum force
NW	38,7%	8Beaufort
W	11,6	8
N	7,6	9
S	7,7	10
SW	7,7	8

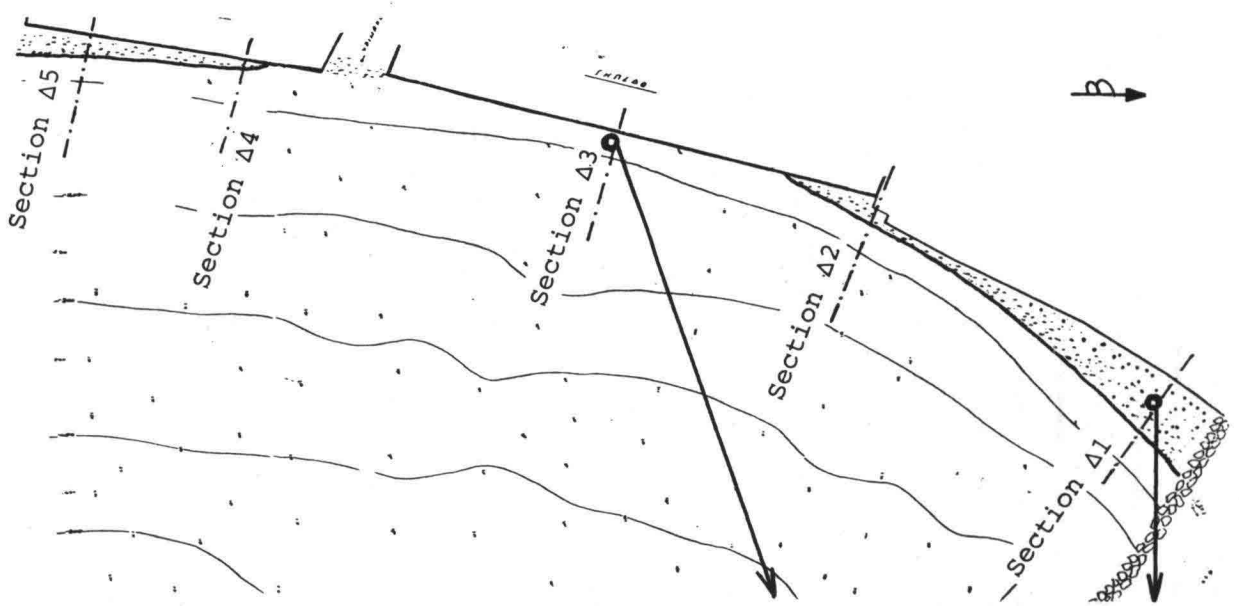

Sample	Mz	st. dev.	S	K
Δ1-1	1.553	0.674	1.600	1.200
Δ1-2	-2.583	1.587	0.450	2.021
Δ1-3α	-1.127	3.310	0.984	0.517
Δ1-3	2.523	0.732	1.736	1.012
Δ1-4	2.577	0.668	1.750	1.013
Δ2-1	-4.647	0.613	-0.665	1.107
Δ2-2	-2.087	2.373	0.909	0.569
Δ2-3	-4.617	0.472	-0.850	1.025
Δ2-4	2.180	0.668	1.711	1.111
Δ3-1	-3.563	0.803	-0.453	1.906
Δ4-1	-4.333	0.413	-1.220	1.139
Δ4-2	-4.197	0.432	-1.127	1.348
Δ4-3	-5.203	0.443	-0.509	0.808
Δ4-4	-6.137	0.506	-0.909	1.051
Δ5-0	0.547	1.914	1.176	1.503
Δ5-1	-5.437	0.506	-0.558	0.852
Δ5-2	-3.617	0.579	-0.364	1.199
Δ5-3	-3.413	0.829	0.212	0.972
Δ5-4	-5.587	0.462	-0.805	0.343

Sample Δ3-1

Sample Δ1-1

Figure 3 Sediment samples from the sea bed along the coast under study

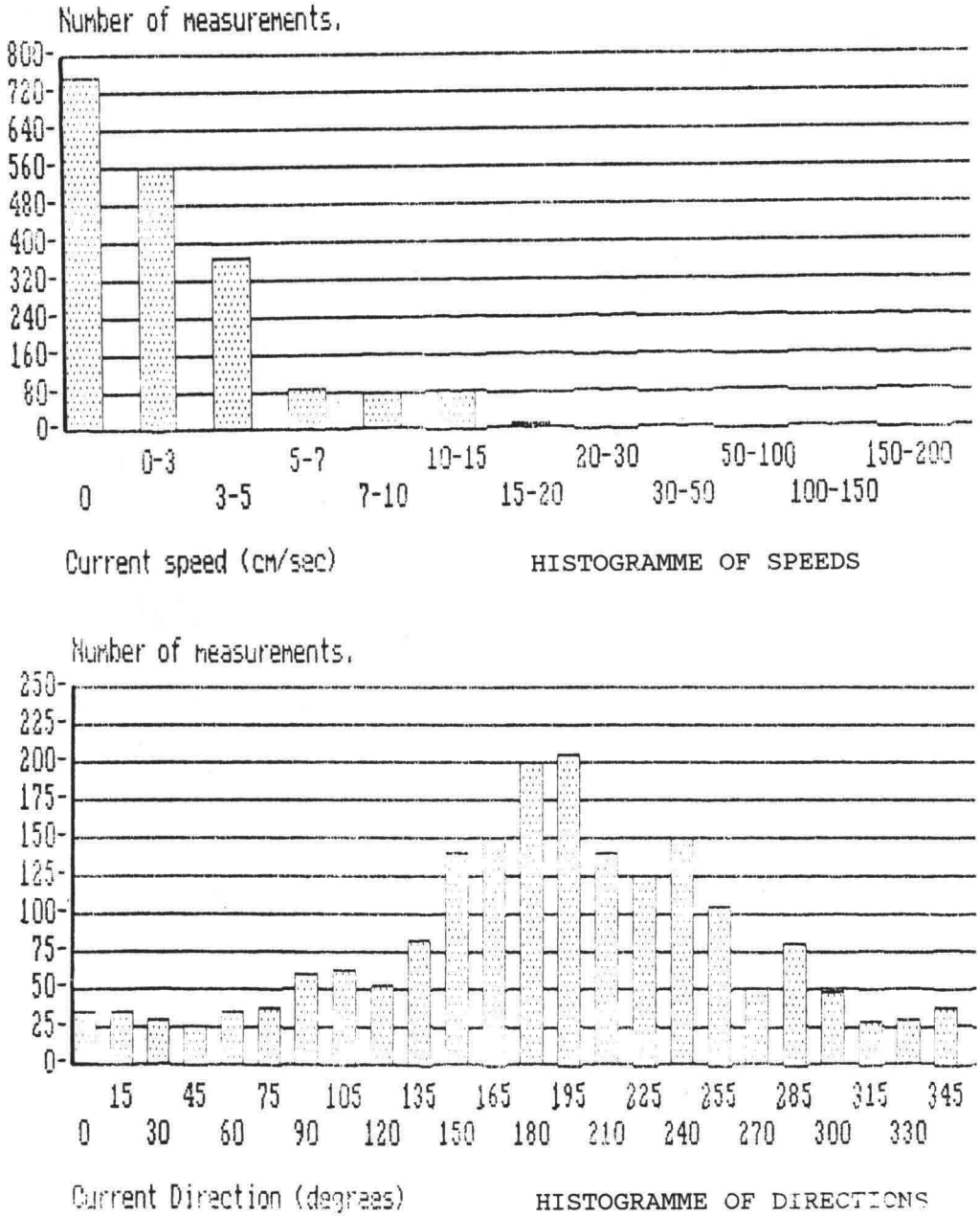

Figure 4 Sea current measurements

Wave parameters were estimated using wind characteristics and fetch considerations. Design waves in deep-sea were chosen as follows:

Directrion	Wave height H_s	Wave period T
N	2,9m	6,6sec
NE	1,8	5,0
E	1,4	4,5
SE	2,1	5,3

Wave approach to the eroding coast was simulated using the refraction-shoalling-breaking model in use at the NTUA. Bathymetric data was collected from the Hydrographic Service and the NTOG. Computations were carried out for conditions before and after the construction of the new marina. Typical results from the computations are shown in Fig.5. The main conclusion drawn from the results of these simulations was that before the construction of the new marina waves were attacking the coast obliquely with a dominant longshore drift southwards. Wave energy was mostly absorbed by the sandy beach. After the construction of the marina the dominant direction of wave-induced longshore flow changed to the left (northwards). Considerable amount of wave energy is found to attack the coast perpendicularly.

3. STRUCTURES TO BE BUILT

Evaluation of the results from the field measurements and computations led to a pattern of nearshore mechanisms. The presence of the mole of the new marina modified the mode of wave action on the beach. Waves started attacking the coast perpendicular and causing suspension of the fine fractions of the bed sediment. Wave-induced dominant longshore flow is now to the north. Suspended sediment migrated northwards (southwards) under the action of waves (currents) and the fine grains in the beach were depleted. The construction of the sea wall eventually caused further erosion.

A system of two detached breakwaters was then designed to provide protection to the coast. The location and orientation of the two structures were defined taking into account the following two conditions:

* location of wave breaking zones
* location of the entrance of the marina

The first parameter imposed the construction distance of the breakwaters from the coastline. This distance was defined following sound coastal engineering principles. The second condition demanded that the breakwaters be built at a distance from the entrance leaving sufficient space for manoevering of small crafts. These two conditions imposed contradicting restrictions. To aggravate the situation, local authorities made it clear that permission would not be granted if the structures were not to be built at a considerable distance from the coast line leaving sufficient space for bathers. A technicosocial compromise was finally reached after long negotiations.

The coastal protection and restoration scheme was completed with a beach replenishment programme. The granulometry of the replenishing sediment was prescribed following the statistical parameters of the in-situ sediment.

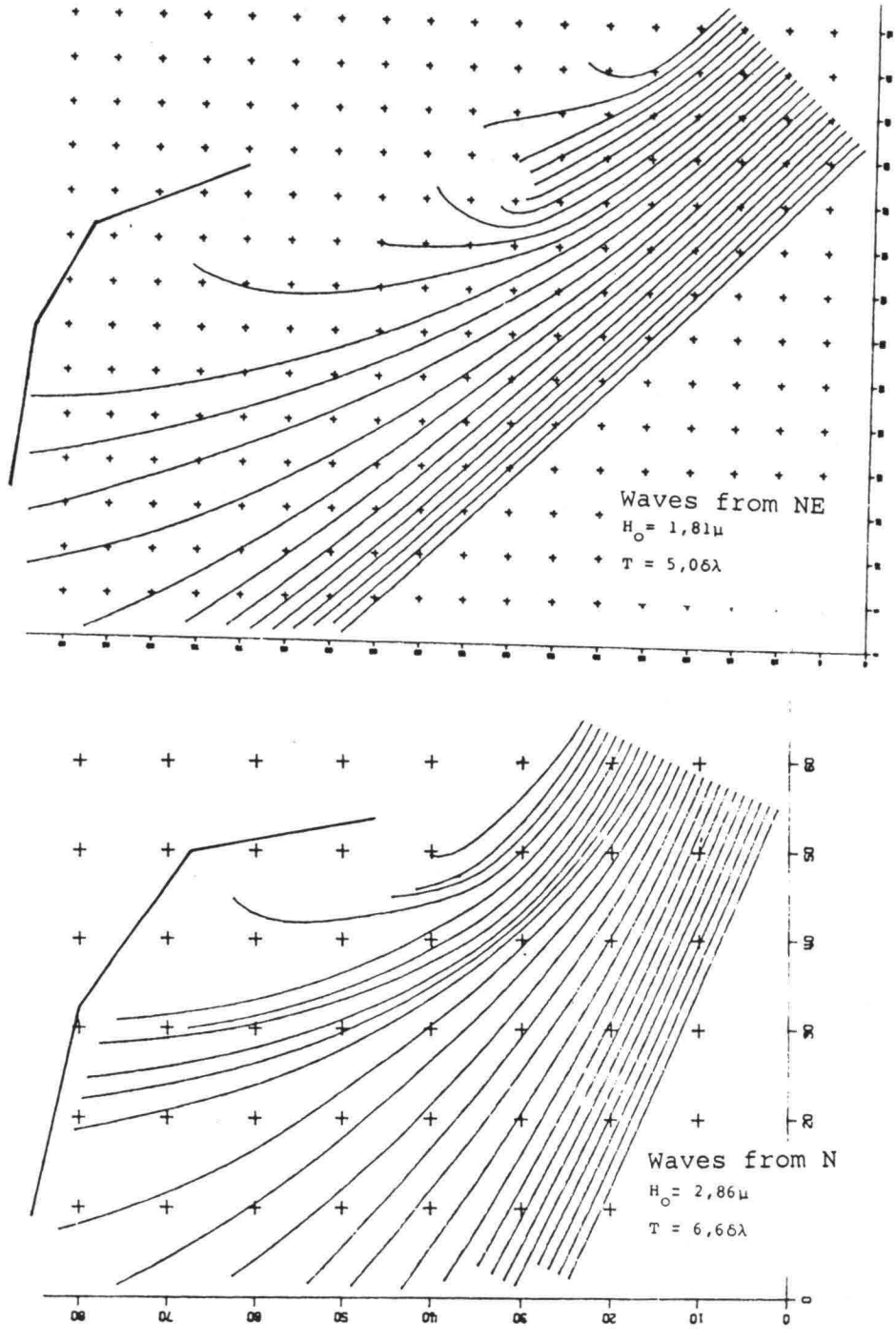

Figure 5 Wave approach simulation

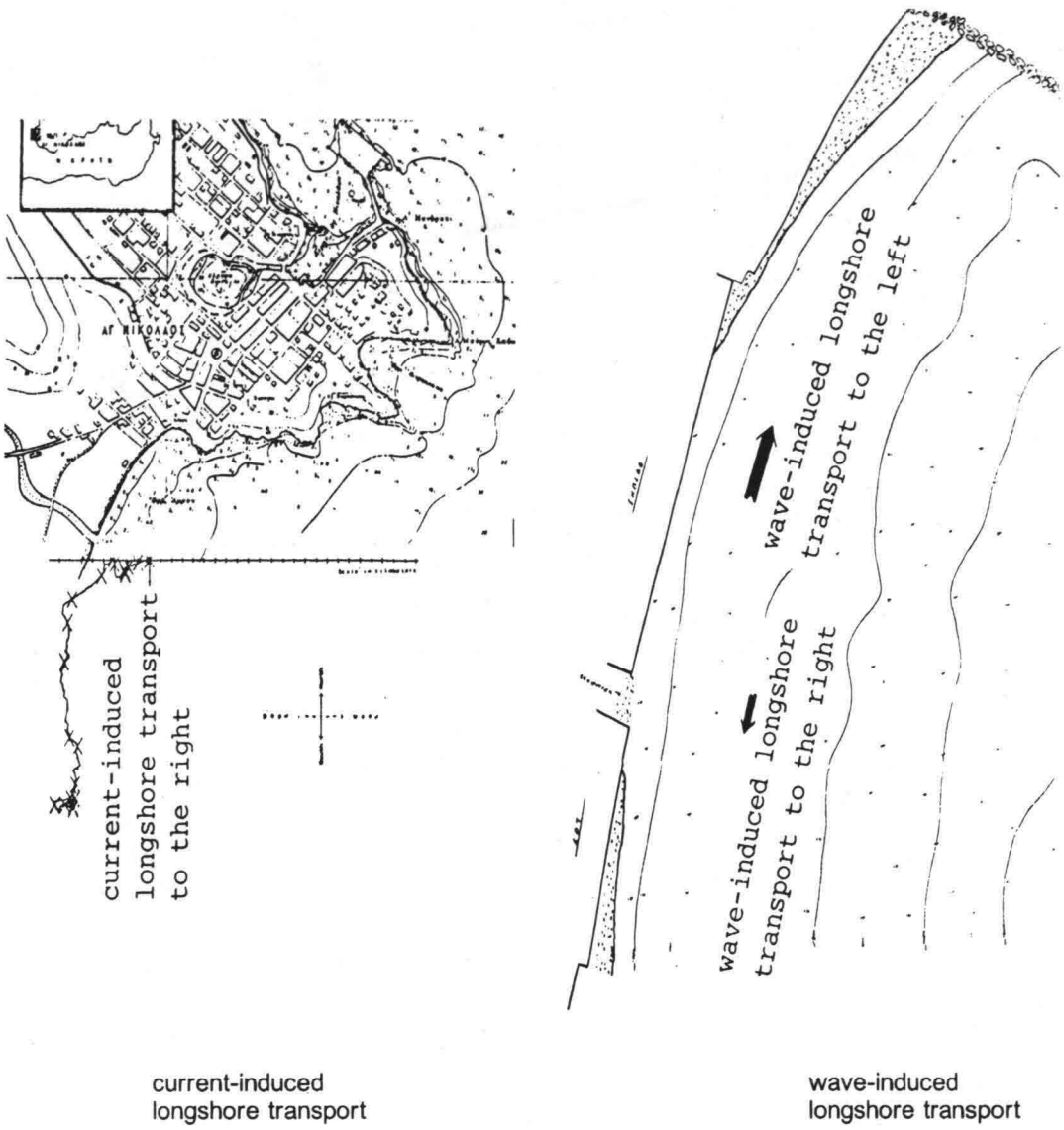

Figure 6 Patterns of longshore sediment transport induced by waves and currents

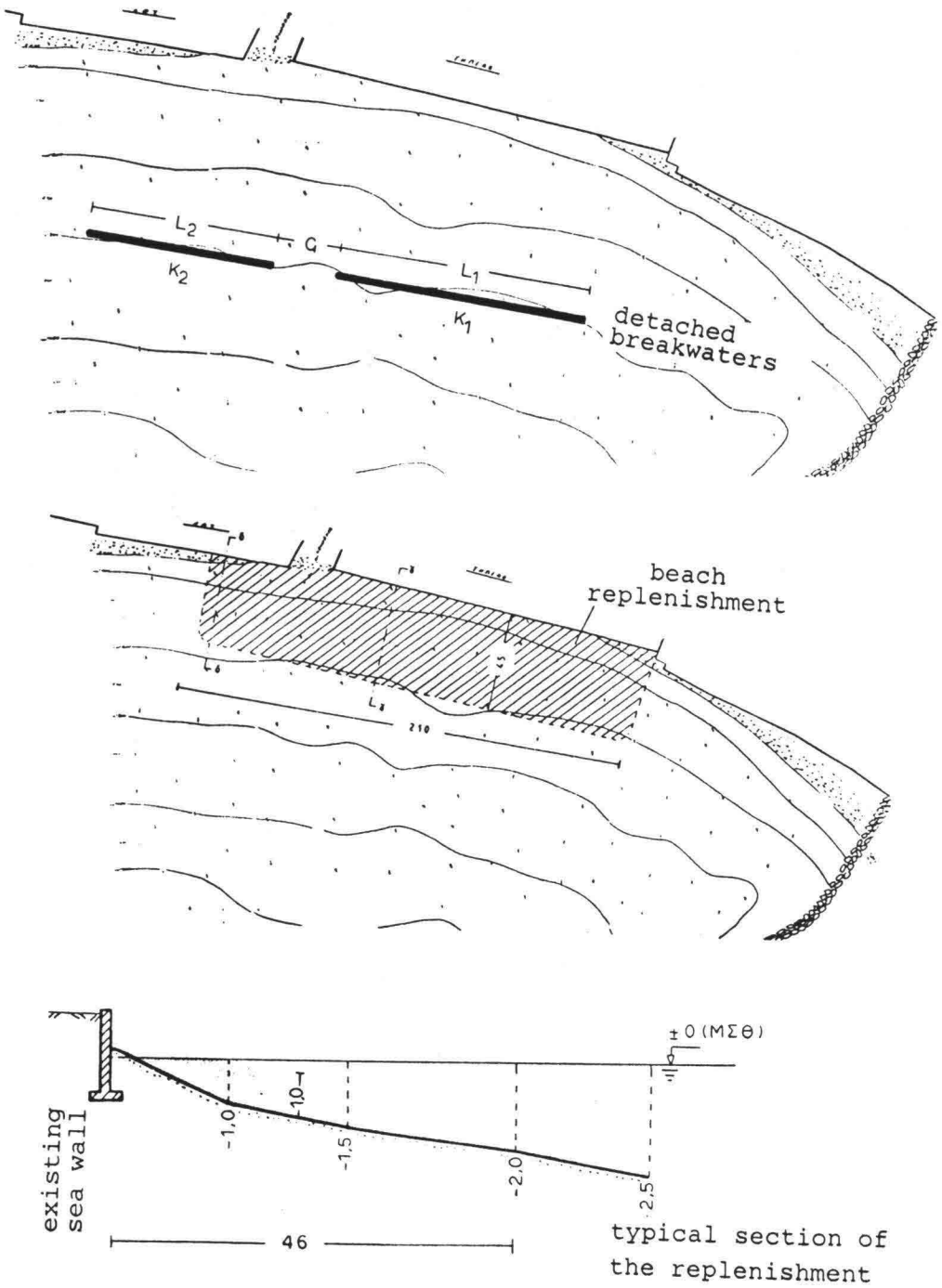

Figure 7 Coastal structures under construction

4. DISCUSSION

The new harbor for small crafts of Ag. Nikolaos caused extensive erosion to the adjacent beach of the town. In 1992 a study was commissioned aiming at restoring the municipal beach. The study included a programme of current and sediment field measurements as well as wave approach modeling in order to gain a sound insight to the physical mechanisms causing the coastal instability. Analysis of the data collected from the programme of measurements showed that the dominant direction of current-induced flow is in the longshore direction to the right (southwards). The simulation of wave approach to the eroding coast in the presence of the harbor structures led to the conclusion that dominant direction of wave-induced longshore flow is to the left (northwards). Considerable amount of wave energy was found to attack the coast perpendicularly. Examination of the grain-size distributions showed that grains can easily be transported by the waves and, in some cases, by the currents.

A patern of nearshore mechanisms was established after evaluation of results from direct measurements and computions. A system of two detached breakwaters was then designed to provide protection to the beach. Restrictions to the selection of the location and orientation of the structures were imposed by the location of the entrance to the harbor. The coastal protection and restoration scheme was completed by a beach replenishment programme. The granulometry of the replenishing sediment was prescribed following the properties of the grains, as found from the field measurements.

ACKNOWLEDGEMENTS

Permission to publish data from the research programme commissioned by the NTOG is acknowledged.

REFERENCES

Moutzouris,C.I. (1992): Research Programme for the Protection of the Eroding Coast of Ag.Nikolaos, Technical Report

NTOG (1990): Design of the Ag.Nikolaos Marina, Technical Report

NTOG (1992): Design of Protective Works for the Eroding Coast of Ag.Nikolaos, Technical Report

HYDRO-PORT'94
International Conference on Hydro-Technical
Engineering for Port and Harbor Construction
October 19 – 21, 1994, Yokosuka, Japan

Protection against Shore Erosion and Channel Shoaling at Port Madero, MEXICO

José Miguel Montoya R [1]
Julio Roberto Vera S [1]
Shoji Sato [2]

[1] Subgerencia de Estudios Básicos e Investigación
Puertos Mexicanos, S.C.T.
Lerdo de Tejada No.6, Col. Marina Nacional, 54180
[2] Nippon Tetrapod Co. LTD.
At present, México Office of Japan International Cooperation Agency
Aristóteles No.77– 403, Col. Chapultepec Morales, 11560

ABSTRACT

The Port Madero has been constructed excavating the sandy beach facing the Pacific Ocean.The port mouth is protected by two parallel rubble mound breakwaters.The depth of access channel is maintained to be more than -9 m by dredging and the west coast is protected by groins and sea-walls of rubble mound.The past shoreline change in the east coast is analysed using eigenfunction and its future change caused by further prolongation of the breakwaters is predicted by one-line theory to check the reasonability of maintenance dredging at the access channel. As for the west coast,the protection measure against erosion is detailed and its effect and reasonability are considered from the analysis of shoreline change using eigenfunction.

Key Words: Littoral drift, shoreline changes, groins and sea-wall.

1. INTRODUCCION

Port Madero is located on the southern part of Mexico, facing the Pacific Ocean, as shown in Fig. 1-1. The port was planned for commercial and fishery activities, and then in 1972 the construction of the east and west breakwaters begun together with dredging of the inner basin. Until 1975 when the port was opened for ships, the east and west breakwaters had been prolonged in 800m and 630m,respectively. The arrangement of port structures in 1993 is shown in Fig. 1-2 with their construction period.

Fig.1-1 Location of Port Madero

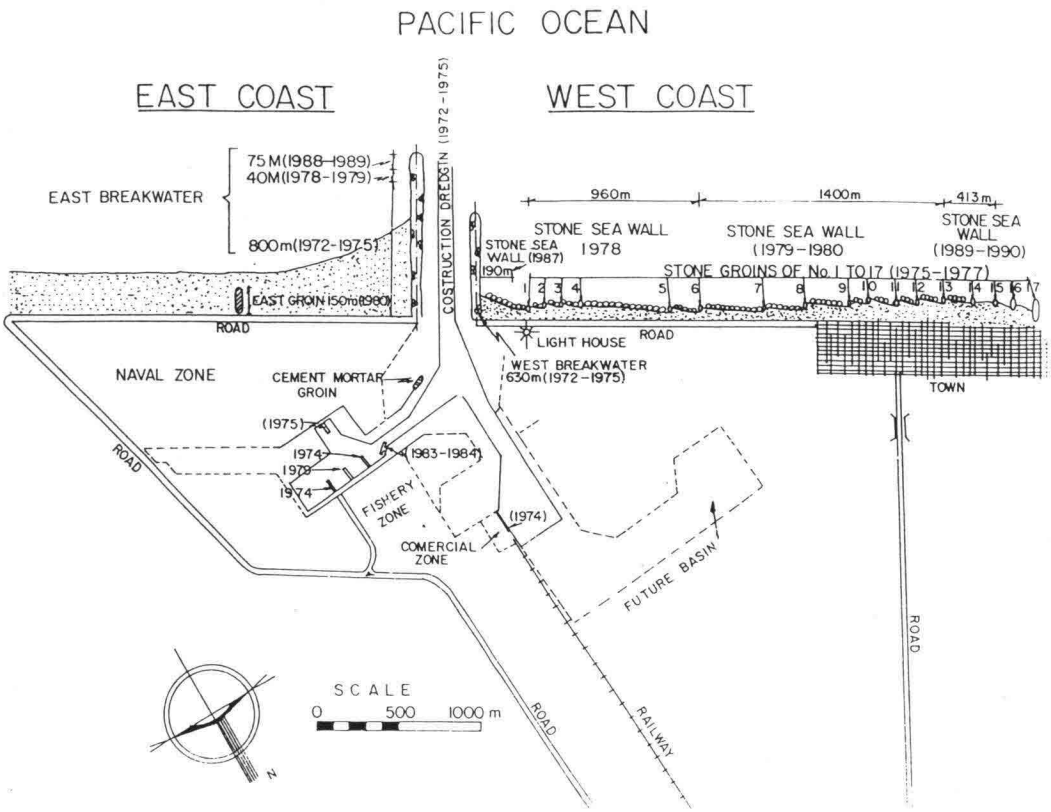

Fig.1-2 Plan of the port at present with the periods of the construction of structures

The first 100m long of the east breakwater is permeable with a core of rubble stone of 500 kg covered by two layers of large stones of 7 ton, the other length of 700m of this breakwater and the total length of 630m of the west breakwater are composed of a core of rubble stones of 250 kg covered by two layers of large stones of 500 kg and two exterior layers of large stones of 7 ton.

Accretion and erosion ocurred respectively in the east and west sides of the breakwaters , and also some part of sand passed trough the voids betwen stones of the east breakwater to deposit in the access channel of the port. In order to reduce the erosion in the west cost, successive construction of stone groins from No. 1 to No. 17 was made from 1975 to 1977, but it wasn't successful, so that from 1978 to 1990 was constructed 2850m long of stone sea-wall betwen the west breakwater and the groin No. 16.

On the other hand, in order to protect the access channel from shoaling, from 1978 to 1989 was prolongated the east breakwater by 115m, and also in 1980 was constructed on the east coast a stone groin of 135m long at 110m apart from the east breakwater. This short groin wasn't successful , and the access channel has been maintained by constant dredging since 1983.

At present, as for the port facilities, there are three piers of 6.5m deep for fishery ships, one pier of 7m deep for military ships, one pier of 7m deep for combustible services, and one pier of 9.5m deep for commercial ships, as shown in Fig. 1-2.

The coast of Port Madero was nearly straight sandy beach with the foreshore slope of nearly 1/13 before the construction of the port. At present the sediments on the backshore is composed of fine sand of 0.38mm in D_{50} in the east coast and mostly coarse sand of 0.50 mm in D_{50} in the west coast.

The astronomical tide of Port Madero are of the semi-diurnal type. The average tidal range is about of 1.47m. The datum level for the port structures and sounding of sea bottom is taken at Mean Lower Low Level, which is 0.693m below Mean Sea Level.

The prevailing directions of the incoming waves are S~SW, and the predominant periods are 10~12 seconds, but in the rainy season from May to October southerly strong waves come causing by cyclones.

2. CHANGES OF SEA BOTTOM CAUSED BY THE CONSTRUCTON OF BREAKWATERS

2.1 Depth contour lines change

Fig. 2-1 shows the change of the contour lines according to the construction of breakwaters. In December of 1971 before the construction of breakwaters, the contour line of 9m deep is located near the tip of the planned east breakwater, whereas the contour line of 8m deep is located on the tip of the planned west breakwater. In April of 1975 when the port was opened for ships, the contour line of 9m deep advances offshore from the tip of the east breakwater, and the contour line of 7m deep is located on the tip of it, whereas near the tip of west breakwater the contour line of 8m deep is located in front of the tip of it. In comparison with

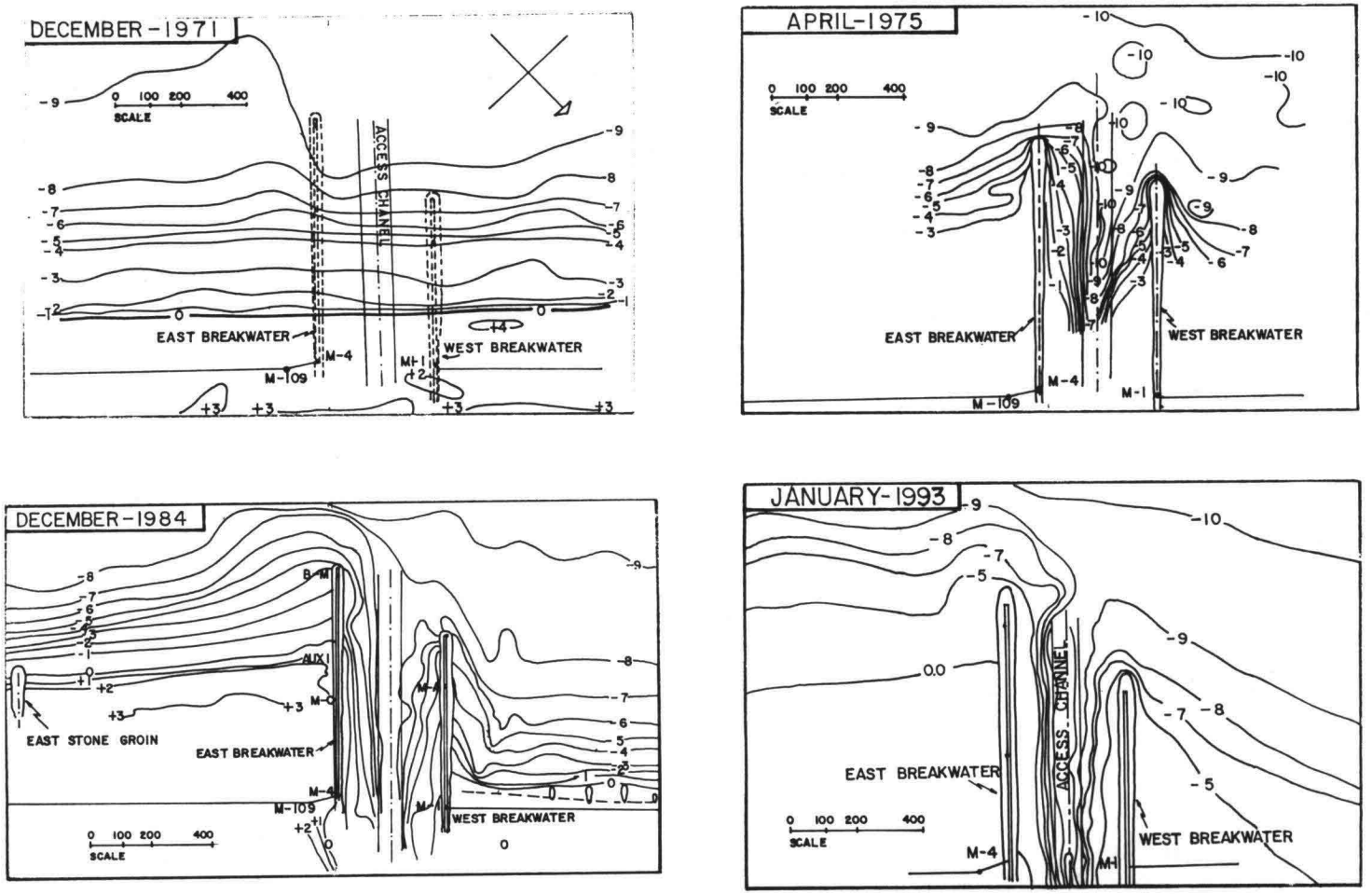

Fig. 2-1 Contour line change according to the construction of breakwaters

December of 1971, erosion and accretion occurred in the west and east coasts, respectively.

In December of 1984 when both breakwaters had been prolonged until the length planned at first; the contour line of 6m passes in front of the tip of the east breakwater and the shoreline of ±0m advances about 300m along the east breakwater compared with December of 1971. In the west coast, the water depth at the tip of the west breakwater does not change compared with December of 1971, but contour lines of 2~5m deep go back landwards.

In January of 1993, the shoreline advances about 100m more in the east coast and the east stone groin already located totally on land. The contour line of 5m deep passes in front of the tip of the east breakwater, although the breakwater was prolonged by about 100m compared with 1984. On the west coast, the countour lines locate without noticeable change compared with December of 1984.

2.2 Shoreline Change

(1) East Coast

Fig. 2-2 shows the change of the shoreline from March of 1983 to December of 1987 in the vicinity of the east breakwater. The shoreline along the east breakwater advanced continuously until 1986 and scarcely changed after 1986, although in the part apart from the breakwater the shoreline changed irregularly.

Fig. 2-3 shows the change of the shoreline after 1989 when the prolongation of the breakwater was suspended. Near the east breakwater the shoreline advanced seaward by about 130m between May of 1989 and January of 1991, but the other shorelines are between these two shorelines. At about 2000m from the breakwater the shoreline advances most in January of 1992 and February of 1993 and retreats most in May of 1989. At about 4000m from the breakwaters, the shoreline advances most in August of 1992 and February of 1993 and retreats most in August of 1991. As a whole, the shoreline seems to have advanced with year from 1989 to 1993.

(2) West Coast

Fig. 2-4 shows the change of shoreline in the west coast from January of 1957 to April of 1991. After the start of the construction works of the breakwater , the shoreline within 1500m from the west breakwater retreated landward by 20~40m until 1973. After 1978 when the stone sea-wall begun to be constructed , the shoreline were stable until 1985, but the shoreline of April of 1991 retreated again in the vicinty of 1000m from the breakwater which was caused by the sinking of the stone sea-wall there. On the other hand, in the west side of groin No. 17 occurred severe erosion after August 1978.

2.3 Beach profile change

Fig. 2-5 shows the change of the beach profile along the east breakwater from December of 1971 to August of 1992. The profile from +3m to -9 or -10m moved in parallel seawards with the slope of about 1/50~1/60 between -0 and -8m, although its yearly advance is very irregular.

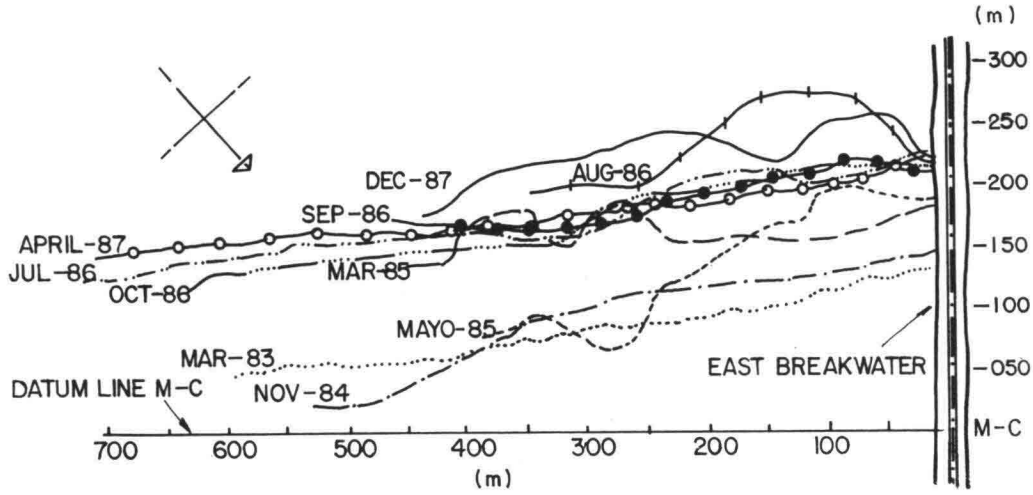

Fig. 2-2 Shoreline change in the east coast near breakwater during March of 1983 to December of 1987

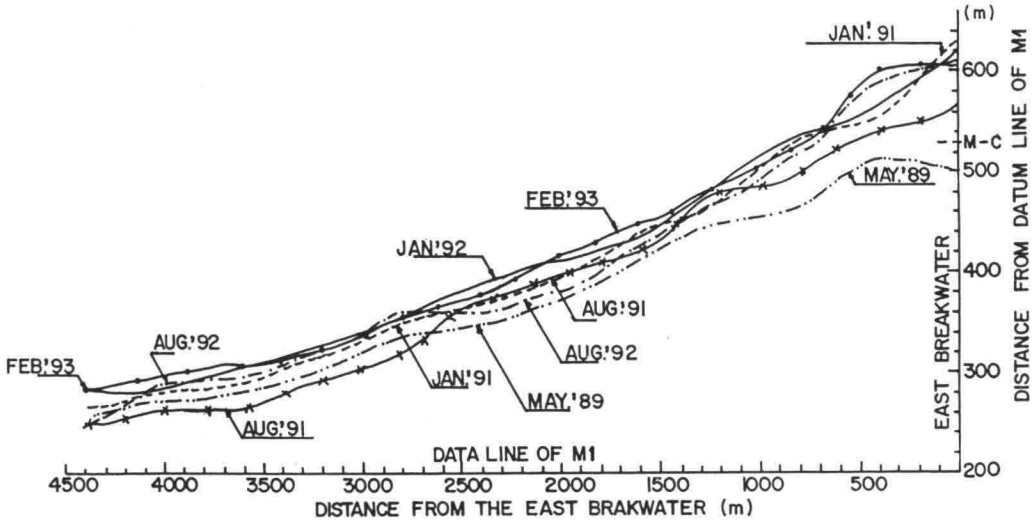

Fig. 2-3 Shoreline change in the east coast after 1989 when the prolongation work of breakwater was suspended

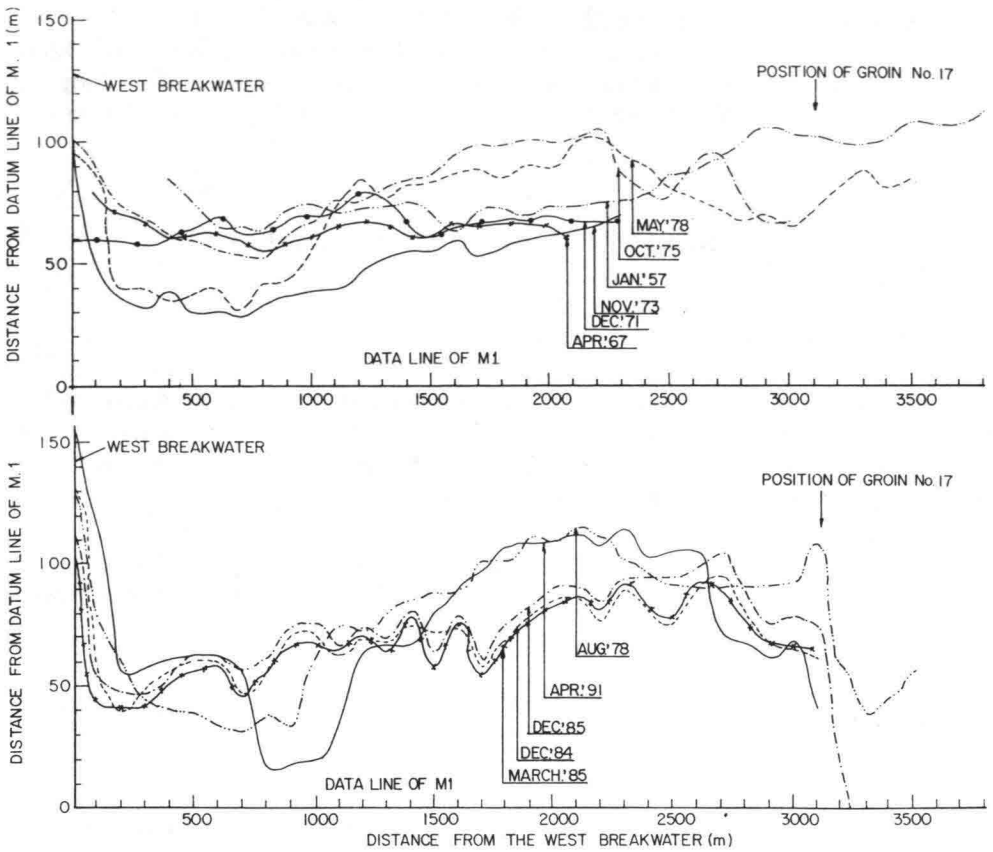

Fig. 2-4 Shoreline change in the west coast

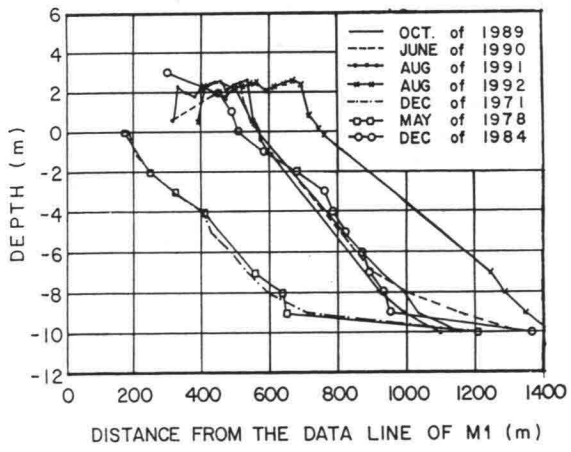

Fig. 2-5 Profile change in the east coast along the breakwater

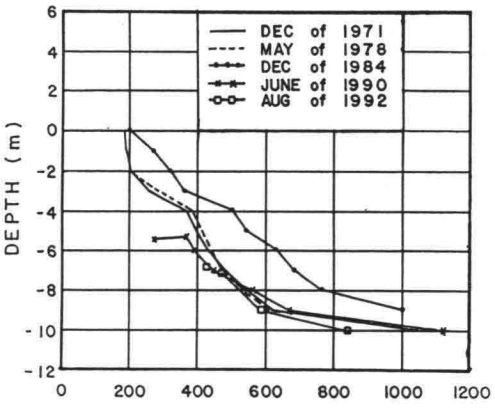

Fig. 2-6 Profile change in the west coast along the breakwater

Fig. 2-6 shows the change of the beach profile along the west breakwater from December of 1971 to August of 1992. The profile only between from -0 or -4m to -10m is shown because the shoreline was protected with stone sea-wall. As a whole, the movements of the slope is not noticiable and its slope changed from about 1/50~1/60 in 1971 to about 1/80~1/100 in 1992.

3. ANALYSIS OF THE SHORELINE CHANGE USING EMPIRICAL EIGENFUNCTIONS

3.1 Method of analysis

In order to make clear the characteristics of the shoreline change , has been found out a set of empirical eigenfunctions which best fits the shoreline data in the least squares sense, following the method which was used by Winant, Inman and Nordstrom (1975) in the description of seasonal beach change using empirical eigenfunctions.

In this analysis, the position I_{xt} of the shoreline from the datum line, where the indexes **t** and **x** indicate the measured time and the distance along the datum line from the breakwater respectively, is expressed in term of a normal mode expansion as follows:

$$I_{xt} = \sum_{p=1}^{n} C_p(t) \cdot e_p(x) \qquad (3\text{-}1)$$

$$(\ 1 \le t \le N,\ \ 1 \le x \le n,\ \ 1 \le p < n\ )$$

But, in the analysis, the deviation from the mean value in time at each position was taken as the value of I_{xt} of the equation (3-1).

Forming the correlation matrix **A** with the following elements:

$$I_{ij} = \frac{1}{n.N} \sum_{t=1}^{N} I_{it} . I_{jt} \qquad (3\text{-}2)$$

$$(\ 1 \le i \le n \ \text{ and } \ 1 \le j \le n\ )$$

$e_p(x)$ of (3-1) is obtained as the eigenvector of the matrix **A** from the following equation:

$$A\ e_p = \lambda_p\ e_p \qquad (3\text{-}3)$$

Where λ_p is eigenvalue and the contribution rate of $e_p(x)$ is calculated as follows:

$$\text{Contribution rate of } e_p(x) = \lambda_p \ / \ \sum_{i=1}^{n} \lambda_i \qquad (3\text{-}4)$$

$C_p(t)$ is calculated as follows:

$$C_p(t) = \sum_{x=1}^{n} I_{xt} \cdot e_p(x) \qquad (3\text{-}5)$$

3.2 Analysis of the shoreline in the east coast

At first, the change of shoreline in the east coast has been analyzed for the data of 50m intervals in the direction of the shoreline until 450 meters from the east breakwater. Those analysed shorelines have been shown in Fig. 2-2 of the chapter 2. Fig. 3-1 shows the values of the first and second modes, which correspond to $C_1(t) \cdot e_1(x)$ and $C_2(t) \cdot e_2(x)$ of Eq. (3-1), respectively.

Mode 1 is 50% in the rate of contribution for the shoreline change, which corresponds to Eq. (3-4), has the following characteristics:

(1) The shoreline of this mode advances seaward with time except the periods between March and May of 1985 and between July and October of 1986. Its reason is not clear, but it is assumed that the materials dredged in the inner basin would be discharged on this beach in May of 1985 and August of 1986. However, in total the shoreline of this mode advances with year.
(2) During 1983 to 1985 the part near to the east breakwater more advance than the other part, but during 1986 to 1987 it is reverse, which shows that the east breakwater could not nearely interrupt materials to pass westward beyond the tip of the east breakwater since 1986.
(3) As a whole, this mode would be assumed to show the yearly change.

Mode 2 of 33% in the rate of contribution shows the following characteristics:

(1) There is a node at the distance of 240m from the east breakwater.
(2) Taking the said node as the boundary, the shoreline of this mode is divided in two groups; the first group which advances in the side of the breakwater and retreats in the other side and the second group which retreats in the side of the breakwater and advances in the other side.
(3) The shorelines of May, July, August, September and October enter in the first group and those of November, December, March and April enter in the second group without relation with year. The period from May to October corresponds to the rainy season when cyclones often attack the coast with highly and easterly waves. The other period corresponds to the dry season when low and westerly waves continue. Therefore, the materials accumalated near to the east breakwater in the rainy season seem to move eastward in the dry season.
(4) As a whole, this mode seems to show the seasonal change of shoreline.

Next, the shorelines after 1989 when the plongation of the breakwater was suspended has been analyzed on the base of the values which have been shown in Fig. 2-3. The result is shown in Fig. 3-2.

Mode 1 has 85.4% in the rate of contribution and the following characteristics:

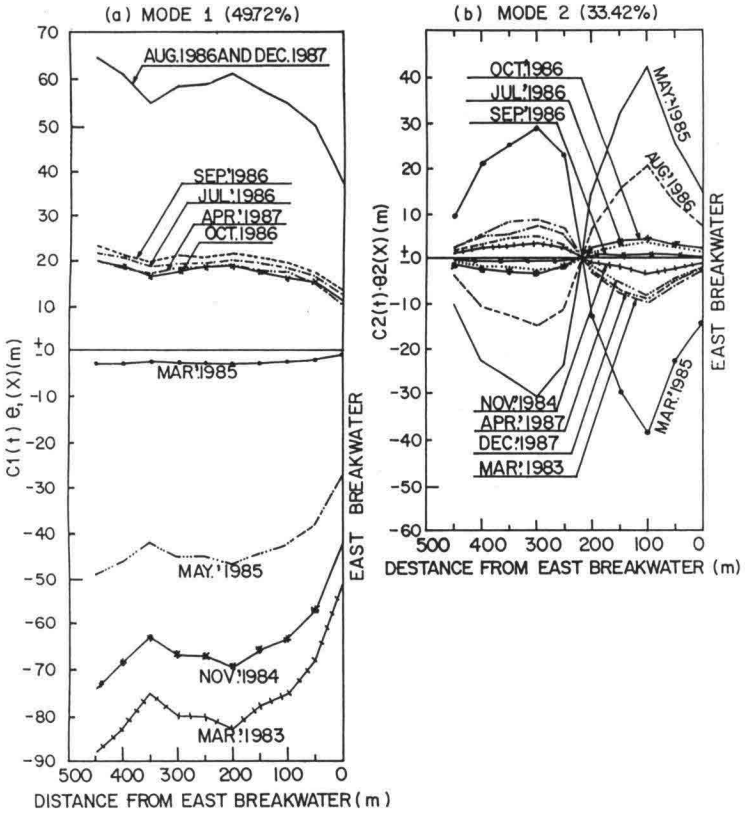

Fig. 3-1 Mode 1 and 2 of the shoreline near to the breakwater in the east coast

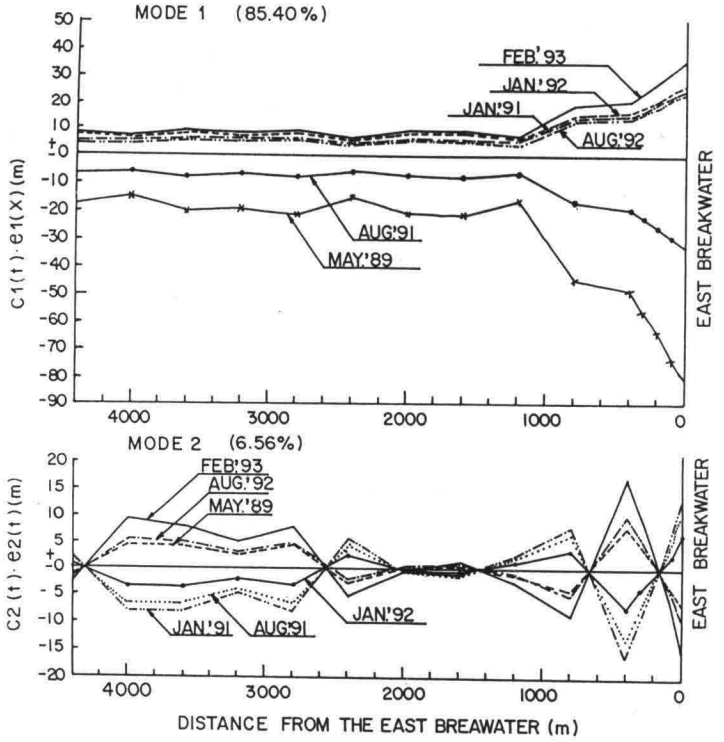

Fig. 3-2 Mode 1 and 2 of the shoreline in the east coast after 1989

(1) The shorelines of this mode advance with time except August of 1992, but, its velocity of advance is very slow.
(2) In the part within 1100m from the east breakwater, the shoreline of the rainy season retreats except August 1992, and it of the dry season advances.
(3) As a whole, this mode seems to show yearly change including some seasonal property.

Mode 2 of 6% in the rate of contribution is difficult to be extracted its property.

3.3 Analysis of the shoreline in the west coast

Data of the shoreline at 100m intervals in the direction of the shoreline have been analyzed within the distance of 2.3 Km from the west breakwaters during from April of 1967 to April of 1991, which have been shown in Fig. 2-4 in the forgoing chapter, where 2.3 Km corresponds about to the situation of the groin No. 12. The results of analysis is shown in Fig. 3-3.

Mode 1 of 49.9% in the contribution rate shows the following characteristics:

(1) There are two nodes in the shoreline of this mode; the first node is situated at 200m from the west breakwater and the second node at 1150m from the same one.
(2) The shorelines of this mode are divided in two groups; the first group retreats within the said two nodes and advances in the both sides of it and the second group advances within the said two nodes and retreates in the both sides.
(3) The first group contains the shorelines of the rainy season such as May, August and October except April of 1991 and the second group contains the shorelines of the dry season such as November, December, January, March and April. As shown in Fig. 1-2, the shoreline between the groins from No. 13 and No. 16 was consolidated by stone sea-wall in 1989 and 1990, so that the shoreline of April of 1991 seems to remain in the first group.
(4) As a whole, this mode seems to show the seasonal characteristics.

Mode 2 of 22.1% in the rate of contribution shows the following characteristics:

(1) The change of the shoreline of this mode becomes smaller with the increase of distance from the west breakwater.
(2) The change of the shoreline becomes much smaller after 1977 than before it. It has relations with the construction of groins of No. 1 to No. 17 during 1975 to 1977 and the construction of stone sea-walls after 1978.
(3) There is not seen seasonal change.
(4) As a whole, this mode seems to express the yearly property including the effect of structures of groins and stone sea-walls.

In the changes of shorelines which show the seasonal change such as Mode 2 of Fig. 3-1 and Mode 1 of Fig. 3-2, the first node is seen in the distance of 200~250m from the breakwater. Assuming that it is caused by edge waves in the coast, their wave length would be about 800~1000m. Mode 1 of Fig. 3-3 has also the second unclear node at 700m and the third clear

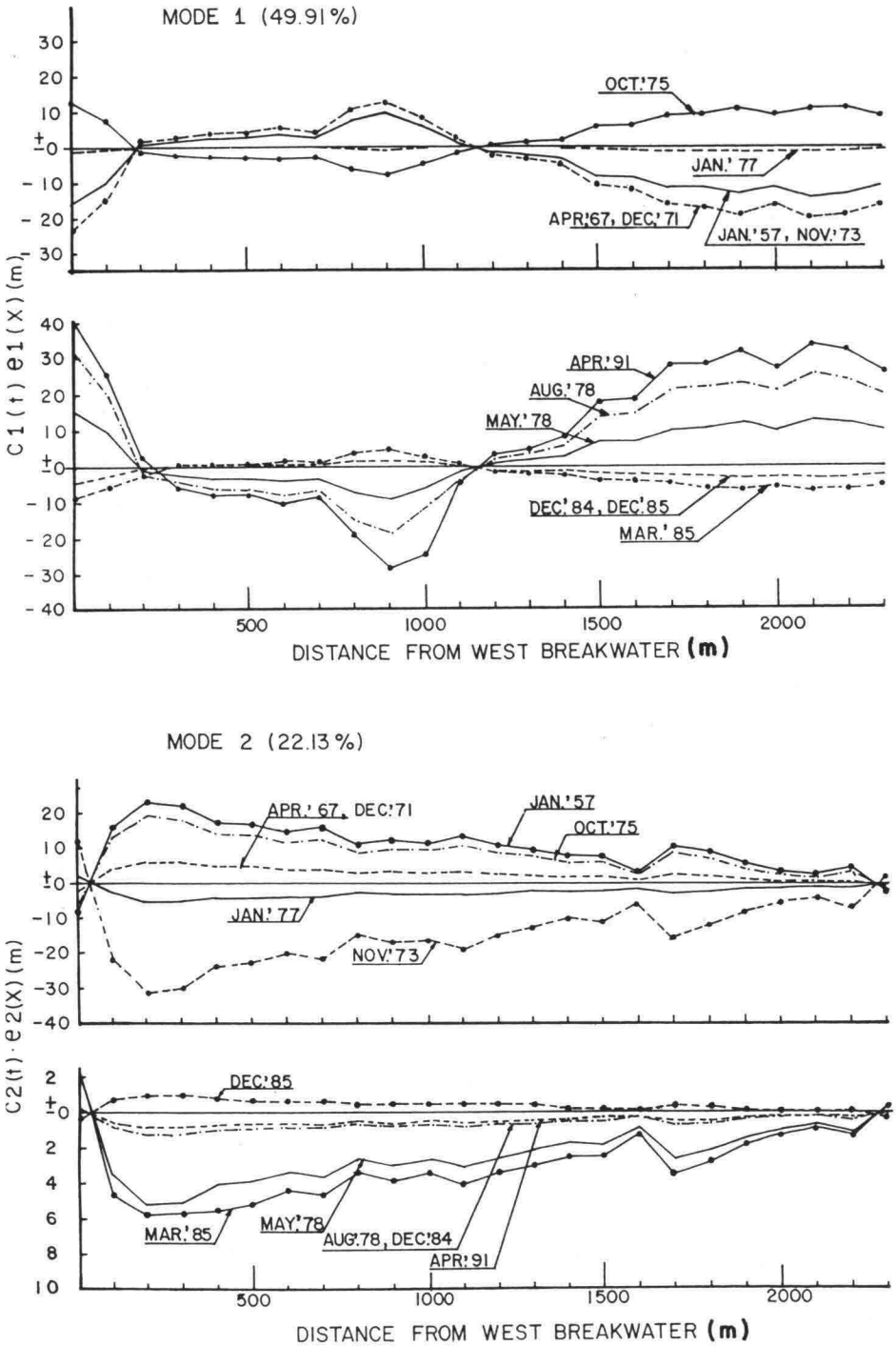

Fig 3-3 Mode 1 and Mode 2 of the shoreline in the west coast

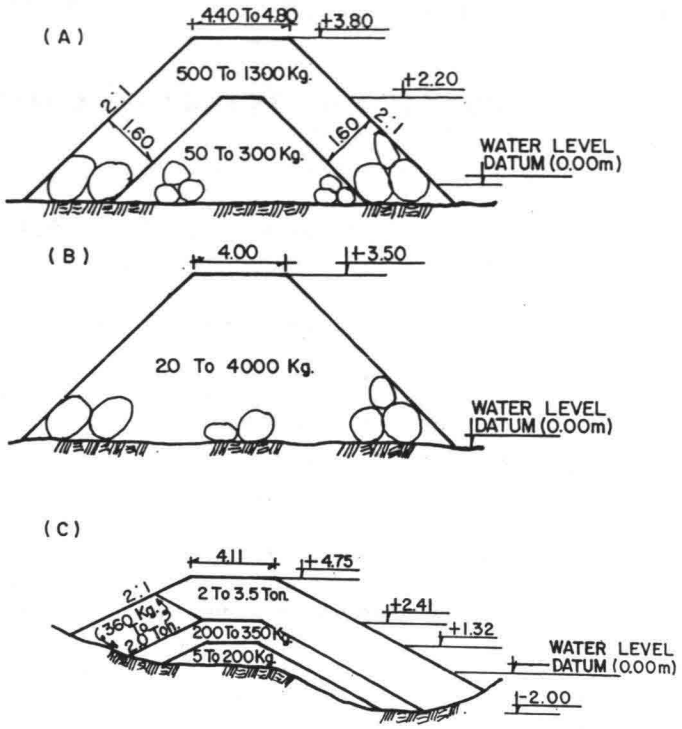

Fig. 4-1 Typicals cross section at the end of 1988 to the begining of 1989 in the west coast

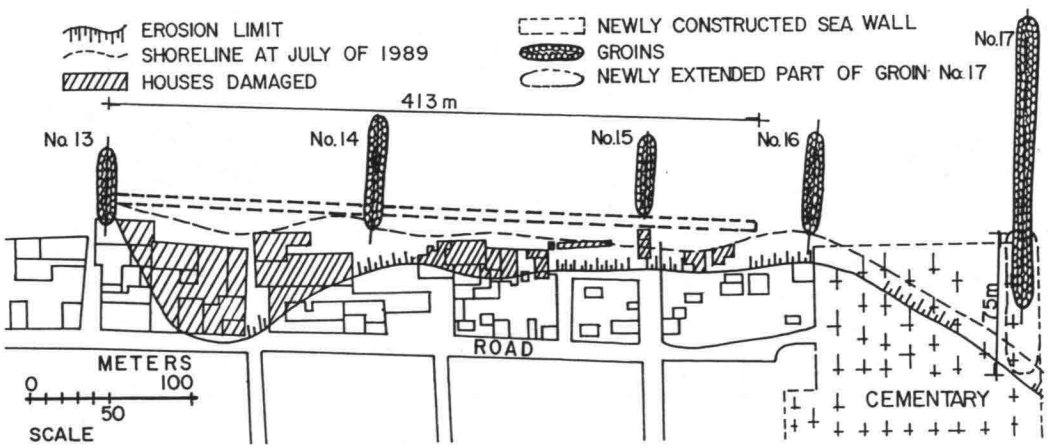

Fig. 4-2 Severe erosion occurred at the end of 1988 to the begining of 1989 in the west coast

node at 1150m. The distance between this two nodes is about 1/2 of the said length of edge waves.

4. PROTECTION AGAINST SHORE EROSION IN THE WEST COAST

4.1 Development of protection against the shore erosion

As have been mentioned before, the coastal protection started on the west coast in 1975 with the construction of seventeen stone groins using the typical cross section shown in (a) Fig. 4-1. Their lengths and the positions have been shown in Fig. 1-2. The construction of groins was completed in 1977, but they weren't successful, so that in 1978 begun the construction of the stone sea-wall .

During 1978 was constructed 960m long of stone sea-wall between groins of No. 1 to 6, using the typical cross section as shown in (b) of Fig. 4-1.

From 1979 to 1980 was constructed 1400m long of stone sea-wall between groins of No. 6 to 13, using the same cross section. In 1980 was carried out the construction of stone sea-wall within 175m from the groin No. 1 using the cross section with the cover layer of 300 to 1000 Kg in the sea side . The protection of 190m long near the west breakwater was completed during 1987 by the typical cross section as shown in (c) of Fig. 4-1.

During the end of 1988 to the begining of 1989 when the east breakwater was prolongated by 75m long, severe erosion occurred within groins of No. 13 to 17. The erosion damaged houses and roads as shows in Fig. 4-2 , and also the embeds of the groins Nos. 15, 16 and 17 were broken and their structures were separated from the land .

Fig. 4-3 Sea-wall in proccess of construction within groin of No.13 to 16

The restoration of the erosion area was carried out by the construction of 413m long of stone sea-wall at the position shown by dotted lines of Fig. 4-2, within groins of No. 13 to 16 from July of 1989 to December of 1990. The Fig. 4-3 shows its restoration works and damaged houses. The restoration included the embed of 75 m long of the groin No. 17. The typical cross section of the stone sea-wall is almost the same as (b) of Fig. 4-1, but 50 to 5000 Kg of stones were used in place of 20 to 4000 Kg of stones.

4.2 Behavior of the shore erosion structures at present

According to the measurement carried out in December of 1992, one year after the above-mentioned restoration works of the area between groins of No. 13 to 16 , the behavior of this structure can be sumarized as follows:

(1) The crest of the sea-wall sinked by almost 0.20m between groins No. 13 to 14, 0.50m between groins No.14 to 15, and almost 0.80m between groins No.15 to 16.
(2) In the east side of groin No. 17 accretion occurred and the shoreline advanced seaward by almost 30m, whereas in the west side of it the shoreline retreated more landward.

According to visual inspection of the shore carried out in September of 1993, the present condition of structures can be sumarized as follows:

(1) The seaward end of the groins of No. 1 to 16 is deteriorated and sinks , whereas the structure of groin No. 17 is good, but the erosion in the west side of this is increasing.
(2) The stone sea-wall is deteriorated and sinks below M.W.L. in the area within groins No. 5 to 8 , and the elevation of the sea-wall sinks by 1 to 1.5m within groins No. 1 to 5 and within groins No. 9 to 10, compared with the designed level.

5. PROTECTION AGAINST SHOALING OF THE ACCESS CHANNEL

5.1 Simulation of the past change of the shoreline in the east coast

In order to determine the factors necessary to predict the change of shoreline near to the east breakwater which will be caused by further prolongation of it, the past change of shoreline has been simulated by the so-called one line theory using data shown in Fig. 2-2. The simulation has been carried out by means of the method of Komar P.D. (1976).

The characteristics of sand transport in the east coast would be sumarized from the matters described in chapter 2 and 3 as follows:

(1) In the rainy season, the alongshore sand transport is generated westward by easterly high waves caused by cyclones, resulting the advance of shoreline in the part near to the east breakwater.
(2) In the dry season, some part of sand accumulated near to the breakwater tends to move eastward by relatively smaller and westerly waves.
(3) The east breakwater could not enoughly interrupt sand to pass itself since 1986, that is, the great part of sand reaching the breakwater passed beyond the tip of it or through the voids of stones of the breakwater.

(4) The sand transport is much more strong in the rainy season than the dry season.

Considering the above characteristics of sand transport, the condition of the simulation was determined as follows:

(1) The direction α_b of breaking waves

In the rainy season from May to October, the direction of waves in the breaking line was taken to be 15 degree against the datum line of **MC** which is a little larger than the inclination of the shoreline in March of 1983 which is about 10 degree against the same datum line. In the dry season from November to April, it was taken to be zero degree so that the some part of the sand accumulated near to the breakwater moved eastwards.

(2) The height **D** of beach profile which moves in parallel and seaward as the result of alongshore sand transport.

From Fig. 2-5, it is seen that the beach profile moves nearely in parallel until -9m. Therefore, adding +3m of the height of backshore, the height **D** was taken to be 12m.

(3) The alongshore wave energy **P** per day and the alongshore transport rate **Q**.

The alongshore sand transport rate is expressed as follows.

$$Q = K.P. \frac{1}{2} \sin (2\alpha_b) \tag{5-1}$$

where P : Alongshore wave energy at breaking line
α_b : Breaking angle
K : Coefficient

The value of **P** per day was taken to be 3×10^4 and 0.5×10^4 ton. m/m in rainy season and in dry season respectively, through trial and error of calculation. Moreover, the coefficient **K** was taken to be 0.4.

(4) Boundary Condition

Dividing the distance of 2 km from the east breakwater in cells of 50m wide as shown in Fig. 5-1, the change of shoreline after the time ΔT was calculated by following equation:

$$Y(I) = Y(I) + (Q(I-1) - Q(I)) \Delta T/(\Delta X * D) \tag{5-2}$$

where Y(I) : Position of the shoreline of X=I

Q(I) : Alongshore transport at the Y(I)
ΔX : Width of each cell, 50m

In the right side of Fig. 5-1, the condition of **Q(NY)**, which is the value of **Q** passing the east

breakwater, was given as follows after trial and error of calculation:

For the rainy season

Q(NY) = Q(NY-1) / 1.5 ; in 1983 and 1984
Q(NY) = Q(NY-1) / 1.2 ; in 1985 and 1986
Q(NY) = Q(NY-1) / 1.05 ; in 1987

For the dry season

Q(NY) = 0 ; for all years

In the left side, Q(0) was taken to be same as Q(1), so that Y(1) did not change through the period of simulation.

(5) Initial position of shoreline

The position of the shoreline in March of 1983 of Fig. 2-2 was taken as the inicial position of shoreline, where from 400m to 2000m it was taken to be 50m which is the same value as it at 400m.

The result calculated with the time step ΔT of one day under the above-mentioned conditions is shows in (b) of Fig 5-2. Comparing with the field data shown in (a) of the same figure, the result of simulation roughly coincides with the field data in the part near to the east breakwater, though the part apart from it does not coincide so well. This descrepancy parcialy would depend to the discharge of the dredged material as mentioned before.

5.2 Estimate of shoreline change caused by the further prolongation of the east breakwater

In order to predict the advance of shoreline caused by the further prolongation of the east breakwater, the simulation has been carried out under the same condition as the forgoing one in Section 5.1, except the follows:

The length of simulated shoreline : 6 km

The condition of Q(NY) : Q(NY) = 0 for all season and all years

The inicial shoreline : The shoreline of December of 1987 which resulted in the foregoing simulation and the part between from 2 km to 6 km was taken to be 50m.

The result of the simulation is shown in Fig. 5-3. In such simulation, the advance of the shoreline tends to become short when the simulated shoreline is short, but the calculation with the shoreline of 4 km resulted to be shorter only by 2m than the case of 6 km at the advance of shoreline along the east breakwater after 15 years.

According to Fig 5-3, the shoreline at the east breakwater advances by 146, 233 and 305m from the position of December of 1987 after 5, 10 and 15 years, respectively.

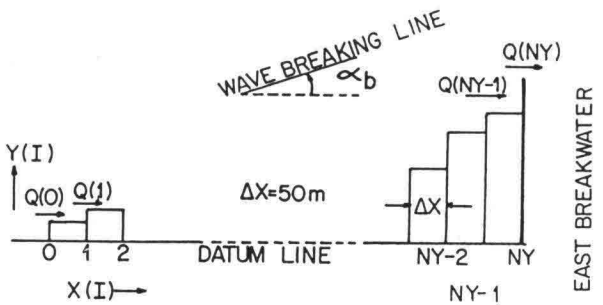

Fig. 5-1 Division of the coast for the simulation of shoreline change

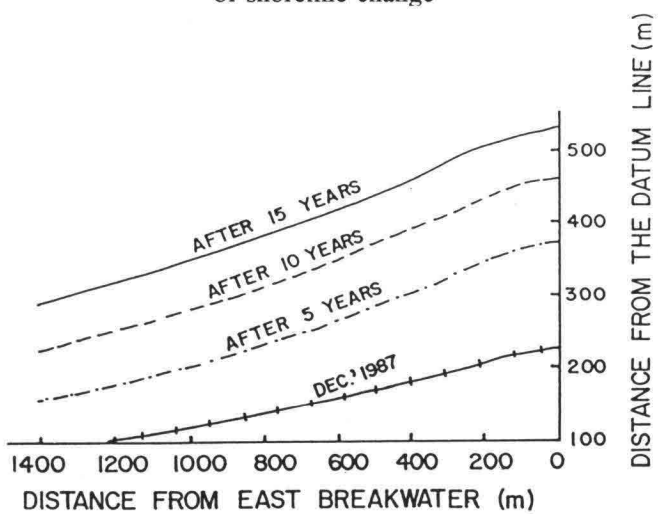

Fig. 5-3 Simulation of the future change of shoreline in the east coast

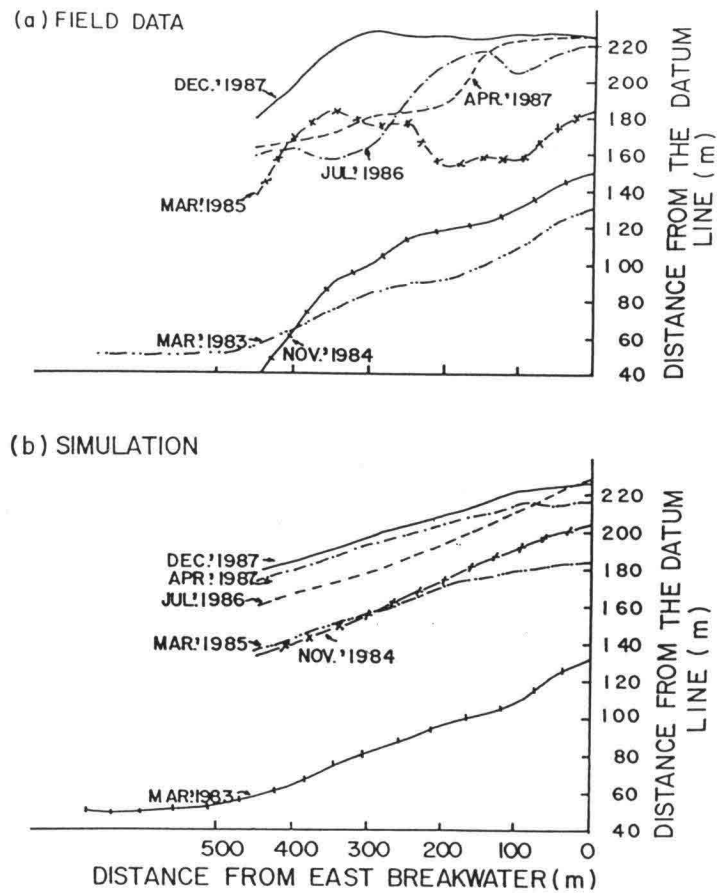

Fig. 5-2 Simulation of the past change of shoreline in the east coast

5.3 Consideration on protection measures against shoaling of the access channel

Using the value of the alongshore wave energy per day **P** obtained in the foregoing section, the alongshore transport per month Q_m in the rainy season is calculated using Eq. (5-1) as follows:

$$Q_m = K.P.\frac{1}{2}.\sin(2\alpha_b) \times 30$$
$$= 0.4 \times (3 \times 10^4) \times \frac{1}{2} \times \sin(2 \times 15°) \times 30$$
$$= 9 \times 10^4 \text{ m}^3 / \text{month}$$

For six months from May to October in the rainy season

$$Q = 9 \times 10^4 \times 6$$
$$= 54 \times 10^4 \text{ m}^3$$

In the above-mentioned simulation, the alongshore transport is supposed to be zero in the dry season, so that the value of 54 X 10^4 m^3 corresponds to the annual transport. That is the net alongshore sand transport is estimated to be about 500,000 m^3 per year from the simulation.

Table 5-1 shows the volume of sand dredged in Port Madero from 1983 to 1991, where 1,671,073 m^3 is the total volume dredged in the access channel during seven years from 1985 to 1991. The access channel is now maintained to be deeper than 9m in the width of 80m. In this case, the average dredging per year become about 240,000 m^3, which corresponds approximately to the half of the net alongshore transport estimated in the above.

Table 5-1 Dredging volume (m^3)

Locations / Years	Access Channel	Expantion of Channel	Inner Basin	Other
1983		232,880	117,690	
1984		558,440	140,098	
1985	80,222	23,180	130,372	
1986		11,830	88,262	
1987	569,939		238,223	
1988	280,170		264,363	79,410
1989		539,900	228,220	119,608
1990	602,787		159,280	101,328
1991 (Until Sep.)	137,955		31,443	
Total	1,671,073	1,365,230	1,397,951	300,346

On the other hand, in the foregoing section, the shoreline has been estimated to advance by about 300m at fifteen years after the present under the assumption that the east breakwater interrupts completely the alongshore sand transport. If the breakwater is prolongated until the depth-line of 10m deep which is at present located at about 400 meters from the tip of breakwater, although such prolongation can not completely interrupt the alongshore transport, the necesary length of such prolongation becomes 300 + 400 = 700m. At the same time, it would be necessary to prolongate the west breakwater by some length.

The cost of such prolongation of breakwaters would surpass the cost for fifteen years of the maintenance dredging which is 240,000 m^3 per year as mentioned above. Therefore, the authority of Madero Port would continue dredging the access channel, although the breakwaters would be prolongated little by little so as to maintain the depth of the tips of the breakwaters deeper than the present. The dredged sand would continue to be discharged in the west coast so as to prevent further shore-erosion.

6. CONCLUSIONS

In the beach of Port Madero,severe accretion and erosion have occurred respectively in the east and west sides of the breakwaters.The alongshore transport rate has been estimated to be about five hundred thousand cubic meters per year from the simulation of past shoreline changes.The present protection measure against the access channel shoaling by means of dredging and the present protection measure against shore erosion by means of groins and sea-walls of rubble mound type seem to be effective and reasonable.

ACKNOWLEDGEMENTS

The field shoreline data analyzed were contributed by the Madero Port Construction Office, Puertos Mexicanos, Ministry of Communications and Transport, MEXICO.

REFERENCES

Dirección General de Obras Marítimas (1971): Field studies to the Project of one Maritime Terminal in Madero Port Chiapas, Rep. of Ministry of Navy of Mexico, (in spanish)

Komar, P.D (1976): Beach Processes and Sedimentation, Prentice-Hall, Englewood Cliffs, N.J.

Winant, D.C., Inman, L.D. and Nordstrom, E. Ch. (1975): Description of Seasonal Beach Changes Using Empirical Eigenfunctions, Journal of Geophysical Research, Vol. 80, No.15.

HYDRO-PORT'94
International Conference on Hydro-Technical
Engineering for Port and Harbor Construction
October 19 - 21, 1994, Yokosuka, Japan

Control of Littoral Drift in Caldera Port, Costa Rica

J. Gilberto Rodoriguez P. [1]
Kazumasa Katoh [2]

[1] Port and River Works Division
Ministry of Public Works and Transport
Direction de Obras Portuarias, Barrio La California
50 metros Norte del Cine California, San José
[2] Chief of the Littoral Drift Laboratory
Hydraulic Engineering Division
Port and Harbour Research Institute, Ministry of Transport
Nagase 3- 1- 1, Yokosuka, Kanagawa 239

ABSTRACT

Caldera Port was constructed in 1981 on the coast of Costa Rica, Central America, facing to the Pacific Ocean. Ever since the beginning of operations, however, there had been a serious problem of sand transportation around the tip of breakwater, into the inner basin due to the northward longshore sand transport under the action of steady and obliquely incident waves. To prevent this situation, the existing breakwater is extended 272 meters based on results of numerical simulation done using the one-line theory. Furthermore, two additional countermeasures are also considered. One is the construction of a jetty located on the upper-side beach to reduce the rate of longshore sand transport. Another is to remove sand from the beach outside of the breakwater. This paper narrates the historical vents that occurred while implementing these these countermeasures.

Key Words: Wing-Breakwater, Longshore Sand Transport, Shoaling of Basin, Jetty
Costa Rica

1. INTRODUCTION

Costa Rica extends roughly from the latitude of 11 ° N to 8 ° N. It is a narrow country, located roughly between the longitude of 83 ° W and 86 ° W, comprising part of the Central American isthmus. Costa Rica is bordered on the north by Nicaragua, on the south by Panama, on the west by the Pacific Ocean and on the east by the Atlantic Ocean. Its minimum width from the Pacific Ocean to the Atlantic Ocean is 119 km. In 1981,

Caldera Port was constructed on the Pacific coast to be a major gateway for the international trade of Costa Rica, as well as the port nearest to the national capital, San Jose. The port began to lead the national economy and industry and support the livelihood of the Costa Rican people through commodity supply. Just after opening the port, however, one of the three berths of the port, which is the deepest and most important, became gradually shallower due to the sand sedimentation in the harbor. Since then, various technical efforts have been done for maintaining the port, through the field survey, repeated dredging of basin, extension of the breakwater, construction of a jetty and so on.

Here, the history of desperate endeavors and its result are reported.

2. NATURAL CONDITIONS AROUND CALDERA PORT

As shown in Figure 1, Caldera Port is located at the latitude of 10.4 ° N and the longitude of 84.7 ° W, and it is situated at the eastern shore of the Gulf of Nicoya, the mouth of which is open to the Pacific Ocean in the south to southwest direction. The natural conditions around the port are as follows, of which some parts are the summary of the report by JICA (Japan International Cooperation Agency) of 1986.

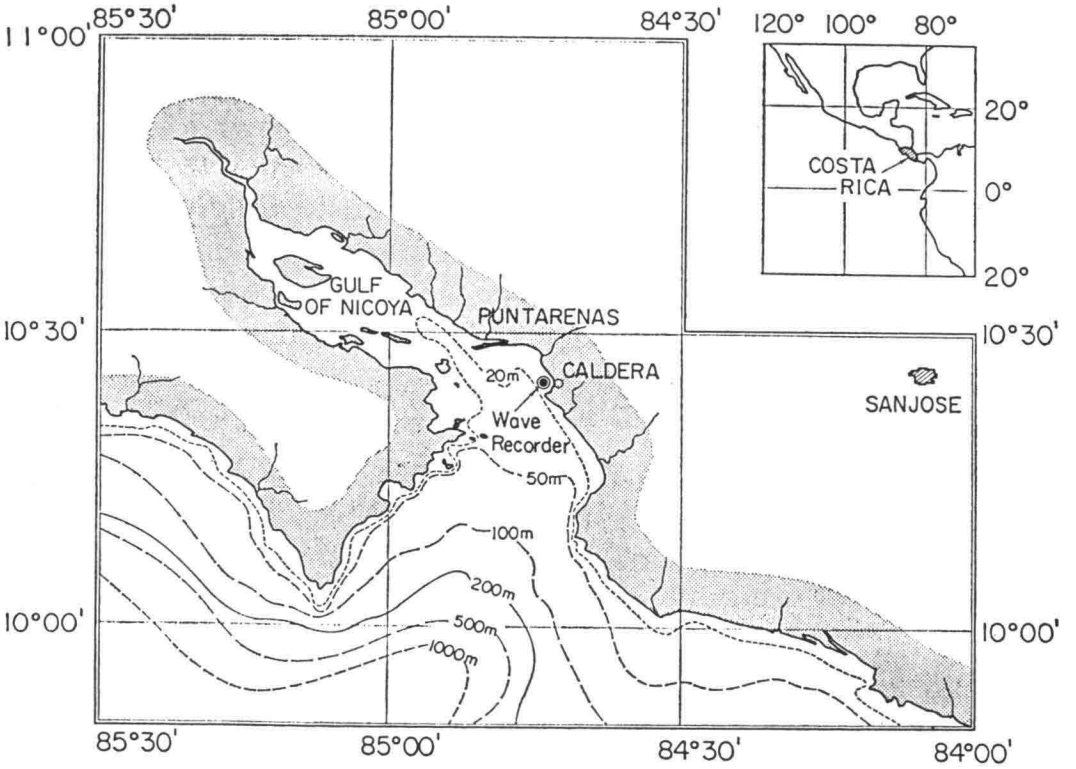

Figure 1 Location map of Caldera Port, Costa Rica (Goda, 1983) .

2.1 Wave Conditions

Waves were intermittently measured at a spot approximately 1.8 km offshore from Caldera Port, at a water depth of 15.5 meters below the datum line, during 7.3 years from June 1978 to November 1985. A total duration of wave observation was 3.3 years. According to the wave data obtained, the probability of significant wave heights between 0.5m to 1.5m is 88.3%, and that of significant wave periods longer than 10.5s is 61.6%. Using the data of the 29 waves of significant wave height greater than 1.8 meters, probable wave heights were estimated by adopting a Weibull distribution with an exponent of 1.25. The results are listed in Table 1. The significant wave period of each probable wave is estimated from the relationship between the significant wave height and the period of extremely large waves as shown in Figure 2.

Table 1 Probable wave heights.

Recurrence Period (years)	Significant Wave Height $H_{1/3}$ (m)	Significant Wave Period $T_{1/3}$ (s)
5	3.692	17.97
10	3.980	18.26
20	4.259	18.50
30	4.419	18.62
50	4.617	18.78

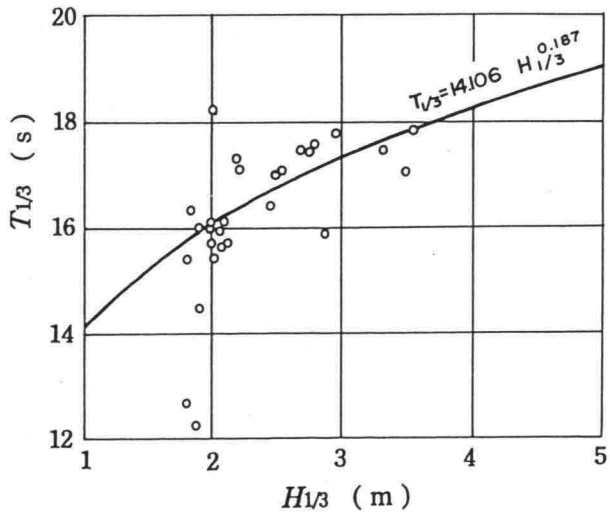

Figure 2 Relationship between significant wave height and period of large waves.

As prevailing wave periods are relatively long, the waves are swells which are coming from the Pacific Ocean through the mouth of the Gulf of Nicoya. Predominant direction of incident waves is considered to be from the SEE to the SW. In the case of extremely

large waves, the significant wave period of 18s or so belongs to a quite long periodicity. By analyzing the wave data obtained in Caldera Port in May 1981 and inspecting the weather charts of the Pacific Ocean, Goda(1983) found that strong winds were blowing over the Southwest Pacific Basin which was 7000 to 9000 km far from Costa Rica, about 5 to 7 days before the coming of extremely large waves to Caldera Port. After some considerations, he concluded that the swells with such a long period were generated by strong winds in a large fetch area near the New Zealand and travelled over a long distance.

2.2 Tidal Conditions

A harmonic analysis was performed using the data obtained by means of a simple water pressure type tide gauge at Caldera Port on 15 days in October 1985. According to the result, a half day $M2$ periodic component is prevailing, while a single day component is of lesser importance. The representative tide levels were calculated with constants of the foue principal tidal harmonics. The large tidal range is 2.59 meters, the mean range is 2.05 meters, and the small range is 1.51 meters, respectively.

The results of field measurements on tidal currents in the offshore area of Caldera Port show that the northward currents during the flood and the southward currents during the ebb are prevailing, respectively. The maximum current velocities are approximately 20 cm/s in the both directions.

2.3 Conditions of Littoral Drift

Due to one way approach of waves, that is northward from the Pacific Ocean as explained above, the sands supplied from rivers and soft sea cliffs are being transported northward along the eastern shore of the Gulf of Nicoya. However, the coast line is not straight but consists of some headlands, river mouths and beaches, which make the condition of littoral drift in this area more complicated.

In order to make a general appraisal in the vicinity of Caldera Port that would help understand the local littoral drift phenomena (specially predominant directions of sand transport) the area was visited and analyzed. This analyses resulted in the conviction that the area should be divided into segments namely the Puntarenas Zone, the Caldera Zone and the Southern Zone as shown in Figure 3. The reasons of these subdivisions are as follows:

1) Boundary between Puntarenas zone and Caldera zone
(a) The foreshore slopes in the Puntarenas zone are about 3 to 5 degrees, while those on Caldera beach between Carballo Cliff and Caldera Port are about 10 degrees or more.
(b) A color of sand on the beach in the Puntarenas zone is light brown. On the other hand, on the backshore higher than the high tide level in the Caldera zone, a large amount of black sand which is heavy and magnetic is accumulated everywhere.
(c) The formation of long sand spit in the Puntarenas zone definitely indicates the

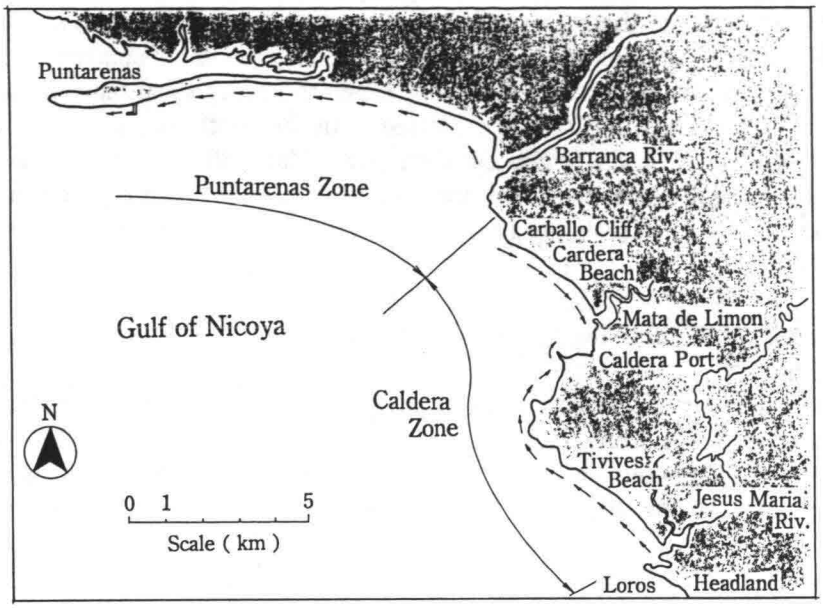

Figure 3 Littoral segments.

westward sand transport which is shown by arrows in Figure 3. On Caldera beach of about 3 km long, the mean diameter of sand is 1.0 mm near Carballo Cliff, which gradually decreases in the southeast direction to be 0.1 mm near the mouth of estuary, Mata de Limon. This change of mean diameter suggests the southeast-ward sand transport as shown by arrows in Figure 3. Then, it can be concluded that Carballo Cliff is the boundary between these two zones.

2) On long sand spit

Since the bed slope of Barranca river, whose mouth is located at the east-end of the Puntarenas zone, is very steep, being 1/160 in the stretch of 6 km from the mouth, it is supposed that the water discharge is fair amount and the flood is fast in the rainy season. Although it is very hard to quantitatively estimate the actual volume of sand discharged from this river due to a lack of information at present, we can infer that a large quantities of sediment must be discharged. Then, the sand spit of 7.5 km long is considered to have been formed with the sand discharged from Barranca river.

3) On the Carballo Cliff

The height of Carballo Cliff is about 60 meters. It consists of sands and rocks with weak interlocking. Thus, the base of the cliff can be easily eroded by the action of waves. As a matter of fact, a railway was constructed around the base of cliff in 1910. Seven years after, however, the route had to be shifted to the hinterland due to the rapid erosion. At present, the trace of railway has completely disappeared. This cliff is the source of sand to Caldera Beach.

4) Boundary between Caldera zone and southern zone

The boundary between these two zones, or the south-end of the Caldera zone, is not so clear. However, we think that Loros Headland may be the boundary between them, because it angles out into the sea and there exists the rocky shoal that extends about 300 meters offshore. Then, the sand transported from the south may go out from this point into the deep sea. Sands originated from Jesus Maria River, which is located in the south-end of the Caldera zone, are transported in the north direction through Tivives Beach and pass by small scale headlands until they reach Caldera Port.

3. Initial Stage of the Shoaling Problem in Caldera Port

The construction of Caldera Port was started in November 1974, with a landfill confined by two external jetties and one sheet pile quaywall of 490 meters long. The rubble mound breakwater of 250 meters in length had been completed in 1981 (see Figure 4). As there exists the northward littoral transport due to the constancy of the wave incidence

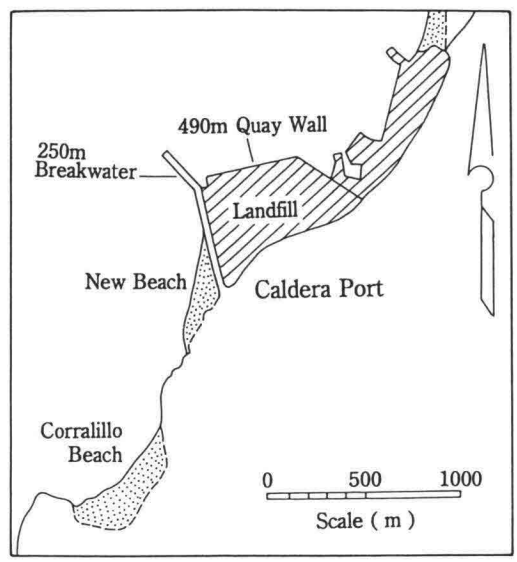

Figure 4 Caldera Port in 1981.

angle, ever since its initial construction in 1974 there has been a process of sedimentation going on at the west sea side of Caldera Port, where New Beach has been formed as seen in Photo 1. New Beach has kept growing and in 1981 the excess sand began to be transported around the tip of breakwater into the port (see Figure 5).

In order to increase the sand holding capacity of New Beach and so diminish the sand transport into the inner harbor, the Ministry of Public Works and Transports (MOPT) initiated construction of a wing-breakwater oriented 45 degrees off the main breakwater (see Figure 6). This expansion of the main breakwater was so designed as to use

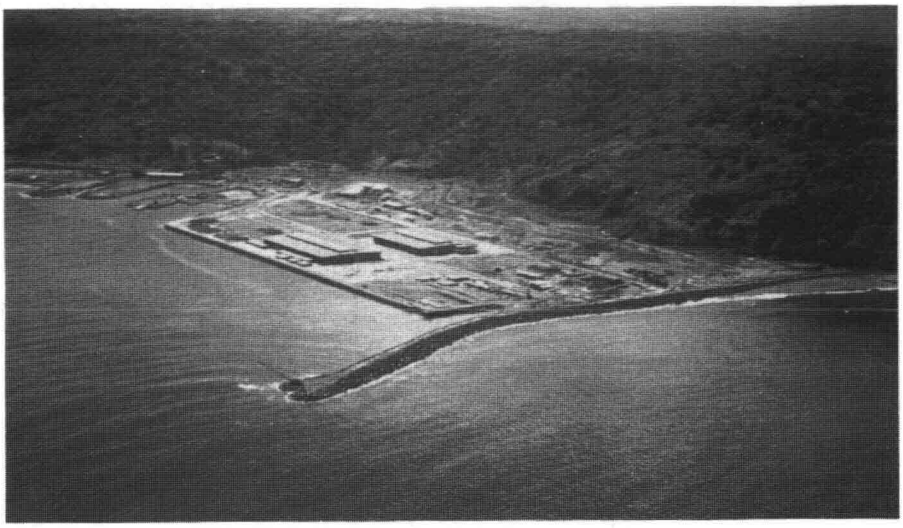

Photo 1 Caldera Port in 1981.

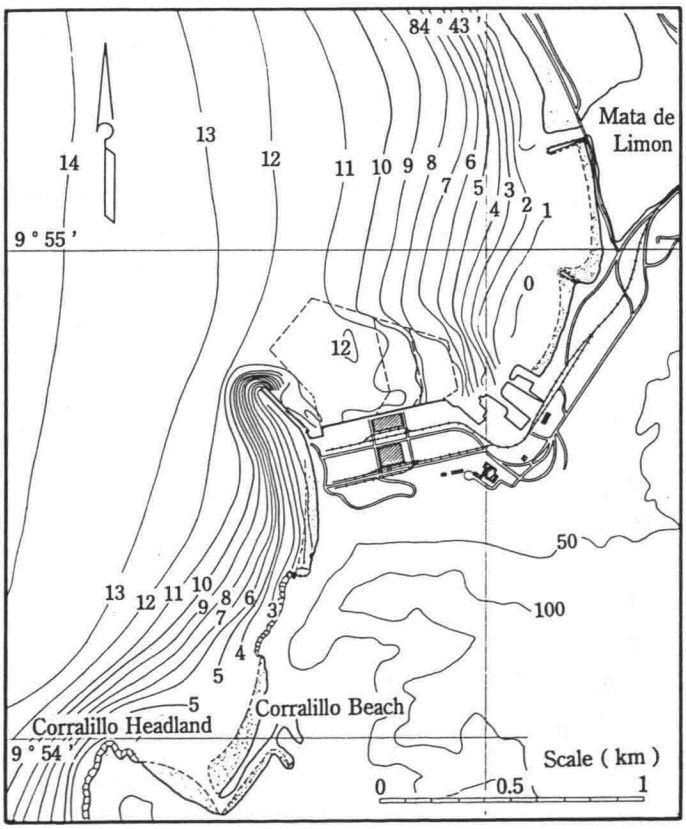

Figure 5 Topography in September 1981.

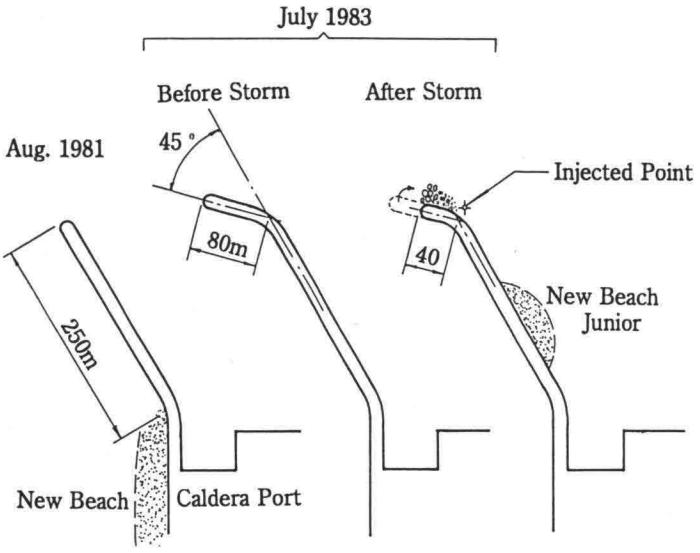

Figure 6 Wing-breakwater before and after large waves.

breaking wave energy to generate a counter flow that should delay growth at the north side of New Beach.

Beginning on July 1983 the breakwater extension reached the 80 meters long. On the 17th and the 18th of July 1983, large waves of 3.5 meters in the significant wave height and 17.5 to 18.5 seconds in a period attacked the port and destroyed the last 40 meters of the wing-breakwater. At the same time, these waves transported a large quantities of sand into the main harbor basin, which built up another small beach, New Beach Junior,

Photo 2 New Beach Junior on the 21st July 1983.

behind the breakwater as shown in Figure 6 and in Photo 2. In order to make fluorescent sand tracer, we took the sand from New Beach Junior, of which diameter is about 0.2 mm. During an attenuation of this storm, on the 26th July, when the breaking waves still diffracted and propagated along the inner side of the breakwater, we injected fluorescent sand tracers of 200 kg at the point near the base of wing-breakwater, which is indicated by an asterisk in Figure 6. On the next day, the sands were sampled from the surface of New Beach Junior. Figure 7 shows a distribution of fluorescent sand tracer, which well agreed with the topography of New Beach Junior. Then, it is inferred that the sand transported from New Beach around the tip of breakwater into the port was carried in suspension farther along the inner side of breakwater to New Beach Junior where the turbulence of diffracted waves well diminished. From here on a subsequent slow process of sand dispersion toward the first berth surely occurred. That is because the scale of New Beach Junior gradually decreased by the action of diffracted waves and disappeared by the beginning of August.

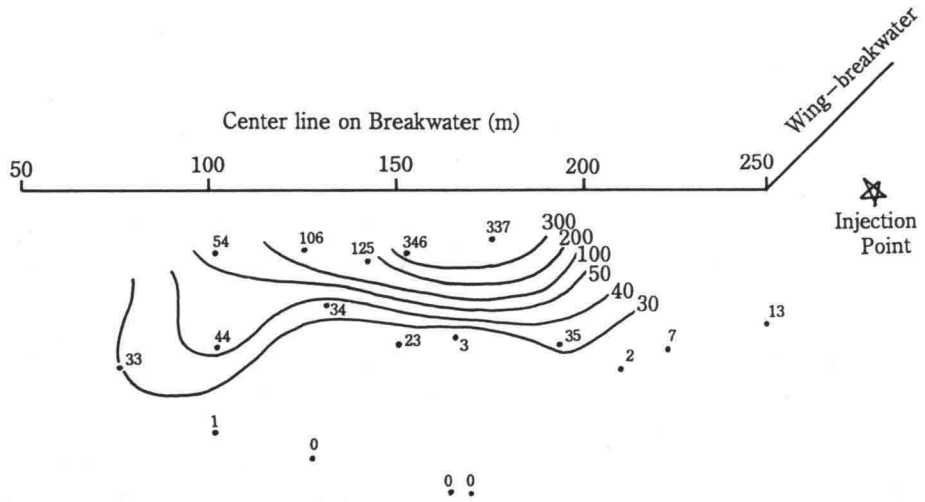

Figure 7 Distribution of fluorescent sand tracer (one day after injection).

It was urgently necessary to extend the wing-breakwater as far as possible to prevent the further shoaling in the basin. Then, MOPT continued construction of the wing-breakwater at a constant but slow pace due to the limited budgets. A slow speed of construction brought a favorable condition: the small deposits on the extension of the center line of the wing-breakwater (2 to 5 meters below mean sea level) reduced significantly the cross sectional areas to be built, when compared to the original breakwater construction depths (which were in the range of 10 to 12 meters). In spite of decreased rock volumes to be placed, construction difficulties increased due to the closeness to the wave breaking zone. Common storm waves easily scoured the breakwater foundations, which made the breakwater unstable.

In order to roughly understand the volume of sand entered into the basin, the volumes of

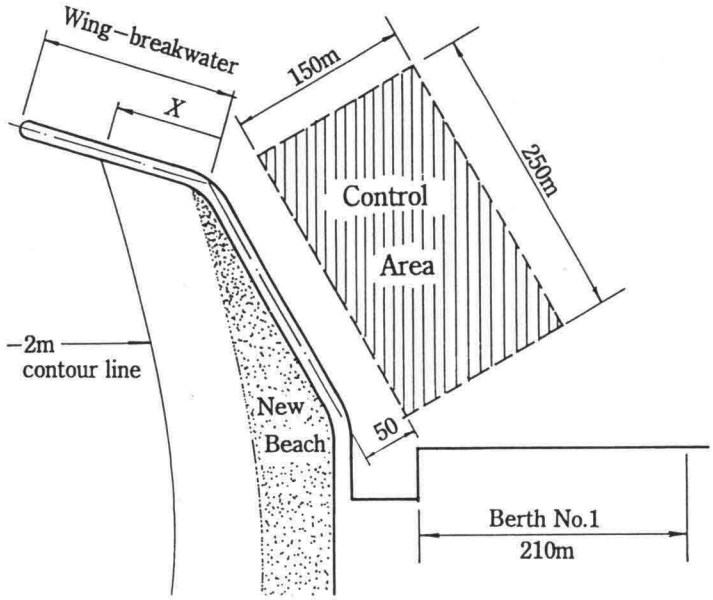

Figure 8 Definition of control area and location of intersection.

sand accumulated in the control area which is located immediately behind the breakwater (250 m x 150 m as shown in Figure 8) were calculated by utilizing the sounding data. In order to roughly indicate the development of New Beach, the location of intersection between the wing-breakwater and the -2 meters contour line is defined as a distance from the corner of breakwater, which is denoted by a symbol X in Figure 8. The results of calculation for the period from 1982 to 1986 are shown in Figure 9, in which the distance of X and the length of wing-breakwater are also shown. During the first three years from February 1982 to February 1985, the sand accumulated with a almost constant rate of 26,000 m^3/yr, or 0.7 m/m^2/yr in the control area. The extension of wing-breakwater was not very effective in preventing the sand from entering into the basin. This is due to the slow construction of the wing-breakwater, which was nearly same as the speed of advancement of -2 meters contour, as shown with a dotted line in Figure 9. In other words, the speed of New Beach developing was nearly same as that of extension of wing-breakwater.

On 13th September 1985, large waves of 2.77 meters in a significant wave height and 17.6 seconds in a period attacked this port, by which the last part of the wing-breakwater was destroyed and at the same time the sands were transported into the basin. This situation induced a loss of adequate depth for docking at the berth No.1. Then, in order to keep designed operational depths at the inner basin of the harbor, an urgent dredging was done until January 1986. A dredging volume was 30,000 m^3 in total. The second full dredging was executed during the months from March to April in 1987 for a total dredged volume of 303,000 m^3, of which 80,350 m^3 were taken from the control area.

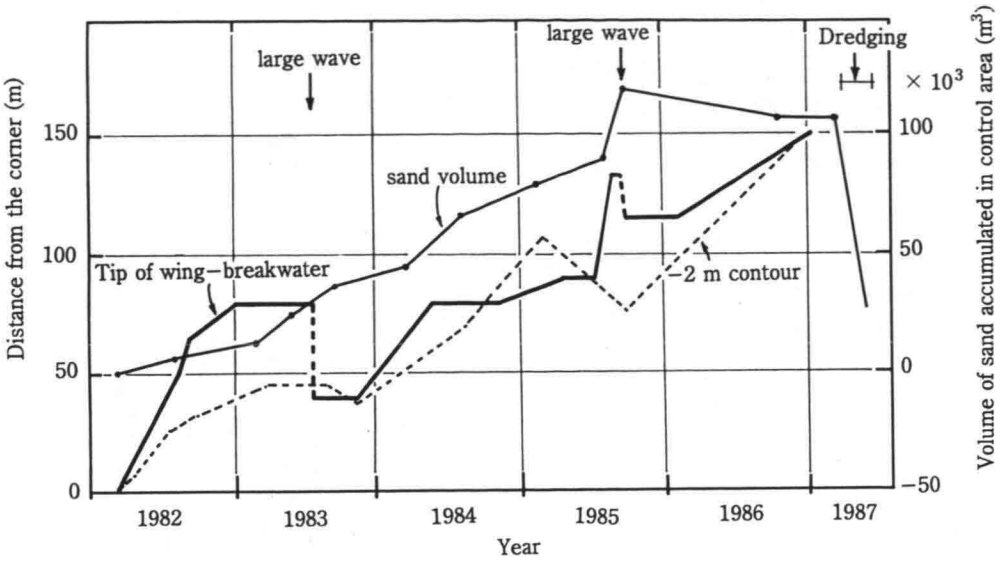

Figure 9 Volume of sand accumulated in the control area, length of wing-breakwater and location of −2 meters contour line.

4. RESULT OF FUNDAMENTAL SURVEY IN 1985

In response to the request of the Government of the Republic of Costa Rica, the Government of Japan decided to conduct a study on the maintenance project of Caldera Port and entrusted the study to JICA. A most important objective of the study was the establishment of adequate strategies to respond to the sedimentation problem. JICA send to Costa Rica a study team during a period from September to November, 1985. The study team conducted a field survey, an analysis of existing data, and numerical simulations on the littoral drift, of which result was reported in JICA Report (1986). Here, we quote important items from JICA Report, which are strongly related to the littoral drift in Caldera Port.

The budget of sand transport in the south side area of Caldera Port is estimated based on the results of soundings which have been executed repeatedly by MOPT since 1981. Figure 10 shows roughly estimated budget of sand transport in areas less than −10 meters deep. The annual northward drift sand volume offshore Corralillo Headland is estimated as 200,000 m^3/yr. Within this volume, the sand volume transported in the zone between the −5 meters and −10 meters contour lines is estimated as 88,000 m^3/yr. A sand volume of 14,000 m^3/yr accumulates at Corralillo Beach, and 98,000 m^3/yr is supplied to New Beach. Part of the sand supplied to New Beach, which is estimated as about 26,000 m^3/yr, accumulated there. The rest passes by the wing tip, goes toward the north side of the foot of the breakwater and accumulates near its foot.

According to Figure 9, it seems on the whole that the sand deposited in the control area at

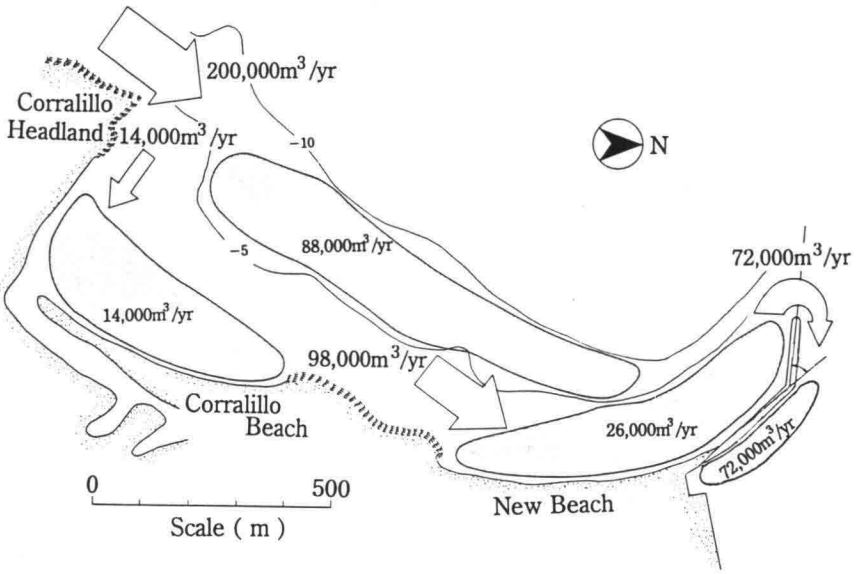

Figure 10 Budget of sand transport at the southern beach of Caldera Port.

a constant rate, being independent of the extension of wing-breakwater. However, it is noticed that rate of sand deposition changed a little from period to period. The volume of sand going into the basin in a short period depends on the relative relation between the sand volume stored in the out side area of port and the location of wing tip. Figure 11 shows the extension progress and the location of -2 meters contour line which is utilized as an indicator for the sand volume stored in the outside area, for the years from 1980 to 1985. From this figure, the distance, D, from the wing tip to the intersection of the

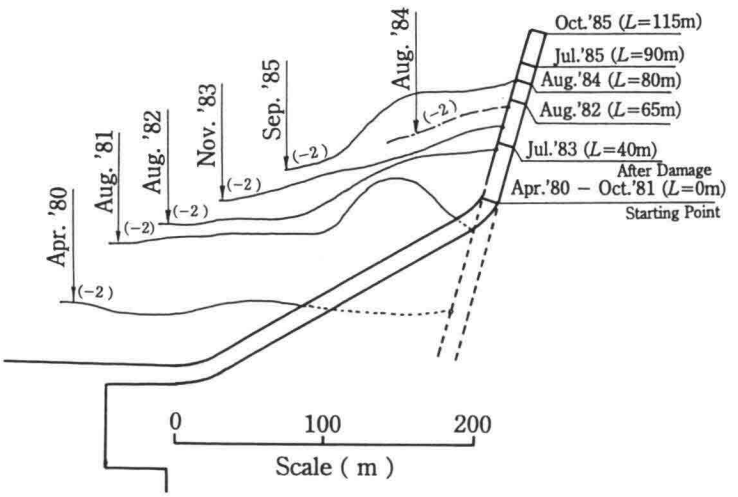

Figure 11 Shoreline changes and wing length.

wing-breakwater and −2 meters contour lines is read for each, of which result is listed in Table 2. The volume of sand accumulated in the basin, which is wider than the area of control area in Figure 7, is calculated for each term and also listed in Table 2, where Q_s is the equivalent volume of sand accumulated in a year.

Table 2 Relation between D and Q_s.

Period	Length of Wing-breakwater (m)	D (m)	Sand Sediment Volume (m^3)	Q_s (m^3/ year)
1980. 4−1981.10	0	45 *2 (Average)	12,000	8,000
1981.10−1982. 7	65	25	21,000	28,000
1982. 7−1983. 8	65 *1 (During damage)	15	40,250	37,000
1983. 8−1984. 8	80	20	24,125	24,000
1984. 8−1985. 9	90	10	94,500 *3	87,000

*1 The length of wing during damage in July 1983 is assumed as 65 meters.
*2 D in 1984.4−1981.10 is assumed as an average value.
*3 This value includes the dredged sand volume.

Figure 12 shows the relation between D and Q_s, which shows that Q_s is depending on D. When D is more than 60 meters, the value of Q_s is zero. If D becomes shorter, then Q_s becomes greater. Finally, Q_s approaches asymptotically to 112,000 m^3/yr, that is the sum of the littoral drift volume at Corralillo Beach and New Beach (see Figure 10). Therefore, under the situation of continuous accumulation of sand in the upper beach, the distance D gradually becomes shorter with time, which brings the undesirable condition; namely that the sand volume of more than 100,000 m^3/yr enters into the basin and deposits there in future. In any case, it is clear that countermeasures must be taken against the sand accumulation in Caldera Port, that is, extension of wing-breakwater or

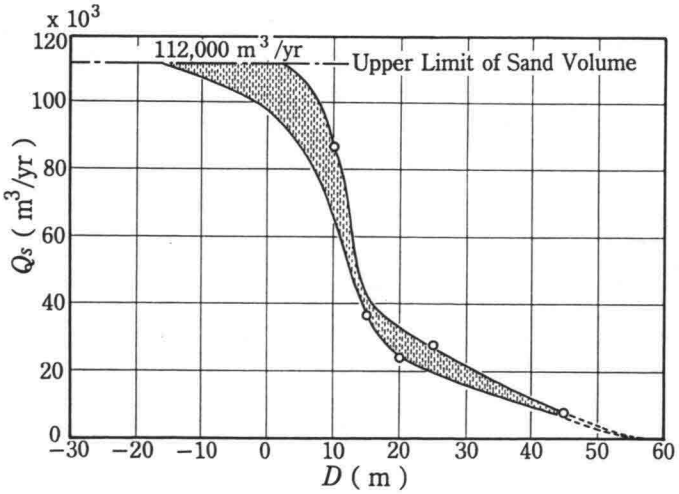

Figure 12 Relation between D and Q_s.

continuous dredging in the basin, or their combination.

If the wing is extended enough in length, the maintenance dredging will not be necessary. The construction cost of breakwater, however, is very high. On the other hand, no extension of wing costs nothing, but the cost of maintenance dredging becomes high. Then, an optimum extension length must be so determined as to minimize the total cost of construction and dredging. For this purpose, the one-line theory was applied. First of all, it was confirmed that the actual shoreline changes and the calculated ones on New Beach and Corralillo Beach were quite similar for the period from September 1981 to September 1985, in which the sand budget shown in Figure 10 was taken into consideration. In this calculation, the shoreline was defined as the contour line of D.L.+1.4 meters. Next, by utilizing the same theory, the further estimations of shoreline change and volume of sand deposited in the basin of Caldera Port were carried out for several cases of varying extension length of the wing-breakwater.

The usual one-line theory can hardly predict the volume of sand which is transported around the wing tip into the basin. Here, however, a smart method of utilizing Figure 12 made it possible to predict it as follow. At first, the location of shoreline on New Beach was calculated by the usual one-line theory. Next, the location of -2 meters contour line was estimated by assuming from the result of data analysis that it is always 68 meters offshore from the shoreline, D.L.+1.4 meters, near the wing-breakwater. When the distance D becomes less than 60 meters, the sand volume which enters into the basin is evaluated from Figure 12. The resultant shoreline is calculated by taking the annual sand volume (Q_s) into consideration. As the distance, D, becomes shorter and Q_s increases with time, this treatment is repeated in every calculation step. Figure 13 shows the result of prediction for the case of 350 meters in total wing length as a typical example. As seen

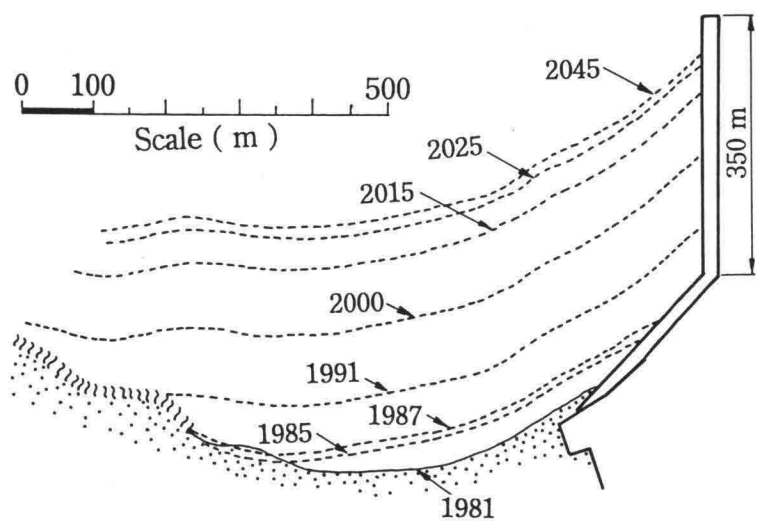

Figure 13 Predicted future shoreline (Wing length = 350 m).

in this figure, the annual shoreline advance rate in the early stage is 7m/yr. It becomes less in the latter because the water depth gradually becomes deeper and also the sand volume going around the wing tip into the basin becomes larger with the advancing of shoreline.

Now, costs are estimated assuming the most reasonable procedures for the wing construction and the dredging for each extension length. In the estimation of dredging cost, not only the dredging of sand coming around the wing tip, but also a primary dredging of sand deposited before 1985 and the usual maintenance dredging every five years are included. The maintenance dredging in the entire basin is necessary because very fine material, being about less than 0.1 mm in diameter, is being accumulated at the rate of 12 to 16 cm/yr. The transport of this fine material is mostly due to tidal currents. Figure 14 shows the wing construction costs, the dredging costs and the total costs of each wing length over the lifetime of 30 years, including the case where the wing-breakwater is not extended at all. From this figure, it is decided that the most economical countermeasure against sand deposition in the basin is to extend the wing-breakwater by a length of 350 meters in total. It is also confirmed in the simulation that the wing extension does not significantly influence on the counter movement of sand from the north side beach, Caldera Beach, into the basin.

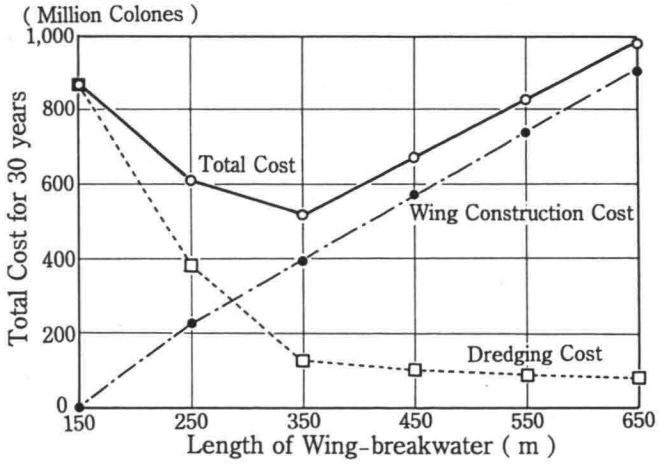

Figure 14 Cost comparison of each wing length.

5. EXTENSION OF WING-BREAKWATER AND OTHER COUNTERMEASURES

According to JICA Report in 1986, two works were urgently required for Caldera Port. One was a primary dredging in order to extract sand which had already deposited. Another was an extension of the wing-breakwater up to be 350 meters in total length. During the first months of 1987, a maintenance dredging program was completed satisfactorily. At this time, the wing of 150 meters in length had been already constructed (see Figure 9),

but the distance D was nearly zero. Then, the extension of wing-breakwater for 200 meters more had to be done as soon as possible. However, as financial prospects for a maintenance for Caldera Port turned meager due to the political and economical difficulties, MOPT eas forced to tackle the construction job for the 200 meters of additional length for the wing on its own, with the reduced resources of the ordinary budget and with old equipments in bad condition.

Figure 15 shows the location of the wing tip during a period from 1987 to 1992. The location of -2 meters counter line is also shown as well as the volume of sand deposited in the control area. As seen in this figure, the extension rate was almost constant, but it was very slow. Only 275 meters reach of wing had been constructed by 1992, which is 75 meters shorter than the target length. Furthermore, the location of wing tip retreated often, which was due to accidents with rubble stones that were scattered to the inside by actions of large waves because the weight of armor stone was too light to overcome the large waves. According to JICA Report (1986), the design weight of armor stone is 17 tons and, particularly for the head of wing, the stones used should be no less than 25 tons in weight. In actuality however the weight of the stones used for construction was 6 to 8 tons. There were large stones more than 20 tons in a quarry and a construction crane on the breakwater had enough capacity for lifting them. However, a loading capacity of trucks which transported the stones from the quarry to the construction site were 8 tons in maximum. Moreover, as the construction of wing was done from its crown, the arm length of crane did not reach the base of breakwater. Then, it is inferred that an execution of its foundation was not necessarily enough.

Figure 16 shows the location of wing tip in detail, during a period from May to August

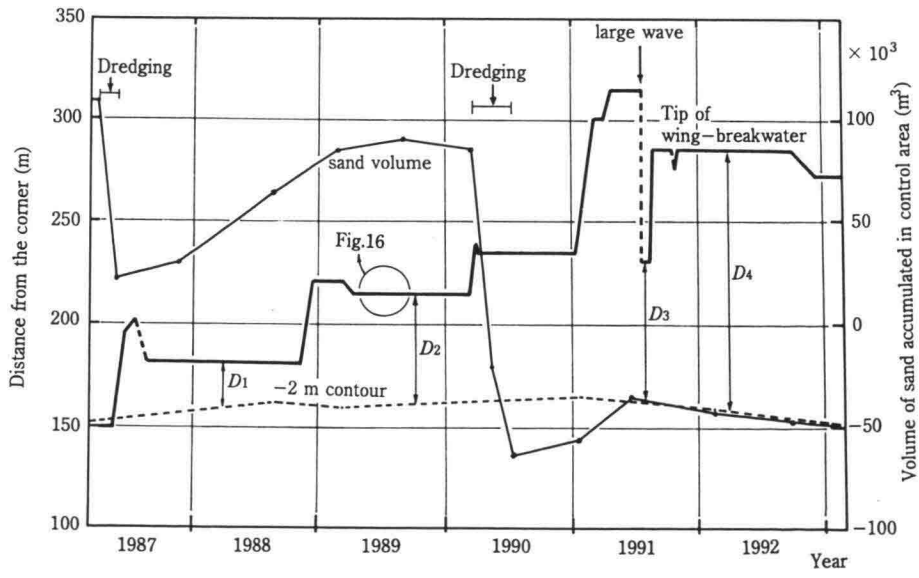

Figure 15 Changes of wing tip location (from 1987 to 1992).

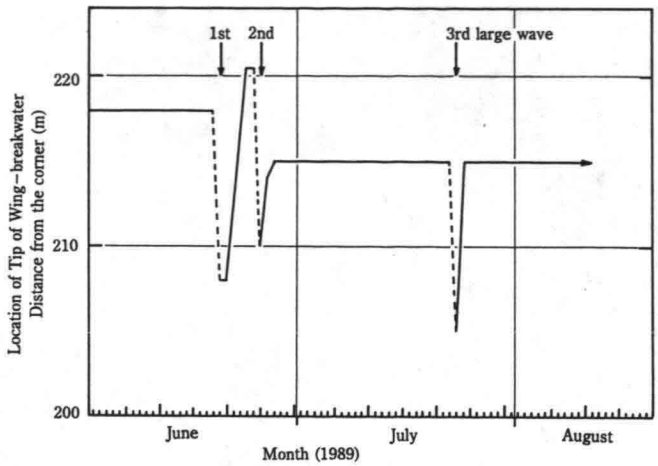

Figure 16 Changes of wing tip location (from May to August 1987).

1987. On the upper side, the days when large waves came are indicated by arrows. At first the large waves came on the day of 18th June, Sunday, by which the rubble stones in the crown of breakwater above L.W.L. and within 10 meters from the wing tip were scattered into the lee side area. As the lower part of wing was still remained, the destroyed part was quickly restored to the former condition and extended a little more by putting other stones on the top. However, the second waves came on the day of 25th June, Sunday, and destroyed again the 12 meters from the wing tip. On the next day, the part of destroyed reach was restored again. Moreover, another large waves came on the day of 23rd July, Sunday, which destroyed the further 10 meters from the wing tip. Also in this case, the restoration work was done on the next day. The fight against the large waves was similar to an ant fighting an elephant. Beside, it is only known that the large waves were long period waves. There is no further information on these waves, because no wave gauge was installed near Caldera Port and every large waves came on Sunday.

The wave on the days of 27th, Saturday, and 28th, Sunday, July were extremely large. According to an eyewitness, a large overtopping occurred over the wing in the reach of about 100 meters from the wing tip. The rubble stones located 85 meters from the wing tip and above L.W.L. were scattered into the lee side area. Also in this disaster, a reach of 56 meters was restored with other stones in a short period. The total length of wing is 272 meters at present (see Photo 3).

As seen in Figure 15 again, the distance from the wing tip to the -2 meters contour line, D_1, was about 20 meters in 1987 and 1988. Under this situation, the sand of bout 64,000 m^3 in volume had been deposited in the control area by the beginning of 1989. The large waves came three times during months from June to July 1989, which transported sand into the port around the tip and made New Beach Junior again just behind the breakwater. However, the distance, D_2, was about 50 meters due to the extension works

Photo 3 Wing-breakwater in 1993.

of wing in 1989. In this conditions, the sand deposition in the control area did not take place. Apart from this preferable situation, as the extension speed of the wing was slow, the sand already accumulated in the basin until 1989. Then, a third full dredging program was carried out in the whole area of basin during the period from March to June in 1990. On this occasion an over-dredging job was accomplished to create a sand trap in the control area with a maximum depth of 16.8 meters. The net dredged volume was about 300,000 m^3, of which 150,000 m^3 were taken from the control area.

In the first half of 1991, the wing was extended 80 meters more from 235 meters to 315 meters in length at a high pace. In July 1991, however, almost full length of newly extended reach was destroyed by very large waves. Although the distance from the wing tip to -2 meters contour line, D_3 in Figure 15, was still about 60 meters, some volume of sand deposited in the control area since the waves were too large. Immediate reconstruction extended the wing to 286 meters, which made the distance, D_4, longer to be 125 meters. After that, in the second half of 1991 and in 1992 there was some erosion in the control area.

Furthermore, the location of -2 meters contour line near the wing retreated onshore as seen in Figure 15. This retreat of the beach is considered to be due to a local counter flow in the southward direction generated by the waves reflected by the the wing. This situation is welcome for reducing the volume of sand transported around the wing tip into the basin. However, we must keep in mind the undesirable possibility that a local scouring at the toe of wing-breakwater may occur in the neighborhood of the tip, which will require us to reinforce the toe of wing for its safety.

As the extension speed of wing was slow and the existing length was still shorter than the designed length, two more countermeasures have been considered. One is the

Photo 4 Small jetty located between New Beach and Corralillo Beach.

construction of new jetty at the upper side of the littoral drift. Another is direct sand extraction from New Beach.

It is also effective to construct a new jetty at the upper side of the littoral drift. The most effective location for this construction is at Corralillo Headland (see Figure 10). However, there is no approach road for the jetty construction there. Temporary works such as the construction of an approach road would be very expensive. Construction of the new jetty from the sea using a construction ship would also be very expensive. Moreover, as you can easily infer from the coastline configuration shown in Figure 3, the wave energy concentrates to Corralillo Headland. The design cross section of the jetty should be as same as that of the wing or more. Then, as the second best location, the new jetty of 90 meters long was constructed on a rocky reef located between New Beach and Corralillo Beach in 1990 (see Photo 4). The jetty could be designed with smaller size rock than that used for the wing by virtue of diffracted small waves. An effect of this jetty has emerged as an advancement of the shoreline on Corralillo Beach (in the foreground in Photo 4). However, its efficiency is not enough, because some of the drift sand is supplied from the offshore of Corralillo Headland to New Beach directly as shown in Figure 10.

Removing the sand at the seashore of New Beach is also an effective way to prevent sedimentation in the harbour. As a complementary step, sand removing by a private industry has been done at New Beach with the objective of reducing its growth. In spite of the small grain size of these sands (d_{50} = 0.2 mm), which makes them of a little use for developers and builders, mean extracted volumes of 3,400 m^3 /month have been noted since 1992. A system of sand extraction is very simple and requires no special machinery. The sand is scraped up to the higher level by bulldozing at the low tide. Because the

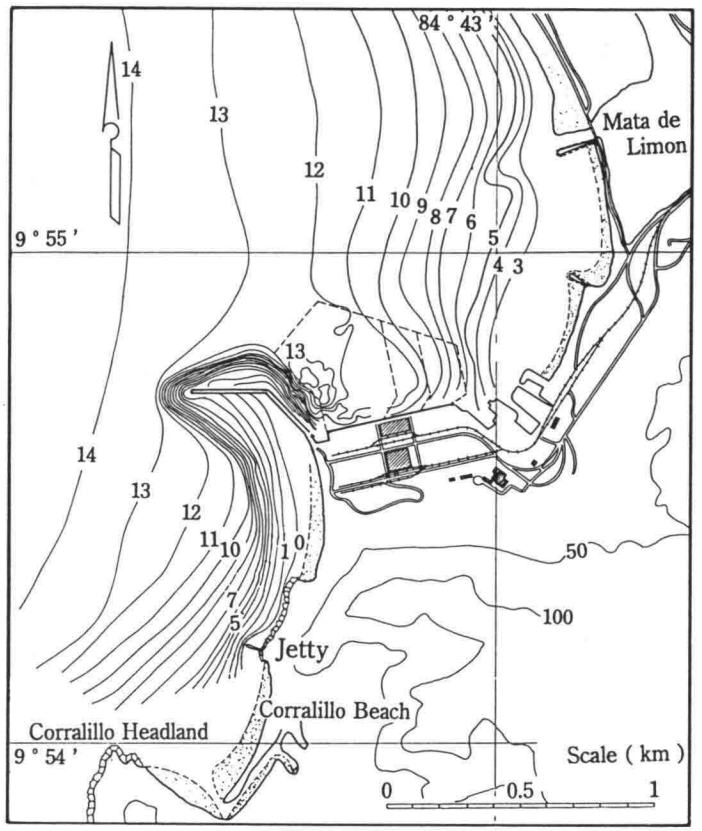

Figure 17 Topography in February 1993.

sand accumulates again during the successive high tide, the process can be continuously done by this simple system.

Figure 17 is a contour map of topography in February 1993. A depositional topography is noticed in a north side area of wing-breakwater, where the rubble stones scattered from the wing were settled due to the repeated disasters and no dredging was conducted in the past. The sand trap topography in the control area, which was formed by over dredging in 1993, is almost unchanged. The sand deposition is not recognized on the basin in front of berth. In short, since February 1992 no shoaling has been detected in the basin, which means that the combination of three kinds of countermeasure is helpful to prevent the further entering of sand into the basin of Caldera Port.

6. SUMMARY AND CONCLUSIONS

Since its completion in 1981, Caldera Port has been exposed to a serious matter of sand

sedimentation in the basin, which is due to the northward littoral drift of about 200,000 m^3/yr by the predominant waves in obliquly incident. To prevent this situation, the extension of wing-breakwater started. According to the result of numerical predictions by the one-line theory, the optimum length of wing-breakwater was 350 meters. However, due to lack of funding, the extension works of wing were done at a slow pace with old equipments in bad condition. The wing was repeatedly destroyed by the large long waves of about 18 seconds in period. At present, the wing has been reconstructed up to be 272 meters in length, which is considered to be not long enough for the near future. Then, other two countermeasures have also been considered to reduce the volume of sand transported into the basin. One is the construction of jetty at the up-side of littoral drift, another is to take sand from New Beach. The latest results of topographic monitoring show that the combination of these three kinds of countermeasure is helpful in preventing further sedimentation in the port.

The valuable experiences piled through the fight against the littoral drift problem in Caldera Port are of fundamental importance. These can be enumerated as follows:

(1) The phenomena of littoral drift are very complicated, so there is very much left to study. The result of sand movement, however, is exceedingly simple, that is to say, either there is resulting erosion or deposition. Then, in order to sufficiently grasp the result of sand movement, it is basically important to monitor the change of topography by conducting repeated sounding survey. In the case of Caldera Port, sounding surveys has been carried out with a high frequency since 1981. Especially the data accumulated by 1985 were very helpful for improving the accuracy of numerical simulation.
(2) An effect of countermeasures for the littoral drift doesn't always appear soon. Then, there is a possibility of making an incorrect decision and taking the haphazard way of doing them. In order to avoid this kind of mistake, it is of importance to examine thoroughly the effect of countermeasures on the topography in advance by a scientific method such as the one-line theory. It is also kept in mind that quantitative predictions of topographical changes are still difficult at present due to the multiplicity and high level of complexity of the various processes involved. To make up for this deficiency, the effect of countermeasures must be followed and checked in the field at regular intervals, during and after their the execution.

ACKNOWLEDGEMENTS

The authors are grateful to Mr. José Chacón L., Director of the Port and River Works Division, Ministry of Public Works and Transport, for his encouragement and support for the present study and to Professor Yoshimi Goda, Yokohama National University, for his important recommendation in 1981 on construction of the wing-breakwater and for his helpful study on the long period waves. The authors are also grateful to Professor Isao Irie, Kyushu University, for his excellent study especially in conducting the one-line theory simulation when he was technical chief of study team sent to Costa Rica in 1985.

Furthermore, this paper is the result of numerous in situ measurements and studies done by the Harbor Works Division in MOPT, and Japanese experts working under the auspices of JICA. Dr. Luis Murillo, University of Costa Rica, gave us the helpful suggestions on our English. A special thanks for all.

REFERENCES

1) Goda,Y.(1983):Analysis of wave grouping and spectra of long-travelled swell, Rep. of PHRI, Vol.22, No.1, pp.3−41.
2) Japan International Cooperation Agency(1986):The study on the maintenance project of the Port of Caldera in the Republic of Costa Rica, 390p.

HYDRO-PORT'94
International Conference on Hydro–Technical
Engineering for Port and Harbor Construction
October 19 – 21, 1994, Yokosuka, Japan

Physical Impact of Bilbao Harbour New Breakwater on Adjacent Beaches

Joan P. Sierra [1]
José A. Jiménez [1]
Agustín Sánchez– Arcilla [1]
José M. Picó [2]
Alejandro Viñuales [2]
Eleuterio J. Villanueva [2]

[1] Laboratori d'Enginyeria Marítima, Catalonia University of Technology
c/. Gran Capitá s/n, mod. D– 1, 08034 Barcelona
[2] Bilbao Harbour Authority, Campo de Volantín 37, 48007 Bilbao

ABSTRACT

Due to the need of new installations and to take profit of several unused areas, the Bilbao Harbour Authority launched an expansion project, which logically consists in the construction of a new breakwater in the left margin of the river. Since this new breakwater can alter the local hydrodynamics, several studies have been undertaken to estimate its influence on two adajacents beaches located inside the harbour. First results indicate that the Ereaga beach will be more stable after the construction of the breakwater. On the other hand, and because the breakwater will increase the wave height in front of the Arrigunaga beach under certain conditions, this beach could be potentially affected. However, since this beach is mainly composed by very coarse sediments, results must be considered as indicative. To estimate the real effects of the expansion works on both beaches a monitoring programme has been launched with a duration of five years.

Key Words: Bilbao Harbour, environmental impact, wave propagation, beach evolution.

1. INTRODUCTION

The Port of Bilbao is the largest harbour in Spain in terms of volume of traffic. It is situated in the Spanish Cantabric Coast, within the Bay of Biscay. Bilbao Docks are over 20 kilometers long, stretching down the Nervion River to the Punta Lucero Breakwater, located at the end of the river inlet (Figure 1).

Originally the Port of Bilbao was a fluvial harbour, but at the end of 19th century it started to expand towards the sea. In 1902, both the Santurce and the Arriluce breakwaters, which close the river mouth, were constructed. After this, the first available information on the harbour expansion toward the Outer Estuary is from the 50's. In 1971 the works for the construction of the Punta Lucero Breakwater and its joined pier started. For this pier, water depths of 32m

were achieved. In 1976 this breakwater was damaged by an exceptional storm. For this reason, the construction of the Punta Galea Breakwater, which would have closed the outer estuary, were permanently stopped. The Punta Lucero Pier was reinforced between 1980 and 1985 and since then it has been used for oil-tankers. Nevertheless a relatively unused space of more than 5 km long and 3 km wide remained among the Punta Lucero and Santurce breakwaters.

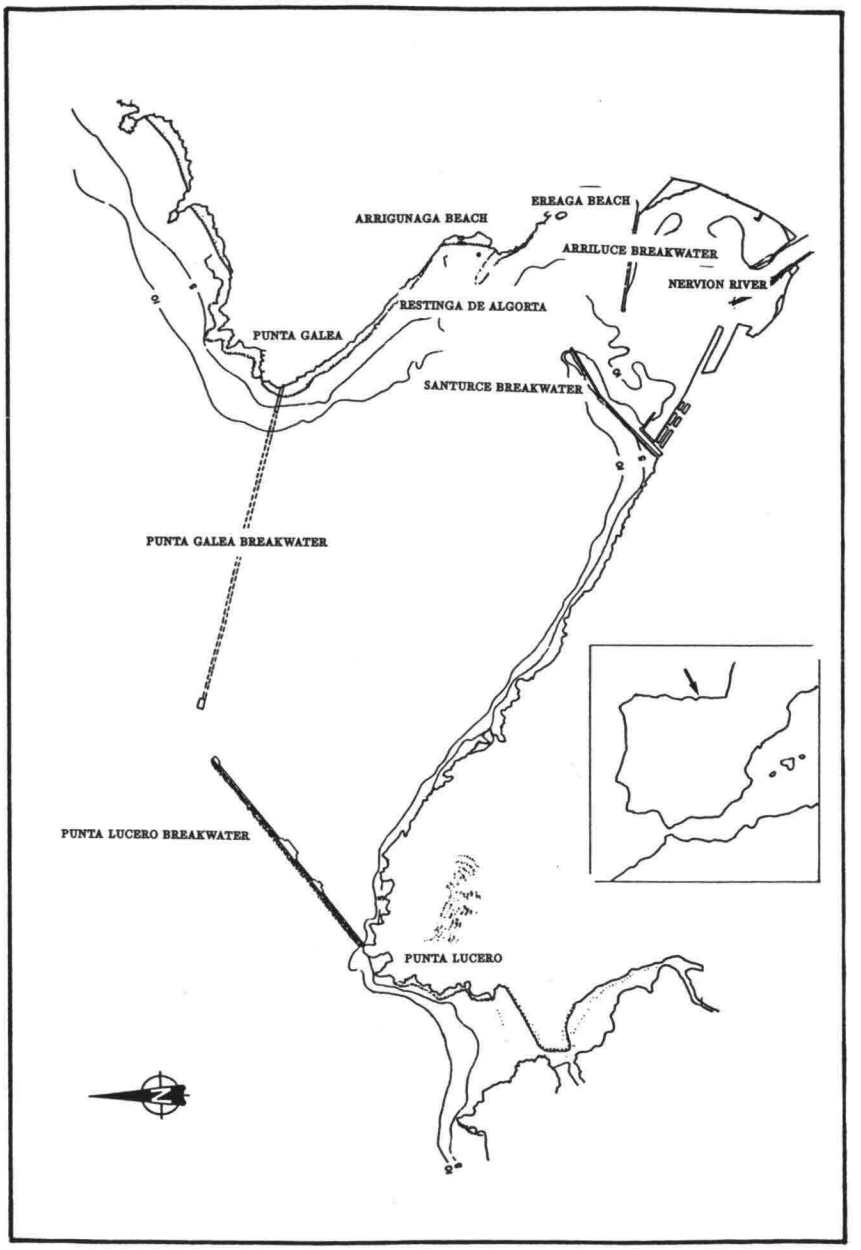

Figure 1 Bilbao Harbour location map

In 1989 the major expansion works were initiated by the Bilbao Harbour Authority in order to satisfy the need of the harbour to expand and to take advantage of the available space in the aforementioned zone. After various technical and economic studies, a solution consisting in the construction of a new breakwater with a length of 3150 m broken in three alignments and a straight counterdike of 1400 m (see Figure 2) was selected. The mouth is 700 m wide and is oriented in direction N15E. This project will make available 8 km more of docks and an additional land surface of 350 Ha.

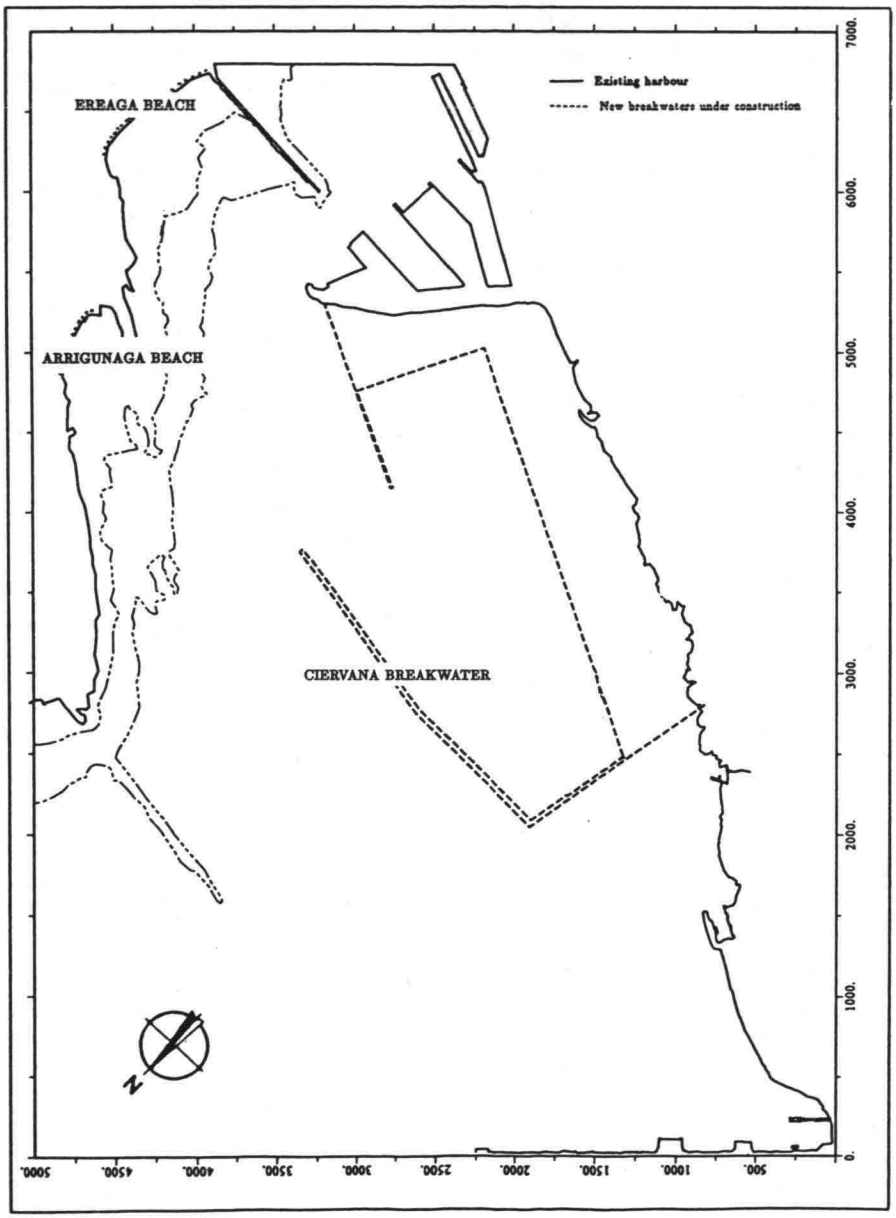

Figure 2 Sketch of the expansion project

In order to have an idea of the magnitude of this expansion works, some order-of-magnitude figures (Villanueva and Uzcanga, 1993) are here included. The construction will require the following volumes (all the amounts are in cubic meters): 1.9 millions of concrete, 7.3 millions of breakwater core, 2.2 millions of rouble mound and 17 millions of soil fill. The term for the execution of the works is 62 months and the total budget is 35,355 millions of pesetas (about U$ 250 millions).

Both breakwaters will be rubble mound-type. They will be protected with concrete blocks of 100 tons weight (in the outer armour layer), which will be able to withstand waves 11 m heigh. No overtopping will be permitted and a shoulder will be placed on top of both breakwaters in order to avoid it. Joined to the breakwaters a wharf with water depths of 21 m will be also constructed.

Wave conditions inside the harbour area will be modified by this new structure. Neighbouring beaches in particular, could be affected by wave reflections coming from the breakwater. The two beaches considered (named Arrigunaga and Ereaga) are facing the new breakwater from the opposite side of the estuary.

Various studies (Sánchez-Arcilla et al., 1991) with a wave propagation numerical model were carried out in order to detect and prevent these effects. The numerical model can simulate the main phenomena involved in wave propagation such as refraction, diffraction and reflection. The results of the model have been employed to estimate the response of both beaches. The estimation of the beach evolution has been done in alongshore and cross-shore directions.

2. BEACH MORPHOLOGY AND ANTECEDENTS

The Arrigunaga and Ereaga beaches are located in the right margin of the mouth of the Nervion River (Figure 1), and they are oriented N-S. The Ereaga beach is about 700 m long and the Arrigunaga beach is about 600 m long.

Both beaches are connected through a rocky outcrop, the *Restinga de Algorta*. This outcrop is a shallow barrier extending down to 2 m depth (with respect to the lowest water level). Since the area of study is a macrotidal coast, with a maximum tidal range of about 4.6 m, this barrier acts as a permeable obstacle, and through this barrier the Arrigunaga beach has fed with sand to the Ereaga beach during the last decades, mainly after the construction of the Punta Lucero breakwater due to the oblique waves incidence in the Arrigunaga beach (CEEOP, 1983, CEDEX, 1990).

At this time the characteristics of both beaches are quite different. The Ereaga beach, located between the Algorta breakwater and the Restinga de Algorta is a sandy beach, with a few submerged rocky outcrops. On the other hand, the Arrigunaga beach is composed by a mixture of several types of sediments: cobbles, pebbles, rocky outcrops and, in a lower percentage, sand. This beach is connected to the north with the Punta Galea cliff, which acts as a source of coarse sediments for the beach.

3. WAVE CLIMATE

Wave climate has been determined using data recorded by a waverider buoy located in open waters, in front of the Punta Lucero Breakwater. Using data recordered by this buoy, the sea-state curves for Hs and Tz of an average year have been obtained (see Figures 3 and 4). 1st October was taken as the origin for this average year.

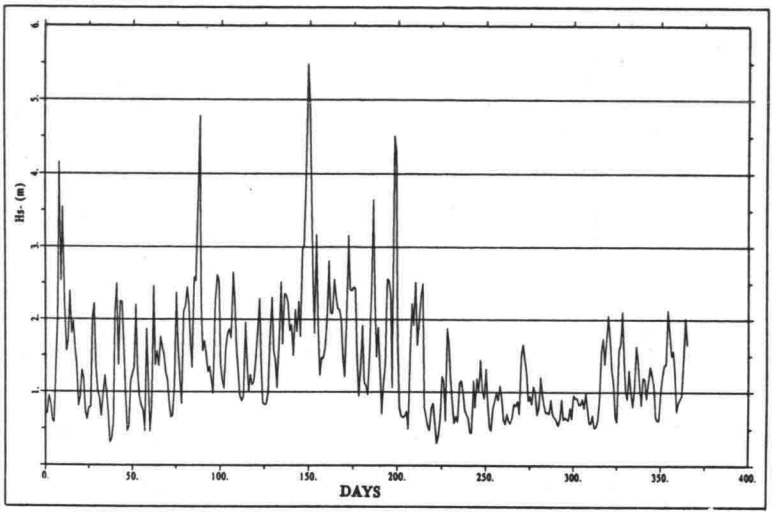

Figure 3 Sea-states curve for H_s

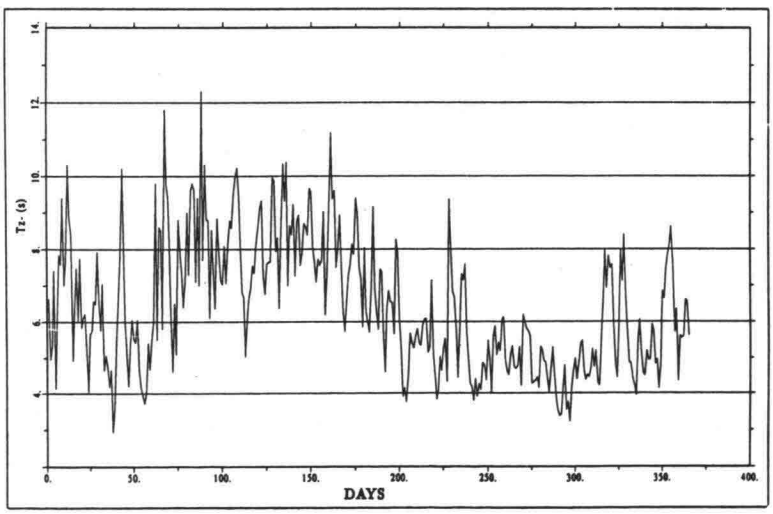

Figure 4 Sea-states curve for T_z

For the wave propagation model application, a reduced number of wave conditions (defined by three parameters: Hs, Tz and direction) was needed. For this reason, a smoothed (average) sea-states curve in terms of the energy flux variable was obtained, with the criteria of maintaining the same area under the curve (see Figure 5).

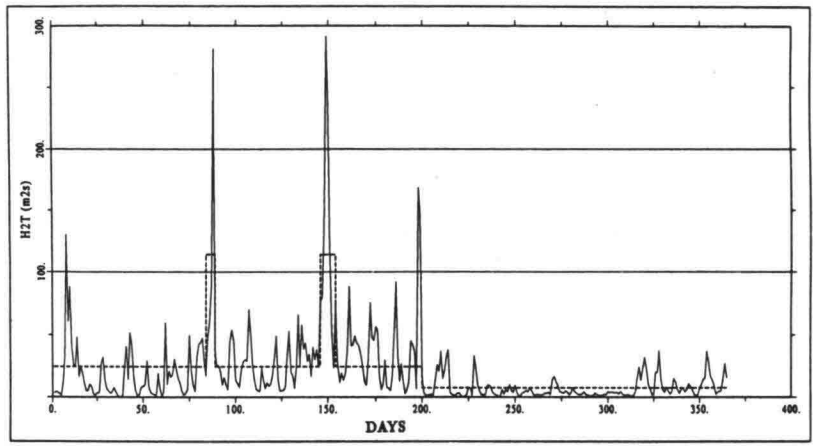

Figure 5 Averaged sea-states energy flux curve

Taking into account visual data, the main directions for wave propagation were determined. Only waves coming from directions between N to NE and W to N are able to penetrate into the harbour. In Table 1, the average annual frequency for each direction is shown. It can be seen that prevailing waves arrive from the fourth quadrant (W to N), with a frequency of almost 92%. In particular, waves from NW and NNW directions are of special importance.

Table 1 Frequency of wave direction.

Direction	Frequency (%)
W	13.9
WNW	18.2
NW	29.7
NNW	22.8
N	12.1
NNE	4.7
NE	3.6

Wave conditions to estimate beach response were selected using the smoothed sea states curve, fixing the more frequents directions which can generate reflections in the new breakwater. With this criterion, the behaviour of both beaches in the most demandig cases from an equilibrium standpoint, could be reproduced. The selected wave conditions can be seen in Table 2.

Table 2 Wave conditions to estimate beach response

Condition	H_s (m)	T_p (s)	θ
C1	3.5	9	N35W
C2	4.0	14	N45W
C3	2.0	7	N45W
C4	3.5	9	N

H_s: significant wave height, T_p: peak wave period,
θ: direction.

4. WAVE PROPAGATION

4.1 Model description

Wave propagation was carried out by applying a well tested numerical model. This numerical model is based on Boussinesq-type equations (Sierra *et al.*, 1988), in which the vertical velocity of the fluid particles is supposed to increase linearly from zero at the bed to a maximum magnitude at the free surface. The Boussinesq equations are formulated in terms of vertically-integrated mass and momentum conservation laws and are obtained with a perturbation technique (Sánchez-Arcilla and Monsó, 1985), yielding the following expressions (Peregrine, 1967):

- Continuity equation

$$\frac{\partial H}{\partial t} + \frac{\partial p}{\partial x} + \frac{\partial q}{\partial y} = 0 \qquad (1)$$

- x-momentum equation

$$\frac{\partial p}{\partial t} + \frac{\partial}{\partial x}\left(\frac{p^2}{H}\right) + \frac{\partial}{\partial y}\left(\frac{pq}{H}\right) + gH\frac{\partial (H-h)}{\partial x} = \frac{Hh}{2}\left[\frac{\partial^3 (hp\ /\ H)}{\partial t\ \partial x^2} + \frac{\partial^3 (hq\ /\ H)}{\partial t\ \partial x\ \partial y}\right] + \frac{h^2 H}{6}\left[\frac{\partial^3 (p\ /\ H)}{\partial t\ \partial x^2} + \frac{\partial^3 (q\ /\ H)}{\partial t\ \partial x\ \partial y}\right] \qquad (2)$$

- y-momentum equation

$$\frac{\partial q}{\partial t} + \frac{\partial}{\partial x}\left(\frac{p\,q}{H}\right) + \frac{\partial}{\partial y}\left(\frac{q^2}{H}\right) + gH\frac{\partial(H-h)}{\partial y} = \frac{Hh}{2}\left[\frac{\partial^3 (hp / H)}{\partial t\,\partial x\,\partial y} + \frac{\partial^3 (hq / H)}{\partial t\,\partial y^2}\right] + \frac{h^2 H}{6}\left[\frac{\partial^3 (p / H)}{\partial t\,\partial x\,\partial y} + \frac{\partial^3 (q / H)}{\partial t\,\partial y^2}\right] \quad (3)$$

where $H = h+\eta$, h is the still water depth, η is the free surface elevation, $p = \int_{-h}^{\eta} u\,dz$ is the mass flux along the x axis, $q = \int_{-h}^{\eta} v\,dz$ is the mass flux along the y axis and u, v are the particle velocities along the x, y axes.

Other terms can be easily included in these momentum equations (Sánchez-Arcilla *et al.*, 1986). With these additional terms (*i.e.* Coriolis acceleration, wind friction, turbulent viscosity or bottom friction) a large number of physical phenomena can be adequately reproduced by the model.

The momentum conservation laws are highly non linear differential equations and they include a third order derivative term, which is due to the existence of a constant vertical acceleration.

The vertical integration of equations (1), (2) and (3) reduces the problem from three to two independent dimensions. These equations are suitable for a wide range of wave lengths. In particular, short wind waves in shallow water provide an acceptable ratio of water depth to wave length except for the shortest waves. These waves can be thus considered as long waves, and their propagation can be correctly simulated by the model.

Considering different terms of the momentum equations and varying initial and boundary conditions, it is possible to reproduce a wide variety of physical phenomena such as Kelvin waves, storm surge, solitary waves, refraction, reflection, diffraction, bottom friction, etc. Analytical solutions of these phenomena were employed in order to calibrate the model (Sánchez-Arcilla *et al.*, 1986, Sierra, 1990).

The equations are solved by means of an implicit centered finite-differences technique with variables defined on a space staggered rectangular grid. A double-sweep algorithm (Abbott and Ionescu, 1967; Abbott *et al.*, 1973) is invoked for solving the system avoiding large and expensive matrix inversion operations.

In open boundaries, an absorbing-reflecting boundary condition (Sánchez-Arcilla and Monsó, 1986) is used. In this way, the multiple reflections due to innerly reflected waves are avoided, because these reflected waves are allowed to escape the domain unhampered.

4.2 Model application

This wave propagation numerical model was employed to analyze the physical impact of the new Ciervana Breakwater on Ereaga and Arrigunaga beaches. For this purpose, wave

parameters (H_s and T_p) included in Table 2 were used as input data for a Jonswap spectrum (Hasselman *et al.*, 1973). The other parameters for this spectral form were average values from the state of art. Once the various spectra were completly defined, irregular wave records were simulated in order to obtain the necessary wave input to feed the propagation model.

Each storm, represented by a typical wave record, was applied to both domain configurations (the present situation and the one with the enlargement works completed). The obtained results were compared, evaluating the wave pattern changes near the two beaches.

In Figures 6 and 7, wave propagation results for a wave spectrum with H_s=4 m and T_p=14 s and waves coming from NW are shown. The results are expressed in terms of amplification coefficients. From the comparison of both figures and similar ones obtained for other NW storm simulations, it was observed that wave heights greatly diminish in the new Ciervana basin due to the lee provided by the new breakwater, as it was expected. Moreover, reflections from the new breakwater and the Galea coast at the opposite side gave a slight increase of wave heights near Arrigunaga. These same storms produced nevertheless a perceptible decrease of wave heights in Ereaga Beach, because of the additional shadow area created by the new breakwater which sheltered the beach.

In Figures 8 and 9, simulations of a storm coming from the N with H_s=3.5 m and T_p=9 s are presented for both configurations. The same effects (*viz.* wave height reduction inside the new basin and wave height increase due to reflections in the area between the breakwater and Galea coast) were observed. In this case, wave conditions on Arrigunaga Beach were quite similar before and after the construction of the breakwater, while on Ereaga Beach, the new structure yielded an appreciable decrease of wave heights.

5. COASTAL EVOLUTION

To study the coastal response of Arrigunaga and Ereaga beaches due to the construction of the new breakwater, a comparative study was performed. State-of-art tools were employed to estimate beach planform and profile changes considering the initial situation (before the construction) and the final one (after the construction). This means that the obtained results are not absolute, in the sense that they only give the evolution trend of the beaches due to the new conditions, (*i.e.* whether or not the beaches will be more stable).

5.1 Shoreline changes

Shoreline changes are usually studied by quantifying the amount of sediment that is transported along the beach, *i.e.* the longshore sediment transport. In pocket beaches, this transport is mainly generated by two mechanisms: (i) longshore transport induced by oblique incidence of breaking waves and (ii) longshore transport induced by currents generated by longshore gradients in the wave height.

To estimate the longshore transport capacity due to the two above mentioned mechanisms, the model due to Osaza and Brampton (1980), which has been succesfully used by several authors (*e.g.* Kraus and Harikai, 1983; Mimura *et al.*, 1983, Hanson and Kraus, 1989), was selected.

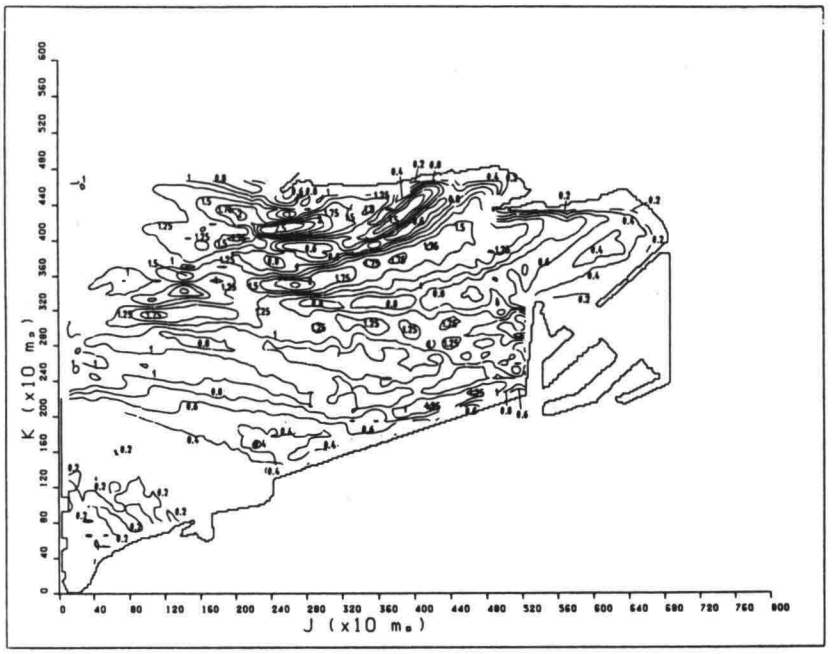

Figure 6 Present situation. NW waves

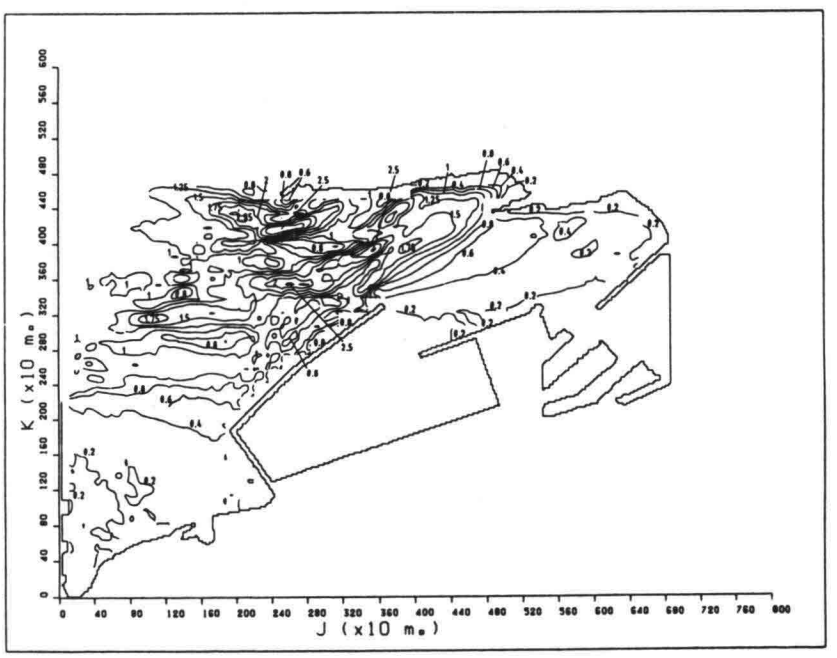

Figure 7 Foreseen situation. NW waves

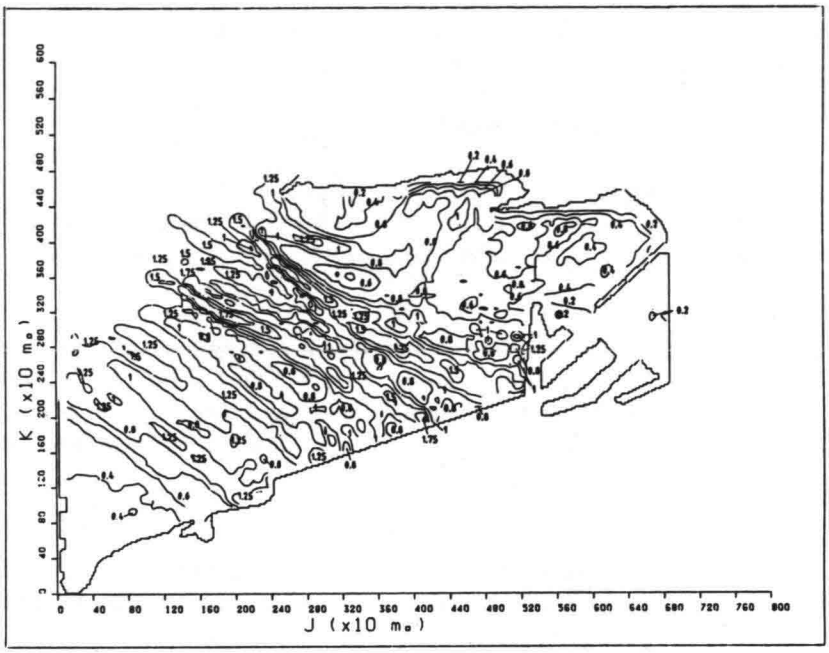

Figure 8 Present situation. N waves

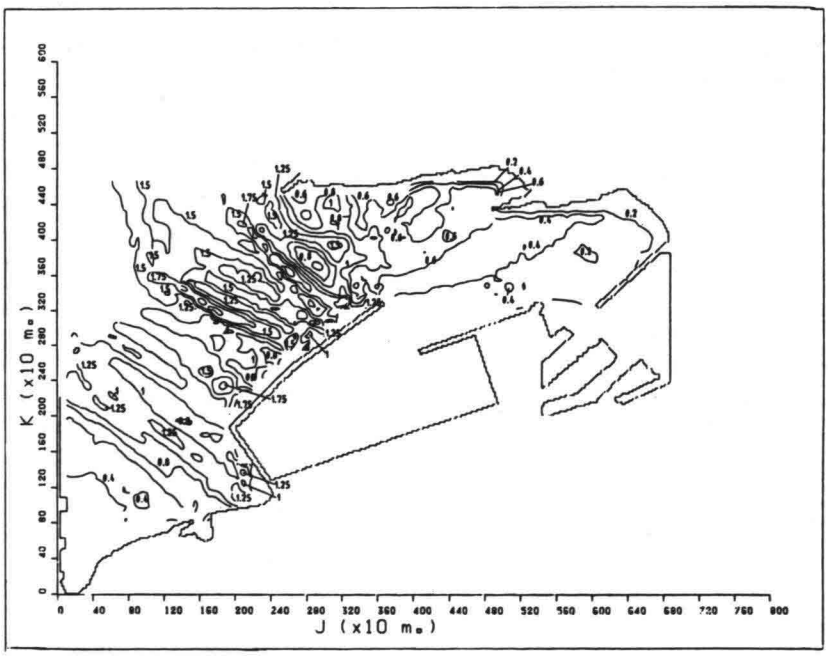

Figure 9 Foreseen situation. N waves

This model uses the CERC formula to estimate the longshore transport (I_l) due to oblique incidence and includes an additional term to estimate the effect of the longshore gradient of wave height. The resulting I_l formula is given by:

$$I_l = (Ec_g)_b \left(K_1 \sin\alpha_{bs} \cos\alpha_{bs} - \frac{K_2}{\tan\beta} \cos\alpha_{bs} \frac{\partial H_b}{\partial y}\right) \quad (4)$$

where I_l is the inmersed weight sand transport rate, $E\ c_g$ is the wave energy flux at breaking, α_{bs} is the angle between the waves and the shoreline at breaking, *tan* β is the beach slope, H_b is the breaking wave height, y is the alongshore coordinate and K_1, K_2 are dimensionless coefficients.

The use of this kind of formulation presents the problem of how to select the values of the various coefficients. A discussion about it can be seen in Kraus (1987), using different test problems. In any case, since this is a comparative study and the objective is to obtain the difference in beach response with and without breakwater, the effect of the selected values will be similarly reflected in both cases.

(1) Boundary conditions
The Ereaga Beach is limited at the southern end by the Algorta breakwater. This structure is long enough to be considered as a total barrier acting as a zero transport boundary condition. Northwards, the Ereaga Beach is limited by the *Restinga de Algorta*, which is a rocky outcrop that acts as a common boundary for both beaches. As it was mentioned before, the offshore limit of this outcrop is relatively shallow, and taking into account the large tidal range, it can not be considered as a total barrier, although the theoretical bypass rate is difficult to evaluate. However, the bypass of sediment, if any, will be directed from the Arrigunaga Beach towards the Ereaga Beach, and will depend on the sediment availability, which is very low. To the north, the Arrigunaga Beach is not limited by any barrier, and it is freely connected with the Punta Galea cliff.

(2) Arrigunaga Beach
This beach is formed by mixed sediments, *i.e.* sand, pebbles and, in some parts of the submerged beach, rocky outcrops. Therefore, the estimation of the longshore transport rate at this beach is not a trivial work. However, several authors have used the CERC formula for this task in similar beaches, with an adequate calibration of the coefficient value (*e.g.* Brampton and Motyka, 1987; Nicholls and Wright, 1991).

Results obtained by Sánchez-Arcilla *et al.* (1991) show that for the selected wave climate (which is typical for storm conditions), longshore transport rates are potentially increased by the construction of the breakwater, specially in the case of the C2 wave conditions (see table 2). In the same way, longshore transport gradients along the beach are also increased, indicating a trend to be more easily eroded, which for a pocket beach means an increase in the wobbling of the beach. The magnitude of this wobbling will depend on the availability of sediment to be transported and on the transport efficiency.

(3) Ereaga Beach
The construction of the breakwater produces, as it was seen before, a decrease in wave height along the beach, and, at the same time, a nearing towards orthogonality of the angles of wave

incidence. This means that longshore transport rates will decrease after the construction of the works. Sánchez-Arcilla *et al.* (1991) showed that this decrease is accompanied by a drastic decrease in the gradients of longshore transport rates, indicating that the beach will be more stable, and with less wobbling between boundaries.

5.2 Beach profile changes

Beach profile changes are associated to cross-shore sediment transport and they usually occur at a short time scale. In general, they can be considered as reversible changes and they can be simply classified into two cases, *viz.* erosion and accretion profiles.

To study beach profile changes the following predictors were used:

-Iribarren's parameter or surf-similarity parameter (Iribarren and Nogales, 1949; Battjes, 1974)

$$Ir = \tan\beta \; / \; \sqrt{H_b/L_o} \tag{5}$$

- Dean's parameter (1973)

$$D = H_b \; / \; Tw_f \tag{6}$$

- Sunamura and Horikawa's parameter (1974)

$$SH = \frac{H_b}{L_o}(\tan\beta)^{0.27}\left(\frac{L_o}{d_{50}}\right)^{0.67} \tag{7}$$

- Hattori and Kawamata's parameter (1980)

$$HK = \frac{H_b}{w_f T}\tan\beta \tag{8}$$

- Dalrymple's parameter (1992)

$$P = \frac{g\,H_b^2}{w_f^3\,T} \tag{9}$$

where H_b is the breaking wave height, T is the wave period, L_o is the deep-water wave length, w_f is the fall velocity of the sediment, d_{50} is the mean grain size, *tan* β is the beach slope and g is the aceleration of the gravity.

Although these parameters are mainly qualitative and can not be used to estimate the magnitude of the profile changes (Jiménez *et al.*, 1993b), their values are an index of the susceptibility of the profile to be eroded by the incident waves. As the value of the parameter increases the profile will be more easily eroded except for Iribarren's parameter. In this case, *Ir* is a morphodynamic index of the beach, and high values will indicate transition towards plunging-collapsing breakers, which are associated to reflective beaches (accretive ones).

These parameters were calculated with the selected wave climate evaluated at the breaking zone and the morphological characteristics of both beaches (beach slope and grain size). They were applied to estimate the response of the two beaches from the values obtained at several points

along the shoreline. Afterwards they were averaged to get a representative value for the entire beach.

(1) Arrigunaga Beach
As it was mentioned before, this beach is characterized by an intertidal zone mainly composed by pebbles, boulders and rocky planforms, with a small percentage of sand. Due to this fact, the application of these parameters is not really a valid procedure. In any case, associated to the wave height increase at the breaking zone expected after the construction of the new breakwater (following the results of the model), the parameters will also increase indicating a higher probability of erosion. However, this must be taken as indicative because the parameters have been derived for sandy beaches, and although their values can be high, the energetic conditions generated by incident waves could not be high enough to move this coarse material.

(2) Ereaga Beach
The application of the presented parameters to this beach give identical results. In all cases (for each parameter and for each wave condition) their value decreased (see Table 3) except for the value of Iribarren's parameter, due to the estimated decrease of wave height at the breaking zone. This decrease means that under similar incident wave conditions, the beach will be more stable in terms of cross-shore movement. The increase in the value of Iribarren's parameter means that the prevailing breaking types will be plunging/collapsing, which are associated to reflective beaches.

Table 3 Estimated averaged values of profile behaviour parameters before and after the construction of the new breakwater for the selected wave conditions (C1, C2, C3 and C4, see chapter 3)

	C1		C2		C3		C4	
parameter	bef.	aft.	bef.	aft.	bef.	aft.	bef.	aft.
Ir	1.9	2.7	3.4	4.7	1.9	3.0	2.3	2.8
D	5.1	2.7	2.6	1.3	3.8	1.5	4.1	2.6
SH	38	19.8	22	11.5	27	10.4	29	19
HK	1.28	0.68	0.65	0.33	0.95	0.37	1.02	0.66
P(*)	55.3	13.7	20.2	5.7	27.2	4.3	28.7	12.2

bef: before the construction, *aft*: after the construction of the breakwater, *(*)*: values in thousands

6. FURTHER WORKS

To supplement this initial theoretical study, a monitoring programme is being now carried out to evaluate the real response of both beaches. This programme will cover a period of 5 years, in which several type of measurements will be performed. The field campaigns are oriented to

cover hydrodynamic and morphological aspects in which the following parameters are being controlled: *waves inside the harbour* (by means of a DATAWELL directional waverider buoy located at shallow water, depth=15 m); *currents* (tidal and wind but not wave induced) *inside the harbour* (by means of two AANDEERA RCM7 currentmeters, located at a depth of about 10 m); *bathymetric response* (by means of periodical campaigns of bathymetry and topography of both beaches); *coastal morphology* (by means of aerial photographs) and *sediment variability* (by means of periodical sediment sampling at the same control points that those used for beach profiling).

These measurements supplement the more general-purpose permannet campaign carried out by the Bilbao Port, which includes *tides*, *meteorology* and *offshore waves*.

This monitoring programme was launched by the end of 1992, and its development will cover the previous situation (before the construction of the new breakwater), the actual situation (during the construction) and the future stage (after the construction). The behaviour of the beaches during all phases of the project is being recorded, and it will serve to estimate the real beach evolution, which will be compared to the predicted behaviour.

7. SUMMARY AND DISCUSSION

Great expansion works have been undertaken by the Bilbao Harbour in order to satisfy its present and future necessities. After various technical and economic studies, a solution consisting in the construction of a new breakwater and the corresponding counterdike was selected.

Wave conditions inside the harbour area will be modified by these new structures. Neighbouring beaches in particular, could be affected by wave reflections coming from the main breakwater. For this reason various studies with a wave propagation numerical model were carried out in order to detect and prevent these effects.

The most energetic waves which penetrate into the estuary are those coming from N and NW. Several wave propagation cases with different periods and heights were performed in both directions, for both harbour layouts (with and without the new breakwater). Numerical simulation showed that waves coming from the NW are reflected from the breakwater and wave heights are thus slightly increased near Arrigunaga beach. On the contrary, these storms produce a remarkable decrease of wave heights in Ereaga Beach. This latter effect is also observed when waves come from the N, while conditions in Arrigunaga Beach are quite similar before and after the construction of the breakwater.

Using the results of the wave propagation study, the response of Arrigunaga and Ereaga beaches was estimated. To do this, the beach response was divided in longshore and cross-shore components. With respect to the beach planform response, results seem to indicate that the Ereaga beach will be more stable under the new situation (*i.e.* after the construction of the new breakwater) due to the decrease in longshore transport rates along the beach and, specially, due to the decrease in transport rates gradients. On the other hand, the potential longshore transport rates along the Arrigunaga beach will increase under the new situation, which implies a potentially higher wobbling of the beach. However, as the beach is composed by different

types of sediment, mainly pebbles, cobbles, rocky outcrops and, in a lower percentage, sand, the real effect can not be directly inferred. The longshore transport formulation should be corrected for this combination of sediment sizes and some treshold criteria for the very coarse sediments should be included. The response of the beach could be significantly less than the one estimated.

Similar results have been obtained for the cross-shore evolution. The Ereaga beach will be more stable under the new situation due to the decrease in the incident waves, whereas the Arrigunaga beach will be more easily eroded. As for the case of shoreline configuration, the response of the Arrigunaga beach must be taken as indicative, because the used criteria have been derived using sandy beaches.

To estimate the real response of both beaches, the Bilbao Harbour Authority has launched a 5 years monitoring programme, in which hydrodynamic and morphodynamic conditions will be permanently controlled. These field campaigns will cover the situation before, during and after the construction of the new breakwaters. Results derived from the field data will serve to validate numerical model results and will be used to design further coastal protection works in both beaches if necessary.

ACKNOWLEDGEMENTS

This study is supported by the Bilbao Harbour Authority. At the begining of the study, Mr. J.J. Uzcanga was the director of the study and the authors wish to acknowledge his support during that period. We extend these thanks to Mr. J. Catasús who worked in the project during the initial stage.

REFERENCES

Abbott, M.B. and F. Ionescu (1967): On the numerical computation of nearly-horizontal flows, J. of Hydraulic Research, 5, pp.97-117.

Abbott, M.B., A. Damsgaard and G.S. Rodenhuis (1973): System 21 Jupiter. A design system for two-dimensional nearly horizontal flows, J. of Hydraulic Research, 11, pp.1-28.

Battjes, J.A. (1974): Surf similarity, Proc. 14th Coastal Engineering Conf., ASCE, pp.466-480.

Brampton, A.H. and J.M. Motyka (1987): Recent examples of mathematical models of UK beaches, Coastal Sediments'87, ASCE, pp.515-530.

CEDEX (1990): Informe sobre las influencia de las obras de la ampliación del Puerto de Bilbao en las playas de Arrigunaga y Ereaga, MOPTMA, Madrid, 26 p. and annexes (in Spanish).

CEEOP (1983): Informe sobre los efectos previsibles de la construcción de los diques de Punta Lucero y Punta Galea sobre las playas de Ereaga y Arrigunaga, MOPTMA, Madrid, 16 p. and annexes (in Spanish).

Dalrymple, R.A. (1992): Prediction of storm/normal beach profiles, J. of Waterways, Port, Coastal and Ocean Engineering, 118, 2, pp.193-200.

Dean, R.G. (1973): Heuristic models of sand transport in the surf zone, Proc. Conf. on Engineering Dynamics in the Surf Zone, pp.208-214.

Hanson, H. and N.C. Kraus (1989): GENESIS-Generalized Model for Simulating Shoreline

Change, Technical Report CERC-89-19, Vicksburg MS, 247p.
Hasselman, K. et al. (1973): Measurements of wind-wave growth and swell decay during the Joint North Sea Wave Project (JONSWAP), Deut. Hydrogr. Z., A8 (no. 12).
Hattori, M. and R. Kawamata (1980): Onshore-offshore transport and beach profile change, Proc. 17th Coastal Engineering Conf., ASCE, pp.1175-1193.
Iribarren, C.R. and C. Nogales (1949): Protection des ports II, Comm. 4, 17th Int. Navig. Congr., Lisbon.
Kraus, N.C. (1987): Prediction models of shoreline change, Nearshore Dynamics and Coastal Processes, K. Horikawa ed., University of Tokyo Press, Tokyo, pp.321-373.
Kraus, N.C. and S. Harikai (1983): Numerical model of the shoreline change at Oarai Beach, Coastal Engineering, 7, pp.1-28.
Jiménez, J.A., V. Gracia and A. Sánchez-Arcilla (1993a): I campaign of sediment sampling in the Ereaga and Arrigunaga beaches (June 93). Preliminary results, Laboratori d'Enginyeria Marítima, Technical Report, 26p. and annexes (in Spanish).
Jiménez, J.A., A. Sánchez-Arcilla and M.J.F. Stive (1993b): Discussion on Prediction of storm/normal beach profiles, J. of Waterways, Port, Coastal and Ocean Engineering, 119, 4, pp.466-468.
Mimura, N., T. Shimizu and K. Horikawa (1983): Laboratory study on the influence of detached breakwater on coastal change, Coastal Structures' 83, ASCE, pp.740-752.
Nicholls, R.J. and P. Wright (1991): Longshore transport of pebbles: experimental estimates of K, Coastal Sediment'91, ASCE, pp.920-933.
Osaza, H. and A.H. Brampton (1980): Mathematical modelling of beaches backed by seawalls, Coastal Engineering, 4, pp.47-63.
Peregrine, D.H. (1967): Long waves on a beach, J. of Fluid Mechanics, 27, pp.815-827.
Sánchez-Arcilla, A. and J.L. Monsó (1985): Flow numerical modelling in nearshore areas, Programa de Clima Marítimo, MOPU, 7, 236p. (in Spanish).
Sánchez-Arcilla, A. and J.L. Monsó (1986): Numerical modelling of coastal flow, Proc. ENVIROSOFT'86, Los Angeles, USA.
Sánchez-Arcilla, A., J.L. Monsó and J.P. Sierra (1986): Non linear numerical model of free surface waves, Programa de Clima Marítimo, MOPU, 17, 125p. (in Spanish).
Sánchez-Arcilla, A., J. Catasús, J.A. Jiménez and J.P. Sierra (1991): Study on the influence of the construction of the Ciervana breakwater on the Ereaga and Arrigunaga beaches, Laboratory d'Enginyeria Marítima, Technical Report, 50p. and annexes (in Spanish).
Sierra, J.P. (1990): Hydrodynamical analysis of non linear wave record transference, Unpublished Ph.D. Tesis, Universitat Politècnica de Catalunya, Barcelona, 310 p. (in Spanish).
Sierra, J.P., A. Sánchez-Arcilla, J.J. Egozcue and J.L. Monsó (1988): Effect of Boussinesq-type equations on wave spectra propagation, Proc. 21st Coastal Engineering Conf., ASCE, pp.350-362.
Sunamura, T. and K. Horikawa (1974): Two-dimensional beach transformation due to waves, Proc. 14th Coastal Engineerging Conf., ASCE, pp.920-938.
Villanueva, E.J. and J.J. Uzcanga (1993): Bilbao Harbour enlargement. Walls against the sea, Cauce 2000, 58, pp.40-47, (in Spanish).

HYDRO-PORT'94
International Conference on Hydro-Technical
Engineering for Port and Harbor Construction
October 19 – 21, 1994, Yokosuka, Japan

Littoral Drift in Fishing Ports and Approach Channels: Problems and Countermeasures

Masatsugu Fukuya
Nobuo Takaki
Kazuo Ota
Soichi Harikai
Masato Ikeda

The Japanese Institute of Technology on Fishing Ports and Communities
6-13-16 Akasaka, Minato-ku, Tokyo

ABSTRACT

Study on littoral drift in fishing ports and approach channels is important both to beach protection and port construction. This paper first reviews on the current state of the drift sand problem and its countermeasures on the basis of a survey questionnaire amongst approximately 3000 fishing ports in Japan. Then, a case study on the littoral drift problem and its countermeasures at Monbetsu fishing port located at a typical sandy drift beach is carried out through field surveys and numerical simulation. Finally, a new type of countermeasure against the drift problem being developed in a few fishing ports is introduced.

Key Words: Littoral Drift, Countermeasures, Field Surveys.

1. INTRODUCTION

There are approximately 3000 fishing ports in Japan. Using a simple calculation, this figure shows an average of about one fishing port for every 10 km of coastline. Actually, sandy beaches make up about 1/3 of the Japanese coastline, and although fishing ports have been constructed along these coasts, development has lagged behind that of rocky coasts.

One reason for this is sand deposition. Fishing ports tend to be small, and the entrances are often located in relatively shallow water of 5-6 meters deep. Littoral drift readily leads to an accretion at port entrances and approach channels, and furthermore results in the function loss of the ports. Much research has been done on the problems of littoral drift, but many engineering issues remain poorly understood, and effective countermeasures are difficult to design and implement.

To bear this idea in mind, this paper examines current state of the problems of littoral drift at fishing ports of Japan, and then focuses on prediction of sedimentation and countermeasures against them.

2. CURRENT STATE OF DRIFT SAND PROBLEMS AND THEIR COUNTERMEASURES IN FISHING PORT OF JAPAN

A questionnaire was conducted at approximately 3,000 fishing ports of Japan in 1990, to assess the most recent conditions of the drift sand problem. The questionnaire focused on the various details of drift sand problems (sand deposition in harbors or/and channels, etc.), the causes, the varieties of improvement work, the histories of drift sand surveys, and the conditions of surrounding beaches.

In order to identify regional characteristics, the results of the questionnaire were classified into four groups of fishing ports which are located in, namely, closed inner bay and inland sea, and open bay and open sea areas (Sea of Japan, Northern Pacific Ocean and Southern Pacific Ocean).

According to the results of this questionnaire shown in Fig. 1, drift sand problems have been encountered at 349 fishing ports, or approximately 12%, and almost all of which involved sand deposition inside harbors and at harbor entrances. The causes identified include longshore drift (in 45% of cases), wave-induced drift toward harbors (sand is carried by waves, transported directly into the harbor and then deposited in it; 35%), the drifts from river flow (35%) and due to nearshore circulation (approximately 30%).

Regionally the frequency of sand deposition problems occurring inside harbors and at harbor entrances was highest in inner bay and inland sea areas, followed by the Japan Sea, Southern Pacific and Northern Pacific areas, in descending order. The occurrence of such problems was higher in inner bay and inland sea areas, but fairly evenly among the other areas.

In regards to countermeasures, more than half of them had resorted to dredging. Most structural improvements involved the installation and extension of

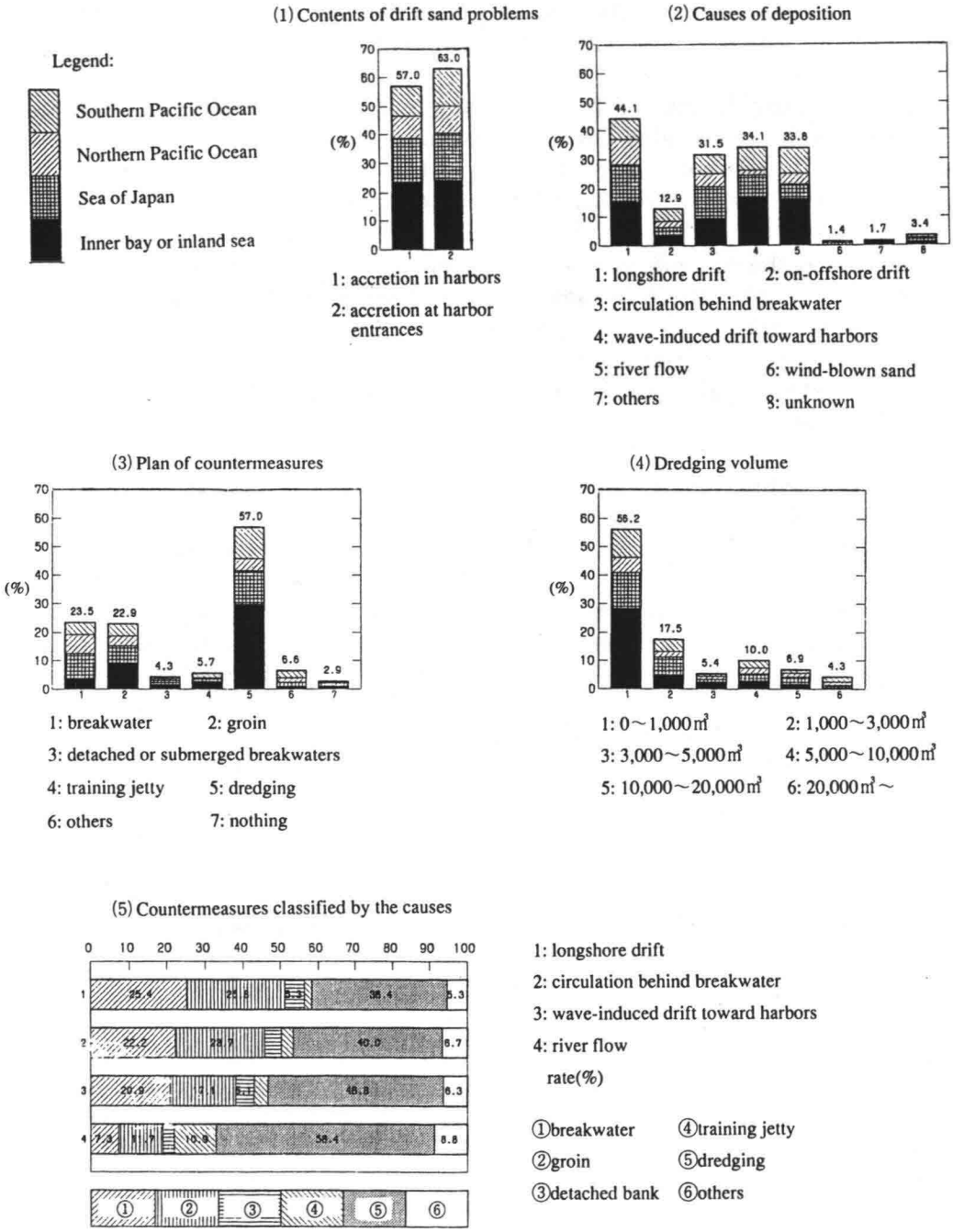

Fig. 1 Results of the questionnaire for drift sand problems

breakwaters and groins, and some cases involved the usage of detached breakwaters or offshore banks. In many cases a combination of several countermeasures were implemented, but the percentage of fishing ports implementing only dredging was high at approximately 40%.

Though dredging is one of the more common countermeasures for various problems, groins were also used for dealing with sand deposition caused by longshore drift and sediment drift due to nearshore circulation. Sand deposition caused by river flow was dealt with by dredging in most cases.

In considering the regional characteristics of countermeasures, it was found that dredging was implemented in most cases at inner bays and inland seas, and the amount of dredging required was relatively limited. However, dredging was less adopted in Northern Pacific areas, where the amount of dredging was fairly great, and structural work such as breakwaters and groins were also used instead in most cases.

As mentioned previously, sand deposition on harbor entrances and inside harbors caused by sediment transport from river flow and by wave-induced drift toward harbors are frequent problems at inner bay and inland sea areas, but the amount of dredging is relatively limited. It should be noted that though drift sand surveys have not been conducted at most of these fishing ports, dredging is planned for coping with drift sand problems in the future. On the other hand, in open bay and open sea areas there were many cases of drift sand carried by high waves and deposited at harbor entrances and inside harbors, and the amount of dredging was considerable. In those cases countermeasures were found to include not only dredging but also structural improvements such as the installation of breakwaters, groins, etc.

In compiling the data structural improvement work according to the various causes of drift sand problems is listed in Tables 1 and 2. Structural improvements are most commonly applied at the updrift side of deposits, at the tip of breakwaters, or at harbor entrances, when attempting to prevent longshore sediment transport.

For the prevention of sediment transport due to nearshore circulation, groins are most commonly used. However, careful consideration must be taken regarding the placement of groins to avoid excessive coverage of main breakwaters and thus to control nearshore circulation caused by the main breakwaters. Though prevention of wave-induced drift toward harbors is difficult to deal with, maintaining sufficient water depth at harbor entrances must be considered when planning fishing port and improvement work.

In regarding the planning and evaluation of improvement work, understanding

Table 1 Types of improvement work for preventing (a) longshore drift

Types	Characteristics	Types	Characteristics
A-1-1: Offshore bank 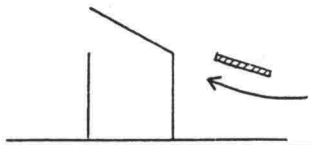	Interception and reduction of longshore drift toward the tip of breakwater by an offshore bank. Cases: Atuga, Yagumo, etc.	A-3-1: Extended breakwater at harbor entrance 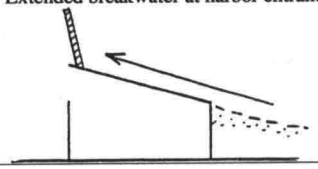	For a considerably great longshore drift to be dealt with on the updraft side of breakwater, a groin is added at the tip of the breakwater. Cases: Miyazaki, Iioka, etc.
A-1-2: Offshore bank 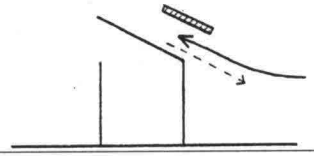	Same as above. In addition, an opposing drift is expected with seasonally changes of wave direction. Cases: Monbetu, Sibetu, Siomi, Settupu, etc.	A-4-1: Offshore harbor entrance (type 1) 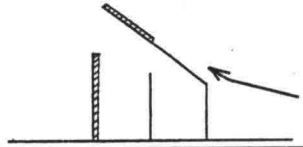	Harbor entrances are extended till to a certain water depth whereby a small littoral drift. Cases: Otosibe, Isohama, Kawaminami, etc.
A-2-1: Groin (land jetty) 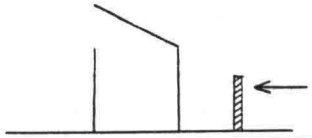	Obstruction and reduction of longshore drift toward the tip of breakwater by a jetty. Cases: Higashiura, Sikanosima, etc.	A-4-2: Offshore harbor entrance (type 2) 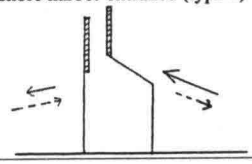	Same as above. For a longshore drift in opposite two directions. Cases: Atunai, etc.
A-2-2: Groin (vaned dike) 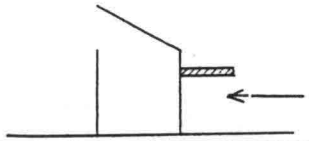	Same as above. (Obstruction by a vaned dike) Cases: Taito, Hamaonisibetu, Reuke, etc.	A-4-3: Offshore harbor entrance (type 3) 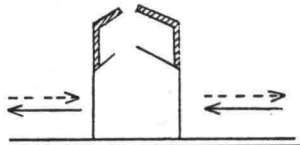	Same as above. Cases: Ootsu, Nagatu, etc.
A-2-3: Groin (port jetty) 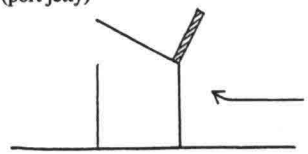	Same as above, but more effective than A-2-1 and A-2-2. Cases: Tomihama, Settupu, etc.	A-4-4: Sand bypass 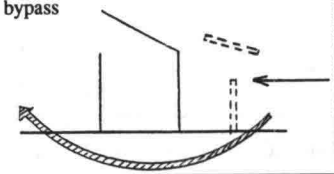	Bypassing the windward deposition caused by longshore drift to the leeward and at the same time preventing erosion on the leeward shore. Cases: Miyazaki , Iioka, etc.

Table 2 Types of improvement work for the prevention of littoral drift (b) due to nearshore circulation and (c) by wave-induced drift toward harbors

Types	Characteristics	Types	Characteristics
B-1-1: Arresting detached breakwater 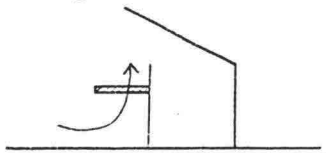	Obstruction and reduction of the sedimentation due to the circulation heading toward the entrance by an offshore bank. Cases: Isozaki, Katagai, Hazaki, etc.	B-3-1: Offshore harbor entrance and groin 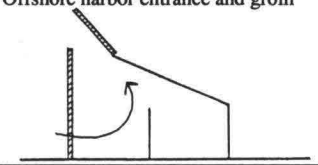	Extension of harbor entrance till to a certain water depth whereby a small littoral drift, and with installation of groin preventing nearshore circulation. Cases: Syari, Isohama, etc.
B-2-1: Sand-blocking groin (type 1) 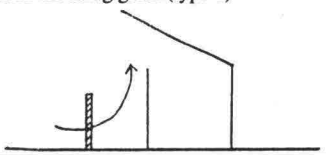	Interception and reduction of sediment transport due to the circulation heading toward the entrance by a jetty. Cases: Seki, Kuwakawa, etc.	B-4-1: Secondary breakwater 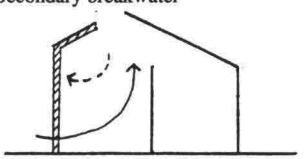	Elimination of deposition at anchorage by a groin controlling nearshore circulation and functioning a key-type secondary breakwater as well. Cases: Nisime, Siina, etc.
B-2-2: Sand-blocking groin (type 2) 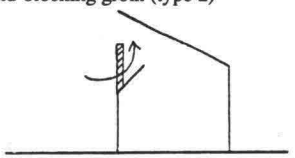	Same as above, and effective for a small circulation limited to a certain area. Cases: Iioka, etc.	C-1: Countermeasure against wave-induced drift toward harbors (1) 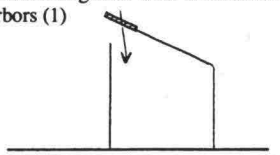	Narrowing of harbor entrance somehow to discourage nearshore circulation.
B-2-3: Groin (type 3) 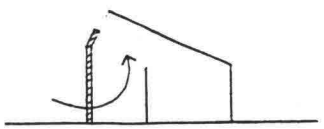	Same as above, and useful only for a large circulation. Cases: Syariki, Wae, Akabane, Maze, etc.	C-2: Offshore bank against wave-induced drift toward harbors. 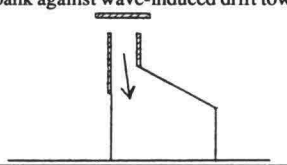	Reduction of wave-induced drift to harbors by reducing wave height at harbor entrances. Cases: Wae, Kitae, Yotukura, etc.
B-2-4: Groin (type 4) 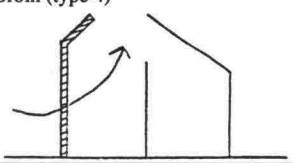	Same as above, and applicable when fishing ports have offshore breakwaters. Cases: Ukedo, etc.	D: Others (such as sand pockets) 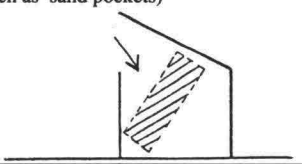	Reduction or restraint of deposition at harbor entrances and in channels by improving dredging methods (responding to different dredging range and location). Cases: Maze, Iioka, etc.

the mechanism of the drift sand phenomenon (deposition) is crucial. And furthermore, though countermeasures may be planned with the mechanism, it is still difficult to completely eliminate the deposition at harbor entrances and inside harbors. A regular monitoring and quantitative evaluation of the effects of improvement work would be important (for example: the volume and the frequency of dredging required each year, the changes in water depth and deposition amounts, etc.).

However, in many cases, the problem of littoral drift could not completely solved, such as the case that improvement work mentioned above was located in shallow water of the entrances, or that accretion at the entrance and inside the port repeatedly occurred with time at the coast with strong drift sand. A common countermeasure adopted against those cases is to extend breakwaters toward offshore, and lay the entrances at a depth of as deep as possible.

3. A CASE STUDY ON LITTORAL DRIFT

Littoral drift was investigated at Monbetsu fishing port in Hokkaido in 1988 and 1992, respectively. The Monbetsu port is located at the western end of the Hidaka coast, which is a prominent littoral drift coast in Japan.

Deposition at the harbor entrances is also considerable at Atsuga fishing port and Seppu fishing port which are located about 12 km and 19 km southeast of the Monbetsu port, respectively. An examination on the arrangement of those two ports had been carried out on the basis of the results of the field investigation and a hydraulics model test untill then.

Along the Hidaka coast, prevailing direction of littoral drift is northwesterly in summer, but in winter littoral drift is recognizable in a southeasterly direction. Therefore, countermeasures against the drift have been taken at the latter two ports by taking advantage of seasonally opposing sediment transport directions, and island banks were built on the offshore side of the breakwaters. As a result, in summer when tombolas occur behind the island bank, the effects of littoral drift at harbor entrances are prevented, and in winter the deposition behind the island bank is discharged to the southeast.

Though the results of these countermeasures have certainly borne fruit, this is not to say that a certain amount of dredging does not also have to be maintained.

Much like the two ports mentioned above, there is a possibility of the sand deposition at the entrance of the Monbetsu port as well. Therefore, countermeasures against the littoral drift for the port construction have been examined for the Monbetsu port.

(1) Review on the Existing Data

In the 1988 survey, the existing data of the observed waves (taken since 1973 at Samani fishing port which is approximately 60 km southeast of the Monbetsu port), the currents, the bed grains, and the topographical changes obtained by aerial photographs, were sorted out to review and analyze them.

It is known, from the data obtained above, that the prevailing wave direction during summer and winter is remarkably different. A SE direction is distinguishable during summer and a SW in winter. Since the Samani and Monbetsu ports are approximately 60 km apart, refraction calculation was conducted for the surrounding areas of the two ports to assess refraction effects. As a result it was confirmed that wave direction was almost the same at both ports.

Surveys of the current characteristics were conducted in 1970 and 1986, respectively, along the surrounding coast of the Monbetsu port, and it was mainly found that the current in the west direction is distinguishable in spring and summer, and in the east in fall and winter, though the directions vary with seasons.

According to a 1985 survey on the bed grains at Monbetsu, the sediments involve a median grain size from 0.125mm to 0.15mm and a fine grain, and they show a uniformly distribution.

Aerial photographs and sounding surveys have been analyzed to reveal characteristics of topographical change. Six pieces of aerial photographs taken in 1947, 1957, 1963, 1971, 1975 and 1983, respectively, indicate that sand accretion has occurred on the east side of the Monbetsu port since it started to be built, while erosion is found on the west side of the port.

Analysis of sounding surveys conducted in 1982, 1983, 1987 and 1988 indicates that in spite of seasonal cycles of sand deposition along the south breakwater in summer, and erosion in winter, overall longshore drift in a year is distinguishably westerly.

(2) Results of Field Surveys

A field survey was conducted. It included the surveys of the incident waves (wave height, period and direction were being observed for 35 days at a station of approximately 10.0m deep), the velocity at a fixed point and direction (observation lasted for one month at three stations shown in Fig. 2), the longshore current (direction and velocity, and wave breaking were observed every 50 m along a 1,100 m shoreline), and the bed grains (at 20 points of the surrounding area of the port).

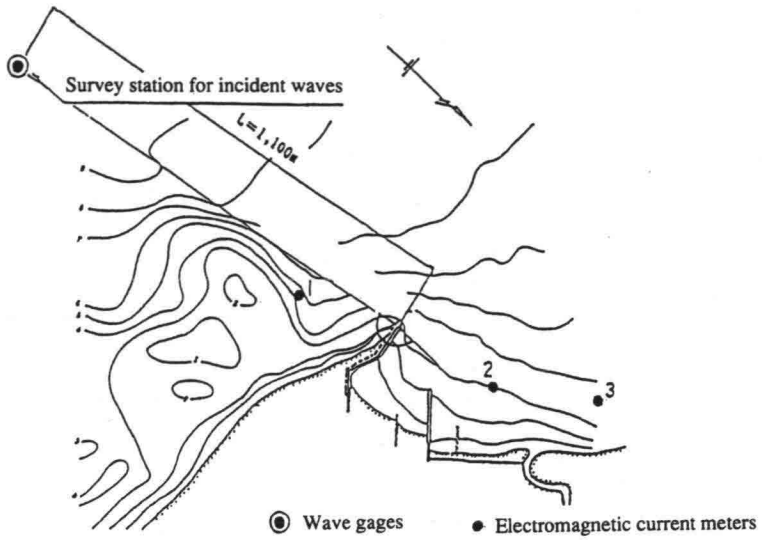

Fig. 2 Locations of measuring instruments in the field survey around the Monbetsu Port

On the basis of the results of the field observation, it is noted that the high wave of more than 2.0m significant wave heights was observed 11 times during the observation period, and its maximum was up to 4.5 m. Amongst the high wave a relatively long period of over 10 sec was observed to last about a week, and a maximum period of $T_{1/3}$ = 16.89 sec.

The prevailing wave direction during the survey ranged from SSE to S. The wave of the Monbetsu port during the survey period was also compared to that of the Samani port, which indicated a strong correlation between the two ports.

Regarding the current during occurrence of high waves, a prevailing wave direction during the survey period was SSE and S, and the nearshore current for both directions was the same. When high waves occur to the S, the current on the east side of the port propagates to the west along the south breakwater, and results in a nearshore circulation near the north breakwater area.

In this way, during summer when wave direction is distinguishably S, it can be reasonably assumed that, by the influence of the S wave the littoral drift direction changes from east to west, whereby sand on the east side of the port is transported to the west along the south breakwater, and deposited within an area from the harbor entrance to the inside of the harbor. However, when wave occurs to the SW in winter, conversely, longshore current is distinguishably easterly (See Fig. 3).

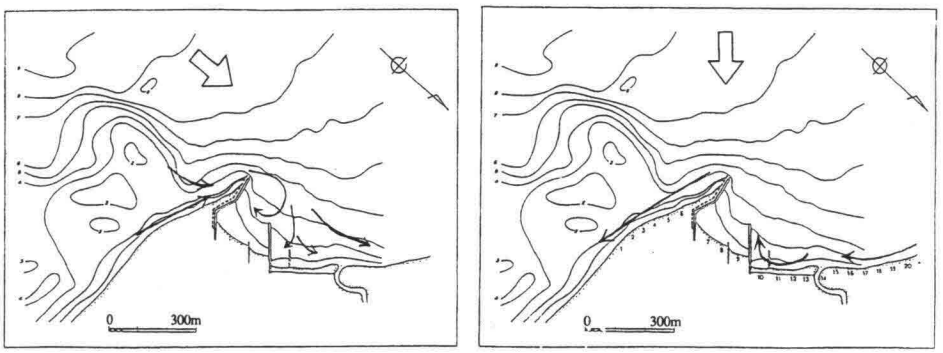

(1) By summer wave (in the S) (2) By winter wave (in the W)

Fig. 3 Diagram of the nearshore current patterns around the Monbetsu Port

(3) Numerical Simulation on Proposals

On the basis of the existing data and the results of the field surveys, the port configuration has been examined by numerical simulation to inhibit sand deposition at the harbor entrance when the fishing port is built.

As mentioned previously, in the surrounding area of the Monbetsu port, longshore sediment transport occurs in opposite directions between summer and winter, and though the direction repeatedly fluctuates throughout the year, overall longshore sediment transport is distinguishably westerly and, due to littoral drift along the south breakwater, sand deposition at the entrance may result in a problem. In consideration of all these factors, an examination based on the following three basic proposals was conducted (Ref. Fig. 4).

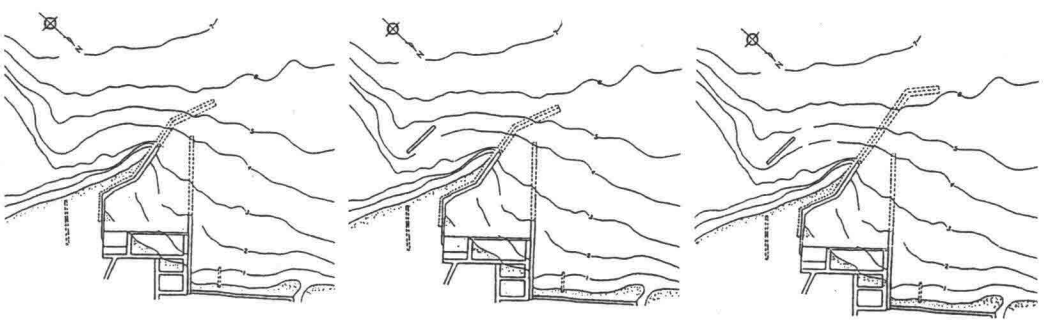

(proposal A) (proposal B) (proposal C)

Fig. 4 Layout of the proposals for the Monbetsu Port

Proposal A: The south breakwater should be further extended to prohibit sand from drifting into the harbor entrance.

Proposal B: A offshore bank or detached breakwater should be added on the offshore side of the south breakwater of proposal A as an additional improvement work of littoral sand. The purpose of the offshore bank is to take advantage of seasonal wave characteristics near the Monbetsu port and to control sand deposition at the entrance through formation of a tombolo in summer, and release the sand of the tombolo to the east in winter.

Proposal C: The south breakwater of proposal A should be extended along the same orientation, and the entrance should be moved to the point where water reaches a depth of 6 m, in order to facilitate currents along the south breakwater by winter waves, and to facilitate an easterly release of the deposited sand in front of the south breakwater.

With the simulation results of proposal A, it has been found that sand will continue to be dropped at along the south breakwater in summer, and that the tip of the south breakwater will eventually lie in a shallow water.

Both proposals B and C were suggested for controlling sand deposition at the harbor entrance through formation of a tombolo behind the offshore breakwater in summer and release the sand of the tombolo to the east in winter. However, the effect was insufficient, therefore further examination was carried out in regards to the length and location of the offshore breakwater.

At the beginning, this type of offshore bank was considered to have two functions. Firstly, it intercepts littoral sand heading toward the harbor entrance when waves occur in summer. Secondly, it causes a current in an opposite direction along the south breakwater when waves occur in winter, and releases the deposits in summer to the east during winter.

Examination on the various layouts of offshore banks was conducted with numerical simulation, but it was found that it is very difficult to achieve the latter of the above functions on the offshore banks. However, as an improvement work to prevent the littoral sand from moving toward the harbor entrance along the south breakwater, the offshore bank is most effective.

When an offshore bank is built there is a current from the back of the offshore bank toward the harbor entrance when waves occur in summer. However, if a groin with a strong sand catch is built, instead, tombolos will be formed behind it, and then eventually develop and become completely connected, and thus can not only shut out the current, but also release the current toward the offshore. Therefore it can be expected that this will reduce the transport of littoral sand toward the harbor entrance, and slow down the accretion on the entrances.

Simulation on the littoral drift before and after the tombolo formation was carried out. The simulation results, as shown in Fig. 5, indicate that regardless of the shape of the south breakwater, if the offshore bank is extended, the quality of the sand interception function is high and effective when wave occurs in summer.

The results of the simulation even revealed that the offshore bank will also function as a jetty after the tombolo formation, and will cause the nearshore current to head toward the offshore. Since the current is not easy to approach the harbor entrance the drift sand does not appear on it. On the basis of those analyses above, therefore, it was judged that the offshore bank can be an effective measure for protecting harbor entrances from drift sand after tombolo formation.

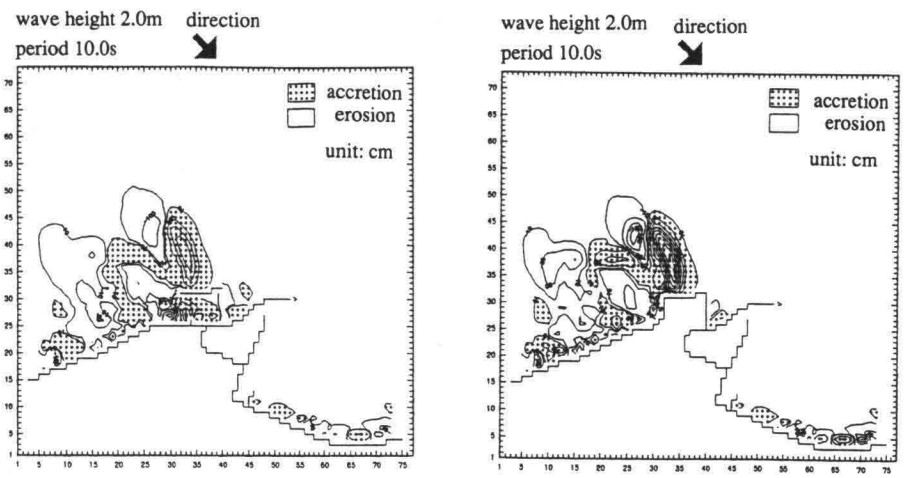

(Before tombolo formation) (After tombolo formation)

Fig. 5 Simulation results of interim proposal for the Monbetsu Port

Regarding the shape of the south breakwater, there was no significant difference between proposal B, C and their interim proposal. When considering, however, that the harbor entrance should be located as far as possible away from the wave breaking zone, and that there is a possibility of longshore wave and reflected wave transporting sand to the east in winter, it is preferable to extend the south breakwater. Thus the interim proposal shown in Fig. 6 was adopted.

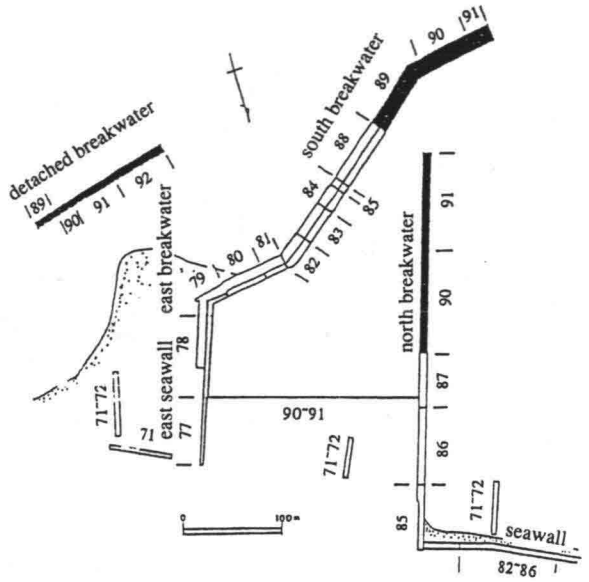

Fig. 6 Progress of the breakwater construction at the Monbetsu Port

(4) Topography Change with Constructed Breakwater

With the interim proposal, as shown in Fig. 6, the development of the fishing port started in 1989. According to the simulation results above, in the front area of the port (from the south breakwater to the east side area), quite a lot of sand was deposited on the east side of the south breakwater extended between 1982 and 1985. Later, during repeated changes between winter accretion and summer erosion, a tendency of sand deposition prevailed.

However, when the offshore bank, which was constructed since 1990, was extended in August of 1992, the effect of the offshore bank has been conspicuous while sand deposition behind the offshore breakwater and in the front of the south breakwater have declined (See Fig. 7).

Approximately 250,000m^3 of sand have been deposited over the last 10 years between the front and the east side of the south breakwater, so there is not so small a sediment transport of littoral sand from the east side toward the port. Sand has also continued to slowly accumulate on the east side of the tip of the south breakwater and on the west side (near the entrance). Since very little time has passed since the construction of the offshore bank, the topography changes must be carefully monitored in the future.

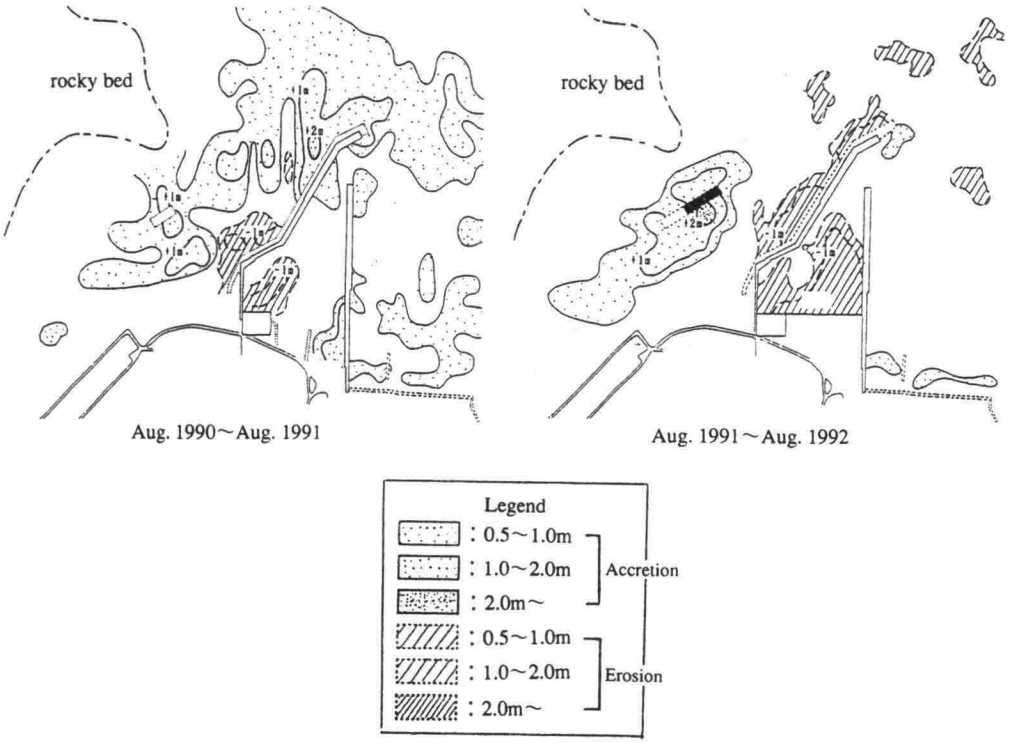

Fig. 7 Topography change between 1990 and 1992 at the Monbetsu Port

4. A NEW TYPE OF COUNTERMEASURE AGAINST LITTORAL DRIFT

Littoral drift countermeasures which have been implemented include dredging, construction or extension of breakwaters and groins, as mentioned before. Even with such steps as those, however, it is difficult to completely eliminate the littoral sand problem. In addition, if the size of groins and so on is increased, the effect of these changes on surrounding beaches will also increase. Therefore, a new type of countermeasure, so-called island fishing port, against littoral drift was recently developed.

For a fishing port it is necessary to not only satisfy the normal functions of the fishing port, but also maintain the continuity of sand transport along coasts and thus minimize the effects on surrounding beaches. It was in light of those goals that the idea of a fishing port on an offshore island, connected to the mainland beach by a bridge, was conceived, and for which planning and development were implemented. An offshore island port not only solves the problems of littoral drift, but also provides a calm water area for marine recreational use and marine life cultivation.

Construction of the island fishing ports is currently underway at the four sites of Kunnui Port (Oshamanbe-cho, Hokkaido), Kizukuri port (Kizukuri-cho, Aomori Pref.), Michikawa port (Iwaki-cho, Akita Pref.) and Kutsuo port (Yukuhashi City, Fukuoka Pref.), and an outline of these fishing ports is shown in Table 3.

Kunnui, Kizukuri and Michikawa ports are designed with the island type to counter littoral drift problems, but Kutsuo port is to reduce the effects of tide flat. All four of these ports are still under construction, the port at Kunnui is the fastest, and it would not be long to be utilized.

The construction of Kunnui fishing port, with the most rapidly progress so far, has been underway since 1988. As shown in Fig. 8, during the construction, the shoreline behind the island is extending forward. However, only at one location along the coastline 150m away from the island, there is a slight tendency of sand deposition, but large-scale beach erosion and accretion have not occurred. At locations 400 m away from the island there are almost no observable effects of the island port construction. As expected at the beginning of the construction, securing the continuity of longshore sediment transport has been found to be successful so far. A survey on littoral drift inside the harbor and on changes of beach topography behind the fishing port is planned as the port construction is completed in the future.

A trace survey on Michikawa fishing port being constructed since 1989 is being conducted over a very wide area to assess the effects and the topographical changes resulting from the port development. To survey over a wide area, 20 observation sites were determined within approximately 45 km of the beach surrounding the Michikawa port, and the changes of the shoreline and the median grain size are regularly observed. In addition, sounding survey is also carried out twice a year as a trace observation of the topographical changes in the surrounding area of the port. Currently there have been no changes detected in the wider area, though a tombolo began to form at the beach behind the port. Continuation of these surveys at the Michikawa port are planned.

Table 3 Outlines of the four island fishing ports

Item	Kunnui port	Kizukuri port	Michikawa port	Kutsuo port
Shape	wine glass type	tulip type	wine glass type	tulip type
Water depth at harbor entrance	6m	7m	7m	3m
Maximum width	approx. 190m	approx. 200m	approx. 240 m	approx. 290m
Offshore distance	247m	172m	350m	400m
Designed wave Height	Ho = 8.0m	Ho = 9.0m	Ho = 11.3m	Ho = 6.2m
Locations	sandy beach, inner bay	sandy beach, inner bay	sandy beach, open sea	tide flat, inner bay
Reasons for construction	promote fisheries, prevent littoral drift inside harbors and reduce effects on surrounding beaches	promote fisheries, prevent littoral drift inside harbors and reduce effects on surrounding beaches	promote fisheries , prevent littoral drift inside harbors and reduce effects on surrounding beaches,	promote fisheries , prevent littoral drift inside harbors and countermeasures against high and low tides, etc.
Survey items	field survey, hydraulic experiments, shoreline change prediction, etc.	field survey, shoreline change prediction, etc.	field survey, shoreline change and 3D beach deformation predictions.	shoreline change and 3D beach deformation predictions, etc.
Conditions of surrounding fishing ports	conducted to maintain approx. 3,000 m³ of dredging per year at Rebun fishing port	conducted to maintain approx. 15,000 m³ of dredging per year at Shariki fishing port	conducted to maintain approx. 11,500 m³ of dredging per year at Matsugasaki fishing port	port was buried by littoral sand at old Kutsuo fishing port, and can not be used during low tide

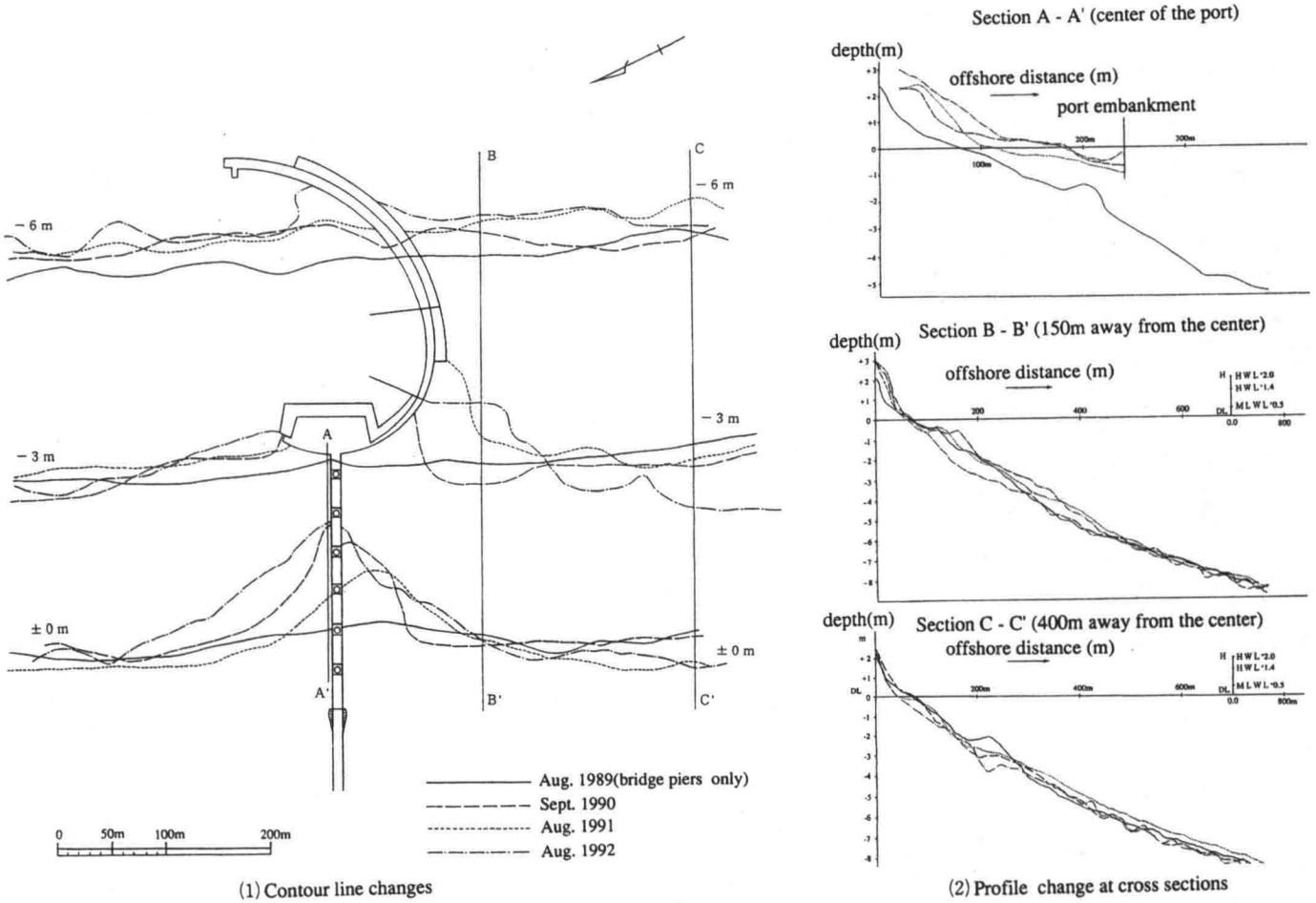

(1) Contour line changes

(2) Profile change at cross sections

Fig. 8 Topography change at Kunnui fishing Port

5. CONCLUSIONS

This paper focuses on the problems of drift sand and their countermeasures at fishing ports of Japan. About 12% of the fishing ports encounter the littoral drift problem according to a survey questionnaire amongst approximately 3000 fishing ports in Japan. In regards to their countermeasures, more than half of them had resorted to dredging, and longshore drift and sediment transport due to nearshore circulation are dealt with by breakwaters and groins in most cases. In addition, an offshore bank or detached breakwater with extension of the breakwaters and groins towards offshore is verified to be effective to prevent longshore drift through a case study on Monbetsu Fishing Port.

However, it is very difficult to completely eliminate the littoral sand problems in case of considerable littoral drifts. Therefore, a new type of countermeasure, so-called island fishing port, against the drift is proposed, and adopted at a few fishing ports being constructed in Japan. It could be expected that this island fishing port is more effective to solve the problems of littoral drift in the future.

Obviously, a great progress has been made on the problem of littoral drift, especially, by numerical simulations. However, the applicability of the numerical models , used in examinations and predictions untill now, to the field conditions is less than perfect due to the problems of the treatment on the wave-induced drift toward harbors, and of the quantitative evaluation on topographical change and the predictive period of the change. Therefore, there is great hope for future research.

There is also concern with land preservation issues in recent years due to the growing problem of beach deformation resulting from beach erosion and the installation of coastal structures. Thus the challenge for fishing port development is not only the concern for maintaining fishing port functions but also reducing the impact of improvement work on surrounding beaches. Therefore the location of fishing port construction work should be recognized within a broad perspective of the drift sand beach. A comprehensive examination also considered the latest development of countermeasures against littoral drift, such as island fishing port mentioned in the paper, should be carried out.

REFERENCES

[1] Nagano, A., M. Ikeda and S. Harikai(1992): Drift sand problem and simulation analysis of fishing ports, Proc. Techno-Ocean'92 Symposium, Yokohama, Japan, pp. 49-55 (in Japanese).

[2] Nagano, A.(1993): Introduction to island fishing ports in Japan, J. Japan Society of Civil Eng.(JSCE), Added Vol. 78-12, pp. 112-113. (in Japanese).

HYDRO-PORT'94
International Conference on Hydro-Technical
Engineering for Port and Harbor Construction
October 19 – 21, 1994, Yokosuka, Japan

Stabilization of Beach in Integrated Shore Protection System

Kazumasa Katoh [1]
Shin-ichi Yanagishima [2]
Satoshi Nakamura [2]
Makoto Fukuta [2]

[1] Chief of the Littoral Drift Laboratory
Hydraulic Engineering Division
Port and Harbour Research Institute, Ministry of Transport
Nagase 3-1-1, Yokosuka, Kanagawa 239
[2] Member of the Littoral Drift Laboratory
Hydraulic Engineering Division
Port and Harbour Research Institute, Ministry of Transport

ABSTRACT

As Japan has a long coastline and is exposed to severe natural conditions, strong efforts on the coastal protection works such as detached breakwaters, jetties, seawalls are necessary to prevent the coastal disasters. However, these concrete structures keep the people away from the waterfront. Then, a new shore protection system, namely Integrated Shore Protection System, is going to be developed. There are many technical difficulties remained to be solved in this new system. The most important and difficult subject is to understand the mechanism of sand movement in a storm, and to develop a technique for stabilizing a beach. So, paying attention to an abrupt beach erosion in a storm, field observations have been being carried out since 1986. Several important results obtained are explained, concerning to the actual condition of abrupt beach erosion, an external force of beach erosion, an effect of ground water table on the beach erosion, and Orientation for new methods of beach stabilization.

Key Words: Infragravity Waves, Berm Erosion, Berm Formation, Water Table, HORF

1. INTRODUCTION ; NATURAL AND HISTORICAL BACKGROUND OF SHORE PROTECTION WORKS IN JAPAN

Japan consists of four main islands of Hokkaido, Honshu, Shikoku, and Kyushu from north to south, and it has other various size islands as many as 3600. The total length of her

coastline is approximately 34,000 km, extremely long despite the small land area. The length of coastline for a person in Japan is about 30 centimeters which is twice longer than that in the world, being about 13 centimeters (Komar, 1976). She is a mountainous country and the area of available lands is no more than 35 percent of the total area. For this reason, the available space for economic and social activities are limited and concentrated along the coastal region. On the other hand, the natural conditions around Japan are too severe. The coasts have been always exposed to the menace of attacks of the large waves due to the typhoon in autumn, the strong monsoon in winter, and the low atmospheric pressure in all seasons, and moreover by the storm surge and tsunami as shown in Figure 1, by which, in fact, a large number of lives and properties were lost in the past. Moreover, the most rivers in Japan are short and fast flowing out. Even the longest, the Shinano River, is a mere 367 km from source to mouth. A localized torrential downpour in the Pacific Ocean side area in a rainy season and the thaw melting snow in the Japan sea side area in the spring consequently floods a river. These are the fatal conditions of natural in Japan.

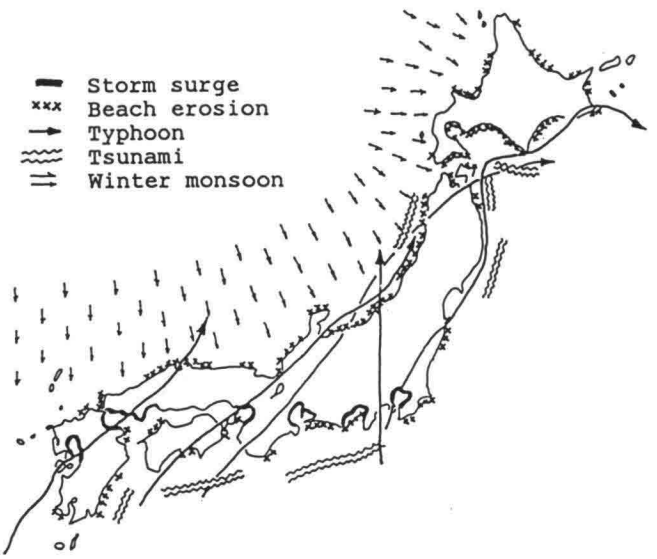

Figure 1 Natural conditions around Japan.

A river improvement has been a matter of major concern historically. The rapid development of river improvement works such as construction of flood channels and dams had gradually reduced the damages due to floods. Such river improvement works, however, brought about extreme decrease of sand volume discharged from the rivers. Also, a large amount of sand was carried away from the river bed to utilize it as the construction material for concrete structures. In addition to that, especially in a period from 1955 to 1964, the ports began to be constructed on sandy beach in earnest on an unprecedented scale in number and size. Furthermore, there were a rapid development of coastal regions by land reclamation. To the matter worse, large−scale disasters happened

concentratedly and continuously during this period. Those are the Toyamaru typhoon (Sep. 1954), the Kanogawa typhoon (Sep. 1958), the Isewan typhoon (Sep. 1959), the Chili Earthquake tsunami (May 1960), and the Second Muroto typhoon (Sep. 1961), etc. Particularly the Isewan typhoon, which hit Ise Bay of the central Japan, brought a tremendous damage of 5,101 killed and completely and partially destroyed houses of 153,893. Due to the combined effects of these factors, the beach erosion problem became more chronically serious in the whole country of Japan.

In the early stage of beach erosion, planned and employed measures were to construct jetties or to place wave breaking works in front of a seawall. The jetties have a function to obstruct the longshore sediment transport by waves, which prevents the sand from being washed away and promotes the sand accretion. They, however, cannot bring their functions into full play for the offshoreward sand transport by the normally incident large waves. Researches on the effects of jetties had been done by the first half of 1960's, of which results have been put in the standard of design in Japan up to this time. Since around 1970, detached breakwaters have been constructed as a general countermeasure for the beach erosion. When the bottom sediment could be expected to be supplied from offshore to onshore side of the detached breakwater, the insular type with gaps was adopted. When it could not, the continuous type without gaps was adopted. In the former case, the sand deposited behind it forming a tombolo or a salient which occasionally reduced the rate of longshore sand transport. As a result, the detached breakwaters were rapidly and widely employed.

In the following undertaking of the shore protection works, it was necessary for the nearly defenseless coast to extend the protected coastline as fast as possible. Many coasts in Japan were protected by most of detached breakwaters, jetties, embankments or seawalls,

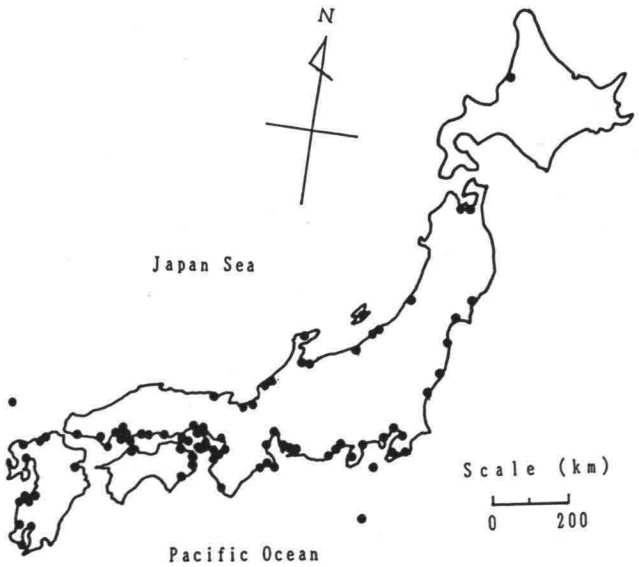

Figure 2 Locations of artificial beach.

and wave energy dissipation blocks. Anyhow, the further erosion to the hinterland had been stopped, but many sandy beaches disappeared.

As the space for sea bathing, which has been the most popular marine leisure in Japan since the old time, decreased little by little in 1960's, suitable beaches for it were demanded to be created. Then, artificial beaches were planned and began to be constructed in many locations. Figure 2 shows the locations of artificial beaches at present. Since volume of sand to be supplied was insufficient and sand was valuable in Japan, it was hard to continuously nourish the artificial beach as it was done in United States of America. Therefore, it was basically important in design to take some facilities into consideration in order to keep the sand inside the beach from being washed away. This was the nearly same technique as those developed as the countermeasures of beach erosion. That is to say, the detached breakwaters and jetties have been constructed to stabilize the artificial beach. It must be said that the purpose of the artificial beach is to make an offer of a recreation zone for people, but not to protect the hinterland from huge waves.

2. CONCEPT OF INTEGRATED SHORE PROTECTION SYSTEM (ISPS)

The constructions of shore protection facilities have been proceeded up to this time. There are, however, some consciousness of problem in the present protection system as follows;

(1) The present shore protection facilities keep the people living in the hinterland away from the waterfront. The views of coastal regions are worse than what it was. The demand for a better quality of protection gets greater along with improvement of a living standard, and multipurpose use of valuable coastal zone comes to be required.

(2) Many artificial beaches have been created to take back the lost beaches. However, they are not designed from a standpoint of prevention of coastal disasters.

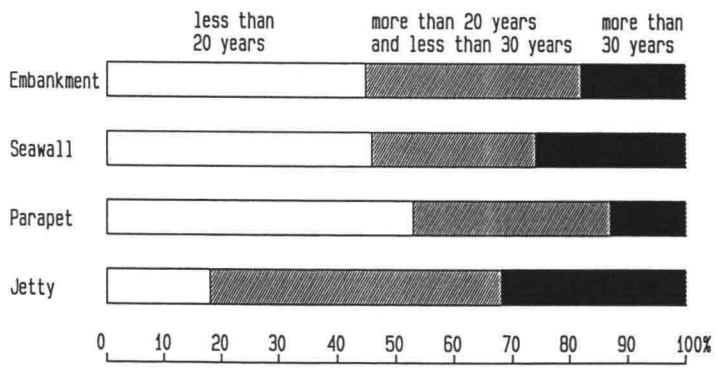

Figure 3 Elapsed years of protective structures around ports (in 1987).

(3) Figure 3 shows the elapsed years since the construction of structures. More than half of facilities were constructed more than 20 years ago. The facilities have been becoming superannuated year by year.

(4) In Japan, there was no severe coastal disaster in last quarter century. This is mainly due to the uplift of coastal improvement level. At the same time, however, it is due to no large typhoon which has attacked the Japanese coast during about the last 30 years. Therefore, it can be said that the present protection system has not been tested yet by a full-scale power of nature.

To solve some of the above stated problem, it is necessary to reinforce the shore protection facilities. For example, to guarantee more safety of life, the shore protection facilities should be designed for a longer return period. The quantity of overtopping against the seawall must be kept much less than what we design now. It needs to enlarge the cross section of coastal structures because of higher crown level. The reinforcement of facilities, however, will diminish the people's desire for more effective utilization and better view of coast. This contradiction motivates us to develop a new shore protection system which must have two functions, that is to say, a prevention of coastal disaster in a huge storm and an acceptance of people to the beach in a calm. Now, a new system, namely a Integrated Shore Protection System (ISPS), is going to be applied to the eroded beach.

The ISPS is the combined system of an offshore structure, a sandy beach and a seawall which brings each protective function into full play as a whole. That is to say, the ISPS works such that the detached breakwater with a low level crown height or submerged breakwater placed at the offshore first suppresses the waves, secondly the natural or

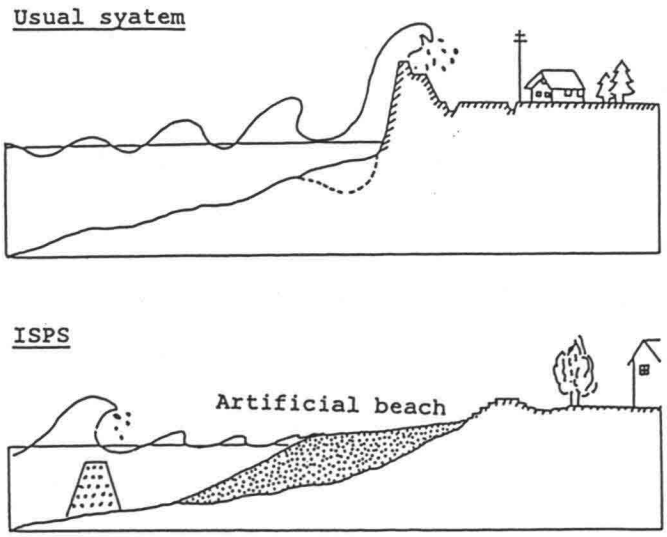

Figure 4 Conceptual comparison between the usual system and the ISPS.

artificial sand beach break the waves propagating onshore, finally a step−type seawall, having the structure with easy access to the beach in a calm, absorbs the rest of the wave energy in a storm(see Figure 4). Since a portion of the protective functions is allotted to each of three facilities, the total system has remarkable features. It can avoid blocking the people's approach to a sand beach and spoiling a beautiful view. We can also take a longer return period of the objective forces at designing facilities. Figure 4 shows the conceptual comparison between the usual system and the ISPS. The former is, so to speak, a line defence which extends in the longshore direction along a coast. Contradictory to this, the latter is a plane defence with the parallel arrangement of plural number of facilities in the cross−shore direction. The crown height of seawall can be made lower in the latter system.

However, there are many technical difficulties which remain to be solved from now so as to make the coasts what people currently desire to be. One of the most important and difficult subjects are to understand the mechanism of topographical changes of sandy beach in the storm and to establish a higher technology for stabilizing it. For these purposes, we have been being carried out the field research since 1986.

3. FIELD OBSERVATION AT HAZAKI OCEANOGRAPHICAL RESEARCH FACILITY

The site of field observation is a entirely natural sandy beach, being exposed to the full wave energy of the Pacific Ocean, and is classified as a micro−tidal beach with the tide range of about 1.4 meters (see Figure 5). The foreshore slope is mild, about 1/50 in average, while the mean bottom slope in the surf zone is a little milder, 1/60. The mean diameter of sediment on a beach is usually 0.18 mm. On this beach, Port and Harbour Research Institute, Ministry of Transport, constructed the Hazaki Oceanographical

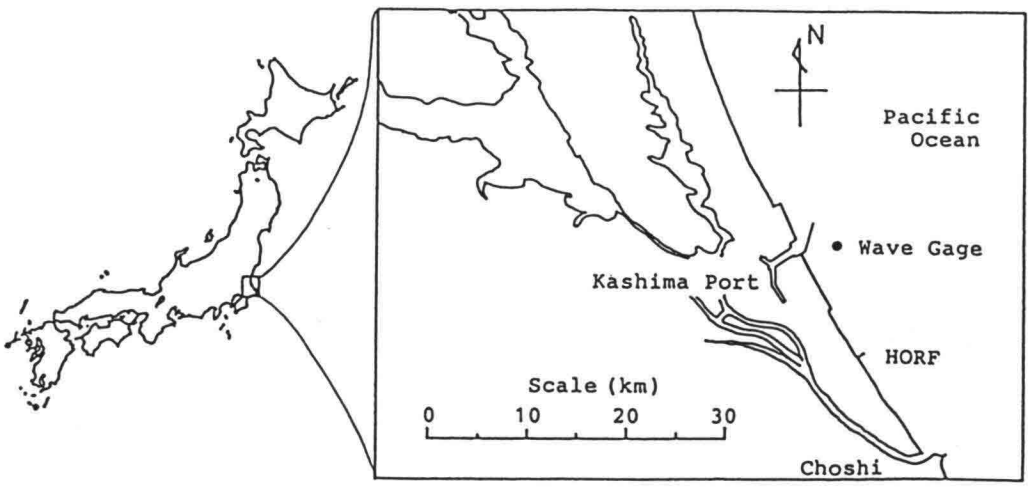

Figure 5 Site of field observation (HORF).

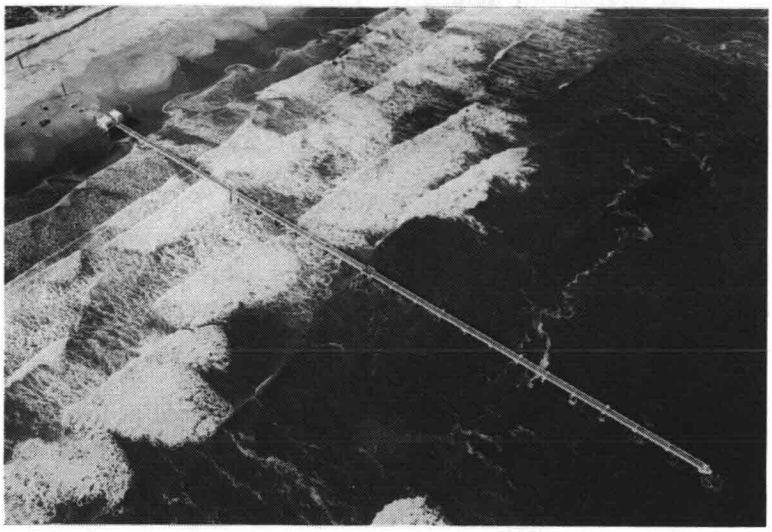

Figure 6 Hazaki Oceanographical Research Facility (HORF).

Research Facility (HORF, see Figure 1) in 1986 for carrying out field observation in the surf zone even under severe sea conditions. The research pier is 427 meters long and supported by concrete−filled steel piles in a single line at 15 meter intervals. The pier deck is 2.5 meters wide and 7 meters above L.W.L. There is a laboratory at the base of the research pier, where two researchers are permanently stationed to measure and observe the many phenomena in the surf zone. The items of observation are as follows;

Beach profile: A beach profile along the research pier was surveyed once daily with a sounding lead from the pier deck. The profile from the backshore to the foreshore was surveyed by using a surveyor's staff and a transit. The cross−shore interval of these measurements was 5 meters.

Waves near the shoreline: An ultrasonic wave gauge was installed on the pier deck at the reference point of +22m as shown in Figure 7. The mean ground level at the observation

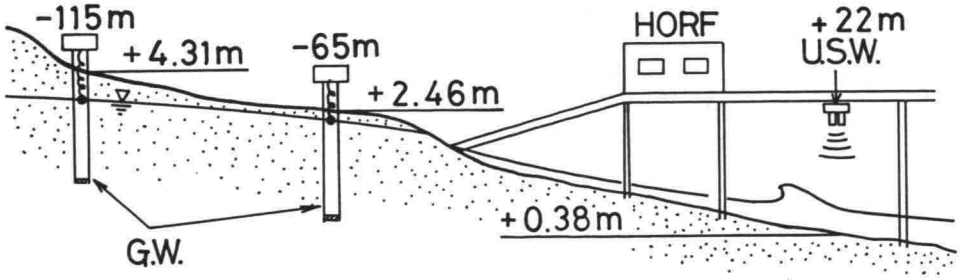

Figure 7 Arrangement of instruments.

point was 0.38 meter above the datum line. The mean water depth was about 0.3 meter at M.W.L. The wave measurements were carried out for 20 minutes of every hour with the sampling time of 0.3 second. By utilizing the data obtained, the significant heights of incident wind waves and infragravity waves were calculated based on the result of spectra analysis (Katoh and Yanagishma, 1992).

Level of water table under the beach : As shown in Figure 7, two pipes of 12.5 centimeters in diameter were sunk into the beach at the horizontal reference point of −65m and −115m. To measure the level of water table at these points, water level meters were installed inside the pipes. The measurements were carried out for 20 minutes of every hour.

Offshore waves: The offshore waves have been being measured at the mean water depth of 23.4 meters offshore the Kashima Port (see Figure 5) for 20 minutes of every two hours.

3.1 Actual Conditions of Abrupt Beach Erosion and Its Recovery

The shoreline position, which is defined at an intersection of beach profile and a level of +1.4 meters above the datum line, is calculated by interpolating the beach profile data of 5 meters interval. Figure 8 shows the daily on−offshore changes of shoreline position. As shown by downward arrows in Figure 8, the shoreline rapidly recessed in one or two days in an erosional process, which was due to the incidence of large waves. On the other hand, on the successive days in the accretionary process, the shoreline gradually advanced with almost constant speed by the action of mild waves, which is approximated by the broken lines in Figure 8 (Katoh and Yanagishima, 1988).

Figure 9 shows the foreshore profiles during the days when the typhoon No.8713 passed near the observation site in September 1987. The berm had been formed at the level

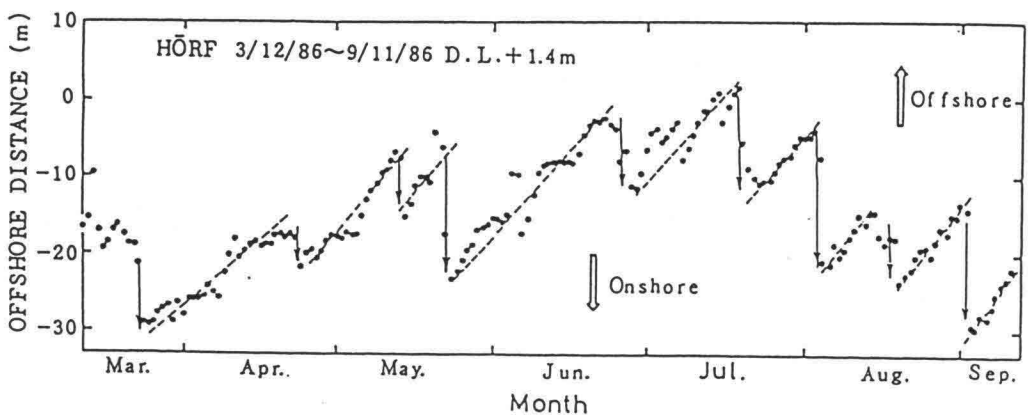

Figure 8 On−offshore changes of shoreline position.

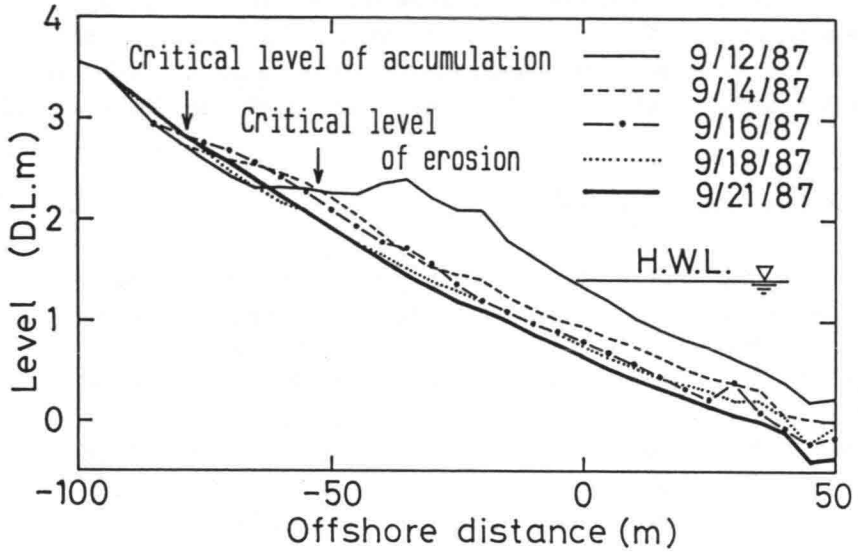

Figure 9 Berm erosion during typhoon No.8713.

higher than H.W.L. by the 12th of September. Disappearance of this berm on the 14th of September means that the berm had abruptly eroded within two days from the 12th to the 14th of September. One more observation must be made concerning Figure 9. There was a interesting paradox that the sand was deposited on the higher elevation when the berm eroded on the 14th and 16th of September.

The eroded beach is not recovered when the incident wave energy is too small, while the beach is eroded further when the incident wave energy is too large. An external force

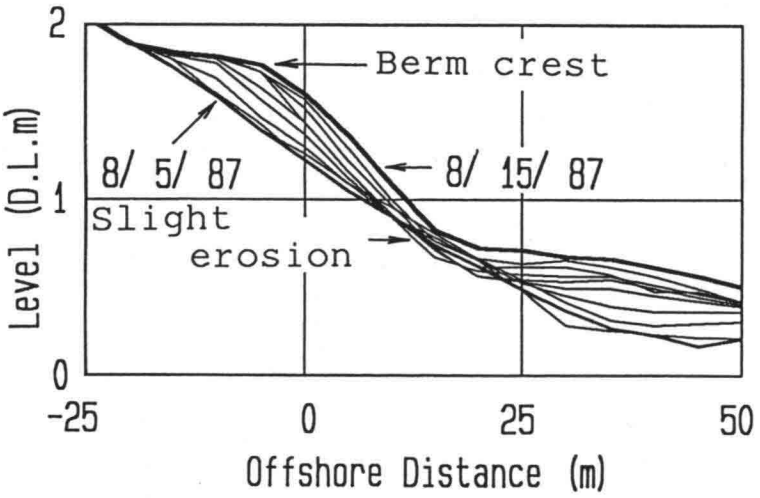

Figure 10 Example of berm formation.

which is necessary for recovery of beach is the waves of moderate energy level. Figure 10 shows a typical example of berm formation during the accretionary process with the incoming of mild waves of about 1 meter in offfshore wave height. The process of berm formation is characterized with a horizontal berm crest and developing of steeper foreshore.

3.2 External Force for Abrupt Beach Erosion

Figure 11 shows the approximate distribution of ocean surface wave energy. The energy in the band of period from 1 to 30 seconds is the largest, which is due to the wind waves. Formerly, the wind waves had been considered to be the main external force of beach erosion in a storm. The wind waves, however, lose their energy when they propagate into the surf zone. Breakers in the surf zone are saturated, that is, the wave height at any point is limited by the local water depth. The larger waves in a storm break further offshore making the surf zone wider but leaving the wave height in the inner surf zone the same. Therefore it is difficult to attribute the abrupt beach erosion in a storm to the offshore wind waves.

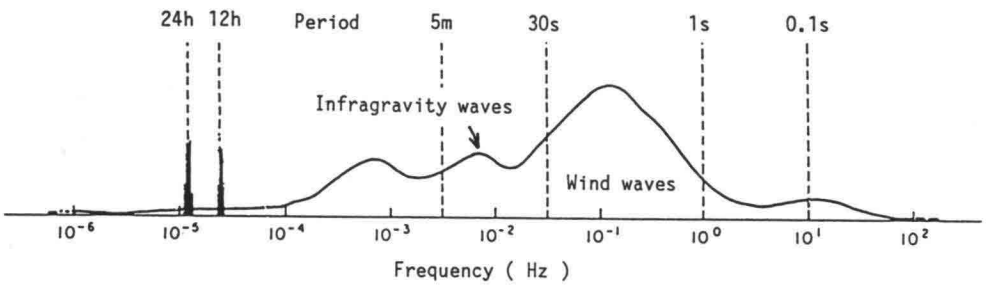

Figure 11 Distribution of ocean surface wave energy.

When an offshore significant wave height was 3.4 meters and a wave period was 11.2 seconds, we conducted the simultaneous measurements of waves at nine locations from the offshore to the shoreline, along a line normal to the beach (Nakamura and Katoh, 1992). Figure 12 shows the cross-shore distribution of the spectral energy densities. The figures on the right-side of Figure 12 are distances from the shoreline to the locations of wave observation. The distribution of spectral energy density at 3.2 km offshore, which is nearly the same as that in Figure 11, has two peaks. The first peak is at 0.1 Hz in frequency and second one is at 0.01 Hz. However, the energy density of wind waves higher than 0.04 Hz in frequency decreases due to wave breaking in the surf zone, being minimum at the location of 10 meters from the shoreline. To make up for this energy decrease in the wind wave band, the energy density in the frequency lower than 0.04 Hz increases in the onshore direction. The waves in this frequency band are called infragravity waves. Figure 13 is the side view of HORF, which was taken when the crest of the infragravity waves ran up on the beach in a stormy conditions. After about one minute, the trough of the infragravity waves came to the beach and the sandy beach emerged. After all, waves which are predominant near the shoreline are not the wind

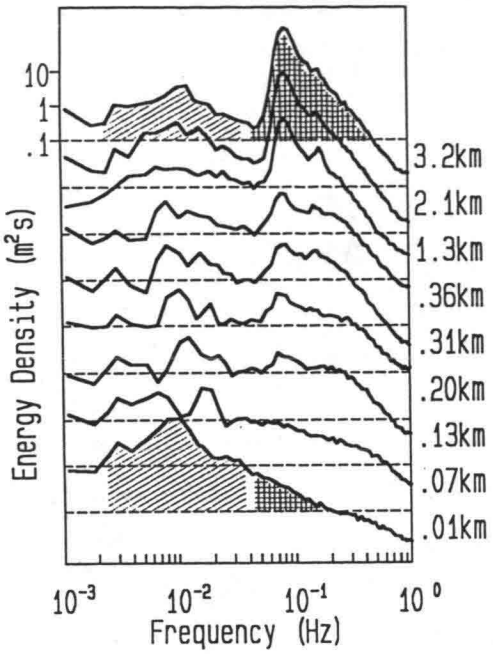

Figure 12 Cross−shore distribution of spectral energy densities.

Figure 13 Isolated HORF due to the run−up of infragravity waves on the beach.

waves but the infragravity waves of 30 seconds to several minutes. Furthermore, it has been already known that the infragravity waves make remarkable growth in a storm (Guza and Thornton, 1982). Accordingly, in the consideration of the mechanism of beach erosion, it should be very important to examine the possibility that infragravity waves act as the external force.

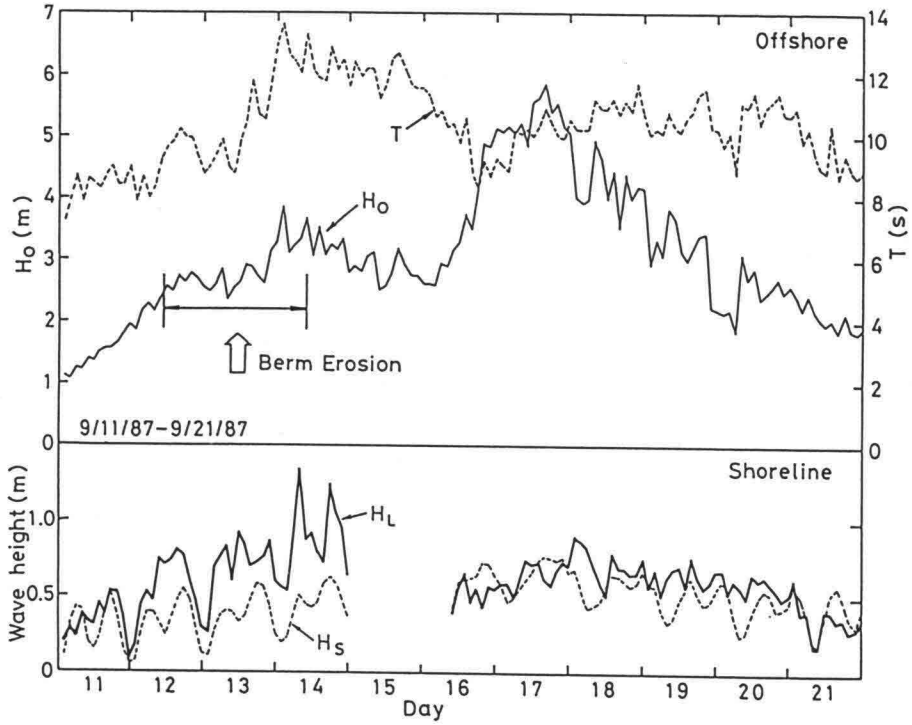

Figure 14 Wave during typhoon No.8713.

To present strong physical evidence of the participation of infragravity waves in berm erosion, a typical example will be shown. Figure 14 shows the change of waves in the offshore and near the shoreline during the period including days when the abrupt berm erosion occurred as shown in Figure 9. The berm had eroded within two days from the 12th to the 14th of September, which is denoted with a blank arrow in Figure 14. First, the significant offshore wave height, *Ho*, reached a peak of 5.98 meters at 4 p.m. on the 17th of September. Therefore, it is rather difficult to explain that the offshore high wind waves were the cause of this berm erosion. Second, the height of incident wind waves, *Hs*, near the shoreline changed periodically independent of the offshore wind waves. That is because the wave height is limited by the shallow water depth which changes with the tide. Therefore we also cannot regard the incident wind waves near the shoreline as the cause of berm erosion. Finally, only the change of infragravity waves near the shoreline, *HL*, which became maximum of 1.3 meters in the morning of 14th September, corresponded to the occurrence of berm erosion. Then, the most important external force that causes berm erosion in a storm is the infragravity waves at the shoreline.

3.3 Relation between Berm Deformation and Infragravity Waves

The sand accumulation at the higher elevation when the berm eroded is considered to be related to a wave run-up level on the beach. It is also considered that the berm crest level, which is the upper limit level of sand accumulation in the process of berm formation

as seen in Figure 10, is also closely related to the wave run−up level. Then, the critical level of sand accumulation (see Figure 9), D_L, and the berm crest level (see Figure 10), A_L, will be examined in conjunction with the wave run−up level.

A maximum wave run−up level, R_{MAX}, on the beach can be assumed conceptually and approximately as

$$R_{MAX} = (\overline{\eta})_0 + a(H_L)_0 + b, \qquad (1)$$

where R_{MAX} is not what is called the run−up level of waves but the upper limit level where the waves may make a significant profile change, $(\overline{\eta})_0$ is the mean sea level at the shoreline, $(H_L)_0$ is the height of infragravity waves at the shoreline, and a and b is the proportional constants. One of the constants, b, corresponds to the run−up effect of the incident wind waves, because the swash excursions of incident wind waves are constant, being independent of the conditions of offshore wind waves (Guza and Thornton, 1982).

Based on the beach profile data obtained everyday at HORF, we selected 48 cases for D_L and 219 cases for A_L respectively, which are assumed to be equal to R_{MAX}. The mean sea level $(\overline{\eta})_0$ and the height of infragravity waves at the shoreline have been being measured every hour by using the ultrasonic wave gauge. By applying the least square method to these data, the values of constants in Eq.(1) have been determined as

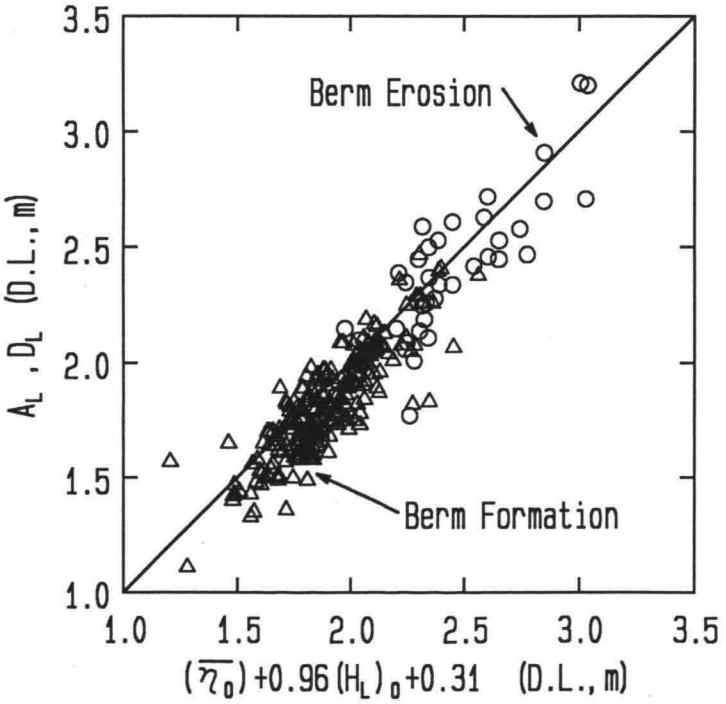

Figure 15 Relation between berm crest level and wave run−up level.

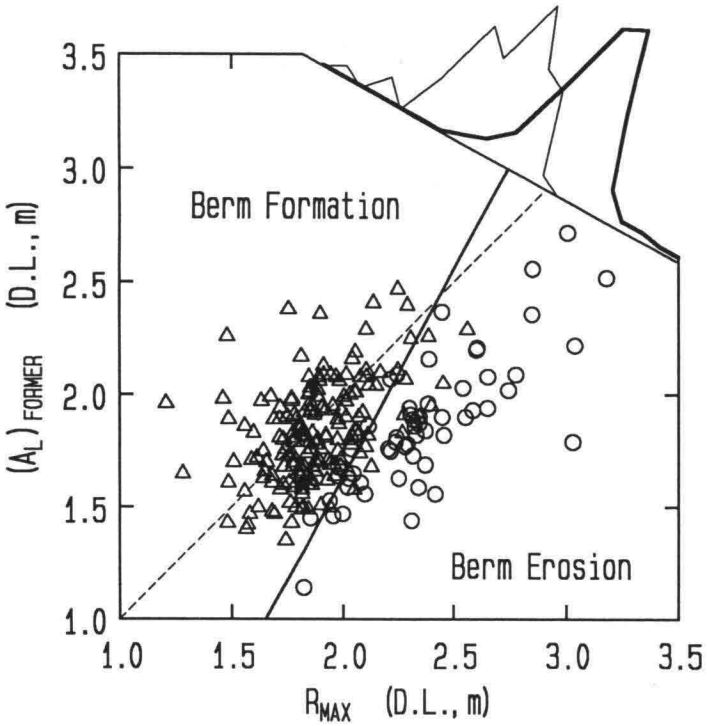

Figure 16 Relation between $(AL)_{FORMER}$ and wave run−up level.

$$DL \text{ or } AL = RMAX = (\overline{\eta})o + 0.96(HL)o + 0.31 \quad (m). \tag{2}$$

In Figure 15, the berm crest level, AL, and the critical levels of sand accumulation, DL, are plotted against the calculated values by Eq.(2), using triangles and circles as respective symbols. Although berm erosion and formation are opposite phenomena, Figure 13 shows that the critical level of sand accumulation in the berm erosion and the berm crest level in the berm formation can be expressed by a single equation, which depends on the sum of the mean sea level, the height of infragravity waves at the shoreline, and the constant run−up of the incident wind waves.

This result leads us to the question what differences are there in the physical conditions between the processes of berm erosion and berm formation. Then, a comparison is made between the berm crest level of the previous day, $(AL)_{FORMAR}$, and the wave run−up level, $RMAX$, which is estimated by Eq.(2). In Figure 16, the relation between them are plotted by distinguishing the cases of berm erosion and berm formation. A linear quadratic discriminant analysis has been done to classify these data into two groups. The result of the analysis, which is the boundary between two groups, is drawn with a straight solid line in Figure 16. Then, we have

$$RMAX > 0.54(AL)_{FORMER} + 1.11 \quad (m), \tag{3}$$

as the condition for the berm erosion. In short, the occurrence that the waves run up beyond the existing berm crest to the higher level is a prerequisite for the berm erosion.

3.4 Relation between Berm Erosion and Ground Water Table

It has long been said that the water table under the beach surface has an important bearing on deposition and erosion of the foreshore and backshore. When the water table under the beach is very high and contiguous with the surface of most of the foreshore, the backwash of the waves is accelerated by addition of water rising to the surface throughout the saturated foreshore. This saturated area is called the effluent zone. The increased volume of backwash by ground water escaping to the surface of the foreshore also dilates the sand and propels the finer grains into the turbulent flow. This enhances the erosion of the foreshore. The causes of high water table which have been pointed out in the past are,

(1) Water from a heavy rain storm in the hinterland flows to the backshore,
(2) As the water table under the beach lags 1 to 3 hours behind the tide, the water table is relatively higher than the tide during the ebb tide,
(3) Hot springs flow out at a beach in Japan.

All of these, however, do not affect the berm erosion during a storm. Now, based on the consideration up to the previous section and our experiences in the field, we can add one more cause of high water table which is directly related to beach erosion during the storm. In the field, it was recognized that the large scale wave run−up beyond the berm crest occurred with a period of 1 to 2 minutes in the storm. The water run−up beyond the berm crest stays on the horizontal area for a good while. As a result, it is not difficult to infer the situation that the level of water table under the beach became higher due to the penetration of sea water into the beach. Then, we examined the data of water table which were obtained on the foreshore and on the backshore as shown in Figure 7. It was soon confirmed that the water table became higher with the increase of run−up height of the infragravity waves in a storm.

Furthermore, it is also inferred that the penetrated water into the beach in turn seeps out through the surface of foreshore. The seepage, however, was not observed in the field. Then, the seepage has been simulated numerically by the finite element method for steady unconfined conditions in two−dimensional case, by utilizing the levels of water table measured at two points and the mean sea level measured near the shoreline. In order to introduce the penetration of water into the beach in the calculation, the steady discharge of penetration through the beach face has been assumed, of which distribution along the beach surface is triangle, being zero at the wave run−up level, R_{MAX}. The value of discharge has been determined by trial and error so that the calculated water table at the reference point of −65m agrees with the measured one in the field (Katoh and Yanagishima, 1993). In this convenient manner, the water table under the beach is calculated for the berm erosion. After that, the seepage level is determined as the intersection of the water table and the foreshore profile, which is denoted by $(GW)o$. In

Figure 17 the seepage levels are plotted against the critical levels of berm erosion in the storm. The plotted data agree approximately with the straight line, on which the seepage level of water coincides with the critical level of berm erosion.

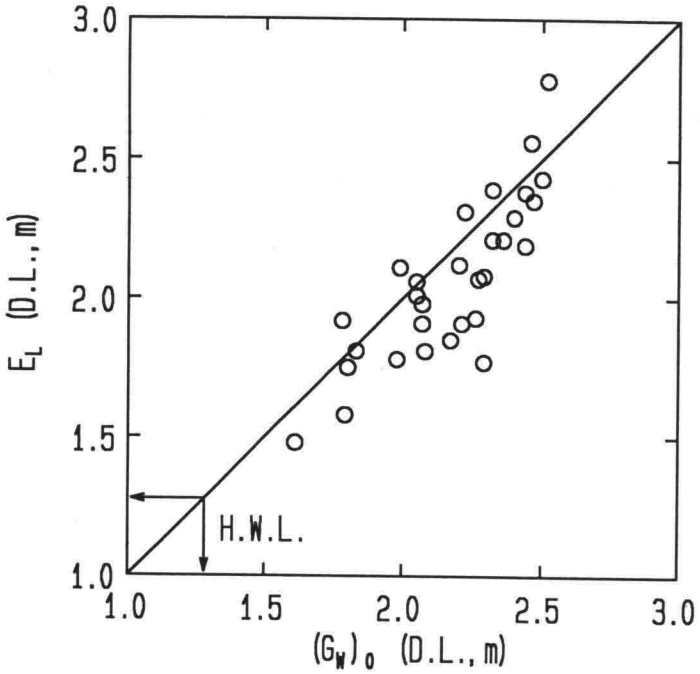

Figure 17 Relation between critical level of berm erosion and seepage level of ground water.

4. POLICIES FOR BEACH STABILIZATION

By considering the mechanism of beach erosion in the storm, new policies of beach stabilization can be introduced, which will be put to practical systems.

4.1 Creation of Wide Beach

If the beach is sufficiently wide, the abrupt erosion will be of no serious consequence because the beach will be successively restored to its previous state under the action of relatively calm waves. Then, to create the wide beach, if possible, is the most fundamental and the most desirable method for shore protection. It is, however, a very hard work to create such a beach by artificial sand nourishment, because it is basically impossible in Japan to guarantee a large volume of sand for nourishment. Even if we could do so under some special circumstances, it is fatally necessary for ever to continue supplying the sand for the beach in order to maintain the beach because the natural supply of sand to beach is not expected any more.

At least, it must be avoided to newly construct structures on the sandy beach. In the case of Japan, as human habitations are crowed as close as the coast, for example, it is a familiar instance that a new road has been constructed on the sandy beach. It is necessary to take thoughtful considerations into account when a step−type seawall, which seems to be desirable for the beach at the first glance, is constructed on the sandy beach.

4.2 Control of Infragravity Waves

Up to present, several kinds of coastal protection facilities such as detached breakwater , submerged breakwater, jetty, artificial reef and so on have been constructed on the coasts in Japan. However, the executions of these facilities are empirically done in the fields, because studies on their hydraulic functions and their effects on the topographies are still insufficient. Now, it is known that the main external force for beach erosion in the storm is the infragravity waves. Then, the study on the functions of these facilities and new−type structures from the point of view of controlling the infragravity waves will enable one to rationally design the coastal protection facility with the high efficiency.

First of all, it is basically necessary to clarify the mechanism of generation of the infragravity waves. We set ten wave gauges from the offshore to the beach along a line normal to the shore at HORF, by which the wave profiles were measured simultaneously and continuously in storms (Nakamura and Katoh, 1992). As a result, it was confirmed that the height of infragravity waves in the surf zone became to large when the length of wave grouping was long. In other words, large waves break in the offshore−side, while small waves come into the shallower area and break in the onshore−side. Then, the location of wave breaking point fluctuates in the cross−shore direction with the same period as a repetition period of wave groups, which generates the infragravity waves in the surf zone. Symonds *et al.*(1982) theoretically explained this generation mechanism of infragravity waves. We have modified the Symonds' theory by taking the effect of propagation of small waves into account, which accurately gives the height of infragravity waves in the surf zone by utilizing the representative values of wave groups. Next, we are going to study the interaction between the wave groups and the coastal protection facilities.

4.3 Control of Water Table under Beach

The ground water table under the beach rises when the foreshore erodes in a storm. Then, lowering the water table by some methods is considered to be one of the new measure for preventing or reducing the abrupt beach erosion in a storm. In this case, as the system of controlling the level of water table will be built under the ground, it will be possible to create the beach of beautiful view without any artificial obstacles.

The system of lowering the level of water table by pumping for preventing the beach erosion, which is called the sub−sand filter system, has been tested in the laboratories and in a small scale field experiment in a calm (Cappell *et al.*, 1979; Vesteby, 1991). However,

the effects of this system on the abrupt beach erosion in a storm have not been understood yet. Then, we carried out the field experiment at HORF in the storm (Yanagishima *et al.*, 1991). While the experiment was going on, the large waves of 5.6 meters in the offshore significant wave height, which was fairly larger than the waves we assumed, came to the beach, and the infragravity waves developed, which run up on the beach and hit the house of pump. Unfortunately the pumping system was broken down. It was, however, confirmed that the erosion on the foreshore was depressed while the pumping system was alive. There is a large problem in this method, that is to say, for the method to function effectively, a continuous pumping of the ground water is required for lowering the water level. Thus, a high operational costs results.

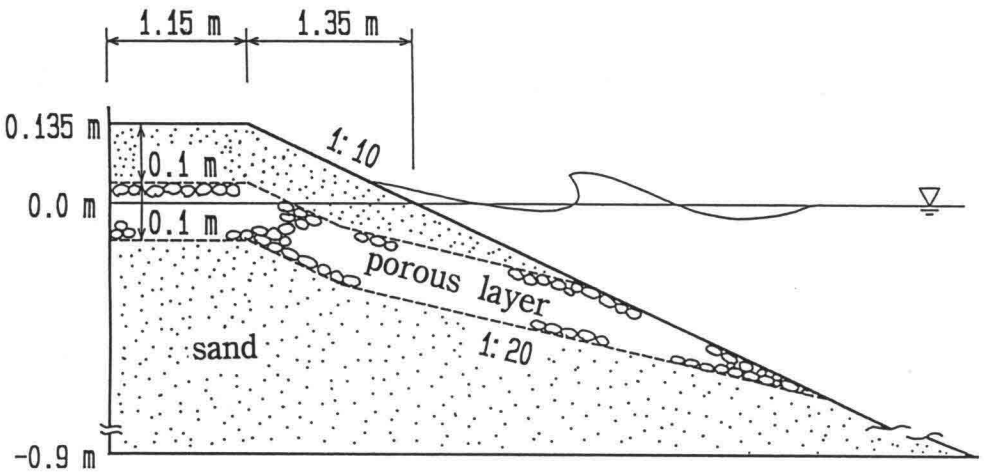

Figure 18 Beach profile in model.

If a gravitational drainage of ground water is possible, we can break through the obstacle of high operational costs. Then, an alternative drainage system is proposed, in which the ground water is naturally drained to the offshore through a porous layer setting up under the beach. An experiment was conducted to examine the functioning of such a porous layer under the sand bed by employing a mobile model beach as shown in Figure 18 in a two-dimensional wave tank (Katayama *et al.*, 1992). The underground drainage layer was made 10 cm thick with crushed stones of from 13 mm to 20 mm in diameter. Figure 19 shows the changes in the beach profile for Run 1 without the underground drainage layer and for Run 11 with the drainage layer. The wave conditions in the experiments were the almost same in both runs. In Run 1, an erosion took place and sand accumulated in the offshore forming a small bar. In Run 11 the profile change is considerably smaller and a berm formed on the foreshore. These observations indicate that the presence of the underground drainage layer prevented erosion on the foreshore. Furthermore, it is recognized that there exists the offshoreward currents in the drainage layer and the wave set-up near the shoreline is well reduced. However, as this new idea is now on a stage of basic research in the laboratory, further studies are needed in order to apply a drainage layer on real beaches.

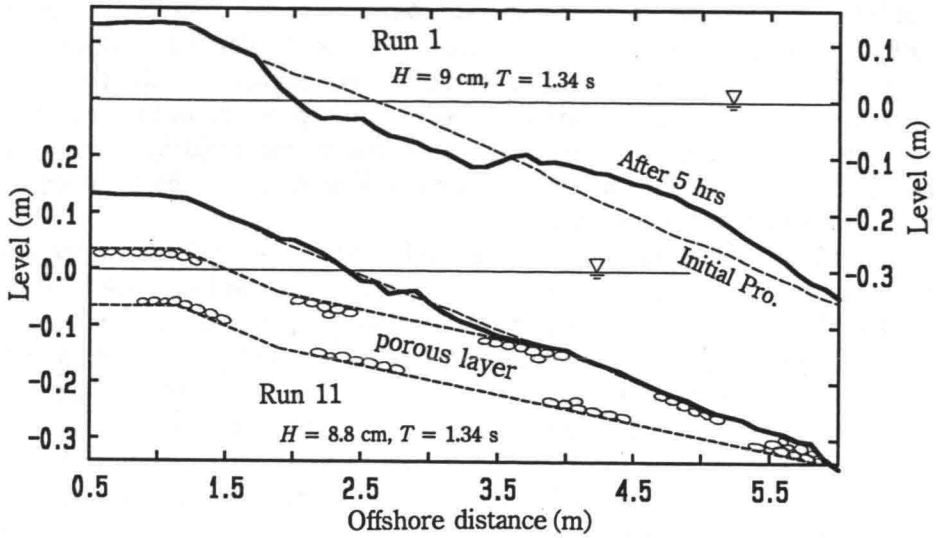

Figure 19 Comparison of changes of beach profiles with and without drainage layer.

6. SUMMARY AND CONCLUSIONS

The summary and main conclusions in this study are as follows;

(1) In Japan, the demand for a better quality of protection gets greater along with improvement of a living standard, and multipurpose use of valuable coastal zone comes to be required. This situation motivates us to develop a new shore protection system which must have two functions, that is to say, a prevention of coastal disaster in a huge storm and an acceptance of people to the beach in a calm. The new system, the Integrated Shore Protection System (ISPS), is the combined system of an offshore structure, a sandy beach and a seawall which brings each protective function into full play as a whole. However, there are many technical difficulties which remain to be solved from now so as to apply the ISPS to the eroded beach. One of the most important and difficult subjects is to understand the mechanism of topographical changes of sandy beach in the storm and to establish a higher technology for stabilizing it.

(2) The most important external force that causes berm erosion in a storm is the infragravity waves at the shoreline. As the infragravity waves run up beyond the berm crest in the storm, the sea water stays for a good while on the horizontal area of the berm, which accelerates the saturation of water into the beach. As a result, the water table becomes higher, and the water flows out through the surface of foreshore. The seepage level of water corresponds to the critical level of berm erosion.

(3) By considering the mechanism of abrupt beach erosion in the storm, two policies for beach stabilization can be introduced.

First, as the main external force for the beach erosion in the storm is the infragravity

waves at the shoreline, the erosion will be avoided or remarkably reduced by suppressing the growth of infragravity waves. In order to develop facilities which can control the infragravity waves, it is basically necessary to clarify the generation mechanism of the infragravity waves. According to the results of field observation in the storms, the infragravity waves were generated in the breaking process of wave groups. Then, as the second step, the effects of facilities on the breaking of wave groups must be immediately studied.

Second, as the ground water table under the beach rises when the foreshore erodes in a storm, the erosion is prevented or reduced provided that we lower the level of water table. For this purpose, the gravity drainage system is proposed, in which the ground water is naturally drained to the offshore through a porous layer setting up under the beach. The result of model experiment on the function of such a porous layer indicates that the presence of the underground drainage layer prevented erosion on the foreshore and the wave set−up near the shoreline is well reduced. This new idea, however, is now on a stage of basic research in the laboratory. Then, further studies are needed in order to apply a drainage layer on real beaches.

REFERENCES

1) Chappell,J., I.G.Eliot, M.P.Bradshow and E.Lonsdale(1979): Experimental constrole of beach face dynamics by watertable pumping, *Eng. Geol., 14. pp.*29−41.
2) Guza,R.T. and E.B.Thornton(1982):Swash oscillation on a natural beach, *Jour. Geol. Res., Vol.87, pp.*483−491.
3) Katayama,T., M.Kurokawa, S.Yanagishima, K.Katoh and I.Hasegawa(1992):Lowering of water table with drainage layer under the foreshore, *Proc. of Coastal Eng., JSCE, Vol.39, pp.*871−875.
4) Katoh,K. and S.Yanagishima(1988):Predictive model for daily changes of shoreline, *Proc. of 21st ICCE, pp.*1253−1264.
5) Katoh,K. and S.Yanagishima(1992):Berm formation and berm erosion, *Proc. of 23rd ICCE, pp.*2136−2149.
6) Katoh,K. and S.Yanagishima(1993):Beach erosion in a storm due to infragravity waves, *Rep. of PHRI, Vol.31, No.5, pp.*73−102.
7) Komar,P.D.(1976):Beach Process and Sedimentation, *Prentice Hall, 429p.*
8) Nakamura,S. and K.Katoh(1992):Generation of infragravity waves in breaking process of wave groups, *Proc. of 23rd ICCE, pp.*990−1003.
9) Symonds,G., D.A.Huntley and A.J.Bowen(1982):Two−dimensional surf beat: Long wave generation by a time−varing breakpoint, *J. Geophy. Res., Vol.87, No.C1, pp.*492−498.
10) Vesterby,H.(1991): Coastal drain system, *Proc. Inter Conf. Geotec. Eng. Coastal Development, pp.*651−654.
11) Yanagishima,S., K.Katoh, T.Katayama, T.Isogami and H.Murakami(1991):Effects of depressing water table on changes of foreshore profile, *Proc. of Coastal Eng., JSCE, Vol.38, pp.*266−270.

HYDRO-PORT'94
International Conference on Hydro–Technical
Engineering for Port and Harbor Construction
October 19 – 21, 1994, Yokosuka, Japan

Scour around the Head of a Vertical– Wall Breakwater

Tunc Gökçe [1]
B. Mutlu Sumer [2]
Jørgen Fredsøe [2]

[1] Technical University of Denmark
Institute of Hydrodynamics and Hydraulic Engineering (ISVA)
2800 Lyngby
Present address: Yüksel Proje International, Ankara
[2] Technical University of Denmark
Institute of Hydrodynamics and Hydraulic Engineering (ISVA)
2800 Lyngby

ABSTRACT

This paper presents the results of an experimental investigation on the near-bed flow patterns and scour around the head of a vertical-wall breakwater. Keulegan-Carpenter number (KC), based on the breakwater width, is found to be the major parameter that governs the flow and the equilibrium scour depth. Basic flow structures are identified as function of KC. The scour depth normalized by the width of the structure is found to increase with increasing Keulegan-Carpenter number. The conventional stone protection is found to be effective in reducing the scour. The scour is practically eliminated when the width of the protection layer is taken to be about 3.5 times the width of the breakwater. Also, the effect of the presence of a co-directional current is investigated. The results indicate that the scour depth is increased considerably with the current.

Key Words: Coastal Engineering, Marine Structures, Scour Protection, Sediment Transport

1. INTRODUCTION

Analysis of breakwater failures has proven that more basic knowledge on scouring around breakwaters needs to be accommodated in the preparation of design guidelines.
A large amount of knowledge has accumulated in the area of scour around offshore structures such as pipelines and piles in the last decade or so (Bijker & Leeuwestein (1984), Herbich et

al. (1984), Sumer and Fredsøe (1992) and Sumer et al. (1992)).

The purpose of the present study is to extend the previously mentioned investigation to the study of scour around the head of a vertical-wall breakwater.

2. EXPERIMENTAL FACILITY

2.1 Flow-visualization experiments

The purpose of these experiments was to get an understanding of the near-bed flow around the head of a vertical-wall breakwater.

The experiments were conducted in a wave flume 0.6 m in width, 0.8 m in depth and 26.5 m in length. The experimental set-up is depicted in Fig. 1. The model structure, located at 13.5 m distance from the wave generator, was a smooth-surface wall, 31.5 cm in length, 3 cm in width and 61 cm in height with a circular round head.

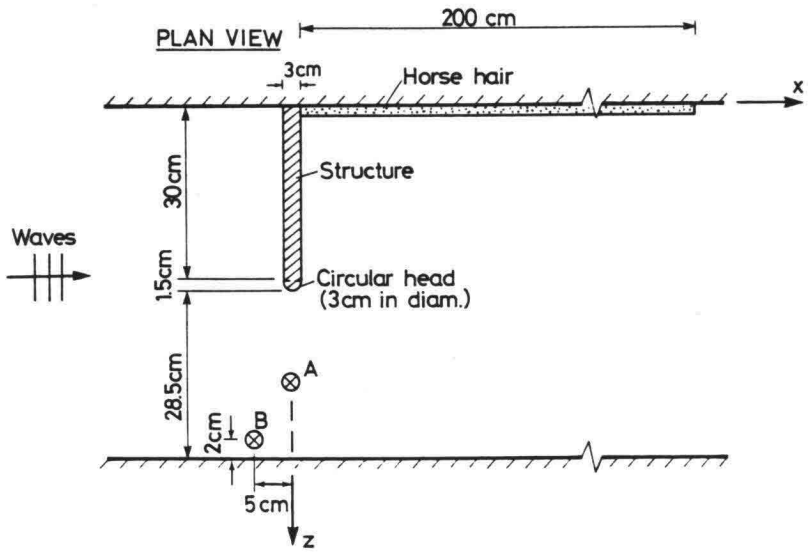

Fig. 1 Test set-up for the flow-visualization experiments. A: location of the underwater mini camera for video recording, approx. 10 cm away from the bed. B: location of velocity measurements.

The hydrogen-bubble technique was used in the experiments. Two bubble wires (30-cm-long and 0.050-mm-diameter copper wires) were stretched in the transverse (z) direction at a vertical distance y = 3 mm from the bottom; one at the upstream side and the other at the downstream side of the model structure, the wires being at distances 1 cm from the side-walls of the model. The lowermost 2 cm portion of the model was made from a transparent material through which the light was spread out.

An underwater pen-size mini camera was used for video recording of the flow processes. It was positioned at an angle to the bottom so that the near-bed flow patterns, visualized by the hydrogen bubbles around and in front of the model structure can be viewed. The flow processes were videotaped for the Keulegan-Carpenter number range from practically KC = 0 to 15 where KC was incremented by 0.5 between KC = 0.5 and 6, by 1 between KC = 6 and 10 and by 5 between KC = 10 and 15. Here, KC number is defined by

$$KC = \frac{U_m T}{B} \qquad (1)$$

in which U_m is the maximum value of the undisturbed orbital velocity of water particles at the bed at the section where the structure is placed, T is the wave period and B is the width of the structure. The calculated values of KC number were based on the U_m velocities measured in the presence of the model structure. The latter velocities were measured by a DANTEC LaserDoppler Anemometer (LDA) at Point B which was located at y = 1 cm away from the bed and at a distance of 5 cm upstream of the structure (Fig. 1). (Experimental constraints necessitated this 5 cm offset in the position of the velocity-measurement point). Also, velocity profile measurements were made at y = 2 cm along the transverse direction over the space between the head of the structure and the opposing side wall (Fig. 2). The figure shows that the velocity attains a constant value (namely the U_m value) for large z distances. So, no

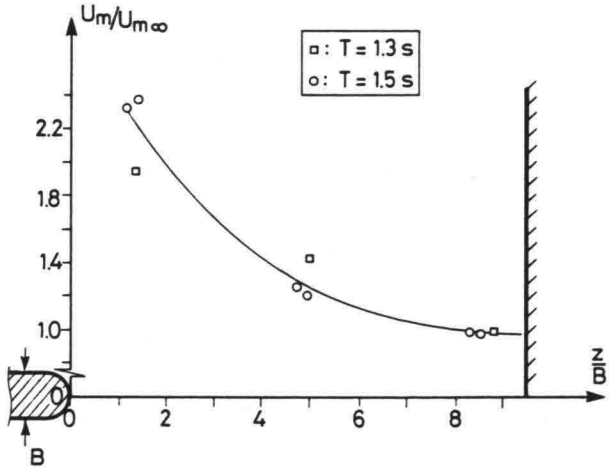

Fig. 2 Velocity distribution over the space between the breakwater and the side wall of the test channel at a distance of y = 2 cm from the bottom in the flow visualization study.

blockage effect was present.

In addition to pure-wave experiments, a few runs were conducted where a co-directional current with 0.1 cm/s velocity was superimposed on waves.

The test conditions are summarized in Table 1.

Test No	Wave period T (sec)	Measured maximum orbital velocity U_m (m/s)	Keulegan-Carpenter number $KC=U_mT/B$	Reynolds number $Re=U_mB/\nu$	Current velocity U_c(m/s)
V1	1.0	0.015	0.5	450	-
V2	1.0	0.030	1.0	900	-
V3	1.3	0.035	1.5	1050	-
V4	1.3	0.045	2.0	1350	-
V5	1.3	0.055	2.5	1700	-
V6	1.5	0.06	3.0	1800	-
V7	1.5	0.07	3.5	2100	-
V8	1.5	0.08	4.0	2400	-
V9	1.5	0.09	4.5	2700	-
V10	1.5	0.10	5.0	3000	-
V11	1.5	0.11	6.0	3300	-
V12	1.7	0.12	7.0	3600	-
V13	1.7	0.14	8.0	4200	-
V14	1.7	0.16	9.0	4800	-
V15	1.7	0.18	10	5400	-
V16	1.7	0.26	15	7800	-
V17	0.8	0.056	1.5		0.1
V18	1.5	0.10	5		0.1
V19	1.7	0.15	8.5		0.1

Table 1. Flow visualization experiments. The mean water depth in the tests was maintained at 40 cm.

2.2 Scour experiments

These experiments were carried out in a large wave flume, 4 m in width, 1 m in depth and 28 m in length. The experimental set-up is illustrated in Fig. 3. The mean water depth in the experiments was held constant at 40 cm. Two kinds of model structures were used: Breakwater 1 and Breakwater 2. In the case of Breakwater 1, the model structure was a simple box, 2 m in length, 1.2 m in height and 0.14 m in width with impermeable walls and with a circular round head. The length of the structure exposed to the flow was 1.7 m (Fig. 3). The structure extended down to the actual bottom of the flume in the vertical section (Fig. 4a).

In the case of Breakwater 2, the previously mentioned box was used as the main part of the breakwater. However, in this case, the box was placed on a protection layer (Fig. 4b); thus, the set-up as such, simulated an actual, vertical wall breakwater with its conventional bedding layer and stone protection (Burcharth (1993)). One important aspect regarding this latter set-up is that an impermeable plate was implemented (Fig. 4b), along the length of the protection layer, to avoid the undermining of the structure due to piping. As regards the protection layer, crushed

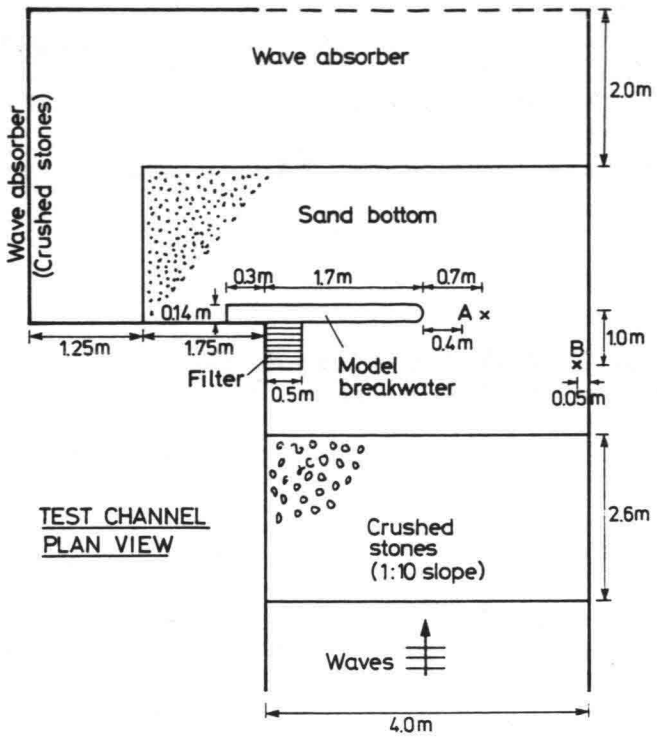

Fig. 3 Test set-up for scour experiments. A: Underwater mini video camera. B: Velocity measurement.

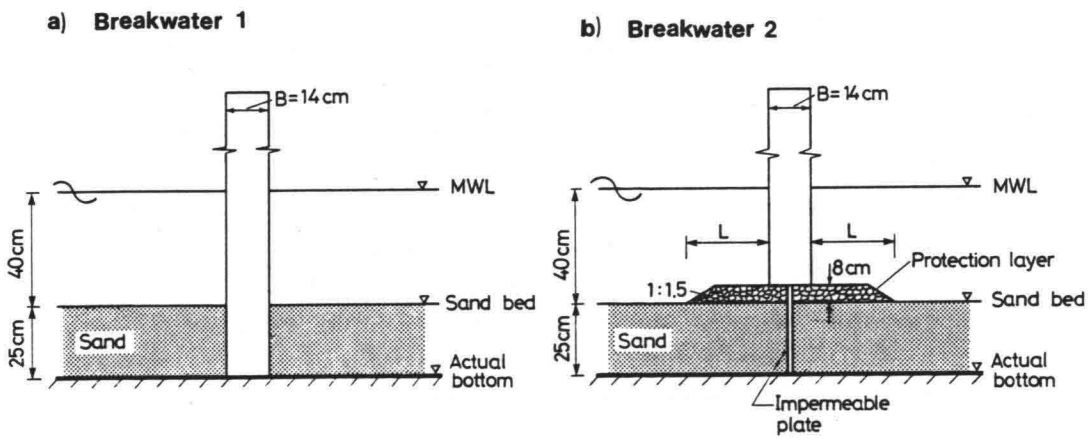

Fig. 4 Cross-section of the model set-ups.

stones the size of approximately d_{50} = 2 cm were used. The experiments were conducted for three different values of the width of the protection layer, namely L = 10 cm, 20 cm and 50 cm.

The experiments were conducted with one size of sand, namely d_{50} = 0.17 mm. Scour process around the head of the structure was continuously monitored with the previously mentioned underwater mini video camera. Velocity measurements were made by a LDA instrument and a bi-directional propeller to determine the velocity amplitude U_m (Fig. 3).

The test conditions are summarized in Tables 2-4. In the tables, θ is the Shields parameter defined by

$$\theta = \frac{U_{fm}^2}{g(s-1)d_{50}} \qquad (2)$$

in which g is the acceleration due to gravity, s = the relative density of sediment, U_{fm} = the maximum value of the undisturbed bed shear velocity, calculated by

$$U_{fm} = \sqrt{\frac{f}{2}} U_m \qquad (3)$$

in which f is the wave friction coefficient (Fredsøe, 1984).

As is seen from the tables, the experiments were conducted under live-bed conditions, namely for $\theta > \theta_{cr}$ in which θ_{cr} is the critical value of the Shields parameter for the initiation of sediment motion at the bed.

Test No	Wave period T (sec)	Measured maximum orbital velocity U_m (m/s)	Shields parameter θ	Keulegan-Carpenter number $KC=U_mT/B$	Reynolds number $Re=U_mB/\nu$	Maximum scour depth S (cm)	S/B
1	1.5	0.22	0.12	2.5	2.9×10^4	1.2	0.092
2	1.7	0.11	0.08	1.4	2.4×10^4	0.7	0.054
3	1.7	0.15	0.10	2.0	2.0×10^4	1.0	0.077
4	1.7	0.175	0.11	2.3	2.3×10^4	1.2	0.092
5	1.7	0.185	0.11	2.4	2.4×10^4	1.5	0.115
6	1.7	0.195	0.11	2.6	2.5×10^4	2.0	0.154
7	1.7	0.22	0.11	2.9	2.9×10^4	2.2	0.169
8	2.0	0.22	0.11	3.4	2.9×10^4	2.1	0.162
9	2.0	0.22	0.11	3.4	2.9×10^4	1.9	0.146
10	2.0	0.275	0.12	4.2	3.6×10^4	3.2	0.246
11	2.0	0.29	0.12	4.5	3.8×10^4	3.3	0.25
12	3.0	0.22	0.09	5.1	2.9×10^4	3.0	0.231
13	3.0	0.30	0.10	6.9	3.9×10^4	4.0	0.308
14	3.0	0.38	0.11	8.8	4.9×10^4	4.7	0.362
15	3.0	0.45	0.11	10.4	5.9×10^4	6.2	0.477

Table 2: Scour tests with pure waves. Breakwater 1.

Test No	Width of protection layer L (cm)	Normalized width of protection layer L/B	Wave period T (sec)	Measured maximum orbital velocity U_m (m/s)	Shields parameter θ	Keulegan-Carpenter number $KC=U_mT/B$	Reynolds number $Re=U_mB/\nu$	Maximum scour depth S(cm)	S/B
16	10	0.71	1.7	0.116	0.07	1.4	1.6×10^4	0.0	0
17	"	"	1.7	0.219	0.16	2.7	3.1×10^4	0.4	0.029
18	"	"	3.0	0.233	0.17	5.0	3.3×10^4	2.8	0.200
19	"	"	3.0	0.277	0.22	6.0	3.9×10^4	2.2	0.157
20	"	"	4.0	0.246	0.20	7.0	3.4×10^4	5.3	0.379
21	20	1.4	1.7	0.118	0.06	1.4	1.7×10^4	0.2	0.014
22	"	"	1.7	0.215	0.16	2.6	3.0×10^4	0.7	0.050
23	"	"	3.0	0.239	0.19	5.1	3.3×10^4	1.4	0.100
24	"	"	3.0	0.297	0.24	6.4	4.0×10^4	1.5	0.107
25	"	"	4.0	0.252	0.20	7.2	3.5×10^4	2.6	0.186
26	50	3.6	1.7	0.121	0.06	1.5	1.7×10^4	0.0	0
27	"	"	1.7	0.211	0.15	2.6	3.0×10^4	0.6	0.043
28	"	"	3.0	0.240	0.19	5.1	3.4×10^4	0.1	0.007
29	"	"	3.0	0.255	0.21	5.5	3.6×10^4	0.7	0.050
30	"	"	4.0	0.240	0.19	6.9	3.4×10^4	0.0	0

Table 3: Scour tests in the pure waves. Breakwater 2.

Test No	Wave period T (sec)	Measured maximum orbital velocity for wave component U_m (m/s)	Shields parameter of wave component θ	Keulegan-Carpenter number for wave component KC	Reynolds number for wave component $Re=U_mB/\nu$	Current velocity U_c(m/s)	Maximum scour depth S (cm)	S/B	$\xi = \frac{U_c}{U_c+U_m}$
31	1.7	0.11	0.08	1.4	1.4×10^4	0.10	8.5	0.65	0.47
32	1.7	0.15	0.10	2.0	2.0×10^4	0.10	9.0	0.69	0.40
33	1.7	0.195	0.11	2.6	2.5×10^4	0.10	9.0	0.69	0.34
34	3.0	0.30	0.10	6.9	3.9×10^4	0.10	13.0	1.00	0.25

Table 4: Scour tests with combined waves and currents. Breakwater 1. Tests were run for only 30 minutes.

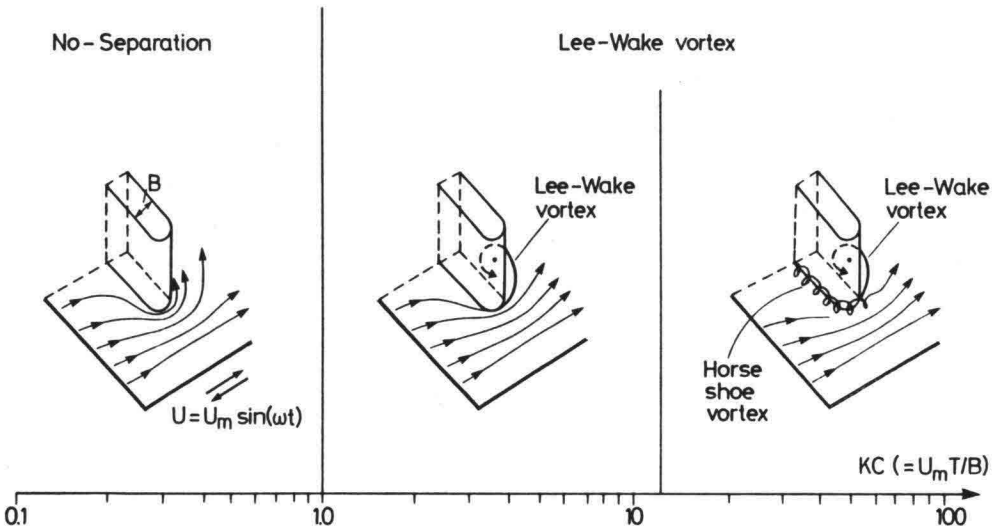

Fig. 5 Near-bed flow regimes around the head of a vertical-wall breakwater.

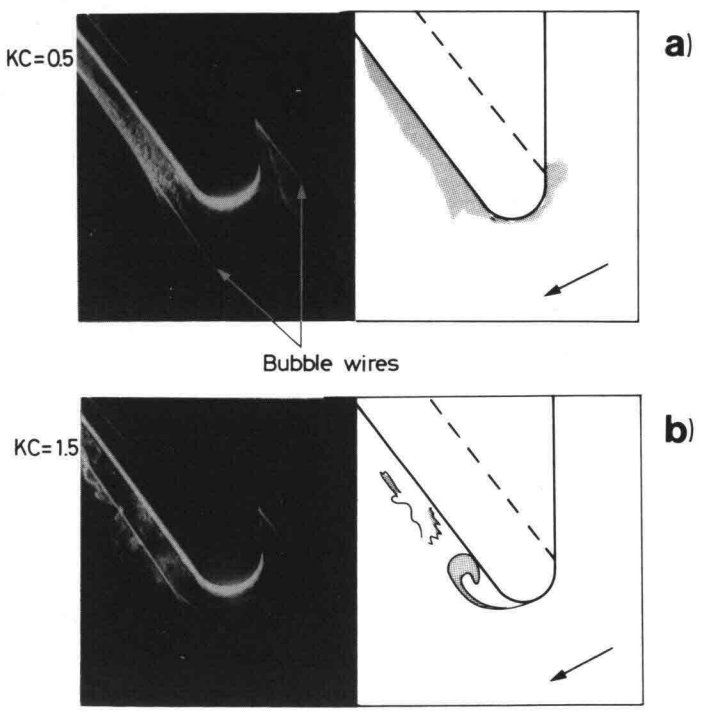

Fig. 6 Video frames. (a): No separation. (b): Separation.

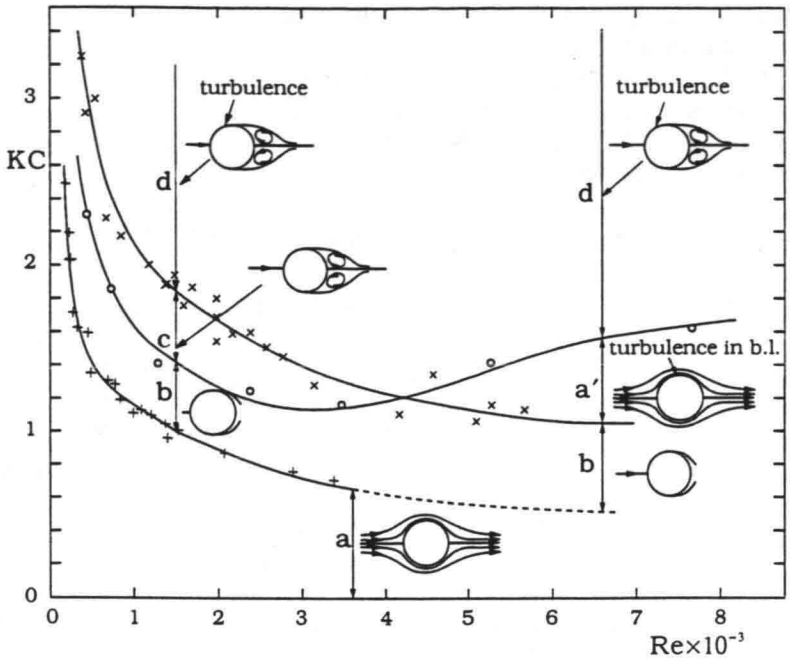

Fig. 7 Regimes of flow around a smooth circular cylinder in oscillatory flows for small KC numbers. The diagram is adapted from Sarpkaya (1986).

In both the flow-visualization experiments and the scour experiments, the upper boundary of the KC range was kept rather large, namely KC = O(10), whereas in practice KC can hardly exceed the values of KC = 4-5. However, experimenting with large KC numbers helped illustrate the trends better with regard to the variation of various quantities with respect to the KC number.

3. FLOW REGIMES

Fig. 5 summarizes the flow regimes observed in the present flow-visualization experiments.

There are three kinds of flow regimes: 1) the non-separated flow regime -- the creeping flow (KC $\lesssim$ 1), 2) the separated flow regimes with a lee-wake vortex formation behind the structure (1 $\lesssim$ KC $\lesssim$ 12) and 3) the separated flow regimes with a lee-wake vortex formation behind the structure and a horse-shoe vortex formation in front of it (KC $\gtrsim$ 12).

3.1 Non-separated flow regime (KC $\lesssim$ 1)

The flow does not separate for KC below approximately unity (Fig. 5). Fig. 6 depicts two video frames, one with KC = 0.5 and the other with KC = 1.5, corresponding to approximately the same instant in the phase space. While there is no sign of separation in the former case, the separation clearly occurs in the latter situation.

The preceding finding agrees rather well with the corresponding result in the case of flow around a circular cylinder (Sarpkaya (1986)). The diagram given by Sarpkaya is reproduced here (Fig. 7) for later use in the paper. From the diagram it is seen that, for the same Reynolds number as in the tests, namely Re $\cong 10^3$ (Table 1), the non-separated flow regime in the case of cylinder terminates at KC = 1.1 (c.f. KC = 1 in Fig. 5). Note that the KC and Re numbers in the cylinder case are based on the cylinder diameter.

3.2 Separated-flow regime with no horse-shoe vortex ($1 \lesssim KC \lesssim 12$)

In this flow regime, a lee-wake vortex forms behind the structure in every half period (Figs. 5 and 6).

The present flow-visualization experiments indicate that the way in which this vortex forms and further develops basically does not vary with the KC number. Fig. 8 depicts a sequence of sketches, illustrating the evolution of the flow picture around the structure during the course of approximately one half period of the motion. (Note that $\omega t = 0$ corresponds to the instant where the wave crest passes the section at which the structure is placed).

The video recordings show, however, that the phase variation of the development of the flow patterns as well as the dimensions of the flow structures are strongly dependent on KC number.

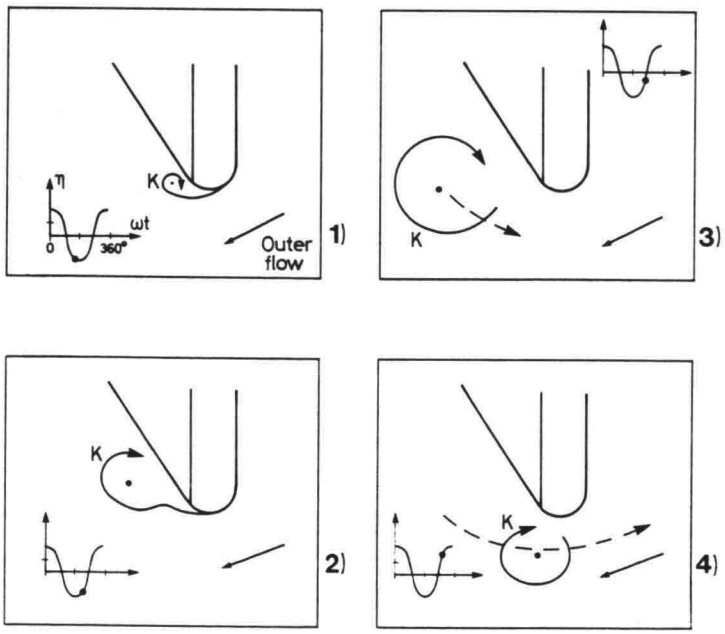

Fig. 8 Development of flow around the head of breakwater KC = 8. η: the surface elevation recorded at the section where the breakwater is placed. Frame 1: Lee-wake vortex forms. Frame 2: It grows in size. Frame 3 and 4: It is eventually washed around the structure.

Fig. 9 presents the data regarding the plan-view extents of the lee-wake vortex normalized by the width of the structure plotted as function of KC number. As seen, the larger the KC number, the larger the size of the lee-wake vortex.

3.3 Separated-flow regime with a horse-shoe vortex (KC $\gtrsim$ 12)

When KC is increased further, a point is reached (namely at KC $\cong$ 12) where, in addition to the lee-wake vortex, a spiral-shape vortex begins to form in front of the structure as sketched

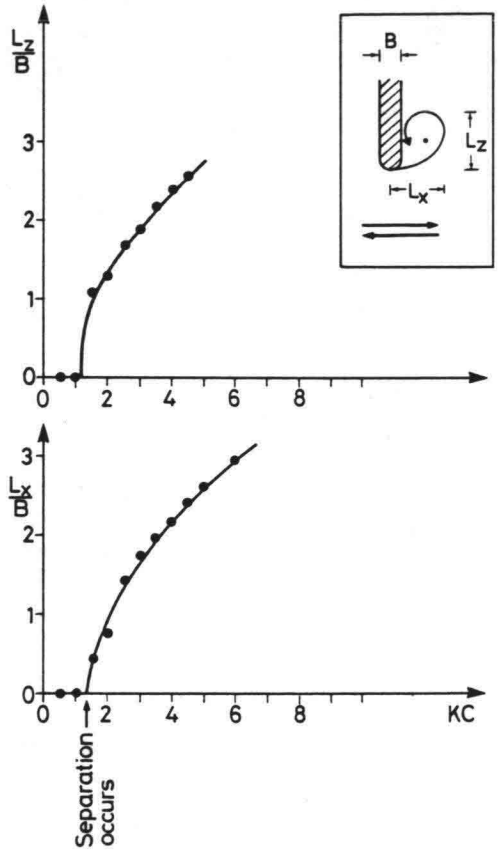

Fig. 9 Dimensions of lee-wake vortex.

in Fig. 10a. This vortex is similar to the horse-shoe vortex in front of a vertical cylinder (Fig. 10b). The latter is known to play an important role in scour around bridge piers and vertical piles (Breusers et al., 1977 and Sumer et al., 1992). As is known, the horse-shoe vortex is formed at the seabed because of the rotation in the incoming flow velocity (Fig. 10). In waves, this rotation is formed in the wave boundary layer. However, the horseshoe vortex is insignificant when the wave boundary layer is thin (Sumer et al. 1992).

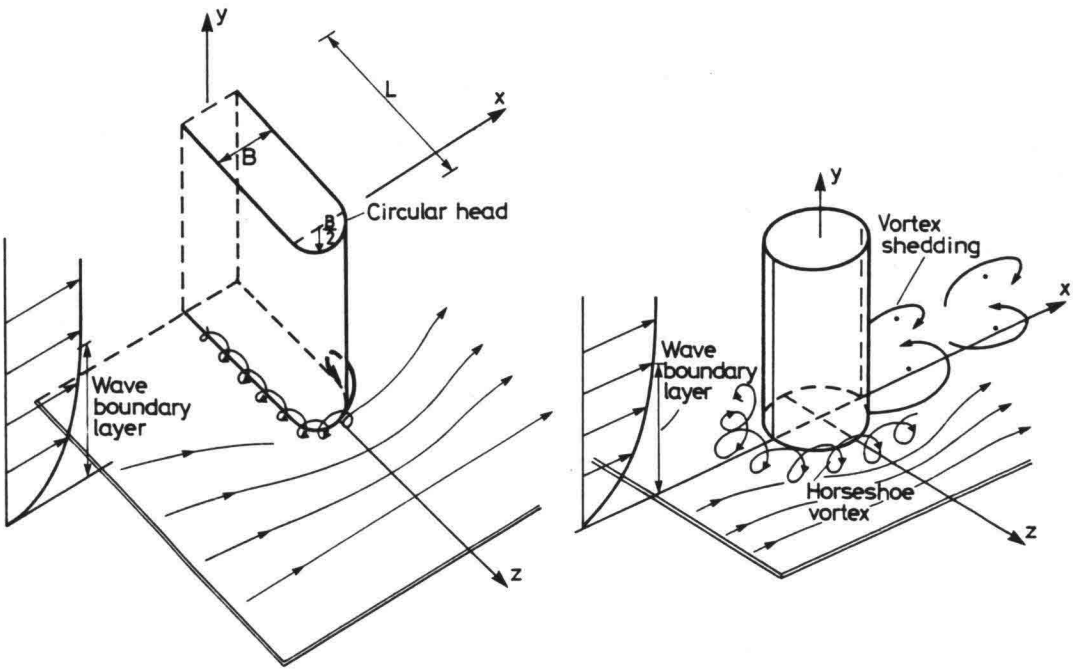

Fig. 10 Flow pattern. a: Vertical-wall breakwater. b: Vertical cylinder.

The present observations indicate that a horse-shoe vortex emerges in front of the structure when KC $\gtrsim$ 12. The observations further indicate that this occurs over a very brief period of time during the course of one half period of the motion. Considering the extremely small values of KC number experienced in real-life situations (KC = O(1)), it may be argued that this flow regime is of no practical significance with regard to scour problems encountered in practice.

3.4 Scale effects

Clearly, when real-life dimensions are considered, some changes may be expected in the values of the critical KC numbers separating the three different flow regimes summarized in Fig. 5.

As for the first critical KC number, namely the KC number beyond which separation occurs, we may deduce from Fig. 7 that, for very large structures where Re number is extremely large and the surface of the structure is rather rough, the flow would remain unseparated for KC $\lesssim$ 2.

We may therefore anticipate that the curves in Fig. 9 may shift slightly to the right, suggesting that the normalized size of the lee-wake vortices would be slightly smaller in the field for the same KC number.

Regarding the second critical KC number, namely the KC number at which the horse-shoe vortex begins to emerge, this may be related to the boundary-layer thickness (Sumer et al.

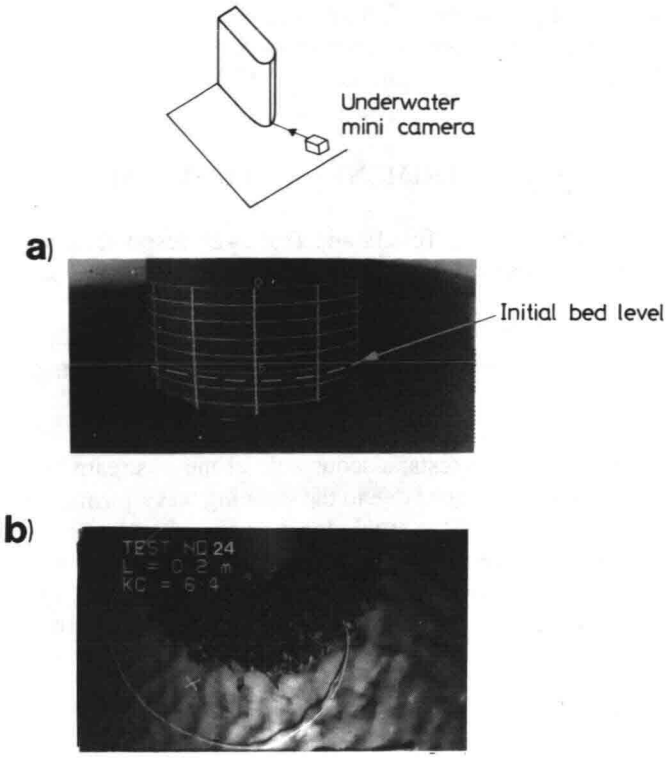

Fig. 11 Scour picture. a: Breakwater 1 (Test 12). b: Breakwater 2 (Test 24).

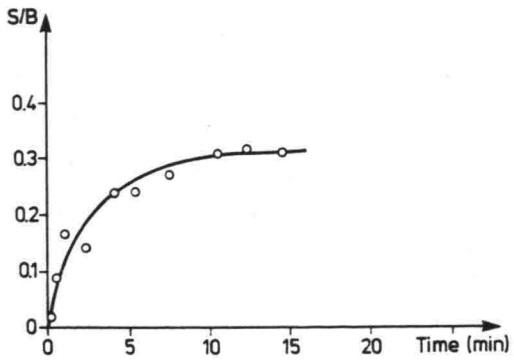

Fig. 12 Scour-depth development. Test 13.

(1992)). In the present flow-visualization experiments, the wave boundary layer was in laminar regime, and the boundary layer thickness δ was estimated to be $\delta/l = O(0.005)$ (Jensen et al. (1989)) in which l is the length of the model breakwater. In the field, this ratio is even smaller, meaning that the horse-shoe vortex can emerge for values of KC which are even larger than

the value indicated in Fig. 5, namely KC $\gtrsim$ 12. As already pointed out, such high KC numbers can not occur in the field, therefore the corresponding flow regime would have no practical significance with regard to the scour processes.

4. RESULTS OF SCOUR EXPERIMENTS AND DISCUSSION

Fig. 11 illustrates the scour holes in Test 12 and Test 24 corresponding to the equilibrium stage. As is seen, the maximum scour depth occurs approximately at the head of the structure.

Fig. 12, on the other hand, illustrates how the maximum scour depth develops with respect to time. As seen, the maximum scour depth attains its equilibrium stage through a transition period.

It may be mentioned that, in the tests, a scour hole at the upstream corner where the model structure joins the side wall developed due to the standing wave formation at this location. This effect was reduced by placing a filter at this location (Fig. 3). It was observed that this scour hole spread gradually along the length of the model structure during the course of the test. However, the scour measurements indicated that the scour process at the head attained its equilibrium stage long before the previously mentioned scour-hole formation reached the head of the model structure.

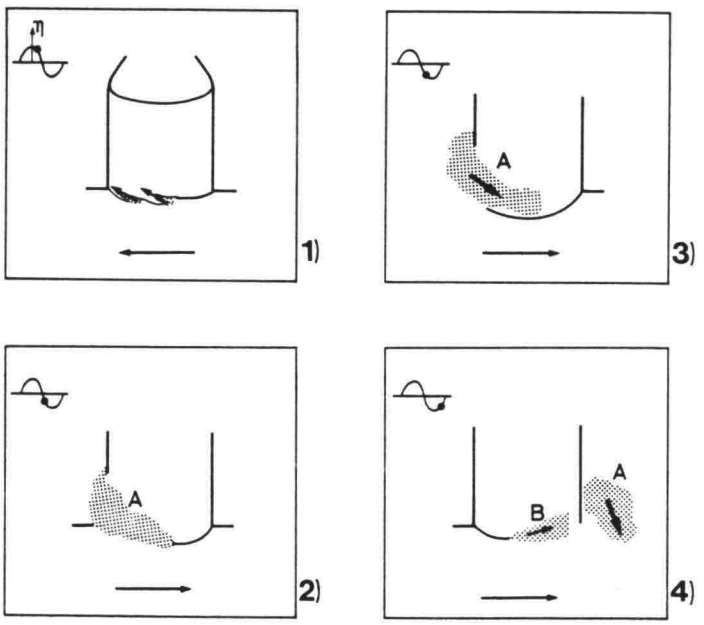

Fig. 13 Sequence of video frames illustrating the way in which scour occurs. The small sketches on the upper left corner of each frame shows the water surface elevation at the section where the breakwater is located.

Fig. 13 schematically illustrates the way in which the scour develops around the structure. The bed at the head of the structure is eroded by the high-speed flow (Frame 1), and the eroded sediment is swept into the lee-wake vortex where the sediment grains are lifted up into the upper portion of the lee-wake vortex (Frame 2). As this vortex is washed around the structure by the flow reversal (Vortex K Fig. 8), the sediment trapped in the vortex will be carried by this vortex (Frame 3) and eventually be deposited away from the structure (Frame 4).

Since the formation and development of the lee-wake vortex is primarily governed by the KC number (as has been discussed in the previous section), it might therefore be expected that the resulting scour, too, is mainly governed by this parameter.

The importance of the KC number in scour problems such as scour below pipelines and scour around vertical piles has been demonstrated previously (Sumer and Fredsøe (1990) and Sumer et al. (1992)). Gökçe and Günbak's (1991) experimental study, and Hansen's (1992) numerical study have later confirmed the relation between the scour depth and the KC number put forward by Sumer and Fredsøe (1990) in conjunction with scour below pipelines.

Fig. 14 depicts the present scour data obtained for Breakwater 1, plotted as function of KC number. S, the scour depth at the head of the breakwater, is normalized by B. As is seen, the correlation is remarkable.

First of all, the scour depth is practically nil for the values of KC number below approximately unity. This may be attributed to the non-separated flow regime observed for such KC numbers (Fig. 5).

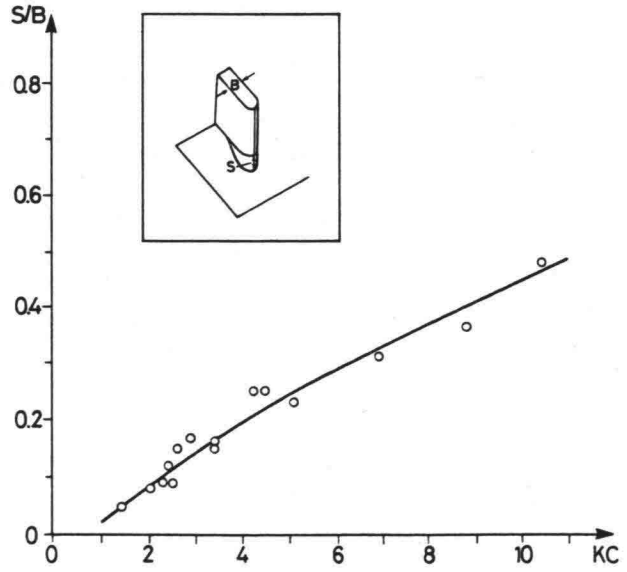

Fig. 14 Normalized scour depth as function of KC, at the head of breakwater with no protection layers. Breakwater 1 experiments. Live bed ($\theta > \theta_{cr}$).

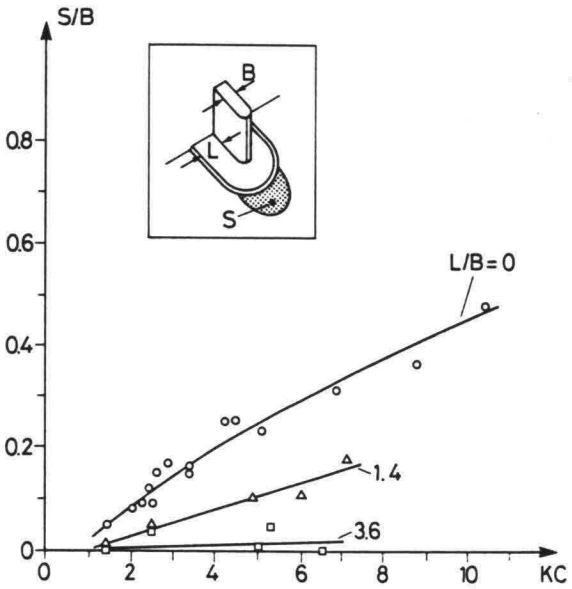

Fig. 15 Normalized scour depth, S/B, at the head of a breakwater with a protection layer. L/B = 0 data: Breakwater 1 (from the previous figure). The rest of the data: Breakwater 2. Live bed ($\theta > \theta_{cr}$).

Secondly, the scour depth increases with increasing KC number. This increase is due to the increased extension of the lee wake (Fig. 9).

Fig. 15 presents the scour data obtained for Breakwater 2 experiments, namely for the case of a breakwater with a protection layer, together with the data presented in the previous figure (L/B = 0 situation). The data corresponding to L/B = 0.71 (L = 10 cm) are not shown in the figure, to keep the figure relatively simple. The scour depths measured for this value of L are mainly below those measured for L/D = 0 (Table 4). Fig. 15 clearly indicates that the larger the width of the protection layer, the smaller the scour depth. In fact, for L/B = 3.6, the scour is practically eliminated for the tested range of KC. This is not entirely unexpected, because the width of the protection layer in this case (Namely, L/B = 3.6) is larger than the vortex dimensions experienced for this range of KC number (namely, L_x, L_y)/B $\cong$ 3), see Fig. 9).

To see the effect of the height of the protection layer, a sensitivity analysis has been undertaken. In this analysis, the Breakwater 2 tests were repeated for a protection layer with zero height (i.e., the surface of the protection layer is flush with the surface of the sand bed). These tests indicated that the results are insensitive to the height of the protection layer. This was indeed expected, since the key point here is to protect the sand bed against the action of the lee-wake vortices. As long as the size of the protection layer is kept larger than the size of the area affected by the vortices (regardless of the height of the protection layer), the bed will be protected.

Considering the maximum KC number which may be experienced in practice, KC = O(5), it may, from the preceding results, be suggested that the width of the protection layer should be

selected at least 3-4 times the width of the breakwater as a measure for protection against the scour at the head of the structure.

Although the present findings indicate that the scour is practically nil for KC $\lesssim$ 1, a slight erosion-deposition pattern as sketched in Fig. 16 may appear for such small KC numbers in the field due to the secondary, steady streaming indicated in the figure.

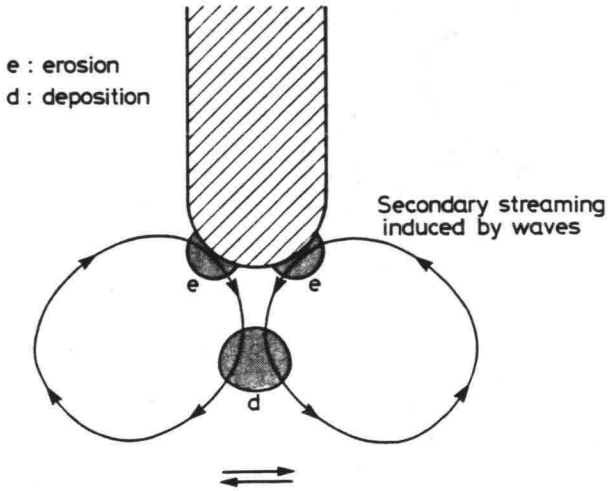

Fig. 16 Anticipated erosion-deposition pattern for very small KC numbers due to streaming.

Finally, it may noted that the effect of the head shape on the scour may be important. This subject is at present under investigation and the results will be reported in a follow-up publication.

Effect of superimposed currents

A few experiments have been conducted to see the effect of the presence of a current on the scour depth (Table 4). The current in the tests was in the same direction as the wave propagation. Each test was conducted for only 30 minutes. Therefore the results regarding the scour depth indicated in Table 4 may not represent the equilibrium values. The data in Table 4 are plotted in Fig. 17 along with the corresponding pure-waves scour data indicated in Table 2.

From the figure it is seen that the presence of a steady current on waves increases the scour depth considerably.

This increase in the scour depth may be attributed partly 1) to the formation of horse-shoe vortex in front of the structure (Fig. 10a) revealed by the present flow-visualization tests made in the presence of a slight current, partly 2) to an increase in the effective KC number in the half period where the wave-induced flow is in the same direction as the current, and partly 3) to the presence of the current itself by which the eroded material is transported away from the structure in the downstream direction.

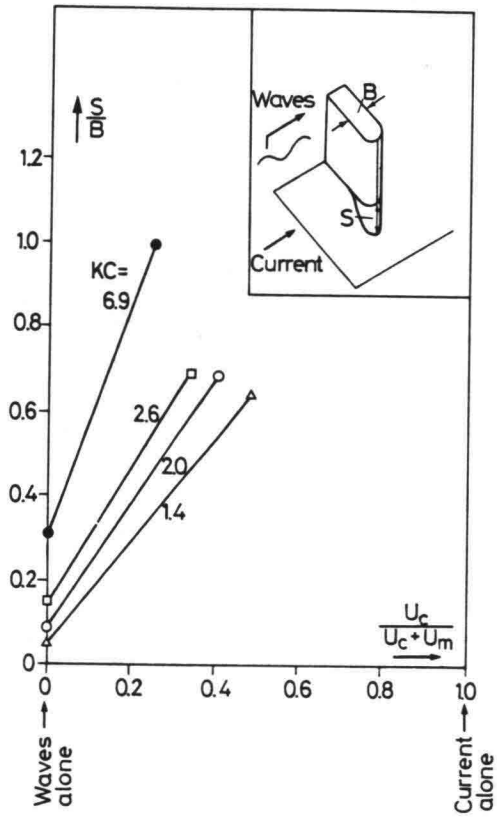

Fig. 17 Effect of current on scour in combined co-directional waves and current. Live bed ($\theta > \theta_{cr}$).

The latter may be an important element in the scour process in the case of extremely small KC numbers. While the net scour around the structure is zero for very small KC numbers (KC $\lesssim$ 1) in the case of pure waves (Fig. 14), substantial scour may occur due to the presence of even a small current, as suggested by Fig. 17. It may be noted that the examined combination of waves and current may be relevant in relation to the scour occurring at the head of a jetty.

Scale effects

In the case of pure waves, the scour process is related directly to the formation and further development of the lee-wake vortex. Therefore the scale effect on the scour must be felt through the scale effect existent with regard to the formation and the development of the lee-wake vortex itself. The latter has been discussed under the heading "Scale effects" in the previous section, and it was concluded that the non-dimensional extents of the lee-wake vortices in the field, namely L_x/B and L_y/B in Fig. 9, may be slightly smaller than those observed in the small-scale laboratory experiments. This suggests that the scour in the field may be slightly smaller than that predicted by the diagrams in Figs. 14 and 15.

In the case of combined waves and current, on the other hand, the major factors are 1) the formation of a horse-shoe vortex in front of the structure and 2) the mere presence of the current itself (so that the sediment can be carried away from the structure), as discussed in the preceding paragraphs. Item (1) is practically unaffected by the scale effect, as long as a current boundary layer is existent. Therefore the results depicted in Fig. 17 might be expected to be unaffected by the change in the scale.

5. CONCLUSIONS

1) Three kinds of flow regimes are identified for flow around the circular-head of a vertical-wall breakwater exposed to waves:

   a) The non-separated flow regime, which is observed for KC $\lesssim$ 1 where KC is the Keulegan-Carpenter number based on the width of the breakwater, B.
   b) The separated flow regime with no horse-shoe-vortex formation in front of the breakwater observed for 1 $\lesssim$ KC $\lesssim$ 12, and finally
   c) the separated flow regime with a horse-shoe vortex formation in front of the breakwater. This flow regime is observed when KC $\gtrsim$ 12.

2) Scour around the head of such a structure is governed by the KC number. The maximum scour depth, S, is found to be practically nil when KC $\lesssim$ 1. For KC $\gtrsim$ 1, however, the normalized scour depth S/B increases with increasing KC number.

3) The scour may be prevented by the conventional stone protection. The experiments indicate that, for a complete scour protection, the width of the protection layer should be selected to be at least 3-4 times the width of the breakwater.

4) The effect of the presence of a current upon the scour depth is found to be extremely important. The results indicate that, given the KC number, the scour depth increases considerably by the introduction of the current.

ACKNOWLEDGEMENT

This work was undertaken as part of the "MAST II Monolithic (Vertical) Coastal Structures" research programme. It was funded jointly by the Danish Technical Research Council (STVF) under the programme "Marin Technique" and by the Commission of the European Communities, Directorate General for Science, Research and Development, under MAST contract No. MAS2-CT92-0047.

The stay of Dr. K. Tunç Gökçe at ISVA as a visiting researcher was financed by the Scientific and Technical Research Council of Turkey with a post doctoral fellowship. Protection work experiments were conducted by Mr. Søren Bo Hansen (M.Sc.).

REFERENCES

Bijker, E.W. and Leeuwenstein, N. (1984). Interaction between pipelines and the seabed under the influence of waves and currents. Seabed Mechanics, B. Denness, ed., Graham and Trotman, Gettysburg, Md., pp. 235-242.

Breusers, H.N.C., Nicollet, G., Shen, H.W. (1977). Local scour around cylindrical piers. Journal of Hyd. Res., Vol. 15, No. 3, pp. 211-252.

Burcharth, H.F. The design of breakwaters. Coastal, Esturial and Harbour Engineer's Reference Book, M.B. Abbott & W.A. Price (Ed.), pp. 381-424, Chapman & Hall, London, 1993.

Fredsøe, J. (1984). Turbulent boundary layers in wave-current motion. Journal of Hydraulic Eng., ASCE, Vol. 110, No. HY8, pp. 1103-1120.

Gökçe, T. and Günbak, A.R. (1991). Self-burial and stimulated self-burial of pipelines by waves. Proc. of the First (1991) International Offshore and Polar Engineering Conf., Edinburgh, U.K., 11-16 August, 1991, II, pp. 308-314.

Hansen, E.A. (1992). Scour below pipelines and cables: A simple model. Proceedings of 11th Offshore Mechanics and Arctic Engineering Conference (OMAE 92), June 7-11, 1992, V-A, Pipeline technology, ASME, pp. 133-138.

Herbich, J.B., Schiller, R.E., Jr., Watanabe, R.K. and Dunlap, W.A. (1984). Sea floor scour-Design guidelines for ocean founded structures (Ocean engineering 4), Marcell Dekker, Inc., New York, N.Y., pp. 203-210.

Jensen, B.L., Sumer, B.M. and Fredsøe, J. (1989). Turbulent oscillatory boundary layers at high Reynolds numbers. J. Fluid Mechn., Vol. 206, 265-297.

Sarpkaya, T. (1986). Force on a circular cylinder in viscous oscillatory flow at low Keulegan-Carpenter numbers, J. Fluid Mech., Vol. 165, pp. 61-71.

Sumer, B.M. and Fredsøe, J. (1990). Scour below pipelines in waves. Journal of Waterway, Port, Coastal and Ocean Engineering, ASCE, Vol. 116, No. 3, pp. 307-323.

Sumer, B.M. and Fredsøe, J. (1992). A review of wave/current- induced scour around pipelines. Coastal Engineering, 1992, Proc. of the 23rd International Conference, Oct. 4-9, 1992, Venice, Italy, vol. 3, pp. 2839-2852.

Sumer, B.M., Fredsøe, J. and Christiansen, N. (1992) Scour around vertical pile in waves. Journal of Waterway, Port, Coastal and Ocean Engineering, ASCE, Vol. 118, No. 1, pp. 15-31.

HYDRO-PORT'94
International Conference on Hydro-Technical
Engineering for Port and Harbor Construction
October 19 - 21, 1994, Yokosuka, Japan

Stability of Beaches Protected with Detached Breakwaters

Yoshiaki Kuriyama [1]
Kazumasa Katoh [2]
Yasushi Ozaki [3]

[1] Senior Research Engineer, Hydraulic Engineering Division
Port and Harbour Research Institute, Ministry of Transport
Nagase 3-1-1, Yokosuka, Kanagawa 239
[2] Chief of the Littoral Drift Laboratory
Hydraulic Engineering Division
Port and Harbour Research Institute, Ministry of Transport
[3] Member of the Littoral Drift Laboratory
Hydraulic Engineering Division
Port and Harbour Research Institute, Ministry of Transport

ABSTRACT

The stability, the shoreline configurations and the beach profiles of beaches protected with detached breakwaters are investigated using the field data on five artificially nourished beaches. There is a relationship between the residual ratio of supplied sand, which represents the beach stability, and a parameter which consists of wave dimensions, detached breakwater dimensions, sediment diameter and beach slope. The geometrically estimated projecting length of a salient agrees with the observed value when the distance between the detached breakwater and the shoreline is larger than half the length of the detached breakwater. The estimated value, however, is larger than the observed one when the distance is smaller than half the length of the detached breakwater. The foreshore slopes and the berm heights predicted with formulae are compared with the observed values, and the validity of the formulae is discussed.

Key Words: Shoreline Configuration, Salient, Berm Height, Beach Slope, Nourishment

1. INTRODUCTION

In Japan, a system called Integrated Shore Protection System (ISPS) which combines detached breakwaters and beach nourishment has been planned and designed as a new type of coast protection system to protect people and property along the coast from wave erosion. A peculiarity of the ISPS is that the protective function of a beach, which reduces the wave energy acting on a seawall located behind the beach, is considered in the design because the

reflection coefficient of a beach is lower than those of any other coastal structures. As a result, seawalls designed using the ISPS need lower crown heights. The ISPS also affords people more opportunities to enjoy marine recreations such as sea-bathing and fishing.

Field investigations on the beach topography changes caused by detached breakwaters provide useful information for more reliable design of the ISPS. Toyoshima (1970) and Seiji et al. (1987) collected field data on detached breakwaters which were constructed to protect the beaches from erosion. They investigated the effect of a detached breakwater on sediment accumulation. However, wave climate, which affects the beach topography change, was not considered in their investigations. Although Kuriyama et al. (1988) have carried out follow-up surveys on five artificially nourished beaches protected with detached breakwaters in order to investigate beach stability, shoreline configurations and beach profiles, the wave climate was not considered.

The main objective of this paper is to study the topographical characteristics of a beach protected with detached breakwaters using wave data. We have collected wave data on the five artificially nourished beaches investigated by Kuriyama et al. (1988), and have rearranged the field data gathered in the follow-up surveys.

2. INVESTIGATED BEACHES

The investigated beaches are Suma Beach, Kataonami Beach, Kashiwazaki Beach, Koikawa Beach and Beppu Beach; their locations are shown in Figure 1. Figures 2 to 6 show their topographies and beach profiles. The figures by the detached breakwaters denote the years of the construction of the detached breakwaters. At Suma Beach and Kataonami Beach, auxiliary

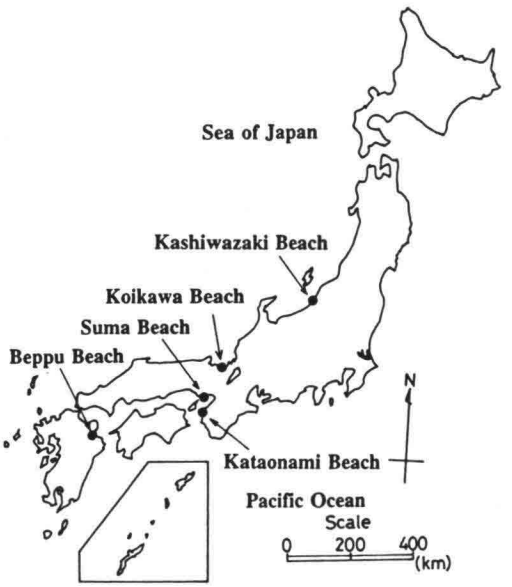

Figure 1 Locations of investigated beaches.

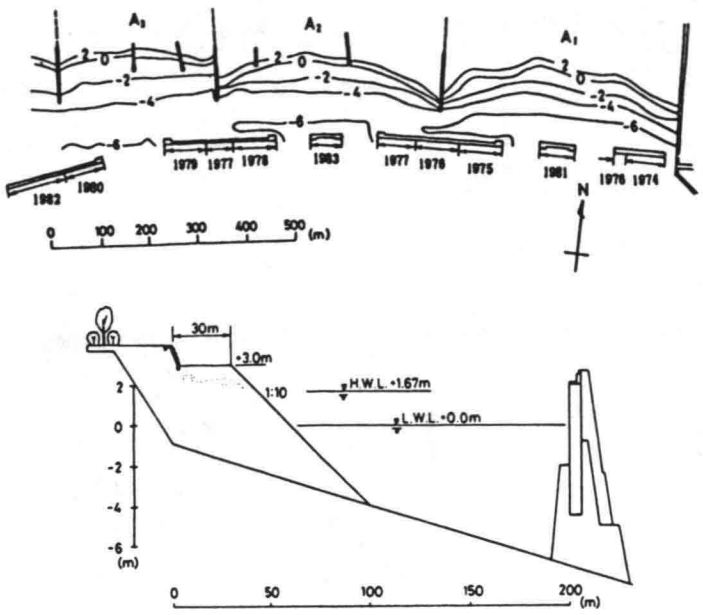

Figure 2 Beach topography and profile of Suma Beach.

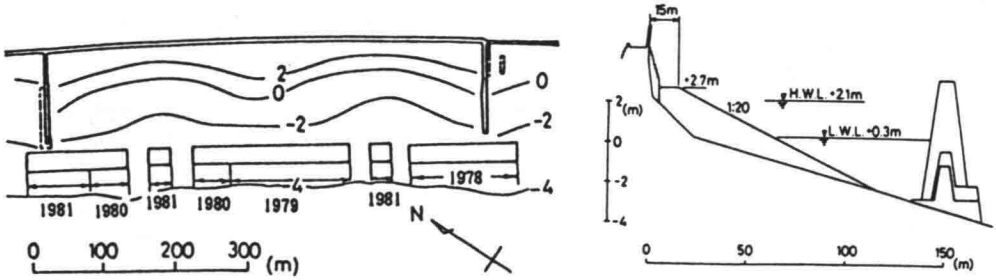

Figure 3 Beach topography and profile of Kataonami Beach.

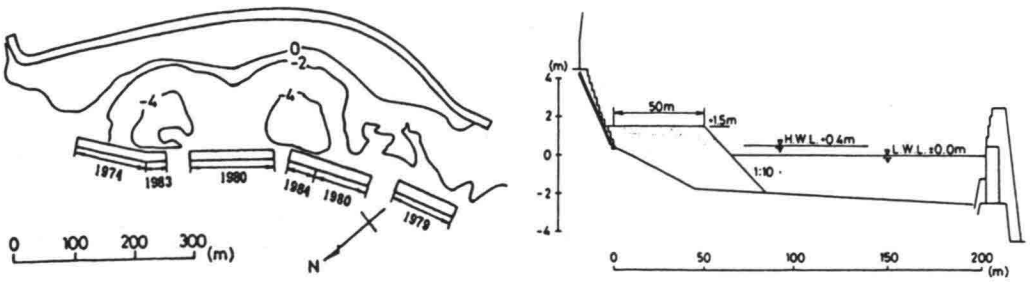

Figure 4 Beach topography and profile of Kashiwazaki Beach.

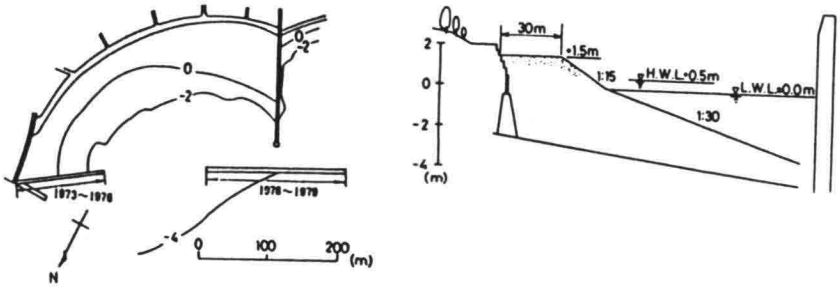

Figure 5 Beach topography and profile of Koikawa Beach.

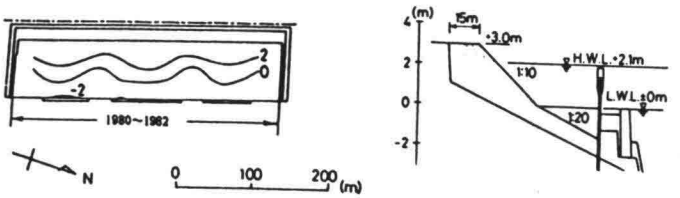

Figure 6 Beach topography and profile of Beppu Beach.

breakwaters were constructed at the openings after the beach nourishment to reduce the run-up heights at the openings. The breakwaters at Kashiwazaki Beach were extended in 1983 and 1984 to decrease the beach topography change.

The wave climates at Suma Beach, Kataonami Beach, Kashiwazaki Beach and Beppu Beach are listed in Table 1. Except for Kashiwazaki Beach, the wave conditions at the three beaches are mild. The high waves at Suma beach and Kataonami Beach are generated by a typhoon or a big extratropical cyclone, and those at Beppu Beach are generated by winter monsoons. At Kashiwazaki Beach, most of the high waves are generated by strong winter monsoons.

Although there are no wave data near Koikawa Beach, the waves at this beach are assumed to be similar to those at Kashiwazaki Beach. The wave heights, however, are assumed to be

Table 1 Wave climate

Beach	Occurrence frequency of waves lower than 0.5m	Maximum significant wave height (m)	Waves that occur twice a year		Investigation period
			height(m)	period (s)	
Suma	70%	2.40	2.0	5	1980~1982
Kataonami	95%	2.87	2.0	15	1980~1982
Kashiwazaki	45%	5.43	4.9	9	Jan.1983~Nov.1983 May1984~May1985
Beppu	75%	3.86	2.0	6	1984~1985

smaller because Koikawa Beach is located at an inner part of a bay.

The dimensions of the investigated beaches are summarized in Table 2. The design water depth is based on the datum line (D.L.) of each beach. The value of d_{50} represents the median sediment diameter. The slopes onshoreward and offshoreward of the shoreline at L.W.L. are expressed by tan α_1 and tan α_2 , respectively, as illustrated in Figure 7. The values of R and B represent the run-up height above D.L. and the backshore width.

Table 2 Dimensions of the investigated beaches

Dimensions \ Beach	Suma	Kataonami	Kashiwazaki	Koikawa	Beppu
Tidal levels (m)					
L. W. L.	0.00	0.30	0.01	0.00	0.00
M. W. L.	1.10	1.10	0.23	0.20	1.30
H. W. L.	1.67	2.10	0.50	0.50	2.10
Detached breakwater					
length (m)	120 ~ 260	130 ~ 220	90 ~ 150	200	65 ~ 95
opening width (m)	204 ~ 223	81 ~ 87	50 ~ 83	126	28
number	4	3	4	1	3
design water depth (m)	7.0	4.4	6.2	4.0	3.0
type	impermeable	permeable	impermiable	permeable	impermeable
crown height (m)	3.2	3.2	2.5	1.8	2.0
crown width (m)	6.5	7.5~8.1	7.5	6.1	2.0
auxiliary breakwater	2	2	2 (submerged)	0	2 (submerged)
d_{50} (supplied sand) (mm)	1.3 ~ 1.6	0.3 ~ 1.4	0.5 ~ 3.0	0.1 ~ 0.2	0.8
Design beach profile					
α_1	1 : 10	1 : 20	1 : 10	1 : 15	1 : 10
α_2	1 : 10	1 : 20	1 : 10	1 : 30	1 : 20
R	3.0	3.1	1.5	1.5	3.0
B	30.0	30.0	50.0	30.0	15.0
Start of nourishment work	1973	1979	1982	1980	1983
Total volumes of supplied sand (m^3)	610000	62000	125000	117000	60000
Investigated period	1978 ~ 1982	1979 ~ 1982	1982 ~ 1985	1981 ~ 1984	1984 ~ 1985

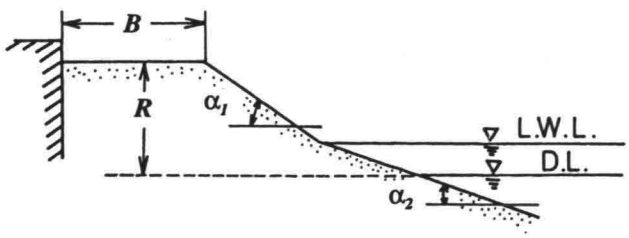

Figure 7 Definition sketch of beach profile.

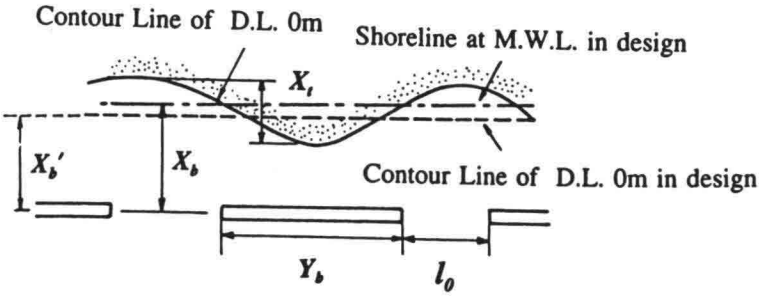

Figure 8 Definition sketch of detached breakwater and shoreline configuration.

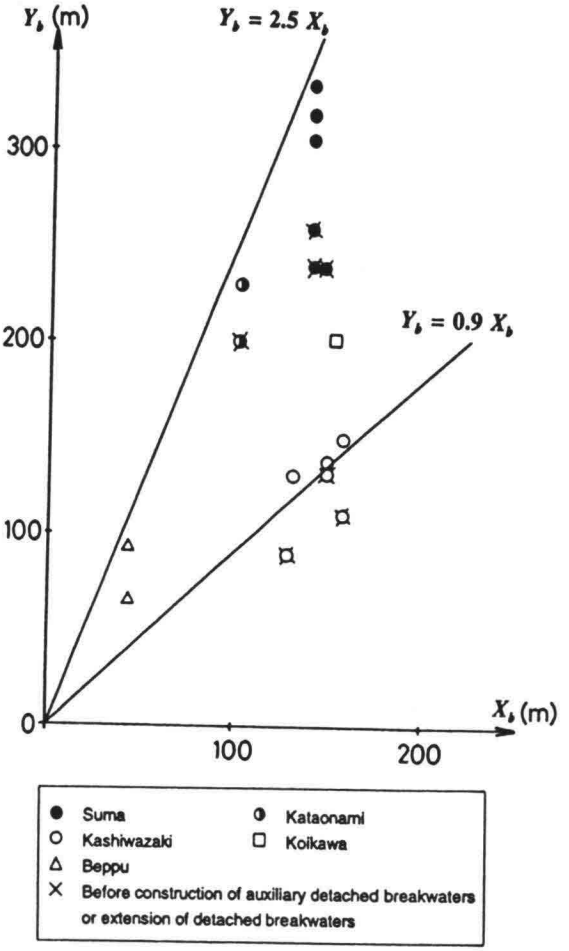

Figure 9 Relationship between X_b and Y_b.

Figure 8 illustrates the definitions of the dimensions of a beach; Y_b is the length of a detached breakwater, l_0 is the width of a breakwater opening, X_b is the distance between a detached breakwater and the shoreline at M.W.L. in design, X_b' is the distance between a detached breakwater and the contour line of D.L.0m in design, and X_t is the projecting length of the D.L.0m contour line. Figures 9 and 10 show the relationships between Y_b and X_b and between l_0 and Y_b. There are relationships among Y_b, X_b and l_0 which can be expressed by $Y_b = aX_b$ and $l_0 = bY_b$,where $0.9 \leq a \leq 2.3$ and $0.2 \leq b \leq 0.5$.

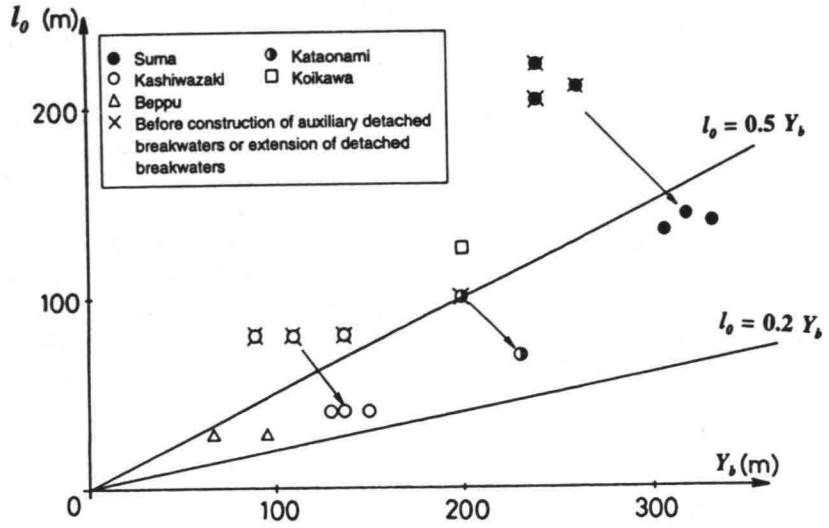

Figure 10 Relationship between Y_b and l_0.

3. BEACH STABILITY

A parameter which represents the stability of the investigated artificially nourished beaches is the residual ratio of the supplied sand, which is expressed as

$$R_V = V_R / V_S, \tag{1}$$

where R_V is the residual ratio, V_R is the volume of the sand remaining in the area shoreward of the detached breakwaters, and V_S is the volume of supplied sand.

Sunamura and Horikawa (1974) investigated the relationship among shoreline change, beach slope, sediment diameter and wave dimensions, and proposed a parameter C_S, which represents shoreline change, given by

$$C_s = (H_0/L_0)(\tan\beta)^{0.27}(d/L_0)^{-0.67}, \tag{2}$$

in which H_0 is the deepwater wave height, L_0 is the deepwater wave length, tanβ is the beach

slope, and d is the sediment diameter. Sunamura and Horikawa (1974) showed with field data that a shoreline advances when C_S is smaller than 18, and retreats when C_S is larger than 18.

We calculated C_S for the investigated beaches by using wave heights estimated by Eq.(3), which considers the wave energy dissipation by a detached breakwater,

$$H_0 = \sqrt{\frac{l_0}{l_0 + Y_B}} H_{01} . \tag{3}$$

The value of H_{01} expresses the height of the deep water wave that occurs twice a year; in the calculation of C_S, we use the dimensions of the waves that occur twice a year, which are listed in Table 2.

Figure 11 shows the relationship between C_s and R_V. The value of R_V decreases as C_s increases. When C_s is smaller than 10, R_V is larger than 0.9, while R_V is smaller than 0.7 when C_s is larger than 30. The value of C_s which demarcates accumulation and erosion is about 5. Although this value is different from that in Sunamura and Horikawa (1974), R_V is also roughly estimated with C_s.

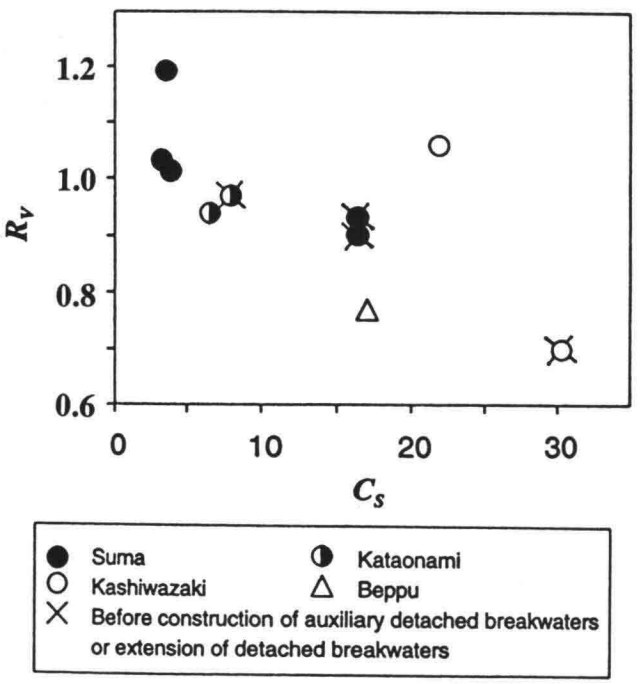

Figure 11 Relationship between C_S and R_V.

4. SHORELINE CONFIGURATIONS

A salient or a tombolo is usually formed behind a detached breakwater. We estimated the projecting length of a salient, X_t, geometrically assuming that a shoreline moves perpendicular to the direction of the diffracted wave. The formula relating Y_b, X_b' and X_t of a salient is

$$\frac{X_t}{X_b'}=\frac{1}{8}\left(\frac{Y_b}{X_b'}\right)^2. \tag{4}$$

The geometrical relationship among Y_b, X_b' and X_t is illustrated in Figure 12. Equation (4) assumes that the alongshore averaged position of the D.L.0m contour line does not change.

Figure 13 shows the comparison between Eq.(4) and the observed values. The solid line represents Eq.(4), while the level broken line represents X_t/X_b' of a tombolo, which is equal to 1. Although the observed values agree with the theoretical ones at Suma Beach, Kashiwazaki Beach and Koikawa Beach, the observed values are smaller than the theoretical ones at Kataonami Beach and Beppu Beach. Equation (4) is valid only when Y_b/X_b' is smaller than 2. The cause of the disagreement when Y_b/X_b' is about 2.5 is probably that the wave heights behind the detached breakwaters were too small to transport sediment. Consequently, the salients did not develop as predicted.

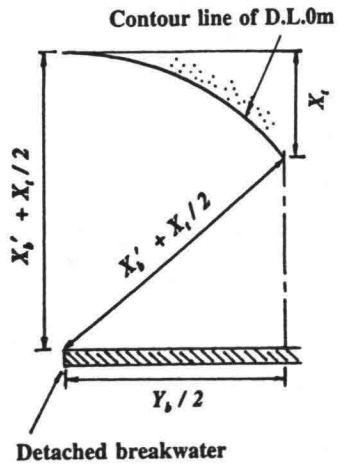

Figure 12 Definition sketch of shoreline configuration.

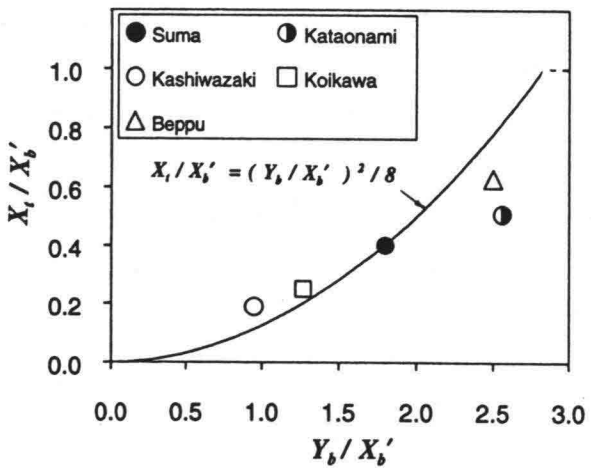

Figure 13 Relationship between Y_b / X_b' and X_t / X_b'.

5. BEACH PROFILES

5.1 Beach Slope in Foreshore Zone

The observed beach slopes in foreshore zone behind the detached breakwaters and the breakwater openings are compared with the values estimated with Eqs.(5) to (7), which were proposed by Port Construction Bureau, Ministry of Transport, Japan (1979), Rector (1954) and Sunamura (Port Construction Bureau, Ministry of Transport, Japan, 1979),

$$\tan\alpha_1=\left(\frac{1}{37.2}\frac{d_{50}}{H_0}\right)^{0.158} \quad :\frac{d_{50}}{H_0}\geq 2.4\times10^{-4},$$
$$\tan\alpha_1=\left(376.6\frac{d_{50}}{H_0}\right)^{0.7856} \quad :\frac{d_{50}}{H_0}<2.4\times10^{-4}, \tag{5}$$

$$\tan\alpha_1=0.3\left(\frac{H_0}{L_0}\right)^{-0.3}\left(\frac{d_{50}}{L_0}\right)^{0.2}, \tag{6}$$

$$\tan\alpha_1=0.45\left(\frac{d_{50}}{H_0}\right)^{0.5}\left(\frac{H_0}{L_0}\right)^{-0.3}. \tag{7}$$

The heights of the equivalent deepwater waves behind detached breakwaters and breakwater openings are estimated by Eq.(8) with the heights of the waves that occur twice a year,

$$H_0=H_{01}\sqrt{\sum K_{oi}^2 r_{si}^2+\sum K_{bj}^2 r_{bj}^2}, \tag{8}$$

where r_{si} is the wave transformation ratio of a submerged breakwater at a breakwater opening, r_{bj} is that of a detached breakwater. The values of K_{0i} and K_{bj} are the diffraction coefficients of the waves that pass through the opening and the detached breakwater; they are the values at the shoreline and are estimated with diffraction diagrams by Goda (1985). The subscripts of i and j indicate the numbers of a opening and a detached breakwater.

The relationship between the observed values and estimated ones is shown in Figure 14. The solid lines, the dash-dotted lines and the broken lines express the values estimated with Eqs.(5), (6) and (7). Since those equations are functions of sediment diameter, several lines are needed to express the estimated values. The symbols with the sign + denote the values behind detached breakwaters, while the symbols without the sign + denote the values behind breakwater openings. The values estimated with Eq.(5) are larger than the observed ones, while the values estimated with Eq.(7) are smaller than the observed ones. The value estimated with Eq.(6) is nearly equal to the average of the observed values at each beach although the value estimated with Eq.(6) at Kashiwazaki Beach is larger than the average.

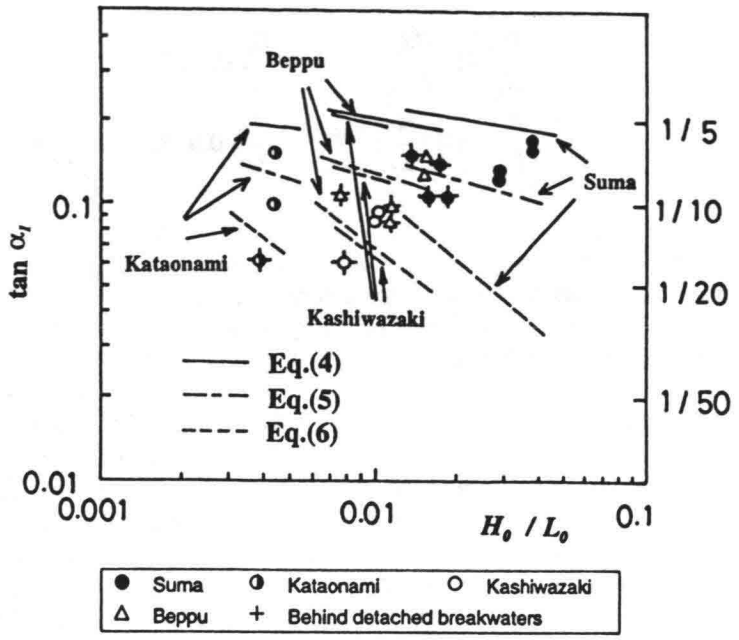

Figure 14 Relationship between H_0 / L_0 and $\tan\alpha_I$.

5.2 Berm Height

Equations (9) and (10) are the formulae for the estimation of berm height, which were proposed by Rector (1958) and Swart (1974), respectively,

$$\begin{aligned} \frac{R'}{L_0} &= 0.024 && : \frac{H_0}{L_0} \geq 0.018, \\ \frac{R'}{L_0} &= 0.18\left(\frac{H_0}{L_0}\right)^{0.5} && : \frac{H_0}{L_0} < 0.018, \end{aligned} \tag{9}$$

$$\begin{aligned} &\frac{R'}{d_{50}} = 7644 - 7706 \exp A, \\ &A = \left(-0.000143 \frac{H_0^{0.488} T^{0.93}}{d_{50}^{0.786}}\right). \end{aligned} \tag{10}$$

The values of R' and T express the berm height above the still sea water level and the wave period. Equation (11) expresses the run-up heights above the still sea water levels observed at open coasts in Japan (Port Construction Bureau, Ministry of Transport, Japan, 1979),

$$\frac{R'}{H_0}=(52\frac{H_0}{L_0})^{-2.7} \quad :\frac{H_0}{L_0}\geq 0.013,$$
$$\frac{R'}{H_0}=(8.25\frac{H_0}{L_0})^{-0.461} \quad :\frac{H_0}{L_0}<0.013. \tag{11}$$

The observed berm heights are compared with the values estimated by Eqs. (9) and (10) with the dimensions of the waves that occur twice a year. The values estimated by Eq.(11) are also compared with the observed berm heights because the run-up heights in storms are supposed to be nearly equal to the berm heights.

Figure 15 shows the comparison between the estimated berm heights and the observed values. The value of R_m denotes the berm height above H.W.L. Equivalent deepwater wave heights were estimated by the procedure mentioned in 5.1. The values estimated by Eq.(9) and Eq.(10) are larger than the observed ones when the values of H_0/L_0 are smaller than 0.01, and smaller than the observed ones when the values of H_0/L_0 are larger than 0.01. The berm heights estimated by Eq.(11) are larger than the observed ones when the values of H_0/L_0 are smaller than 0.013. However, the estimated berm heights at Suma Beach, where the values of H_0/L_0 are larger than 0.013, are smaller than the observed ones.

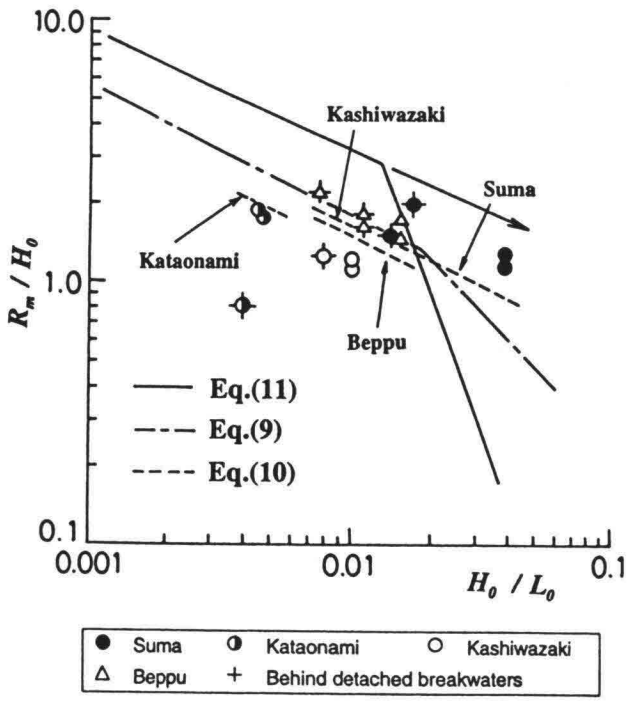

Figure 15 Relationship between H_0 / L_0 and R_m / H_0.

The berm height should be designed so that waves do not reach the seawall behind the beach because the waves reflected by the seawall erode the beach. Beaches where the berm heights are larger than the values estimated with Eq.(11) are safe when the design values of H_0/L_0 are smaller than 0.013. The beaches are not safe when the design values of H_0/L_0 are larger than 0.013 because the values estimated by Eq.(11) are smaller than the observed ones. Hence, when the design wave steepness is larger than 0.013, we recommend designing the berm height to be larger than the value estimated with the lower equation of Eq.(11), which is for the waves whose steepness is larger than 0.013; the value estimated with the lower equation of Eq.(11) is shown by the arrow in Figure 15.

6. CONCLUSIONS

The residual ratio of the supplied sand can be roughly estimated using the parameter C_S, which is expressed by Eq.(1). The ratio increases as C_S decreases; the ratio is larger than 0.9 when C_S is smaller than 10, while the ratio is smaller than 0.7 when C_S is larger than 30.

The estimated projecting length of a salient using Eq.(4), which was derived geometrically, agrees with the observed value when Y_b/X_b' is smaller than 2. The estimated value, however, is larger than the observed one when Y_b/X_b' is about 2.5. Equation (4) is valid only when Y_b/X_b' is smaller than 2.

The foreshore slope predicted with Eq.(6) approximately agrees with the mean of the observed values at each beach. The slopes estimated with Eq.(5) are larger than the observed ones, while the values estimated with Eq.(7) are smaller than the observed ones.

The berm heights estimated by Eq.(11) are larger than the observed ones when the values of wave steepness are smaller than 0.013. The estimated ones, however, are smaller than the observed ones when the values of wave steepness are larger than 0.013. Thus, we recommend using the lower equation of Eq.(11), which is for the waves whose steepness is smaller than 0.013, in order to estimate the berm height even when the design wave steepness is larger than 0.013.

ACKNOWLEDGEMENT

The authors would like to thank the provincial governments for providing the useful data, and Dr. N. Tanaka and Prof. I. Irie, former Directors of Marine Hydrodynamics Division, Port and Harbour Research Institute, for their valuable advice. Further acknowledgement is extended to Dr. Robert Christian Faucette, Research Scientist, Conrad Blucher Institute, Texas A&M University -Corpus Christi, for his useful comments that improved this paper.

REFERENCES

Goda Y. (1985): Random Seas and Design of Maritime Structures, University of Tokyo Press, pp.51-66.

Kuriyama Y., I. Irie and K. Katoh (1988): Follow-up Surveys of Artificially Nourished

Beaches, Coastal Eng. in Japan, Vol.31, No.1, pp.105-120.
Port Construction Bureau, Ministry of Transport, Japan (1979): Manual for Artificially Nourished Beach, pp.29-34. (in Japanese)
Rector R. L. (1954): Laboratory Study of Equilibrium Profiles of Beaches, Technical Memorandum No.41, Beach Erosion Board, 38p.
Seiji M., T. Uda and S. Tanaka (1987): Statistical Study on the Effect and Stability of Detached Breakwaters, Coastal Eng. in Japan, Vol.30, No.1, pp.131-141.
Sunamura T. and K. Horikawa (1974): Two-dimensional beach transformation due to waves, Proc. 14th ICCE, pp.920-938.
Swart D.H. (1974): A Schematization of Onshore-Offshore Transport, Proc. 14th ICCE, pp.884-900.
Toyoshima O. (1970): Statistical Investigation on Detached Breakwaters, 17th Japanese Conf. on Coastal Eng., pp.323-330. (in Japanese)

HYDRO-PORT'94
International Conference on Hydro-Technical
Engineering for Port and Harbor Construction
October 19 - 21, 1994, Yokosuka, Japan

Gros Beach Nourishment (San Sebastian, SPAIN)

José María Medina Villaverde

Ingeniero de Caminos, Canales y Puertos
Centro de Estudios de Puertos y Costas- CEDEX
C/ Antonio López, 81, 28026 Madrid

ABSTRACT

Since the beginning of the century, Gros beach, in San Sebastián, has been invaded by the development of the city. Streets and buildings went towards the sea in several hundred of meters. Also the construction of sea walls along the coast has induced reflections and erosions. Now a sand nourishment project has been drawn up, for which the author of this paper has studied the most feasible and reliable solutions.

1. INTRODUCTION

Gros beach is located close to the east edge of the Cantabrian Spanish shore, at the pretty city of San Sebastian -Donostia, in the local language- (Guipúzcoa).

At 1.901, the shoreline was placed in the today Colon's Avenue, which lies today behind several building blocks, some 300 meters far from the present day shoreline.

This situation involves the destruction of the beach, as the century went by.

2. STUDIES UNDERTAKEN

The previous studies were necessary to be made, with the aim of knowing as perfectly as possible the main physical and hydrodynamic features. The referred works can be summarized as follows:

a) Visual Checking
b) Historical data referring to Gros Beach and Guipuzcoa's coast
c) Sea climate
d) Wave propagation
e) Shoreline evolution
f) Physical modelling

In the following paragraphs, those studies will be summarized and commented.

3. VISUAL CHECKING

The beach morphology were very well known, since the author lived close to the beach for several months. We were also helped by people from the General Directorate on Shores of the Spanish Ministry of Public Works and Transports, who provided us with several graphic

documentation related to the beach. Some of them (see final pages) were taken at low tide (we performed an harmonic study of the tidal wave in the date and hour in which the photo was made). After that studies we check the existence of strong reflections at the Kursaal (west edge of the beach), in which a sea wall was constructed. Reflected waves go from west to east with an obliquity of some 90 degrees, provoking a strong sand transport.

The conclusion of the visual checking was that there was a big need of making a sand nourishment as soon as possible. ***Every complete beach is the best civil work on coastal defence***. ***The dune destruction should be avoided***.

4. SEA CLIMATE

To make this study we used the database of the National Weather Records Center)(North Caroline, U.S.A.), and the directional buoy of the RED ESPAÑOLA DE MEDIDA Y REGISTRO DE OLEAJE (R.E.M.R.O. Centro de Estudios de Puertos y Costas-CEDEX, Madrid, Spain), placed in front of the Bilbao (Vizcaya, Spain) coast.

The geographical coordinates to collect data were from 43°24' to 44°24' North and from 2°06' to 4°06' West.

From these sources we could made the wave roses which can be seen at the end of the paper.

The most frequent storms use to come from the N.W. quadrant. The most usual periods are 8 to 10 seconds.

5. STUDY OF SOLUTIONS

Since the only way to have a Beach at Gros was nourishing it, and since underwater there is no room enough to place sand, constructing a breakwater was quite necessary. Several plan shapes were checked, as can be seen in the next paragraph. The different layouts are shown at the end of the paper.

6. WAVE PROPAGATION

Wave propagation studies were made with **REFDIF10** and **MDS2D32P** mathematical models, developed at Cepyc by its present Director, D. José María Grassa Garrido, who kindly allow us to use them. The inputs to the models came from the sea climate study.

Three different grids were used to make the study: the first one was very big and coarse, in order to involve the whole Guipuzcoa coast, the second one affecting only the San Sebastian beach and the final, the most fine involved only the Gros beach.

Several N.W. storms, whose periods fitted between 10 and 20 seconds, were tested. Two tidal conditions were used (high and low tide, with some 4.00 m between them).

Results show that waves arrive to the beach with a very, very low obliquity (less than 5°). The lower periods the highest obliquities due to the fact that refraction appears latter in propagation.

Among the results, we select the most representative: the storm N-70°-W (the highest initial obliquity) and T = 14 s. In the figure can be seen how the final obliquity (at the beach) is very low.

MDS2D32P includes also the effect of reflection on the walls. The figures show the wave propagation corresponding to the storm NW, T = 16 s, with sea level 3.5 m due to high tide. Energy loss due to bottom friction is also included.

Wave propagation studies showed the need of placing an obstruction to waves in order to induce a diffraction effect, which aim is to place wave fronts parallel to the shoreline. Thus the best solution was constructing a breakwater, whose effect is diffracting waves and also supporting the nourished beach, to avoid the loosing of sand into the mouth of Urumea River, nearby the beach.

Several layout of breakwaters were tested in order to choose the best plan.

7. SHORELINE EVOLUTION

Among the several possible solutions we had to choose the best, from the point of view of the stability of the beach. Thus, we performed a shoreline evolution study, helped by the GENESIS[1] mathematical model.

The initial shoreline was defined by means of Silvester's theories on shaping of bays. The incoming waves had an obliquity from -5° to +5° respecting to the normal to the initial shoreline, according to the wave propagation studies.

The best solution places the top of the breakwater in the active zone of the beach (see figures). From the point of view of hydrodynamics the best solution is likely to be a curve breakwater, in order to avoid disturbances in the mouth of Urumea River. In addition, the curve breakwater should save sand.

8. PHYSICAL TEST

A physical test was performed. In it, two different breakwaters were tested: a straight one, following the right bank of Urumea river, and the proposed curve one. The result of the test showed that the theoretical study was right.

9. CONCLUSIONS

1. Urban planning has been historically the guilty of the erosive situation of the Gros beach.
2. Thus, is very important to pay attention to the effects of civil works on Nature
3. There is two main dangers derived from construction of civil works: the first one consists of cutting the natural sand supply to beaches, destroying an effective device of coastal defence, the second one consists of invading the beach, destroying it directly. These two situations should be avoided.
4. The nourishment of Gros beach is necessary to get a stable beach in the Zurriola bay.
5. Constructing a breakwater is indispensable, in order to induce diffractions, to get wave fronts parallel to the proposed new shoreline.
6. The best plan for the breakwater is curve, in order to avoid disturbances in the mouth is the curve one.
7. After constructing the embankment is necessary to nourish the beach with some 1.000.000 m^3.

---

[1] CERC. Department of the Army. Vicksburg, Mississippi, USA

10. FIGURES

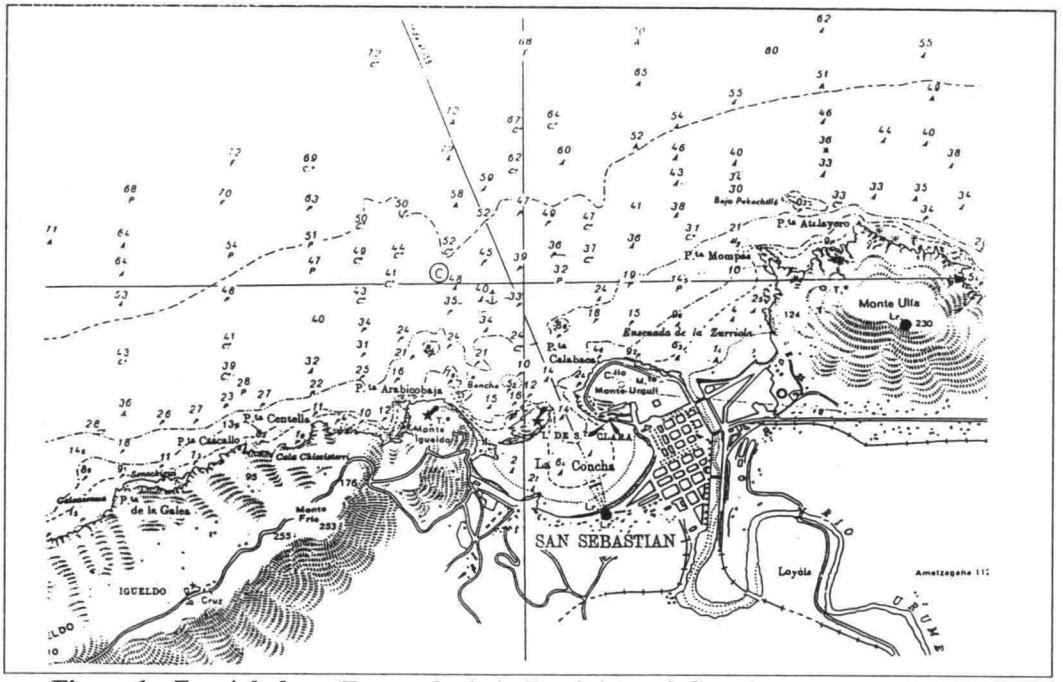

Figure 1.- Zurriola bay *(Ensenada de la Zurriola)* and Gros beach *(Playa de Gros)*

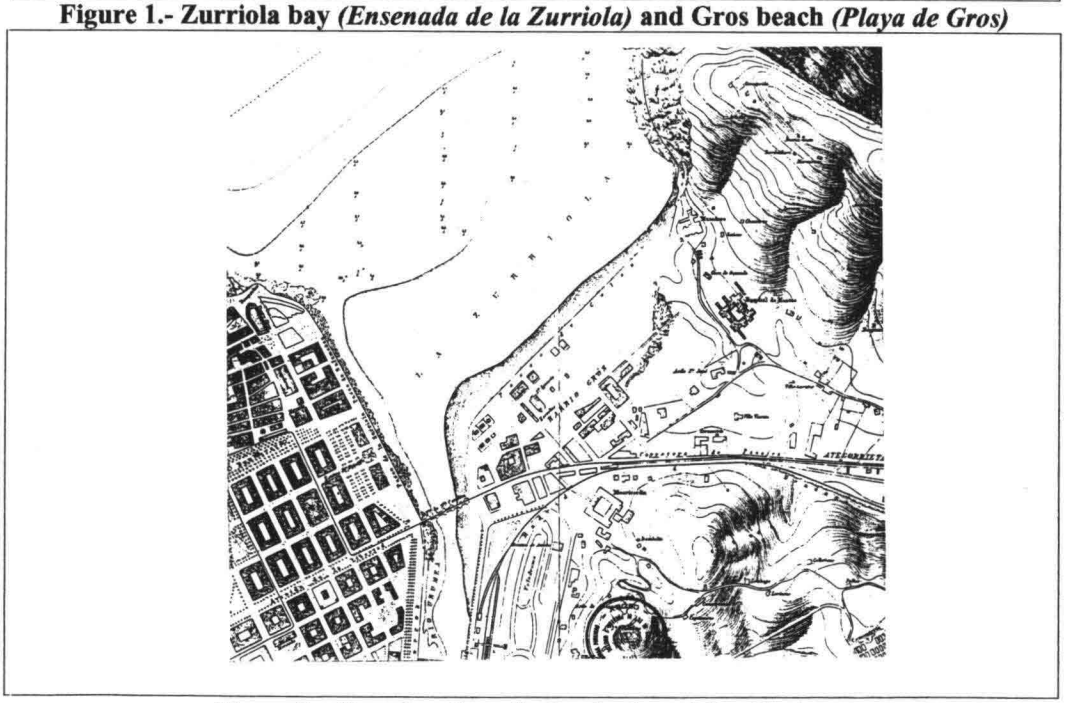

Figure 2.- Gros beach at the beginning of the Century

Figure 3.- Gros beach as it looks today

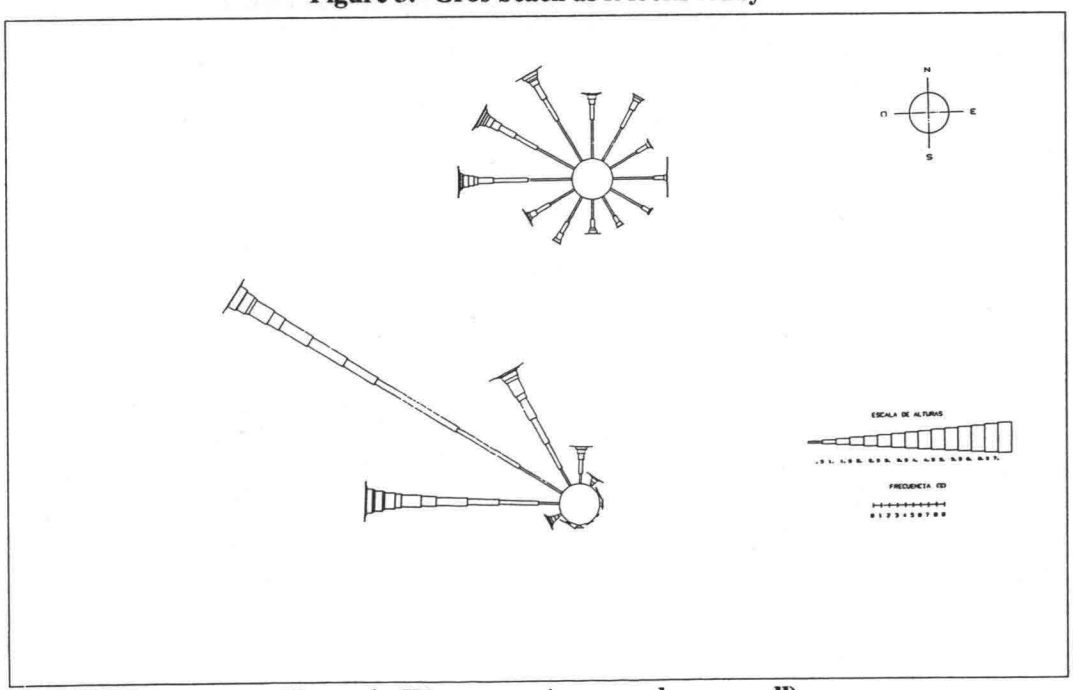

Figure 4.- Wave roses (up: sea; down: swell)

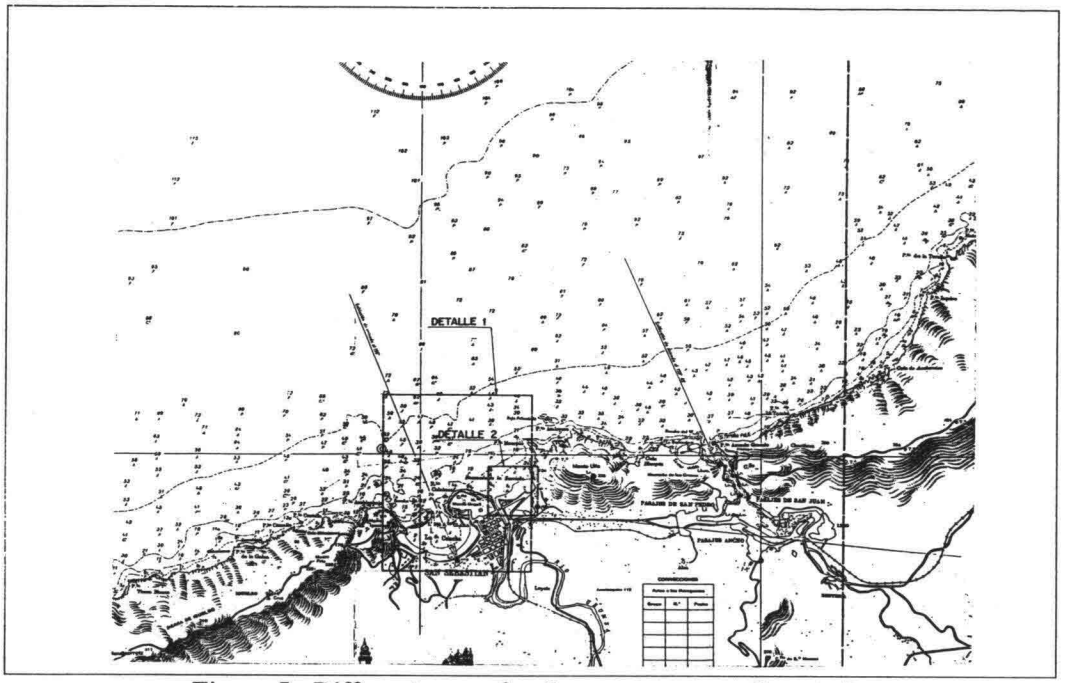

Figure 5.- Different zones for the wave propagation study

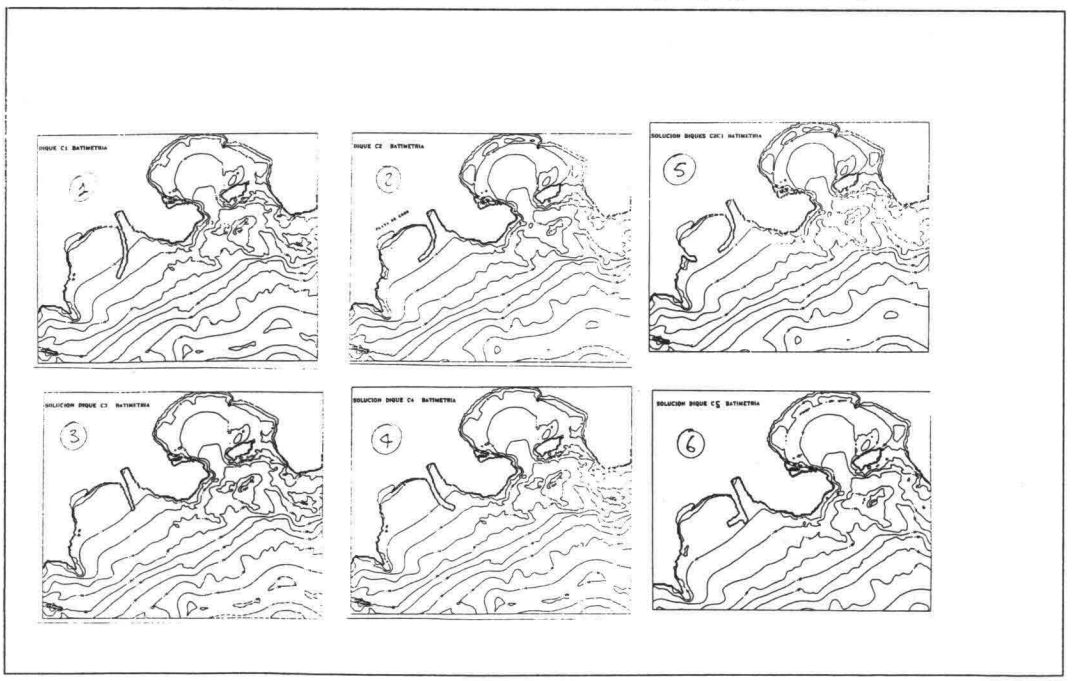

Figure 6.- Different tested solutions

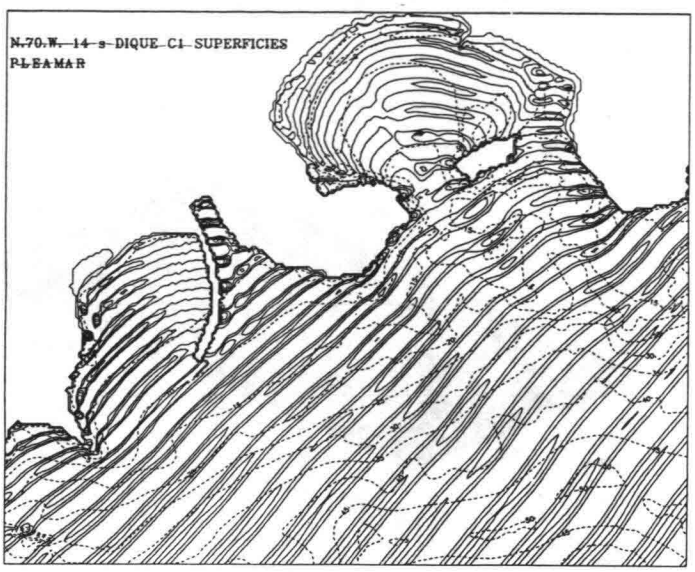

Figure 7.- Wave propagation: N-70°-W / 14 s / high tide

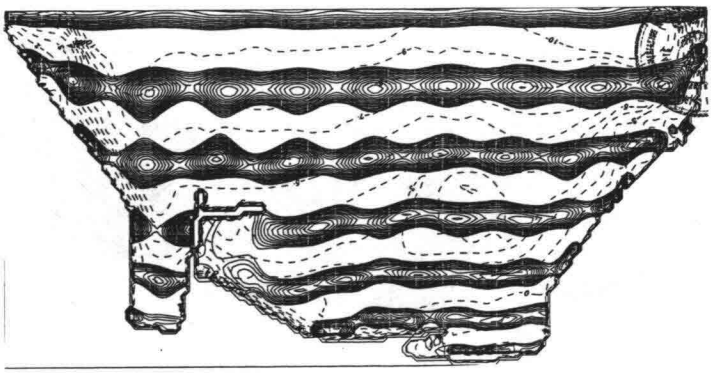

Figure 8.- Wave propagation NW / 16 s / high tide / with friction, reflection and breaking (MDS2D32P)

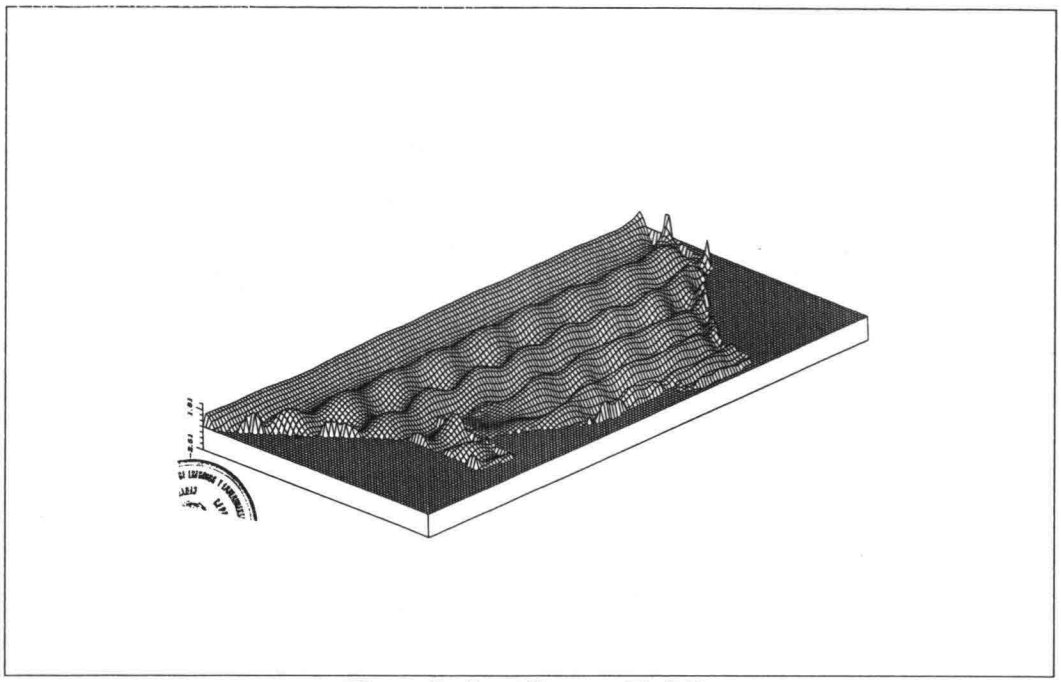

Figure 9.- Last figure with 3-D

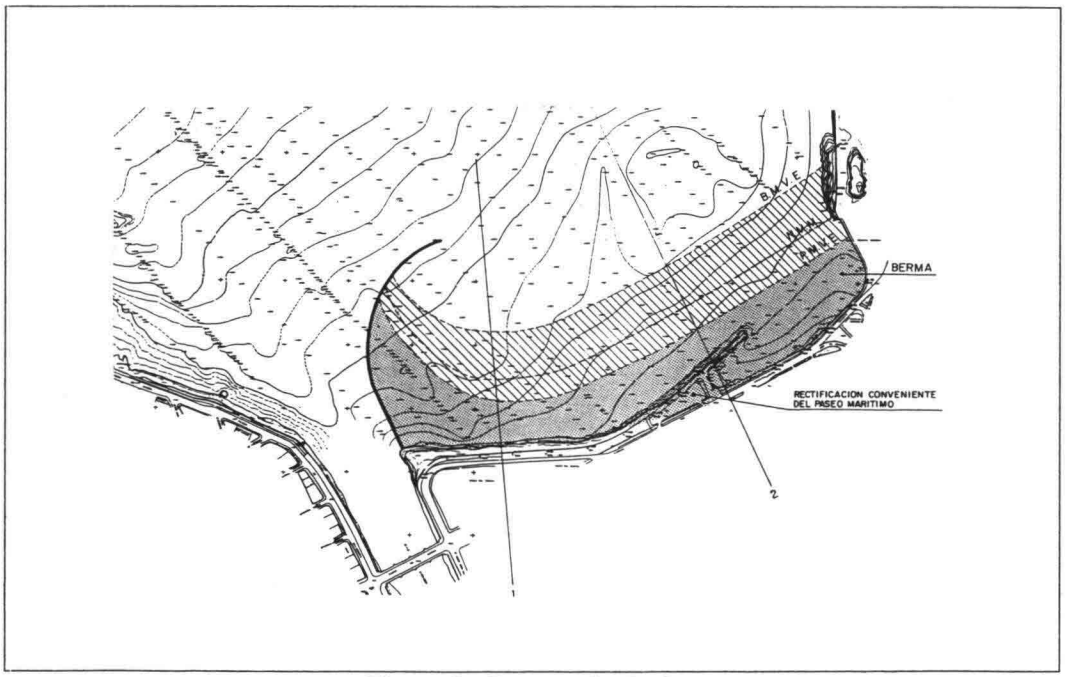

Figure 9.- Proposed solution

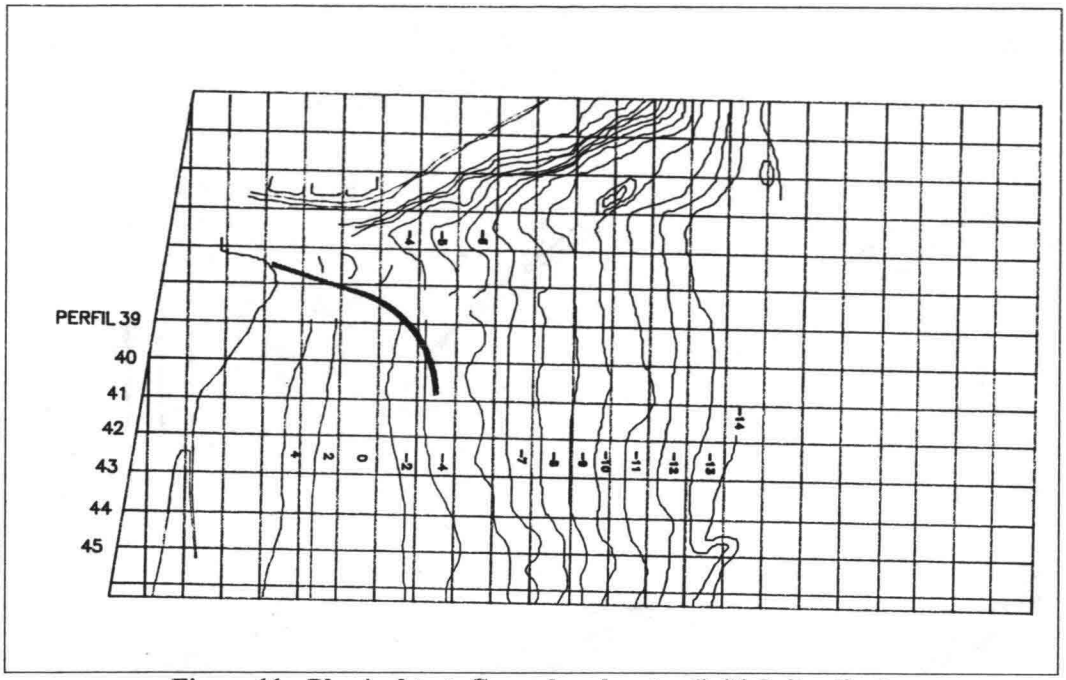

Figure 11.- Physical test. Curve breakwater (initial situation)

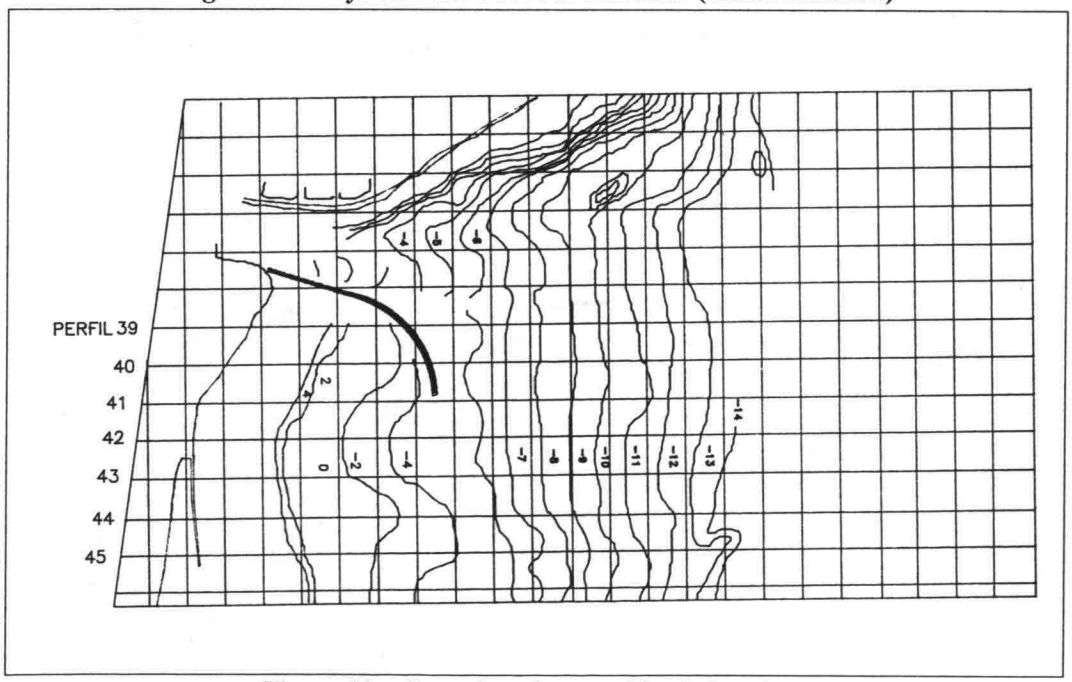

Figure 12.- Curve breakwater. Final situation

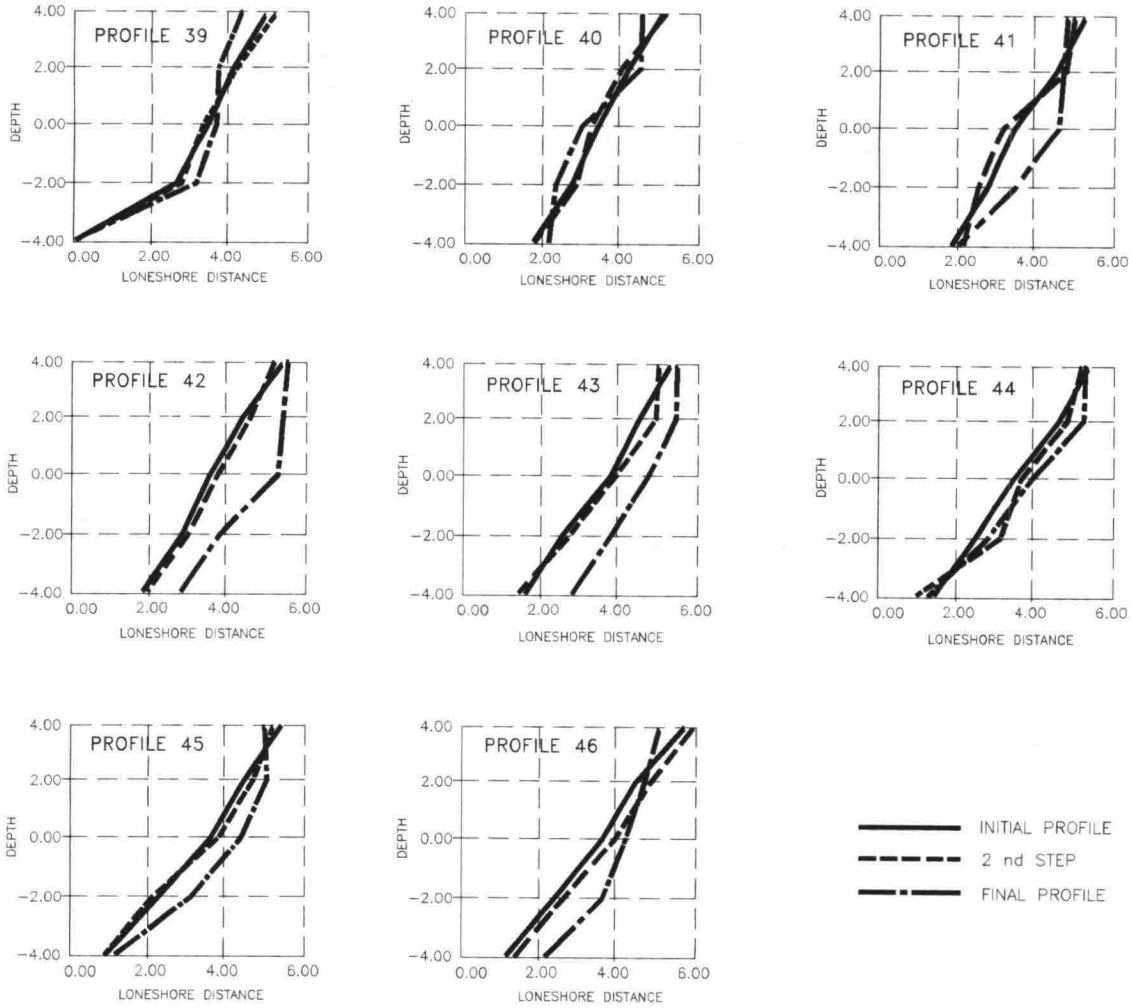
PROFILE 39
PROFILE 40
PROFILE 41
PROFILE 42
PROFILE 43
PROFILE 44
PROFILE 45
PROFILE 46
DEPTH
LONESHORE DISTANCE
4.00
2.00
0.00
-2.00
-4.00
0.00
2.00
4.00
6.00
INITIAL PROFILE
2 nd STEP
FINAL PROFILE

HYDRO-PORT'94
International Conference on Hydro-Technical
Engineering for Port and Harbor Construction
October 19 - 21, 1994, Yokosuka, Japan

Development and Application of a Numerical Model for Shoreline Simulation

K. Janardanan
V. Sundar

Ocean Engineering Centre, Indian Institute of Technology
Madras 600 036

ABSTRACT

A numerical model for predicting the shoreline oscillation due to the presence of shore connected structures has been developed based on the approach proposed by Kraus and Harikai (1983). Even though, this is an oneline model considering only the longshore sediment transport in predicting the shoreline evolution due a structure normal to the shore, it is well entrenched in the Coastal Engineering Practice. As the action of regular waves is unrealistic, a more appropriate method of Monte Carlo simulation of the wave characteristics has been used, wherein, the daily wave characteristics form the basic input parameters. The above method of simulation is effected by changing the sequential occurrence of wave characteristics. The developed model is applied to the major port at Madras, India for its verification and prediction of shoreline changes. The shoreline evolution predicted for the Madras port using the Monte Carlo simulation is compared with that obtained due to average wave data. The salient results obtained as stated above are reported in this paper.

Key Words: Shoreline Evolution, Monte Carlo Simulation, Wave Characteristics, Erosion, Accresion, Shore Conneted Structures.

1. INTRODUCTION

Prediction of shoreline oscillation due the presence of structures is very important because of the high cost involved for the protection of coast from erosion. Peninsular India has a vast coastal line of length about 6000 Km, considerable portion of it especially stretches along the east coast, experiences severe erosion due to the presence of natural headlands or man made shore connected structures. In addition, the existence of the major ports, as well as developing ports formed by breakwaters has a significant effect on adjacent shoreline. The next major activity of aquaculture come up in a big way, needs continuous pumping of seawater through pipelines or through open trenches. These pipelines are sometimes being supported on rubble mound groins which again alter the configuration of the shorelines. Hence, there is an urgent need to investigate the shoreline changes due to shore connected structures.

Numerical models offer the capability to incorporate the wave characteristics and sediment transport and has the potential of providing reasonable estimate of the shoreline response.

Due to the importance of order of sequential wave events, a Monte Carlo simulation of wave characteristics is used to determine the shoreline response similar to the methodology proposed by Le-Mehaute et al (1981). The use of monthly or yearly wave data averages are highly questionable, because, the phenomenology linking the wave forcing function to the longshore transport and other related effects are highly nonlinear and the principle of super position is no longer valid. For instance, a long wave followed by a short wave does not yield the same result as a short wave followed by a long wave. The present study deals with the result obtained by applying the developed numerical model for the prediction of shoreline response adjacent to the Madras port breakwater. The daily visual observation of wave characteristics, viz., wave height, wave period and wave direction for ten years (1980-1990) has been used for studying the shoreline response. In the case of Monte Carlo simulation, the sequence of occurrence wave characteristics are changed using a random seed number twenty times and leading to twenty simulated shorelines, the average of which is taken as the representative shoreline response.

2. DEVELOPMENT OF NUMERICAL MODEL

2.1 General :

Mathematical modeling of shoreline change has proven to be a useful engineering technique for understanding and predicting the evolution of sandy beaches. The mathematical modeling of shoreline evolution essentially relates the change in the shoreline, to the rate of material transported from the beach. In oneline model, the longshore sand transport is assumed to occur uniformly over the whole beach profile down to a certain critical depth called depth of closure or depth of active sediment transport. The governing differential equation of oneline model will take the following form

$$(b + D_c)\frac{\partial y}{\partial t} = -\frac{\partial Q}{\partial x} + q(x) \qquad (1)$$

where y is the shoreline position, positive towards the offshore is the function of x measured along the shore and time t, b: height of berm, D_c: Limit of active sand transport beyond which sand transport changes can be assumed to be negligible (Depth of closure), Q: wave induced longshore sediment transport and q(x): quantity of sediment added per unit length of shoreline by various agencies like sand deposited or dredged during the beach nourishment, loss or gain of sand by wind etc.

The value of D_c depending on wave characteristics according to the Hallermier (1981) is expressed as

$$\frac{D_c}{H_s} = 2.28 - 67.5 * \frac{H_s}{gT_s^2} \qquad (2)$$

in which H_s and T_s are significant wave height and period respectively.

In this paper, D_c which depend on the grain size of the sediments, D_{50}, is taken as a depth at which sediment starts lifting from the sea bed given in -----(1984).

The longshore sediment transport based on the longitudinal energy flux according to ----- (1984) is given by

$$Q = 1290 \times P_l \, m^3 / year \qquad (3)$$

where P_l = longitudinal energy flux $= \frac{\rho g^2}{32\Pi} H_0^2 T K_R^2 \sin(\alpha_b)\cos(\alpha_b)$

ρ = mass density of sea water in $N sec^2 / m^4$

g = gravitational constant in m / sec^2

H_0 = deep water wave height in meters, T = wave period in seconds

K_R = refraction coefficient $= \sqrt{\frac{\cos(\alpha_0)}{\cos(\alpha_b)}}$

in which α_b and α_0 are the wave angles at the breaker depth and deep water respectively Le-Mehaute and Koh (1981) approximated breaker angle α_b as

$$\alpha_b = \beta \alpha_0 \qquad (4)$$

where $\beta = 0.25 + 5.5(\frac{H_0}{L_0})$, in which, L_0 is deep water wave length.

The effects of diffraction are accounted by replacing the refraction coefficient K_R by $K_R K_D$.

$$Q = AK_D^2 \cos(\alpha_0)\sin(\alpha_b) \qquad (5)$$

in which $A = \frac{1290}{32\Pi} \rho g^2 H_0^2 T$ and K_D is diffraction coefficient

The value of K_D is calculated by the method proposed by Dean and Dalrymple (1984).

Setting the scale factors for y,x,t,Q and eq. 1 may be written in a nondimensional form as

$$\frac{\partial \bar{y}}{\partial \bar{x}} = -\frac{\partial \bar{Q}}{\partial \bar{x}} + \bar{q}(x) \tag{6}$$

where, $\bar{y} = \frac{y}{(b+D_c)}, \bar{x} = \frac{x}{(b+D_c)}, \bar{t} = t^*\left(A/(b+D_c)^3\right), \bar{Q} = \frac{Q}{A}$ and

$$\bar{q} = q(x) \times (b+D_c)/A$$

2.2 Numerical Model of Kraus and Harikai (1983)

The nondimensional equation of shoreline evolution is expressed in the finite difference scheme as

$$\bar{y}_{n,\bar{t}+1} = B^*\left\{\bar{Q}_{n,\bar{t}+1} - \bar{Q}_{n+1,\bar{t}+1}\right\} + C_n \tag{7}$$

where $B^* = \frac{\delta \bar{t}}{2 \times \delta \bar{x}}$ and $C_n = B^*\left[\bar{Q}_{n,\bar{t}} - \bar{Q}_{n+1,\bar{t}+1} + 2\delta \bar{x}\bar{q}_{n,\bar{t}}\right] + \bar{y}_{n,\bar{t}}$

The nondimensional shoreline is divided into N grid points at equal nondimensional interval $\delta \bar{x}$. Then shoreline changes over a nondimensional time $\delta \bar{t}$ is calculated using the above finite difference formula.

In this method model $\bar{Q}$ at the time interval $\bar{t}+1$ is expressed in term of shoreline co-ordinate of $\bar{y}$, first isolating the term involving α_{sp}(angle of shoreline normal to x-axis) using trigonometric identities. One of the term involving α_{sp} is then expressed as first order quantities in $\bar{y}$ at the time step $(\bar{t}+1)$.

$$\bar{Q} = K_D^2 \cos(\alpha_o)\sin(\alpha_b) \tag{8}$$

where $\alpha_o = \alpha - \alpha_{sp}$ and α = wave direction with respect to x-axis.

The angles α_o, α and α_{sp} are defined in Fig. 1.

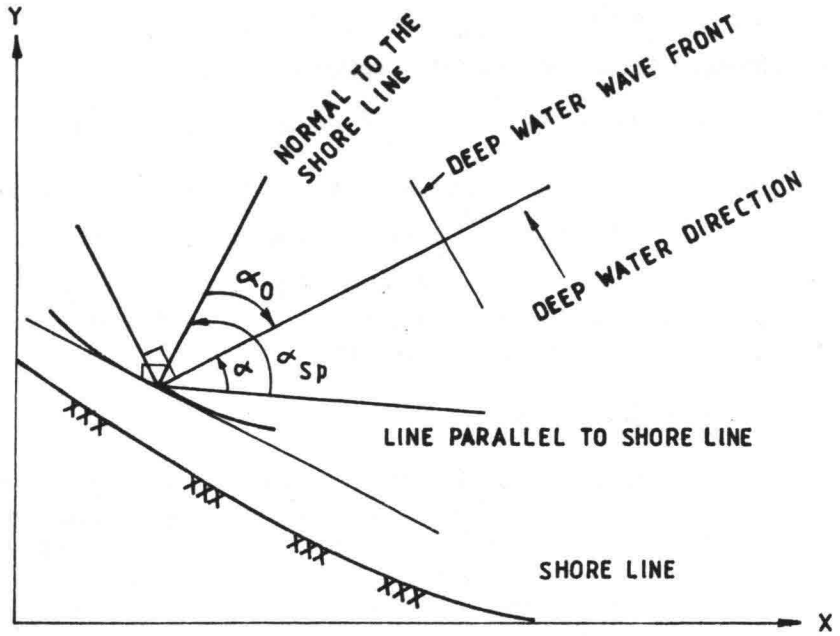

FIG. 1. SKETCH DEFINING ANGLES α_0, α, AND α_{sp}.

$$\bar{Q} = K_D^2 \cos(\alpha - \alpha_{sp}) \sin(\alpha_b)$$

$$\bar{Q} = K_D^2 \sin(\alpha_b) \{\cos(\alpha)\sin(\alpha_{sp})\cot(\alpha_{sp}) + \sin(\alpha)\sin(\alpha_{sp})\}$$

$$\bar{Q} = E_n \left\{\bar{y}_{n-1,\bar{t}+1} - \bar{y}_{n,\bar{t}+1}\right\} + F_n \qquad (9)$$

where $E_n = K_D^2 \left[\cos(\alpha)\sin(\alpha_{sp,\bar{t}})\sin(\alpha_{sp,\bar{t}})\right] / \delta x$ and

$$F_n = K_D^2 \left[\sin(\alpha)\sin(\alpha_{sp,\bar{t}})\sin(\alpha_{b,\bar{t}})\right]$$

Substituting eq.9 in eq.5 will result in an expression of the form

$$BE_n \bar{Q}_{n-1,\bar{t}-1} - (1 + 2BE_n)\bar{Q}_{n,\bar{t}+1} + BE_n \bar{Q}_{n,\bar{t}+1} = E_n \left[C_n - C_{n-1}\right] - F_n \qquad (10)$$

The above equation represent a set of (N-1) linear equation for(N-1) unknowns. The end values are specified as boundary conditions i.e. $\bar{Q}_1 = 0$ and $\bar{Q}_{N+1} = \bar{Q}_N$. The eq.10 resulted into a tridiagonal form which is solved to $\bar{Q}$ values. The $\bar{y}$ is then calculated using eq.7. This process is repeated entire time duration and nondimensional quantity is converted into real quantities using scale factors.

2.3 Monte Carlo Simulation

Le-Mehaute et al(1981) proposed Monte Carlo simulation technique in order to predict shoreline oscillations for a number of wave characteristics which yield a number of time histories of the shoreline evolution, the average of which is taken as the best representative shoreline evolution. In the present case wave data namely wave heights, period and direction of the Madras port are used to predict shoreline change for a period of five years from 1989 shoreline by taking the average of simulated shoreline position.

3. RESULTS AND DISCUSSIONS

3.1 Model Verification:

The developed user friendly software is verified with analytical model of Le-Mehaute and Soldate(1978). These results and salient features of the user friendliness has been presented in detail by the investigators (1993) earlier. After the validation is found to be good, the numerical model is validated for field data for the Madras port, India. The layout of the Madras port given in fig. 2 shows the location of sand screen south of the harbour breakwater which is treated as the effect of a groin due to which the changes in the shoreline was computed based on the methodologies discussed earlier.

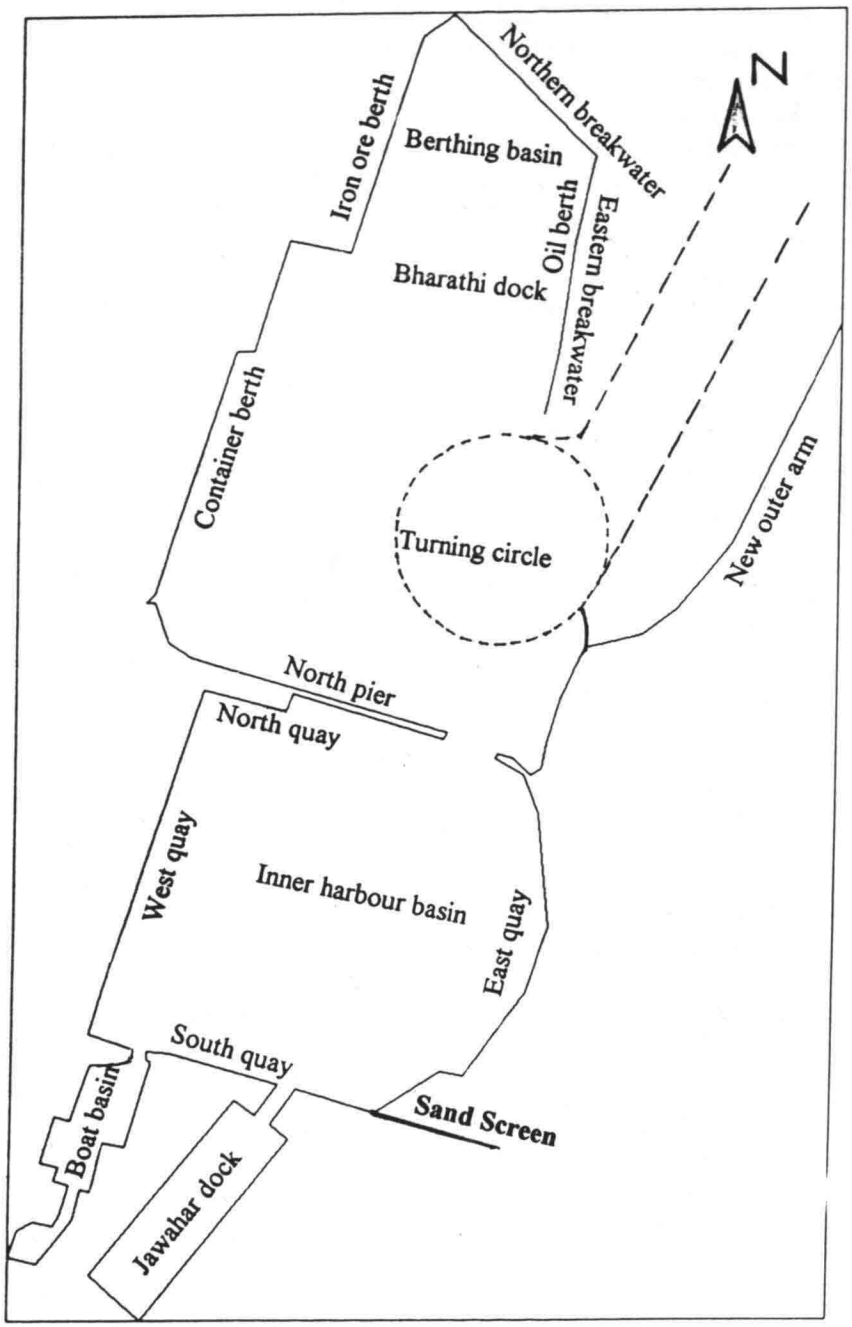

Fig. 2. Geometric configuration of Madras Port, India

The initial shoreline observed in 1980 was used to run the model with the daily wave characteristics observed for the year 1981. The shoreline is predicted for a time span of one year using the Monte Carlo simulation technique with twenty simulations, the average of which is treated as the representative shoreline evolution due to the presence of the structure. These results along with the measured shoreline for the year 1981 are depicted in fig.3. The results demonstrates that the deviation between twenty shoreline is minimum. The trend in the variation of the predicted shoreline is similar to that of the measured. It is observed that near the tip of the structure and the tail of shoreline, the comparison is good, whereas at other locations slight deviations are observed with a maximum deviation of upto 14%. When dealing with coastal engineering problems, modeling all the associated parameters are highly complex and even the measurements may lead to considerable deviations from the nature. This explains the reasons for the observed deviations.

The plots showing the initial shoreline along with the ones predicted with average wave characteristics and Monte Carlo method are presented in fig. 4. It is observed that the predicted shoreline based on the latter method is in closer agreement with the measured shoreline of 1981.

3.2 Application of the Model:

The developed numerical model after its validation has been used to predict the shoreline changes of the updrift of sand screen of the Madras port. In this case, the shoreline measured in 1989 form the initial input and the daily means of 10 years wave data has been consider as the wave characteristics of each of the day. The stretch of shoreline of 1500 m is divided into 75 grids and its co-ordinates at the center of each grid form the basic input for the initial shoreline. The model was run to establish the monthly variation in the shoreline evolution. The results thus obtained is shown in fig. 5(a) and fig. 5(b).

The results shows that, during the months January to February, upto distance of about 300m, updrift of the sand screen erosion is noticed beyond, which, there is not much of difference is observed between initial and predicted shorelines.

During the months of June to October, according to the numerical model, deposition is observed over the entire stretch of the shoreline considered. This is attributed due to the fact that during June to September the littoral drift along the Madras coast is towards the north contributing nearly to the extent of about 75% of the annual littoral drift. This huge drift due to the interception of harbour breakwater lead to the advancement of the shoreline.

Though one would anticipate erosion at the location of the study area during the months of November and December since the littoral drift is towards the south. the model predicts deposition for these months. The results obtained from the present model shows a similar

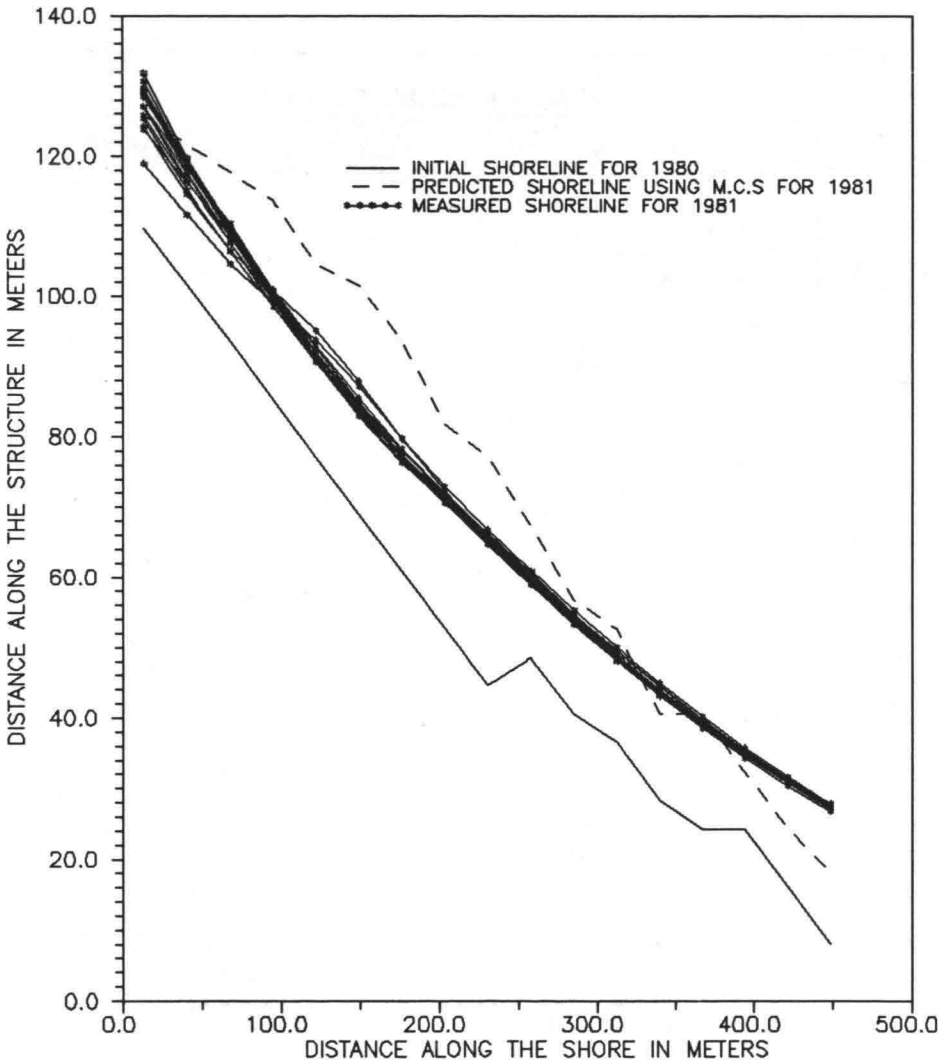

Fig.3 Comparison of Measured and Predicted Shoreline by Monte Carlo Simulation

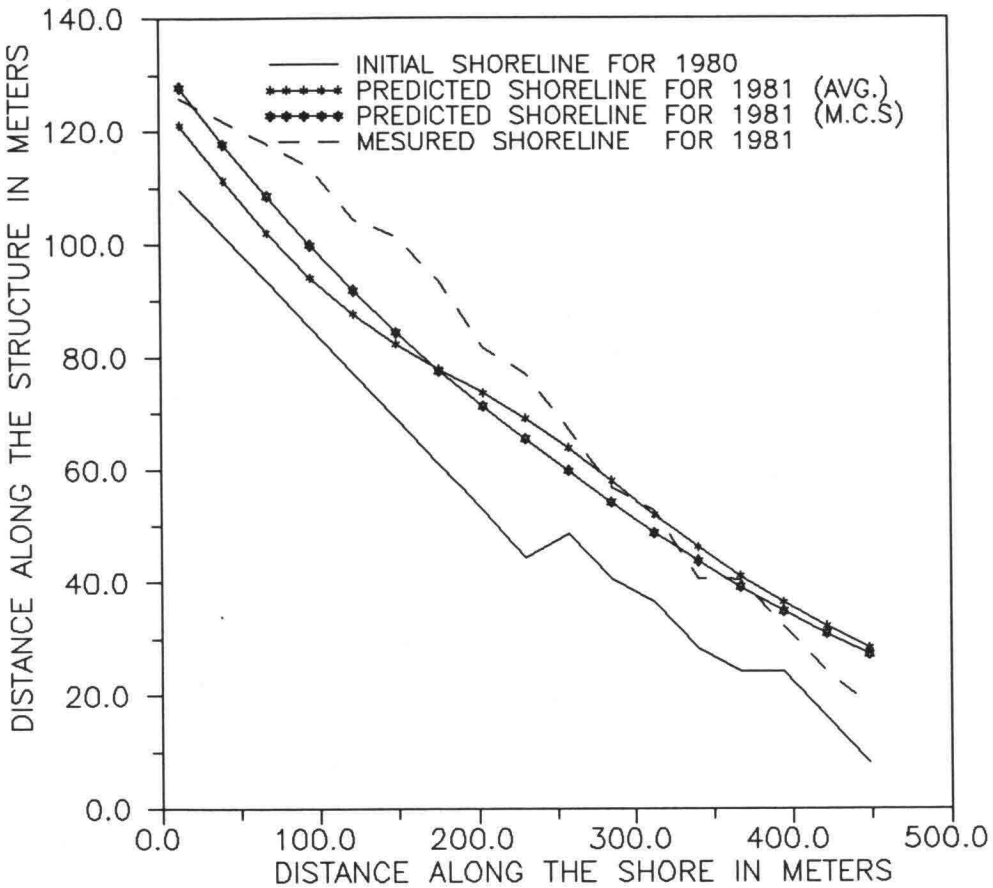

Fig.4 Comparison between Measured and Predicted Shoreline with Averaging method and Monte Carlo Simulation Method

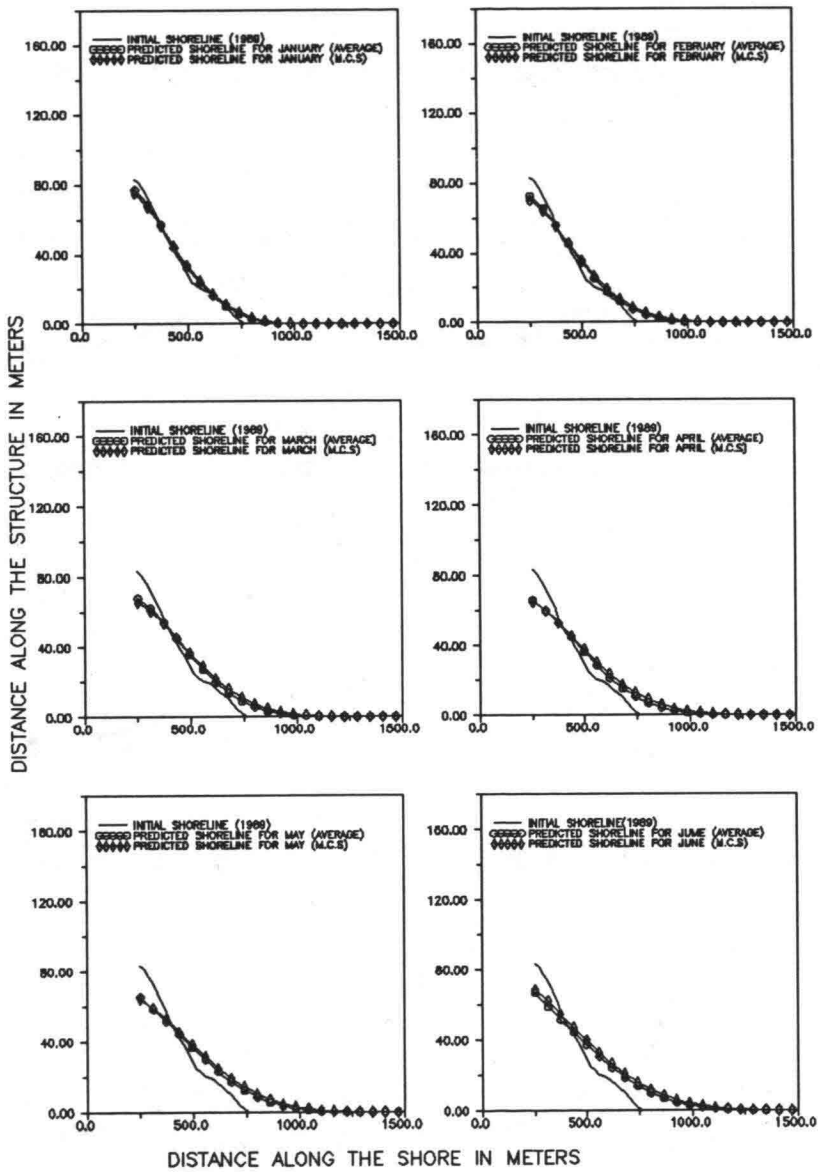

Fig.5(a) Monthly Variations in the Predicted Shoreline near Madras Port, India.

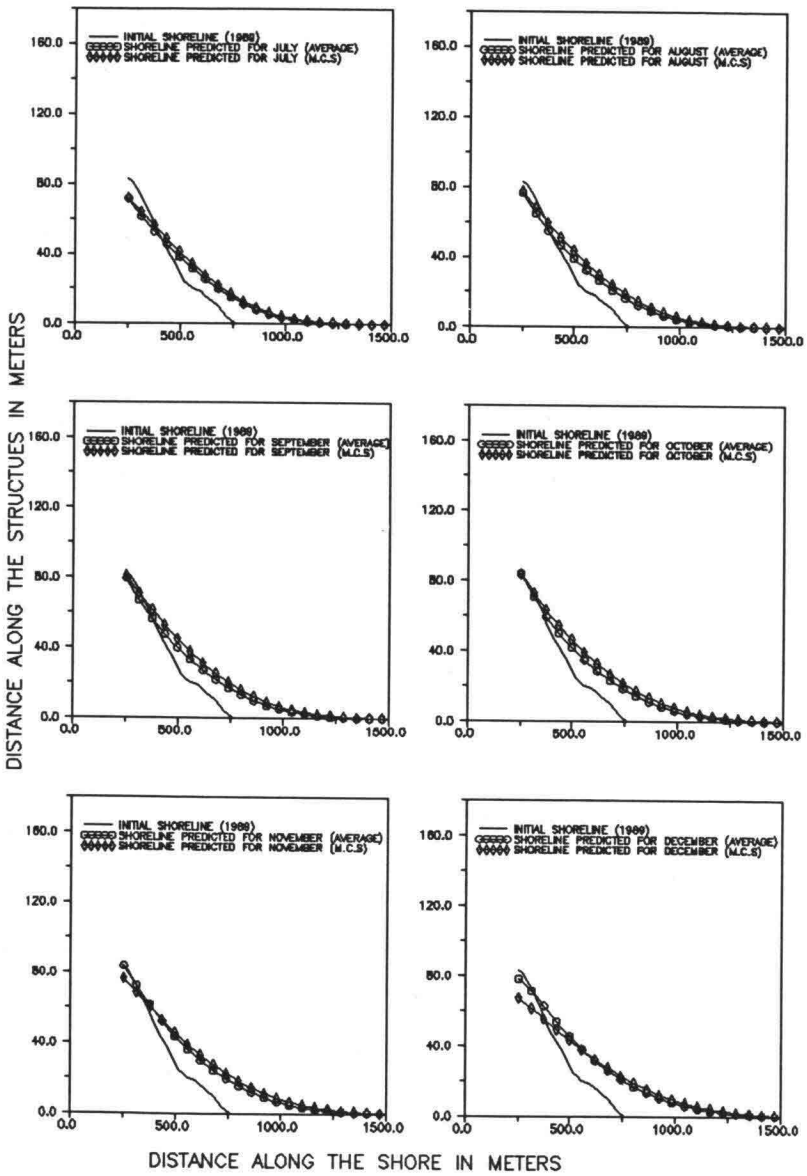

Fig.5(b) Monthly Variations in the Predicted Shoreline near Madras Port, India.

trend during the months of January to May except that persistence of advancement of shoreline beyond 300 m from south of sand screen is noticed for these months.

The foregoing discussions has demonstrated clearly the variation of the shoreline changes over a year which also reflect the effects of monsoons.

The east coast of India experiences two monsoons namely south west monsoon (June-September) and north east monsoon (October-December). The wave characteristics are effected by this monsoons, whereas during the non monsoon season (January-May) the wave characteristics are similar to that of north east monsoon. As regard to the sediment transport, the littoral drift during the non monsoon and south west monsoon is towards the north, whereas, during the north east monsoon littoral drift is towards the south, with the annual net drift moving towards the north.

Due to the above phenomena, all the ports on the east coast of the India experiences deposition or advancement of shoreline on its southern side, resulting erosion on the north of the harbours.

To account for the seasonal variation the present numerical model is used to predict shoreline evolution with measured shoreline of 1989 as the initial shoreline. The seasonal effects on the simulated shoreline are presented in fig. 6.

The procedure adopted is as follows. With initial measured shoreline of 1989, shoreline evolution is predicted for non monsoon season . This is consider as the initial shoreline for predicting the final shoreline due to the effect of south west monsoon. The predicted shoreline of south west monsoon is the initial shoreline for the north east monsoon. However, in the plots the initial shoreline of 1989 is taken as the basic reference line for discussion. From the fig. 6 it is observed that irrespective of season deposition is found to be taken place about 300m away from the sand screen. During the north east and non monsoon seasons, slight erosion is observed adjacent to the sand screen where as deposition is observed during the south west monsoon near it. Slight amount of deviation are observed between two methods of simulation near the structure.

The annual variation of shoreline evolution is shown in fig. 7, from which, it is observed that the predicted shoreline advanced towards the sea, the rate at which it advances slightly reduces with increase in time.

4. CONCLUSIONS

Exact solution to the most of the Coastal Engineering problem are often difficult. The solution mainly depend both on numerical modeling as well as physical modeling while uncertainties still exist in exactly modeling near shore phenomena.

In this paper efforts has been made in developing a numerical model for shoreline oscillation by changing the sequential occurrences of wave characteristics. The developed

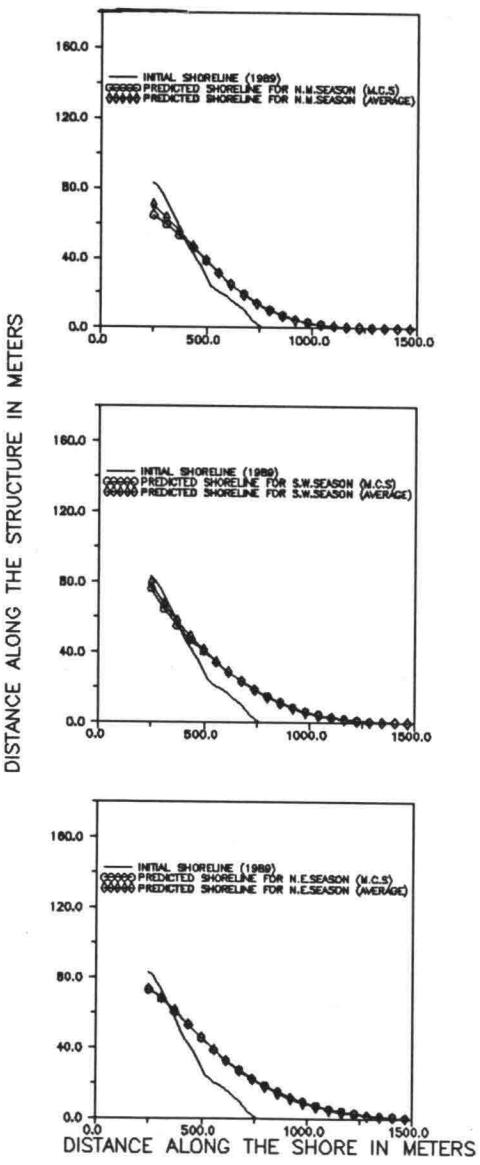

Fig.6 Seasonly Variations in the Predicted Shoreline near Madras Port, India.

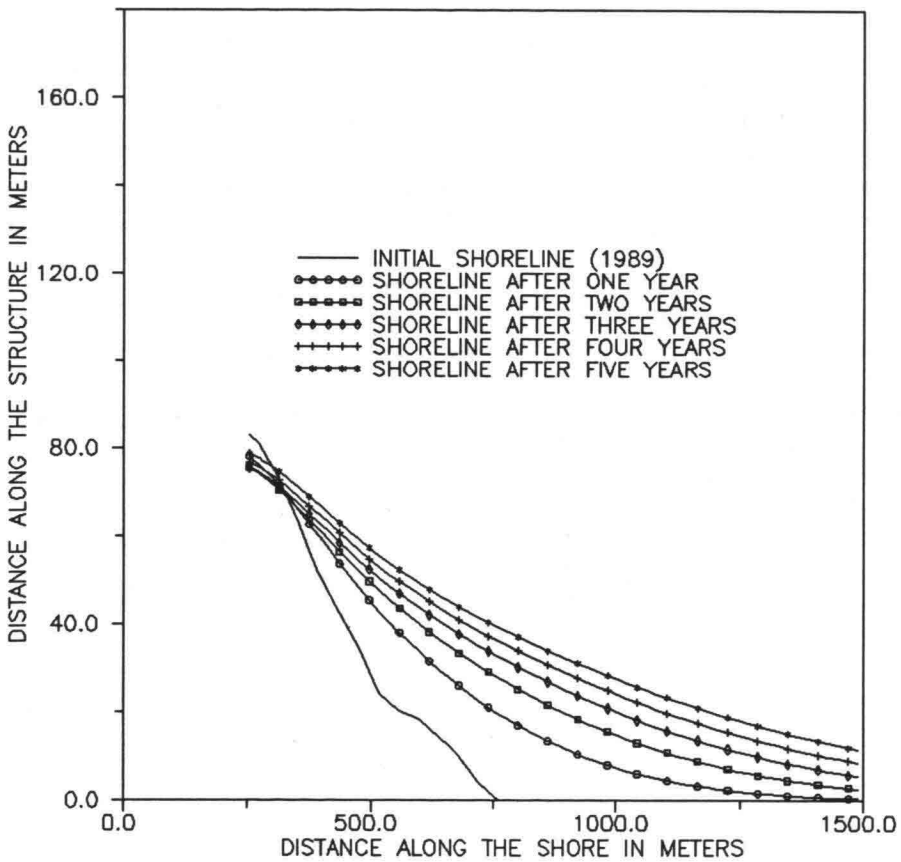

Fig.7 Yearly Variations in the Predicted Shoreline near Madras Port, India.

model is applied to Madras port. It is felt that developed numerical model reported in this paper will be useful in planning for construction of structures considering the wave induced sediment transport.

ACKNOWLEDGMENT

The work reported in this paper is a part of the research work funded by Department of Ocean Development, Government of India. The authors acknowledge their support. The authors also thank the Madras port authorities for supply of data used in this study.

REFERENCES

Dean, R.A and Dalrymple, R.G.(1984): Water Wave Mechanism for Scientist and Engineers, Prentice - Hall Inc.

Hallermeier, R.J. (1981): Uses for a calculated limit depth to beach erosion . Proc. 16 th Coastal Engineering Conf. ASCE, pp 1493-1512.

Janardanan, K.and Sundar, V. (1993): Development of userfriendly software for the shoreline evolution using oneline model, SMCE, Institution of Engineers(India), Visakpatnam, India. pp 109-117.

.Kraus, N.C. and Harikai, S. (1983): Numerical model of the shoreline changes of Oarai beach, Coastal Engineering , Vol. 7, pp 1-28.

Le-Mehaute, B. and Koh, R.(1967): On the breaking of the waves arriving at an angle with the shoreline. J. of Hydraulic Research Vol. 5.

Le-Mehaute, B. John, D. and Chia-Chu Lu. (1981): Monte Carlo simulation of shoreline process, Proc. Conf. on Directional Wave Spectra Applications, California, pp 269-280.

Le-Mehaute, B. and Soldate, M.(1978): Mathematical modeling o shoreline evolution, Proc. 16 th Coastal Engineering Conf., ASCE, pp 1163-1179.

-----Shore Protection Manual.(1984): Coastal Engineering Research Center, US Army corps of Engineers, Vickcsburg, Miss.,U.S.

HYDRO-PORT'94

International Conference
on
Hydro-TechnicalEngineering
for
Port and Harbor Construction

CONFERENCE TIMETABLE
(FINAL VERSION)

'94
HYDRO-PORT

OCTOBER 19–21, 1994
YOKOSUKA, JAPAN

CONFERENCE TIMETABLE

Wednesday, Oct.19

Opening Ceremony 10:00 - 10:30		
Coffee Break 10:30 - 10:50		
Keynote Lecture 10:50 - 11:50	A Plea for Engineering-minded Research Efforts in Harbor and Coastal Engineering Professor Yoshimi Goda, Yokohama National University, Japan	
Lunch 11:50 - 13:00		
Technical Session 1 on Theme 1 13:00 - 15:25	Theme : Acquisition and Analysis of Wave Information for Structural Design Chairman : Akira Watanabe, University of Tokyo, Japan Secretary : Toshihiko Nagai, Port and Harbour Research Institute, Japan	
	(1-1) 13:00-13:20	Introduction of Japanese NOWPHAS System and its Recent Topics (Nationwide Ocean Wave information network for Ports and HArbourS) T. Nagai, K. Sugahara, N. Hashimoto, T. Asai, S. Higashiyama and K. Toda, Japan
	(1-2) 13:20-13:40	Wave Monitoring System of the Korea Maritime and Port Administration K. S. Park, D. Y. Lee, C. S. Kim, S. W. Kang, K. S. Bahk, K. C. Jeon, S. I. Kim, J. S. Shim and B. C. Oh, Korea
	(1-3) 13:40-14:00	Cooperation on the Improvement of the Wave Measurement and Analysis Technology between PHRI and KORDI D. Y. Lee[1], K. S. Bahk[1], K. S. Park[1], B. C. Oh[1], K. D. Seo[1], T. Nagai[2], N. Hashimoto[2], T. Asai[2] and T. Horie[2]; [1]Korea, [2]Japan
	(1-4) 14:00-14:20	Reliability of Wave Forecasting by Autoregressive Model Represented in Wave Energy H. Ohashi, S. Akamura, M. Suzuki and H. Inada, Japan
	(1-5) 14:20-14:40	On the Extreme Wave Height Analysis H. F. Burcharth and Z. Liu, Denmark
	(1-6) 14:40-15:00	Evaluation of Directional Wave Measurements - a Comparative Field Exercise A. van Tonder and J. Davies, South Africa
	(1-7) 15:00-15:20	Measured Transformation of Deep Water Wave Spectra Across a Shallow Coral Reef Flat D. D. McGehee, U. S. A.
	(Remarks) 15:20-15:25	
Coffee Break 15:25 - 15:45		
Technical Session 2 on Theme 2 15:45 - 18:10	Theme : Wave Transformation Analysis for Port Construction Chairman : Robert G. Dean, University of Florida, U. S. A. Secretary : Yasumasa Suzuki, Port and Harbour Research Institute, Japan	
	(2-1) 15:45-16:05	Field Application of Angular Spectrum Model to Directional Wave Transformation K. D. Suh, B. C. Oh and J. S. Shim, Korea
	(2-2) 16:05-16:25	Time Domain Simulation of Directional Wave Propagation into Harbours O. G. Nwogu and E. P. D. Mansard, Canada
	(2-3) 16:25-16:45	The Development and Application of a Computational Model of Directional Wave Transformation in Harbours N. P. Tozer and J. V. Smallman, U. K.
	(2-4) 16:45-17:05	Applicability of Multi-directional Wave Experiment for Port Design Y. Suzuki, T. Hiraishi, T. Takayama and N. Ikeda, Japan
	(2-5) 17:05-17:25	Field Applicability of Wave Models to Estimating the Wave Fields Outside and Inside a Harbor T. Shimizu, A. Ukai, Y. Kubo and M. Shimada, Japan
	(2-6) 17:25-17:45	Development and Application of a Numerical Model for Wave Diffraction through Breakwater Gaps D. Anand and V. Sundar, India
	(2-7) 17:45-18:05	Penetration of Long Waves into a Lagoon Harbour and Resulting Ship Motions V. Barthel, E. P. D. Mansard and D. D. MacDonald, Canada
	(Remarks) 18:05-18:10	
Reception 18:20 - 20:00	On the 5th Floor of the Yokosuka Prince Hotel	

Thursday, Oct.20

Technical Session 4 on Theme 4 9:00 - 11:25	Theme : Harbor Water Quality and Seawater Quality Improvement Chairman : Desmond A. Lord, D. A. Lord and Associates, Australia Secretary : Kazuo Murakami, Port and Harbour Research Institute, Japan	
	(4-1) 9:00- 9:20	Characteristics of Wind Induced Upwelling in Tokyo Bay based on Analysis of NOAA-AVHRR data S. Ueno, K. Nadaoka, H. Ohtani and H. Katsui, Japan
	(4-2) 9:20- 9:40	3-Dimensional Modelling of Heated Water Discharges into Coastal Waters of Yellow Sea S. W. Kang and T. S. Jung, Korea
	(4-3) 9:40-10:00	Development of Water-Intake Works with Submerged Mound (WWSM) A. Nakayama, M. Yamamoto, J. Yamamoto and A. Moriguchi, Japan
	(4-4) 10:00-10:20	Water Quality in Penang Harbor P. M. Sivalingam and S. V. Charles, Malaysia
	(4-5) 10:20-10:40	Environmental Monitoring of the Lagunar Complex of the South Region of the Santa Catarina State D. Accetta, W. S. S. Dias, B. M. Vargas and J. A. dos. Santos, Brazil
	(4-6) 10:40-11:00	Channel Experiments on Coastal Water Purification by Stone Bed with Biofilm Y. Hosokawa, T. Ootsuki and C. Niwa, Japan
	(4-7) 11:00-11:20	Sand Covering for Improving Quality of Bottom Sediments in Japanese Harbors S. Inoue, T. Horie, K. Murakami, Y. Hosokawa, S. Sato and Y. Sega, Japan
	(Remarks) 11:20-11:25	
Coffee Break 11:25 - 11:40		
Special Lecture 1 11:40 - 12:20	Management of Coastal Waters in Western Australia : The Use of Integrated Models Dr. Desmond A. Lord, Director of D. A. Lord and Associates, Australia	
Lunch 12:20 - 13:30		
Technical Session 5 on Theme 5 13:30 - 15:55	Theme : Beach Stabilization in the Vicinity of a Harbor Chairman : Norio Tanaka, Nippon Tetrapod Co., Ltd., Japan Secretary : Kazumasa Katoh, Port and Harbour Research Institute, Japan	
	(5-1) 13:30-13:50	Change of the Ag. Nikolaos Beach in the Vicinity of a New Harbor for Small Crafts C. I. Moutzouris, Greece
	(5-2) 13:50-14:10	Protection against Shore Erosion and Channel Shoaling at Port Madero, MEXICO J. M. Montoya R.[1], J. R. Vera. S.[1] and S. Sato[2]; [1]Mexico, [2]Japan
	(5-3) 14:10-14:30	Control of Littoral Drift in Caldera Port, Costa Rica J. G. Rodoriguez P.[1] and K. Katoh[2]; [1]Costa Rica, [2]Japan
	(5-4) 14:30-14:50	Physical Impact of Bilbao Harbour New Breakwater on Adjacent Beaches J. P. Sierra, J. A. Jiménez, A. Sánchez-Arcilla, J. M. Picó, A. Viñuales and E. J. Villanueva, Spain
	(5-5) 14:50-15:10	Littoral Drift in Fishing Ports and Approach Channels: Problems and Countermeasures M. Fukuya, N. Takaki, K. Ota, S. Harikai and M. Ikeda, Japan
	(5-6) 15:10-15:30	Stabilization of Beach in Integrated Shore Protection System K. Katoh, S. Yanagishima, S. Nakamura and M. Fukuta, Japan
	(5-7) 15:30-15:50	Scour around the Head of a Vertical-Wall Breakwater T. Gökçe, B. M. Sumer and J. Fredsøe, Denmark
	(Remarks) 15:50-15:55	
Poster Session 16:00 - 18:00	Council Rooms of Yokosuka Industrial Plaza on the 3rd Floor of the Bay Square Yokosuka Building (Posters will be exhibited from 9:00 to 18:00.)	

Friday, Oct.21

Technical Session 3 on Theme 3 9:00 - 12:20	Theme : Design Wave Forces on Composite Breakwaters Chairman : Hans F. Burcharth, University of Aalborg, Denmark Secretary : Shigeo Takahashi, Port and Harbour Research Institute, Japan	
	(3-1) 9:00- 9:20	Caisson Breakwaters: Integrated Design and Wave Load Specifications H. Oumeraci, A. Kortenhaus and P. Klammer, Germany
	(3-2) 9:20- 9:40	Experimental Study and Theoretical Comparison of Irregular Wave Pressures on Deepwater Composite Breakwaters H. S. Hou, Y. D. Chiou and C. H. Chien, Chinese Taipei
	(3-3) 9:40-10:00	A Proposal of Impulsive Pressure Coefficient for the Design of Composite Breakwaters S. Takahashi, K. Tanimoto and K. Shimosako, Japan
	(3-4) 10:00-10:20	A Comparative Study on Wave Forces and Overtopping of Caisson Breakwaters J. Juhl, Denmark
	(3-5) 10:20-10:40	Design of Harbour Entrances: Breakwater Design and Vessel Safety M. W. McBride, J. V. Smallman and N. W. H. Allsop, U. K.
	(Remarks) 10:40-10:45	
	(Coffee Break) 10:45-10:55	
	Chairman : Katsutoshi Tanimoto, Saitama University, Japan Secretary : Shigeo Takahashi, PHRI, Japan	
	(3-6) 10:55-11:15	A New Type of Breakwater with a Step-Shaped Slit Wall R. Fujiwara, T. Yoshida, K. Kurata, S. Kakuno and K. Oda, Japan
	(3-7) 11:15-11:35	Hydraulic Experiments for Basic Design of Offshore Breakwater for Protecting Artificial Island D. S. Lee, W. S. Park, K. D. Suh and Y. M. Oh, Korea
	(3-8) 11:35-11:55	New Types of Breakwater Two Projects in MONACO R. Bouchet, P. Cellario and J. L. Isnard, Monaco
	(3-9) 11:55-12:15	Field Demonstration Test on a Semi-Circular Breakwater H. Sasajima, T. Koizuka, H. Sasayama, Y. Niidome and T. Fujimoto, Japan
	(Remarks) 12:15-12:20	
Lunch 12:20 - 13:30		
Special Lecture 2 13:30 - 14:10	Engineering Devices for a Smooth Port Operation with Focus on Developing Countries Professor Isao Irie, Kyushu University, Japan	
Coffee Break 14:10 - 14:30		
Technical Session 6 on Theme 6 14:30 - 16:15	Theme : Countermeasures against Shoaling due to Siltation and Sedimentation in the Harbor and Waterway Chairman : Isao Irie, Kyushu University, Japan Secretary : Hiroichi Tsuruya, Port and Harbour Research Institute, Japan	
	(6-1) 14:30-14:50	Criteria and Methods to Determine Navigable Depth in Hyperconcentrated Sediment Layers W. R. Parker and P. M. Hooper, U. K.
	(6-2) 14:50-15:10	Field Surveys on Siltation-Prevention Effects in Waterway and Anchorage by Submerged Walls T. Kihara, H. Sasajima, K. Yoshinaga, T. Koizuka, H. Sasayama, H. Yoshinaga and T. Fujimoto, Japan
	(6-3) 15:10-15:30	Case Study on Channel Improvement in the Mouth of the Yongjiang River J. Jiang, China
	(6-4) 15:30-15:50	Field Survey on Estuarine Mud Transport Process around Navigation Channel, Banjarmasin, Indonesia H. Tsuruya, K. Murakami, K. Nagai and I. Irie, Japan
	(6-5) 15:50-16:10	Modelling Cohesive Sediment Transport in Tidal Waters K. P. P. Pathirana, J. C. S. Yu and J. Berlamont, Belgium
	(Remarks) 16:10-16:15	
Closing Ceremony 16:20 - 16:40		

HYDRO-PORT'94
International Conference on Hydro-Technical
Engineering for Port and Harbor Construction
October 19 – 21, 1994, Yokosuka, Japan

Drifting Characteristics of Littoral Sand Around Submerged Breakwater (Field Survey on Niigata West Coast)

Haruyo Funakoshi [1]
Toshihiko Siozawa [2]
Atsuhiro Tadokoro [1]
Shuichi Tsuda [1]

[1] Niigata Investigation and Design Office
The 1st District Port Construction Bureau, Ministry of Transport
1-332 Hakusan-ura Niigata, 951
[2] The 1st District Port Construction Bureau, Ministry of Transport
1-332 Hakusan-ura Niigata, 951

ABSTRACT

Detached breakwater was installed on the Niigata West Coast to prevent erosion of the seashore. Various studies were made to understand the movement of the surrounding sand and the change of current flows caused by construction of the submerged breakwater. The main interim results of site surveys are as follows: The wave height behind the submerged breakwater was deduced which is almost as same as the results of hydraulic model test. The directions of littoral current flows around the breakwaters are closely related to those of waves. It was observed at some points behind the breakwaters that the current flows became large or the direction of currents turned reversely according to the wave development. A trend was found that the wave depth behind the breakwaters was deepened by 1 meter after the construction. These results show that the waves are dissipated by submerged breakwater as excepted. It is, however, suffered that the turbulence of littoral current in the behind might increase during construction stage of a half width of submerged breakwater.

Key Words: submerged breakwater, shore protection works, site observation, littoral sediment transport

1. INTRODUCTION

The Niigata West Coast faces the Sea of Japan and is located westward of the mouth of the Shinano river, which is the longest river in Japan. Previously, the West Coast had sand dunes that were several hundred meters wide which were formed with large amounts of sands discharged from the Shinano river. However, the completion of the two diversion channels (Ohkouzu and Sekiya) of the Shinano river and development of the Niigata port decreased the amount of discharged sediment. In addition, land subsidence occurred due to the exploitation of natural gas. As a result, the shoreline retreated up to 350m from that of 1890. At one time, the coastline retreated close to residential areas.

Large-scaled countermeasures to reduce erosion have been started around 1950, after the end of World War II. Detached breakwaters were constructed along the entire length of the West Coast to prevent the coastline from retreating. However, high waves, which are caused by strong winds of winter monsoon and atmospheric depressions, constantly cause settlement and scattering of the wave dissipation blocks of the detached breakwater. The cost of restoring the blocks is very high. Observations in recent years have revealed that the water depth in the offshore side of the breakwaters has been gradually increasing. This may result in a serious disaster if it is continued. Therefore, submerged breakwater and groins with beach nourishment are planned as new measures against erosion. The erosion prevention works will be more stable against high waves and cause less erosion to sea bottom of the surrounding area.

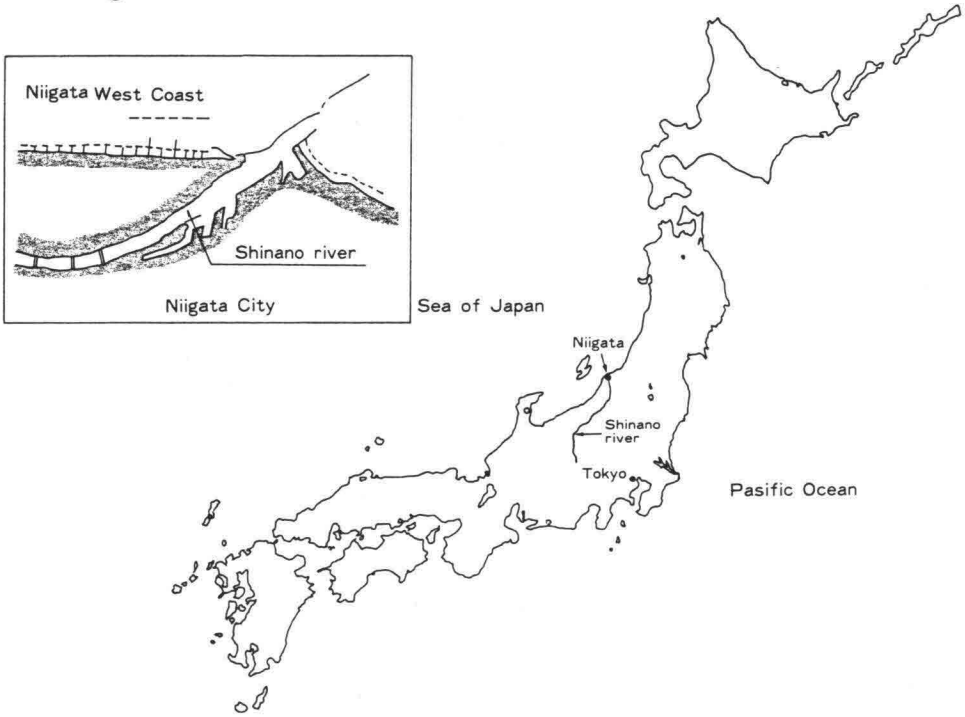

Figure 1 Location Map of Niigata West Coast

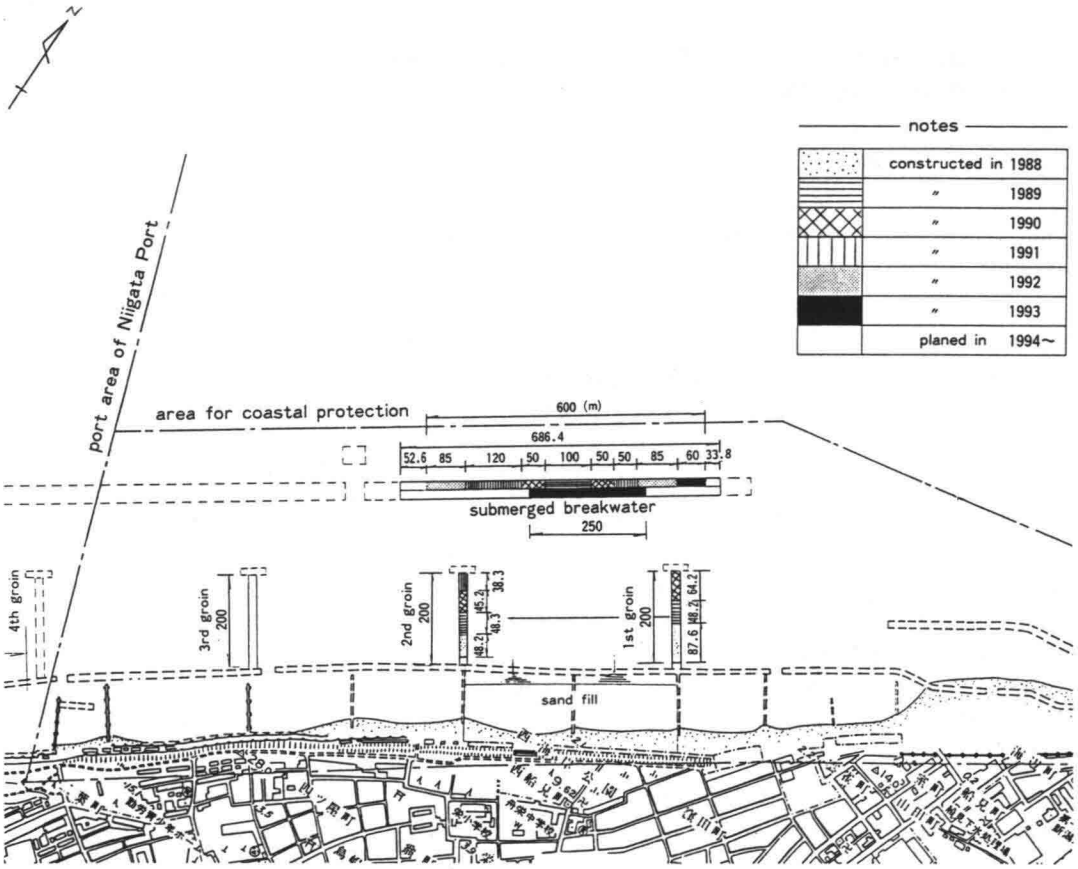

Figure 2 Shore Protection Works against Erosion at Niigata West Coast

This report presents an outline of the design and construction of the erosion prevention works on the Niigata West Coast. It also clarifies the characteristics of currents and topographic changes around the submerged breakwater. These characteristics were analyzed based on the observed current flow and water depth of the surrounding area. This report is an interim report of our study since about half of the submerged breakwater cross section has been completed.

2. DESIGN AND CONSTRUCTION OF COUNTERMEASURE WORKS AGAINST EROSION

2.1 Design Method

The design method for the erosion control facilities on the Niigata West Coast is described below.

<Design waves>
Two design waves were determined; one is to control erosion and another is to design structures. The peak energy wave is adopted for erosion control, which is 3.0m in a significant wave height and 8.0sec in period. The peak energy wave has a statistical one which has the maximum energy among the classified wave heights of observed annual wave data. A wave with a return period 50 years was adopted for the structural design.

<Dimension of submerged breakwater by calculation>
The crown height of the submerged breakwater is set at −1.5m and the width is 40m wide considering the stability of shoreline and sea bottom and the safety for small vessels. The −1.5m crown height was decided so as to reduce wave reflection almost to that of natural shoreline in order to stabilize for the front sea bottoms against erosion, and to provide small vessels such as rowing boats and dinghy-type yachts with sufficient bottom clearance. The width was decided to reduce the energy peak wave height to 1.5m so as to protect the shoreline from erosion after the stability calculation of sand of shoreline. These functions of submerged breakwater were confirmed by two-dimensional hydraulic model test.

<Three-dimensional hydraulic model test for littoral transport>
A three-dimensional hydraulic model test with a movable bed was carried out to study the stability of shoreline after the completion of submerged breakwater. As a result, the littoral drift along the shoreline was more significant than expected. Therefore, impermeable groins were designed to prevent the long shore sand movement near the shoreline. The length, width and interval were determined by the model test.
Through these studies, a layout plan in Figure 2 were adopted as the countermeasure works against erosion of the shoreline and sea bottoms. Figure 3 shows the cross section of facilities with beach nourishment plan.

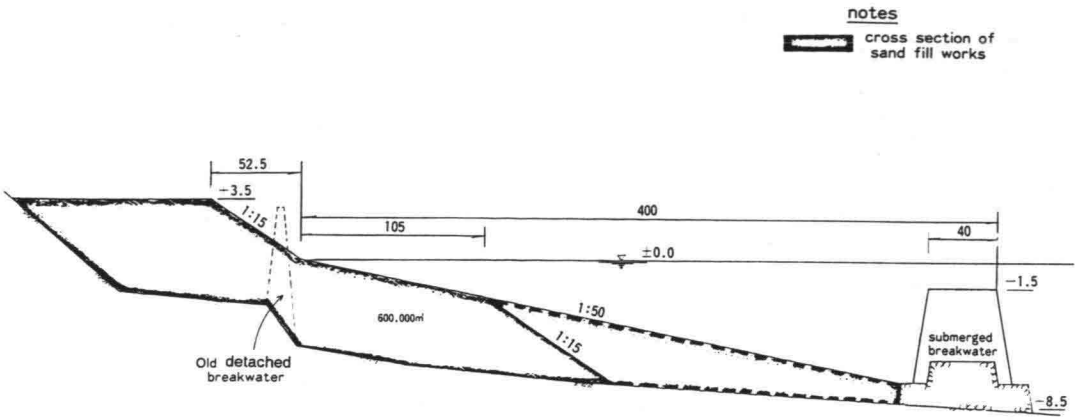

Figure 3 Cross Section of Shore Protection Works

2.2 Construction Procedure

The construction works are carried out in several stages with careful observations to confirm no false effects; coastal destruction, erosion in sea bottoms, etc. to the adjacent areas. The construction work of 600m long submerged breakwater is divided in two stages as shown Figure 4 which is the typical cross section of the breakwaters. The first was to construct a provisional breakwater with half-wide cross section in order to study the actual effects on the surrounding sea bottom topography and shoreline. The second was to complete the breakwater as planned after confirming no false effects. Figure 2 shows the construction history by year. The provisional breakwater of 600m length was completed and the planned of 250m was completed by 1993. This report presents the site observation results and the analysis by the completion of 540m long provisional breakwater of half width in 1992.

3. SITE OBSERVATION

Wave height, currents and sea bottom level changes were observed around the submerged breakwater. Waves and winds were also observed at the offshore observation point of -35m depth off the Niigata port. The observation points around the submerged breakwater are shown in Figure 5. The observation was carried out during rough seas in October to December since 1989. The observation at St.8 and St.9, however, were started in 1991 after the breakwater was constructed long enough near to those points. A sounding survey in the wide area was performed once a year in May to June to study the topographical changes of sea bottom around the submerged breakwater. Grain size analyses were also carried out to get the grain size distribution of sands in the shoreside.

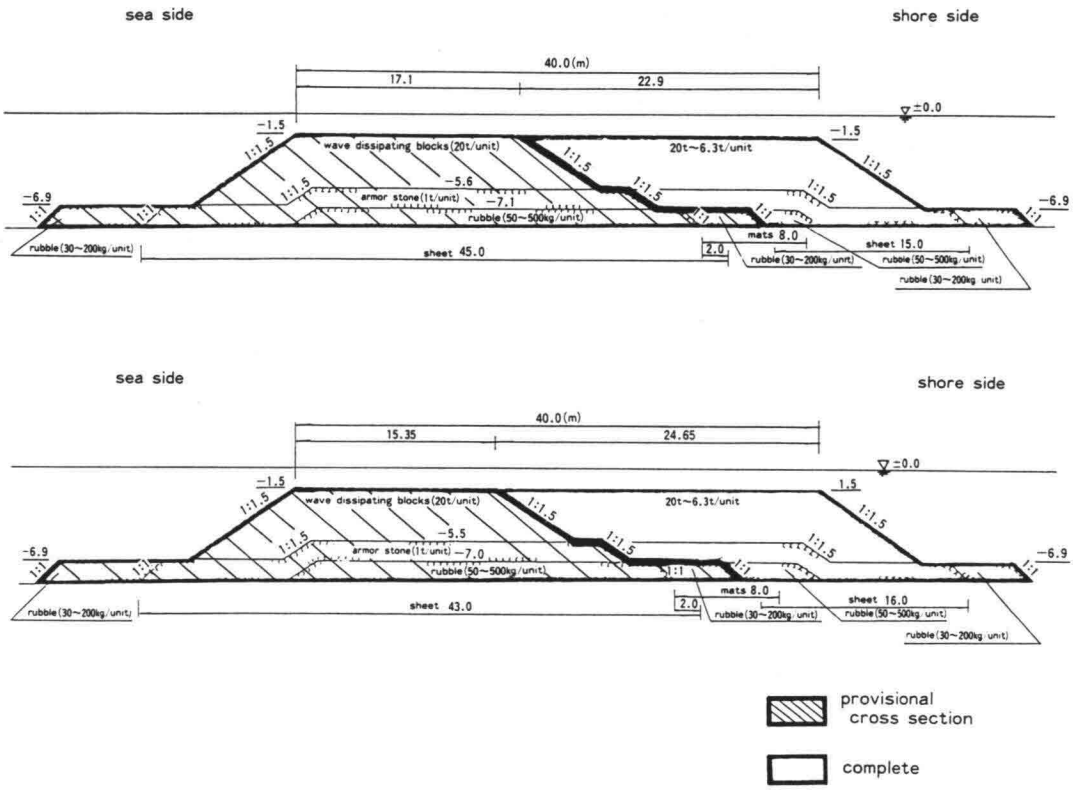

Figure 4 Cross Section of Offshore (Submerged Breakwater)

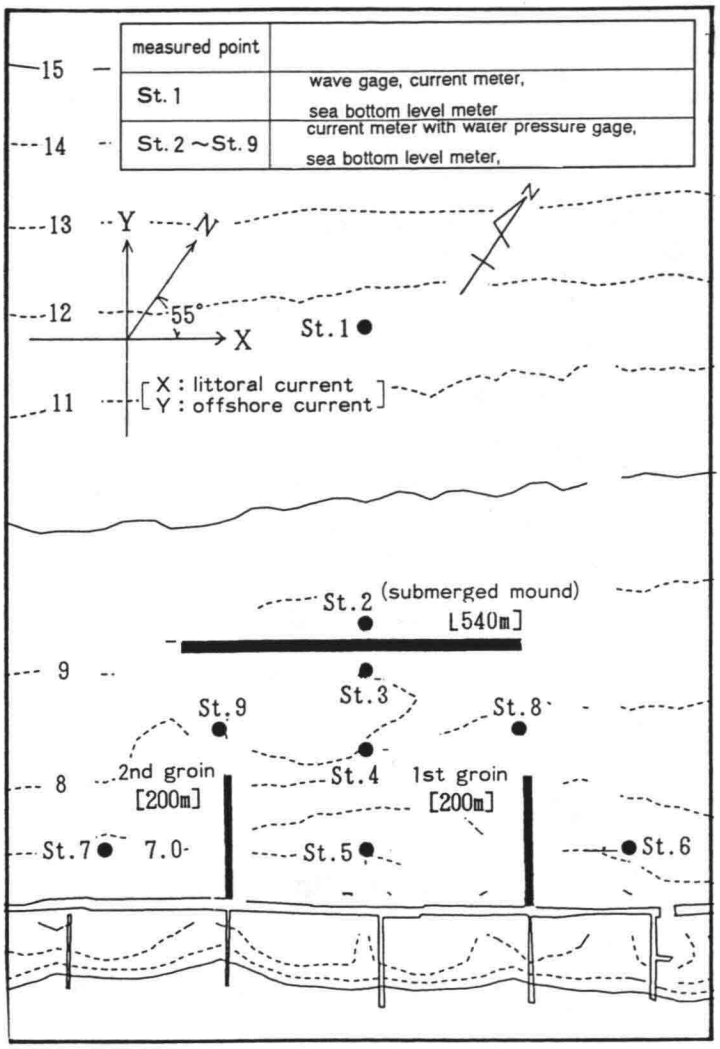

Figure 5 Measuring Points of Waves, Currents and Sea Bottom Surface

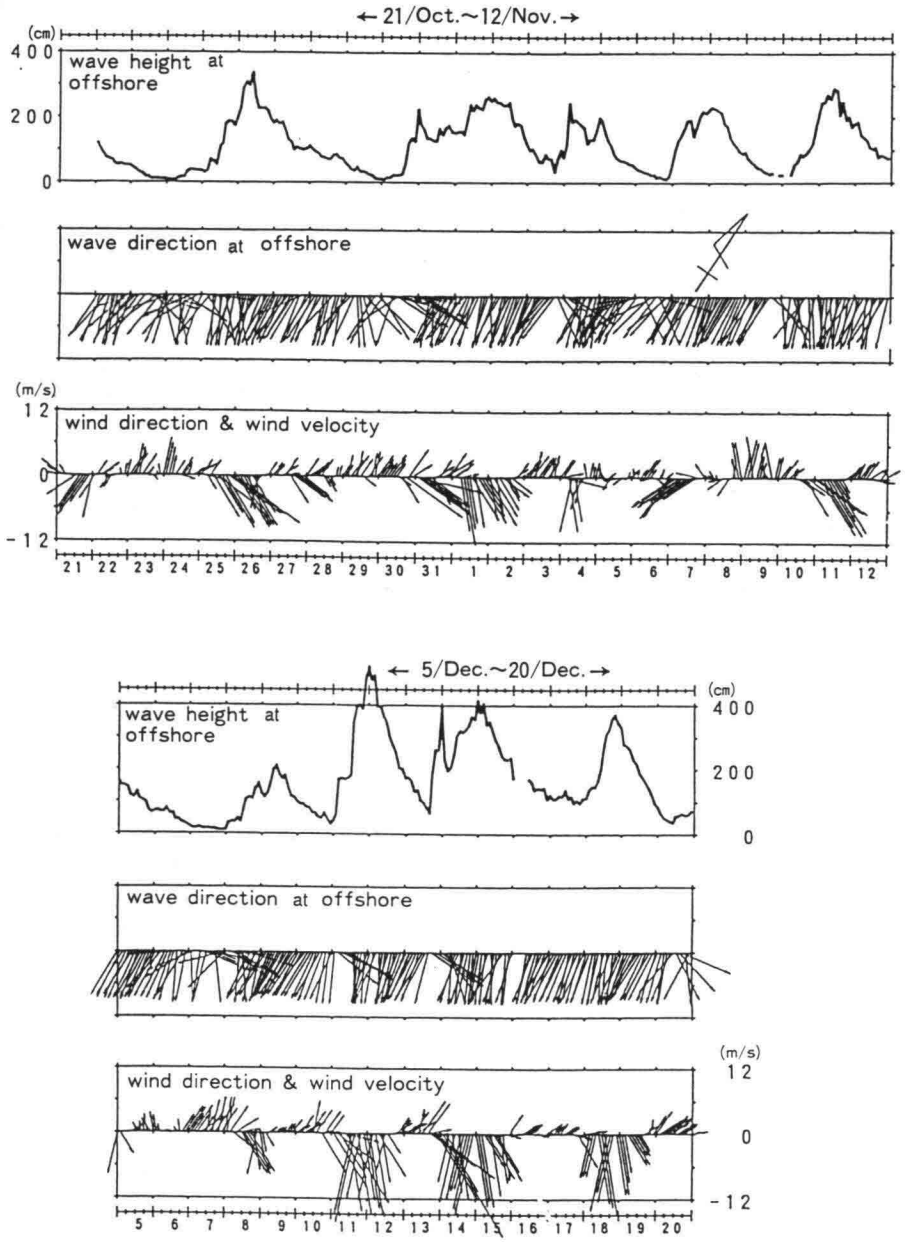

Figure 6 Features of the waves and winds in Niigata West Coast

4. RESULTS OF OBSERVATION AND ANALYSIS

4.1 Waves and Winds Observation

Large waves caused by seasonal strong winds attack frequently and for a long period at the Niigata Coast in autumn to winter. Figure 6 shows the observed wave height, wave direction, wind direction and wind velocity at the observation point of -35m depth off the Niigata port. In the figure, large waves more than 2m height occurred observed five times during the 23 days from 21st October to 12th November and four times during the 16 days from 5th to 20th December.

The condition of rough seas continued often for two days or more. During the development stage of waves, the wave directions were between W and WNW and turned to NNW to N when waves became the peak stage. The wind directions changed from W to N according to the wave development. With the results of the observation, the change of wave directions from W to N during wave development is considered to have significant effects on the littoral drift on the Niigata West Coast.

4.2 Wave Height Reduction Effect Of Submerged Breakwater

Figure 7 shows the changes of wave height by the submerged breakwater. The wave heights at St.3 and St.4 behind the breakwater are apparently lower than those of St.1 and St.2 before it.

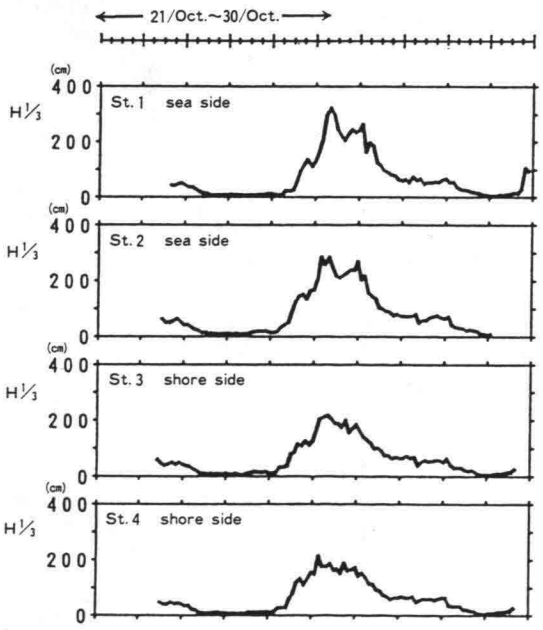

Figure 7 Significant Wave Height at the Sea Side and Shore Side of the Submerged Breakwater

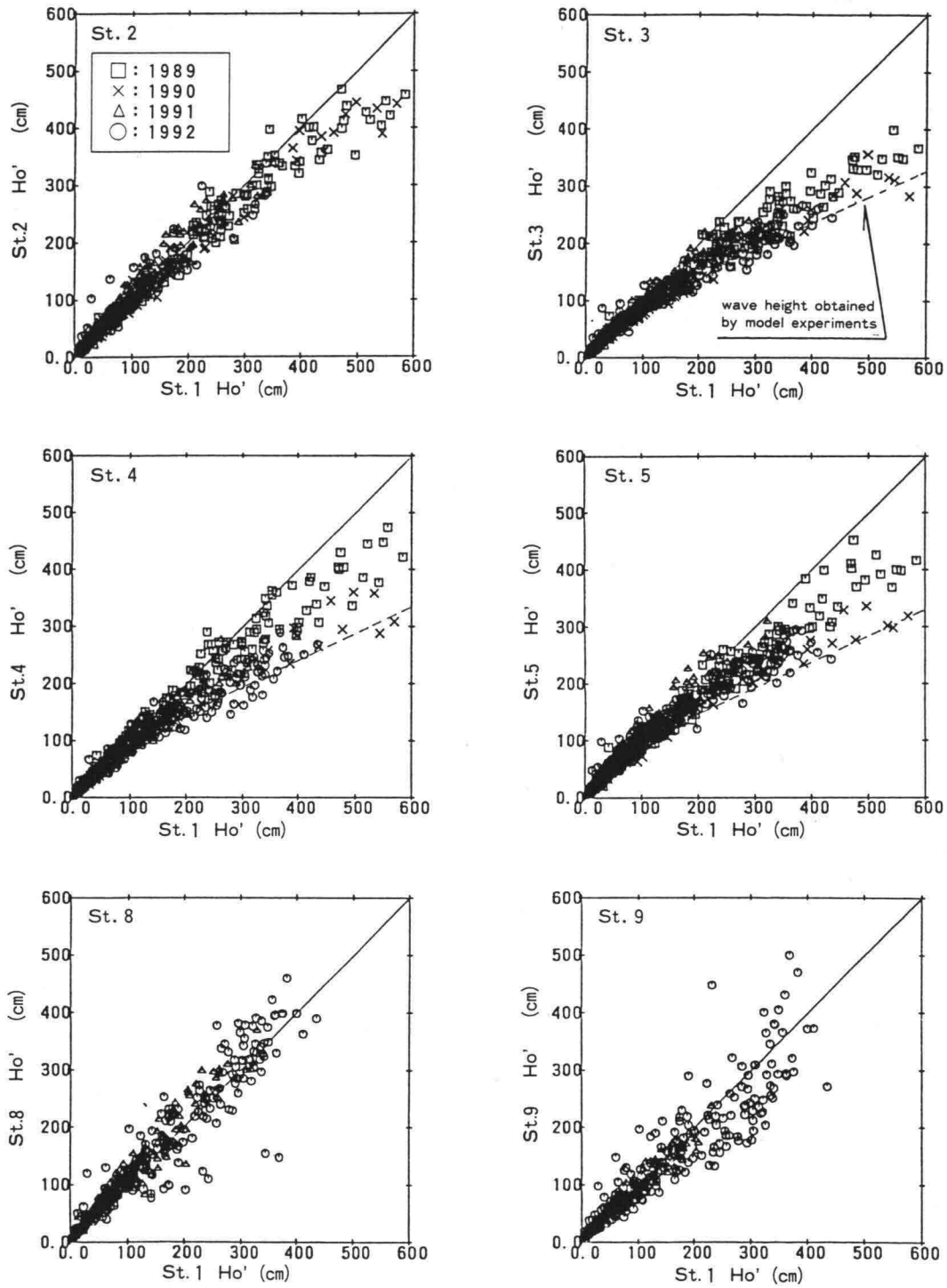

Figure 8 Comparison of Equivalent Deepwater Wave Height at St.1 with Other Points

Figure 8 compares the wave height at St.1 with those at other observation points. The observed wave heights at St.3 and St.4 are lower than that of St.1. The wave height reduction effect is more evident when the wave heights at St.1 are 2m or more. The dotted line indicates the wave heights behind the planned breakwater predicted by the model test. Although only half width of the submerged breakwater has been completed, the observed values in site are close to those of the model test. It is the wave reduction effect of submerged breakwater.

4.3 Current Flow Observation

Figure 9 shows the chronological changes of mean flows observed at the levels of 10cm above the sea bottom. The eastward flow is shown in positive and the westward flow negative in the figure. This shows that the eastward flows were predominant at St.1 and the relative large eastward flows were observed at St.1 and St.3 during the wave development stage. The eastward flows were predominant at St.9 during the wave development stage and the large westward flows appeared when the waves were developed and reached to the peak.

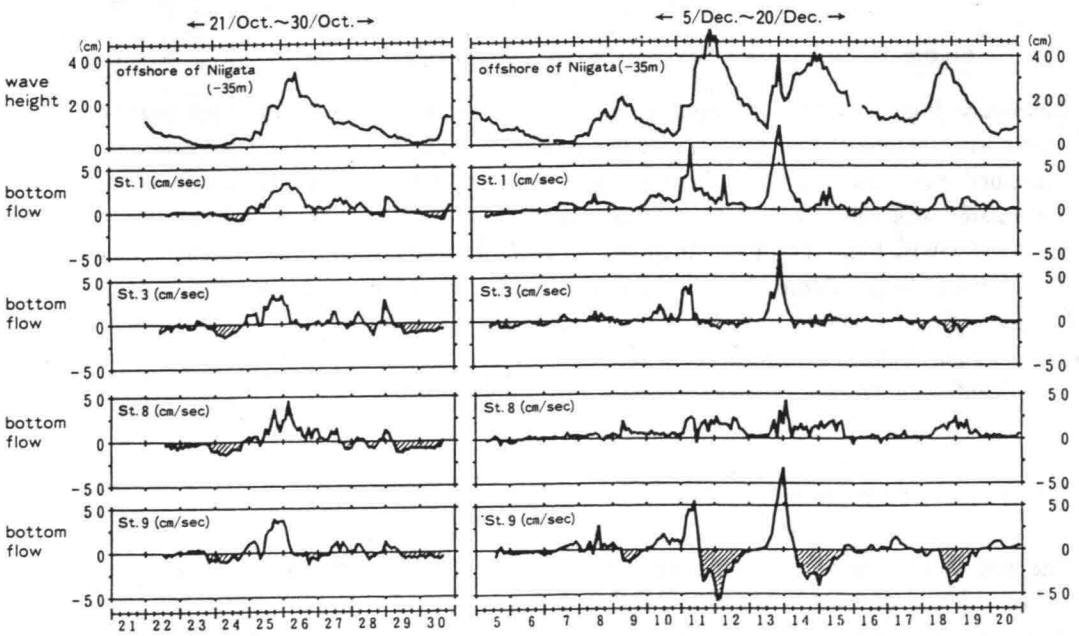

Figure 9 Longshore Bottom flow around the Submerged Breakwater

Figure 10 shows the typical patterns of the bottom flows in each storm. The flow directions are eastward when the waves are in development stage and they turn westward at St.9 when the waves are at the peak stage. It is considered that the flows caused by wave breaking over the submerged breakwater turn to divide the direction to right- and left- ward according to the change of the wave direction.

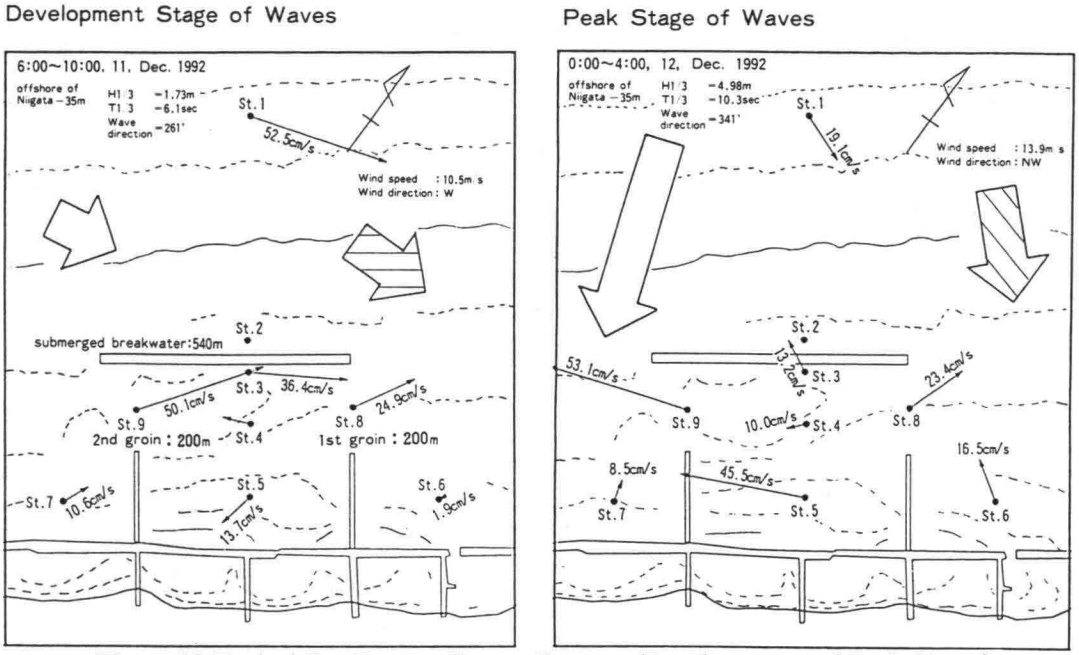

Figure 10 Typical Sea Bottom Current Patterns (Development and Peak Stages)

Relatively high velocity appeared behind the submerged breakwater. Figure11 shows the relationship between long shore velocities and wave heights for the last 4 years. At St.5, the velocities were not large in spite of large waves in 1989 because the length of submerged breakwater was short. The velocities, however, were large and westward in 1992 when the breakwater was long. The flow directions of St.8 and St.9 were reverse each other when the waves were large. Although it is rather difficult to get conclusion since the submerged breakwater is provisional one, the bottom flow behind the breakwater as shown St.5 and St.9 becomes large and changes it's direction after the construction. And this is considered to have significant influence on the sand movement of sea bottom.

4.4 Changes of Sea Bottom Surface

The results of observations on changes of the sea bottom level are shown in Figure 12. It is noticed that the sea bottom level changed about 10cm everywhere and went down 20 cm or more in a short time at areas where the change was great. At St.1 and St.2 in the offshore side of the submerged breakwater, a relationship between wave height and changes of the sea bottom level is not clear. So wave heights are considered to have fewer effects on the changes of the sea bottom surface in the offshore side. At St.4, St.5, and St.8 in the shore side of the submerged breakwater, the sea bottom surface tends to be scoured when the wave heights increases and to recover its original level when those decrease. Then wave heights are considered to have significant effects on the changes of the sea bottom surface in the shore side. At St.9, the sea bottom surface does not change even if the wave heights change, although it is in the shore side of the submerged breakwater.

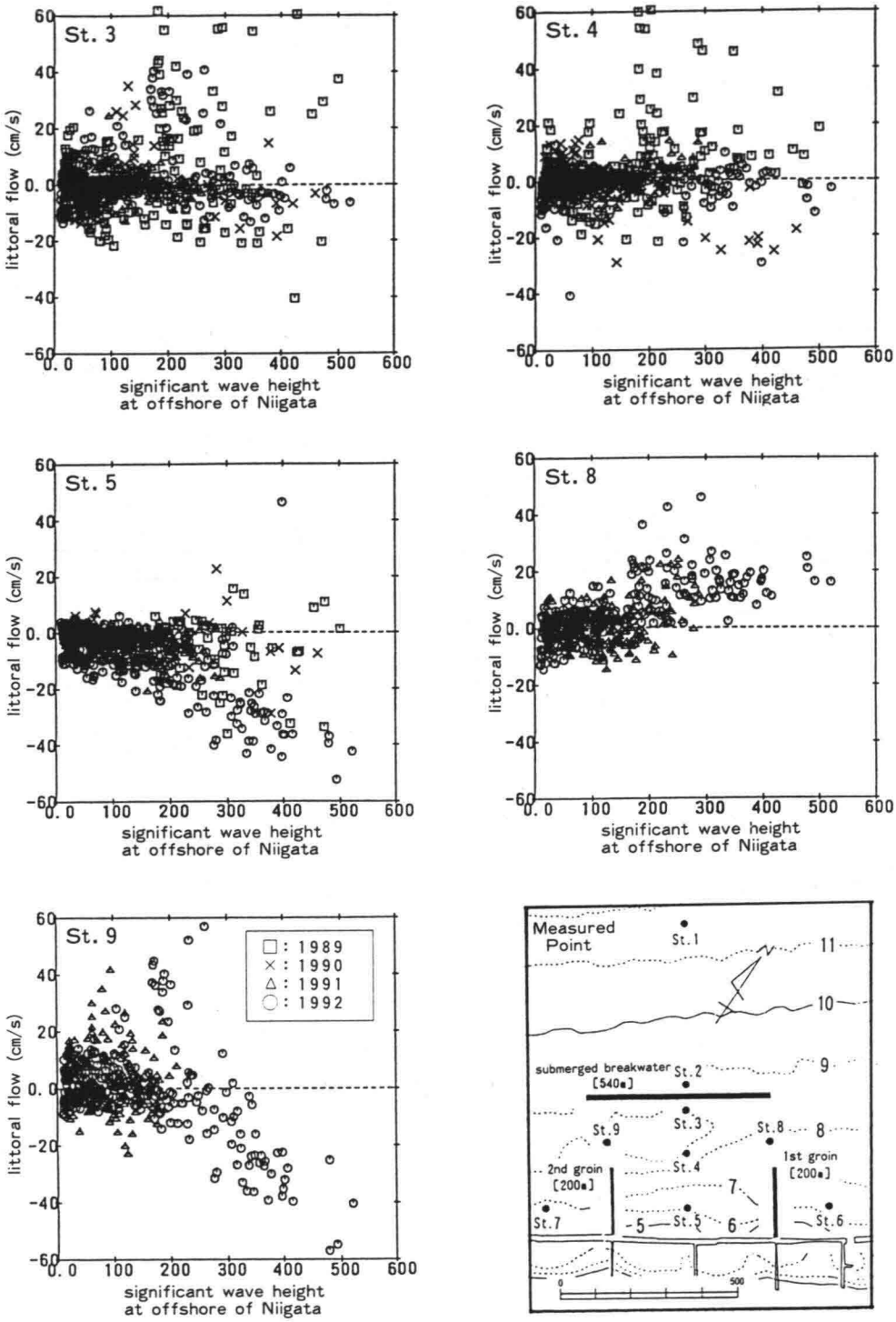

Figure 11 Relation Between the Wave Heights and longshore Currents

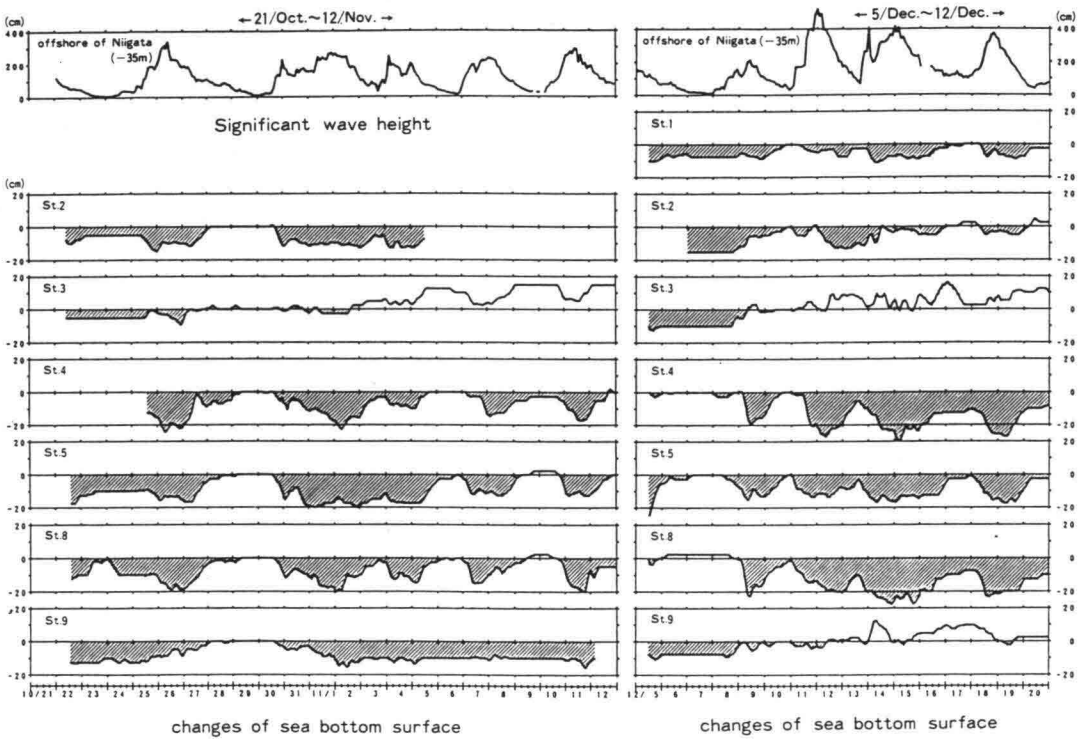

Figure 12 Changes of the Sea Bottom level around the Submerged Breakwater

Figure 13 shows changes of the bottom level surface caused by a storm. It indicates that the bottom surface at St.4, St.5, and St.8 tends to be scoured as the wave heights increase and recover to the original level as the wave heights decrease. A relationship between wave heights and the changes of the sea bottom surface was not clear at St.1, St.2, St.3, and St.9.

4.5 Topographical Changes due to Construction of Submerged Breakwater

Figure 14 shows topographical changes in the surrounding areas by the construction of the submerged breakwater. The data were obtained by sounding surveys from 1987 to 1992 after the start of the construction of the submerged breakwater. Along the lines No.2 and No.3, scouring began behind the submerged breakwater in 1990 (when the length reached 200m), increased in 1991 and became stable in 1992. On the line No.1, scouring in the area of submerged breakwater in 1991 occurred before the construction of it. When the length reached 370m, heavy scouring occurred behind it in 1992. The line No.4 had less topographical changes than the other lines, but undergone erosion in 1992. Thus, as the construction of the submerged breakwater was proceeded, the area behind the submerged breakwater was suffered to large-scaled scouring locally, particularly at the shore side of the west end. The area in front of the submerged breakwater was not so much scoured although slight topographic changes were observed.

The submerged breakwater area was divided into small zones to investigate the changes of the average water depth in each zone. The results are shown in Figure 15. This figure indicates that zones No.12 and No.13 were greatly scoured, while zones No.2 and No.3 had a tendency for deposition. Slight scouring were found in zone No.16 to 20, but there was a tendency for recovering except for zone No.16. The changes were also very small in zone No.21 through No.25. These facts suggest that construction of the submerged breakwater has a small effect on the scouring in front of it.

Sand volume were calculated over the measurement lines to investigate topographical changes over a wider area. Figure 16 shows the difference of the sand volume between 1989 and each surveyed year. This figure indicates that the lines of scouring or deposition change in each period, and that there was no lines where the tendency was changed greatly by the construction of the submerged breakwater. The bottom sounding chart in Figure 16 does not show unusual changes of water depth in front of the submerged breakwater.
Such a tendency suggests that the topographical features in front of the submerged breakwater are not affected by construction of the submerged breakwater as expected in the initial design.

4.6 Characteristics of Sand Around Submerged Breakwater

Figure 17 shows the results of analysis on the grain size and ignition loss of the sand collected around the submerged breakwater. At sampling point 1, the silt content was high

and the median grain size was small in the surface layer. These characteristics differ greatly from those at depths of 20 cm or more and those of other point in the West Coast. In the surface layer at point 2, the median grain size is large, and the silt content is relatively low. The sand at point 2 is considered to be representative of West Coast sand. At point 3, the median grain size is slightly smaller, but the silt content and ignition loss are almost the same as those at point 2.

5. CONCLUSION AND ISSUES TO BE SOLVED

The results of observations in this study are summarized as follows:

1)The wave height decreased by the submerged breakwater became small as predicted by the hydraulic model test.

2)The current direction behind the submerged breakwater is closely related to the wave direction. While the wave direction is west at the development stage and turns to north at the peak stage, the current direction turns eastward to westward.

3)At observation points behind the submerged breakwater, the sea bottom was scoured 20 cm or more as the waves developed and recovered their original level as the waves decayed.

4)Comparing the sounding results, a tendency is found that the sea bottom behind the submerged breakwater is scoured more than 1 m after the construction.

5)Topographical features of the sea bottom in front of the submerged breakwater were not so much affected by the construction, as expected in the design.

The results of observations in this study suggest that turbulence of current flows behind the submerged breakwater may increase during the construction. Then, it is very important to monitor the topographical changes of the sea bottom during the course of construction of submerged breakwater.
Works for completing the submerged breakwater have been started in 1993. Beach nourishment is planned to be carried out since around 1995. We plan to continue to study the flow and topographical changes around the submerged breakwater during the works. We will also study the stability of beach nourishment planned in the future.

ACKNOWLEDGMENTS

Authors would like to express our sincere gratitude to the member of Committee of Niigata West Coast Erosion Prevention Study and the staff of the Port and Harbor Research Institute who willingly gave advice and guideline to this study.

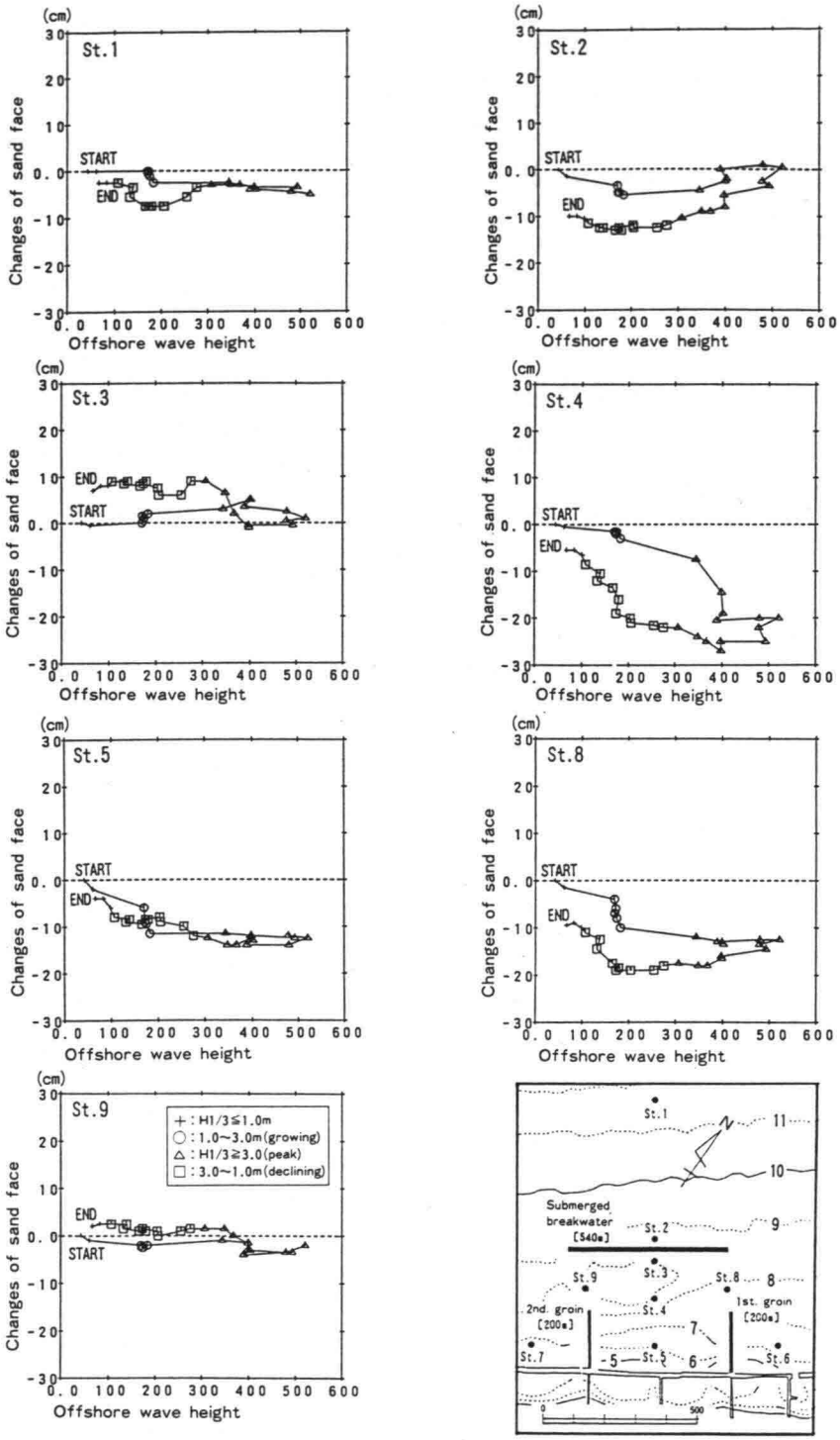

Figure 13 Changes of the Sea Bottom Level related with Significant Wave Height (11 ~ 13 / Dec.'92)

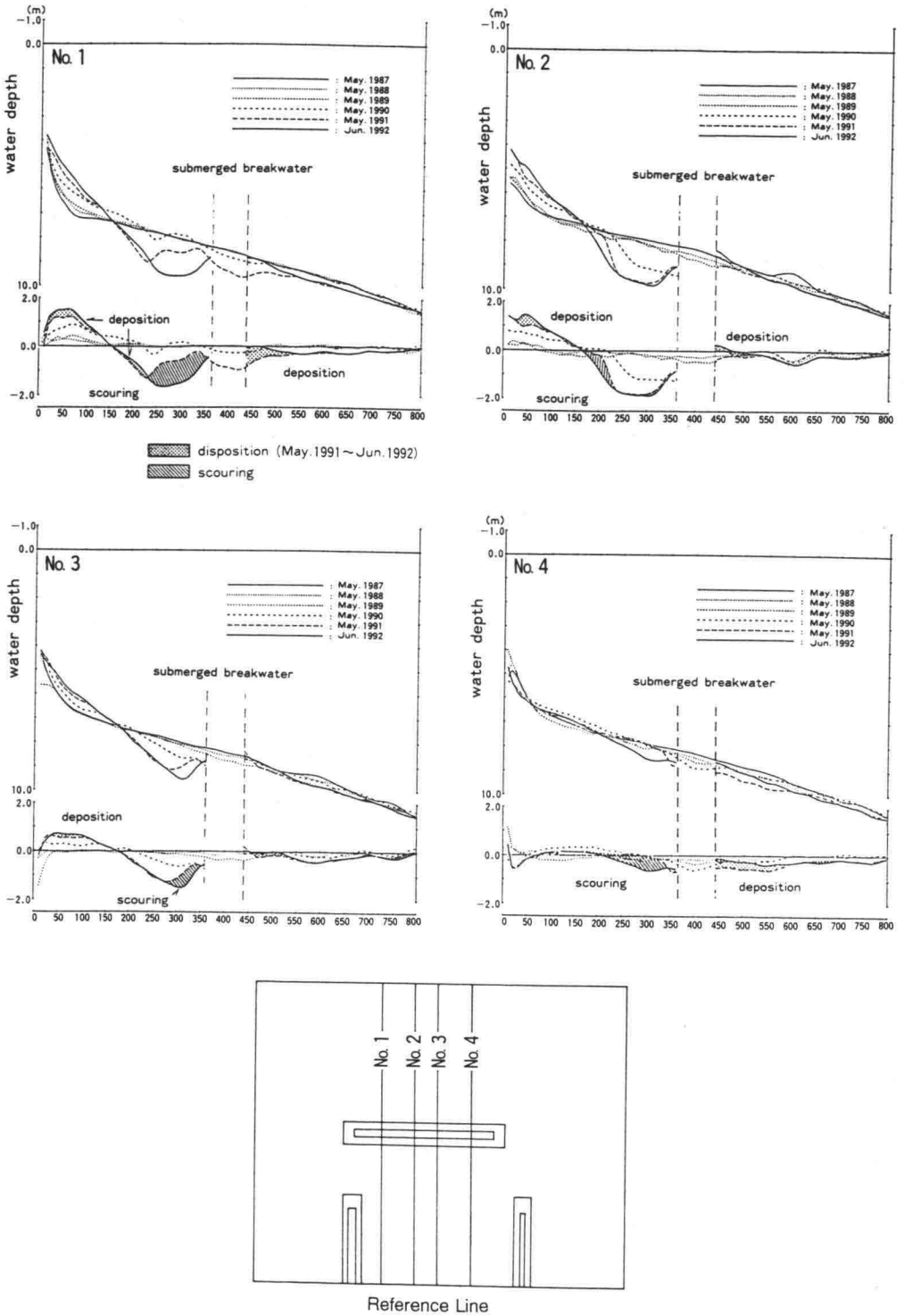

Figure 14 Profile Changes in the Surroundings due to Construction of the Submerged Breakwater

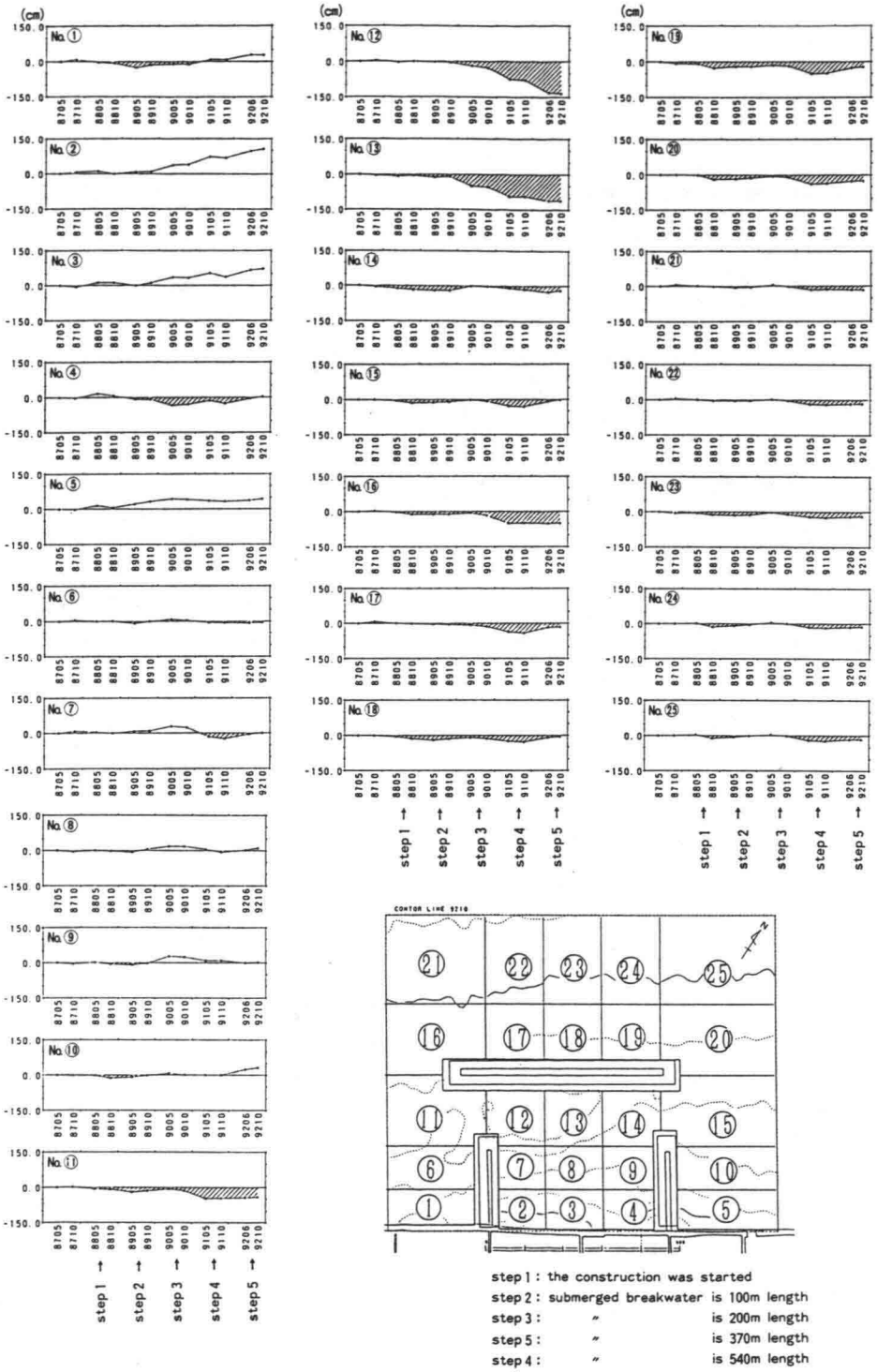

Figure 15 Changes of the Average Water Depth around Submerged Breakwater

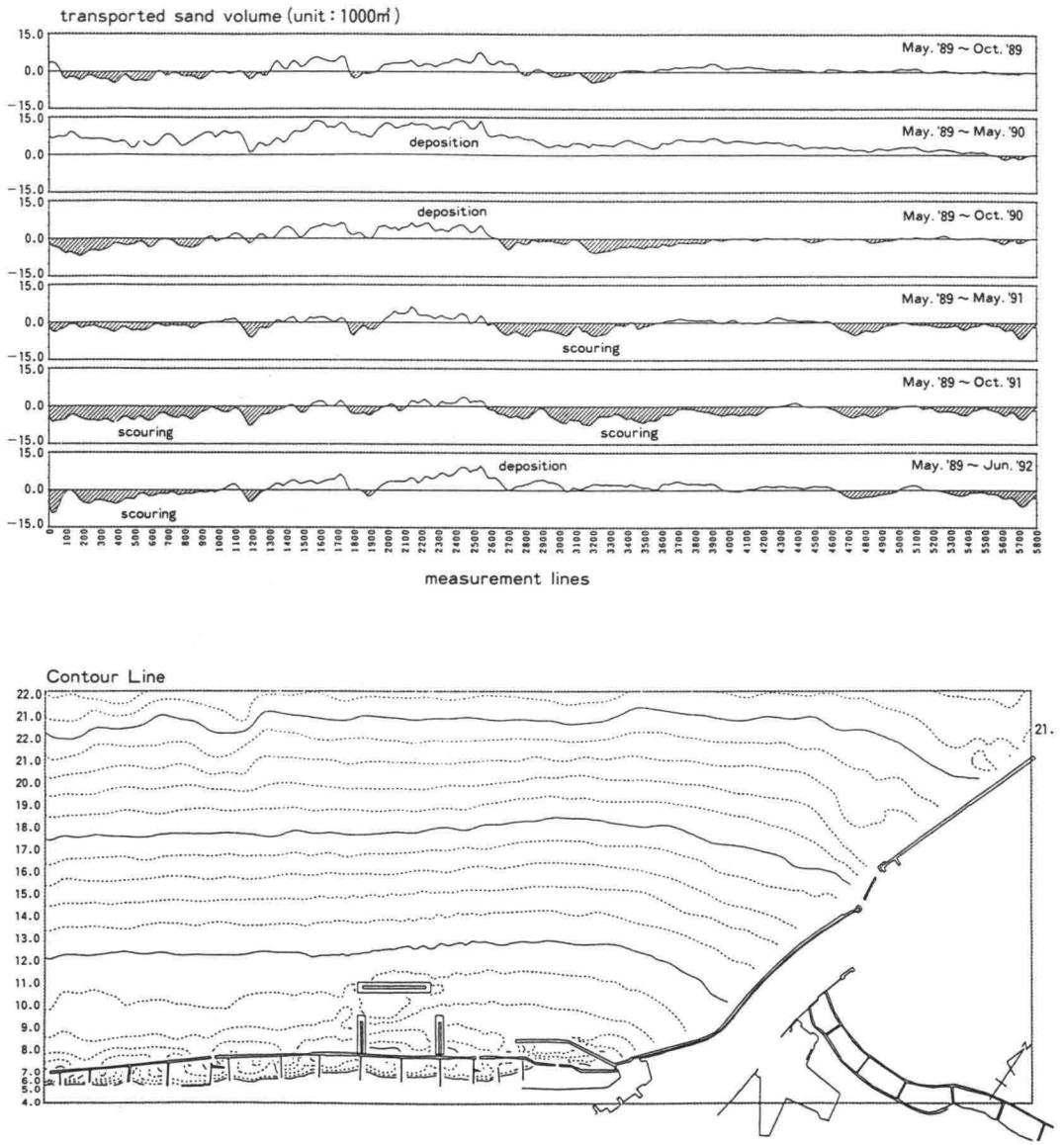

Figure 16 Total Littoral Sediment Transport Rate

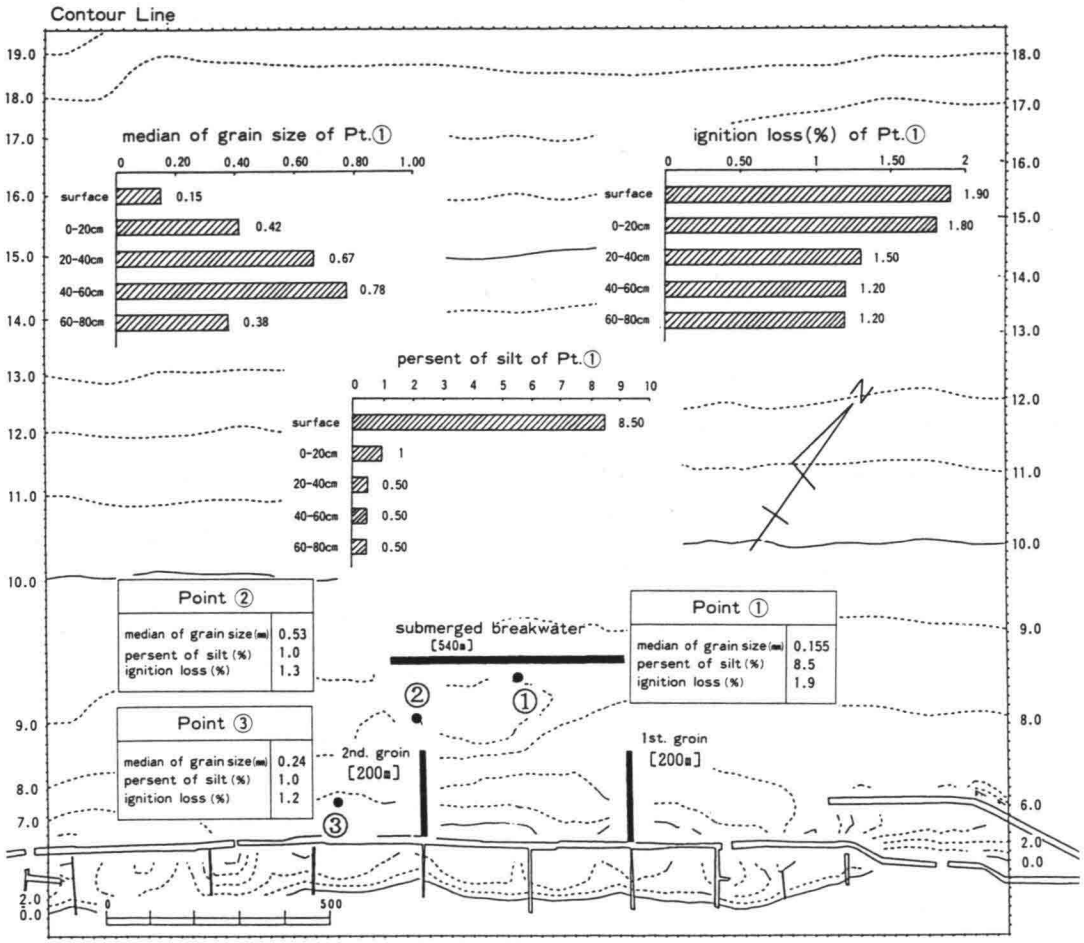

Figure 17 Characteristics of Sea Bottom Sands

REFERENCES

Iwatani,F.,T.Miyamoto,M.Matsushita,S.Yoshinaga,R.Kawamata and Y.Adachi: Prediction of Waves, Currents and Topographical Change around Submerged Offshore Breakwater, Coastal Engineering in Japan Vol.32, No.2, December 1989,JSCE.

Arai,Y.,M.Tanaka,H.Iwamoto and R.Kawamata: Sea Bottom Change Caused by Waves at the Niigata West Coast, Proc. 34th Japanese Conf. on Coastal Eng.,1987.(in Japanese)

Nakata,H.,M.Suzuki, K.Abe,R.Kawamata and M.Minami: Field Survey on Topographical Changes around Submerged Breakwater comparing with Prediction Model, Proc. 39th Japanese Conf. on Coastal Eng.,1992.(in Japanese)

HYDRO-PORT'94
International Conference on Hydro-Technical
Engineering for Port and Harbor Construction
October 19 - 21, 1994, Yokosuka, Japan

Investigation of Current and Particle Velocity near the Surf Zone

Chien-Kee Chang [1]
Fu-Tung Chang [2]

[1] Director, Institute of Harbour and Marine Technology
Wu-Chi, Taichung
[2] Assistant, Institute of Harbour and Marine Technology
Wu-Chi, Taichung

ABSTRACT

Three research piles are installed on the shallow water of mild beach for a reseach group to carry out field measurement near surf zone. The main purpose in this study is to measure and analyze water particle velocity induced by waves. The particle velocities induced by waves are filtered by a narrow frequency band width. The plots of the ratio between calculated and measured values of particle velocity amplitude show quite scattering. Finally, it is found that the relationships between velocity transfer function $(U/H\omega)$ and dimensionless parameter $(\omega^2 z^2/gD)$ of field data have consistent tendency in comparing with Chiu and Kou (1993) laboratory experiment results.

Key Words : Particle Velocity, Surf Zone, Velocity Transfer Function, Observation Piles

1. INTRODUCTION

The kinematics of shallow water waves plays very important role for coastal phenomena such as sediment transport, wave forces on structures, diffusion of material. Field experiment to measure instaneous particle velocity induced by water wave is quite difficult before electromagnetic current meter and data acquisition were developed. By using electromagnetic flowmeter, sampling rate 0.5Hz, Thornton and Krapohl (1974) conducted field experiment to measure wave induced water particle velocity at research tower located at mean water depth 19^m. The results show wave and particle velocity have high coherence at the range of significant energy density, but have larger discrepency at higher and lower

frequency. Cavaleri et al (1978) measured wave pressure and three components particle velovity at water depth 16^m. Recorded velocities are about 10% less than expected on the basis of linear wave theory. The difference does not appear to be caused by finite amplitude effect but rather the influence of turbulent fluctuation near the surface. Isobe and Horikawa (1982) carried out laboratory tests and two field experiments, the measured water particle velocities were used to compare with the results calculated by energy flux method. In the surf zone, the field experiment results show the relative velocity amplitude approaches a constant for mild bottom slope.

In the past decade, water particle velocity induced by regular and irregular waves have been studied in the laboratory by many authors. Vis (1980) carried out experiment investigation to measure wave induced orbit velocities near the bottom by using Laser Doppler meter instead propeller type flow meter used in the past. Comparision between theory and measurement was executed in frequency and time domain. Anastsiou (1982) equipped a two-channel Laser Doppler anemometer to investigate water particle kinematics near and above MWL, and the results are in good agreement with theorical approaches. Daemrich et al (1982) developed a simulation method based on linear wave theory to calculate the maximum postive and negative orbit velocity of the individual wave of a wave train, the result shows good correlation with experiment data, except at the location near free surface, a tendency towards over or underestimation. Koyama amd Iwata (1985) proposed a modified transfer function method (MTFM), the laboratory experiments show that MTFM is a simple and highly reliable approximate method to calculate water wave particle velocity. Y-F Chiu and Yi-Yu Kuo (1993) measured water particle velocities of progressive waves. By comparing data obtained from experiment and calculated by linear and finite wave theories, it exists some degree of discrepency. A dimensionless velocity transfer function ($U/H\omega$), which composed of particle velocity U, wave height H and angular wave frequency ω was proposed. It is found that the experiment data and velocity transfer function have good correlation for regular and significant wave of irregular wave train, but rather scattering for individual wave of irregular wave train.

The main purpose of this study is to carry out field measurement of waves and particle velocities near the surf zone of mild slope beach. Water particle velocities induced by wind wave are filtered out and the maximum orbit velocities are compared with those calculated values of based on linear and finite wave theories. Finially, by using field data, the relationship between velocity transfer function and dimensionless parameter will be investigated its applicability.

2. FIELD MEASUREMENT

In order to carry out the field measurements of wind, wave, wave pressure and current, observation piles are installed near the tip of the North Groin of Taichung Harbour. The locations are shown in Fig 1, and the depths are 1.0^m, 3.0^m and 6.0^m LLWL respectively.

The maximum tidal range in Taichung area is about 5^m; hence, by tidal variation, wave and current at different water depth can be measured.

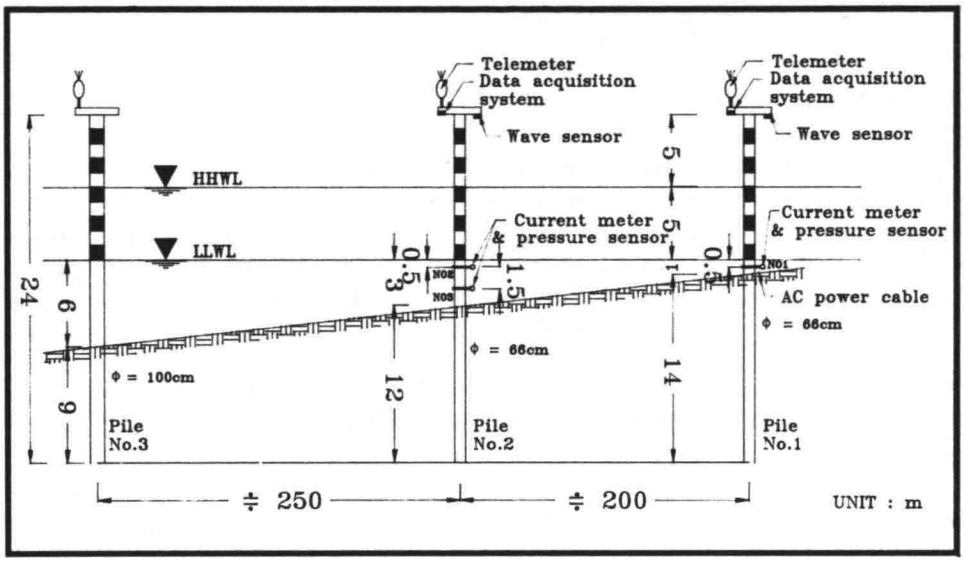

Fig 1 Layout of intruments for field measurement

Ultrasonic wave transducers are mounted on the platform at the top of the pile; and the real time wave signals are sent to land station by using telemeter which developed by Professor Kao of Cheng Kuang University. Current meters of electromagnetic type and pressure sensors are installed at piles No.1 and No.2 which located at 1.0^m and 3.0^m LLWL as shown in Fig. 1. Data acquisition system consists of IBM compatible PC-386, with 100MB hard disc, 14 bit A/D convertor and the integration of the system is shown in Fig. 2. The sampling rate of both current and pressure are 5 Hz, and recorded 10^{min}

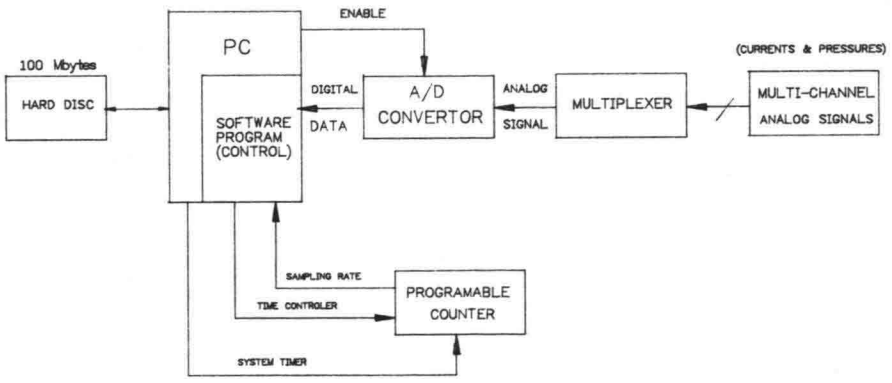

Fig 2 BLOCK DIAGRAM OF DATA ACQUISITION SYSTEM

for every 2 hours interval. In this study, water sruface level is transferred from presure data, because wave data are not recorded synchronously. The water surface level and particle velocity for two time steps 7-23-2 and 7-23-10 are plotted as shown in upper two diagrams of Fig. 3 and Fig. 4 respectively.

3. DATA ANALYSIS

Figure 3 and 4 show that at the same time step waves recorded at shallower water (Pile No.1) are smaller than those obtained at deeper water (Pile No.2), but water particle velocities of channel No.1 are greater than the coresponding particle velocities of channel No.3. On the other hand, wave climates at two time steps are quite similiar, but the particle velocity increases tremendously due to decreasing of water depth during ebb tide, especially for channel No.1 located at the shallower water.

In order to analyze the orbit velocity induced by wind waves, high frequency particle velocity component within the band width between 0.5 Hz and 0.05 Hz is filtered. The time series particle velocities are plotted as shown in the third diagram of Figure 3 and Figure 4. After filtering, the orbital velocity changes its direction and magnitude in according with the profile of surface wave. The velocities of low frequency components between 0.05 Hz 0.005 Hz due to long period water surface variation are plotted as shown in the bottom diagram of Figure 3 and Figure 4, which will be analyzed further in the future.

Based on wave records the horizontal water particle velocity amplitudes for sorted out individual waves are calculated by using linear wave theory (U_L) and second order finite amplitude wave theory (U_2), the results are used to compare with the corresponding velocity amplitudes obtained from field measurement (U_F). The ratio of (U_L/U_F) and (U_2/U_F) are plotted against the relative water depth (d/L) as shown in Figure 5, for channel No.1. Channel No.1 installed on the pile No.1 located at shallower water, in the period of investigation the water depth varies from 2.08^m to 4.08^m. Figure 5 shows the range of relative water depth between 0.05 to 0.4, the ratios of particle velocity between calculated and measured have wide range of scattering and the particle velocities calculated by using second order finite amplitude wave theory do not have much improvement.

Figure 6 and 7 are the plots between the ratio (U_L/U_F) and relative depth (d/L) for channel No.2 and No.3, which are mounted on pile No.2 located at deeper water, and water depth varies from 5.29^m to 7.29^m for field experiment. Channel No.2 equipped at the upper position of the pile and the water depth of current meter ranges from 1.58^m to 4.79^m. Figure 6 shows calculated velocity amplitudes are over or under-estimation in comparing with field measured data. Channel No.3 installed at the lower position of pile No.2, water depth of current meter changes from 3.08^m to 6.29^m. Figure 7 shows that the calculated values have a tendency towards measured data for increasing of relative water depth (d/L).

By using the method applied in wave statistics, the significant particle velocity amplitude of wave train is analyzed. The ratios between significant particle velocity amplitude

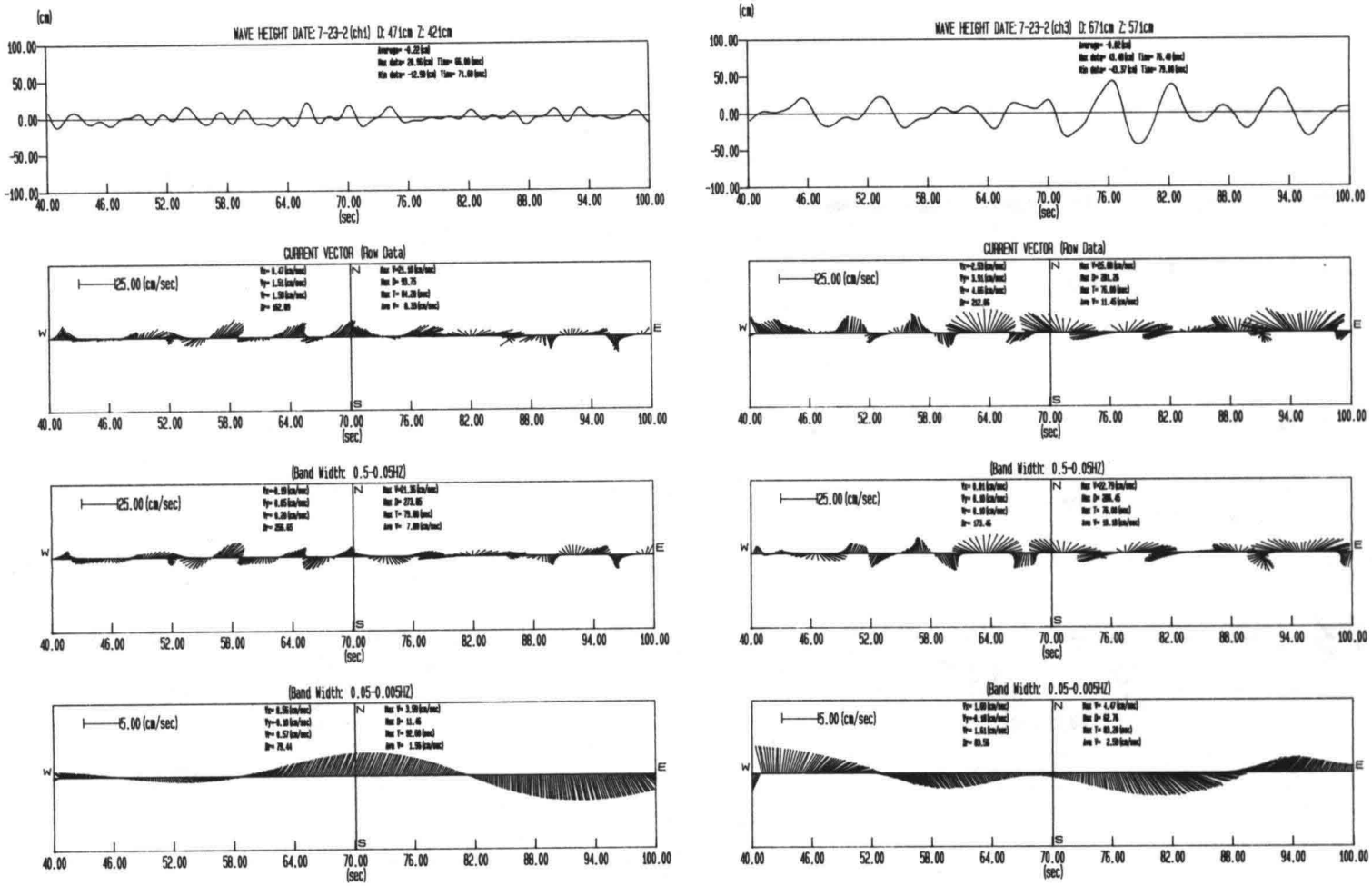

Fig.3 Time Series of Water Waves and Paticle Velocities (High Tide)

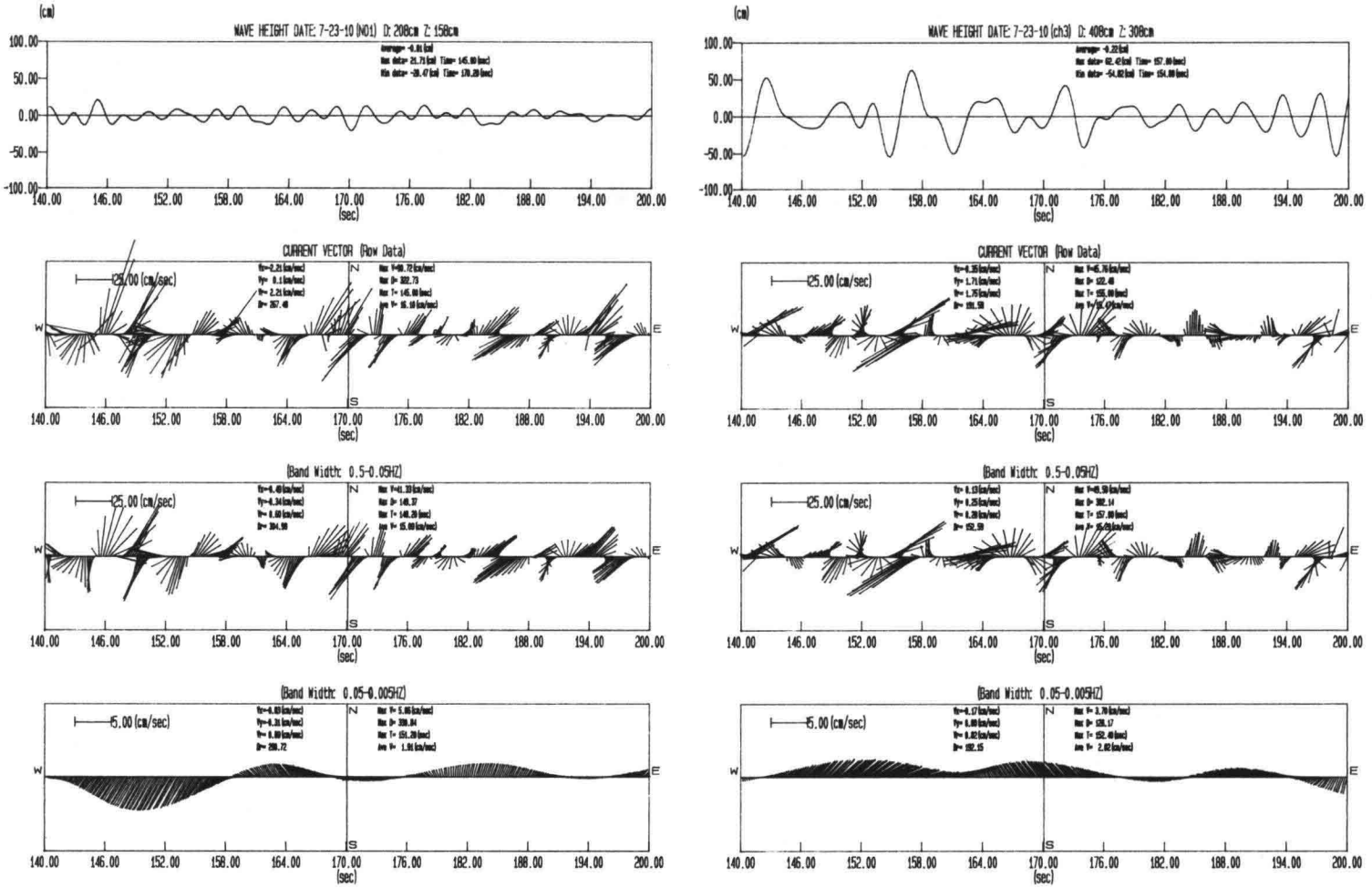

Fig.4 Time Series of Water Waves and Paticle Velocities (Low Tide)

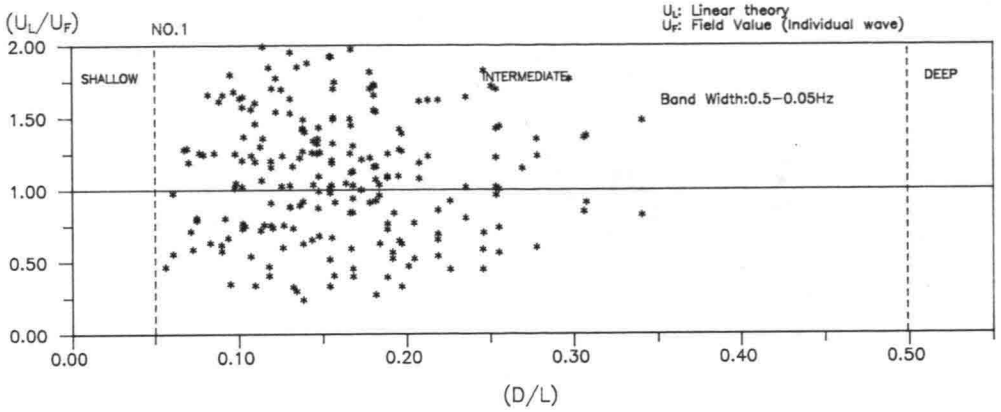

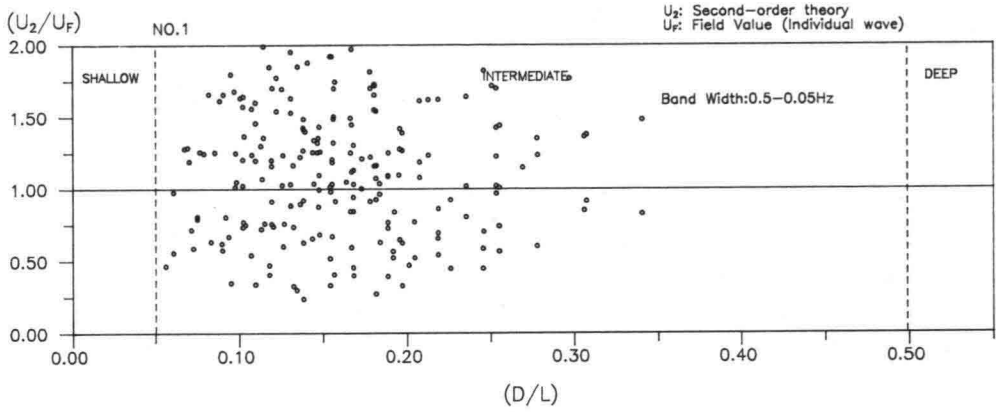

Fig 5 Relationship Between the-Ratio of Calculated and Measured Velocities and Relative Depth for Current Meter No.1

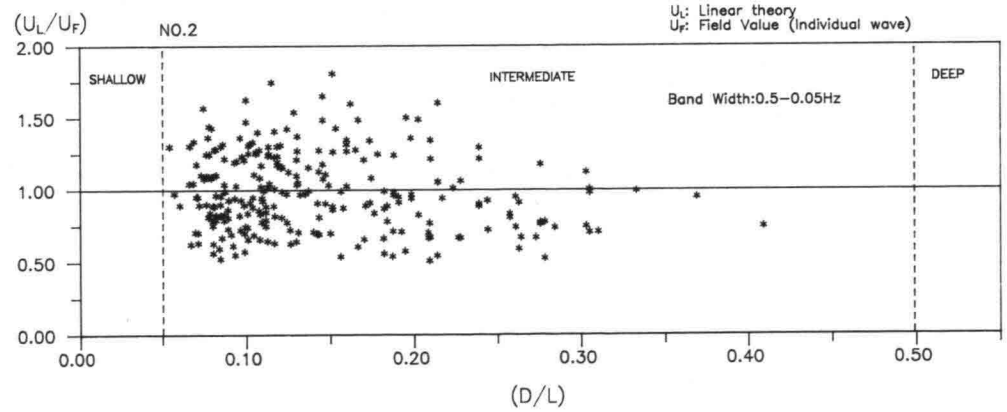

Fig 6 Relationship Between the-Ratio of Calculated and Measured Velocities and Relative Depth for Current Meter No.2

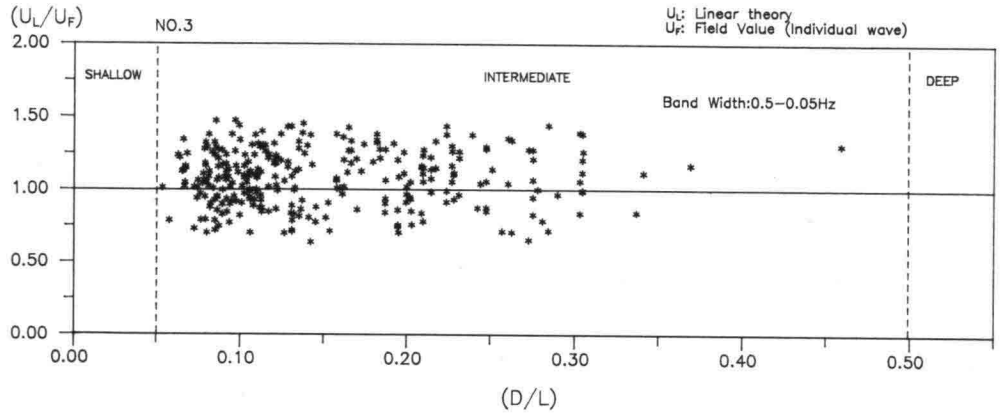

Fig 7 Relationship Between the-Ratio of Calculated and Measured Velocities and Relative Depth for Current Meter No.3

obtained by field measurement and those calculated by wave data for three channels are plotted in Figure 8. The result shows that the calculated velocities can not estimate quite well in comparing with field measured velocities.

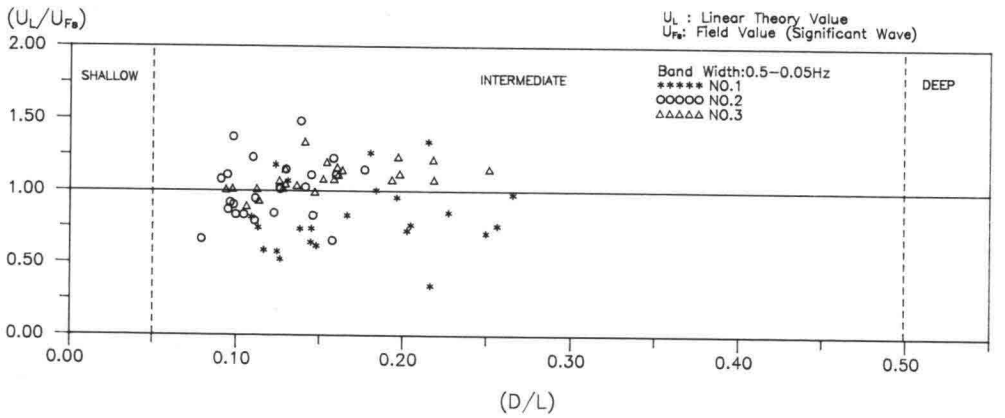

Fig 8 Relationship Between the-Ratio of Calculated and Measured Velocities and Relative Depth for Signigicant Wave

4. VELOCITY TRANSFER FUNCTION

Water particle velocity (U) induced by waves is function of wave height (H), angular wave frequency (ω), water depth (D), depth of the particle (Z), water density (ρ) and gravitational constant (g), which can be written in function form as

$$F(U, H, \omega, D, Z, \rho, g) = 0 \tag{1}$$

By applying Π - theorm dimensional analysis, four dimensionless parameters are as follow.

$$\Pi_1 = \frac{U}{H\omega}, \qquad \Pi_2 = \frac{D}{H}, \qquad \Pi_3 = \frac{Z}{H}, \qquad \Pi_4 = \frac{\omega^2 H}{g} \tag{2}$$

Recombine Π_2, Π_3 and Π_4 obtain the following new parameter

$$\Pi_5 = \frac{\omega^2 Z^2}{gD} \tag{3}$$

Hence, the velocity transfer function, VTF can be written as

$$VTF = \frac{U}{H\omega} = F'(\frac{D}{H}, \frac{Z}{H}, \frac{\omega^2 Z^2}{gD}) \tag{4}$$

Chiu and Kuo (1993) carried out laboratory experiment and proved VTF does not have good relation with D/H or Z/H, but has good correlation with $\omega^2 Z^2/gD$.

Figure 9 shows the relationship between VTF and dimensionless parameter $\omega^2 Z^2/gD$ for significant waves and its corresponding particle velocity amplitudes of wave trains which measured at three different locations of pile No.1 and No.2. The best fitting curves of exponent form are drawn by using solid line and dash line for field observation and laboratory experiment respectively. Although it exists slight difference between two curves, but the tendency is quite consistency. Some individual waves and its corresponding particle velocities are sorted out from time series records. The relationships between VTF and dimensional parameter for individual waves and their corresponding velocities are plotted as shown in Figure 10, 11 and 12 for current meter No.1, No.2 and No.3 respectively. Figure 10 shows that wave and current measured in the shallower water, data points and the fitting curve of laboratory data have consistent exponent tendency, but the VTF values have wide range of scatting. Figure 11 and 12 show large part of the VTF values are located under the regression curve of laboratory experiment, but the data points do not have wide range distribution. Current meter No.3 installed 1.5m below No.2, the results show the coherence increases with increasing of water depth. Figure 13 shows the relationship between VTF and dimensionless parameter $\omega^2 Z^2/gD$ for individual waves and its corresponding particle velocity amplitudes recorded at three currentmeters. Regression curve is plotted by solid

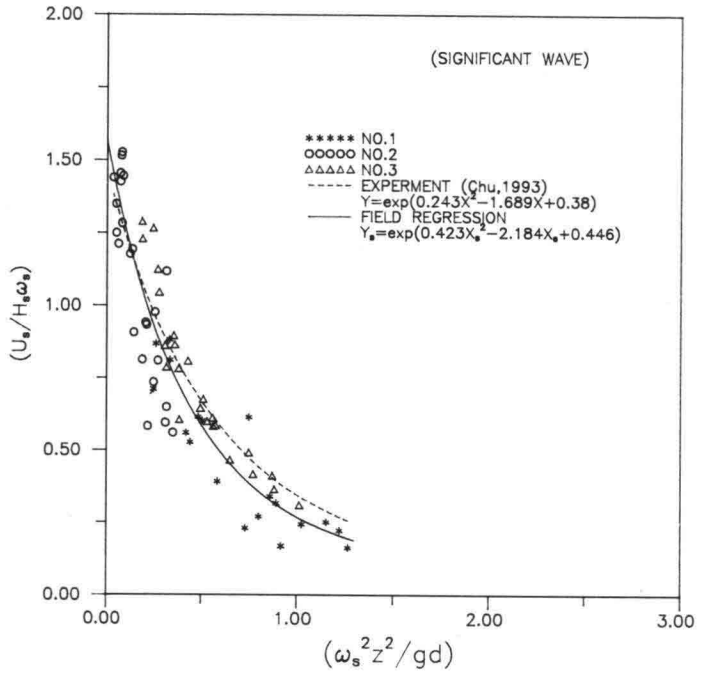

Fig 9 Relationship Between VTF and $\omega^2 Z^2/gd$ for Significant Wave

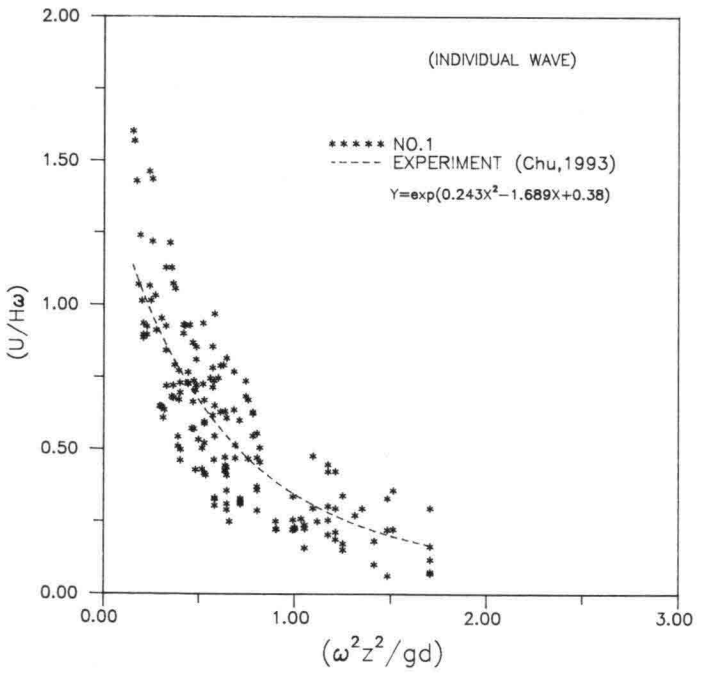

Fig 10 Relationship Between VTF and $\omega^2 Z^2/gd$ for Individual Wave of Current meter No.1

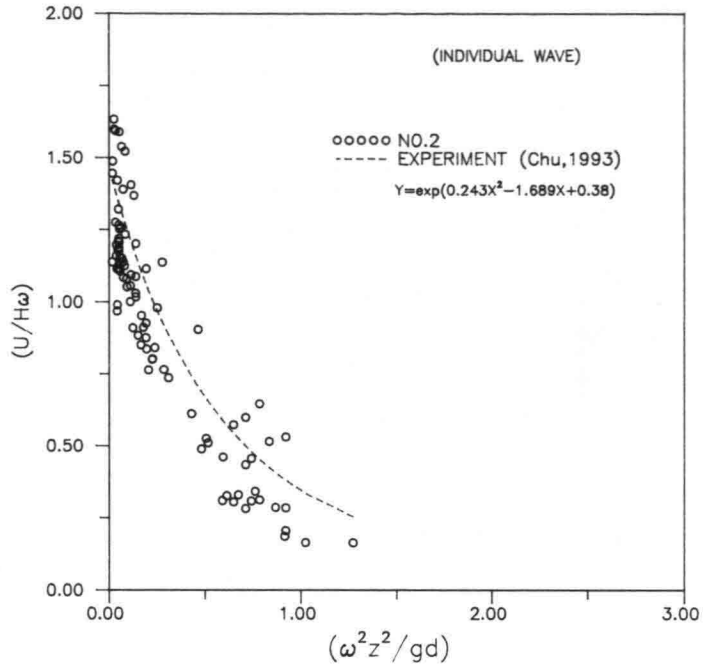

Fig 11 Relationship Between VTF and $\omega^2 Z^2/gd$ for Individual Wave of Current meter No.2

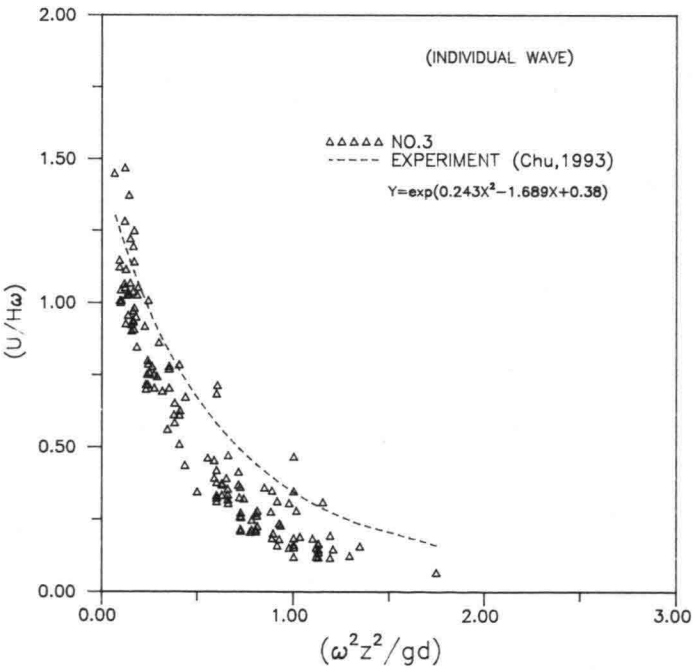

Fig 12 Relationship Between VTF and $\omega^2 Z^2/gd$ for Individual Wave of Current meter No.3

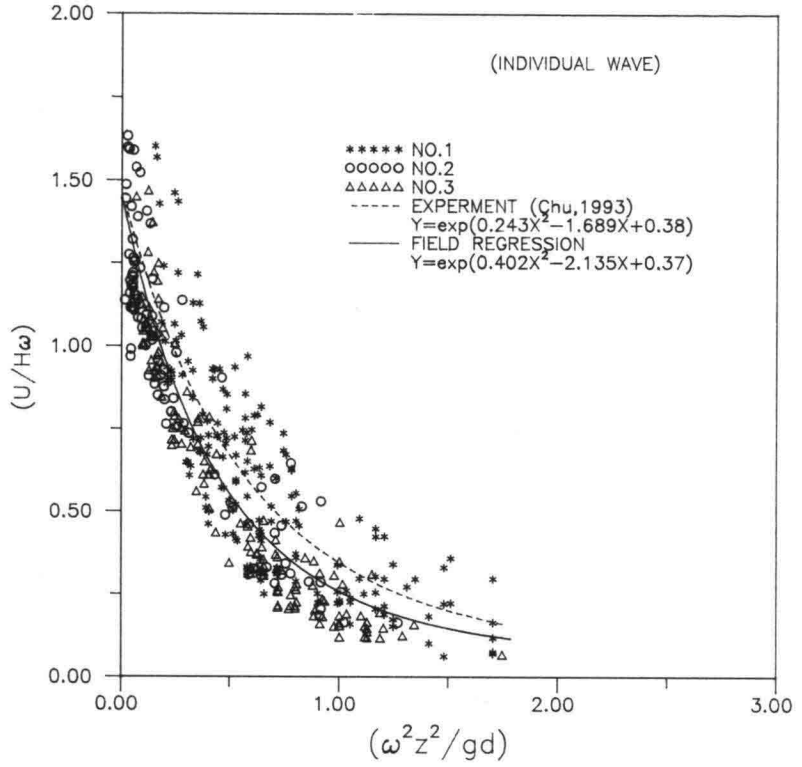

Fig 13 Relationship Between VTF and $\omega^2 Z^2/gd$ for Individual Waves

line in comparing with the dash line curve of laboratory experiment. The best fitting curves of Figure 9 and Figure 13, the velocity transfer function (VTF) can be expressed by the following equations.

$$VTF = \frac{U_s}{H_s \omega_s} = Exp[0.423(\frac{\omega_s^2 Z^2}{gD})^2 - 2.184(\frac{\omega_s^2 Z^2}{gD}) + 0.446] \tag{5}$$

For significant wave and its corresponding particle velocity amplitude.

$$VTF = \frac{U}{H\omega} = Exp[0.402(\frac{\omega^2 Z^2}{gD})^2 - 2.135(\frac{\omega^2 Z^2}{gD}) + 0.37] \tag{6}$$

For individual wave and its corresponding particle velocity amplitude.

5. CONCLUSION

1) In shallower water, the ratio of particle velocities between measured in the field and those calculated by linear or finite wave theory, and have wide range of scattering.

In deeper water, the observed particle velocities have a tendency towards calculated values when d/L approaches 0.5.

2) Either significant or individual wave and its corresponding particle velocity have good correlation between velocity transfer function $(U/H\omega)$ and dimensionless parameter $(\omega^2 Z^2/gD)$. Practically, the regression equation can be used to evaluate particle velocity induced by water waves.

3) Low frequency component water particle velocities which may created by group waves, further analysis is requird for better understanding.

ACKNOWLEDGEMENTS

This research was supported by National Science Council of the Republic of China, under the Contract NSC-82-0209-E-124-003. The authors sincerely wish to express their gratitude to the working group of the Utilization of Coastal Zone, for hard work of field measurement.

REFERENCES

1. Anastasiou, K, et al (1982): Measurements of Particle Velocity in Laboratory - Scale Random Waves, Coastal Engineering, 6 (1982), PP233-254.
2. Cavaleri, F. et al (1978): Measurement of the Pressure and Velocity Field Below Surface Waves, Turbulent Fluxes Through the Sea Surface, Wave Dynamics and rediction, Plenum Press, New York, PP257-272.
3. Chiu, Y-F and Kou, Y-Y (1993): A Study of Character of Water Particle Velocity, Proc. 15th Conf. on Ocean Engineering 1993, (in Chinese), PP29-42.
4. Daemrich, K.-F. et al (1982): Investigation on Orbital Velocities and Pressures in Irregular Waves, Coastal Engineering 1982, PP297-312.
5. Isobe, M. and Horikawa, K. (1982): Study on Water Particle Velocities of Shoaling and Breaking Waves, Coastal Engineering in Japan, Vol.25, 1982, PP109-123.
6. Koyama, H. and Iwata, K. (1985): Estimation of Water Particle Velocities by a Modified Transfer Function Method, Coastal Engineering in Japan, Vol.28, 1985, PP1-13.
7. Thornton, Edward B. and Krapohl Richard F. (1974): Water Particle Velocities Measured Under Ocean Waves, Journal of Geophysical Research, Vol.79, No.6, PP847-852. Vis, F. C. (1980): Orbital Velocity in Irregular Waves, Coastal Engineering (1980), PP173-186.

HYDRO-PORT'94
International Conference on Hydro-Technical
Engineering for Port and Harbor Construction
October 19 - 21, 1994, Yokosuka, Japan

Two Dimensional Change of Swash Slope

Susumu Kubota [1]
Yukimasa Hida [2]
Mitsuo Takezawa [1]

[1] College of Science and Technology, Nihon University
Kanda-Surugadai 1-8-14, Chiyoda-ku, Tokyo 101
[2] Tohoku Electric Power Co., Inc.
Ichiban-chyo 3-7-1, Aoba-ku, Sendai 980

ABSTRACT

Topographical changes of an artificial beach slope mounded on natural beach were measured including the measurement of its external force. The artificial slope was went back as the original slope of natural beach with time. The obtained data were used for decision of coefficient in the on-offshore transport rate formula proposed by Sunamura(1984).

Key Words:beach face change, field experiment, sediment transport rate formula, artificial beach slope,

1. INTRODUCTION

For preventing the beach erosion and utilizing the coastal zone, the estimation of topographical change in the swash zone is important. However, mechanism of change in beach profile is not well understood because of its complexity and difficulty of measurement of sediment transport and waves. For understanding the mechanism it is needed to observe the detailed beach change including its external force. This kind of studies based on field observation have been rarely performed except the study of Sallenger and Richmond(1984). They found that the oscillation of beach face level propagated landward in the swash zone from measuring change of the elevation at eleven sticks installed on the swash slope. Their field experiment lacked the measurement of incident waves and currents.

Thus, authors have conducted field observations for swash profile change and its external force since 1988. At an observation on Hasaki Beach in 1988, a new measuring method using a stick array and video movie cameras was developed. However, significant beach change did not occur during the period of experiment. In 1990, an observation on Hiratsuka Beach was carried out after swash slope was artificially converted from steep (approx. 1/8) to gentle (approx. 1/10). Results of the observation showed that swash slope went back as original slope of natural beach.

In 1992, A field observation at Hasaki Beach was conducted again for tracing the profile changing of a beach artificially mounded on a natural slope. In this paper, Results of the observation are described.

2. FIELD OBSERVATION

A field observation was conducted on July 29 1992, at Hasaki Beach located about 100 km east of Tokyo facing the Pacific Ocean (Fig. 1). On this beach, the research pier belonging to the Port and Harbour Research Institute, is located. The sea water surface movement at a pole in the surf zone during the measurement was recorded by a pair of 16 mm memo-motion cameras mounted on this pier.

Figure 2 shows a plan view of experiment site and arrangement of measuring instruments. The offshore wave condition was measured by an ultrasonic wave gage installed on the seabed near the pier at a distance of 370 m offshore (St.0). An artificial beach which had steeper slope than original beach slope, was mounded by bulldozers during a low tide (Photo 1). The scale of artificial beach was 30 m alongshore and 20 m on-offshore. The slope of artificial beach was approximately 1/10 (the original or natural beach slope was approximately 1/20). The median diameter of sand in the swash zone were 0.17 mm to 0.19 mm, a sorting coefficient, defined as $S=d_{75}/d_{25}$, where d_p is the grain diameter at which $_p$ percent of the sand weight is finer, were 1.15 to 1.25, and the specific gravity were 2.65 to 2.75.

Change of foreshore topography were measured on two survey lines. One was located on the center of the artificial beach (line B) and another was located on the natural beach about 15 m south from the artificial beach (line D). On the line B, vertical sticks made of iron bar with diameter of 12 mm, fixed a measuring tape in mm unit was installed normal to the shoreline at an interval of 0.5 m (see Fig.3(a)). A total of 37 sticks were installed covering the entire swash zone. Two or three video movie cameras were employed for measuring the topographical change. Each camera was S-VHS video movie camera with more than 500 scanning lines and 360000 pixels. A cameraman shot, as closely as possible, a graduation of stick meeting with sand surface when a wave went out (Photo 2).

To obtain incident waves and currents, a capacitance typed wave gage (CWG) and an electromagnetic current meter (EMCM) were collocated at St.1A (Photo 3(a)). In the swash zone, two hemisphere shaped EMCM with bottom plate to prevent from scouring were installed (St.2A and St.3A), as shown in Photo 4.

The same measurement was simultaneously done on a natural beach face (line D) for comparing with the data each other. The beach profile of line D is shown in Fig.3(b). A total of 35 sticks were installed at an interval of 1 m in the swash zone. The measuring instruments for incident waves and currents are shown in Photo 3(b).

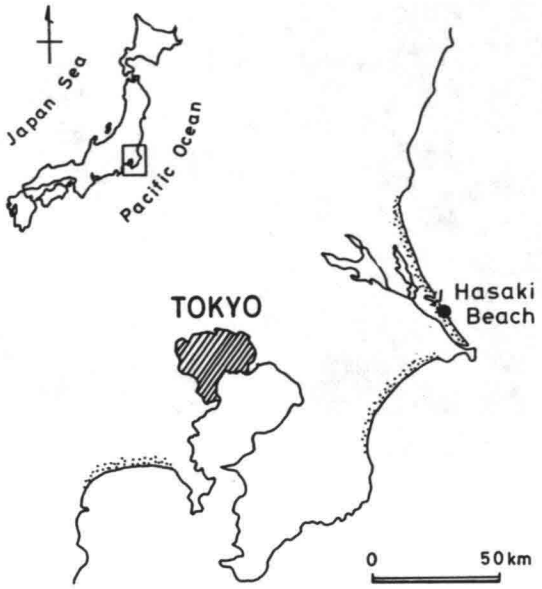

Fig.1 Location map of field site.

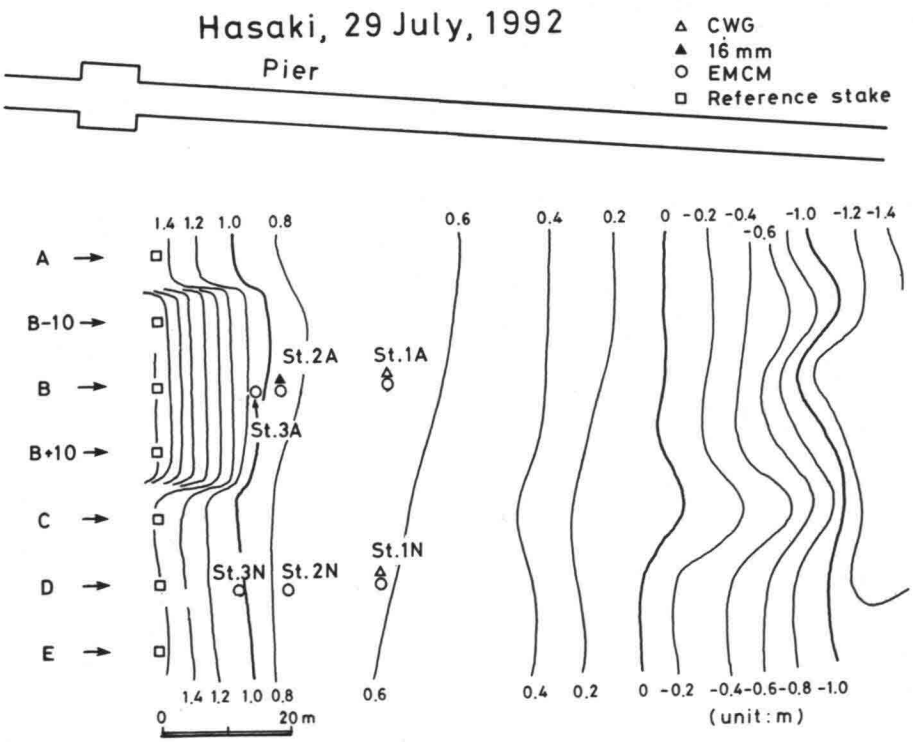

Fig.2 Beach plan view and arrangement of instrument.

Photo 1 Artificial beach made by bulldozers.

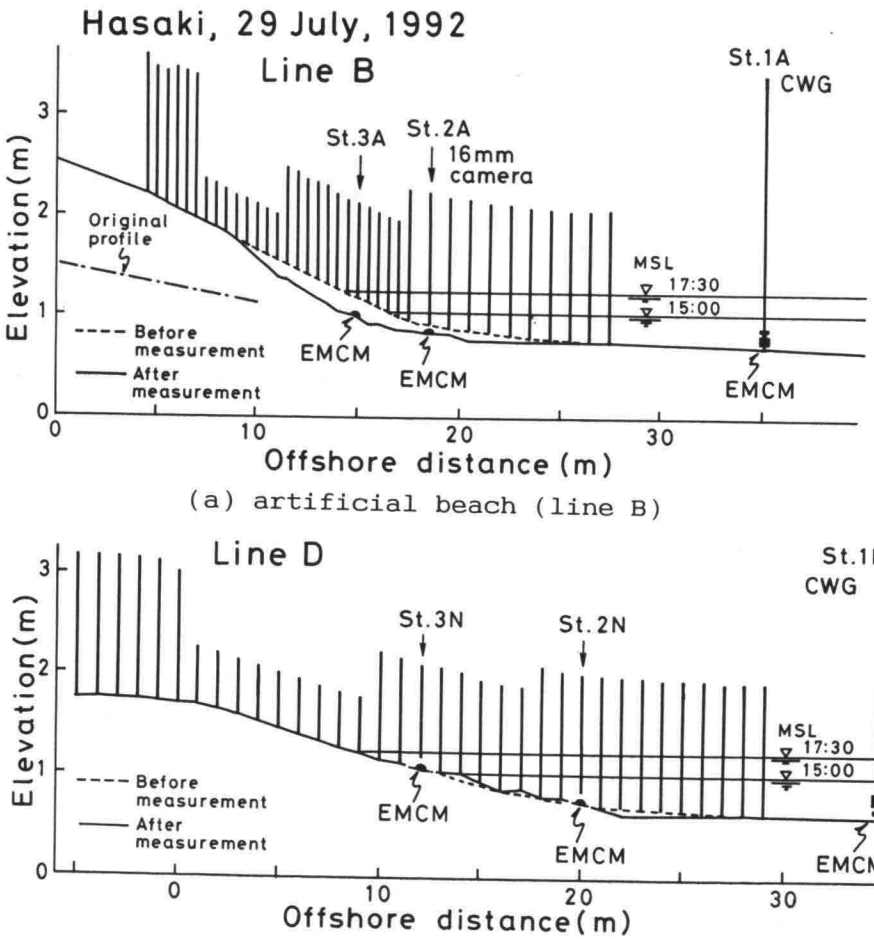

Fig.3 Beach profiles and arrangement of the sticks and measuring instruments.

Photo 2 Measurement for the bottom surface level using video movie cameras.

(a) artificial beach (line B)

Photo 3 A set of a capacitance typed wave gage and an electromagnetic current meter installed in front of the swash slope.

(b) natural beach (line D)

Photo 3 A set of a capacitance typed wave gage and an electromagnetic current meter installed in front of the swash slope.

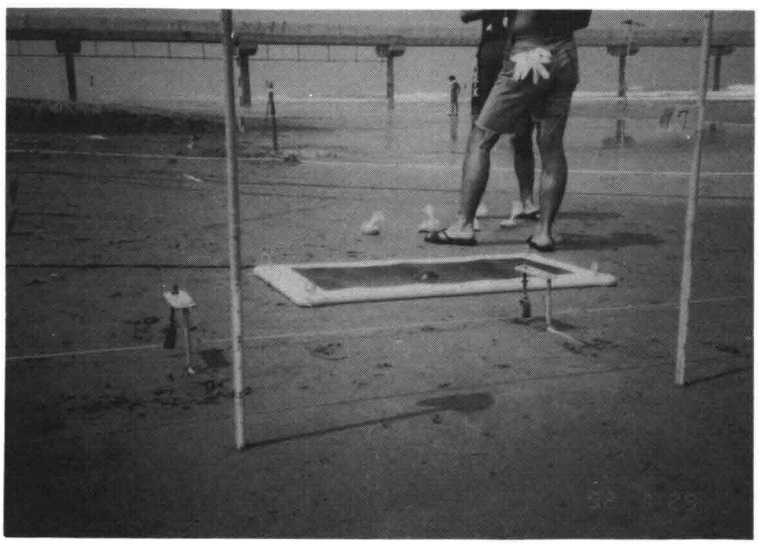

Photo 4 A hemisphere shaped electromagnetic current meter with bottom plate installed on the swash slope.

The data collection was started at 15:00 and ended at 17:30, giving a 150 min experiment duration. During the experiment the tide rose about 0.2 m. Average breaking wave height and period by visual observation were 0.8 m and 10.6 s. Average breaker line was located approximately 80 m offshore from the shoreline. The type of breaker was spilling and the wave direction was almost normal to the shoreline. Output of the electrical instrument was recorded on an open-reel digital data recorder. The data sampling interval was 0.2s.

3. RESULTS AND DISCUSSION

3.1 Characteristic of Incident Waves and Currents

Figure 4 shows the time series of mean sea level from the seabed obtained at the measuring point about 370 m offshore (St.0) and the St.2A. A dashed line indicates 1 min averaged values and a solid line indicates 10 min moving averaged values. The mean sea level both in and out of the surf zone quickly rises 0.2 m during 50 or 60 minutes at the beginning of measurement. After 50 or 60 minutes the rising of it is very slowly.

Figure 5 shows the mean square of surface variations at St.0 and the St.2A. One min averaged values at both stations indicate large fluctuation. This is due to long period waves which has the significant power in the range from 0.015 Hz (67s) to 0.035 Hz (29s) in the power density function shown in Fig. 6. Ten min averaged values at St.2A are almost constant, although that at the offshore measuring point sometimes fluctuates.

Figure 7 shows the mean flow velocities, $\bar{u}$ and $\bar{v}$ at Sts. 2A and 2N. u and v denote on-offshore and longshore component of current velocity, respectively. The value of $\bar{v}$ at both stations are negligibly small.

Figure 8 shows the time series of mean square of water particle velocity, $\overline{u^2}$ at St.2A and St.2N. One min averaged values at both stations indicate large fluctuation as well as the wave power. Magnitude of 10 min averaged $\overline{u^2}$ at St.2A decreases during first 40 or 50 min. This is due to the rising of sea level. After 50 min, $\overline{u^2}$ becomes a constant value of 0.185 m^2/s^2. This value are 2 times as large as the value of $\overline{u^2}$ at St.2N.

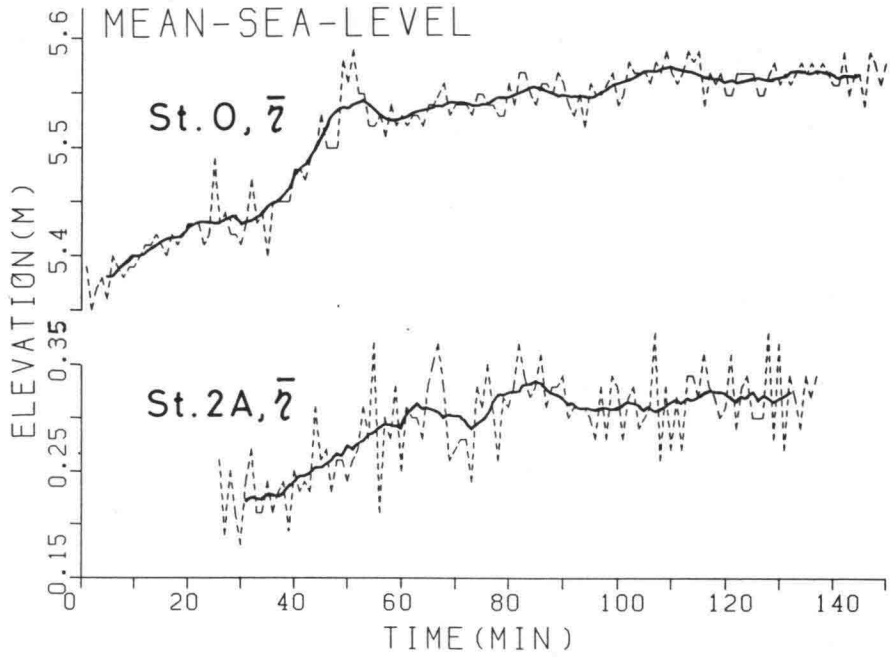

Fig.4 The time series of mean sea level from the seabed at the offshore measuring station (St.0) and St.2A.

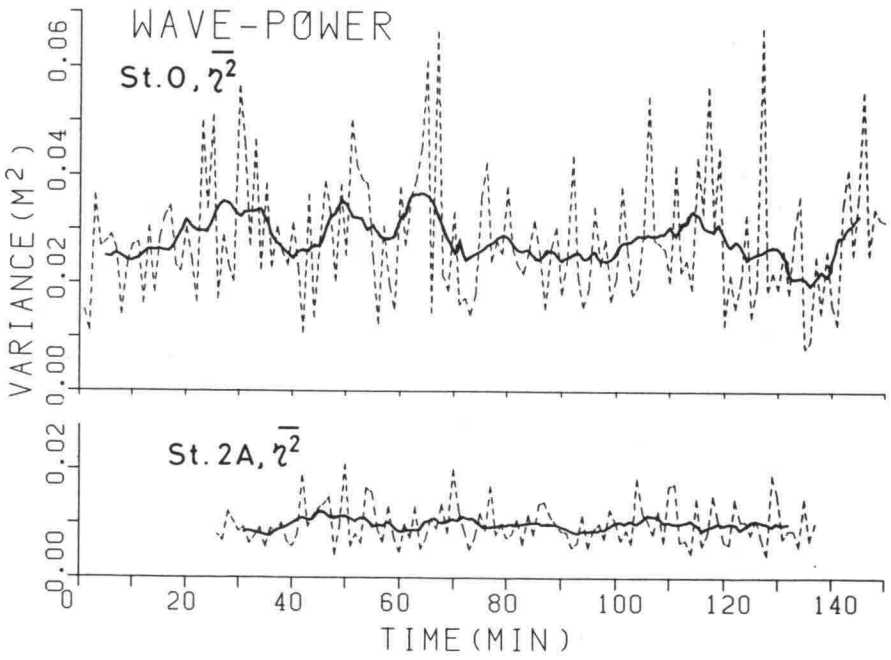

Fig.5 The time series of mean square of surface variations at the offshore measuring station (St.0) and St.2A.

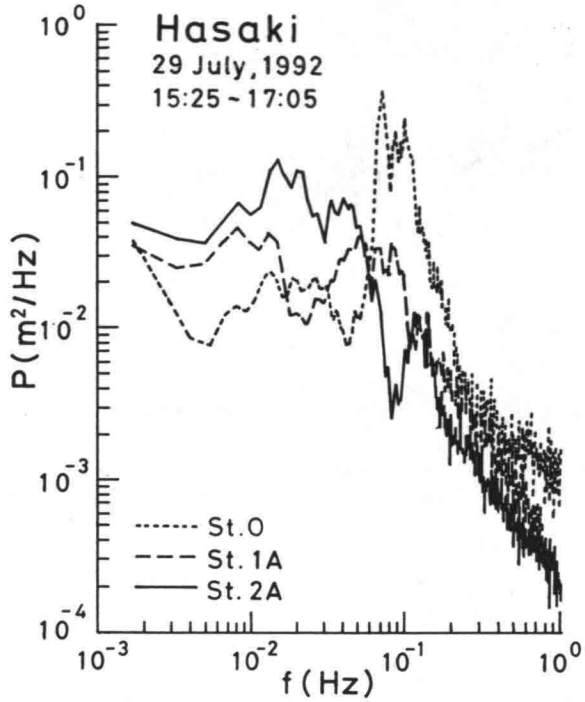

Fig.6 Power spectral density functions of the sea water surface variations at the offshore measuring station (St.0), St.1A, and St.2A.

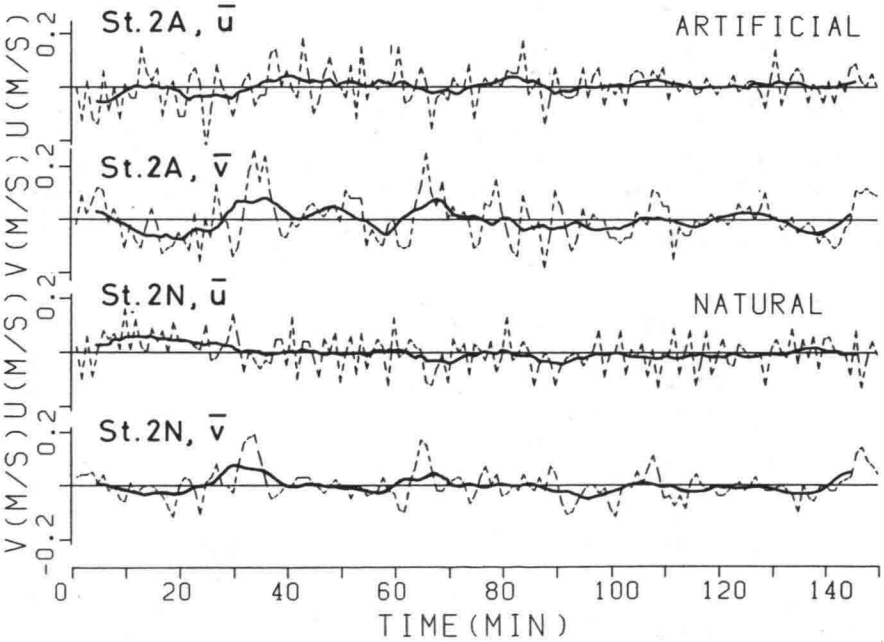

Fig.7 The time series of mean flow velocity, $\bar{u}$ and $\bar{v}$ at St.2A and St.2N.

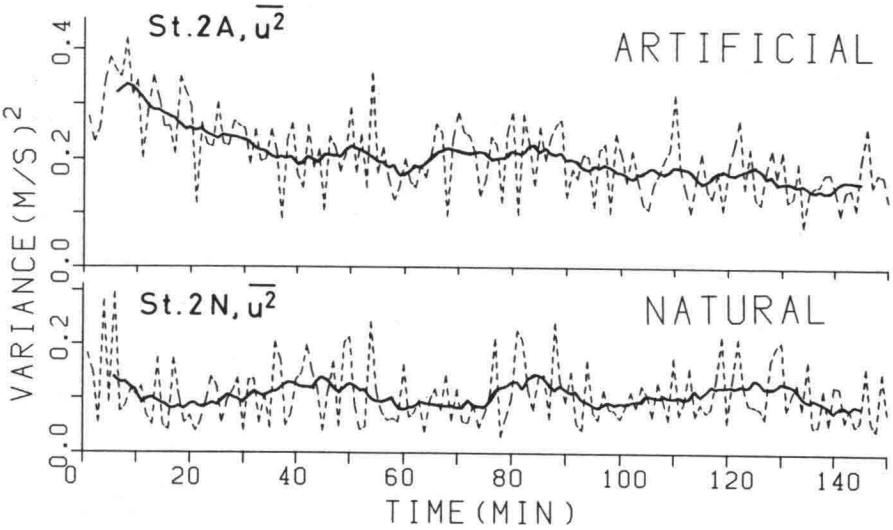

Fig.8 The time series of mean square of water particle velocity, $\overline{u^2}$ at St.2A and St.2N.

3.2 Topographical Change in the Swash Zone

Bottom surface elevations at each sticks in the video image were read every 1 min. The previous data was hold when the data was malfunctioned. These data were converted to the elevation on the reference level.

Figures 9(a) and (b) show the profile changes of line B on the artificial beach and line D on the natural beach every 30 min. The natural beach profile has no significant change. On the contrary, at the artificial beach, the beach face slope sets back toward the land with the time. The lower the position of slope goes down, the larger the erosion occurs. It is considered that the beach face slope was approaching to original slope of natural beach corresponding with the incident wave condition.

Figure 10 shows the cumulative elevation change in the swash zone opposite to the initial profile on line B (a) and on line D (b). At the natural beach, significant beach change does not occur during this experiment. The artificial beach also does not change at the first stage of the measurement as well as the natural beach. After 50 min, the sea side tip of artificial slope is firstly eroded. The erosion of the slope is increased and extended landward.

Figure 11 shows cumulative sediment volume for profile change in the swash zone. The dashed line and the solid line denote the volume on the natural beach and on the artificial beach, respectively. Ratio of the erosion at the artificial beach after 50 min is a constant value of $1.14*10^{-4}$ $m^3/m/s$.

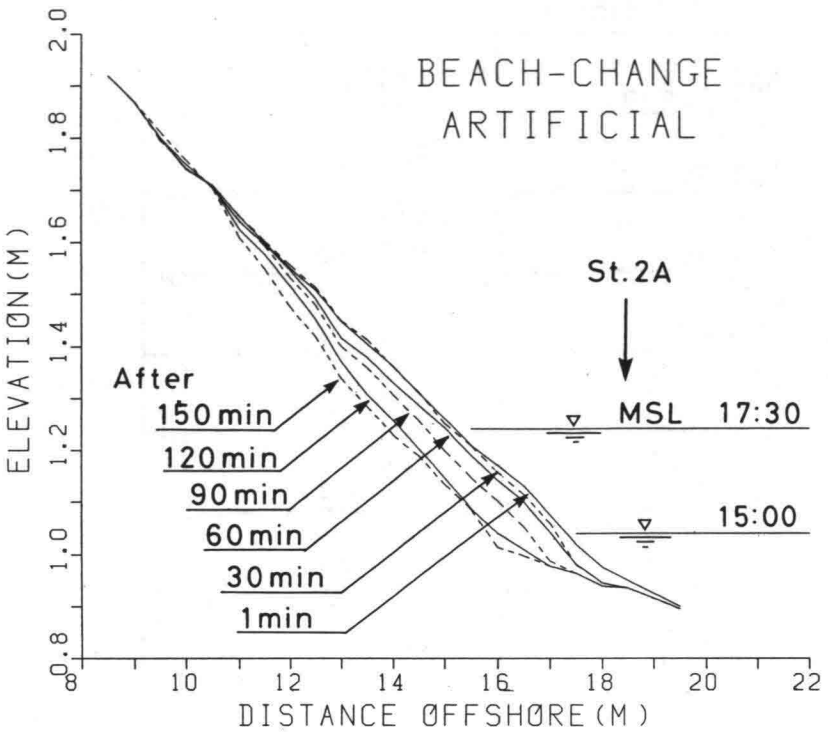

(a) artificial

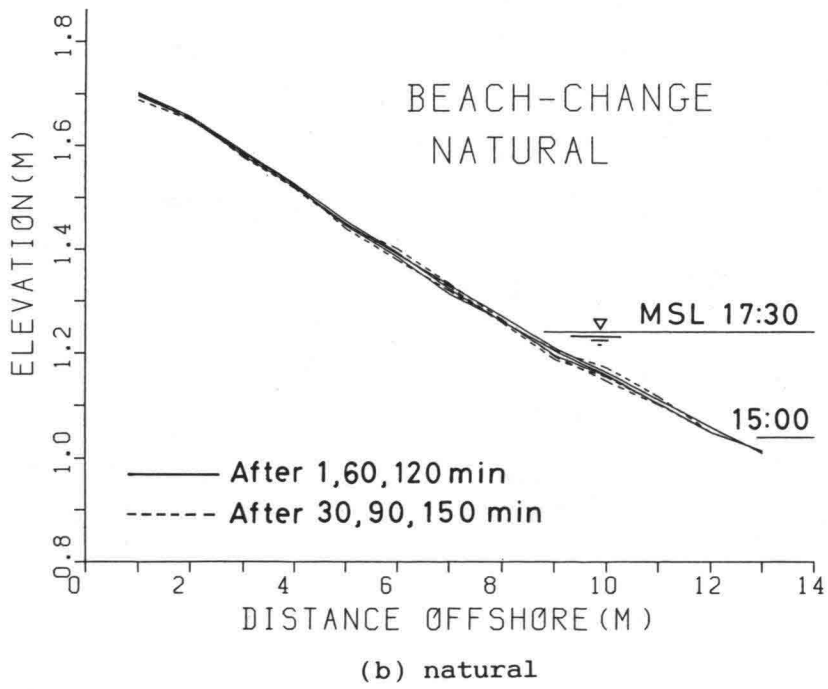

(b) natural

Fig.9 Profile change in the swash zone.

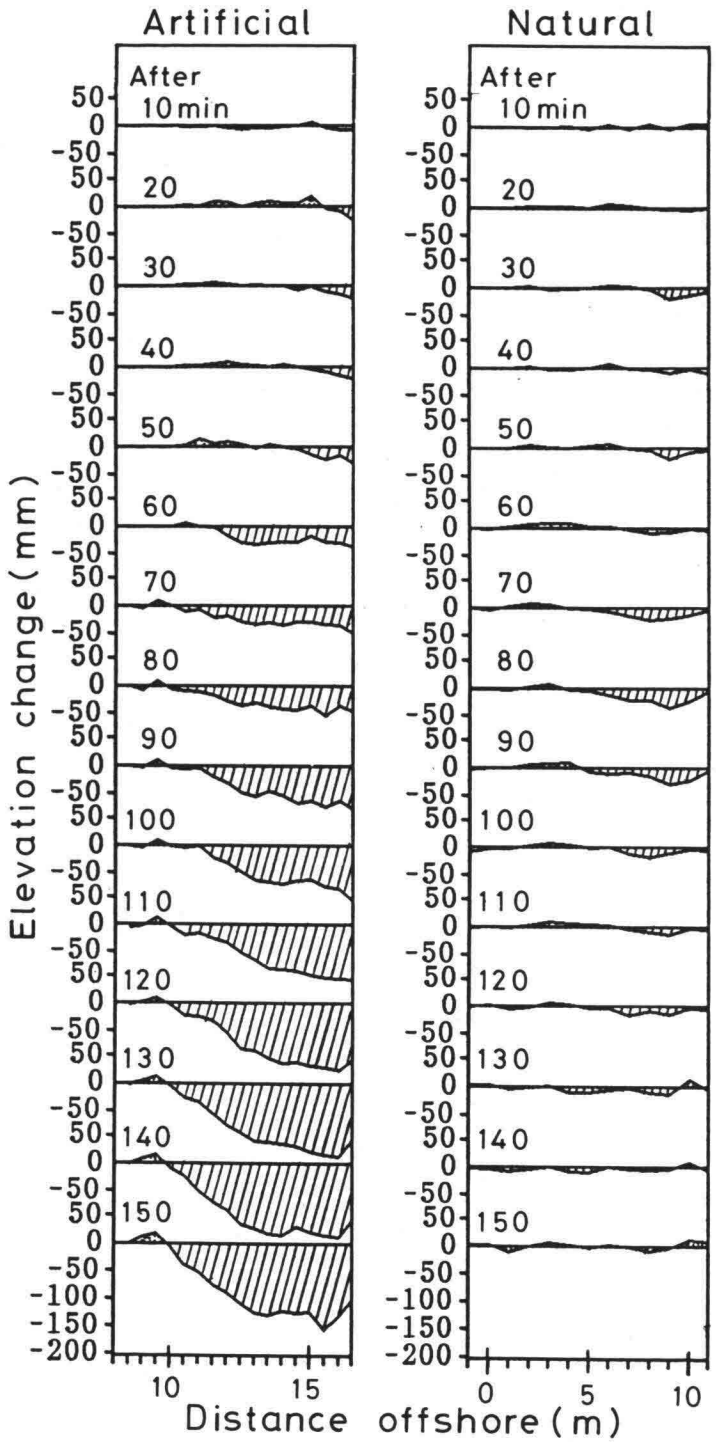

Fig.10 Elevation change in the swash zone.

At the artificial slope, St.2A located at the seaward end of the slope, at which the bottom topography change almost composes as shown in Fig.8(a). Considering that the longshore current velocity was negligibly small, integration of the elevation changes from landward point to St.2A obtains the sediment transport rate through St.2A. At the natural slope, the sediment transport rate through St.2N can be obtained by the same method on St.2A. Figure 12 shows the time series of the sediment transport rate, $\overline{q}$ at St.2A and St.2N. The sediment transport rate, $\overline{q}$ through St.2N on the natural beach is alternately positive (onshore) and negative (offshore) values. At the artificial beach, $\overline{q}$ is almost constant negative value of approximately 1.07×10^{-4} $m^3/m/s$ after 50 min. It is certainly that a fluctuation period of more than 15 or 20 min is inherent in the time series of $\overline{q}$ at both stations. The reason for this fluctuation is not clear.

3.3 Relationship of Sediment Transport Rate and its External Force

In order to find a lag time of sediment transport rate and its external force, cross-correlation coefficient between 10 min averaged values of $\overline{u^2}$ and $\overline{q}$ was calculated. Where, data for calculation were used those obtained after 50 minutes, since it was considered that first 50 minutes of the experiment was in transitional stage. The result showed that no significant lag time existed. More detailed data for the sediment transport rate, e.g. the data by every wave, may be needed for this purpose.

Figure 13 shows the relationship between 10 min averaged values of $\overline{u^2}$ and $\overline{q}$ in the artificial beach (a) and the natural beach (b). Values of $\overline{q}$ scatter higher than that of $\overline{u^2}$. It shows that the sediment transport rate changed though the external force did not change.

The many previous formulas for on-offshore sediment transport are expressed with the nondimensional on-offshore transport rate, Φ ($=q/wd$) and the Shields parameter, Ψ ($=f_w u_b^2/(2sgd)$. where, q is the net transport rate, w is the fall velocity, the f_w is bottom friction factor, u_b^2 is the fluid velocity in the vicinity of bed, s is the sediment specific gravity in still water, g is the gravitational acceleration, and d is the grain size.

Values of Φ and Ψ calculated using the data for the constant erosion (after 50 min) occurred on the artificial beach slope are

$$\Phi = 1.54 \qquad \text{and} \qquad \Psi = 30.57$$

These values are similar to the value from $\Phi = 12.5\ \Psi^3$ by Madsen and Grant (1976).

A formula for the net transport rate in the swash zone was proposed by Sunamura (1984). This formula is as follows:

$$q/wd = (-1)\cdot 10^{-5} U_r^{0.2}\, \Phi'(\Phi' - 0.13 U_r) \qquad (1)$$

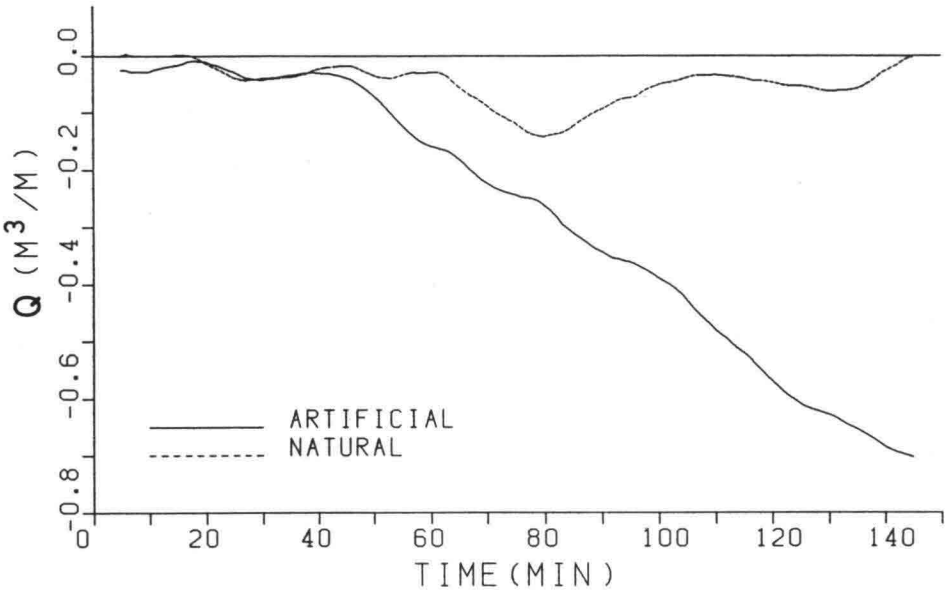

Fig.11 Cumulative volume of beach change.

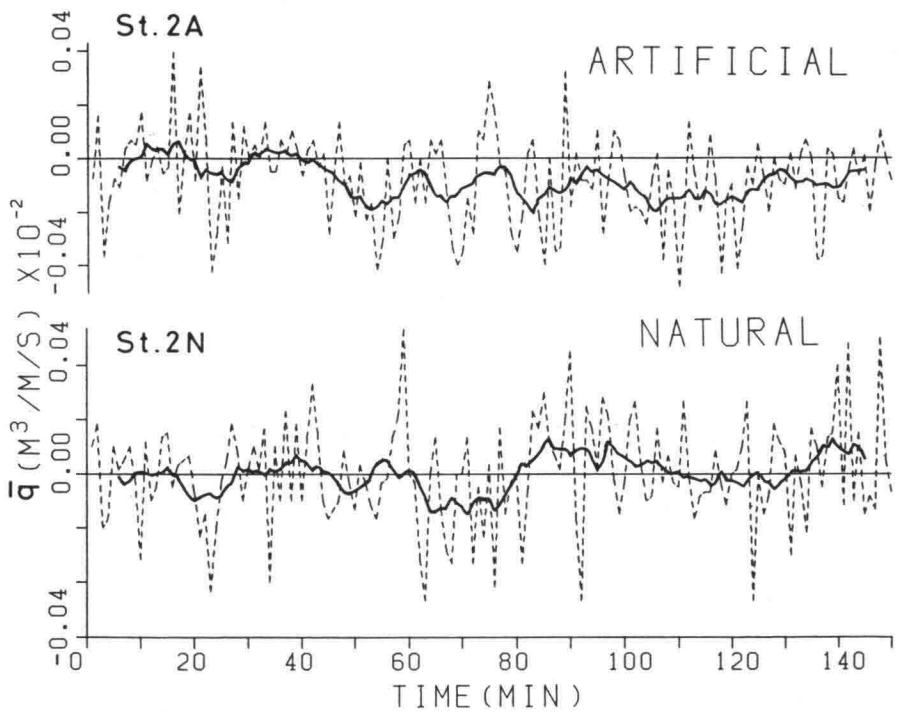

Fig.12 The time series of the sediment transport rate, $\bar{q}$ at St.2A and St.2N.

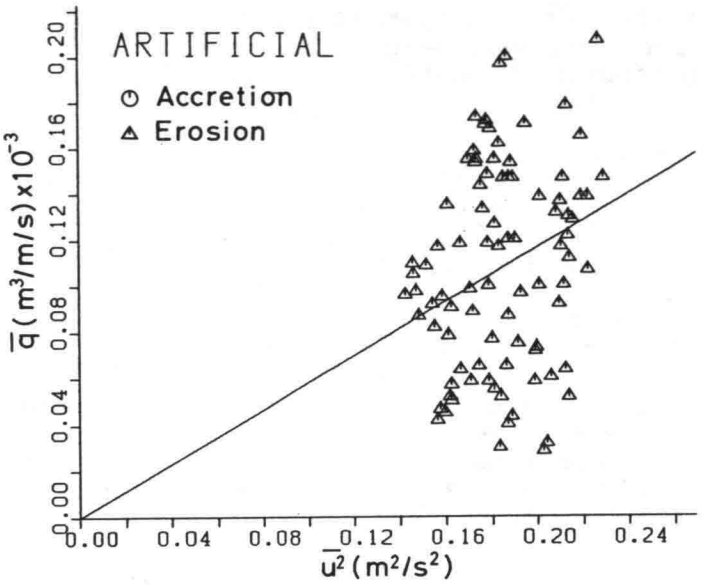

(a) artificial

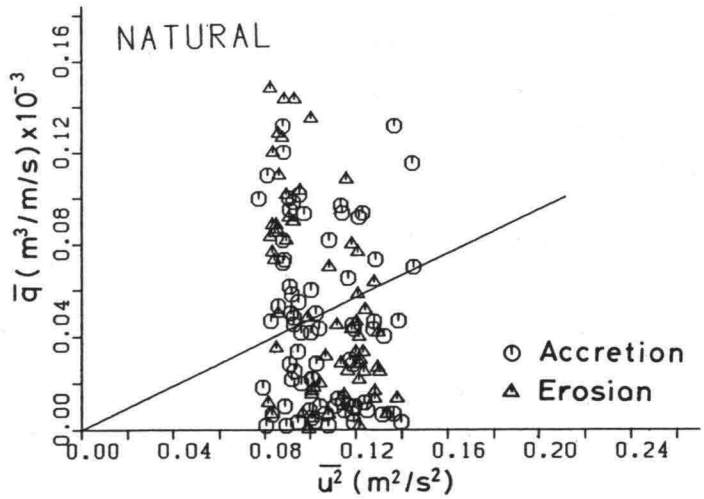

(b) natural

Fig.13 Relationship between $\overline{u^2}$ and $\overline{q}$.

where, q is the net sediment flux, U_r is the Ursell parameter ($=gHT^2/h^2$:H and T are wave height and period at water depth h), and $\Phi'$is the parameter($=H^2/shd$) for sediment transport rate by Hallermeier (1982).

H and h are obtained as

$$H = 2.5\ (\tan\beta\ )H_b \qquad (2)$$

$$h = -(3.85\ \tan\beta\ -0.985)h'+(1.63\ \tan\beta\ +\ 0.048)\ H_b \qquad (3)$$

where $\tan\beta$ is the beach slope, h' is the still water depth, and H_b is the braking wave height.

This formula was applied to the field data, although the formula assumed the uniformed beach slope. Values of q calculated by this formula were larger than the field data of the artificial and natural beaches, respectively. Then, modifying the coefficient to judge the direction of sediment transport rate,

$$q/wd = (-1)\cdot 10^{-5}U_r^{0.2}\,\Phi'(\,\Phi'-0.06U_r) \qquad (4)$$

Calculated values by this formula agree with the field data as shown in fig.14.

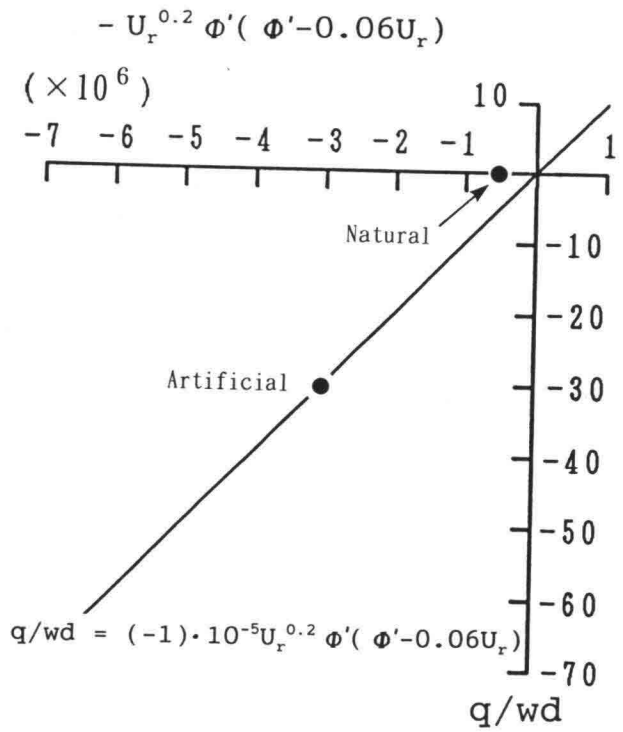

Fig.14 Relationship between sediment transport rate measured and predicted.

4.CONCLUDING REMARKS

Results in the observation are as follows;

1) Mean velocity of longshore current on both natural and artificial beaches were negligible small. However, mean square of on-offshore velocity component on the artificial beach was about two times of that on the natural beach.

2) With rising the tide, the artificial beach was eroded, and its slope went back as original slope of natural beach.

3) The offshore sediment transport rate at the toe of artificial beach face were constantly $1.14*10^{-4}$ $m^3/m/s$ throughout the experiment period.

4) The non-dimensional sediment transport rate was explained by the flow intensity parameter. The sediment transport rate in the swash zone and its direction can be estimated using the model by Sunamura(1984).

ACKNOWLEDGEMENTS

The authors would like to thank the Port and Harbour Research Institute, Ministry of Transport, for permission to use the observation pier. We also acknowledge to Dr. M. Mizuguchi, Professor, Dept. of Civil Eng., Faculty of Science and Engineering, Chuo University, for helpful comments. We would also like to express our appreciation to students of Nihon University and Chuo University who provided considerable supports during the field work.

REFERENCES

Hallermeier, R.J(1982): Oscillatory bedload transport: Data review and simple formulation, Continental Shelf Res., Vol., pp. 159-190.

Madsen, O.S. and W.D.Grant(1976): Quantitative description of sediment transport by waves, Proc. 15th Coastal Eng. Conf., ASCE, pp.1093-1112.

Sallenger, A.H. and B.M.Richmond(1984): High-frequency sediment oscillations in the swash zone, Marine Geology, 60, pp.155-164.

Sunamura, T.(1984): Prediction of on/offshore net sediment transport rate in the swash zone, Proc. 30th Japanese Conf. on Coastal Engineering, JSCE, pp.316-320 (in Japanese).

Theme 6

COUNTERMEASURES AGAINST SHOALING DUE TO SILTATION AND SEDIMENTATION IN THE HARBOR AND WATERWAY

HYDRO-PORT'94
International Conference on Hydro-Technical
Engineering for Port and Harbor Construction
October 19 - 21, 1994, Yokosuka, Japan

Criteria and Methods to Determine Navigable Depth in Hyperconcentrated Sediment Layers

William Reginald Parker
Peter Michael Hooper

Blackdown Consultants Ltd, Georges Farm, West Buckland
Wellington. Somerset. TA21 9LE.

Abstract.

In areas where hyperconcentrated benthic layers form, the depth apparently available for navigation may vary according to the methods and criteria used for its definition. Rheological parameters may be the ideal determinants but are not realistically achieved in situ or in useful survey mode: in situ density determination is a practical tool with a proven track record. Rheological and densimetric parameters, though not uniquely related, may be related empirically for practical purposes. Non-nuclear and nuclear survey systems are now available to optimise navigable depth and minimise and control dredging where hyperconcentrated benthic layers form.

Key Words: Navigable Depth, Rheology, Density, Criteria, Methods.

1. INTRODUCTION.

In estuaries or coastal areas local energy and an available sediment population combine to produce a significant solids load and the development of stratified suspensions (Parker & Kirby 1977; Parker et al 1980; Kirby & Parker 1983) which evolve to form hyperconcentrated benthic layers (HBL). In otherwise low suspended load environments, wave energy is particularly effective in generating or sustaining HBL(Kendrick 1980;Wells 1986; Maa and Mehta 1987).

In contrast to sandy sediment, these fine sediment slurries have strongly time dependent characteristics (Parker & Kirby 1977, 1982; Bean & Sills 1981) which affect their density structure, their physical (rheological) properties, their acoustic properties and their response to hydrodynamic stresses. They consequently present special, though quite widespread, problems to repeatable and cost effective determination of depths available for navigation and, thereby, the control and cost effectiveness of dredging. In this paper we examine the basic depth requirement for safe navigation, the parameters relevant to determining at what level within an HBL the material becomes non-navigable, practical meth-

ods to achieve this and a critical path to assess the cost benefits of applying the "nautical depth" concept.

2. GENERAL CRITERIA FOR NAVIGABLE DEPTH.

In shallow or confined waters, the hydrodynamic interaction of a vessel with the boundaries (bed and/or walls of the channel) leads to a number of effects upon the performance and handling of the vessel. From a wide range of studies it has been recommended by P.I.A.N.C. that vessels require a minimum underkeel clearance of approximately 10% of the draught of the vessel (P.I.A.N.C. 1983). In areas of firm seabed (gravel, sand, boulder clay, etc) there is in general no doubt where navigable water ends and the non-navigable seabed starts. However in muddy areas, and especially in areas where HBL development occurs, there may arise considerable doubt over the altitude of the seabed. This has its origins in

a) what precisely constitutes the sea bed.
b) the various methods used to define the sea bed altitude.

Thus the question "where is the seabed?" may only be answered following resolution of the query "what is the seabed?".

3. DEFINITIONS OF DEPTH IN MUDDY AREAS.

Various definitions of depth in muddy areas have been proposed e.g. Parker 1989 and 1993. These are

Hydrodynamic Depth : the level of the interface between moving muddy water and stationary watery mud.
Parametric Depth : the bed level determined by some material parameter e.g. target strength, shear strength, density, etc.
Operational Depth : the depth of a particular parameter relevant to some specific operation, e.g. navigation.

In areas where the mud bed is firm these 3 definitions will coincide. However in areas of HBL development, transport or deposition, the natural characteristics, behaviour and evolution of HBL can lead to gross differences between the depths defined above (Parker 1989).

4. RELEVANT CHARACTERISTICS OF HYPERCONCENTRATED BENTHIC LAYERS.

A hyperconcentrated benthic layer is a high concentration slurry of fine sediment. Known also as "creme de vase" (Allen et al 1974; Migniot 1968), "fluid mud" (Inglis and Allen 1957), "slib and sling mud" (Delft 1962), this type of material is widely reported in estuaries and coastal waters around the world.

The original "fluid mud" (Inglis and Allen 1957) was identified from echosounder records and confirmed as a mud slurry by Kirby and Parker (1974). Because the term fluid mud arises from an acoustic signature it is based on a gradient parameter not an absolute parameter. The target strength which produces an echo is, for a given apparatus, dependent upon a critical reflection coefficient. This is determined by the local vertical gradient in acoustic impedance which in turn is predominantly a function of the local vertical densi-

ty gradient (Parker and Kirby 1977, 1982). The critical values of impedance gradient vary with acoustic frequency as has been discussed elsewhere(Parker and Kirby 1977). Consequently a wide range of material types have been referred to as fluid mud such that the term is now largely devalued. It is perhaps better to refer to benthic layers of a particular character which may be acoustically detected.

HBL have characteristics which present particular problems for depth determination and definition of navigable depth. These may be identified as

a) the material in them is usually aggregated. This gives rise to concentration dependent non-Newtonian rheological properties.
b) they have a strongly time dependent density structure arising from selfweight consolidation (Parker 1989; Bean & Sills 1981; Parker and Kirby 1977).
c) they exhibit time dependent changes in acoustic propagation properties arising from changes in density structure (Parker & Kirby 1977, 1982) and bacterially mediated generation of gas microbubbles (Sills et al 1991).
d) they exhibit time dependent changes in physical (rheological) properties arising from consolidation which may affect navigability and response to hydrodynamic stresses.

Of particular importance is the change within the HBL from the condition of a suspension(aggregates supported by fluid forces e.g. viscous drag or turbulent momentum exchange) to a structured condition (long range continuous structure where the material is supported by mechanical strength and excess pore pressure). This change propagates upwards through the HBL as a consequence of settling and consolidation (Bean & Sills 1981; Parker & Kirby 1977, 1982). This change occurs at a concentration known as the critical concentration which varies from one mud to another.

5. THE CONCEPT OF NAUTICAL DEPTH.

Practical experience has shown that vessels may navigate with their keel altitude below the level of the acoustically detected surface of the HBL. This practice was recognised and formalised in the Nautical Depth Concept (Kirby et al 1980; P.I.A.N.C.1983).

6. CRITERIA FOR DETERMINING NAVIGABLE DEPTH IN HYPERCONCENTRATED BENTHIC LAYERS.

The requirement is to identify the limiting level within the HBL where the material properties are such that the medium may deleteriously affect the manoeuvering or passage of the vessel. Examination of vessel streamlines reveals complex patterns of flow around the hull and fluid displacement extending significant distances away. In confined circumstances complex return flows may be associated with vessel passage. The vessel is required to displace the HBL material. The greatest displacement of material is from the vessel centreline, the least is at some distance away from the vessel. The most rapid displacement occurs along the bow section of the vessel.

The varying distributions of strain amplitude and rate (displacement and velocity) lead to local shear rate gradients. When the displaced medium is clear water the important forces are inertial and viscous. The viscous forces, being for a Newtonian fluid, are not shear rate dependent. However, where the displaced medium is an HBL then the inertial forces involved are time and space dependent and because of the non-Newtonian characteristics of the medium the viscous forces are a time and space varying function of solids concentration, strain rate and strain amplitude.

The spectrum of response of materials to stress is embodied in the Deborah Number (De) (Reiner 1964).

$$De = \frac{Tr}{To}$$

where Tr is the relaxation time of the material and To is the period of the stress.

If De is $>>1$ then the material behaves as an elastic solid whereas if De $<<1$ then the material behaves as a viscous fluid.

Thus the response of the HBL to the passage of the vessel may vary, according to its relative position, from elastic to viscous. This presents difficulties in defining the relevant values of parameters and the simulation of the relevant processes and effects.

6.1 Relevant Material Parameters.

Rheological Properties.

Two principal rheological material parameters may be defined as being relevant to the Nautical Depth concept. They are
i) apparent viscosity (also known as plastic viscosity or differential viscosity) is the quotient of shear stress (T) divided by the shear rate (Y), (Fig 1A, Fig 1B).

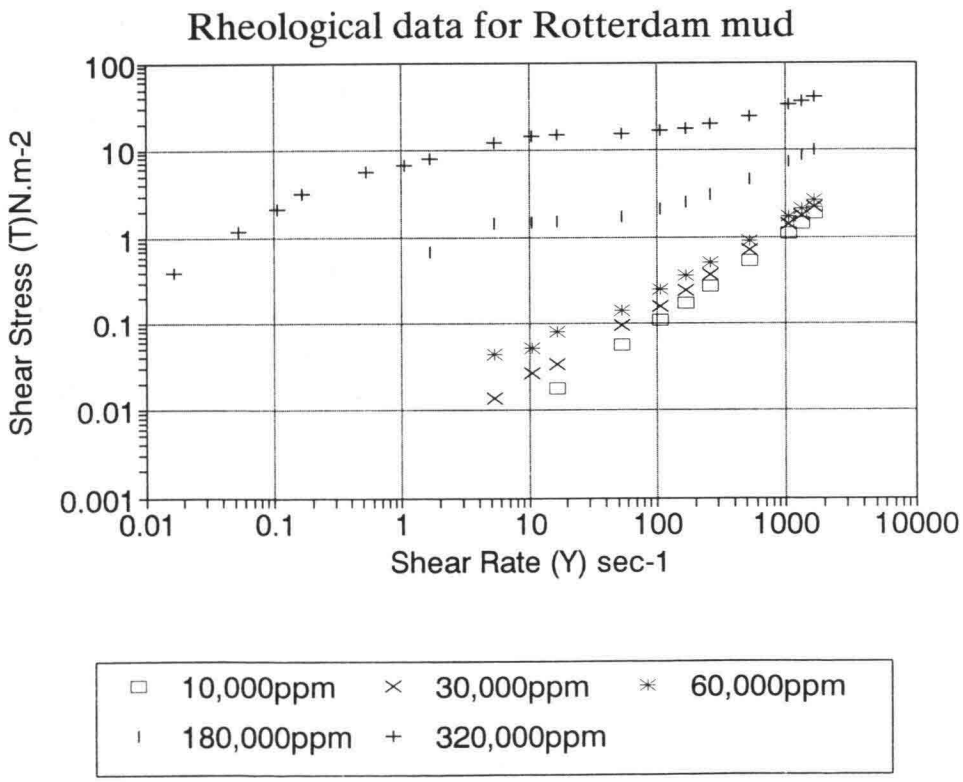

FIGURE 1A Equilibrium flow behaviour of natural mud. Plot of shear stress vs shear rate.

ii) yield stress : the yield stress is the stress required to induce and sustain irrecoverable strain in a material. This therefore implies both an amplitude and a duration of stress at,or above, yield.

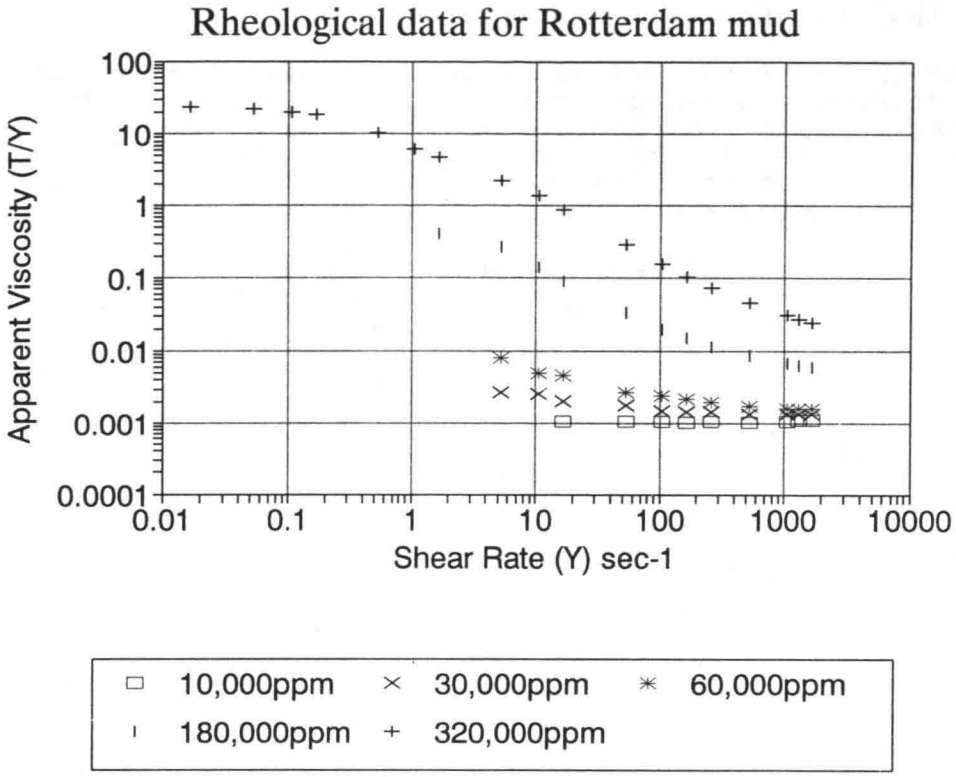

FIGURE 1B Apparent viscosity (T/Y) vs shear rate for natural mud showing Newtonian behaviour at low solids content (10,000 ppm) and non-Newtonian behaviour at high solids content.

The rheological behaviour of fine particle dispersions is complex. At low volume concentrations they exhibit Newtonian or mildly non-Newtonian (pseudoplastic) shear thinning behaviour. As the solids volume concentration increases the flow behaviour becomes increasingly non-Newtonian in character(Williams & Williams 1989). At, and above, the critical volume concentration a yield stress may be detected and with increasing solids volume concentration the material becomes elastico-viscous (Williams & Williams 1989). The critical solids volume concentration at which long range structure forms can be assessed using shear wave propagation (Adler et al 1949). Below this solids content the flow behaviour may be examined using equilibrium imposed shear rate rheometry. However, large particles may present operational problems to the requirements for the homogeneous shear field in the couette. Above the critical solids content, yield and flow behaviour are more complex and are more appropriately evaluated using controlled stress rheometry (Davis et al 1968).

Identification of the critical volume concentration separates two regimes of properties. At solids content less than critical the HBL material has pseudoplastic characteristics. For practical purposes it has no yield stress. Above the critical solids content the material has

increasing structural and elastic properties and the yield stress determined by controlled stress methods rises exponentially with solids content.

Solids Concentration.

Rheological properties vary with solids content. In practical situations the determination of the relevant solids concentration may present problems. From a sediment transport or dredging standpoint the relevant solids concentration is the mass of solids per unit volume. From a behavioural or rheological (and hence navigation) viewpoint the solids volume concentration is important. More specifically it is the effective volume concentration (volume of aggregates and occluded fluid) that is of importance.

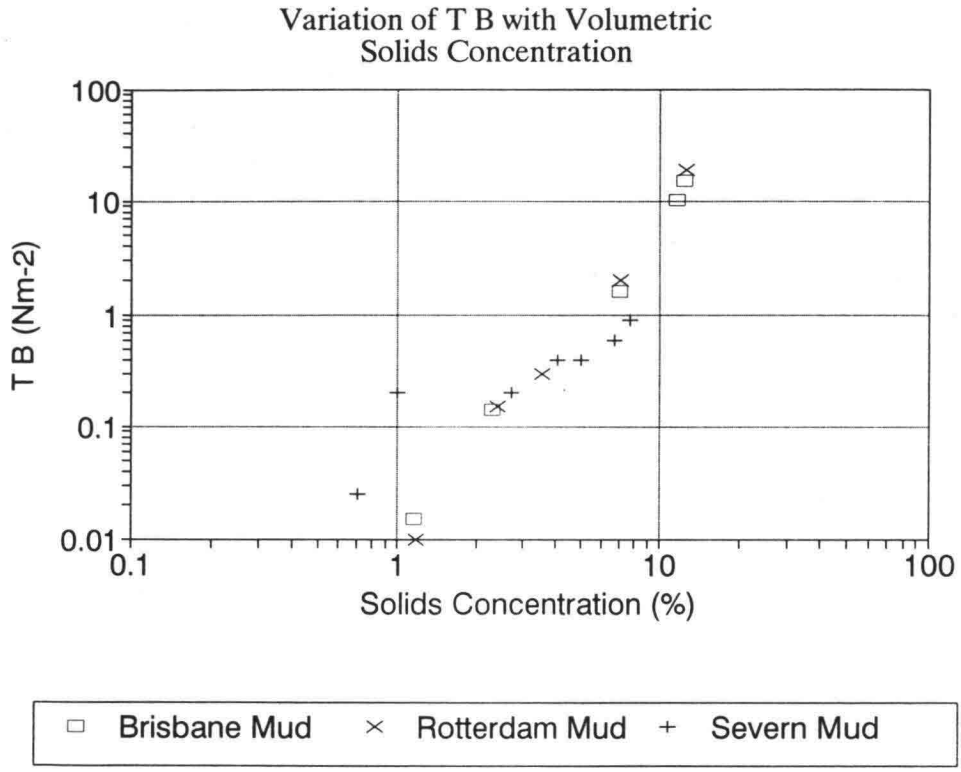

FIGURE 2 Variation in residual stress with volumetric solids concentration for 3 natural muds.

The transform between solids content, solids volume fraction and effective volume fraction is non unique. It depends initially on the interparticle bond lengths as influenced by particle parameters (mineralogy, size, shape) and electrolyte parameters (pH, ionic strength) through the distribution of total interaction potential. This basic multiparameter dependence is amplified by the range of aggregate structure, porosity and density, arising from the turbulent stress history of the aggregate and also the variable densities of particles comprising the aggregate. Thus although solids volume fraction can be determined, the effective volume fraction is more problematical. In practice the bulk density of the material is determined for correlation with field measurement. This encompasses the role of varying volume fraction.

6.2 Determination of Material Parameters.

a) Equilibrium Imposed Shear Rate Rheometry.
The methods to be adopted depend upon the nature of the material. At solids concentration less than critical concentration the essential parameter is the apparent viscosity (shear stress divided by shear rate). This is best determined using equilibrium techniques and an analytical geometry such as the Mooney Cell (Mooney and Ewart 1934). Care must be taken to ensure gap size appropriate to the particle spectrum. Fig 1A shows curves of shear stress vs shear rate and Fig 1B apparent viscosity curves for varying solids content of natural muds.

From such curves may be derived an extrapolated residual stress (often referred to as the Bingham Yield Stress). Figure 2 shows data for various muds. These data do not reflect a yield stress in the Hookean sense but indicate the relative magnitude of the electrostatic and other interparticle forces (Hunter & Nicol 1968). As such they reflect the energy dissipated by the breaking of interparticle bonds during the shearing suspension. It is interesting to note the similarity between differing materials at intermediate and higher shear rates and the differences at low shear rates.

b) Controlled Stress Rheometry.
For the determination of static yield stress, controlled stress measurements and the use of a cruciform vane are found to be most appropriate and effective (James et al 1987, 1988).

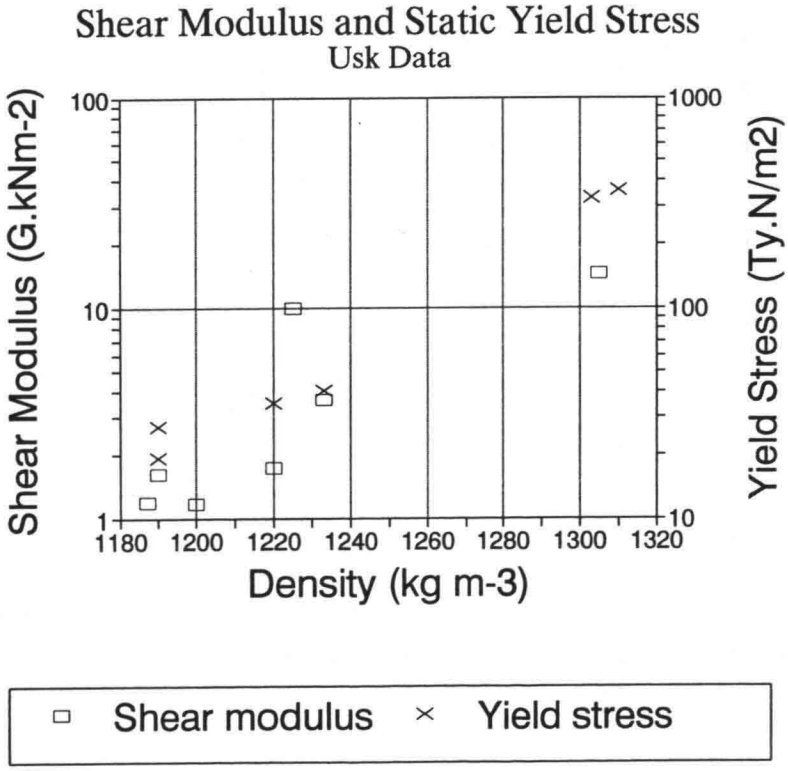

FIGURE 3 Shear modulus and static yield stress as a function of bulk density for Usk mud.

c) Shearometry.
A key transition in behaviour occurs at the development of long range structure. This can be examined using shear wave propagation (James et al 1987, 1988; Joseph et al 1986). Fig 3 shows a relationship between shear modulus and solids content (in this case bulk density). As the value of shear modulus approaches the limits for detection, the boundary between the suspension/non-suspension solids content (density) is approached.

d) Effect of Particle Size Spectrum.
A wide particle spectrum which includes large particles can present severe problems to concentric cylinder measurements, especially at high solids content.
In Fig 4, values of static yield stress measured by controlled stress rheometry are compared with the so called "initial rigidity" determined by cylindrical imposed shear rate rheometry.

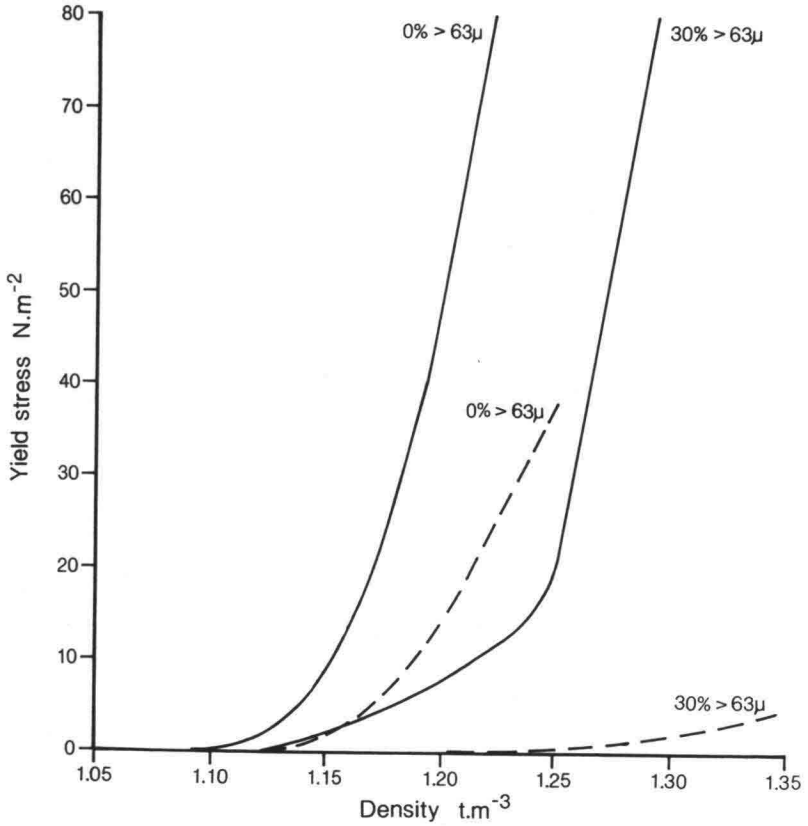

FIGURE 4 Comparison of static yield stress (solid lines) and "Initial Rigidity" (dashed lines) with density for Zeebrugge mud covering the range 0% to 30% content greater than 63 microns. Static yield stress determined using controlled stress rheometer and cruciform vane. Initial rigidity determined using concentric cylin der and imposed shear rate methods.

For each method the effects of particle size can be demonstrated. Particle size spectra also affect the values of shear modulus measured by shearometry. In Fig 5 we show the effect of varying proportions of fine sand on the shear modulus of media of nominal constant density. Results in Fig 4 and 5 are consistent with the different electrostatic bonds be-

tween different particles. The strongest bonds are between clay minerals. Increasing the sand content reduces the relative number of clay/clay bonds thereby reducing the bulk strength at a given density.

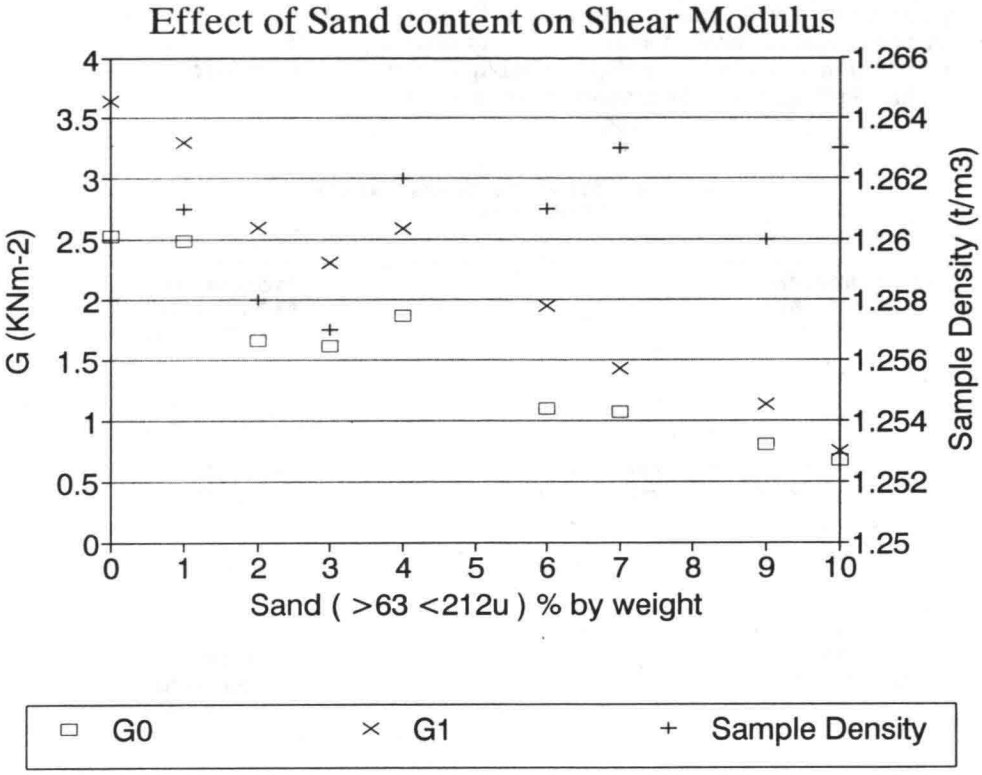

FIGURE 5 Effect of coarse particles (>63 microns <212 microns) on shear modulus. "G0" is the initial shear modulus at the start of readings; G1 is the first equilibrium value. The density of samples used is also shown to indicate the sensitivity of the results to density. This is because the shear modulus (G) is calculated from

$$G = V^2 D$$

where V is the shear wave speed and D is density. The experiments were attempted around a nominal density of 1.260 t/m^3.

e) Effects of Sampling.
As rheological measurements must be executed in the laboratory, it is necessary to obtain samples. Sampling disturbance can severely affect the results. The destructive nature of coring has been described by Parker & Sills (1990) and Parker (1991).

7. PRACTICAL METHOD TO APPLY THE NAUTICAL DEPTH CONCEPT.

The objective of applying the Nautical Depth concept is to identify the depth to which vessels may pass through the HBL thereby avoiding unnecesary dredging and unnecessary restrictions on navigation. In Fig 6 we outline a critical path developed and successfully used by Blackdown Consultants. The presence of HBL is usually first detected by hydrographic survey echosounder data and the possible magnitude of depth discrepancies can be

assessed from such records. However it should be borne in mind that sound speed in the HBL can be lower or higher than in the overlying water column so that the apparent thickness of the layer may be greater or less than its actual thickness. If there appears to be significant potential depth gain then it is worth proceeding to the next stage where this is confirmed by preliminary assessment of the density structure and rheology of the HBL. This assessment of shear modulus vs density derives preliminary relationships for critical concentration and allows the depth of navigable material to be assessed. From this the potential depth gains can be assessed more securely.

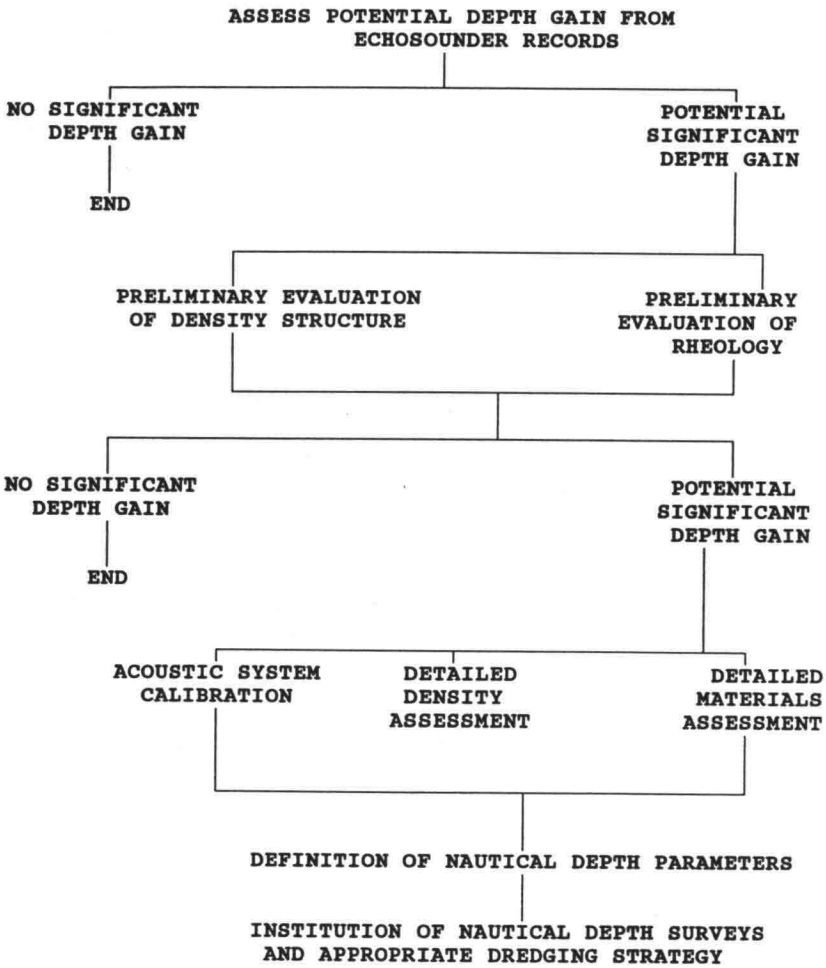

FIGURE 6 Blackdown Consultants Critical Path for investigating the applicability of the Nautical Depth concept and its implementation.

If this leads to an indication of a potentially significant depth gain then a detailed assessment is undertaken in a third stage which includes

i) calibration of acoustic systems to identify threshold impedance gradients and relate acoustic records to HBL structure.

ii) detailed density assessments to identify characteristic density structures and their relation to acoustic signatures, using both laboratory and field measurements.
iii) detailed materials assessment to identify critical yield values, particle size effects and temporal variations in material characteristics.
iv) sediment dynamics assessment to identify the sources, formation and transport mechanisms and timing of the HBL development.

From these assessments an appropriate Nautical Depth parameterisation can be developed and sedimentation management strategies evolved, for example methods to exclude HBL. It is generally the case that the cost of such investigations is only a small percentage of the savings in dredging costs. The critical path approach optimises the cost benefits of the study.

8. PRACTICAL EXAMPLES.

Port of Zeebrugge in Belgium.

An extensive sedimentological and rheological investigation has been undertaken to identify the appropriate Nautical Depth parameter to define navigable depth in the port of Zeebrugge. This included evaluation of the relationships between density and dry solids, seasonal variations in sand content, sand content as a function of density and the relationship between static yield stress and density.

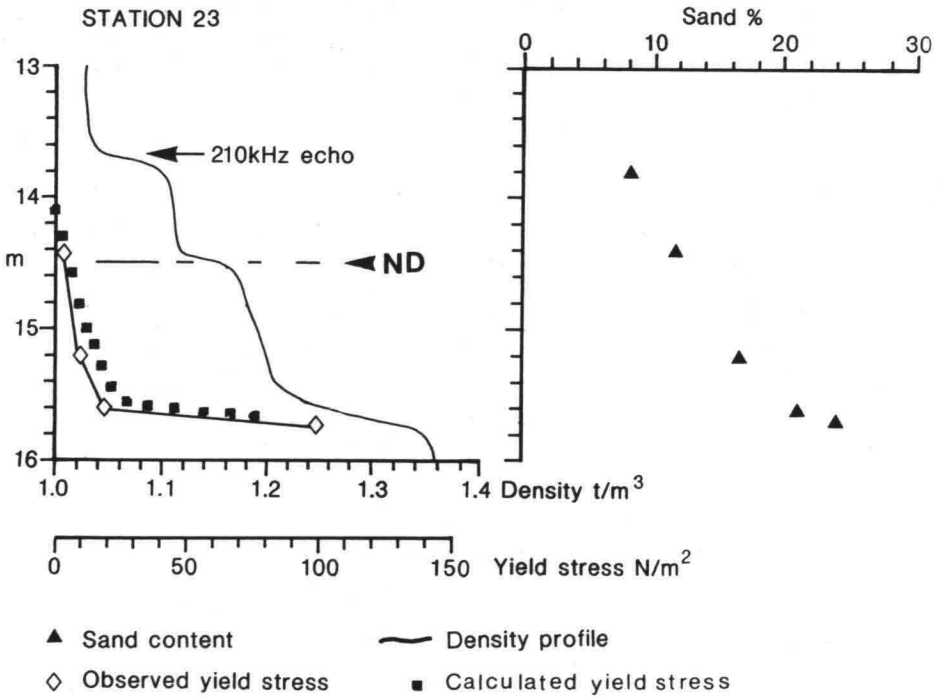

FIGURE 7 Comparison of echosounder (210 kHz) defined depth with density defined Nautical Depth (N.D.), also showing the static yield stress measured on isokinetic samples and a yield stress calculated from the empirical density/static yield stress relationship of Fig 4.

On the basis of rheological tests a density of 1.14 t/m^3 was adopted for the practical determination of Nautical Depth. In a separate study (Kerckaert and Vandenbosche 1988), full scale sailing trials with a deep draught vessel showed safe navigation with the keel at the 1.15 t/m^3 level. This gave greatly increased draught when compared to an echosounder determination of bed.

In Fig 7 we show the relationship between a density profile, a profile of sand content, yield stress determined by measurement and yield stress derived from the density vs yield stress curves. Also shown is the depth indicated by the 210 KHz echosounder. It is evident from this figure that significant depth gains can be achieved by the application of Nautical Depth criteria.

In this project a full application of the Nautical Depth concept was achieved (Kerckaert and Vandenbosche 1988).

Port of Harwich.

Echosounder records from the port of Harwich show up to 2 metres separating the first and second reflectors. At first sight the potential depth gains appear significant. In stage 2 of the evaluation it was found that shear modulus values were 0.05 kNm^{-2} at a bulk density of 1.1t/m^3 and 0.1 kNm^{-2} at a bulk density of 1.15 t/m^3. However, comparison of echosounder data and density data show that the bed surface as defined by the echosounder and the densimeter agree to within the combined experimental resolution of the 2 systems (+ or -5cm) and that values of density corresponding to non-navigable material occur within 20-30 cm of the sediment/water interface. In these circumstances no benefits could be demonstrated for the application of the Nautical Depth concept and the echosounder was shown to provide reliable estimates of navigable depth. The investigation was completed at the end of stage 2.

CONCLUSIONS.

In areas where hyperconcentrated benthic layers form different techniques can give different results in the determination of depth available for navigation purposes. Acoustic systems tend to underestimate available depth. Evaluation of relevant material properties suggests that muds of similar appearance have differing material properties relevant to the determination of nautical depth. The cost benefits of applying nautical depth can be quickly and economically assessed by appropriately designed investigation. Full application requires detailed evaluation of the relevant physical and behavioural properties of the HBL but can result in very substantial cost benefits through reduced dredging, more effective dredging and better guaranteed depths for port entry. This methodology is fully tested and can be applied to any port.

ACKNOWLEDGEMENT.

We are grateful to the Belgian Ministry of Public Works for permission to use data from the studies in Zeebrugge and to Harwich Haven Authority for permission to quote from studies undertaken on their behalf.

REFERENCES

Adler, F.T., W. M Sawyer and J.D.Ferry (1949): Propagation of transverse waves in viscoelastic media. J.of Applied Physics, Vol.20, pp.1036-1041.

Allen, G.P.,R. Bonnefille,G. Courtois and C.Migniot (1974): Processes de sedimentation des vases dans l'estuaire de la Gironde, La Houille Blanche, Vol 1/2, pp.129-136.

Been, K. and G.C.Sills (1981): Selfweight consolidation of soft soils, Geotechnique, Vol.31(4), pp.519-535.

Davis, S.S., J.J. Deer and B.J. Warburton (1968): A concentric cylinder air-turbine viscometer. Journal of Scientific Instruments (J. of Physics E),Series 2(1), pp.933-936.

Delft (1962): Demerara Coastal Investigation. Hydraulics Lab. Delft. 240 pp.

Hunter, R.J. and S.K.Nicol (1968): The dependence of plastic flow behaviour of clay suspensions on surface properties. J.Coll.Sci. vol.28, pp.250-259.

Inglis, C.C. and F.H. Allen (1957): The regimen of the Thames Estuary as affected by currents, salinities and river flow, Proc.I.C.E., Vol 7, pp.827-868.

James A.E., D.J.A. Williams and P.R.Williams (1987): Direct measurement of sttic yield properties of cohesive suspensions. Rheol.Acta., pp.437-446.

James, A.E., D.J.A.Williams and P.R.Williams (1988): Small strain low shear rate rheometry of cohesive sediments. In Dronkers, J. and W. van Leussen (Eds). Physical Processes in Estuaries. Springer-Verlag, pp.488-500.

Joseph, D.D., A.Narain and O. Riccius (1986): Shear wave speeds and elastic moduli for different liquids. Jour. Fluid Mech., Vol.171, pp.289-308.

Kerckaert, P. and D. Vandenbosche (1988): Maintenance Dredging at the port of Zeebrugge. Procedures to achieve an operational determination of nautical bottom. Proc. 9th KVIV Harbour Congress. Antwerp.

Kendrick, M. (1980): Port of Belawan, Indonesia. 3rd report on Hydraulic Studies. Report EX 879 1 & 2, H R Wallingford, pp. 103.

Kirby, R. and W.R. Parker (1974): Seabed density measurements related to echosounder records. Dock and Harbour Authority, Vol. LV(641), pp. 423-424.

Kirby, R and W.R. Parker (1983): The distribution and behaviour of fine sediment in the Severn Estuary. Canadian Journal of Fisheries and Aquatic Science, Vol. 40, Suppl 1, pp. 83-95.

Kirby, R., W.R. Parker and W.H.A.van Oostrum (1980): Definition of the seabed in navigation routes through mud areas. Int.Hydrographic Review, Vol.LVIII(1), pp. 107-117.

Maa, P.-Y. and A.Mehta (1987): Mud erosion by waves: a laboratory study. Continental Shelf Research, Vol. 7, Nos 11/12, pp. 1269-1284.

Migniot, C (1968): Etude des proprietes physiques de differents sediments tres fins et de leur comportement sous des actions hydrodynamique. La Houille Blanche, Vol. 23(7), pp. 591-620.

Mooney, M and R.H.Ewart (1934): The conicylindrical viscometer, J. of Physics, Vol.5, pp. 350-354.

Parker, W.R. (1989): Definition and determination of the bed in high concentration fine sediment regimes. J. of Coastal Research, Special Issue No, Vol.5, pp. 175-184.

Parker, W.R. (1991): Quality control in mud coring. Geo-Marine Letters, Vol. 11, pp. 132-137.

Parker, W.R. (1993): Determining depth and navigability in fine sediment areas, in Abbott, M.B. and W.A.Price (Eds), Coastal, Estuarial and Harbour Engineers Reference Book. Chapman Hall, London, pp. 611-613.

Parker, W.R. and R.Kirby (1977): Fine sediment studies relevant to dredging practice and control. Second Int. Conf. Dredging Technology, B.H.R.A., Cranfield, U.K. pp. 15-26.

Parker, W.R. and R.Kirby (1982): Time dependent properties of cohesive sediment relevant to sedimentation management, in: Estuarine Comparisons, V.S.Kennedy (Ed), Academic Press, New York, pp. 573-589.

Parker, W.R. and G.C.Sills (1990): Observation of corer penetration and sample entry during gravity coring. Marine Geophysics Researches, Vol.12, pp.101-107.
Parker, W.R., T.J.Smith and R.Kirby (1980): Observation of density stratification due to suspended fine sediment. In: Second Int. Symposium on Stratified Flows, T Carstens and T.McClimans (Eds),Tapir, Trondheim, pp.955-966.
P.I.A.N.C. (1983): Navigation in muddy areas. Report of Working Group 3A, in PIANC Bulletin, 43, General Secretary of PIANC, Brussels.
Reiner, M. (1964): The Deborah Number, Physics Today, Vol.1, pp.62.
Sills, G.C., S.J. Wheeler, S.D.Thomas and T.N. Gardner (1991): The behaviour of offshore soils containing gas bubbles. Geotechnique, Vol. 41(2), pp.227-241.
Wells, J.T.and G.P. Kemp (1986): Interaction of surface waves and cohesive sediment, in Mehta (Ed), Estuarine Cohesive Sediment Dynamics, Springer-Verlag, pp.43-65.
Williams, P.R. and D.J.A.Williams (1989): Rheometry for concentrated cohesive suspensions, J. Coastal Research, Special Issue 5, pp. 151-164.

HYDRO-PORT'94
International Conference on Hydro-Technical
Engineering for Port and Harbor Construction
October 19 – 21, 1994, Yokosuka, Japan

Field Surveys on Siltation-Prevention Effects in Waterway and Anchorage by Submerged Walls

Tsutomu Kihara [1]
Hiroshi Sasajima [2]
Kiyoto Yoshinaga [3]
Takashi Koizuka [2]
Hiroshi Sasayama [2]
Hiroshi Yoshinaga [2]
Takahiro Fujimoto [2]

[1] Technical Section, Bureau of Ports and Harbours, Ministry of Transport
2-1-3, Kasumigaseki, Chiyoda-ku, Tokyo, 100

[2] Shimonoseki Investigation and Design Office
4th District Port Construction Bureau, Ministry of Transport
4-6-1, Takezaki-cho, Shimonoseki, Yamaguchi, 750

[3] Kumamoto Port Construction Office
4th District Port Construction Bureau, Ministry of Transport
1259-7, Yahata-cho, Kumamoto, 861-41

ABSTRACT

Kumamoto Port is under construction as an artificial island in Ariake Bay, Japan. In Ariake Bay, bottom materials in the seabed consist of silt and clay. In such a sea area, bottom materials are eroded by waves and currents and deposit in the waterway and anchorage (i.e. siltation). Hence, in Kumamoto Port, submerged walls were installed on both sides of the waterway, 100 m wide and 4.5 m in water depth, to prevent siltation. The submerged walls consist of inverted T-shape concrete blocks 1.0 or 1.5 m in height and 2,000 m in length. After installation of the submerged walls, a series of field surveys was conducted from 1991 to 1994, to investigate the mechanism of the siltation in the waterway and anchorage and to verify the siltation-prevention effects by the submerged walls.

Key Words: Kumamoto Port, Siltation, Bottom Materials, Erosion, Deposition

1. INTRODUCTION

The site of Kumamoto Port thus lies under forbidding natural conditions for the construction of a port and, as a result, for years all construction plans had been given up. However, the development of the Kumamoto urban area triggered practical consideration of port construction in 1971, and the port and harbor planning was approved by the Minister of the Ministry of Transport in January 1974. The plan was revised in 1987 to the existing port and harbor planning to cope with great changes in socioeconomic circumstances including a shift in

Figure 1 Location of Kumamoto Port

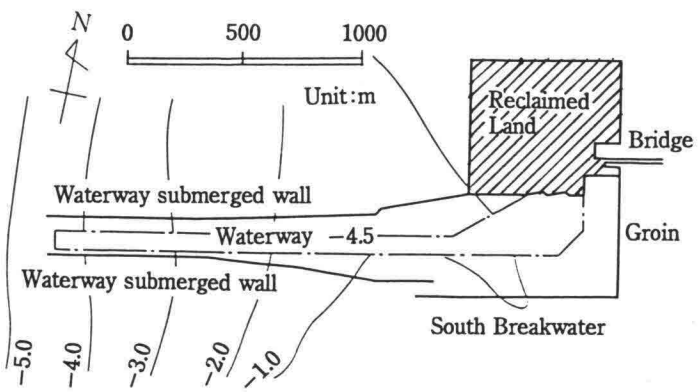

Figure 2 Plan of Kumamoto Port

In the sea area around Kumamoto Port, soft bottom materials consisting of silt and clay are eroded by waves and currents. Eroded bottom materials resulting in suspended mud are carried to the waterway and anchorage, and eventually deposit there. This causes siltation in the waterway and anchorage, obstructing the passage, docking and undocking of ships. Hence, submerged walls were constructed in Kumamoto Port in 1991 to prevent siltation in the waterway and anchorage. After installation of the submerged walls, a series of field surveys was conducted for three years from 1991. The purposes are to investigate the mechanism of the siltation in the waterway and anchorage and to verify the siltation-prevention effects by the submerged walls. The field surveys have the following specific aims:

① Characteristics of bottom materials
Accomplished by measuring the grain size distribution, median diameter, specific gravity, water content and ignition loss of bottom materials sampled at a number of locations, including the waterway and anchorage, to investigate the characteristics of bottom materials.

② Conditions of siltation in waterway and anchorage
Accomplished by water depth by echo sounder periodically to analyze the siltation in the waterway and anchorage.

③ Conditions of suspended mud flow
Accomplished by SS concentration, current conditions (current velocity and direction), wave height and water depth around the waterway and anchorage, to analyze the suspended mud flow fluxes and to confirm the effect of the submerged walls in reducing the suspended mud intrusion in the waterway and anchorage.

2. DETAILS OF FIELD SURVEYS

2.1 Kumamoto Port

As shown in Figure 1, Kumamoto Port is under construction in Ariake Bay off the coast of Kumamoto City. The city, hinterland to the port, has a population of about 630 thousand and is the center of the economy and culture of Kumamoto Prefecture. Approximately 14 km away from downtown Kumamoto, the port is located off the coast in Ariake Bay between the mouths of two rivers: the Shirakawa originating in Mt. Aso, and the Midorikawa originating in the Kyushu Highlands.

Ariake Bay, the site of Kumamoto Port, constitutes an inner bay surrounded by the Shimabara and Uto Peninsulas and various Amakusa islands. Thus, the effect of swell in the bay is negligible. Also the locally generated waves are not large, namely, significant wave height of 0.4 to 1.0 m and wave period of 3 to 4 s. With the tidal range (difference between H.W.L and L.W.L.), however, being approx. 4.5 m, this sea area is characterized by the largest tidal level variation in Japan. Under the seabed lies a 30 to 40 m thick soft clay layer, known as Ariake clay. The seabed near the coast slopes very gently, at 1/1,000 specifically, thus creating the largest tidal flat in Japan during ebb tide. Moreover special attention should be paid for the sea water quality in the port construction works, because this area is famous for green laver farming.

industrial structure. In this plan, Kumamoto Port is designed as an artificial island with 140 ha land reclamation for wharves as a base for the distribution of commodities for consumers and industry in the northern area of Kumamoto Prefecture, port-related facilities, marina and greenery with a tidal flat and artificial beach. Harbor facilities include a -10 m waterway and an approx. 80 ha anchorage. The total length of the north and south breakwaters is about 4000 m. Figure 2 presents the plan in March 1993 when the ferry berth (-4.5 m) was opened for tentative use.

2.2 Mechanism of Siltation in Waterway and Anchorage

Siltation in the waterway and anchorage is greatly affected by the surrounding natural conditions. In the sea area around Kumamoto Port, significant shear stress acts on the seabed in stormy weather, such that bottom materials are likely to erode, agitating silt and clay. Bottom materials thus eroded area in suspension in the water and are carried to the waterway and anchorage, settling and depositing there.

The settling characteristics of bottom materials differ greatly from those of sand. The settling velocity of sand can be expressed by a settling velocity formula dependent on grain size and specific gravity. The settling velocity of bottom materials consist of silt and clay is subject to grain-to-grain interaction. Figure 3 shows an example of the relationship between the settling velocity of bottom materials and the SS concentration (Thorn, 1981). When the SS concentration is sufficiently small, the greater the SS concentration, the more the grains coagulate, thus forming flocks and eventually increasing grain weight, with the result of increased settling velocity. When the SS concentration is sufficiently large, grains interact each

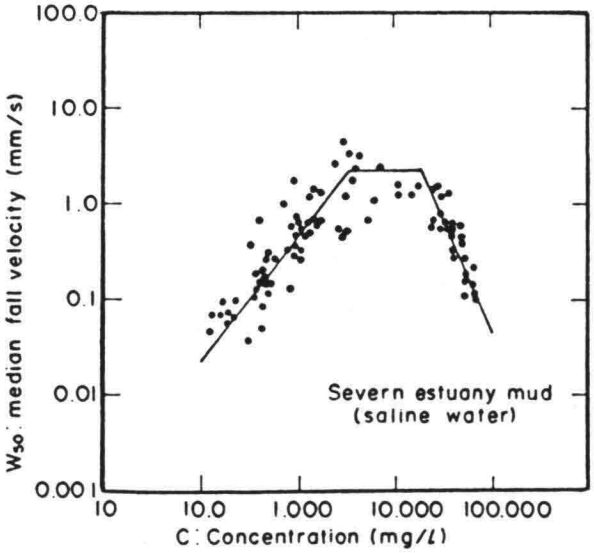

Figure 3 Settling velocity and SS concentration

other, pore water escapes through clearances between grains, an ascending current results (i.e. hindered settling), and therefore the greater the SS concentration, the smaller the settling velocity. Thus, the settling characteristics of bottom materials consist of silt and clay are very complicated.

2.3 Siltation-Preventive Effects by Submerged Walls

It is desirable that the measures for siltation in the waterway and anchorage are accommodated in the port planning, with a balance achieved between cost of port and harbor facilities and effective siltation-prevention facilities. That is an economic comparison should be made between the installation of siltation-prevention facilities and maintenance dredging, to find the optimal approach (Irie *et al*, 1991). In Kumamoto Port, the dredging of the waterway and anchorage is required before constructing breakwaters to put the ferry berth into tentative use. Hence, it was proposed that the submerged walls are installed as tentative structures to prevent the siltation in the waterway and anchorage, until completion of the breakwaters. The effects of the submerged walls include their role as a weir to hinder the fluid mud layer that is formed in stormy weather, and to prevent deposition in a waterway by carrying out the suspended sediments with the upwelling currents developed behind the submerged walls.

To identify the effects of a submerged wall, the amount of deposition was observed from December 1986 until March 1988 at trenches (W 30 m × L 50 m × D 2 m) in the area where the waterway would be installed. Figure 4 shows the time variation of deposition heights during the observation period. Trench No. 1 is located at a water depth of 4 m, trench No. 2 at 2 m, and trench No. 3 at 2 m at the same depth but surrounded by the 1.0 m high submerged walls. With regard to the siltation, trench No. 1 exhibits virtually the same tendency as trench No. 2. In stormy weather, more than 60 cm siltation a day is observed. Throughout the observation period, more than 150 cm siltation occurred. In contrast, trench No. 3 underwent only less than 30 cm siltation during the same period, thereby proving that the submerged walls are effective in preventing the siltation (Toshima *et al*, 1992).

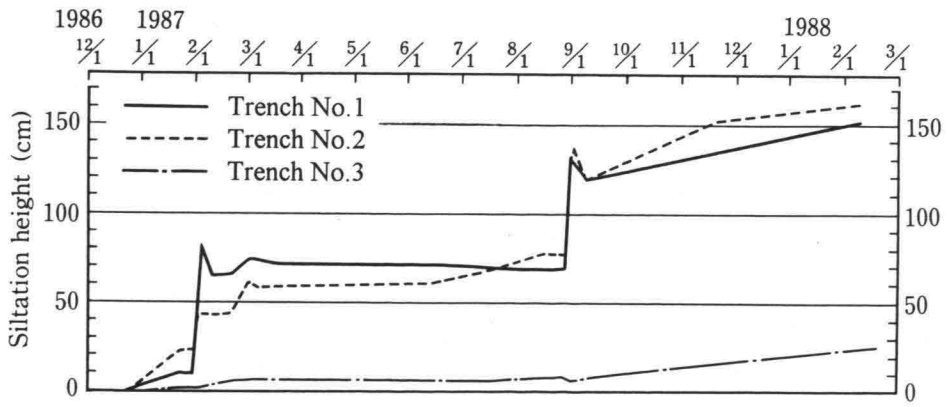

Figure 4 Time variation of deposition heights at trenches

Thereafter, to obtain the optimal arrangement of the submerged walls, a numerical simulation of siltation-prediction was conducted for the case that Kumamoto Port is put into tentative use. Calculation conditions are those in stormy weather on August 31, 1987, within the siltation observation period. The case with the less siltation is the one when the submerged wall height off the coast side is 1.0 m while that on the coast side is 1.5 m. This case assumed the flush effect, which forcibly flushes bottom materials off the coast during ebb tide. In this case, the siltation height is less than 5 cm throughout the waterway and anchorage, with the total siltation registering 8% of the case without submerged walls. These studies suggested that the arrangement of the submerged walls in Kumamoto Port should be considered with reference to the results of the numerical simulations (Toshima *et al*, 1992).

Based on the field investigations and the numerical simulation inverted T-shape concrete block submerged walls, as shown in Figure 5, are installed in Kumamoto Port on both sides of the waterway, 100 m wide and 4.5 m in water depth over 2,000 m in length. Submerged walls with 1.5 m height are placed at a water depth of less than 3 m, where erosion is considered to be dominant, and those with 1.0 m height are placed at a water depth deeper than 3 m. Installation works of the submerged walls was completed by July 1991. For three years after the installation in 1991, field surveys on siltation-prevention effects in the waterway and anchorage by the submerged walls were conducted (Shimonoseki Investigation and Design Office, 1992a and 1993a).

3. CHARACTERISTICS OF BOTTOM MATERIALS

3.1 Outline of Observation

In practical sea areas including Kumamoto Port, bottom materials are a mixture of sand, silt and clay. As described in Section 2.2, the settling characteristics of sand, silt and clay differ greatly

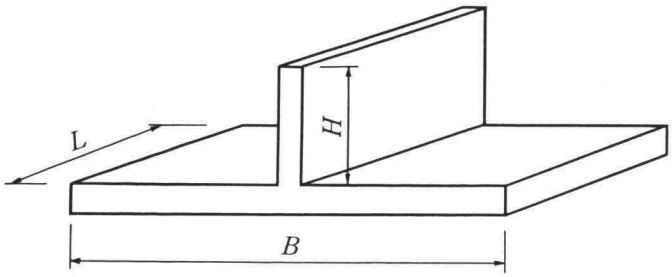

L (m)	*B* (m)	*H* (m)
4.5～7.0	4.0～9.0	1.0～1.5

Figure 5 Submerged wall block

from one another and, therefore, understanding of the siltation mechanism requires knowledge of bottom material characteristics in the siltation area. Bottom materials distributed in and around the waterway and anchorage are sampled and the analysis was made for grain size distribution, median diameter, specific gravity, water content and ignition loss. (Shimonoseki Investigation and Design Office, 1993b).

Sampling was performed at four points in the waterway, four points in the anchorage, and 16 points in other areas, during flood and ebb tides in normal and stormy weather, both during spring tides. Bottom materials were sampled 350 ml at each point in the range from the seabed to 2 cm thereunder. Sand is defined as 0.075 to 2 mm in diameter, silt as 0.005 to 0.075 mm, and clay as less than 0.005 mm, and respective content is measured.

3.2 Results and Discussion

Figure 6 shows the grain size distribution at each sampling point based on the content of sand, silt and clay. Although there is little difference in grain size distribution among sampling times, there is a noticeable difference among sampling points. A high content of silt and clay is found in the waterway and anchorage. In the latter, in particular, their content exceed 90%. A high content of sand is found on the coast side of the original ground. Near the opening section between the south breakwater and submerged walls, the sand content measured as much as more than 85%.

In the anchorage, where the content of silt and clay are relatively high, the median diameter ranges from 0.011 to 0.023 mm, specific gravity from 2.66 to 2.72 g/cm^3, water content from 139 to 198%, and ignition loss from 8.4 to 13.5%. The waterway has a median diameter of 0.019 to 0.036 mm, specific gravity of 2.61 to 2.73 g/cm^3, water content of 98 to 174%, and ignition loss of 6.3 to 11.7%. Near the opening section between the south breakwater and submerged walls, where sand content is the highest, the median diameter is 0.150 to 0.275 mm, specific gravity 2.73 to 2.83 g/cm^3, water content 31 to 46%, and ignition loss 2.6 to 4.3%. To examine the uniformity of grain sizes, d_{25} and d_{75} are read from the grain size accumulation curve, and then uniformity of grain size index, S_0, given by the following equation is calculated:

$$S_0 = (d_{75} \diagup d_{25})^{1/2} \qquad (1)$$

The grain size index S_0 ranges from 2.24 to 3.20 in the waterway, from 3.34 to 6.08 in the anchorage, and 1.23 to 1.48 near the opening section between the south breakwater and submerged wall. Comparing with Figure 6, bottom materials containing much sand have S_0 closer to 1.0, and the grain size distributions are relatively uniform. Those containing much silt and clay, on the contrary, have wide distributions.

These results show that bottom materials causing the siltation in the waterway and anchorage consist of fine-grained silt and clay. This is because that the waterway and anchorage relatively free from the forces of waves and tidal currents are subject to small external forces; because of this, once silt and clay have settled, they do not easily be eroded, thus allowing deposition to persist. In contrast, at the location near the opening section between the south breakwater and submerged wall, the bottom is subject to strong currents and strong shear stress. Because of this, it is difficult for fine-grained silt and clay to deposit, whereas coarse sand is easy to stay where

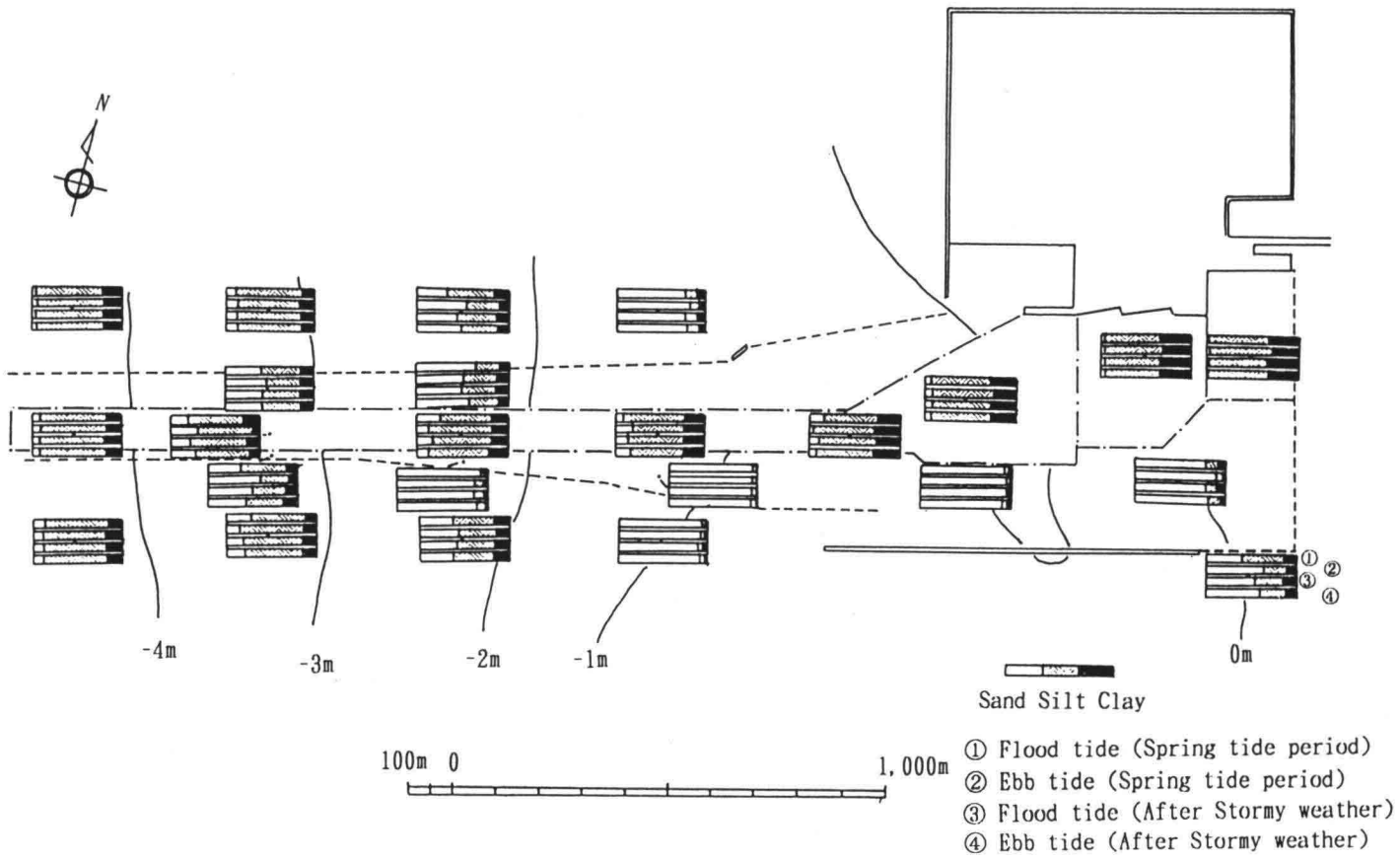

Figure 6 Grain size distributions of bottom materials

it is.

4. SILTATION IN WATERWAY AND ANCHORAGE

4.1 Outline of Observation

In Kumamoto Port, dredging of the waterway and anchorage for the ferry berth to be put into tentative use was initiated after installation of the submerged walls, and almost completed by September 1992. The water depth at that time measured 5.0 to 5.5 m in the waterway and 3.0 to 6.0 m in the anchorage. The bottom sounding works to trace the changes in water depth in the waterway and anchorage were carried out four times in 1992, namely September, October, November, and December, and six times in 1993, namely January, February, March, June, August, and October. In and around the waterway and anchorage, a total sounding area is 1,742,000 m^2 (Shimonoseki Investigation and Design Office, 1993c).

An echo-sounder of 200 kHz is used for the bottom sounding. When the SS concentration has vertical distribution, measured water depth vary with the frequency of the sounder. This is because, where vertical distribution of SS concentration noticeably changes, reflection points of sound wave vary with the frequency of the sounder. In Kumamoto Port, a sounding lead with the bottom area of 113 cm^2 weighing 2.7 kg is used to calibrate echo-sounders of 12, 28, 110, 190, and 210 kHz. As a result, differences in measurements according to frequencies virtually disappeared. Thus, a high-frequency sounder, with high measurement precision, is used. The sounding direction is approx. north to south, vertical to center line of the waterway.

4.2 Results and Discussion

Figure 7 shows the change in water depth from September 1992 to October 1993. Since September 1992, three locations have been dredged and are marked as areas having undergone more than 50 cm erosion. The waterway and anchorage tended to undergo deposition as a whole. Deposition in the waterway is 10 to 50 cm, more at the central part than elsewhere. Deposition in the anchorage is greater than in the waterway, measuring more than 50 cm on the front side of the quaywall and the waterway side of the anchorage. In areas except the waterway and anchorage, the south side of the anchorage and on the coast side of the south submerged walls is 30 to 50 cm erosion, and deposition on the coast side of the south submerged walls receives 30 to 50 cm deposition.

Figure 8 shows the time series of water depth at each area with reference to the level in September 1992. The anchorage is divided into seven areas (1 to 5, 1' and 2'), and the waterway is divided into five areas (6 to 10). Water depth change in the waterway is more moderate than in the anchorage. The change rate for all areas from September 1992 to October 1993 does not exceed 3.0 cm/month. The change rates in areas 8 and 9 from January to February 1993 and from June to August are relatively high, at more than 10.0 cm/month. The change rates in areas 3, 4 and 5 from August to October 1993, register more than 20.0 cm/month. In January to February 1993, when deposition is great in the waterway, significant wave height of 0.5 to 1.0 m appears 14 times, which indicates severer wave conditions than in other periods. In June to October 1993, four typhoons passed through the Kyushu district, to which Kumamoto Port

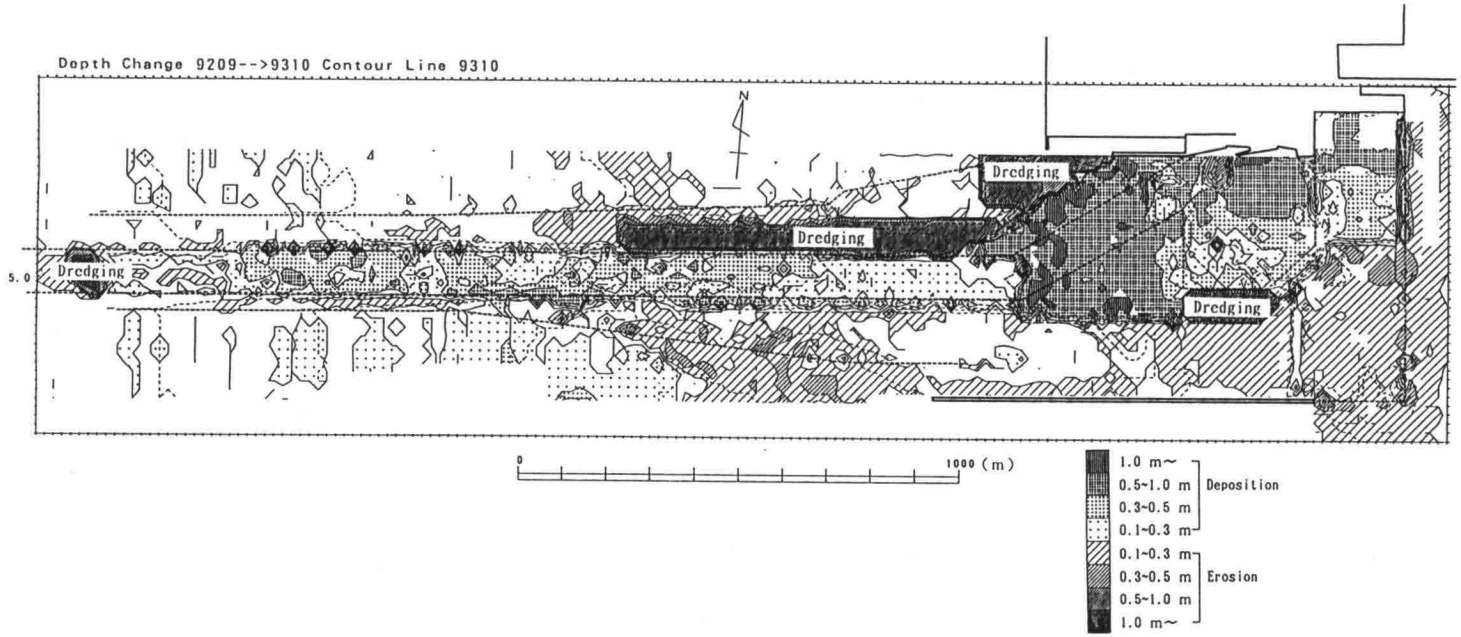

Figure 7 Change in water depth in and around waterway and anchorage

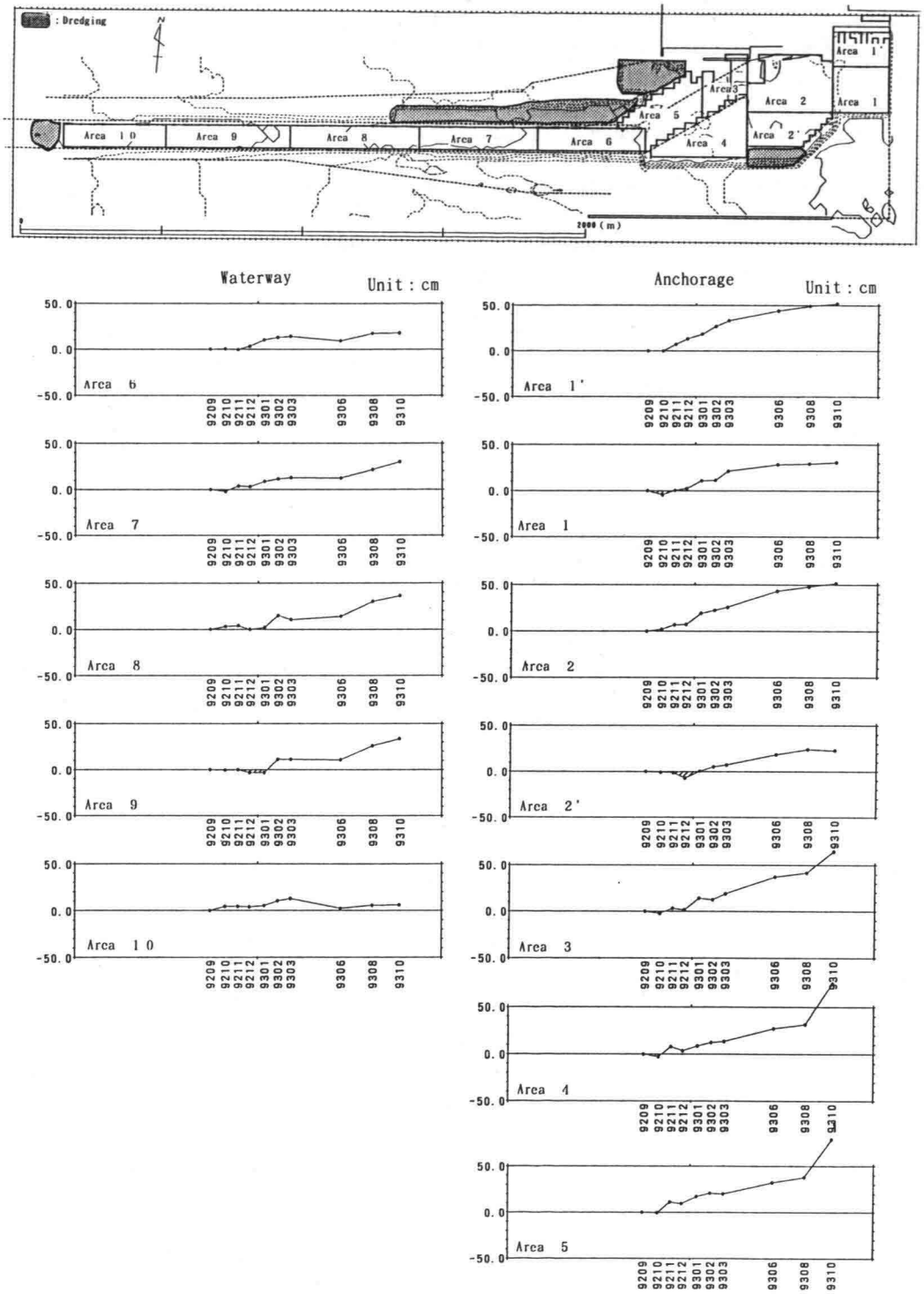

Figure 8 Time series of water depth in waterway and anchorage

belongs, eventually causing more deposition in the waterway and anchorage than in other periods. These observations imply that the waterway and anchorage siltation is strongly related to the weather conditions.

In June to August 1993, more deposition occurs in the waterway than in the anchorage, where the changes in water depth are small. The fact that erosion is scarcely occurred in the same period within the bottom sounding range suggests that the deposition in the waterway is the result of the movement for bottom materials from outside of the sounding area. In contrast, in August to October 1993, much deposition occurs in the anchorage, whereas deposition in the waterway is relatively limited. In this period, the volume of erosion nearly equals to that of deposition within the sounding area. These findings show that deposition in the anchorage is the result of the movement of bottom materials from the sounding area. To elucidate what is the main cause of deposition in the waterway and anchorage, there is a need for detailed analysis of waves, currents, winds and so on during the bottom sounding period.

5. OBSERVATION OF SUSPENDED MUD FLOW

5.1 Outline of Observation

Consideration of siltation-prevention effects in the waterway and anchorage by the submerged walls requires understanding of bottom material behavior in the process of the siltation. Siltation in the waterway and anchorage occurs as a result of the deposition of suspended mud, produced by the erosion of bottom materials. Hence, the effects of wave and current conditions on bottom materials are studied by measuring the time series of SS concentration ,current velocity, current direction, wave height and water depth. Further, the current velocity flux (current velocity $\times$ 1 m) and SS flux (SS concentration $\times$ current velocity $\times$ 1 m) are calculated to estimate the total SS flux in the port area. Moreover, the SS flux is compared between outside and inside the submerged walls so as to evaluate the siltation-prevention effect by the submerged walls (Shimonoseki Investigation and Design Office, 1992b and 1993d). Possible causes of siltation include the deposition of the suspended mud directly in the waterway and anchorage, and inflow of a fluid mud layer formed during mud settling. Although it is well known that the fluid mud layer exists near the seabed, details in the case of Kumamoto Port are not known. Hence, an attempt to observe the fluid mud layer is made by measuring the vertical distribution of SS concentration after stormy weather.

The SS concentrations are estmated from the turbidity measurements obtained with the scattered type turbidity meter with reference to the calibration performed in laboratory experiment. The current velocity, wave height and water depth is measured with the electromagnetic current meter. The vertical distribution of SS concentration is obtained from samples taken by the water column sampler. Water column samplings are carried out after stormy weather. Samples are taken 12 h, 15 h and 18 h after the maximum wave height is recorded.

5.2 Results and Discussion

Figure 9 shows the time series of SS concentrations measured at 0.5 and 0.25 m above the

seabed, and wave and current conditions in stormy weather inside and outside the south submerged wall. The SS concentrations increase when the water depth is less than 5 m. Although they decrease once when the current direction changes, they continue increasing until the water depth is more than 5 m. This is because the bottom shear stress on the seabed is large when the water depth is shallow, thus causing erosion of bottom materials. Between SS concentration peaks, and wave height and current velocity peaks, a time lag of about 6 h is confirmed. This is because a certain period is needed from when bottom materials are eroded by waves and currents, until the resulting suspended mud settles, forming a fluid mud layer and thus increasing SS concentration near the seabed. Current velocity is a little higher inside the submerged walls than outside, whereas SS concentration peaks are inversely higher outside the submerged walls than inside. The SS concentration inside the submerged walls differs only little according to the height above the seabed. Outside the submerged walls, however, SS concentration peak at 0.25 m above the seabed is greater than at 0.5 m. It is because the submerged walls hindered the flow of the fluid mud layer near the seabed.

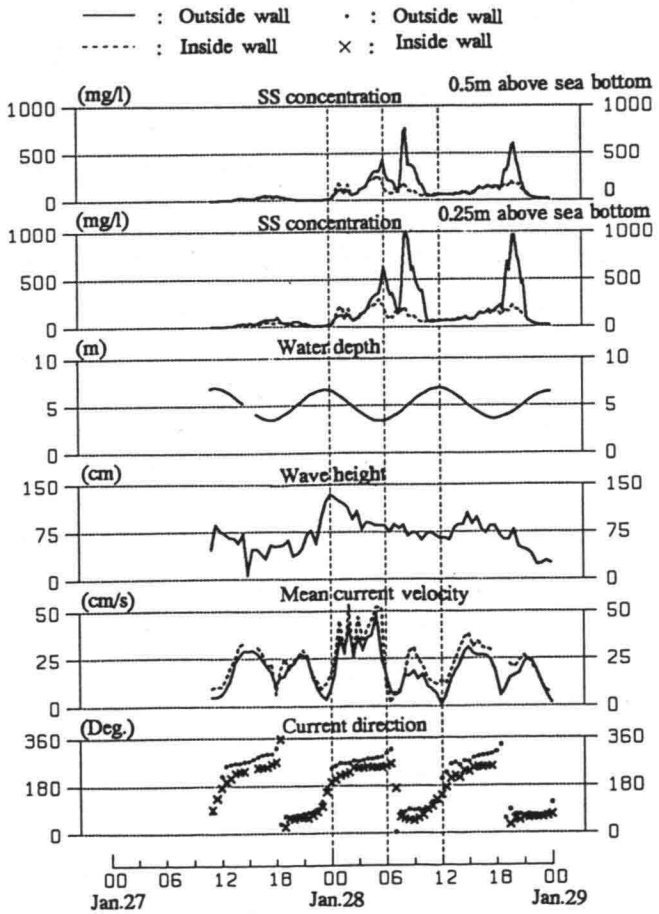

Figure 9 Time series of SS concentrations and, wave and current conditions during stormy weather

Figure 10 (a) shows the suspended mud flow during the ebb tide as represented by the current velocity flux and SS flux. Near the opening section between the south breakwater and the submerged wall, the fluxes fluctuate in direction. This occurs because currents owing to ebb tide are concentrated at the opening section, causing strong currents. Therefore, it is considered

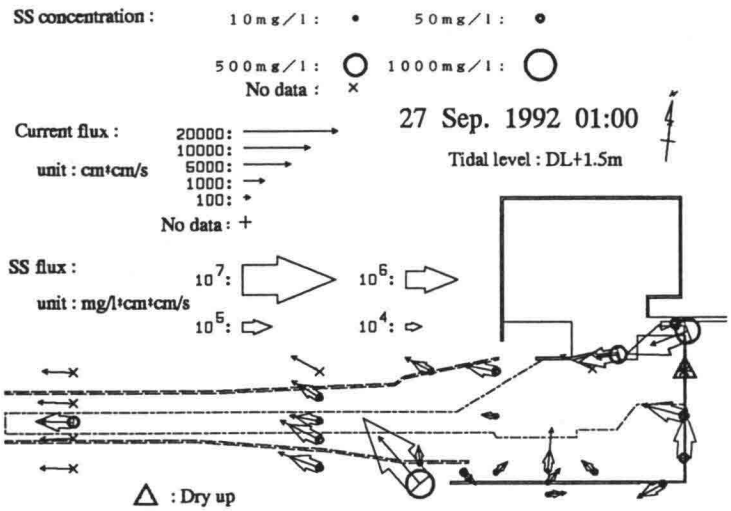

Figure 10 (a) Suspended mud flow during spring tide period (Ebb tide)

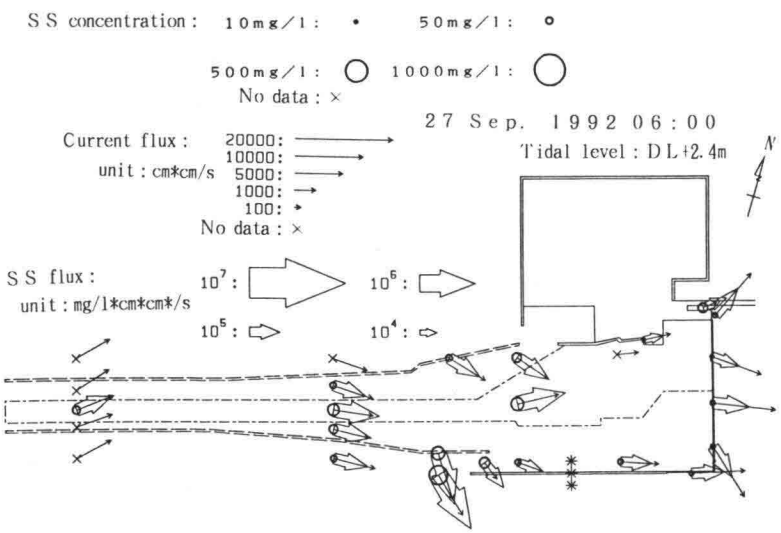

Figure 10 (b) Suspended mud flow during spring tide period (Flood tide)

that the areas around the opening section are eroded. The SS flux entering the waterway is relatively great outside the submerged wall at the opening section, whereas it is limited inside the submerged wall. This shows the shield effect of the submerged walls blocking suspended mud. Influx of suspended mud from the coast side into the anchorage is greater than that from the anchorage to the waterway; this fact indicates that, during ebb tide, siltation occurs mainly in the anchorage.

During flood tide shown in Figure 10 (b), SS flux is oriented toward the outside of the waterway near the opening section between the south breakwater and submerged wall. The amount of the SS flux running from the waterway to the anchorage is relatively large and,

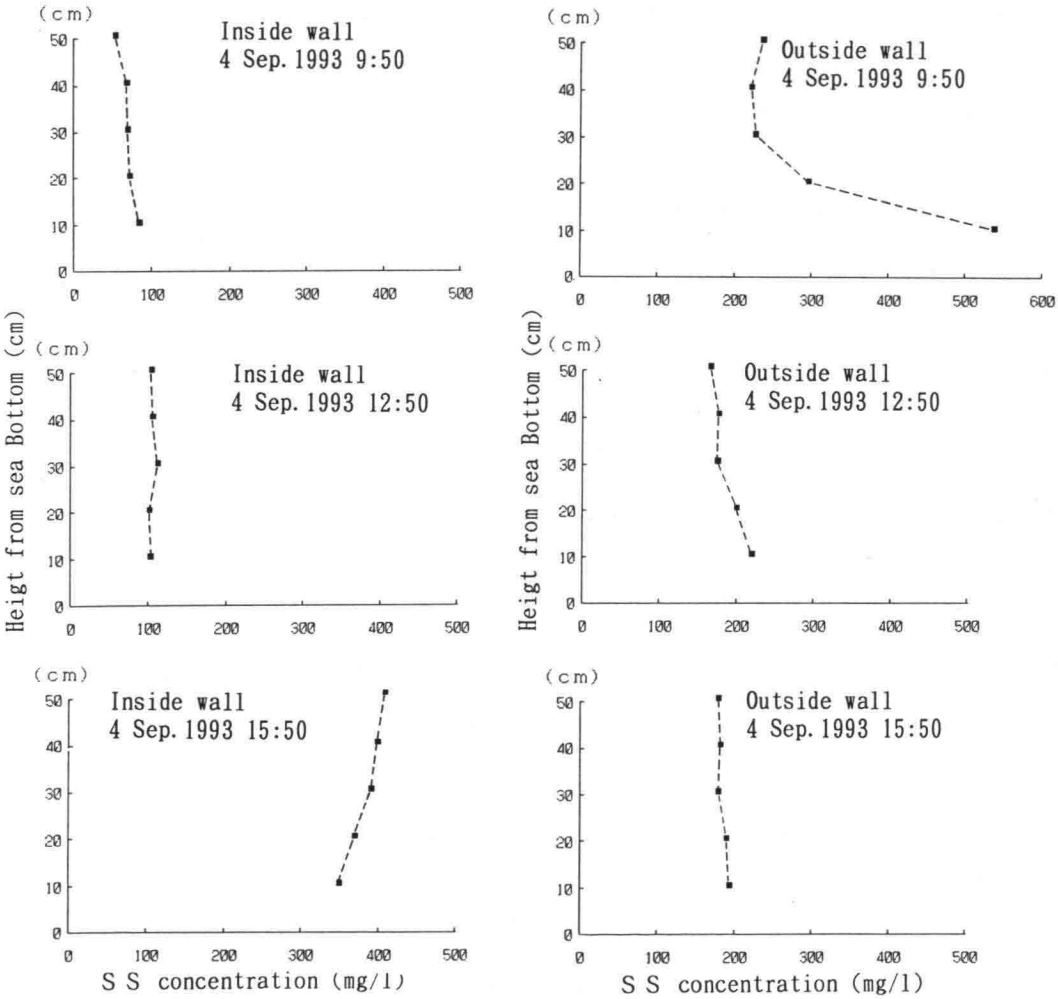

Figure 11 Vertical distributions of SS concentration

therefore, it is considered that more suspended mud flows into the anchorage than into the waterway during flood tide as well. These findings imply that the anchorage is more likely to silt up than the waterway, throughout a cycle of ebb and flood tides. This inference concurs with the conditions of the siltation in the waterway and anchorage described in Section 4.2.

Figure 11 shows the vertical distribution of SS concentration after stormy weather. Water column samples are taken from five strata into which the range from the seabed to 50 cm thereabove is divided, both inside and outside the south submerged walls. Outside the submerged walls, SS concentrations decrease with time whereas the concentration inside increases more at the third sampling than at the first and second. This is because that the third sampling is taken during fall nearing the ebb tide, when the current velocity grows large, thus allowing suspended mud to flow more easily than otherwise. As a result, the current direction changes from outward to inward relative to submerged walls, as shown in Figure 10 (a); the result is promoted suspended mud influx and eventual increased SS concentration inside the submerged walls. Since the suspended mud supposedly enters the submerged walls, rising above the walls, SS concentration measures higher at 50 cm above the seabed than closer to it. In the comparison of SS concentration between inside and outside the submerged walls, the former is smaller than the latter, excluding the third sampling. Since, outside the submerged walls, a fluid mud layer is assumed to exit near the seabed, the SS concentration there at the first sampling, in particular, exhibited a vertical distribution higher near the seabed than elsewhere. Inside the submerged walls, however, SS concentrations are virtually constant in the vertical direction, faring around 100 mg/l; this fact concurs well with the measurements in Figure 9. Thus, it is proved that, excluding cases where a large amount of suspended mud can flow as in the third sampling, the submerged walls are capable of preventing the influx of a fluid mud layer and suspended mud itself, as demonstrated in Figures 9 and 10.

6. CONCLUSIONS

In Kumamoto Port, field surveys were conducted to study the mechanism of the siltation in the waterway and anchorage, and the siltation-prevention effects by the submerged walls; the characteristics of bottom materials are investigated by measuring the grain size distribution and so on. Water depth in the waterway and anchorage is measured periodically to know the total amount of siltation. Furthermore, conditions of the suspended mud flow is analyzed from SS concentration and current data. The conclusion obtained by the present field surveys are as follows:

① Bottom materials deposited in the waterway and anchorage consist of silt and clay. In the anchorage in particular, such fine-grain constituents account for 90% of bottom materials, This is because keeping low the shear stress on the seabed in the waterway and anchorage, which makes bottom materials erosion unlikely and therefore maintains the tendency of deposition.

② Siltation in the waterway and anchorage is affected by the natural conditions in the surrounding sea areas. Water depth change is greater in the anchorage than in the waterway. The source of siltation in the anchorage is considered to be bottom materials eroded around the waterway and anchorage.

③ Locations where the SS flux is large are under erosion in most cases. It may be that such locations serve as a source of the supply of bottom materials that silt the waterway and anchorage. The direction of SS flux indicates that there is a tendency for more suspended mud flows into the anchorage than into the waterway throughout a cycle of ebb and flood tides.

④ After stormy weather, SS concentration outside the submerged walls grows larger near the seabed than elsewhere, forming a fluid mud layer there; whereas, inside the submerged walls, SS concentration, smaller than outside, remains almost constant in the vertical direction. This is because the submerged walls are effective in preventing the influx of the fluid mud layer.

ACKNOWLEDGEMENTS

The field surveys on siltation-prevention effects in the waterway and anchorage by the submerged walls described in this paper are reported to the Kumamoto Port Technical (Siltation) Committee. The authors are grateful for useful advice and guidance given by the committee chairman, Prof. Isao Irie, Kyushu University and committee members concerned. In this regard, special thanks should go to chief of Environmental Hydraulics Laboratory, Dr. Kazuo Murakami and chief of Hydrodynamics Laboratory, Dr. Hiroichi Tsuruya, both of the Port and Harbour Research Institute, Ministry of Transport.

REFERENCES

Irie, I., K. Murakami and H. Tsuruya (1991): Hydraulic mechanism of siltation in approach channels and harbors, Proc. of Japan Society of Civil Engineers, No.438, II -17, pp.1-12. (in Japanese).

Shimonoseki Investigation and Design Office (1992a): Report of field surveys on siltation-prevention effects in waterway by submerged walls, 4th District Port Construction Bureau, Ministry of Transport, 143p. (in Japanese).

Shimonoseki Investigation and Design Office (1992b): Report of investigation on suspended mud flow in Kumamoto Port, 4th District Port Construction Bureau, Ministry of Transport, 97p. (in Japanese).

Shimonoseki Investigation and Design Office (1993a): Report of field surveys on siltation-prevention effects in waterway by submerged walls, 4th District Port Construction Bureau, Ministry of Transport, 173p. (in Japanese).

Shimonoseki Investigation and Design Office (1993b): Report of investigation on characteristic of bottom materials in Kumamoto Port, 4th District Port Construction Bureau, Ministry of Transport, 46p. (in Japanese).

Shimonoseki Investigation and Design Office (1993c): Report of investigation on siltation in Kumamoto Port, 4th District Port Construction Bureau, Ministry of Transport, 57p. (in Japanese).

Shimonoseki Investigation and Design Office (1993d): Report of investigation on suspended mud flow in Kumamoto Port, 4th District Port Construction Bureau, Ministry of Transport, 118p. (in Japanese).

Thorn, M. F. C. (1981): Physical process of siltation in tidal channels, Proc. of the Conf. on Hydraulic Modelling Applied to Maritime Engineering Problems, Institution of Civil Eng.,

pp.47-55.
Toshima, H., H. Ozasa, K. Yoshinaga and M. Iwasaki (1992): Technical development for construction of Kumamoto Port, Civil Engineering in Japan 1992, Japan Society of Civil Engineers, pp.129-145.

HYDRO-PORT'94
International Conference on Hydro-Technical
Engineering for Port and Harbor Construction
October 19 - 21, 1994, Yokosuka, Japan

Case Study on Channel Improvement in the Mouth of the Yongjiang River

Jiang Jiyao

Tianjin Research Institute for Water Transport Engineering
Ministry of Transport, 37 Xingang Er Hao Road, Tanggu, Tianjin

ABSTRACT

The dynamic conditions of the Yongjiang Estuary had been worse and worse and serious situation occured due to the construction of the Yaojing Lock and Zhinhai Harbor. so Zhenhai Harbor could not be put into operation after its completion. Hence, for the purpose of navigation of 10,000 tonners, some construction and training works were used for regulation. Within 5 years, the successful results have been gained and experiences are also provided for the tidal estuary regulation.
Key Words: Estusry, Waterway, Siltation, Regulation.

1. HISTORICAL BACKGROUND

Yongjiang River, situatid in the Ningbo region of Zhejiang Province, is a important waterway in the south—east China, especially for foreign trade. There are two big tributaries, i. e. Yaojiang River and Fenghua River. Yaojiang River belongs to a plain river, Fenghua River is mountain stream. Yongjiang River with the length of 22km is the name given to the confluence of these two tributaries in the Ningbo City. The river width at the middle tide livel varies from 200m to 510m. In the river basin, the rainfall is rich and the flow — in sediment is small. There are vast fertile farm land along the banks.

The reach of Yongjiang River out of the Zhenhai Bay is widened into the shallowest channel, i. e. the Zhaobaoshan Shoal. Out of this, the water area is separated by the Zhanbaoshan, the Hudunshan, the Youshan and the Lishan, forming a complex field of flow and sediment with multi—entrances. The topography under water is undulant. Pools and shoals appear alternatively from the inside to the outside, such as, the Zhaobaoshan Shoal, the Hudun Pool, the Hu—You Shoal, the Youshan Pool, the Youshan Out Shoal (called a bar) and Jintang Waterway. The 5km—long water area from the Zhenhai Bay to Jintang Waterway is called the Yongjiang Estuary (see Fig. 1)

For the development of farmland and economy, a tide lock was built at Yaojiang River which is 25 km away from the estuary to block the salt water in 1959. In 1974, the Ningbo New Harbor—Zhenhai Harbor was built at the estuary, which turned the estuary with multi—entrances into one with a single entrance. These two engineering projects, especially the harbor construction, seriously disruoted the dynamic condition of the estuary, and caused the heavy aggradation. So, the two coal docks set up in 1978 could not be put into operation due to the insufficient water depth.

Since 1979,according to the dredging and regulating combination principles,a series training works have been used based on analysis and model test study. The Zhenhai Harbor was turned from a dead harbor into a active harbor within five years. The two coal docks were put into operation in Apr. 1982. By the end of 1985. the whole channel depth of the estuary has fulfilled the requirement of navigation for 10,000 tonners。Now six 10,000—ton docks,three 5,000—ton docks and one chemical terminal have been completed. Under the normal maintance dredging conditions,10,000—ton ships(the max. 20,000 tons)can berth for operation. In 1990,the handling capacity of the Zhenhai Harbor was over 4,000,000 tons and better economic benefits are gained.

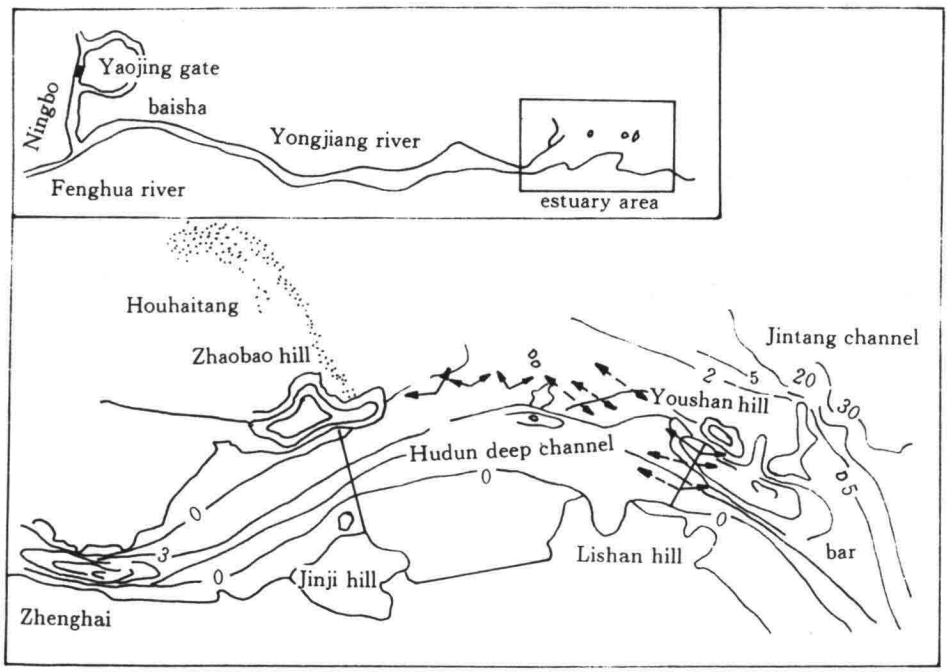

Fig. 1Topographical Features of Yongjang Estuary

2. HYDROGRAOHY OF THE ESTUARY

2.1 TIDE

The tide of the estuary is non—regular semidiurnal tide of a weak type with the average range of 1.76m,beloning to weak tide mouth. The average high tidal level is 3.03m and the average low tidal level is 1.26m. The average discharge is 1,400m^3/s in the Lishan cross section and 830m^3/s in the Zhaobaoshan cross section. The complicated flow patterns can be shown from Fig. 1. The Maximum tidal velocity is 1.2m/s and flood and ebb velocity is about 0.5m/s on average. The ebb velocity is greater than the flood velocity. In addition,the tidal flow of the estuary arrives about 40—80min later than that the outside of the estuary due to the action of the flow of the Jintang Waterway against the flow out of the Yongjiang River.

2.2 WAVE

Influenced by the hills around, the wave direction is mainly WNW—ENE with the frequency of 70. 3%. The frequency of other direction are only 7. 0% and the calm seas are 22. 7%. The wave height greater than 0. 5m are all wind waves of WNW—ENE. Table 1 indicates the wave frequence with different height. The max. wave height over 50 years is

Table 1 wave Frequency at Different Heights

wave height(H)	<0. 5m	0. 6—1. 0m	1. 1—1. 4m	>1. 5m
frequence(%)	80. 7	14. 4	3. 5	1. 4

established to be Hmax. =5. 0m with the relevant period of 8 sec.

2. 3 SEDIMENT

The north of the eatuary is bounded by the broad Hangzhou Bay which is the main source of the sedinent in the estuary. The flow—in sedinent from upstream are very small. The sediment amount transported into the Lishan cross section from the open sea is about 14,000,000 tons per year. The sediment amount carried into the estuary by tide varies with different seasons. In winter, the concentration is high due to much north—west strong wind and big waves. The max. concentration can reach to 4. 8kg/m^3. Whereas, in summer, as most winds are south—east and there are only small wind waves and the conncentration is small and the max. value is below 0. 1kg/m^3. The month average concentrtation of the Lishan cross section can be shown in Table 2 based on the field measurement in 1975—1976.

Table 2 Concentration of the Lishan Cross Secton on Month Average

month	1	2	3	4	5	6	7	8	9	10	11	12	ave.
conce	1. 28	1. 39	1. 49	1. 28	0. 98	0. 74	0. 48	0. 47	0. 78	1. 06	1. 11	1. 26	1. 03

The bed materials of the estuary are medium and fine silt (d_{50}=0. 017—0. 20mm)except for the fine sand and coarse sand (d_{50}=0. 053mm)in the bar.

2. 4 RUNOFF

For many years, the average runoff volume has been 82m^3/s corresponding to one tenth of the average tide intake amount of the Zhaobashan cross section. In the flood season from June to Sep. the sediment deposited in the Yongjiang channel in the dry period is moved and transported into the estuary by a great amount of flood water, which forms the basic process of siltation in the flood season and erosion in dry season.

3. SILTATION OF THE ESTUARY

3. 1 After the Yaojiang tide lock was built at the Yaojiang tributary in 1959, the tidal amount coming in Yongjiang River decreased greatly. According to the field measurement of the Zhenhai section at the estuary, it decreased by about 40%, Moreover, as the tide wave characterstics and runup downstream the lock were changed, the Yongjiang Channel which is 22 km away from the lock was aggraded by the sediment of 40,000,000m^3 and mean silting thickness was 2. 3m, which made a grest influence on the estuarine area.

By comparison between the three charts of 1959, 1962 and 1970, and taking the chart of 1956 as the topography before the lock construction, up to May of 1970 the total siltation

amount of 3,740,000m³ had been found at 5 km—long reach of the eatuary with low tidal level and the average silting thickness reached 1. 28m(see Table 3).

Table 3 Estuary Siltation due to the Yaojiang Lock Construction

time	topograpic change	dredged volume	silting volume	silting thickness(m)
lock const. Aug. 1962	1,440,000	160,000	1,600,000	0. 54
Aug. 1962 Aug. 1970	1,620,000	520,000	2,140,000	0. 74
In total	3,060,000	680,000	3,740,000	1. 28

3. 2 When the Zhenhai Harbor was started to be built in 1974, a brekwater with the height of +5. 0m and the length of 3. 3km was built along the Zhaobaoshan—Hudunshan—Youshan, which blocked the two gaps of the Zhao—Hu and Hu—You, making the estuary a single You—Li entrance (see Fig. 2). After the completion of the breakwater in Sep. 1957

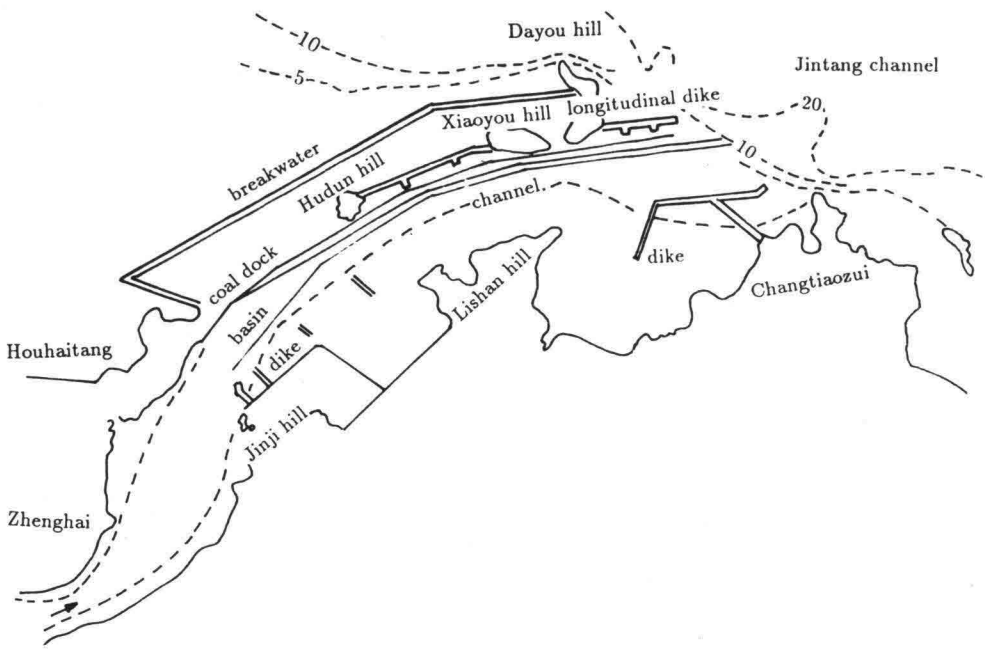

Fig. 2 General Arranement of Regulation in the Yongjiang River

the flood and ebb volunes were reduced by 29% and 42% respectively and there were no change in the sediment coming into Yongjiang River from the sea, so the river bed was rapidly silted. According to the three charts of 1973. 1975 and 1976, under the condition of the medium tide level, the total siltation amount was 3,600,000m³ with the average silting thickness of 1. 25m from the time of the breaskwater construction to Apr. 1976, in which 2,710,000m³ were found in the range of the depth contour of ±0m, accounting for 75% of the total (see Table 4).

As the water depth conditions at each area of the estuary were different as well as the change of the dynamic condition caused by the harbor construction, the siltation were also quite different. Heavy siltation occured in the Huyoushan—Dayoushan area.

Table 4 Estuary Siltation due to Harbor Construction

range	silting duration	topographical change(m^3)	dredging volume(m^3)	silting amount	mean silt thickness
medium tide under +2.0m	1973.3—1975.5	1,930,000		1,930,000	0.66
	1975.7—1976.4	840,000	830,000	1.670,000	0.59
	1973.3—1976.4	2,770,000	830,000	3,600,000	1.25
under ±0m	1973.3—1975.7	1,660,000		1,660,000	0.68
	1975.7—1976.4	220,000	830,000	1,050,000	0.49
	1973.3—1976.4	1,880,000	830,000	2,710,000	1.17

especially in the Youshan deep pool section. Only in the two years from the beginning of building the breakwater to Apr. 1976, the average water depth under the medim tidal level reduced from 7.2m to 4.1m and the average silting height was 3.1m, The river bed below ± 0m was raised by 4.2m on average. The water carring section was narrowed by 45%, it can be seen that the silting speed was very fast.

In the harbor construction, except for the breakwater the harbor basin and channel were also cut to widen the water carring section. This caused the extensive siltaiton in the basin and channel. The most serious siltation occured at the coal dock and the channel of the Youshan Outer Shoal. The cut of the basin and channel had been completed by the end of 1976. Only in the three months from Jan. 16 to May 1, the average silting height of the dock basin(410m ×230m)reached 1.92m. The daily average silting density was1.8cm. In the flood season of May in the same year, the general silting height was 1.0m within a half month. The channel of the Youshan Outer Shoal was very difficult to dredge and was redeposited quickly after dredging. Even continuous dredging was kept on, it was impossible to maintain the designed depth(−7.2m)for ship navigation.

4. TRAINING WORKS AND RESULTS

The above serious siltation caused the newly built Zhenhai Harbor out of operation. From 1979, the units of researching, designing and contruction proposed to use a series of training works as shown in fig. 2 based on the analysis of a great number of field investigation and model test studies, the main training works will be presented as followes.

4.1 OVERALL DESIGNING THE DOCKFRONT AND IMPROVING THE FLOW PATTERNS

For the north bank, a longitudinal dike with a length of 480m was set up along the dockfront and the Huyou section. For the south bank, a series of spur dikes and longitudinal dikes were used to improve the flow regimes reforming a stable channel with a slight bend, and to increase the water carring capacity of the north bank remaining navaigable depth of the berthing area and channel. The right beach was also strengthened, so that a deep pool with a height beach could be formed. The width of the river was widened progressively from 290, to 340m to prevent the tidal volume into Yongjiang River from decreasing.

4.2 BUILDING THE SPUR DIKE AT THE JINJISHAN

Spur dike 1# and 2# were built at the Jinjishan of the south bank, turning the ebb to the north bank, which can make the flood and ebb unform and change the silting location to increase the water depth of the dockfront.

The sediment carried by ebb tide was firstly deposited at the dock basin (the desinged depth of 7.2m) which is located at the end of the Zhaobaoshan Shoal with a depth of about 3.0m, Accordingly, the dynamic axis of the flood and ebb in this area was different. The natural deep water area was 160m away from the dockfront. In order to increase the water depth of the dockfront and improve the regime of the section, the downturned spur dikes with the length of 105m and 102m respectivcely, were built at the Jinjishan. centering the flood and ebb flow at the main north pool to increase the velocity at the dockfront. After the construction of it, the dynamic axis of the flood and ebb became uniform, the deep water area was turned north about 100m. and the average depth of the basin wa increased by 2.0m with the maximun depth of 9.5m. Only small dredging needed can keep the dock in operaion.

4.3 REMOVING THE HARMFUL STRUCTURES

There was a measuring pier at the upper part of the coal dock. Effected by the pile base of this pier, the river bed formed a sand spit under water. When the water level dropped to some extent, the spit leaded the ebb current southwards, and in the north, there was a backwater area with 100m in length and 50m in width, causing a heavy siltation in the dockfront. The minimum depth was only about 1.0m. To solve this problem, the measuring pier was removed to dislodge the poit and the slope connecting the basin with the Zhaobaoshan Shoal was flated. After that the backwater area disappeared and siltation rate was greatly falled down. Spur dikes 1# and 2# have also made the results even more successtul than what is expected.

4.4 BUILDING THE YOUSHAN JETTY

In the entrance, a mouth bar was formed with the crest of about 3.5—4.0m in natural depth due to the effects of the north wind waves and the Jingtang waterway. Through the model test, it was found that there was a backwater area over the crest of the bar. As d_{50} of the bar was 0.053mm and the water content was only 26%, it was very difficult to dredge. So the contracting works for stream fluting were used to weaken the influence of the wind wavaes. Firstly, a short jetty with length of 462m was built on the north bank with two 40m—long short spur dikes inside, directing towards the bar. The bar was shrinking and the cresl height was towering gradually with the extension of the jetty. After the completion of the jetty, the bar was lowered by 1.7m—1.9m. Then, a series of spur dikes and longitudinal were set up at the south band. The crest height was further lowered and the water depth was abut 6.0m. Based on the analysis of teh field data, the relationship of the river facies was obtained:

$$H = 3.69 \frac{Q^{2/3}}{B^{2/3} \quad S^{1/3}}$$

where H=the average depth ovcer the crest section of the bar (m)

B=the river width (m)

Q=the ebb volume (m^3/s)

S=the sediment concentration (kg/m^3)

5 MAIN EXPERIENCES OF THE REGULATIONS

The successful regulation of the Yougjing Estuary has been obtained with in five year. It not only gains the wonderful economic benefit of turning a "dead harabor"into a "active harbor", but alsò provides some experienses and basis for tidal estuary regualtion. The main experiences are summarised as follows.

5.1 FORMING A SLIGHT BEND RICER SITUATION CAN INCREASE AND STABILIZE CHANNEL WATER DEPTH

In the training works designing, a 3km—long jetty designed refering to the width of normal line had been planned to be built on the south bank. But as the river situation has a little bend and the flow is moving towards the north bank(concave side), the side shoal on the south bank which was gradually aggraede acted as a jetty. So the jetty planned to be built was withdrawn because it was found to be useless in the model test. It economized the engineering investment. Under the river situation of the slight bend, the channel depth from the Zhaobaoshan to the Dayoushan has been maintained to be 6m—8m.

5.2 RATIONAL PLACEMENT OF THE TRAINING WORK COULD NOT CAUSE A SIGNIFICANT CHANGE IN THE TIDE WAVES OF THE ESTUARY

Table 5 The Characteristic Values of the Estuary Tide Brfore and After the Regulation

item	before regulation	after regulation
meam high tide level(m)	2.90	2.95
mean low level (m)	1.13	1.17
mean tide range (m)	1.77	1.78
mean flood duration(h)	6.25	6.25
mean ebb duration(h)	6.17	6.17
flood volume ($10^4/m^3$)	1868	1883
ebb volume ($10^4/m^3$)	1865	1882
mean flood discharge(m^3/s)	830	835
mean ebb discharge(m^3/s)	840	855

As the tide water volume is the main dynamic force of the Yongjiang Estuary Attention must be given to the effect on the tidal intake in the placement of the training woks. Considering the balance of the sediment transport by tide, followimg relationship of the regulated width can be obtained:

$$B_2 = (H_1/H_2)^{4/3}B_1$$

Where H_1, H_2, B_1 and B_2 are expressed as the water depth and river width defore and after the

regulation respectively. From the above relationship, the upper mouth width of the Yongjing Estuary was defined as 290m, which was wider than that of the Zhenhai Bay channel (180m). The lower mouth width was widened to 340m. Therefore, there was no great change in tidal waves of the Estuary (see Table 5).

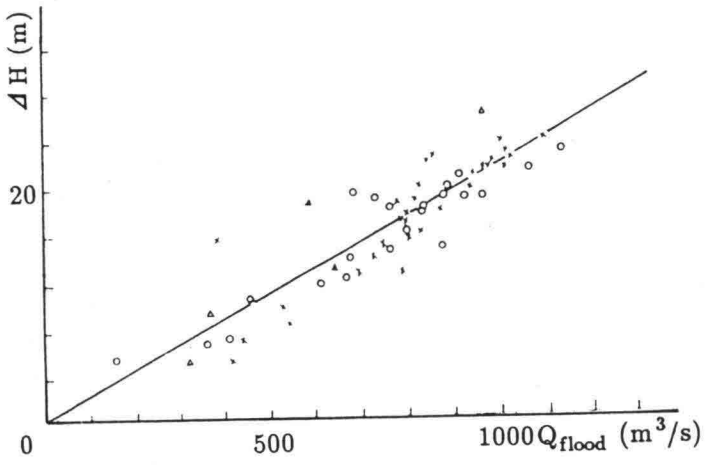

Fig. 3 Relationship between Q_{flood} and ΔH in Zhaobaoshan Section

The discharge has been not changed since the regualtion. The average water depth of each section of the regulated reach and the channel depth can be calculated by the following formulas respectively:
the depth after the regulation

$$H_2 = (B_1/B_2)^{3/4} H_1$$

the depth of the channel

$$H_{channel} = H_{average} + 1.80$$

5.3 THE UNIFORMITY OF THE DYNAMIC AXIS OF THE FLOOD AND EBB CAN ENLARGE THE WATWE CARRING SECTION AND DEEPEN THE CHANNEL WATER DEPTH

It is considered that the water carring section depends on the tidal volume. A certain tidal volume produces a certain stable water carring section. before the regulation, the stable cross section under the medium tidal level of the Zhaobaoshan was 1800m². After the completion of the spur dikes at the Jinjishan, the width to turn the flow (start to calculate from the head of a dike) was about 100m, covering one third of the whole river width, The original flow paths of the flood to the north and ebb to the south tended to be centered at the basin and channel. As the dynamic axis was uniformed, the water carring section under the medium tidal levle was increased to 2000m² by 25% and the water depth of the stable section (below the base surface of the Wusong) was greatly increased from 2. 8m before the regulation to 5. 9m. The water depth of the coal dock was also increased.

5.4 THE AVERAGE VALUES OF THE FLOOD AND EBB CURRENT VELOCITY OF THE STABLE SECTION SHOULD BE DEFINED AS THE VELOCITY

Rational determination of the regulated velocity can gain the economical result in regualtion. According to the regulation of the Yongjing Estuary, It is appropriate to use the average values of the velocity of the flood and the ebb of the stable cross section as the regulated velocity. For example, before the regulation, the velocity of the Zhaobaoshan cross section was 0. 49m/s which was stable (see table 6). After the harbor construction the decrdase of the tide velocity caused the harbor silted. Since the regulation, the average velocity has been 0. 44m/s approaching the average velocaity before the harbor construction and the bed has been stable. In addition, it was proved from the circle flume test that the threshold velocity which could not cause the siltation in the basin was 0. 45m/s that is corresponding to the velocity before the construction.

Table 6 The Average Velocity of the Zhaobaoshan Cross Section(m/s)

time	flood	ebb	aver	situation
before harbor const	0. 40	0. 50	0. 49	stable
after harbor const	0. 27	0. 35	0. 31	unstable heavy siltation
after regulation	0. 41	0. 47	0. 44	basically non—siltation

5.5 REGULATED WATER LEVEL

Regulated level was defined based on the ebb. Analyzing the history of tidal level and velocity measured in the estuary, the water level in the maximun velocity was defined as +2. 0m—+2. 3m for spring, medium and slack tides. The maximum velocity is 0. 75—0. 95m/s for spring tide, 0. 80m/s for medium tide and 0. 75m/s for slack tide, which all exceed the mean starting velocity of $d_{50}=0.46$m/s. The utilization of the maximun velocity of ebb current to wash out the channel can greatly strengthen the channel washing capacity by dike—like structure. Based on this analysis, the regulated water level of the Youngjiang channel was defined as +2. 3m. It is verified from practice that the regulated waterlevel is appropriate, which not only provides a good washing condition by the trainging waorks, but also keep the tidal waves of the estuary from obvious changing.

6. CONCLUSION

In summary, with purpose of getting navigable water depth for 10, 000 tonners in the Yongjiang Estuary, successful results have been obtained by measuring, i. e. rationally placing the training works, fully using the exiting flow dynamics to contract water and transport sediment, and combining dredging with regulation.

REFERENCES

Jiang Juyao, "Analysis on the Siltation Problems of Zhenhai Harbor", 1976
Jiang Juyao, "Preliminary Suggestion on the Regulation of Zhenhai Harbor", 1976
Engineering Department of Ningbo Harbor Authority "Preliminary Nanlysis on the Con-

struction Proceeding of the Channel Regulation of Zhenhai Harbor and its Results",1981
Cai Jiaxi,Xia Jingen and Pan Xinbei,"Analysis on the Beneficial Results of the North Jetty of Zhenhai Harbor ",1981
Zhang Dingbang and Yuan Meiqi "Channel Regularion of Zhenhai Harbor at Yongjiang Estuary",1982
Cao Zude,"Research on the Regulation of the Mouth Bar of the Yongjiang Estuary",1983

HYDRO-PORT'94
International Conference on Hydro-Technical
Engineering for Port and Harbor Construction
October 19 - 21, 1994, Yokosuka, Japan

Field Survey on Estuarine Mud Transport Process around Navigation Channel, Banjarmasin, Indonesia

Hiroichi Tsuruya [1]
Kazuo Murakami [1]
Kohei Nagai [2]
Isao Irie [3]

[1] Port and Harbour Research Institute, Ministry of Transport
1-1, Nagase 3-chome, Yokosuka, 239
[2] Japan Port Consultants, LTD., 3-1-4 Shibuya, Shibuyaku, Tokyo, 150
[3] Kyushu University, 6-10-1, Hakozaki, Higashiku, Fukuoka, 812

ABSTRACT

A comprehensive field survey was performed for one year from September 1988 in order to reveal the mechanism of siltation in and around the navigation channel constructed on the muddy tidal flat formed in front of the mouth of the Barito River in the Republic of Indonesia. The 14 km long approach channel of Banjarmasin Port which locates 26 km upstream from the river mouth has been suffering from siltation requiring dredging works at a rate of 2 to 3 million m^3 every year. Problems related to the siltation of harbors and navigation channels with high dredging costs accentuate the necessity to elucidate the transport of fine sediments in estuaries. From the field survey, it can be concluded that the fine sediments are supplied from the Barito River and the widely spread fine sediments form a fluid mud layer on the tidal flat. The fluid mud layer thus formed is easy to move by external forces and accumulate in the navigation channel together with the resuspended bed materials which are transported by convection and diffusion.

Key Words: Access Channel, Banjarmasin, Siltation, Fluid Mud

1. INTRODUCTION

In many riverine ports and their approach channels, huge investments have been made for maintenance dredging every year due to siltation. The 14 km long access channel of Banjarmasin Port, which is a typical example of such ports, has been suffering from the heaviest siltation in Indonesia, requiring dredging works at an annual rate of 2 to 3 million m^3, and still the planned profile of 6 m in depth and 60 m in bottom width is hardly maintained. The causes and results of the siltation were not clear enough. In order to reveal the mechanism of siltation and to develop measures for the reduction of siltation, extensive field surveys were carried out for one year from September

1988 to September 1989. There are many interesting facts found through the study and some of the results of field surveys are introduced in the present paper. The city of Banjarmasin locates at the south east of Kalimantan as shown in **Fig. 1.**

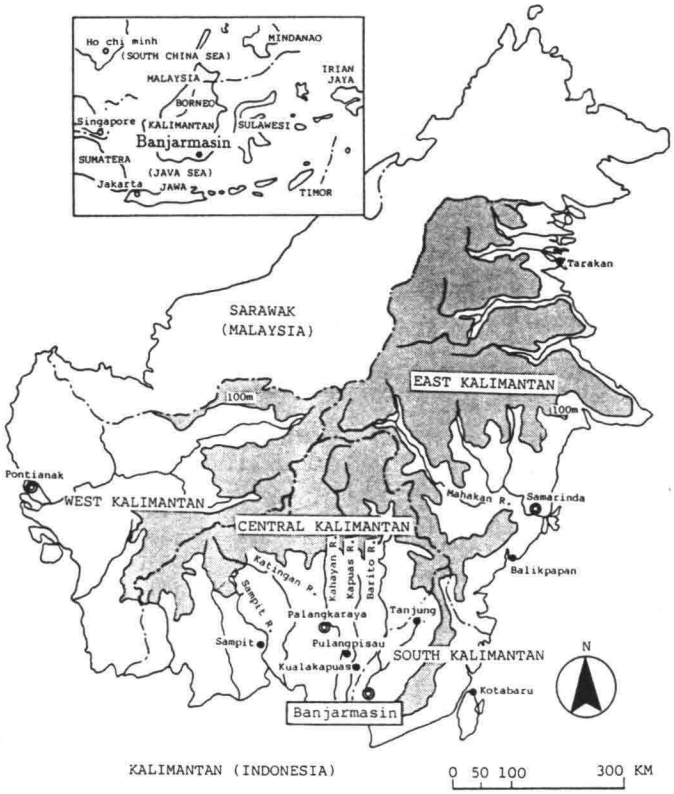

Fig. 1 Kalimantan

Photo 1 The Mouth of Barito River and Estuary

Photo 1 shows the mouth of the Barito River and estuary taken in the rainy season at December 6, 1988. Turbid water can be seen on the tidal flat. Banjarmasin port locates approximately 26 km upstream from the mouth of the Barito River. Inside the river, the water depth is deeper than 7 m and there are no problems for navigation. However, there is a large tidal flat in front of the river mouth. Very shallow area of which water depth is less than 1 m widely spreads on the flat.
Figure 2 shows the access channel which connects the river mouth with offshore. In the figure, some observation points are also expressed. The details of the field survey will be explained in the following chapter.
The rainy season usually starts from November and lasts until April of the next year.

2. ITEMS OF SURVEY

Hydraulic mechanism of siltation in an estuary is summarized in **Fig. 3.**

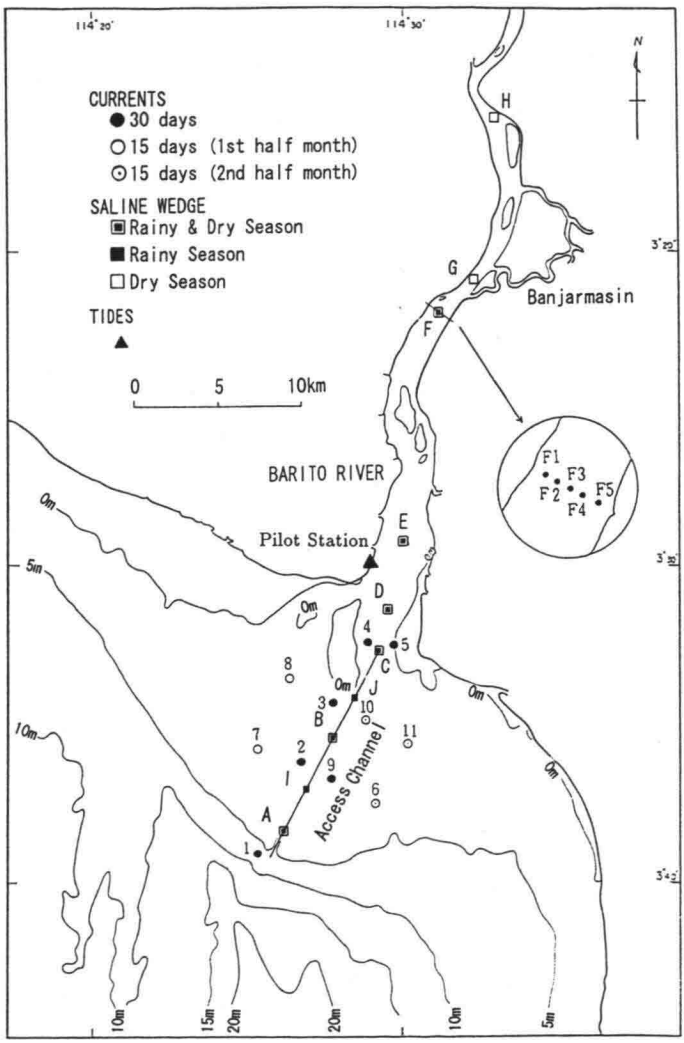

Fig. 2 Banjarmasin, Barito River, and Observation Points

The amount and characteristics of sediment carried to the estuary depend on the geology, the topography and the climate. If a large amount of fine sediments such as clay and silt are carried by river water, they flocculate and deposit in an estuary and a shallow tidal flat is usually formed in front of the river mouth. This phenomena is dominant in the rainy season in a tropical area.
To investigate the mechanism of siltation, many kinds of data should be collected such as river discharge, velocity, saline wedge, turbidity, tidal currents, waves, etc. Erosion from the bed and deposition mainly depend on the bed shear stress which will be a function of currents in the river and of both currents and waves in the sea area.
Natural condition survey in the present study consists of Yearlong Survey, Monthly Survey, General Survey, and Other Surveys. The contents of each survey are as follows;

2.1 Yearlong Survey

a) Tides
b) Wind
c) Waves

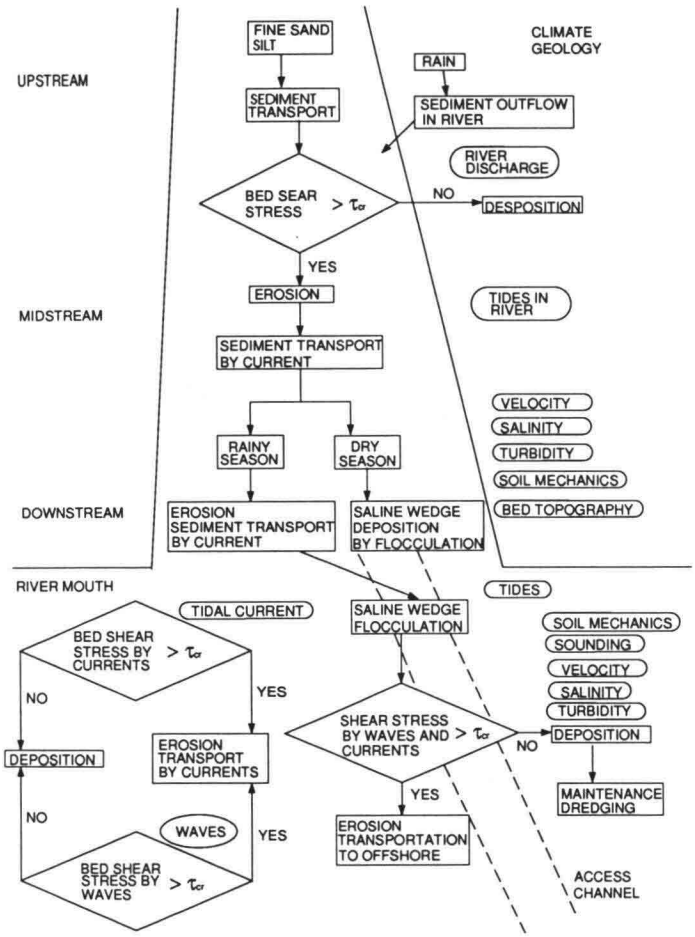

Fig. 3 Natural Conditions in Estuary and Field Survey Items

Tide and wind observations were carried out continuously for one year at the pilot station (**Fig.2**). A self-recording type tide gauge (LFT-III) was used to measure the tidal level near the river mouth. The tidal level at the offshore side was determined by the average value of the water depth measured continuously at 0.5 second interval for one minute burst every two hours by using the wave height recorder. It was installed at St.1 in **Fig.2**. The water depth here was 6 m. The harmonic analysis was made for the both data at the pilot station and St.1.
Wave height and wave direction were observed continuously for one year by using a self-recording wave height recorder (SSW-II) and an electro-magnetic current meter (EMC-108) at St.1 in **Fig.2**. Wave height and period were determined by zero-up crossing method. Dominant wave direction is considered to be the averaged direction of the measured orbital wave motion.

2.2 Monthly Survey

a) River Discharge
b) Saline Wedge
c) Bottom Material
d) Echo-sounding in Narrow Area

Measurements of river discharge were carried out along a transverse line at St.F as shown in **Fig.2**. Before the observation, water depth was measured along the line by an echo-sounding and five points of measurement (from F1 to F5) were set as shown in **Fig. 4**.

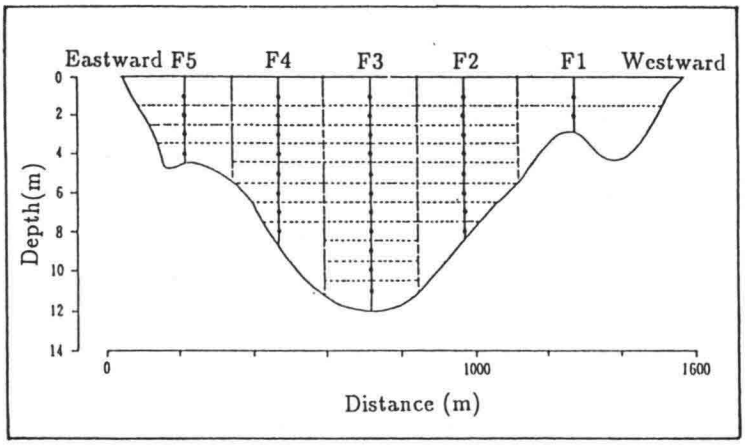

Fig. 4 River Discharge Survey Points on Line F

At each observation point, the velocity was measured at each location every 1 m below the water surface and 0.5 m above the bottom for 24 hours at an interval of 1 hour.
Saline wedge observations were carried out along the access channel and the river.
The points of observation are expressed in **Fig. 2** from St.A at the offshore side of the channel to St.H at the upstream side of the observation area in the river.
Current was measured with a current meter, salinity and water temperature with a salinometer, and turbidity with a turbid meter.
All these apparatuses are direct-reading type.
The total number of the observation point is 8 for both the dry and rainy season. In a dry season,

as saline wedge deeply intrudes in the river the points of measurement G and H were newly set instead of points I and J only for a rainy season. The saline wedge observation was carried out for 24 hours at every 1 hour. At each observation point, measurements were made vertically at every 1 m pitch from the water surface to the elevation 2 m above the bed and at every 0.5 m pitch downward from there to the bed.
Echo-sounding was carried out by using an echo-sounder (ATLAS DESO 10, Frequency: 33 kHz and 210 kHz) in the narrow area covering the access channel. Sounding lines were set at an interval of every 25 m transverse to the access channel. Tide corrections were made to the measured depths by using the observed tide data at the pilot station.

2.3 General Survey

a) Tidal Current Distribution
b) Buoy Tracking
c) Bottom Material, Salinity and Suspended Solids

The points of measurement for tidal currents are shown in **Fig. 2**. Solid circles show the points where 30 days measurement were conducted and open circles for 15 days.
The current meters which can measure the horizontal two components were installed 0.5 m above the seabed. The time of measurement is 2 minutes and 8 seconds and an interval of the measurement is 1 hour.
Current observations by buoy tracking survey near the mouth of the Barito River were conducted by tracking floats released from ships.
Bottom sampling was carried out by a grab type bottom sampler at 26 points and vane test was done onboard. The sampled bottom materials were analyzed for grain size distribution, water content, ignition loss, specific gravity, and cumulative distribution of grain size.

2.4 Others

a) Echo-sounding in Wide Area
b) Soil Boring
c) Seabed Level
d) Bottom Sampling

3. RESULTS

3.1 Tide, Wind and Waves

Figure 5 shows an example of measured time series of significant wave height, period, dominant wave direction, tide, and wind in the rainy season. From the measured wave data, frequency distributions of significant wave heights and period for the rainy, dry, and all seasons were obtained. In the dry season, significant wave height is less than 1 m. On the contrary, wave heights greater than 1 m sometimes appear in the rainy season as shown in **Fig. 5**.
The dominant direction of wave attacking is from the south (S) in the dry season and south-west (SW) in the rainy season. The total wave energy flux in the rainy season is approximately two times greater than that in the dry season.
Results of the tidal harmonic analysis in a year at the Pilot Station and St. 1 at the offshore side of

the access channel (see **Fig. 2**) are listed in **Table 1**. The diurnal component K_1 is dominant and the semi-diurnal component M_2 is the second largest one in the tidal flat area.

Table 1 Principal Four Tidal Constants at Pilot Station and St. 1

Position	Pilot Station				Station 1			
Components	K1	O1	M2	S2	K1	O1	M2	S2
Amplitude (cm)	59	30	32	2	63	33	32	4
Phase (deg.)	33	287	159	69	331	282	139	63

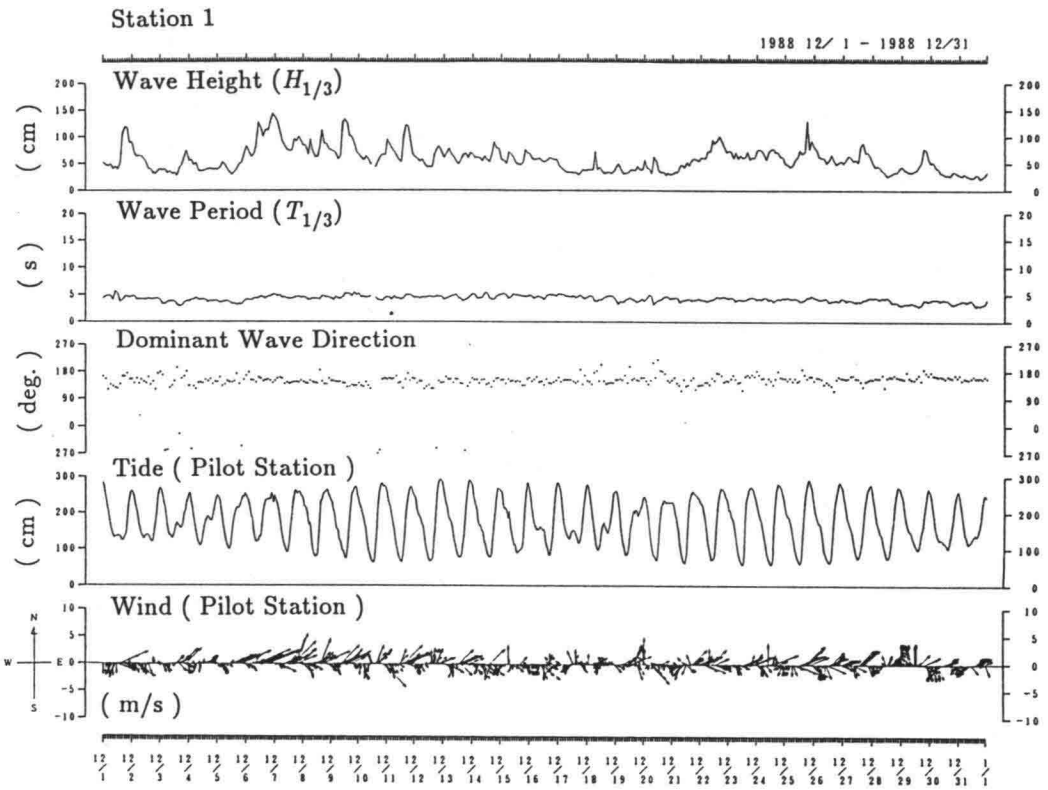

Fig. 5 Time Series of Measured Waves, Tide and Wind

3.2 River Discharge

The water surface elevation measured at the Trisakti wharf at Banjarmasin port about 26 km upstream from the river mouth, and the river discharge measured at the observation station F during the river discharge survey (25 hours continuous observation) are shown in **Fig. 6** as a representative case of the rainy season.

The total transportation quantity of suspended materials passing through the section F is also estimated by adding up the multiplied value of the current velocity and SS concentration at each segment in **Fig. 4**. The result is shown in the lowest section in **Fig. 6**.
The daily variation of the river discharge shows the strong flow-out except in the flood tide. The

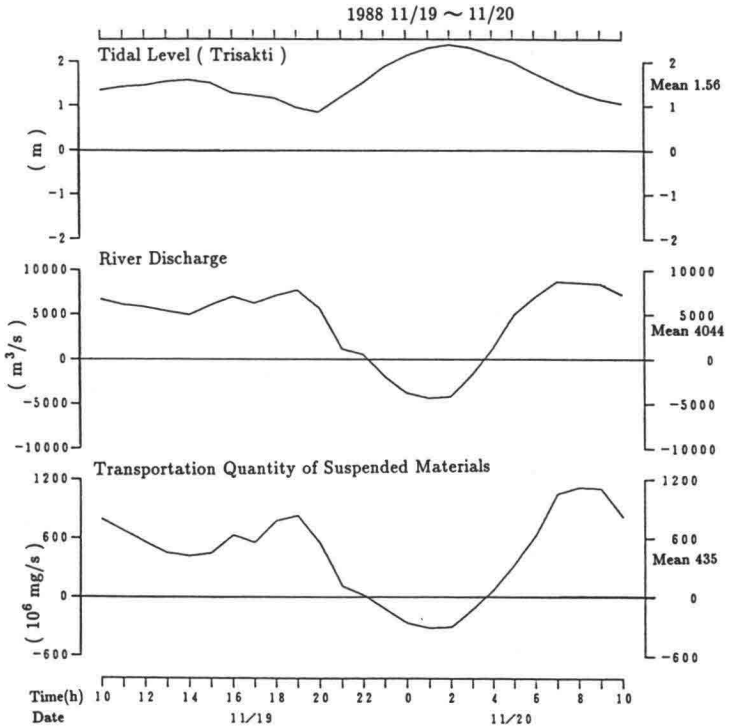

Fig. 6 Time Series of Tidal Level, River Discharge, and Transportation Quantity of Suspended Materials (1988. 11.19~20)

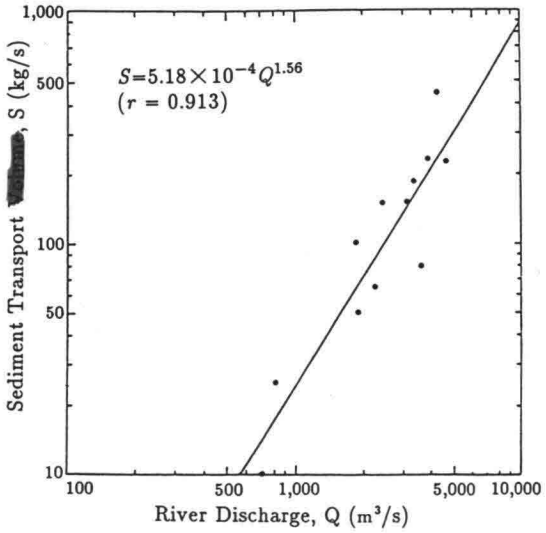

Fig. 7 Daily Mean River Discharge and Transportation Quantity of Suspended Materials

daily mean river discharge is 4,044 m^3/s. The maximum flow-out volume reaches 8,696 m^3/s which is about two times larger than the daily mean discharge.
Although the measured data in the dry season are not shown, the daily mean river discharge in August 1,989 is 731 m^3/s which is about one sixth of the discharge in the rainy season.
Figure 7 shows the relationship between the daily mean river discharge and the transportation quantity of suspended materials.

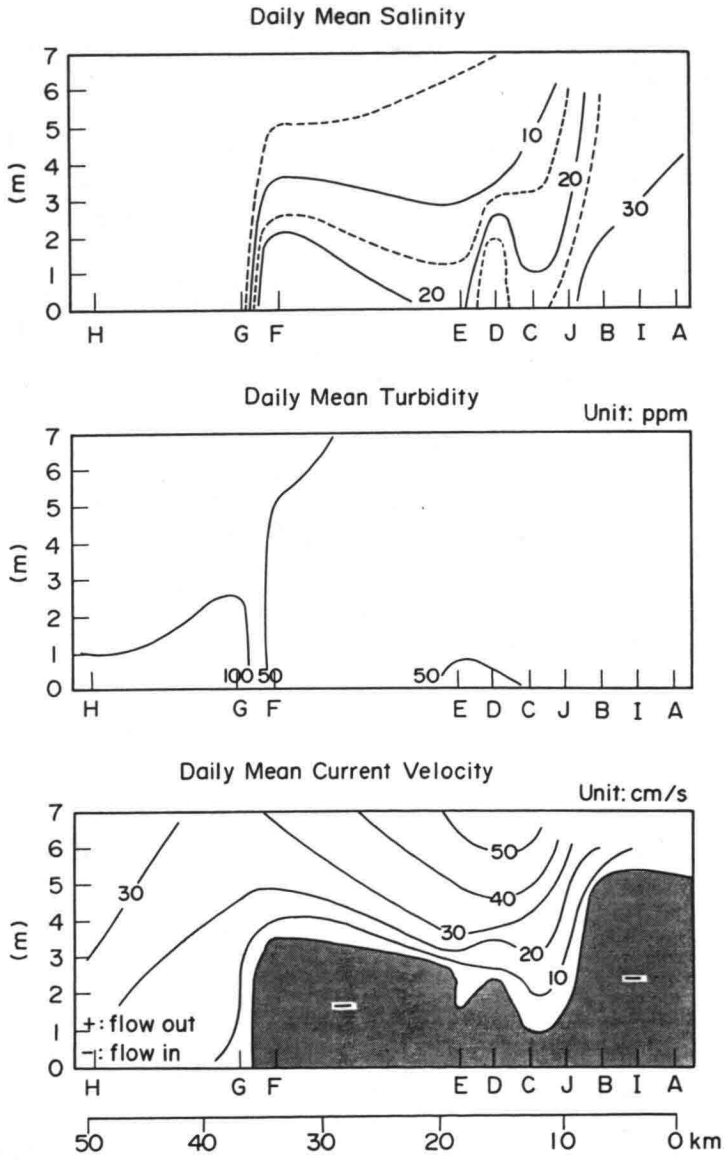

Fig. 8 Distributions of Daily Mean Salinity, Turbidity, and Velocity along River and Access Channel (Dry Season, 10th and 15th Oct. 1988)

In the rainy season, the roughly estimated sediment transport rate W by river water will be

$W = 450$ kg/s,
$= 1.2$ million ton/month,

which is equivalent to a mud volume of 1.7 million m^3/month with a bulk density of 1.45 ton/m^3

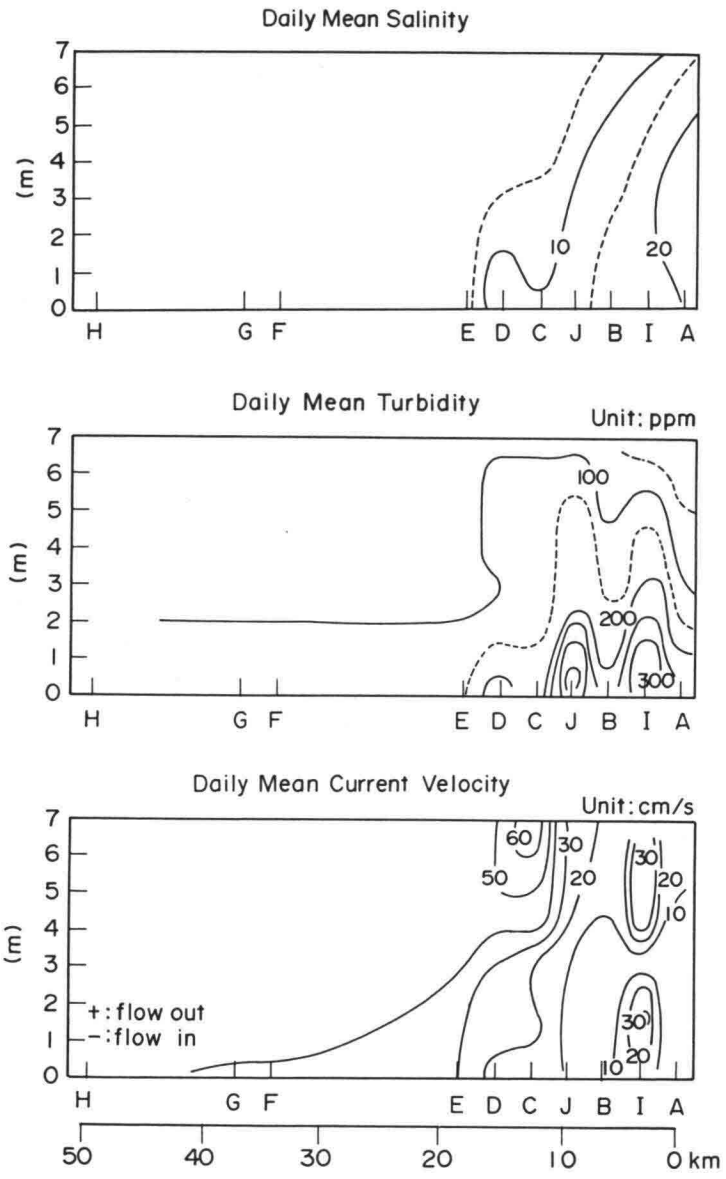

Fig. 9 Distributions of Daily Mean Salinity, Turbidity, and Velocity along River and Access Channel (Rainy Season, 10th and 13th Dec. 1988)

and a water content of 110%.

3.3 Saline Wedge

The import factor of siltation in estuaries is the turbidity maximum. This area generally locates near the head of the salt intrusion. The suspended sediment concentration near the zone is higher than that in the river or that further seaward in the estuary (*Dyer* (1988)).
Saline wedge surveys were carried out from September 1988 to August 1989 once a month. Vertical distributions of salinity, turbidity, and velocity along the river and the access channel axis averaged in a day are expressed in **Figs. 8** and **9** for the dry and rainy season, respectively. In the dry season (**Fig. 8**), the front of saline wedge deeply intrude in the river at St.G near Trisakti wharf in Banjarmasin Port.
The structure of the saline wedge from St.C in the river mouth to St.G shows a weakly mixed-type. The maximum daily mean turbidity shows 100 ppm near the head of salt intrusion. The height of the saline wedge near the head is approximately from 2 to 3 m. The river water overrides the saline wedge of which velocity is negative (to the upstream direction) as indicated in the daily mean current velocity in **Fig. 8**.
A typical observation results in the rainy season are expressed in **Fig. 9**. With regard to the salinity distribution in the rainy season, a front of salinity of the level 20 is pushed away to the offshore end of the access channel owing to the increased river water discharge. The saline wedge in the access channel shows a well mixed-type.
The daily mean turbidity reaches 300 ~ 350 ppm in the offshore region of the access channel. There is no inflow of sea water in the river and access channel in the rainy season.

3.4 Bathymetric Change in the Access Channel

Sounding in the access channel was carried out from Oct. 1988 to Aug. 1989 about once a month for a total of twelve times. The sounding area (0.3×15 km) covers the access channel and sounding lines are at intervals of 25 m transverse to the access channel.
The distance is measured from the offshore side of the access channel. The location of measurement is expressed as the distance from the offshore side (in metric unit). Therefore, the location at the onshore side of the access channel is represented as 14,000.
The longitudinal channel bottom profiles along the center line and 100 m west and east side, from the 5th to 7th stage during the intermission period of dredging are expressed in **Fig. 10**.
The 5th to 7th stage observations are from February 28th to May 24th, 1989. The duration of the intermission period of dredging is 85 days.
At the 6th and 7th stage, two surfaces of the seabed appeared in the reflected planes along the center line. The upper reflected planes are for the 210 kHz sounding and the lower ones are for the 33 kHz sounding. At the 6th stage, the upper surface for the 210 kHz echo shows some scatter, but at the 7th stage the upper surface appears over most of the area in the access channel. At the 7th stage, the discrepancies between the two reflected planes are about 2~3 m and are presumed to show a fluid mud layer.
In the upper figure in **Fig. 10** a very shallow area exists near Sp. 11,000. This shallow area is formed in front of the river mouth because of the sudden decrease in the river current velocity and of the effects of waves mainly attacking from south-west. Grain size here is coarser than that in another area. The median diameter is greater than 1,000 μm (*Tsuruya et. al.* (1992)). In the east side of the channel, on the contrary, the area from Sp. 5,000 to 9,000 is shallower than the west

side. This important feature can be confirmed by **Fig. 11**. The seabed level in the west of the channel at Sp. 10750 is about 2 m higher than that in the east. However, from Sp. 9,750 to Sp. 4,750, the seabed level in the east is higher than that in the west. The river flow shows meandering in accordance with these shallow area.

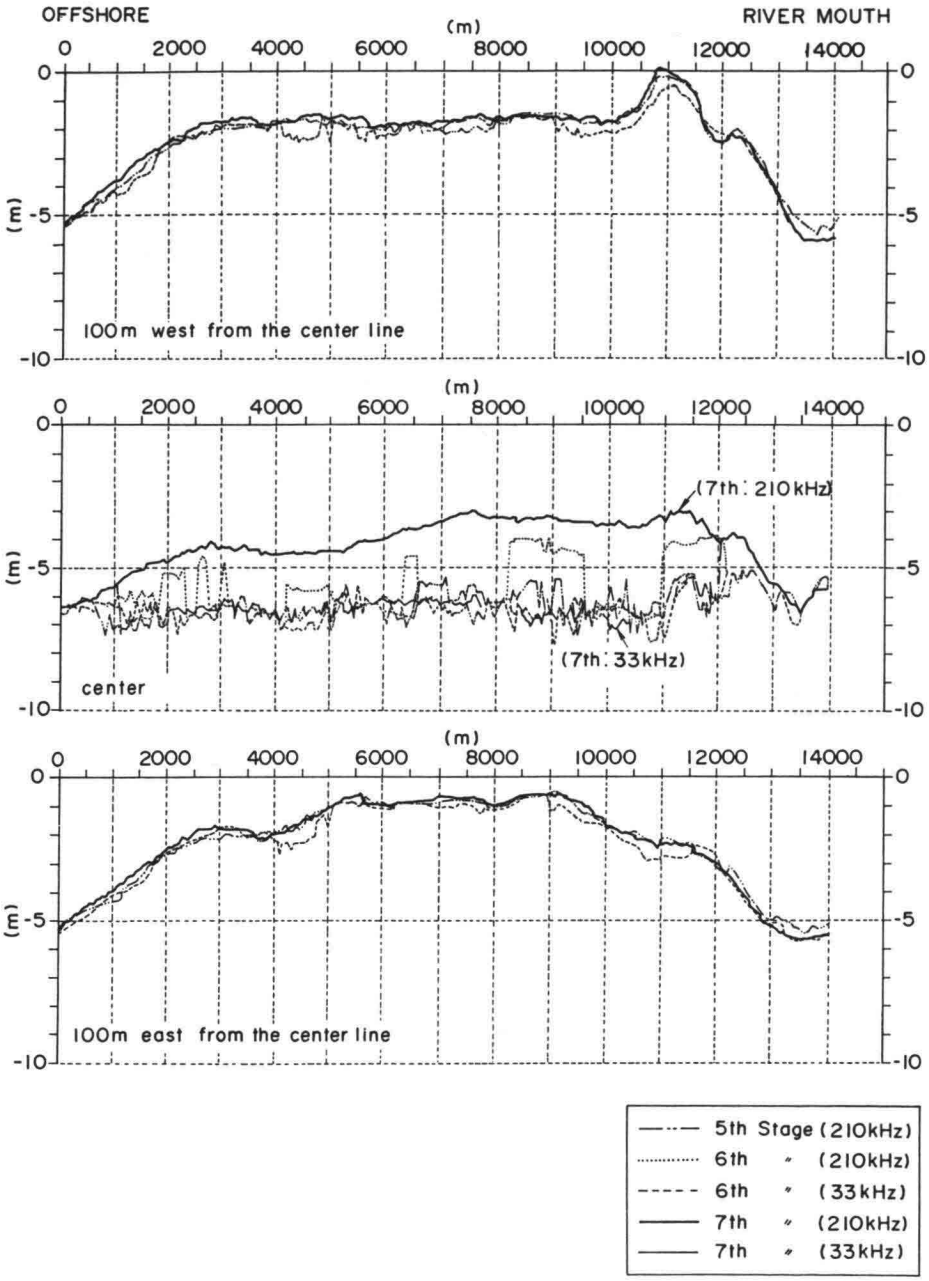

Fig. 10 Longitudinal Bed Profile in Access Channel

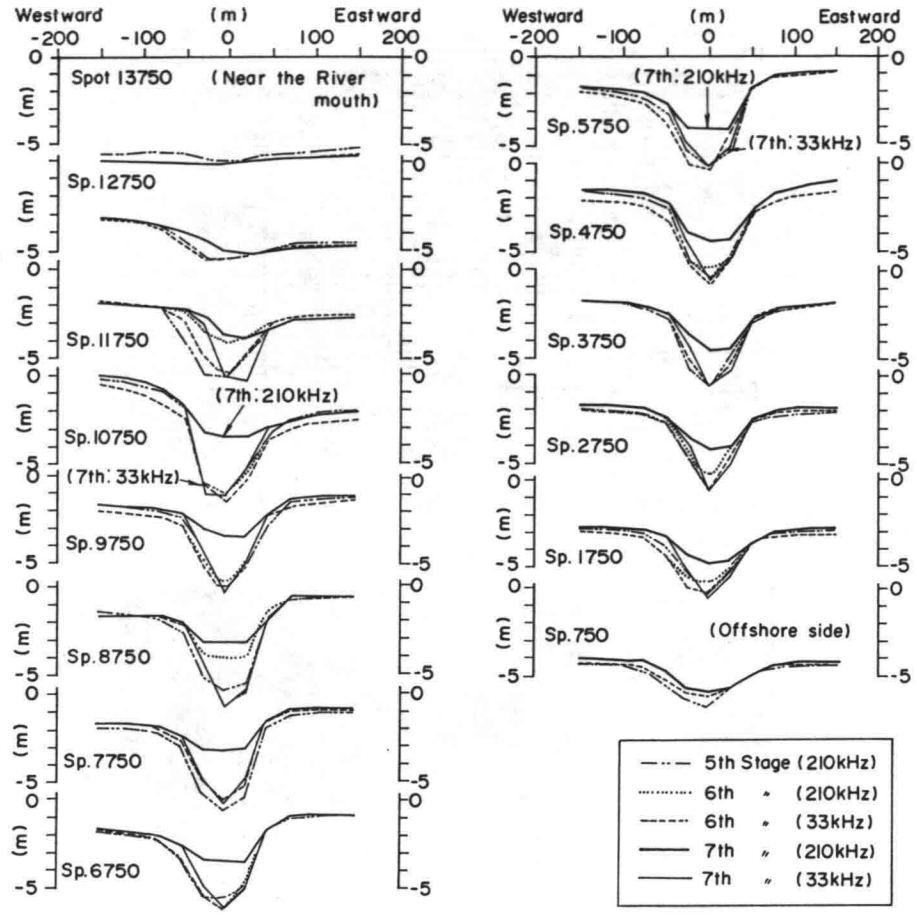

Fig. 11 Lateral Profile of Access Channel

3.5 Fluid Mud and Siltation Volume in the Access Channel

As explained in the previous section, a fluid mud layer was detected from the echo sounding. **Figure 12** shows a record of cross-sectional echo soundings with 210 and 33 kHz emitters at Sp. 5,000. The measurement was conducted 2.5 months after the completion of dredging works. It was confirmed that the bottom level detected by a lead was nearly coincident with the 33 kHz reflected level. The surface of the 210 kHz echo sounding near the center of the channel is nearly horizontal and slopes on both sides of the channel suggest that a dense layer is flowing in from both sides of the channel. **Photo 2** shows bottom mud sampled on the flat 4.5 km onshore from the offshore side of the access channel and about 1 km east from the channel. The water depth here is 3.1 m. On the black-colored relatively hard mud layer at the seabed sampled by a grab-type sampler, there is a brown-colored fresh mud layer of which thickness is about 2 cm.

The color of this fluid mud layer is similar to that of the river water. It can be considered that this type of dense and movable fluid mud layer is the main cause of siltation in the access channel.

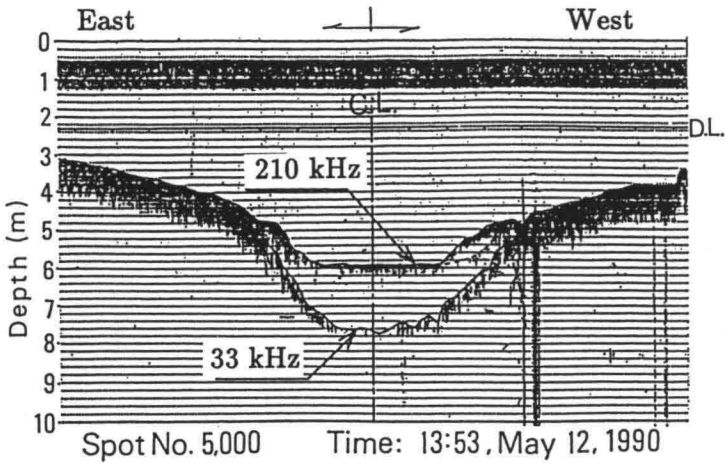

Fig. 12 Fluid Mud Layer Recorded by Echo Sounder

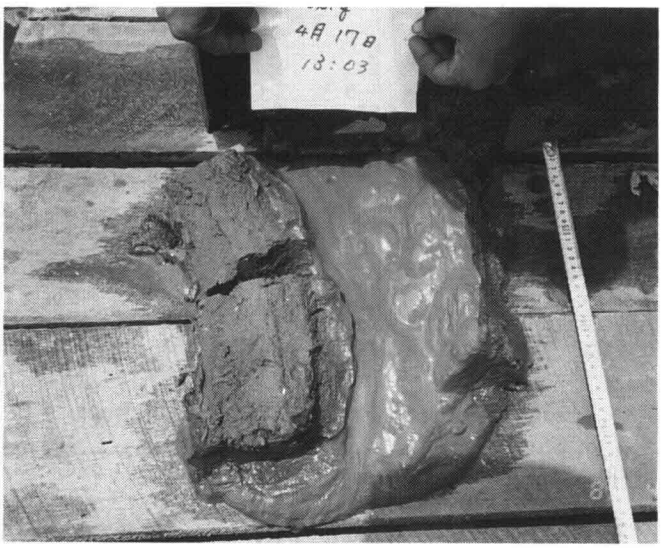

Photo 2 Sampled Bottom Mud and Movable Fluid Mud

Figure 13 shows vertical distributions of bulk density, current velocity, salinity, and temperature measured at the center of the access channel of Sp.10,000 on May 15, 1990. The measurement of bulk density was made with a bamboo sampler which consists of separate segments with a length of about 50 cm. For each bamboo segment, a hole was made at an upper part, and many pieces of adhesive tape linked with a thread covered the holes. After the bamboo was inserted in a mud layer vertically, the thread was pulled away and mud was sampled layer by layer. At the same time, echo sounding and lead level test were conducted. The upper most surface layer consists of mainly river water with a salinity of less than 10. Below this layer down to the depth just above the 210 kHz surface, there is sea water layer. Then underneath this echo surface, there is a bottom layer in

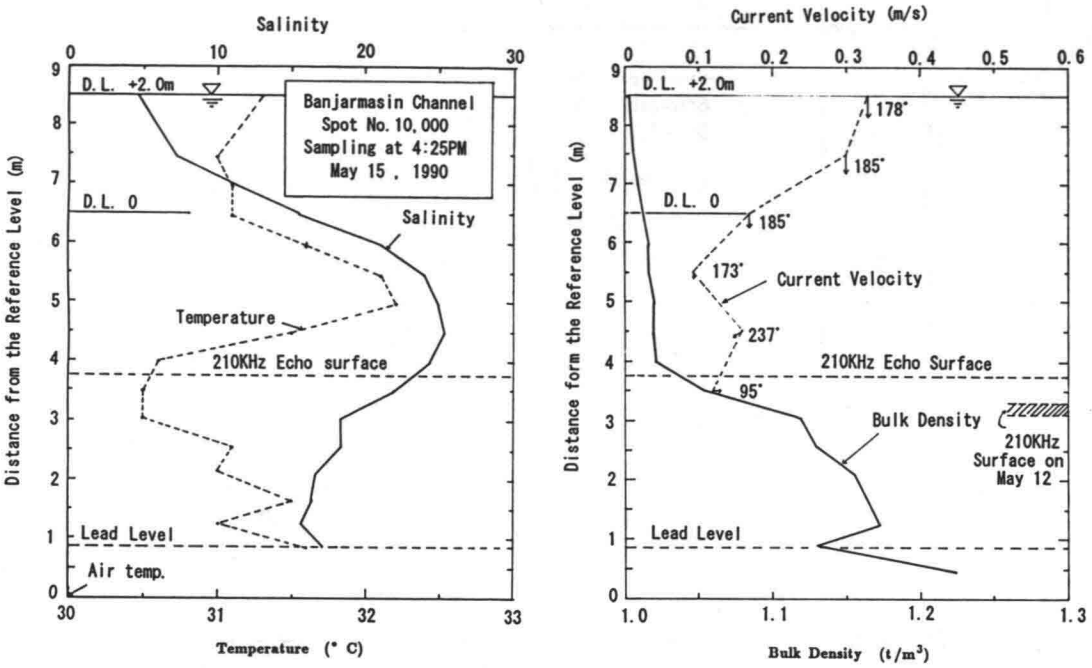

Fig. 13 Vertical Distribution of Fluid Mud in the Channel

which the bulk density increases sharply from around 1.02 to over 1.20 t/m^3. The surface of this layer is just the sea water containing suspended materials, and the bottom is very soft mud. The layer has a thickness of about 3 meters in this measurement. This is the fluid mud. Fluid mud is defined by *Krone* (1962) as having a suspended solids SS of more than 10,000 ppm, and by *Kirby and Parker* (1974) as when the bulk density γ_t is 1.05 t/m^3 $\leq \gamma_t \leq$ 1.3 t/m^3.
The echo sound with 210 kHz frequency is reflected near the upper boundary of the fluid mud layer, because of the sharp and large change in density of acoustic impedance. It sometimes disappears due to disturbances and mixtures of the sea water and fluid mud, which are caused by ships' propellers. It is to be noted that the boundary most possibly moves up and down according in accordance with the movement of the fluid mud due to the action of a shear stress of the upper current in the sea water, gravity force, etc.

During the intermission period of dredging from march to May 1989, the siltation process in the access channel was monitored by means of a echo-sounder with 210 kHz and 33 kHz as previously mentioned in **3.4.**
Longitudinal distributions of siltation volumes for each section 500 m along the channel and ±50 m in transverse direction from the center are shown in **Fig. 14.** The total volume of siltation during the period is about 1,730,000 m^3 within a width of 100 m. The amount of harder materials detected by 33 kHz, however, is rather small: 320,000 m^3 in total, of which approximately 150,000 m^3 or 46 % of the total, is between Spots 11,000 and 13,000.

4. CONCLUSIONS

Main conclusions of the present study are summarized as follows:

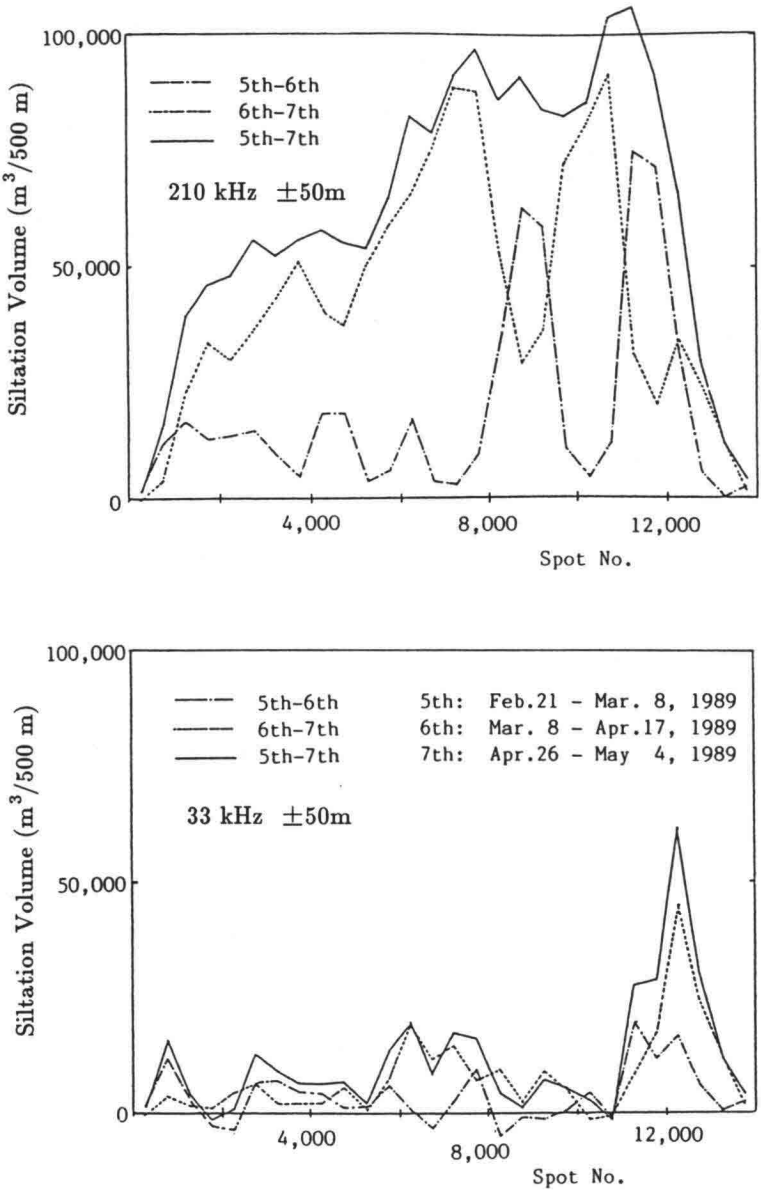

Fig. 14 Siltation Volume along the Channel Axis (width ±50 m)

1) The relationship between the daily mean river discharge and the transportation quantity of suspended materials is obtained. In the rainy season, the sediment transport rate by river is about 1.2 million ton/month, which is equivalent to a mud volume of 1.7 million m^3/month with a bulk density of 1.45 ton/m^3.

2) Saline wedge deeply intrude in the Barito River and shows a weakly mixed-type in dry season. In rainy season, on the contrary, a front of salinity of the level 20 is pushed away to the offshore end of the access channel owing to the increased river discharge. The saline wedge in the access channel shows a well mixed-type.

3) Fluid mud was observed in and around the access channel which is the main source of siltation. During the intermission period of dredging in 85 days, the total volume of siltation is estimated. The estimated volume of siltation is 1,730,000 m^3 for the 210 kHz echo sounding data. The amount of harder materials detected by 33 kHz is rather small: 320,000 m^3 in total, of which approximately 150,000 m^3 or 46% of the total, is between Spots 11,000 and 13,000.

ACKNOWLEDGEMENTS

The authors are greatly indebted to Japan International Cooperation Agency for the support of the present study in connection with "The Study on Maintenance Dredging in the Access Channel of Banjarmasin Port in The Republic of Indonesia".
We also should like to express our grateful thanks to the members of the Directorate General of Sea Communications of the Government of Indonesia and those of the Study Team organized by the Overseas Coastal Area Development Institute of Japan.

REFERENCES

Dyer, K. R. (1988): Fine Sediment Particle Transport in Estuaries, Physical Process in Estuaries, Springer-Verlag, pp.295-310.

Kirby, R. and W. R. Parker (1974): Seabed Density Measurements Related to Echo Sounder Records, The Dock and Harbour Authority, Vol. LIV, No. 641, pp. 423-424.

Krone, R. B. (1962): Flume Studies of the Transport of Sediment in Estuarial Shoaling Processes, University of California Hydraulic Engineering Lab. and Sanitary Research Lab., Barkeley, 110p.

Tsuruya, H., K. Murakami, I. Irie and K. Katoh (1992): Siltation Study in a Long Approach Channel on Large Scale Muddy Tidal Flat, Proc. of 23rd Int. Conf. on Coastal Eng., ASCE, pp.2879-2892.

HYDRO-PORT'94
International Conference on Hydro-Technical
Engineering for Port and Harbor Construction
October 19 - 21, 1994, Yokosuka, Japan

Modelling Cohesive Sediment Transport in Tidal Waters

K.P.P. Pathirana
C.S. Yu
J. Berlamont

Laboratory of Hydraulics, Katholieke Universiteit Leuven
de Croylaan 2, B-3001 Leuven

ABSTRACT

A two-dimensional, depth-averaged, finite element transport model has been developed which simulates the cohesive sediment transport in estuaries and coastal waters. The cohesive sediment processes in coastal enviornment are incorporated in the transport model. The transport model is driven by a two-dimensional, depth-averaged, finite difference hydrodynamic model. The model results have been verified by the experimental data obtained from laboratory flume studies on cohesive sediment transport under uniform and alternating currents. The complete model has been applied to the Western Scheldt estuary and the results have been presented.

Key Words: Suspended Sediments, Settling Velocity, Deposition, Erosion

1. INTRODUCTION

The behaviour of cohesive sediments in estuaries is rather complex as they are strongly affected by the hydrodynamic field, the chemical composition of suspending fluid and the physio-chemical properties of sediments (Mehta, 1986). The suspended clay particles become more cohesive as the salinity of the sediment suspending waters increases and the collision of cohesive particles with each other, can result in the formation of much larger aggregates. These larger aggregates generally possess higher settling velocities relative to those of individual sediment particles which eventually lead to higher siltation rates. Therefore, cohesive sediments entered an estuary, undergo various processes including, flocculation/ aggregation, deposition, consolidation, erosion and advective and dispersive transport which are typically linked by the nature of the tidal flow.

Problems related to fine, cohesive sediments in estuarine environments can be broadly classified into two major categories. The first one relates to erosion, transport and deposition dependent processes, and the consequences include the erosion and sedimentation of estuarine navigation

channels, harbours and waterways. The second category refers to the role of cohesive sediments in transporting contaminants in estuarine waters, and the degradation of water quality that is being used for consumption or recreational purposes. The understanding of these problems and their quantification for engineering purposes can be accomplished by modelling the movement of cohesive sediments in estuarine waters.

In recent years, there has been an increasing emphasis on using numerical models to study a wide range of flow and transport problems rather than physical models. This paper describes a two-dimensional, depth-averaged, finite element transport model which simulates the temporal and spatial distribution of cohesive sediments and bed level changes in estuaries and coastal waters. As the cohesive sediments have low settling velocities, these particles are highly sensitive to hydrodynamic field. Therefore, the flow fields must be simulated with a reasonable accuracy. The proposed transport model is driven by a two-dimensional, depth-averaged, finite difference flow model based on a falsified alternating direction implicit (FADI) solution method. The model predictions are quite reasonable and are discussed in this paper.

2. FLOW MODEL

The classical shallow water equations are generally used to describe the flow in estuaries and coastal waters. The two-dimensional, depth-averaged shallow water equations can be written on the Cartesian plane as;

$$\frac{\partial u}{\partial t} + u\frac{\partial u}{\partial x} + v\frac{\partial u}{\partial y} - fv = -g\frac{\partial \zeta}{\partial x} - \frac{\tau_{bx}}{\rho H} + \frac{\partial}{\partial x}(\nu_h \frac{\partial u}{\partial x}) + \frac{\partial}{\partial y}(\nu_h \frac{\partial u}{\partial y}) \tag{1}$$

$$\frac{\partial v}{\partial t} + u\frac{\partial v}{\partial x} + v\frac{\partial v}{\partial y} + fu = -g\frac{\partial \zeta}{\partial y} - \frac{\tau_{by}}{\rho H} + \frac{\partial}{\partial x}(\nu_h \frac{\partial v}{\partial x}) + \frac{\partial}{\partial y}(\nu_h \frac{\partial v}{\partial y}) \tag{2}$$

and the conservation of mass,

$$\frac{\partial \zeta}{\partial t} + \frac{\partial (Hu)}{\partial x} + \frac{\partial (Hv)}{\partial y} = 0 \tag{3}$$

Where, t = time (s), ζ = water surface elevation with respect to mean sea level (m), H = total water depth (m), u,v = mean velocity components along the x and y directions (m s^{-1}), f = Coriolis parameter (s^{-1})(= $2\omega \sin \phi$), g = acceleration due to gravity (m s^{-2}), ρ = density of water (Kg m^{-3}), ν_h = kinematic eddy viscosity ($m^2 s^{-1}$), τ_{bx} and τ_{by} = shear stresses due to bottom friction in the x and y directions (N m^{-2}).

The shear stresses due to bottom friction are computed using the quadratic friction law, and are illustrated below.

$$\tau_{bx} = \frac{\rho g\, u \left(\sqrt{u^2 + v^2}\right)}{C_h^2} \quad ; \quad \tau_{by} = \frac{\rho g\, v \left(\sqrt{u^2 + v^2}\right)}{C_h^2} \tag{4}$$

Where C_h is the Chezy coefficient which can be estimated in shallow estuaries, using the Manning's coefficient n as;

$$C_h = \frac{H^{\frac{1}{6}}}{n} \tag{5}$$

2.1 The FADI-Model

The FADI (Falsified Alternating Direction Implicit) model has been constructed based on the conventional ADI scheme [Dronkers, 1969], which is a six equation scheme, but further simplified into a four equation solution [Yu, 1993]. The simplification has been carried out by falsifying the continuity equation into two falsified difference equations. The governing differential equations are splitted into two sets of two difference equations in both x- and y-directions respectively. The difference forms of the equations are discretized on a fully staggered C-type grid. The computations proceed first with the momentum equation in the x-direction:

$$\frac{u_{i-1/2,\,j}^{n+1} - u_{i-1/2,\,j}^{n}}{\Delta t} + (adv)^n + g\,\frac{\zeta_{i,\,j}^{*} - \zeta_{i-1,\,j}^{*}}{\Delta x} - f\,\overline{v}^{\,n} + \frac{\tau_{bx}^{n}}{\rho\, H} = 0 \tag{6}$$

and the falsified continuity equation :

$$\frac{\zeta_{i,\,j}^{*} - \zeta_{i,\,j}^{n}}{\Delta t} + \frac{(h+\zeta_{i+1/2,\,j}^{n})\, u_{i+1/2,\,j}^{n+1} - (h+\zeta_{i-1/2,\,j}^{n})\, u_{i-1/2,\,j}^{n+1}}{\Delta x} = 0 \tag{7}$$

where i and j are the space indices in x and y direction respectively; n and n+1 indicate the old and new time-levels; the * shows a transient stage of the falsified continuity equation which has to be further integrated to another transient stage to get consistency with the original differential equation. This is followed by solving the following set of equations in the y- direction:

$$\frac{v_{i,\,j-1/2}^{n+1} - v_{i,\,j-1/2}^{n}}{\Delta t} + (adv)^n + g\,\frac{\zeta_{i,\,j}^{n+1} - \zeta_{i,\,j-1}^{n+1}}{\Delta y} + f\,\overline{u}^{\,n+1} + \frac{\tau_{by}^{n}}{\rho\, H} = 0 \tag{8}$$

and

$$\frac{\zeta_{i,\,j}^{n+1} - \zeta_{i,\,j}^{*}}{\Delta t} + \frac{(h+\zeta_{i,\,j+1/2}^{*})\, v_{i,\,j+1/2}^{n+1} - (h+\zeta_{i,\,j-1/2}^{*})\, v_{i,\,j-1/2}^{n+1}}{\Delta y} = 0 \tag{9}$$

Both sets of difference equations are formulated implicitly. These sets of equations can also be re-arranged into a set of tridiagonal systems. These sets of tridiagonal systems can be solved efficiently by using the ``*Thomas algorithm*". Since there are only two sets of four implicit

equations to be solved, the computational cost is much reduced as compared to the six-equation ADI scheme.

3. TRANSPORT MODEL

The concentration of suspended sediment is assumed to be low, so that the influence of sediment particles on the flow field can be neglected. This allows the sediment transport model to be decoupled and run independently of the flow model. In the transport model, the advection-dispersion equation is solved with an appropriate sink and source term which represent the sediment exchange rates at the bed.

Assuming that the cohesive sediments are well mixed throughout the water depth, the advective and dispersive transport of suspended sediments in a turbulent flow field are described by;

$$\frac{\partial C}{\partial t} + u\frac{\partial C}{\partial x} + v\frac{\partial C}{\partial y} = \frac{1}{H}\frac{\partial}{\partial x}\left[HD_x\frac{\partial C}{\partial x}\right] + \frac{1}{H}\frac{\partial}{\partial y}\left[HD_y\frac{\partial C}{\partial y}\right] + S \qquad (10)$$

Where, C = concentration of suspended sediment (Kg m^{-3}), D_x and D_y = sediment dispersion coefficients in the x and y directions respectively (m^2 s^{-1}), and S = sink-source term (Kg m^{-3} s^{-1}). The sink-source term represent the sediment exchange processes at the bed, and can be expressed as;

$$S = \left[\frac{\partial C}{\partial t}|_e + \frac{\partial C}{\partial t}|_d\right] \qquad (11)$$

Where, $[\partial C/\partial t]_e$ is the rate of sediment erosion from the bed (*i.e.* source) and $[\partial C/\partial t]_d$ is the rate of sediment deposition (*i.e.* sink).

A bed is considered to be composed of a number of layers of known thickness, each having a specified density. A correlation between bed density and shear strength has to be specified so that the bed shear strength can be determined at each bed elevation during simulation. This provides a reasonable estimation of erosion rates on sediment beds. Due to the complexities of sediment processes in estuarine environments, the majority of investigations, particularly on settling, deposition and erosion, have been oriented towards the laboratory. Thus, the rate expressions related to these sediment processes are developed based on experimental investigations. The algorithms used to quantify the different sediment transport processes, are illustrated in the next section.

3.1 SEDIMENT PROCESSES

3.1.1 Erosion

Three modes of erosion have been identified, namely, *surface erosion, mass erosion* and *re-entrainment of a high density suspension* (Mehta, 1988). Surface erosion is particularly evident in low concentration environment and is prevalent in estuaries subject to currents of low to

moderate strength. At higher concentrations, under strong tidal currents and also under storm generated flows, mass erosion is dominant (Mehta, 1986).

The erosion rate ε, can be expressed in terms of the time-rate of change of the suspension concentration $[\partial C/\partial t]$, as;

$$\epsilon = H \frac{\partial C}{\partial t} ; \qquad (Kg\ m^{-2}\ s^{-1}) \qquad (12)$$

Where H is the total depth of water. Various erosion rate expressions are reported in the literature based on many laboratory experiments which have been carried out on different states of cohesive sediment beds. For *dense, consolidated* cohesive beds, the rate of erosion can be reasonably described by the following relationships (Ariathurai and Arulanandan, 1978);

$$\frac{\partial C}{\partial t} = M \left[\frac{\tau_b}{\tau_{ce}} - 1 \right] ; \qquad \tau_b \geq \tau_{ce} \qquad (13)$$

$$\frac{\partial C}{\partial t} = 0 ; \qquad \tau_b < \tau_{ce} \qquad (14)$$

Where M is an erosion constant (Kg m^{-2} s^{-1}), τ_b is bed shear stress (Nm^{-2}) and τ_{ce} is the critical shear stress for erosion (Nm^{-2}). The magnitude of these parameters vary with the type of sediment, water content, total salt concentration, ionic composition in the water, pH and temperature. Although the consolidation of sediment beds has a certain influence on the erosion rates at the bed particularly for long term simulations, the consolidation process is not presently considered in this study.

For *soft, partially consolidated* cohesive sediment beds, the following empirical relationship has been recommended to estimate the erosion rates (Parchure and Mehta, 1985) instead of Eq.(13);

$$\frac{\partial C}{\partial t} = \epsilon_0 \exp\left[\alpha(\tau_b - \tau_{ce})^{\frac{1}{2}}\right] ; \qquad \tau_b \geq \tau_{ce} \qquad (15)$$

Where, ε_0 and α are empirical constants which are also dependent on the same physio-chemical factors as M and τ_{ce} in Eq.(13). This exponential form of the erosion rate expression is particularly suitable for estimating the erosion rates on slake water deposits.

3.1.2 Deposition

The depositional behaviour of fine, cohesive sediments is distinctly different from that of cohesive sediments. This distinction arises primarily due to the effect of flocculation of cohesive particles. After performing a series of depositional experiments in a straight, recirculating flume using San Francisco Bay mud, Krone(1962) proposed the following deposition law;

$$\frac{\partial C}{\partial t} = \frac{W_s C}{H}\left[1 - \frac{\tau_b}{\tau_{cd}}\right]; \qquad \tau_b < \tau_{cd} \tag{16}$$

Where W_s is the settling velocity of sediment particles (ms^{-1}) which depends on the concentration, and τ_{cd} is the critical shear stress for deposition (Nm^{-2}).

The deposition law given in Eq.(16) implies that all initially suspended sediments must eventually deposits when $\tau_b < \tau_{cd}$, and no deposition occurs when $\tau_b \geq \tau_{cd}$. However, a log-normal relationship proposed by Mehta and Partheniades (1973) for the determination of deposition rates, is an extension to the deposition law proposed by Krone (1962). The log-normal relationship is based on the concept of equilibrium concentration (C_{eq}) which mainly represents a partial deposition of suspended sediments when the bed shear stresses higher than the critical shear stress for deposition. The log-normal deposition law can be briefly illustrated as (Mehta and Partheniades, 1973);

$$\frac{\partial C}{\partial t} = -\left[1 - erf\left(\frac{1}{\sigma_1\sqrt{2}}\log_{10}\left[\frac{(\tau_b^*-1)}{(\tau_b^*-1)_{50}}\right]\right)\right]\cdot$$

$$\left[\frac{0.434\ \exp\left(\frac{-T^2}{2}\right)}{2\sqrt{2\pi}\ t\ \sigma_2}\right]C_0\ ; \qquad \tau_b \geq \tau_{cd} \tag{17}$$

where, $T = \log_{10}\left[\frac{t}{t_{50}}\right]^{\frac{1}{\sigma_2}}$, $\tau_b^* = \frac{\tau_b}{\tau_{bmin}}$, $(\tau_b^*-1)_{50} = 4\ \exp(-12.7\tau_{bmin})$, C_0 = initial suspended sediment concentration, *erf*= error function, t_{50} = time required for deposition of 50% of the depositable sediments, τ_{bmin} = bed shear stress below which all suspended sediments eventually deposits, σ_1 = standard deviation of a plot of C_{eq}^* against (τ_b^*-1) on log-probability coordinates, σ_2 = standard deviation of a plot of C^* versus t/t_{50} on log-probability coordinates, $C_{eq}^* = \frac{C_{eq}}{C_0}$ and $C^* = \frac{1}{2}\left[1 + erf\left(\frac{T}{\sqrt{2}}\right)\right]$.

3.1.3 Settling velocity

Settling velocity is an important parameter in estuarine sediment transport as it greatly influences the deposition rates. Settling velocities of cohesive sediments are properties of a

suspension rather than on grain size. Three types of settling have been identified based on suspension concentration which represent the effect of particle flocculation in estuarine waters (Mehta, 1986).

$$W_s = Constant \; ; \qquad C < C_1 \tag{18}$$

$$W_s = K_1 C^n \; ; \qquad C_1 \leq C \leq C_2 \tag{19}$$

$$W_s = W_{s0}(1 - K_2 C)^{\beta} \; ; \qquad C > C_2 \tag{20}$$

Where, K_1, n, K_2 and β are empirical constants dependent on the sediment composition and the turbulent structure of the suspending flow field. W_{s0} is a reference settling velocity. The concentration ranges C_1 and C_2, generally depend on the type of sediment-fluid mixture. In-situ measurements on settling velocities are very important for the predictive transport modelling as they are particularly sensitive to the hydrodynamic condition. The settling velocity - concentration relationship (Eq.(19)) varies considerably between estuaries, which may be the result of floc density or organic content variations and different tidal situations (Dyer, 1989). It is, therefore, important to estimate appropriate values of settling velocities to be used in numerical modelling.

3.2 SOLUTION TECHNIQUE

The finite element technique is used to solve the depth-averaged advection dispersion equation in the transport model by applying the Galerkin's weighted residual method. Nine nodes, quadrilateral elements are chosen to discretize the domain. The mixed interpolation is adopted where the concentration of suspended sediments and the velocity components, are approximated using quadratic polynomials and linear approximation is used for the water depths. Time descritization is performed using a finite difference scheme. The Crank-Nicholson scheme shows improved results than that of the first order implicit scheme for the advection dispersion equation (Pathirana, 1994). The frontal technique is chosen as the solution technique. This solution method generally overcomes the problem of large memory requirement, however, this significantly increases the computational costs for large scale simulations. To overcome this problem, the applicability of parallel computers in estuarine sediment transport simulations, has also been investigated (Pathirana, 1992).

The hydrodynamic data, two velocity components (u,v) and the water depth (H), are transferred from the flow model as input parameters. A bilinear interpolation function is used to interpolate these flow fields from the finite difference mesh to the finite element mesh.

4. MODEL VERIFICATION

The transport model has been verified by simulating two different laboratory experiments and comparing the measured and predicted results. These experiments were carried out in SOGREAH, Grenoble, France in the framework of G8 Coastal Morphodynamics research programme of the MAST-2 project which was funded by the commission of the European Communities. These experiments included the cohesive sediment transport in an annular flume under uniform and alternating currents (Gallissaires et al., 1993).

4.1 Mud transport in an annular flume under uniform currents

The experiments on mud transport were carried out in an annular flume which comprised with two straight sections of 30m long and two 180^0 bends, each 12m long. The cross section is rectangular with a width of 1m and a depth of 0.4m. Currents were generated by an Archimedean screw submerged in the central part of the straight sections. The flow rate and direction of flow were determined by the screw speed and direction of rotation, respectively.

The mud used in this study were taken from the river Garonne at the mouth of the Bordeaux wet dock in France. Rheological measurements were carried out by using a rotating viscometer (Brookfield) in order to determine the yield stress of mud. The density profile of sediment deposits was estimated by settling column experiments. The mud bed in the flume was prepared by deposition from a suspension. At the end of a certain consolidation period, flow velocity in the flume was increased in discrete steps by increasing the speed of the Archimedean screw. Once the velocity was increased to a particular value, it was maintained for more than 40 minutes. The velocity and turbidity measurements were taken. A total of six erosion tests were performed based on different consolidation periods (t_s), ranging from 0.25 to 7.6 days. Out of these, three erosion tests are presented in figures 1 to 3. These figures are related to the erosion experiments on sediment beds which were consolidated to 0.25, 1.75 and 4.9 days, respectively.

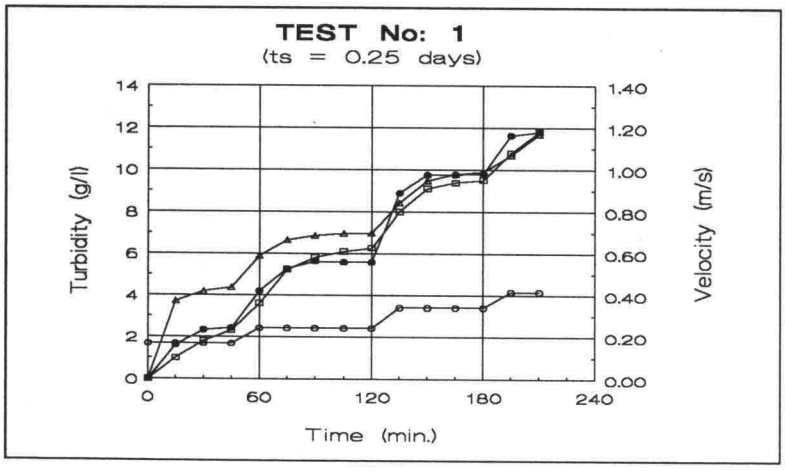

Figure 1 Time variation of concentration and velocity of erosion test no.1 (t_s =0.25 days) (o = Velocity, • = Experimental results, Δ = Erosion model given in Eq.(13), □ = Erosion model in given Eq.(15)).

The test reach of the annular flume was divided into 60 quadrilateral elements. A zero concentration gradient was imposed for the downstream flow boundary. The suspension concentration at the downstream boundary was used as the upstream boundary condition for the next time step in order to represent the recirculating system. Two erosion models described in Eq.(13) and Eq.(15) were used for the simulation of each erosion experiment. This allowed the possibility of comparing the behaviour of different erosion models with the same set of input data. A comparison of the predicted and measured suspended sediment concentration is given in figures 1 to 3.

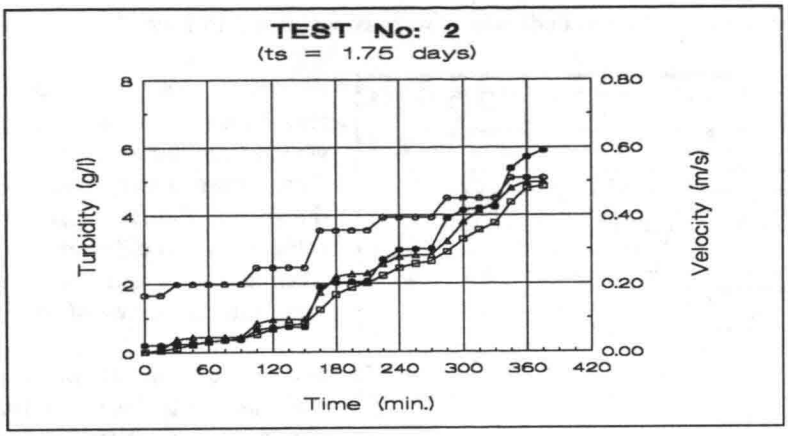

Figure 2 Time variation of concentration and velocity of erosion test no.2 (t_s =1.75 days) (o = Velocity, • = Experimental results, Δ = Erosion model given in Eq.(13), □ = Erosion model in given Eq.(15)).

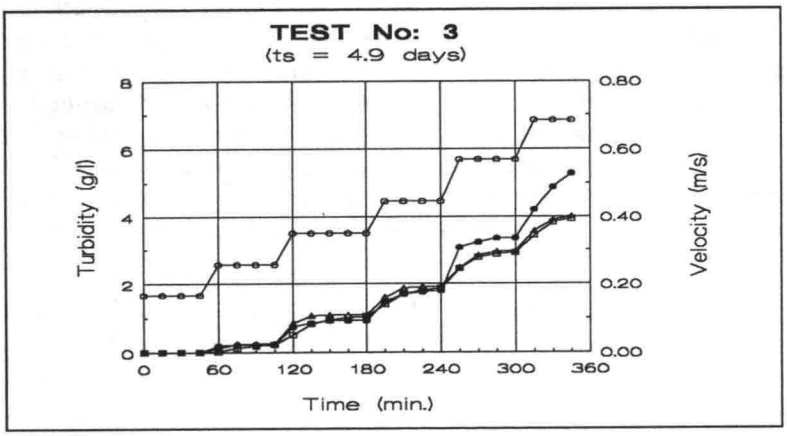

Figure 3 Time variation of concentration and velocity of erosion test no.3 (t_s =4.9 days) (o = Velocity, • = Experimental results, Δ = Erosion model given in Eq.(13), □ = Erosion model in given Eq.(15)).

A reasonable agreement was achieved between the experimental and model results for the temporal variation of suspended sediment concentration, for all test cases. The exponential form of the erosion rate expression gave a good agreement between the measured and the predicted suspension concentrations on relatively soft sediment beds, as shown in figure 1. The density profile in the sediment bed appeared to be highly sensitive to the simulated concentration profiles as it determined the critical shear stress for erosion.

4.2 Mud transport in an annular flume under alternating currents.

The same experimental set-up described in the previous section was used to perform a series of experiments on cohesive sediment transport under alternating currents (Gallissaires et al., 1993). The sediment bed in the flume was formed as in the previous tests. Four experiments

were carried out on sediment beds which were consolidated to four different time periods.

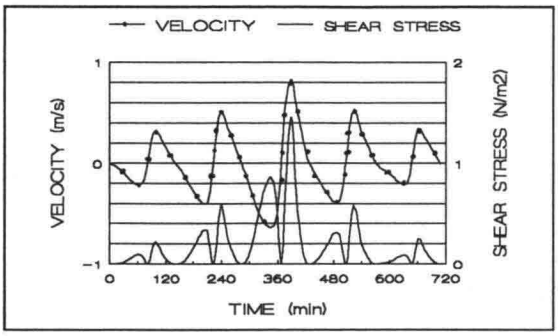

Figure 4 The distribution of mean velocity and bed shear stress during five tides (Gallissaires et al., 1993).

For each test, five tidal cycles were reproduced , successively. The mean velocity distribution and corresponding bed shear stress during five tidal cycles are shown in figure 4. During each test, velocity and turbidity measurements were taken at 2,5 10 and 25cm above the bed along the centre line of the flume.

The finite element mesh used in the previous tests was utilized for the simulation of these experiments. The boundary conditions for the transport model were the same as in the pervious tests. Density profiles of the sediment beds prior to the start of each experiment were estimated from a non-dimensional density profile based on a settling column experiment. Since the water depth in the flume was shallow and the slack water period was relatively short, aggregation of sediment particles during the test was assumed to be negligible. The settling velocity is, therefore, assumed as a constant in the deposition algorithm in this particular simulation. In addition, the log-normal deposition law described in Eq.(17) is also considered. Figures 5 and 6 show the comparison of the simulated suspension concentrations with the experimental results (depth-averaged) for the mud transport experiment under alteranating currents.

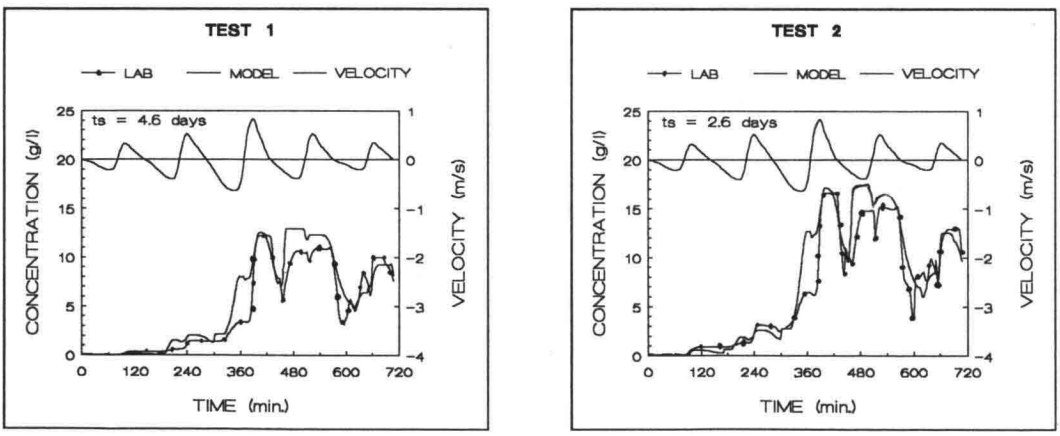

Figure 5 Time variation of the measured and predicted depth-averaged suspended sediment concentration in tests 1 and 2.

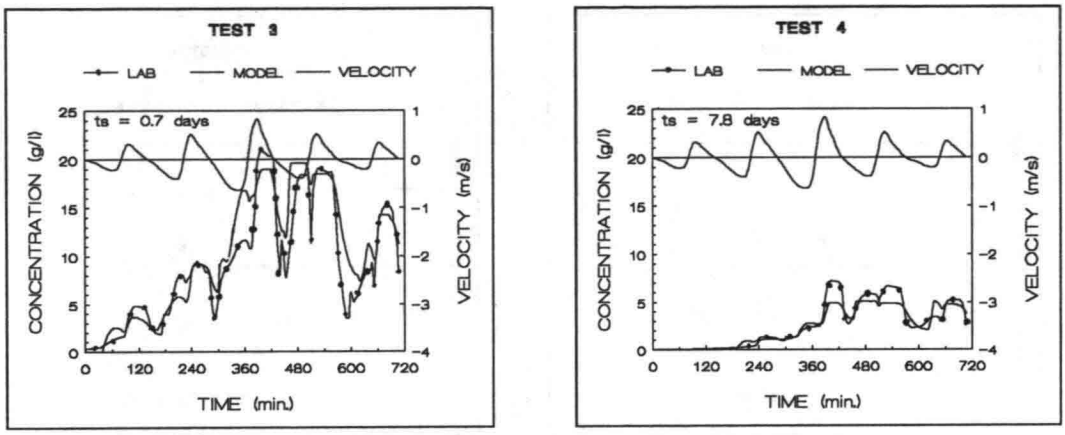

Figure 6 Time variation of the measured and predicted depth-averaged suspended sediment concentration in tests 3 and 4.

Good agreement was obtained between the experimental and the model results for variation of suspended sediment concentration of four tidal experiment. The discrepancies among the simulated and measured results were mainly associated with the estimation of bed density profile and the omission of the consolidation process of sediment deposits in the model. The concentration peaks appeared to be always lagged the velocity peaks during tidal experiment. This is caused by the scour lag which expressed the lag time between the erosion of sediment and the vertical diffusion of this sediment to the upper layers. The detailed analysis of the results is given in Pathirana (1994).

Comparison of actual and predicted sediment fluxes across the flume for all four experiments are shown in figures 7 and 8. The actual sediment flux across the flume was determined by the measured concentration profiles at 2, 5, 10 and 15cm above the bed, and also by the velocity profiles at the same location estimated from the depth-averaged velocity profile given in figure 4. Good agreement was observed between the actual and the predicted sediment fluxes for all four experiments.

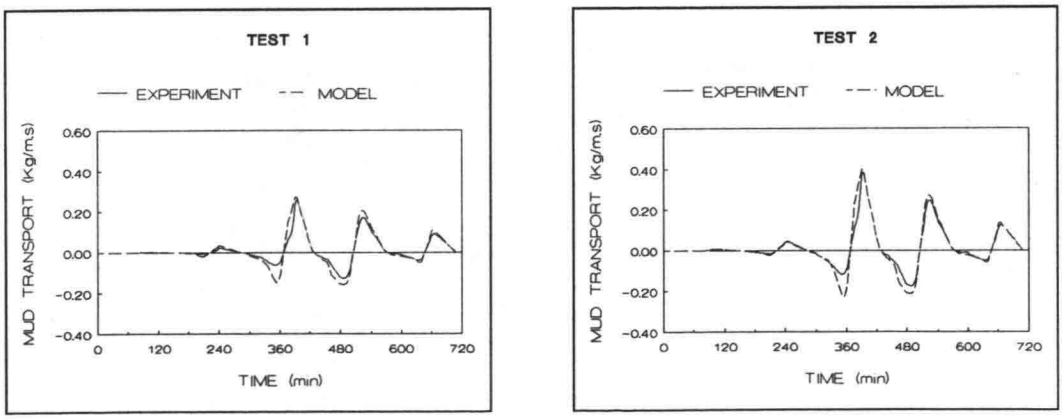

Figure 7 A comparison of mud transport between the laboratory and the model results for tests 1 and 2.

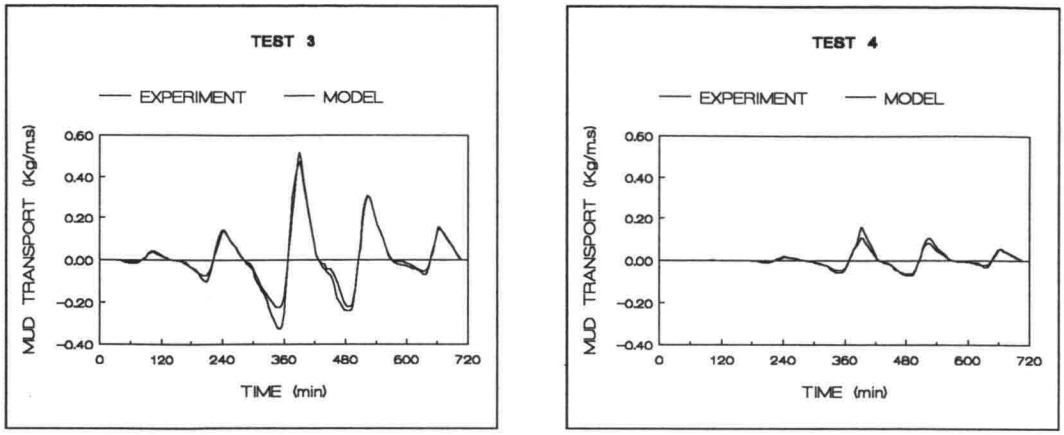

Figure 8 A comparison of mud transport between the laboratory and the model results for tests 3 and 4.

5. A REAL LIFE APPLICATION

5.1 Model description

The model was applied to a part of the Western Scheldt estuary from the Liefkenshoek in Belgium to Bath in the Netherlands to simulate the temporal and spatial variation of suspended sediment transport and sedimentation patterns (Figure 9). The problems related to the fine, cohesive sediments in this part of the estuary are reported to be severe as a result of heavy siltation.

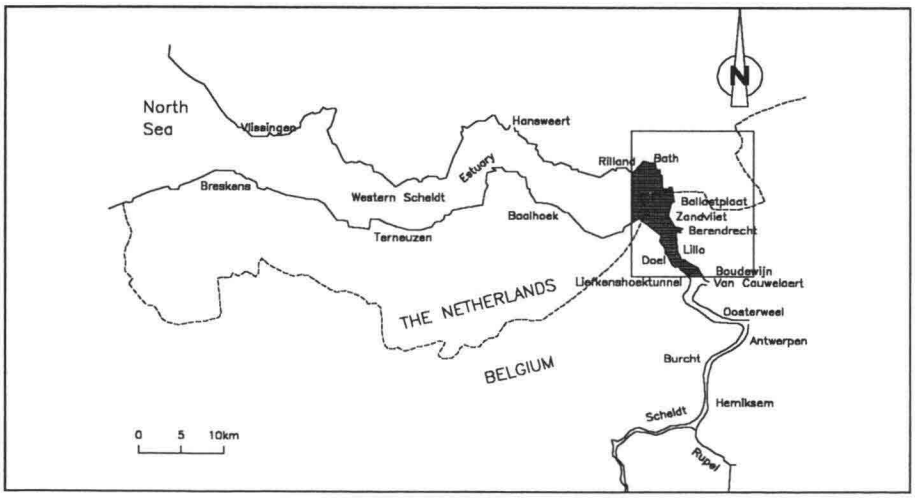

Figure 9 Location of the model area.

The Western Scheldt estuary is generally categorized as a well mixed to partially mixed estuary

due to its very low vertical salinity stratification, which only occur over short periods of tide, mostly during high water slack (Wartel, 1977). Moreover, hydrodynamic forces exerted by tides are the dominant forces in transporting suspended sediments in this estuary.

Although some of the hydrodynamic and sediment data required for the model simulation were collected from different sources, these field measurements were found to be insufficient to perform a complete model simulation and verification. The available measurements mostly covered only short time periods. Continuous measurements on mud transport and bed level variations for a sufficiently long period, are rare. This could be partly due to the very high cost involved in field measuring campaigns and partly due to frequent dredging works and ship movements which make it more difficult for accurate in-situ measurements on mud transport to be carried out. However, the field data collected during this study for the proposed model area, were fairly sufficient to perform a typical model simulation, but were not enough to verify the accuracy of the simulated results. However, typical model predictions are presented here in order to illustrate the applicability of the proposed model to real life engineering problems.

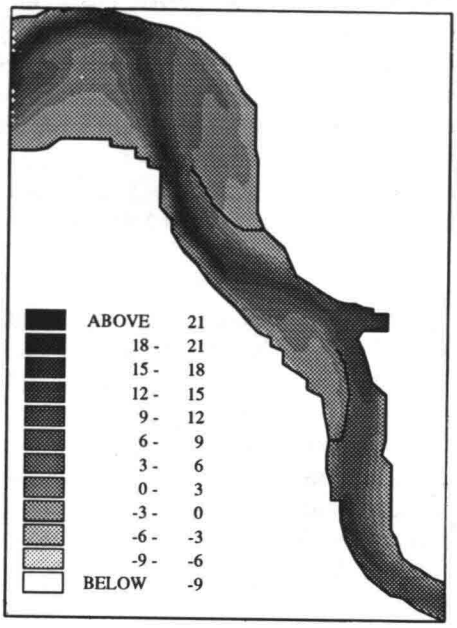

Figure 10 Bathymetry of the model area. Datum N.A.P. (in meters)

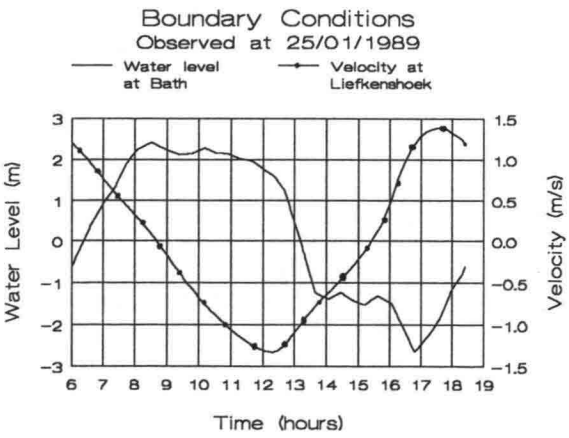

Figure 11 The boundary conditions used for the flow model.

The length of the model area is about 18 Km, and its bathymetry as reported in 1991, is shown in figure 10, which clearly indicates a deep navigation channel. The two submerged dikes shown, are used to conduct the flow during ebb. The flow model uses a regular grid size of 100m by 100m. The boundary conditions for the flow model were based on field measurements. The water level variations at Bath and the flow velocities at Liefkenshoek were used as the downstream and the upstream boundary conditions, respectively (Figure 11).

The finite element mesh used for the simulation of cohesive sediment transport, is shown in figure 12, which consists of nine noded quadrilateral elements. The required sediment data were chosen based on field measurements and literature (An., 1988; Mulder and Udink, 1990) as follows: settling velocity of cohesive particles was taken as constant and as equal to 2 mm/s, an erosion rate constant of 0.5 g/m^2 was used, and the critical shear stresses for deposition and erosion were taken as 0.2 Pa and 0.4 Pa, respectively.

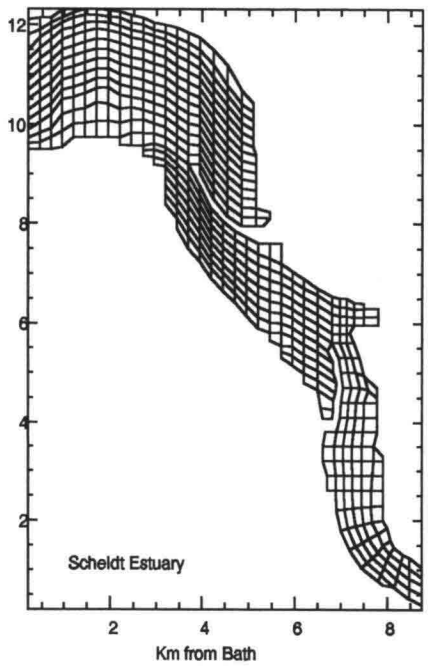

Figure 12 Finite element mesh used for the transport model.

The concentration boundary conditions used for the model simulation were based on the data found in Van Eck et al., (1991). According to this, a constant sediment concentration of 200 mg/l was imposed at the upstream boundary, and the downstream boundary was treated as a free flux condition during the ebb tide. Similarly during flood tide, the downstream boundary was fixed at 100 mg/l of sediment concentration and a free flux boundary condition was implemented at the upstream boundary. The simulations started with zero initial concentrations. It was assumed that no sediment particles would be eroded from the main body of the estuarine mud bed below the existing bathymetry, as the densities and shear stresses of these mud layers were reported to be sufficiently higher. The erosion process included in the model simulation was, therefore, only for the slack water deposits.

5.2 Results and discussion

The model results of the spatial variations of suspended sediment concentrations at various stages of a tidal cycle, are shown in figures 13 to 16. The velocity profiles of the model area at low water and high water are illustrated in figures 17 and 18. Figure 19 shows the deposition patterns predicted by the transport model after ten tidal cycles.

The field application revealed that the model predicted reasonable results on the spatial distribution of suspended sediment concentrations and deposition patterns over the model area during tidal cycles. According to the figures 13 to 16, large quantities of cohesive sediments entered into the estuary with the upstream river discharge and were advected and dispersed seaward due to downstream currents. The areas of high sediment concentration gradually moved downstream along the estuary, and finally reached close to the Zandvliet lock at low water slack.

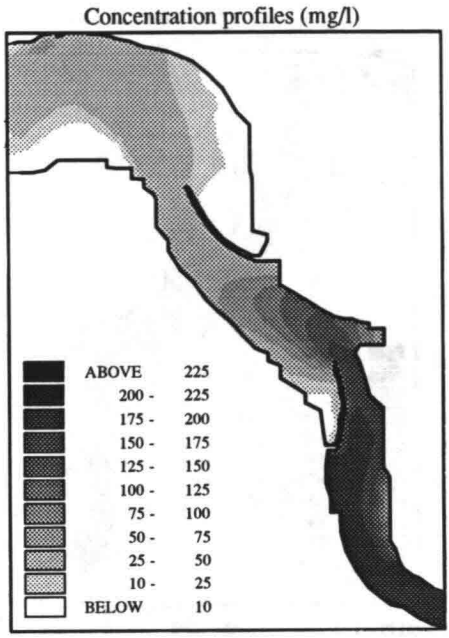

Figure 13 Concentration profiles at 3 hrs before low water.

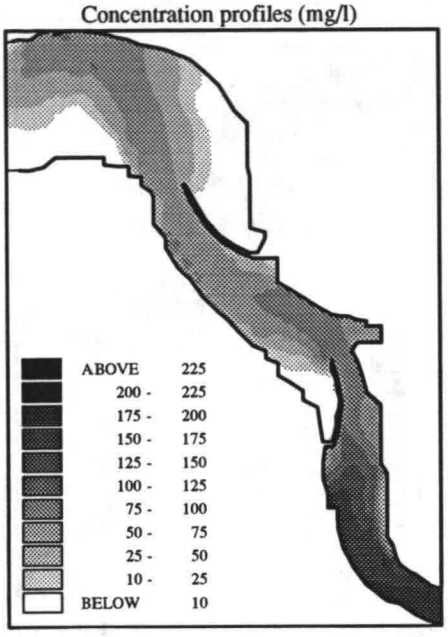

Figure 14 Concentration profiles at low water.

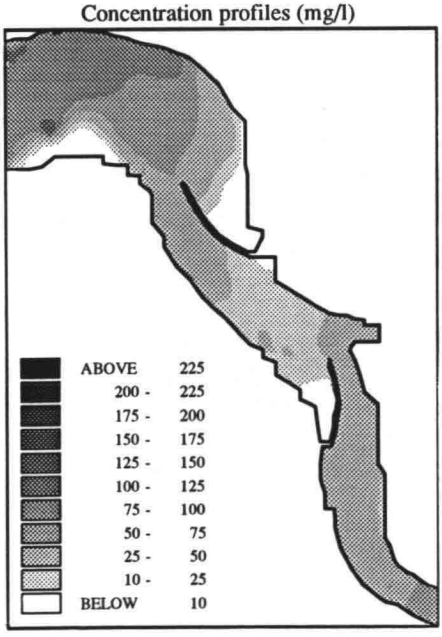

Figure 15 Concentration profiles at 3 hrs after low water.

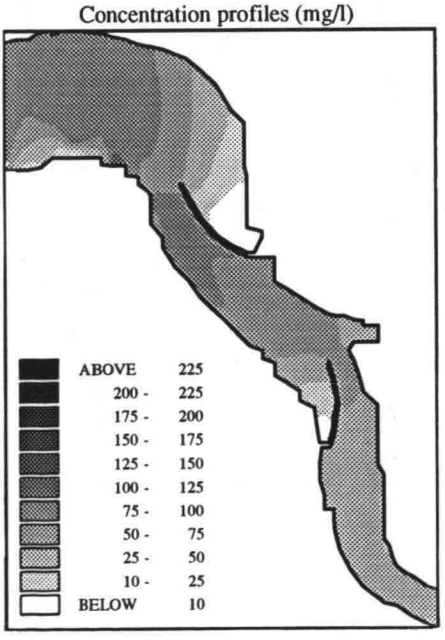

Figure 16 Concentration profiles at high water.

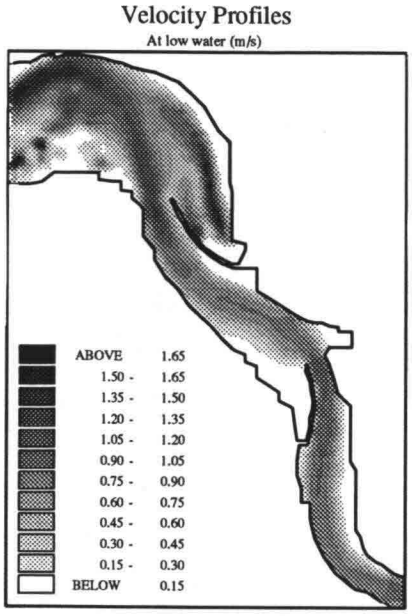

Figure 17 Velocity profiles at low water.

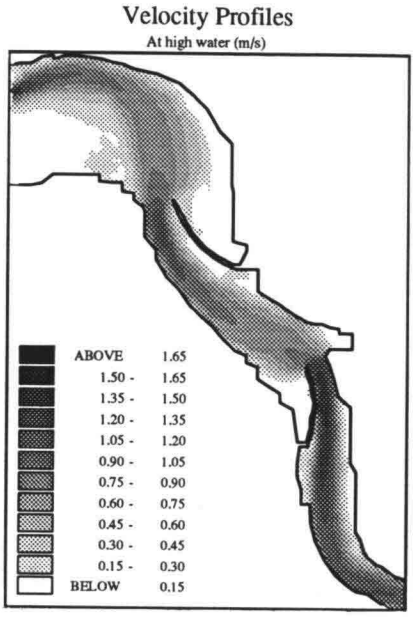

Figure 18 Velocity profiles at high water.

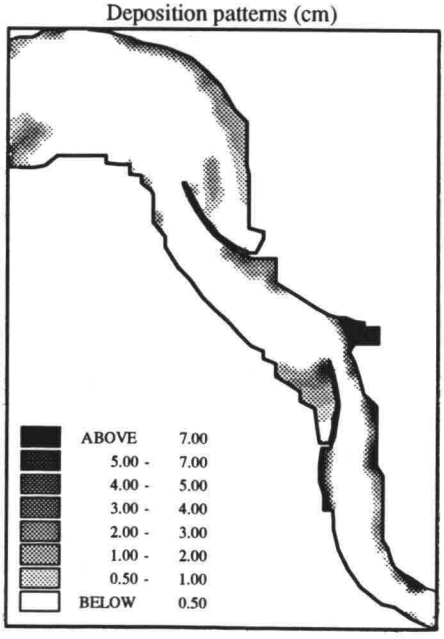

Figure 19 Deposition patterns predicted by the transport model after 10 tides.

However, when the flow direction was changed during high water, this sharp concentration front was gradually pushed upstream and fine sediments then entered into the model area from the downstream boundary. These sediments were advected and dispersed upstream due to tidal currents and eventually reached up to Ballastplaat during high water slack. However, the magnitude of the sharp concentration front during high water was relatively low as compared to the upstream concentration front predicted during low water. This behaviour was commonly observed during the entire model simulation.

Since the sharp concentration front moved into the estuary from the upstream boundary during low water, was completely moved out from the model area during high water, it would be reasonable to conclude that the area of turbidity maximum would be located outside of this model area, further upstream. This prediction is correct and is in accordance with the observations reported in the literature. According to Wartel (1977), the area of maximum sediment concentration was located between Antwerpen and Zandvliet. Similar observations made by Van Leussen et al. (1989), indicated that the high concentration zone was situated near the port of Antwerpen. It was further reported that the lowest sediment concentrations occurring during the tidal cycle were downstream of Zandvliet as far as the North Sea (Wartel, 1977). The simulated results followed a similar trend in the spatial distribution of suspended sediments to those reported in the literature.

The deposition pattern simulated by the model (figure 19), is not unexpected, as a larger amount of sediment deposition would be expected along the river banks, particularly close to the downstream boundary and entrance channels of the Berendrecht-Zandvliet locks. Similarly, the area close to the entrance channel of the Van Cauwelaert-Boundewijn locks appeared to be silted up. The deposition patterns observed in the model area were mainly due to the presence of relatively low flow velocities. These results are confirmed by the observations reported in the literature. Frequent dredging operations are carried out to maintain navigable depths in the entrance channels to these locks.

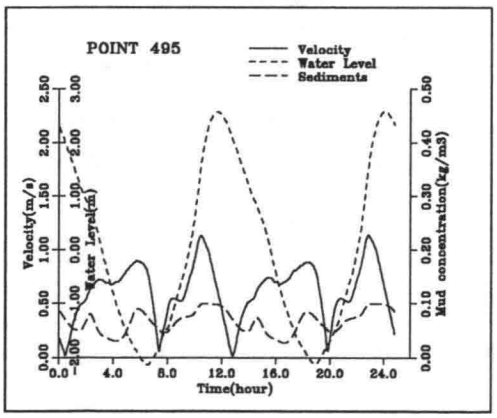

Figure 20 Model predictions at point 495.

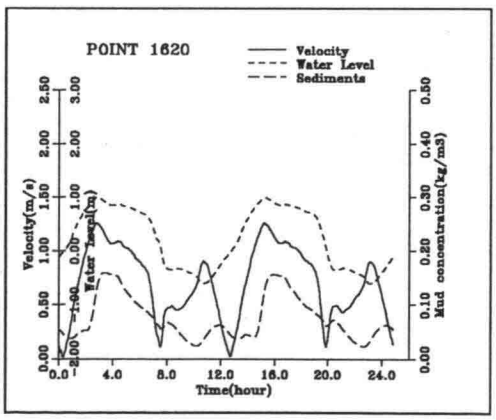

Figure 21 Model predictions at point 1620.

The suspension concentration-time record simulated by the transport model at nodes 495 and 1620 in the main navigation channel, are shown in figures 20 and 21. There were no

consistent measurements available from this area to verify these results. However, the concentration profiles simulated by the model appear to be reasonable. Both concentration peaks lag the corresponding velocity peaks, representing the effect of scour and settling lags in cohesive sediment transport, which occur due to the slow response of sediment particles to the flow (Dyer, 1988).

The above application shows that the model is capable of yielding reasonable results. This has been already confirmed by comparing these model predictions with two other transport models (Fettweis et al., 1993).

6. SUMMARY AND CONCLUSIONS

A numerical model has been developed which simulates the temporal and spatial distribution of fine, cohesive sediments and bed level changes in well-mixed estuaries. The sediment processes which includes. the erosion and deposition, have been incorporated in the model. The model has been verified through the experimental data. The simulated results of two laboratory experiments indicate that the algorithms used to describe the different sediment processes have successfully combined to predict the behaviour of a mud bed during uniform and alternating currents. The density profile of sediment bed largely influences the simulation results. In addition, a correlation between the critical bed shear stress for erosion and the dry density also plays an important role in the model predictions. The model has been applied to a part of the Western Scheldt estuary and the results have been discussed. Although the availability of field measurements was insufficient to verify the model results quantitatively, the model predictions were quite reasonable. However, a proper calibration of the model parameters is of considerable importance in modelling cohesive sediment transport in estuaries.

ACKNOWLEDGMENTS

The laboratory data used in this study were received from SOGREAH, Grenoble, France within the framework of G8 Coastal Morphodynamics research programme of the MAST-2 project which was funded by the commission of the European community. The authors wish to thank IMDC (International Marine and Dredging Consultants N.V., Antwerp, Belgium) in providing them with the measurement data for the Western Scheldt estuary. We also wish to thank Mrs. L.Van Rentergem in the University Computing Centre, for her assistance in visualization of the model results.

REFERENCES

An. (1988): Optimalisatie van de Onderhoudsbaggerwerken in de Toegangsgeul naar de Kallosluis- Mathematisch Model SLIBTRANS, IMDC Report, No. 906-88.01.02, IMDC, Antwerp, Belgium (in Dutch).

Ariathurai, R. & K. Arulanandan (1978): Erosion rates of cohesive soils, Technical notes, J. of Hydraulic Engineering, Vol.104, HY2, pp.279-283, ASCE.

Dronkers, J.J. (1969) : Tidal computations for rivers coastal areas and seas, J. of Hydraulic Engineering, Vol.95, HY1, ASCE, pp.29-77.

Dyer, K.R. (1988): Fine sediment particle transport in estuaries, "Physical processes in estuaries", (Job Dronkers & W. Van Leussen, eds.), Springer-Verlag,pp.295-310.

Dyer, K.R. (1989): Sediment processes in estuaries: Future research requirements, J. of Geophysical Research, Vol.94, No:C10, pp.14,327-14,339.

Fettweis, M., M. Sas, K.P.P. Pathirana, E. Jabbari & C.S. Yu (1993): Sediment transport modelling in the Scheldt estuary: Comparision of different models, Proc. of the Int. Conf. on Hydro-Science and Engineering, Vol. 1-Part B, (Sam S.Y. Wang, ed.), Washington DC., USA, pp.1705-1710.

Gallissaires, J.M. & J. Viguier (1993): Flume measurements of mud transport on a flat bottom under uniform and alternating currents, Internal Report No. 7285.1, MAST2-G8M, Project 4-Topic E, Mud Morphodynamics Modelling, SOGREAH, Grenoble, France.

Krone, R.B. (1962): Flume studies of the transport of sediment in estuarial shoaling processes, Final report, Hydraulic Eng. Laboratory & Sanitary Eng. Research Laboratory, University of California, Berkley.

Mehta, A.J. (1986): Characterization of cohesive sediment properties and transport processes in estuaries, Estuarine cohesive sediment dynamics', (Mehta A.J., ed.), Lecture notes on Coastal and Estuarine studies, No.14, Springer-Verlag, pp.290-325.

Mehta, A.J. (1988): Laboratory studies on cohesive sediment deposition and erosion, "physical processes in estuaries", (Job Dronkers & W. Van Leussen, eds.), Springer-Verlag, pp.427-445.

Mehta, A.J. & E. Partheniades (1973): Depositional behaviour of cohesive sediments, Technical Report No. 16, Coastal and Oceanographic Engineering Laboratory, University of Florida, Florida, USA.

Mulder, H.P.J. & C. Udink (1991): Modelling of cohesive sediment transport, A case study: The Western Scheldt Estuary, Int. Conf. on Coastal Engineering, July, pp.2-6.

Pathirana, K.P.P. (1994): Modelling cohesive sediment transport in estuaries and coastal waters, PhD Dissertation, Civil Engineering Department, Catholic University of Leuven, Belgium.

Pathirana, K.P.P., Z.W. Song & C.S. Yu (1992): Modelling tidal induced currents and transport on parallel computers, ENVIROSOFT 92, Proc. of IV Int. Conf. on Development and Applications of Computer Techniques in Environmental Studies, (P.Zannetti, ed.), Southampton (UK), pp.191-204.

Parchure, T.M. & A.J. Mehta (1985): Erosion of soft cohesive sediment deposits, J. of Hydraulic Engineering, Vol.111, No.10, ASCE, pp.1308-1326.

Van Eck, G.T.M., N. De Pauw, M. Van Langenbergh & G. Verreet (1991): Emissies, Gehalten, Gedrag en Effecten van (Micro) Verontreinigingen in het Stroomgebied van de Schelde en het Schelde-Estuarium, Water, No.60 (in Dutch).

Van Leussen, W. & E. Van Velzen (1989): High concentration suspensions: their origin and importance in Dutch estuaries and coastal waters, J. of Coastal Research, Special Issue No.5, Fort Lauderdale, Florida, USA, pp.1-22.

Wartel, S. (1977): Composition, transport and origin of sediments in the Scheldt Estuary, Geologie en Mijnbouw, Vol.56(3), pp.219-233.

Yu, C.S. (1993): Modelling shelf sea dynamics and estuarine circulations, PhD Dissertation, Civil Engineering Department, Catholic University of Leuven, Belgium.

Yu, C.S., K.P.P. Pathirana & J. Berlamont (1992): Tidal flow simulations and transport modelling in the Western Scheldt Estuary, Proc. of IX Int. Conf. on Computational Methods in Water Resources, (T.F. Russell et al., eds.), Denver, Colorado, USA, pp.649-656.

HYDRO-PORT'94
International Conference on Hydro-Technical
Engineering for Port and Harbor Construction
October 19 – 21, 1994, Yokosuka, Japan

Viscous Damping of Irregular Waves Propagating over Mud Seabeds

Zhao Zidan
Li Heqing

Tianjin University, Tianjin, 300072

ABSTRACT

The viscous damping of waves propagating over mud seabeds have been investigated in several papers, but nearly all of them only considered the case of regular waves propagating over mud seabeds, which is different with practical conditions in coastal areas. Therefore, the present authors try to investigate the case in which waves are irregular. Basic assumptions for this study are assumed as follows: (1) Water surface elevations can be expressed by the superposition of an infinite number of component regular waves with different periods; (2) Viscous damping of all the component waves can be treated as that of independent regular waves; (3) Water is treated as viscous fluid and mud as plastic fluid.

Key Words: Regular waves, Irregular waves, Bingham fluid, Wave damping coefficients, Wave spectrum.

1. INTRODUCTION

In muddy coatal areas there usually exists non-consolidated mud layer under water. In most cases mud behaves like a Bingham plastic fluid. Under the action of water waves, mud fluctuates and dissipates the energy of waves so that waves attenuate when they propagate over a muddy bottom. This paper focuses on the viscous damping of irregular waves propagating over mud seabeds, modeling the mud as Bingham fluid. The solution of this subject is extended from that given by Zhao and Jiang(1988) for the case of regular waves which had been awarded for the most outstanding paper by the 6th Congress of the Asian and Pacific Regional Division of the International Association for Hydraulic Research (1988, Kyoto, Japan) and also for the Scientific and Technical Advance by the State Council of Education of China(1991). The theory was reverified experimentally by the present authors(1993).

2. THORETICAL CONSIDERATION

Basic equations for the component regular waves in the case of irregular waves can be written

as follows:

$$\frac{\partial u_1}{\partial x}+\frac{\partial v_1}{\partial z}=0, \tag{1}$$

$$\frac{\partial u_1}{\partial t}=-\frac{1}{\rho_1}\frac{\partial p_1}{\partial x}+\nu_1\nabla^2 u_1, \tag{2}$$

$$\frac{\partial v_1}{\partial t}=-\frac{1}{\rho_1}\frac{\partial p_1}{\partial z}+\nu_1\nabla^2 v_1, \tag{3}$$

$$\frac{\partial u_2}{\partial x}+\frac{\partial v_2}{\partial z}=0, \tag{4}$$

$$\frac{\partial u_2}{\partial t}=-\frac{1}{\rho_2}\frac{\partial p_2}{\partial x}+\nu_2'\nabla^2 u_2, \tag{5}$$

$$\frac{\partial v_2}{\partial t}=-\frac{1}{\rho_2}\frac{\partial p_2}{\partial z}+\nu_2'\nabla^2 v_2, \tag{6}$$

in which the footnote 1 and 2 represents the upper layer(water) and the lower layer(mud) respectively (coordinate system as shown in Fig.1), ρ_1 is the density for water and ρ_2 is that for mud, ν_1 is the viscous coefficient for water and ν_2' is the equivalent viscous coefficient for mud, it can be expressed as:

$$\nu_2'=\frac{\eta_2}{\rho_2}+\frac{1}{\rho_2}\frac{\tau_B}{\overline{N}}. \tag{7}$$

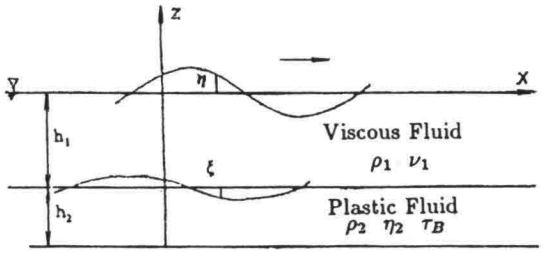

Fig.1 Coordinate system

Where η_2 is the rigid coefficient, τ_B is the Bingham yielding stress. According to Zhao and Jiang(1988), the parameter $\overline{N}$ can be determined by

$$\overline{N}=\frac{1}{2}kH_r\frac{|\overline{\omega}^2\cosh kh_1-gk\sinh kh_1|}{\overline{\omega}\sinh kh_2}\left(\frac{\sinh 2kh_2}{kh_2}\right)^{\frac{1}{2}}, \tag{8}$$

wave number k can be obtained by the following wave dispersion equation,

$$\begin{aligned}&[\rho_2\overline{\omega}^2\cosh kh_2-(\rho_2-\rho_1)gk\sinh kh_2](\overline{\omega}^2\cosh kh_1-gk\sinh kh_1)\\&+\rho_1\overline{\omega}^2\sinh kh_2(\overline{\omega}^2\sinh kh_1-gk\cosh kh_1)=0,\end{aligned} \tag{9}$$

and, $\overline{\omega}=2\pi/\overline{T}$, $\overline{T}$ is the wave period in average, H_r is the root-mean-square wave height.

According to the assumption that the water surface elevation can be expressed by the superposition of an infinite number of component regular waves with different periods, the water surface elevation at any fixed point can be expressed as

$$\eta(t) = \sum_{i=1}^{M} a_j \cos(\omega_j t + \theta_j), \tag{10}$$

where a_j is the amplitude of the j-th component wave, ω_j and θ_j its corresponding angular frequency and initial phase, θ_j is a uniform and random distribution in the area of $(0, 2\pi)$, M is a positive and large enough number.

Similar as that for the case of regular waves, the amplitudes of component waves for irregular waves can be given as

$$a_{sj} = a_{0j} \exp(-\varepsilon_j / s), \tag{11}$$

in which a_{0j} is the amplitude of the j-th component wave at initial position, a_{sj} is also the amplitude of j-th component wave but far from the initial position with the distance of s, and, ε_j is the corresponding wave attenuation coefficient, its calculating method had been introduced by the previous papers (see Zhao and Jiang,1988; Zhao *et al*,1993). Therefore, the water surface elevation at any point far from the initial position with distance s can be expressed by

$$\eta_s(t) = \sum_{i=1}^{M} a_{0j} \exp(-\varepsilon_j / s) \cos(\omega_j t + \theta_j). \tag{12}$$

Thus the transformation of irregular waves over mud bottom can be determined if a_{0j} and ω_j are known. In fact, the amplitudes and angular frequencies for component waves can be determined from theoretical or experimental wave spectra. As a matter of convenience, the authors take the frequency f instead of angular frequency ω ($\omega = 2\pi f$) and divide the region f_L–f_H(which includes the most part of energy, see Fig.2) into M sub-regions, thus the frequency interval $\Delta f_j = f_j - f_{j-1}$. Let $\hat{f}_j = (f_j - f_{j-1})/2$, and treat the waves between f_j and f_{j-1} as a component wave whose frequency is $\tilde{f}_j$, where $\tilde{f}_j$ can be selected by random sampling in the domain of f_{j-1} to f_j, the amplitude $a_j = \sqrt{(S(\hat{f}_j) \cdot \Delta f_j)}$.

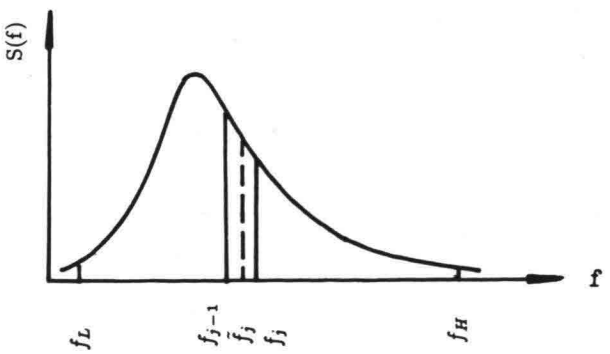

Fig.2 Sketch used for dividing the frequency interval for wave spectrum

After the suitable time interval Δt is selected, the wave surface at initial position and another position far from the former with the distance of s at $t = n\Delta t$ can be given by

$$\eta_0(n\Delta t) = \sum_{i=1}^{M} \sqrt{2S_0(\hat{f}_j)\Delta f_j}\cos(2\pi \tilde{f}_j n\Delta t + \theta_j), \tag{13}$$

and

$$\begin{aligned}\eta_s(n\Delta t) &= \sum_{i=1}^{M} \sqrt{2S_s(\hat{f}_j)\Delta f_j}\cos(2\pi \tilde{f}_j n\Delta t + \theta_j') \\ &= \sum_{i=1}^{M} \sqrt{2S_0(\hat{f}_j)\Delta f_j}\exp(-\varepsilon_j/s)\cos(2\pi \tilde{f}_j n\Delta t + \theta_j'),\end{aligned} \tag{14}$$

respectively, where $S_0(\hat{f}_j)$, $S_s(\hat{f}_j)$ are their corresponding wave spectrum and $\sqrt{2S_0(\hat{f}_j)\Delta f_j}$, $\sqrt{2S_s(\hat{f}_j)\Delta f_j}$ their corresponding wave amplitudes, thus the propagation of irregular waves' spectrum can be given as

$$S_s(\hat{f}_j) = S_0(\hat{f}_j)\exp(-2\varepsilon_j/s). \tag{15}$$

It is obvious that the absolute value of the transfer function of wave spectrum in the propagation processes for irregular waves is

$$|T(\hat{f}_j)| = \exp(-\varepsilon_j/s). \tag{16}$$

Of course, the relationship between wave spectrum expressed by the frequency and that by the angular freqency is

$$S(\omega) = S(2\pi f) = \frac{1}{2\pi}S(f). \tag{17}$$

3. EXPERIMENTS

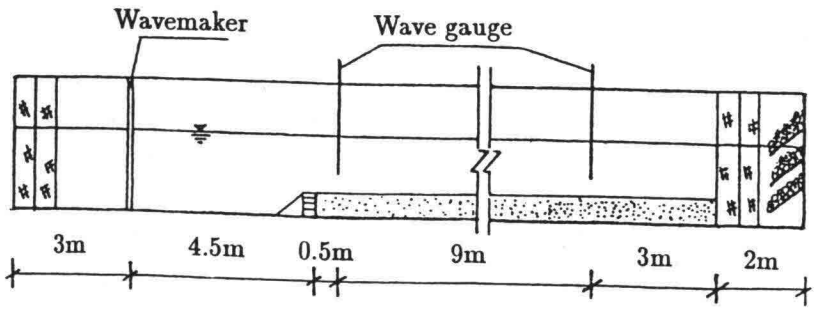

Fig.3 Sketch for experimental arrangements

The experimental work was carried out at the State Key Laboratory on Offshore and Coastal Engineering at Dalian University of Technology. The flume is 22m long, 0.45m wide and 0.50m deep. At the end of the flume, a wave maker which can produce irregular wave motion was installed. The soils were taken from the New Port of Tianjin and their median diameter was 0.0036mm. Wave heights are observed by four gages at equal apart 3m. Experimental arrangements are shown in Fig. 3.

In order to model irregular wave motion, the Jonswap wave spectrum is used, it can be expressed as

$$S(f) = \alpha {H_{1/3}}^2 \frac{1}{{T_p}^4 f^5} \exp\left[-\frac{5}{4}\left(\frac{1}{T_p f}\right)^4\right] r^{\exp\left[-\frac{(T_p f-1)^2}{2\sigma^2}\right]}, \tag{18}$$

in which

$$\alpha = \frac{0.0624}{0.230 + 0.0336r - 0.185(1.9+r)^{-1}}, \tag{19}$$

$$\sigma = \begin{cases} \sigma_a : & f \le f_p \\ \sigma_b : & f > f_p. \end{cases} \tag{20}$$

f_p is the peak spectrum frequency, T_p is the period of peak spectrum, i.e., $T_p = 1/f_p$; r is a parameter and is used to express the tip degree of the spectrum (r=1–7), here the average value $r = 3.3$ is selected; $\sigma_a = 0.07$ and $\sigma_b = 0.09$.

Values of water surface elevation at four positions were recorded by the computer. The time interval for sampling is $\Delta t = 0.05$, and sampling time is 102s, thus 2048 values at each position for each experiment are recorded. The statistical values from experimental waves and wave spectra were also analysed by computer.

The density of mud used for the experiment is 1.029–1.316 g/cm^3.

4. ANALYSIS ON THE CALCULATED AND EXPERIMENTAL RESULTS

Here the present authors treat the waves observed at the initial position as incident waves and numerically model the observed wave spectrum by Eq.(13), thus the calculated component waves for irregular waves can be obtained. The observed wave spectrum can be obtained by Fast Fourier Transform (FFT), i.e., the wave spectrum can be determined by

$$S(\frac{r}{N\Delta t}) = \frac{2\Delta t}{N}|A_r|^2, \quad r = 0, 1, 2, \cdots, \frac{N}{2}, \tag{21}$$

in which

$$A_r = \sum_{k=0}^{N-1} \eta_k \exp(\frac{2\pi}{N} rk), \tag{22}$$

η_k is the k-th value of the recorded water surface elevations (k=0,1,$\cdots$,N-1), N is the total number of the recorded data of the water surface elevation. According to the requirment of

FFT, $N = 2^m$, m is a positive integer.

After the measured wave data being analysed, it was found that the periods of waves in most cases are over 0.5s, thus the cut-off frequency can be taken as $f_c = 2.0$Hz. Sampling time interval used for experiments is $\Delta t = 0.05$s, then the following equation is satisfied

$$f_c \leq \frac{1}{2\Delta t}, \tag{23}$$

therefore, the folding effect of frequency can be ignored. Based on the results of spectral analysis, when

$$f = \frac{r}{N\Delta t} \geq \frac{204}{2048 \times 0.05} = 1.9921875, \tag{24}$$

the spectral energy can be omitted, thus the preceeding 204 records of scattered values in this range(f less than 1.992Hz) can be taken and then smoothed by the rectangular method, hence the observed spectrum at initial position can be obtained. The former methods can also be used for analysing the wave spectrum at other positions.

Here the dividing section number used for numerically modelling observed wave spectrum at initial position was taken as $M = 40$. It was indicated that this dividing section number can be used for obtaining good results. In order to divide the section, The method of equi-dividing energy was used, where $\tilde{f}_j$ was obtained by random selecting at the second half region for every divided section, the initial phase (random value) θ_j was given by computer.

In order to caculate irregular waves, $\Delta t = 0.05$s was also selected. Water surface elevations for $n = 0, 1, \cdots, 2047$ at every observed position were caculated by Eq.(14) and wave spectra at the same position were caculated by Eq.(15) .

4.1 Comparisons between Observed and Calculated Statistical Wave-heights

The statistical analysis of a series of observed and calculated water surface elevation values for waves was carried out by the method of zero-up-crossing. Table 1 shows parts of the results, in which H_{me}, H_{re} and H_{se} represent the experimental values for mean wave height, root-mean-square wave height and significant wave height, H_{mcl}, H_{rcl}, H_{scl} are their corresponding calculated values respectively. In Table 1, wave heights, water depth(h_1) and mud layer depth(h_2) are measured by cm, the density of mud(ρ_2) by g/cm^3, the rigid coefficient of mud(η) by 10^{-5} N$\cdot$ s/cm^2 and the Bingham yielding strss(τ_B) by 10^{-5} N/cm^2. The difference between H_{me} and H_{mcl}, H_{re} and H_{rcl}, and H_{se} and H_{scl} at initial position denotes the difference between experimental and numerically modelling waves. It can be found that the agreement between them seems quite well. It can also be found out that the larger the density of mud becomes, the more rapidly wave heights attenuate (see Table 1).

4.2 Comparisons between Observed Wave Heights and the Results Calculated by the Method of Representative Waves

Based on the method of representative waves, the irregular wave attenuation was also studied, in which the wave period at initial position was expressed by average wave period, and the representative wave heights by average wave heights, or by root-mean-square wave heights or by the highest one-third wave heights(i.e., significant wave heights). Parts of the

Table 1 Observed and calculated wave heights

T09254	h_1=20.00		h_2=10.00	ρ_2=1.078		η_2=0.0110	τ_B=1.890	
No.	H_{me}	H_{mc1}	H_{mc2}	H_{re}	H_{rc1}	H_{rc2}	H_{se}	H_{sc1}	H_{sc2}
0	4.90	4.75	4.90	5.21	5.10	5.21	6.96	6.95	6.96
1	4.85	4.51	4.54	5.18	4.84	4.84	7.14	6.60	6.54
2	4.41	4.19	4.22	4.82	4.41	4.50	6.71	5.69	6.14
3	4.44	4.06	3.91	4.77	4.27	4.19	6.46	5.58	5.77

T07108	h_1=20.00		h_2=10.00	ρ_2=1.120		η_2=0.0202	τ_B=3.722	
No.	H_{me}	H_{mc1}	H_{mc2}	H_{re}	H_{rc1}	H_{rc2}	H_{se}	H_{sc1}	H_{sc2}
0	5.76	5.72	5.76	6.26	6.21	6.26	8.67	8.48	8.67
1	5.73	5.18	5.24	6.21	5.65	5.71	8.48	7.86	8.03
2	5.26	4.83	4.76	5.70	5.16	5.22	7.77	7.02	7.44
3	4.93	4.61	4.32	5.38	4.90	4.76	7.37	6.51	6.90

T07172	h_1=22.50		h_2=7.50	ρ_2=1.167		η_2=0.0260	τ_B=8.614	
No.	H_{me}	H_{mc1}	H_{mc2}	H_{re}	H_{rc1}	H_{rc2}	H_{se}	H_{sc1}	H_{sc2}
0	3.27	3.33	3.27	3.48	3.52	3.48	4.69	4.65	4.69
1	2.77	2.83	2.65	2.97	2.99	2.85	4.09	3.99	3.96
2	2.83	2.31	2.15	2.97	2.42	2.33	3.86	3.18	3.35
3	2.26	2.22	1.75	2.38	2.30	1.90	3.14	2.99	2.83

T07235	h_1=24.60		h_2=5.40	ρ_2=1.234		η_2=0.0410	τ_B=31.800	
No.	H_{me}	H_{mc1}	H_{mc2}	H_{re}	H_{rc1}	H_{rc2}	H_{se}	H_{sc1}	H_{sc2}
0	4.32	4.34	4.32	4.66	4.63	4.66	6.45	6.12	6.45
1	3.17	3.27	3.17	3.43	3.47	3.42	4.81	4.67	4.85
2	2.53	2.77	2.32	2.71	2.92	2.51	3.65	3.83	3.65
3	2.17	2.44	1.70	2.26	2.52	1.85	2.91	3.10	2.75

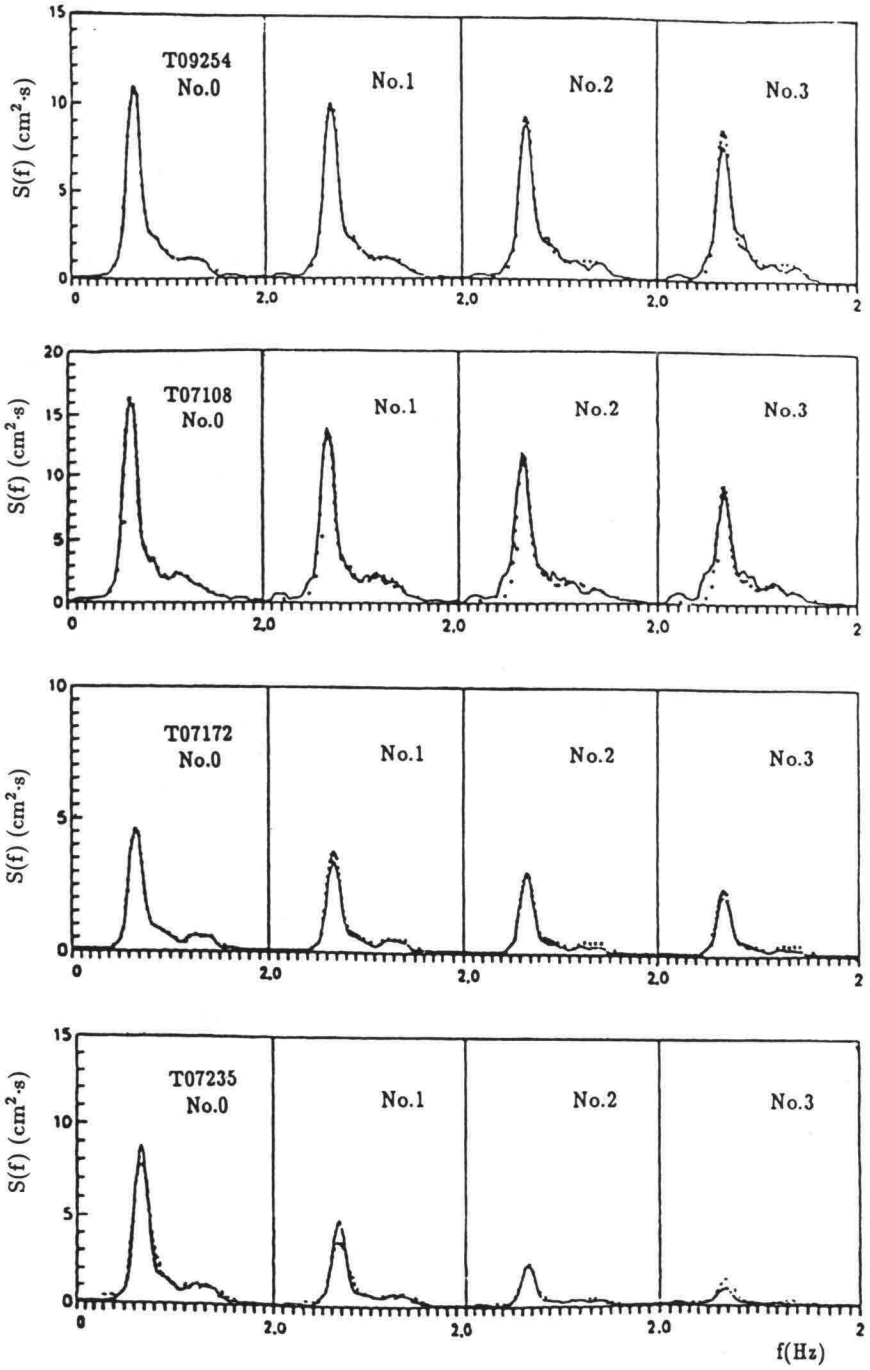

Fig.4 Measured and calculated wave spectra

calculated results were shown in Table 1, in which H_{mc2} represents the calculated average wave heights, H_{rc2} the calculated root-mean-square wave heights and H_{sc2} the calculated values of the highest one-third wave heights. It seems that the agreement between observed and calculated significant wave heights is better.

4.3 Comprarisons between Observed and Calculated Wave Spectrum

Fig. 4 shows parts of the observed and calculated wave spectra, in which the solid lines denote the observed results and the points denote the calculated results. It can be found out that they are very close to each other. In the 9m long experimental section in flume, the peak frequencies of spectra along wave direction are nearly the same, but the peak values of spectra along wave direction gradually decrease, and decrease faster with the increase of the density of mud. The wave attenuation coefficients for different component waves are different since their corresponding periods are different in general. In fact, this can be found out from Eq.(15). Fig.5 shows the relationship between wave attenuation coefficient and wave frequency, it indicates that the main parts of the waves decrease faster.

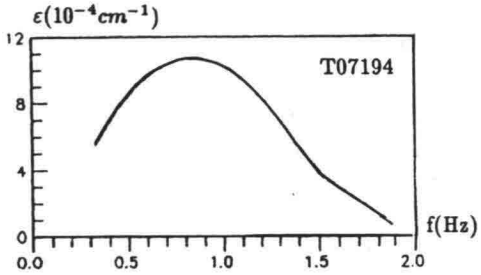

Fig.5 The relationship between wave attenuation coefficients and wave frequencies

Wave spectrum can also be calculated by FFT from the values of water surface elevation given by Eq.(14), the dotted lines in Fig.4 show the calculated results by this method.

5. CONCLUSIONS

Main conclusions of the present study are summarized as follows:

1) The theoretical results for regular waves over mud seabeds given by Zhao and Jiang(1988) were successfully extended to the case of irregular waves propagating over mud seabeds when the water surface elevation for irregular waves were expressed by the superposition of an infinite number of component waves with different periods.

2) If irregular waves propagating over mud seabeds were expressed by the representative wave with average period and significant wave height, the viscous damping of this wave along its own propagating direction can be directly determined by the theory of Zhao and Jiang(1988).

ACKNOWLEDGEMENTS

This study was finacially supported by the State Key Laboratory on Offshore and Coastal Engineering at Dalian University of Technology, Dalian, China; the authors are grateful to Madam Meiyi Guo, an engineer of that laboratory, for her help on the experimental work.

REFERENCES

Zhao,Z. and L. Jiang(1988): Study on the interaction between waves and mud bottom, Procedings of the Sixth Congress of the Asian and Pacific Regional Division of International Association for Hydraulic Research, Kyoto, Japan, Vol.IV, pp.105–111.

Zhao,Z.,H. Li and M. Guo(1993): Transformation of waves over fluid mud beds, Marine Science Bulletin, Vol.12, No.1, pp.1–9(in Chinese).

Zhao,Z.,H. Li and M. Guo(1993): Experiment study on transformation of irregular waves over fluid mud beds, Marine Science Bulletin, Vol.12, No.4, pp.1–8(in Chinese).

AUTHOR INDEX

A

Accetta,D. 871
Adachi,Kazumi 377
Adachi,Kumiko 977
Akahoshi,T. 443
Akamura,S. 107
Allsop,N.W.H. 525
Amin,Z. 405
Anand,D. 317
Aono,T. 217
Asai,T. 67, 93, 203

B

Bahk,K.S. 83, 93
Barthel,V. 333
Berlamont,J. 1271
Bouchet,R. 581
Burcharth,H.F. 123

C

Cellario,P. 581
Chang,C.-K. 1179
Chang,F.-T. 1179
Charles,S.V. 843
Chen,C.C. 721
Chien,C.H. 473
Chiou,Y.D. 473

D

Davies,J. 143
Dias,W.S.S. 871

F

Fredsøe,J. 1097
Fujimoto,T. 593, 1225
Fujisaki,H. 707
Fujiwara,R. 543
Fukuta,M. 1077
Fukuya,M. 1059
Funakoshi,H. 673, 1157
Furukawa,K. 953

G

Geshi,H. 707
Goda,Y. 1
Gökçe,T. 1097
Gomyoh,M. 977
Goto,C. 217
Guangwen,H. 423

H

Harikai,S. 1059
Hashimoto,N. 67, 93, 203
Hida,Y. 1193
Higano,J. 977
Higashiyama,S. 67
Hiraishi,T. 281
Hitachi,S. 765
Hong,S.K. 941
Hooper,P.M. 1211
Horie,T. 93, 907
Hosokawa,Y. 885, 907, 953
Hosoyamada,T. 733
Hou,H.S. 473, 721
Hu,T.M. 721

I

Iida,I. 967
Ikeda,M. 1059
Ikeda,N. 281
Ikeya,T. 353
Imberger,J. 23
Inada,H. 107
Inoue,S. 907
Irie,I. 43, 1253
Isnard,J.L. 581
Isozaki,I. 227
Istiyanto,D.C. 641
Ito,K. 203
Iwase,K. 353

J

Janardanan,K. 1141
Jeon,K.C. 83
Jiang,J. 1243
Jiménez,J.A. 1041
Juhl,J. 505
Jung,T.S. 805

K

Kakuno,S. 543
Kang,S.W. 83, 805
Katoh,K. 1019, 1077, 1117
Katsui,H. 785
Kawada,M. 765
Kawahara,T. 443
Kihara,T. 1225
Kim,C.S. 83
Kim,S.I. 83
Kimoto,K. 977
Klammer,P. 453
Kobayashi,A. 203
Koizuka,T. 593, 1225
Komoto,Y. 691
Kono,T. 405
Kortenhaus,A. 453
Kubo,Y. 303
Kubota,S. 1193

Kunisu,H. 393
Kurata,K. 543
Kuriyama,Y. 1117
Kwon,J.G. 175

L

Lee,D.S. 563
Lee,D.Y. 83, 93
Lee,J.N. 941
Li,H. 1291
Liu,Z. 123
Lord,D.A. 23

M

MacDonald,D.D. 333
Mansard,E.P.D. 253, 333
McBride,M.W. 525
McGehee,D.D. 165
Minami,J. 353
Miyazaki,S. 377
Montoya R.J.M. 999
Mori,S. 707
Moriguchi,A. 823
Moutzouris,C.I. 987
Murakami,K. 907,921,1253
Mutoh,A. 707

N

Nadaoka,K. 785
Nagai,K. 1253
Nagai,T. 67, 93, 203
Nakagawa,M. 977
Nakamura,Satoshi 1077
Nakamura,Shigehisa 187
Nakayama,A. 823
Niidome,Y. 593
Niwa,C. 885
Nwogu,O.G. 253

O

Oda,K. 543
Oh,B.C. 83, 93, 239
Oh,Y.M. 563
Ohashi,H. 107
Ohnaka,S. 365
Ohtani,H. 785
Ojima,R. 691
Okuyama,Y. 377
Ootsuki,T. 885
Ota,K. 1059
Otsuki,T. 977
Oumeraci,H. 453
Owaki,T. 691
Ozaki,Y. 1117

P

Park,K.S. 83, 93
Park,W.S. 563
Parker,W.R. 1211
Pathirana,K.P.P. 1271
Pattiaratchi,C. 23
Picó,J.M. 1041
Pilarczyk,K.W. 617

R

Rodoriguez P.,J.G. 1019

S

Sánchez-Arcilla,A. 1041
Sano,K. 673
Santos,J.A.dos. 871
Sasajima,H. 593, 1225
Sasayama,H. 593, 1225
Sato,N. 217
Sato,Seiji 907
Sato,Shoji 999
Sega,Y. 907
Seo,K.D. 93
Sekimoto,T. 393
Shibata,T. 203
Shim,J.S. 83, 239
Shimada,M. 303
Shimizu,K. 921
Shimizu,T. 303
Shimosako,K. 489, 747
Shin,M.S. 941
Shiozawa,T. 1157
Shiraishi,S. 443
Sierra,J.P. 1041
Sigurdarson,S. 651
Simizu,N. 673
Sivalingam,P.M. 843
Smallman,J.V. 267, 525
Suda,Y. 977
Sudarpo 641
Sugahara,K. 67
Sugiura,S. 443
Suh,K.D. 239, 563
Sumer,B.M. 1097
Sundar,V. 317, 1141
Suzuki,M. 107
Suzuki,Yasumasa 281
Suzuki,Yasushi 227

T

Tadokoro,A. 1157
Takahashi,S. 489, 733, 747
Takaki,N. 1059

Takayama,T. 281
Takezawa,M. 1193
Tanahashi,T. 227
Tanimoto,K. 489
Teruya,M. 377
Tobiki,I. 203
Toda,K. 67
Tonder,A.van 143
Toue,T. 203
Tozer,N.P. 267
Tsuda,H. 405
Tsuda,S. 673, 1157
Tsuruya,H. 765, 1253

U

Ueda,S. 443
Ueno,S. 785
Uesugi,T. 967
Ukai,A. 303

V

Vargas,B.M. 871
Vera S.,J.R. 999
Viggosson,G. 651
Villanueva,E.J. 1041
Villaverde,J.M.M. 1131
Viñuales,A. 1041

W

Weibing,F. 423
Widagdo,A.B. 641

Y

Yamada,K. 921
Yamagata,N. 691
Yamamoto,J. 823
Yamamoto,M. 823
Yamamoto,S. 733
Yamazaki,T. 393
Yanagishima,S. 1077
Yang,Y.M. 175
Yauchi,E. 967
Yokobori,K. 967
Yoshida,Tadashi 673
Yoshida,Toshiharu 543
Yoshinaga,H. 1225
Yoshinaga,K. 1225
Yoshizawa,T. 365
Yu,C.S. 1271

Z

Zhao,Z. 1291